Syntheses and Properties of Conjugated Polycyclic Molecules Containing Heptazethrene, Indacene, and Azulene Cores

A Thesis Submitted

In Partial Fulfillment of the Requirements

for the Degree of

DOCTOR OF PHILOSOPHY

by

Priyank Kumar Sharma

2019CYZ0005

DEPARTMENT OF CHEMISTRY

INDIAN INSTITUTE OF TECHNOLOGY ROPAR

May, 2024

Priyank Kumar Sharma: *Syntheses and Properties of Conjugated Polycyclic Molecules Containing Heptazethrene, Indacene, and Azulene Cores*

DEDICATED

TO

MY PARENTS & ALL LOVED ONES

Declaration of Originality

I hereby declare that the work which is being presented in the thesis entitled **Syntheses and Properties of Conjugated Polycyclic Molecules Containing Heptazethrene, Indacene, and Azulene Cores** has been solely authored by me. It presents the result of my own independent investigation/research conducted during the time period from July 2019 to May 2024 under the supervision of Dr Soumyajit Das, Assistant Professor, IIT Ropar. To the best of my knowledge, it is an original work, both in terms of research content and narrative, and has not been submitted or accepted elsewhere, in part or in full, for the award of any degree, diploma, fellowship, associateship, or similar title of any university or institution. Further, due credit has been attributed to the relevant state-of-the-art and collaborations with appropriate citations and acknowledgments, in line with established ethical norms and practices. I also declare that any idea/data/fact/source stated in my thesis has not been fabricated/ falsified/ misrepresented. All the principles of academic honesty and integrity have been followed. I fully understand that if the thesis is found to be unoriginal, fabricated, or plagiarized, the Institute reserves the right to withdraw the thesis from its archive and revoke the associated Degree conferred. Additionally, the Institute also reserves the right to appraise all concerned sections of society of the matter for their information and necessary action (if any). If accepted, I hereby consent for my thesis to be available online in the Institute's Open Access repository, inter-library loan, and the title & abstract to be made available to outside organizations.

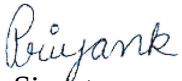

Signature

Name: Priyank Kumar Sharma
Entry Number: 2019CYZ0005
Program: PhD
Department: Chemistry
Indian Institute of Technology Ropar
Rupnagar, Punjab 140001

Date: 23/08/2024

Acknowledgments

I would like to take this opportunity to acknowledge some very special people who have been integral parts of my journey so far.

First and foremost, I would like to express my deepest gratitude to my supervisor, **Dr. Soumyajit Das**, for his constant support, guidance, inspiration, and encouragement throughout this journey. His enthusiasm, expertise, patience, depth of knowledge, and scientific curiosity have been truly inspiring.

Besides my supervisor, I am also thankful to my doctoral committee members: **Dr. T. J. Dhilip Kumar**, **Dr. Avijit Goswami**, **Dr. Indranil Chatterjee**, and **Dr. Rajesh V. Nair**, for their insightful feedback, valuable time, and useful suggestions that have significantly contributed to the refinement of this thesis.

It is my privilege to thank the present director of IIT Ropar, **Prof. Rajeev Ahuja**, and the former director of IIT Ropar, **Prof. Sarit K. Das**, for providing world-class research infrastructure.

I also express my gratitude to **Prof. Subhajit Bandyopadhyay**, **Dr. Dibyendu Mallick**, and **Dr. Tullimilli Y. Gopalakrishna** for their excellent collaboration. It was a great experience to work with them.

I acknowledge the central research facilities (CRF) of IIT Ropar. I want to thank the convenor of the NMR facility, **Dr. Manoj Kumar Pandey**, for his cooperation. I sincerely thank the HRMS facility committee members, **Dr. Avijit Goswami** and **Dr. Anupam Bandyopadhyay**. I am grateful to the current head of the department, **Dr. Tharamani C.N.**, the former head of the department, **Dr. T. J. Dhilip Kumar**, and other faculty members of the Chemistry Department for facilitating the use of various departmental instruments and their valuable suggestions.

I acknowledge the help and support provided by the technical staff, especially **Mr. Manish**, **Mr. Kamlesh**, and **Mr. Nazre**, for their timely help with NMR, Single-crystal and HRMS data, and the non-teaching staff, **Mrs. Poonam**, **Mr. Nagendra**, **Mr. Sushil**, and **Mrs. Samita** of the Department of Chemistry.

My extraordinary lab mates deserve special thanks for their friendly cooperation and invaluable help whenever required. I cannot express in words how fortunate I am to have talented former and current lab members: **Himanshu**, **Hemonta**, **Sakshi**, **Neha**, **Rashmi**, **Pooja**, **Rakesh**, **Nikhil**, **Akanksha**, **Vishal**, **Vishvajeet**, **Annapurna**, and **Suman**. Their support in maintaining a healthy environment and engaging in useful discussions in the lab has greatly aided my learning and understanding of various aspects of research. I will always

cherish these memories and wish them great success in every aspect of their lives. I am grateful to my co-authors for their contributions to my work. I also thank all the summer trainees and project students who worked on short-term projects in our lab.

As the first student of Dr. Soumyajit Das's lab, I had no immediate seniors to guide me. Therefore, I am especially grateful to seniors from other labs, including **Dr. Suman**, **Dr. Soumen**, **Dr. Gautam**, **Dr. Sourav**, **Dr. Debarshi**, and **Dr. Prasoon**, for their invaluable guidance and assistance. Their help in troubleshooting reactions and navigating research challenges was crucial in my progress.

I owe a special debt of gratitude to my dear friends at IIT Ropar, **Shivangi**, **Sandeep**, **Gulshan**, and **Arijit**. Your unwavering support, encouragement, and belief in me have been a constant source of motivation throughout this doctoral journey. From late-night research-free discussions to endless cups of coffee, thank you for being my cheerleaders and confidants.

Finally, I would like to express my heartfelt gratitude to my parents, **Mr. Ashwani Sharma** and **Mrs. Suman Sharma**, for their eternal blessings, unconditional love, unwavering support, and encouragement in accomplishing my dream. They have always shown me the best path to follow, and they truly mean the world to me. I am also deeply grateful to my brother **Ishu** and my sister **Riya** for their love, support, and constant encouragement throughout this journey.

Lastly, I would like to extend my thanks to everyone who may have been inadvertently omitted from this list. Your contributions, support, and encouragement have been invaluable to me, and I deeply appreciate all that you have done.

Certificate

This is to certify that the thesis entitled **Syntheses and Properties of Conjugated Polycyclic Molecules Containing Heptazethrene, Indacene, and Azulene Cores**, submitted by **Priyank Kumar Sharma (2019CYZ0005)** for the award of the degree of **Doctor of Philosophy** of Indian Institute of Technology Ropar, is a record of bonafide research work carried out under my guidance and supervision. To the best of my knowledge and belief, the work presented in this thesis is original and has not been submitted, either in part or full, for the award of any other degree, diploma, fellowship, associateship or similar title of any university or institution.

In my opinion, the thesis has reached the standard fulfilling the requirements of the regulations relating to the Degree.

Soumyajit Das.

Signature of the Supervisor

Dr. Soumyajit Das

Department of Chemistry

Indian Institute of Technology Ropar

Rupnagar, Punjab 140001

Date: 23/08/2024

Lay Summary

Understanding aromaticity is crucial to realizing the stability and physical characteristics of π-conjugated molecules. Similarly, the fundamental understanding of antiaromaticity is of great importance in terms of both biological research where researchers have lately been able to answer the intrinsic instability of DNA, caused by the relieving of antiaromaticity; as well as in materials science where Breslow had shown evidence that antiaromatic π-systems may result in high carrier mobility because unlike benzene with the special stability called aromaticity, there is no question of loss of stability for antiaromatic core. Pro-aromaticity is a relatively new term, and according to the pro-aromatic theory, the process that leads to the formation of diradicals is the aromaticity gain of successive non-aromatic rings. This process involves minimizing net energy, which can eventually exceed the energy needed to break a double bond and result in the formation of a diradical.

In my thesis, I explored the design and synthesis of π-conjugated polycyclic molecules with interesting optoelectronic properties for organic electronics applications. While in Chapter 1, a general introduction regarding the recent progress of pro-aromatic heptazethrene, antiaromatic indacene, and aromatic azulene core embedded polycyclic hydrocarbons are presented, the following chapters contained the syntheses and properties of new polycyclic molecules bearing these cores that were invented during my doctoral research work. My research was focused on the syntheses of newer arrays of π-conjugated molecules embedded with heptazethrene, indacene, and azulene cores. These new molecules were fully characterized using various spectroscopic techniques in order to investigate the ground-state photophysical and electronic properties. Furthermore, density functional theory calculations were performed to give a clear conclusion on the actual ground state electronic configurations of the new molecules, in order to support the experimental findings.

Abstract

The investigation of π-conjugated systems has gained significant attention in recent times due to the intriguing optoelectronic properties and tunable ground state characteristics. These systems have a wide range of applications in various fields, such as organic electronics, spintronics, photovoltaics, and sensors. Understanding the concepts of aromaticity, pro-aromaticity, and anti-aromaticity is crucial and has a significant impact on the stability and ground-state electronic properties of these systems. **Chapter 1** presents an introduction to the background of zethrene and its higher homologues, specifically heptazethrene. The subsequent discussion is related to indacene- and azulene-embedded polycyclic arenes (PAs) and polycyclic heteroarenes (PHAs). Based on the aforementioned topics, a series of novel PAs and PHAs are designed, wherein the heptazethrene, indacene, and azulene cores are incorporated into the π-backbone.

Higher-order zethrenes exhibit diradical character in the ground state, which can only be modulated by π-ring annulation, whereas substitution did not affect the electronic ground state of the zethrene molecules. In **Chapter 2**, we have shown the isolation of a dibenzoheptazethrene derivative in the closed-shell ground state bearing push-pull substituents, which results in a zero diradical character and a low-lying zwitterionic form. In **Chapter 3**, attempts were made to isolate highly reactive dicyclopenta[*b*,*d*]thiophene (DCPT) core by fusion of naphthalene and phenanthrene units. However, unexpected decomposition products were obtained. DCPT is a heteroatom-modified *as*-indacene in which one of the central C_{sp^2}–C_{sp^2} double bonds of the *as*-indacene unit is replaced with an isoelectronic sulfur atom. Extending this indacene chemistry to the **Chapter 4**, we reported a formally aromatic dicyclopenta[*c*]fluorenothiophene, which exhibits a dominant antiaromatic character of the *as*-indacene subunit due to the inclusion of thiophene unit in the π-backbone. Finally, in **Chapter 5**, a tribenzo-extended non-alternat isomer of *peri*-acenoacene was reported with a formal azulene unit embedded in the polycyclic backbone, making it the newest non-hexagonal nanographene accessed through a Scholl-type oxidation approach. All the reported molecules exhibit remarkable photophysical properties with tunable (anti)aromatic or diradical characters that make them promising materials for applications in organic electronics and photonics.

List of Publications from Thesis

Journals

1. **Sharma, P. K.,** Das, S. Unveiling a Quinoidal 2,3:10,11-Dibenzoheptazethrene. *J. Org. Chem.* **2022**, *87*, 5430–5436.
2. **Sharma, P. K.**, Mallick, D., Sharma, H., Das, S. Dominating Antiaromatic Character of *as*-Indacene Decides Overall Properties of a Formally Aromatic Dicyclopenta[*c*]fluorenothiophene. *Org. Lett.* **2023**, *25*, 2201–2206.
3. **Sharma, P. K.**, Babbar, A., Mallick, D., Das, S. Constructing 1-Ethoxyphenanthro[9,10-*e*]Acephenanthrylene for the Synthesis of a Polyaromatic Hydrocarbon Containing a Formal Azulene Unit. *J. Org. Chem.* **2023**, *88*, 5473–5482.
4. **Sharma, P. K.**, Mallick, D., Das, S. A Thiophenoradialene-Embedded Polycyclic Heteroterphenoquinone Exhibiting Dominant Antiaromatic Traits. *Org. Lett.* **2023**, *25*, 5089–5093.
5. **Sharma, P. K.**, Jana P., Bandyopadhyay, S., Das, S. Cyano Disubstituted Tetrabenzoindeno[2,1-*a*]fluorene: Open-shell or Closed-shell?. *Chem. Commun.* **2024**, *60*, 7319–7322.

Table of Contents

List of Figures

List of Schemes

List of Tables

Notations and Abbreviations

ACID	anisotropy of the induced current density
APCI	atmospheric pressure chemical ionization
Å	angstroms
BBr_3	boron tribromide
BLA	bond length alternation
Bu_4NPF_6	tetra-*n*-butylammonium hexafluorophosphate
1,2-DCE	1,2-dichloroethane
CD_2Cl_2	deuterated dichloromethane
CP	cyclopentannulated
CS	closed-shell
CHF	cyclohepta[*def*]fluorene
CV	cyclic voltammetry
DBHZ	dibenzoheptazethrene
DCM	dichloromethane
DCPT	dicyclopenta[*b*,*d*]thiophene
DDQ	2,3-dichloro-5,6-dicyano-1,4-benzoquinone
DFT	density functional theory
DIBAL-H	diisobutylaluminium hydride
EPR	electron paramagnetic resonance
ESI	electron spray ionization
HB	hydrogen bonding
HRMS	high resolution mass spectra
HOMA	harmonic oscillator model of aromaticity
HOMO	highest occupied molecular orbital
HZ	heptazethrene
IDN	indacenodinaphthalene
IDF	indacenodifluorenes
ICT	intramolecular charge transfer
IF	indenofluorene
LUMO	lowest unoccupied molecular orbital
MesMgBr	mesitylmagnesium bromide
NICS	nucleus independent chemical shift
NIR	near-infrared
NMR	nuclear magnetic resonance
NPA	natural population analyses
OLED	organic light-emitting diodes
OFET	organic field-effect transistors
OPV	organic photovoltaics
OS	open-shell

PA	polycyclic arene
PAH	polycyclic aromatic hydrocarbons
PAP	phenanthroacephenanthrylene
PCC	pyridinium chlorochromate
PININ	poly(indenoindene)
PHA	polycyclic heteroarene
PH	polycyclic hydrocarbon
PHTPQ	polycyclic heteroterphenoquinone
QDM	quinodimethane
SCXRD	single-crystal x-ray diffractometry
SCLC	space-charge-limited current
TDDFT	time-dependent density functional theory
THF	tetrahydrofuran
TIPSE	triisopropylsilylethynyl
TLC	thin layer chromatography
TPQ	terphenoquinone
UV-vis	ultraviolet-visible

1.1 Introduction

Benzene **1** is the simplest, fully conjugated monocyclic hydrocarbon that follows the Hückel 4n+2 rule of aromaticity (Figure 1.1).[1] The fusion of **1** with multiple hexagonal rings (**2**-**3**), or rings other than the benzene ring (**4**-**5**), gives rise to higher-order π-conjugated ring systems known as polycyclic arenes (PAs) (Figure 1.1).[2,3] Substitution of these π-conjugated carbocycles with heterocycles, such as furan, pyrrole, or thiophene, results in polycyclic heteroarenes (**6**-**7**, PHAs) with different properties in comparison to the isoelectronic carbocycles, e.g. **2** and **6** (Figure 1.1).[2b,4]

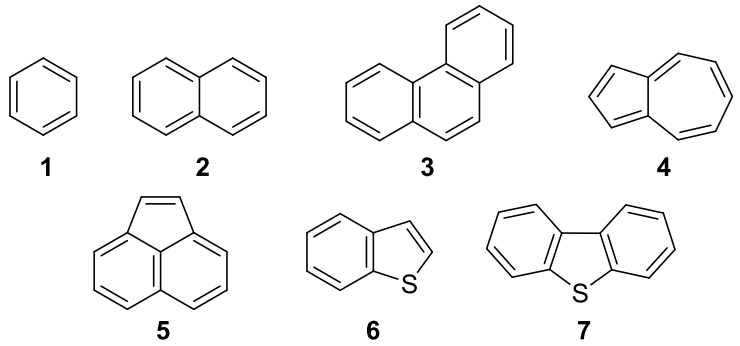

Figure 1.1 Examples of PAs (**1**-**5**) and PHAs (**6**-**7**)

The initial investigation of π-conjugated systems commenced with the detection and separation of polycyclic compounds from petroleum by-products.[5] In the early 20th century, R. Scholl and E. Clar made a significant contribution to the synthesis and characterization of polyarenes. They used harsh conditions like high temperatures and strong oxidants to synthesize these compounds. Moreover, due to the low solubility and stability of large polyarenes, the exploration of these compounds was limited to low molecular weight polyarenes.[5] Over the past two decades, research on PAs and PHAs has witnessed a significant resurgence in the scientific literature due to the development of advanced synthetic methods and analytical techniques that have made it significantly easier to efficiently synthesize and characterize atomically precise, fully conjugated polycycles under mild conditions.[6,7] The intriguing optoelectronic properties of these compounds, resulting from extended π-conjugation and delocalization, have made them valuable candidates for various material applications, including organic light-emitting diodes (OLEDs), field-effect transistors (OFETs), and photovoltaics (OPVs).[8] Consequently, there has been significant development and expansion within various classes of PAs, including higher-order acenes and condensed polycyclic aromatics.

PAs and PHAs hold significant relevance in the scientific community for various reasons. Firstly, the theoretical investigation of π-conjugated systems provides valuable insight into the concepts of (anti)aromaticity. Secondly, these compounds can serve as building blocks for a wide range of carbon-based nanostructures, such as graphene, carbon nanotubes, carbon nanobelts, fullerenes, and carbon schwarzites. Thirdly, PAs and PHAs can self-assemble into complex supramolecular structures due to intermolecular π–π interactions that are not yet fully understood. Lastly, these compounds have a wide range of significant applications in several fields, such as organic chemistry, biology, and materials science.[9] The stability of PAs and PHAs is a critical factor in their synthesis and practical applications. Molecules with zigzag edges may experience instability in comparison to molecules all armchair edges. For examples, the higher order acenes undergo oxidation in the presence of oxygen and light thereby disrupting the conjugation.[10] This inherent instability presents a considerable challenge for their extensive application in organic devices. Therefore, various bulky substituents are introduced at the reactive centers to stabilize these systems. In addition to stabilization, these substituents also help to improve the solubility of these compounds. It is important to understand the intrinsic reactivity and optoelectronic properties of these species for designing novel PAs and PHAs that could be used as organic functional materials. Meanwhile, various alternative of acenes have been developed such as heteroacenes,[11] thienoacenes,[12] zethrenes[13] and indenofluorenes.[14]

1.1.1 Zethrene

Zethrene is a Z-shaped PA, which can be regarded as the two naphthalene units connected via a *trans*-1,3-butadiene unit,[13] as shown in Figure 1.2. It was first reported by Clar *et al.* in 1955.[15] Afterward, many synthetic methods were devised for the synthesis of stable Zethrene derivatives.[16] The density functional theory (DFT) calculations at B3LYP/6-31G(d) level of theory predicted that the highest occupied molecular orbital (HOMO)−lowest unoccupied molecular orbital (LUMO) energy gap of zethrene was nearly equal to that of the well-known semiconductor pentacene.[16a,17] This makes it a potential material for organic semiconductors. Furthermore, in 1995, Burt and coworkers predicted, using Pariser-Parr-Pople (PPP) molecular orbital method, that zethrene and its derivatives would exhibit near-infrared (NIR) absorption and emission.[18] Higher-order zethrenes, for example, heptazethrene **9**, octazethrene **10**,

nonazethrene **11**, and so on, can be obtained by extending the central butadiene core (shown in red, Figure 1.2).[13] As predicted by Maksić *et al*. in 2006, zethrene and higher-order zethrenes would show large absolute proton affinity and second-order hyperpolarizability.[19]

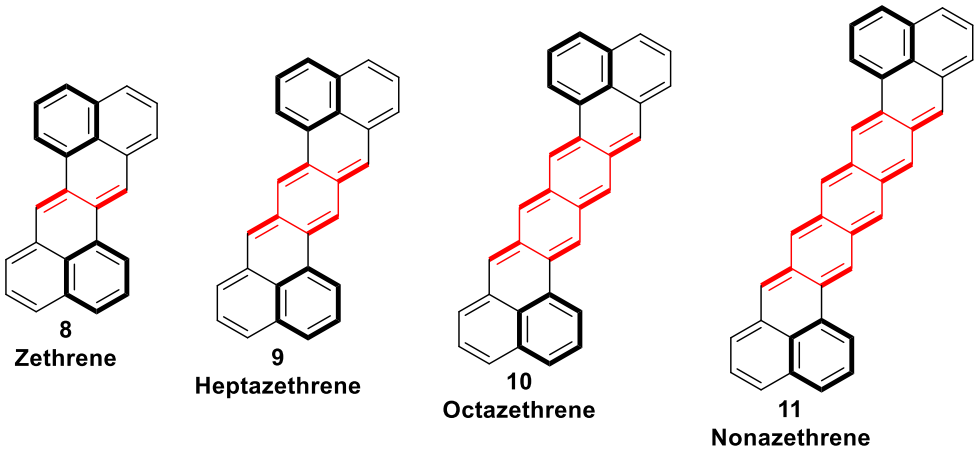

Figure 1.2 Structures of Zethrene and its higher homologues. Bold benzene rings denote the aromatic π-sextet rings.

Generally, π-conjugated polycycles can exist in two electronic states: closed-shell (CS) and open-shell (OS) states. In a CS ground state, bonding electrons are paired. In contrast, if there are one or more unpaired electrons, then it is referred to as an OS state. Zethrene can exist in a variety of resonance forms, including CS (quinoidal) and OS (diradical) forms, as shown in Figure 1.3. As per Clar's aromatic sextet theory,[6a,b] the higher the number of aromatic π-sextets, the greater the stability of that resonance form. Zethrene doesn't have an extra aromatic π-sextet ring in the OS-I resonance form compared to the CS resonance form. Furthermore, it loses an aromatic π-sextet ring in the OS-II resonance form, which means that the diradical form is destabilized. As a result, all zethrene derivatives documented thus far have exhibited a CS ground state.[16]

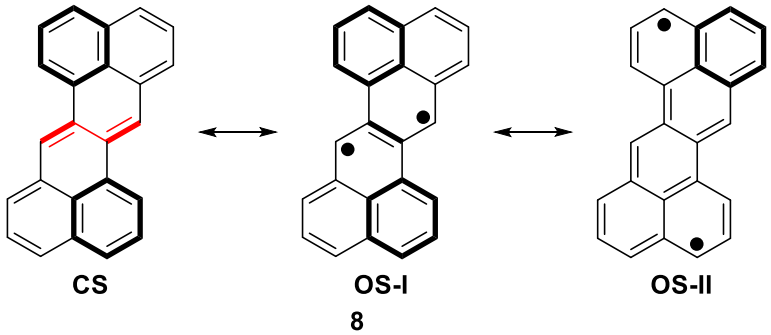

Figure 1.3 Resonance structures of zethrene **8**.

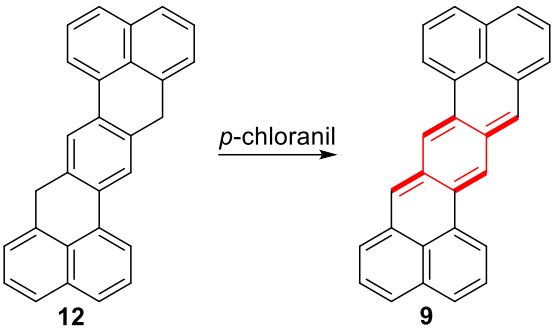

Scheme 1.1 Clar's route for parent heptazethrene **9**.

Heptazethrene **9** is the next homologue of zethrene (Figure 1.2), featuring two naphthalene moieties that are bridged via a *para*-quinodimethane (*p*-QDM, shown in red for Scheme 1.1) unit, having seven condensed benzenoid rings.[13] The parent heptazethrene was synthesized by Clar and Macpherson in 1962 through the oxidative dehydrogenation of its dihydro precursor **12** using *p*-chloranil in benzene or xylene. It was isolated as a dark green solid compound and exhibited an absorption maximum at 586 nm in solution. However, due to its high reactivity, it easily decomposed in the air.[20] Later, studies showed that the high reactivity of heptazethrene was due to its inherent OS diradical character. As per the analysis, heptazethrene was predicted to exhibit a small diradical character in the ground state. In order to quantify the contribution of the OS resonance form to the ground state of a molecule, the concept of diradical character index (y_0) is employed, a theoretical calculation based on natural orbital occupation numbers of the LUMO.[21]

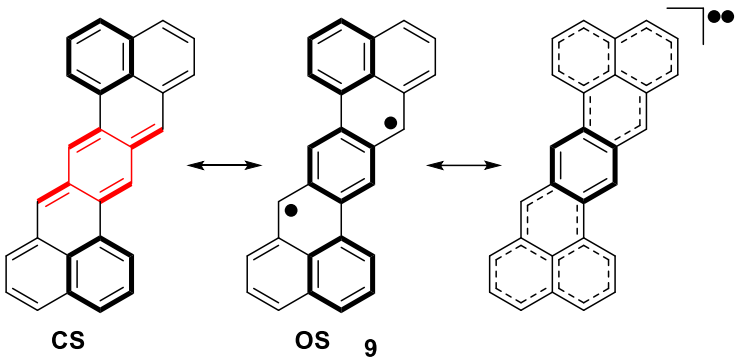

Figure 1.4 CS and OS canonical forms of heptazethrene.

As shown in Figure 1.4, heptazethrene possesses two aromatic π-sextets in the CS quinoidal resonance form and one additional aromatic sextet ring in the OS singlet diradical form. This will provide the extra aromatic stabilization effect, along with thermodynamic stabilization facilitated by radical delocalization throughout the entire

π-backbone. As a result, heptazethrene possesses a diradical character in its ground state, which was found to be 0.17.[22] Furthermore, in order to increase the stability of heptazethrene, these radical centers need to be kinetically protected.

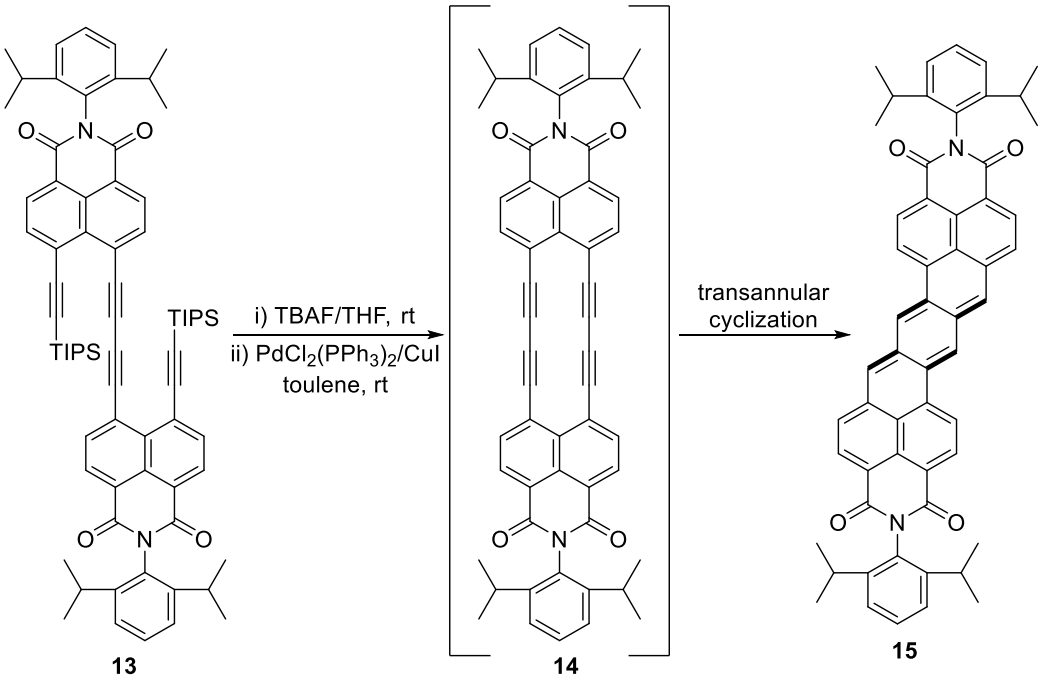

Scheme 1.2 Synthesis of a heptazethrenebis(dicarboximide) **15**.

In 2011, Wu *et al.* documented the synthesis of heptazethrenebis(dicarboximide) **15**, which was the first stable and soluble heptazethrene derivative bearing dicarboximide electron-withdrawing substituents on the peri-position of the heptazethrene π-scaffold.[23] As depicted in Scheme 1.2, the synthesis begins with the *in-situ* deprotonation and Pd-catalyzed homo-coupling reaction which afforded the key intermediate octadehydronaphtho[14]annulene **14**, which undergoes spontaneous intramolecular transannular cyclization to give the final compound **15** as a green-colored solid in 22% yield. Here, close orbital overlap within the diacetylene units facilitates spontaneous cyclization. The UV-Vis absorption spectrum of **15** in dichloromethane (DCM) was bathochromically shifted compared to zethrene diimide, which was attributed to extended conjugation. Additionally, **15** does not exhibit photoluminescence, whereas zethrene diimide shows a fluorescence quantum yield of 50%.[16e] More interestingly, the ^{1}H nuclear magnetic resonance (NMR) spectrum of **15** in deuterated dichloromethane (CD_2Cl_2) showed no ^{1}H signals in the aromatic region at ambient temperature. However, signals started to appear and sharpen upon gradual cooling, indicating a singlet diradicaloid ground state. Moreover,

unrestricted symmetry-broken DFT calculation revealed that the energy of the singlet OS singlet diradicaloid state was 5.8 and 7.5 kcal.mol^{-1} lower than that of the CS state and OS triplet state, respectively, indicating the OS singlet state as the ground state.

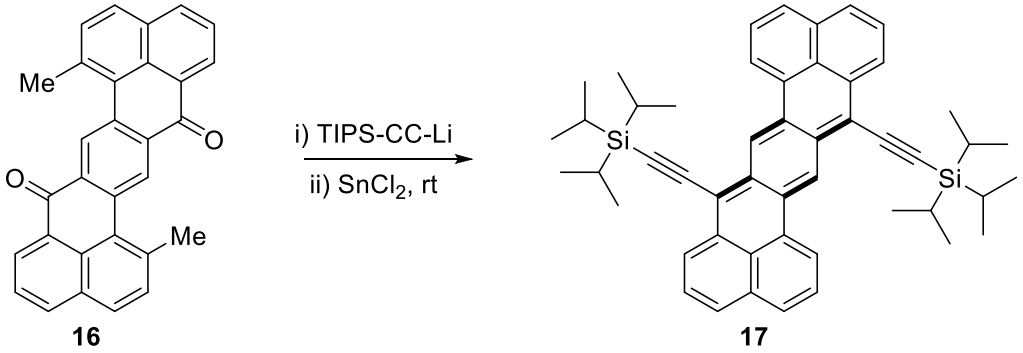

16 **17**

Scheme 1.3 Kinetically blocked heptazethrene derivative.

Although compound **15** was found to be more stable as compared to the parent heptazethrene due to HOMO level stabilization by the electron-withdrawing dicarboximide substituent, the reactive radical sites were not kinetically blocked, which resulted in the slow decomposition of this heptazethrene derivative on storage. As a result, it was deemed unsuitable for materials applications. In order to address the stability issue, Wu and co-workers implemented a strategy wherein highly reactive radical positions were substituted with bulky triisopropylsilyl (TIPS) acetylene groups using heptazethrene diketone as a key intermediate.[24] As shown in Scheme 1.3, the nucleophilic addition of the TIPS acetylene groups to the diketone compound **16**, followed by $SnCl_2$ mediated reductive elimination to afford the kinetically protected heptazethrene derivative **17** in 87% yield. The stability of **17** was significantly enhanced by kinetic protection of the reactive radical sites and due to the extended spin delocalization to the acetylene unit. It is worth noting that both experimental and theoretical results indicated that TIPS-heptazethrene **17** has a CS electronic ground state, unlike heptazethrene diimide **15**. This observation can be ascribed to the variation in the HOMO−LUMO energy gap of heptazethrene diimide **15** (0.99 eV) and TIPS-heptazethrene **17** (1.47 eV). Due to the larger HOMO−LUMO energy gap in TIPS-heptazethrene **17**, the admixture of HOMO−LUMO energy levels in the ground state is less efficient, leading to a closed-shell ground state with reduced diradical character. Furthermore, the UV-vis absorption spectra of compound **17** exhibited a typical *p*-band feature with a low-energy absorption maximum at 634 nm, which is a typical feature of various closed-shell PAs, including acenes.[25]

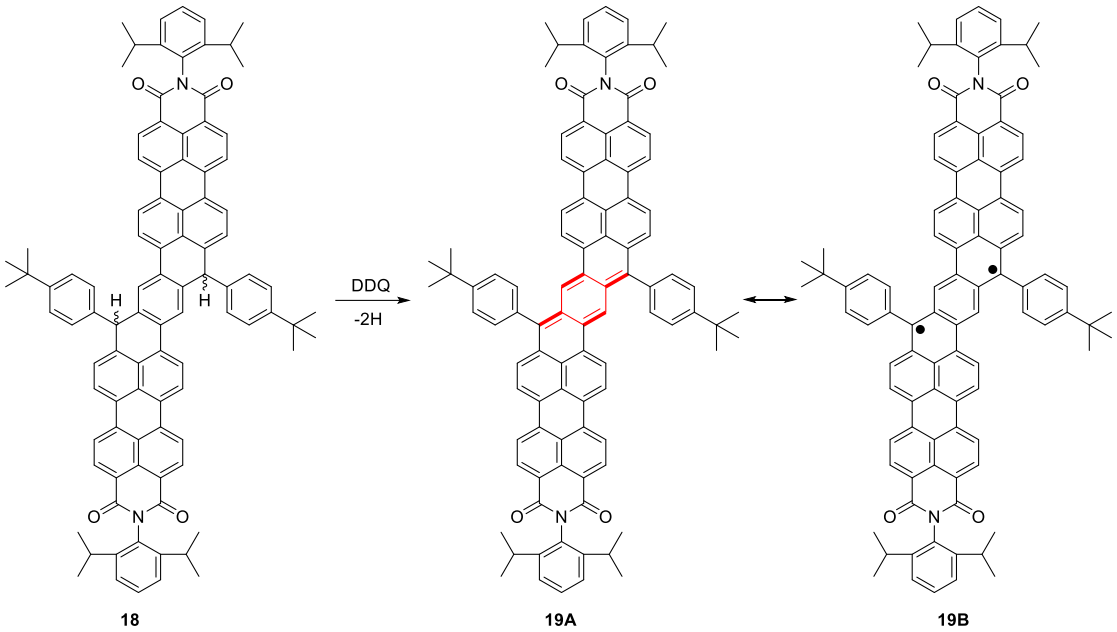

Scheme 1.4 Synthesis of perylene monoimide dimer **19**.

In an effort to investigate the effect of core modification on the electronic ground state of singlet diradicaloid PAs, Wu *et al.* synthesized a *p*-QDM-bridged perylene monoimide dimer **19**.[26] The aforementioned structure can be viewed as an extended heptazethrene derivative, wherein the pro-aromatic *p*-QDM unit acts as a bridge connecting the two perylene monoimide units. As demonstrated in Scheme 1.4, the dimer was obtained by the oxidative dehydrogenation of its precursor **18** using DDQ with a yield of 27%. By introducing an electron-withdrawing imide group at the *peri*-position of perylene and a 4-*tert*-butylphenyl group at the methylene position in the *p*-QDM moiety, they were able to obtain a soluble and stable compound **19**. Compound **19** exhibited an OS singlet diradical ground state as it recovered additional aromatic π-sextet on the central pro-aromatic *p*-QDM moiety in the OS form **19B**, similar to heptazethrene diimide **15**. Theoretically (at UCAM-B3LYP/6-31G*), compound **20** demonstrated a singlet diradical character index (y_0) of 0.465. Moreover, using SQUID measurement, the experimental singlet-triplet energy gap ($\Delta E_{S_0-T_1}$) was estimated to be −2.97 kcal/mol. Compound **19** showed a strong absorption band at 915 nm (ε = 2.5 x 10^5 M^{-1} cm^{-1}) accompanied by two shoulder bands at 1008 and 1157 nm in the NIR region. This band structure is a characteristic of many singlet open-shell PAs, which likely originates from the admixture of doubly excited electronic configuration (H,H→L,L) into the ground state.[27] As a result of its largely delocalized electronic structure and moderate singlet biradical character, compound **19** showed a

large two-photon absorption cross-section ($\sigma^{(2)}_{max}$ = 1300 GM at 1800 nm) and ultrafast excited-state dynamics.

As mentioned previously, the parent heptazethrene **9** is predicted to exhibit an OS singlet diradical ground state. However, it is important to note that the ground state of heptazethrene derivatives is significantly influenced by the core modification and the HOMO–LUMO energy gap. Additionally, the peripheral π-extension of the heptazethrene core through the naphthalene rings could also have a substantial impact on its ground-state electronic properties. It is worth noting that the symmetrical π-extension of the heptazethrene core through the benzene *cata*-fusion at the peripheral naphthalene rings provides up to four regioisomers of dibenzoheptazethrene (DBHZ); 1,2:9,10-DBHZ **20**, 5,6:13,14-DBHZ **21**, 2,3:10,11-DBHZ **22** and 4,5:12,13-DBHZ **23**, as shown in Figure 1.5.

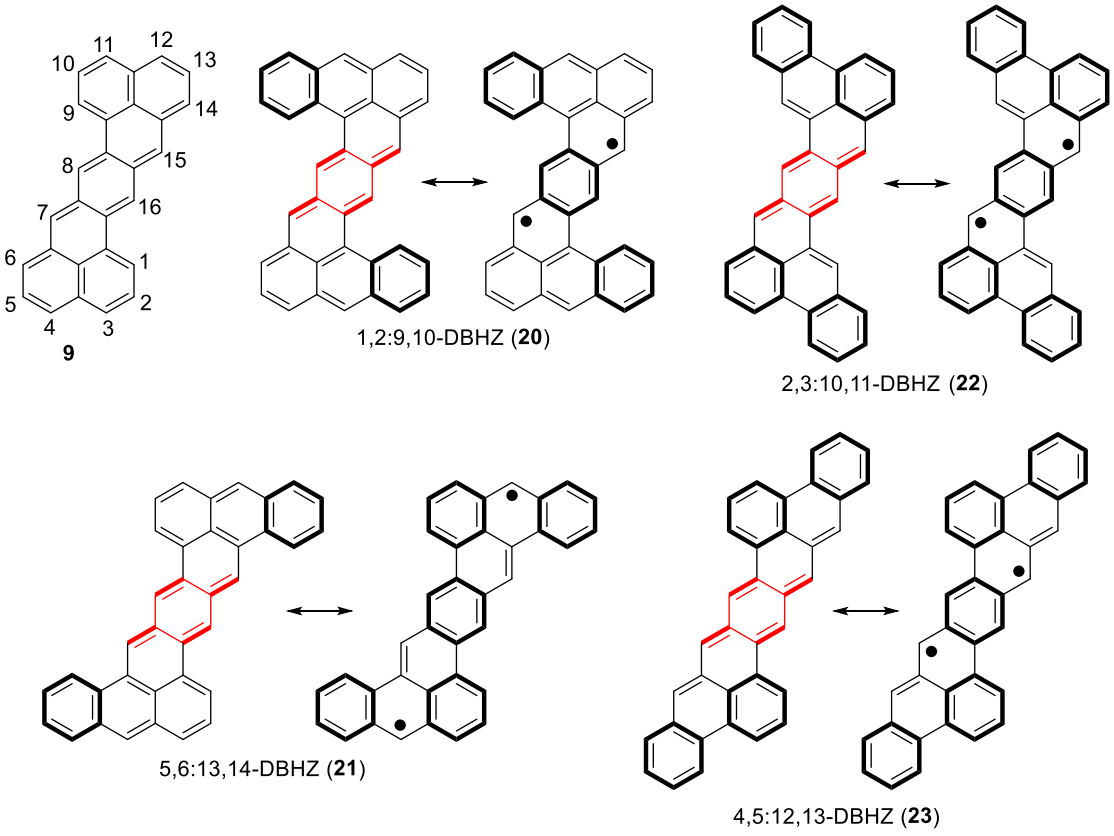

Figure 1.5 Closed-shell and open-shell resonance structures of dibenzoheptazethrene (DBHZ) regioisomers.

In order to evaluate the validity of Clar's aromatic sextet rule for π-extended OS singlet diradical molecular systems, Wu *et al.* investigated the anthracene-based 1,2:9,10-DBHZ **20** and 5,6:13,14-DBHZ **21** isomers, which can be regarded as the lateral π-extended heptazethrene.[28] They synthesized derivatives that were kinetically

protected with aryl or TIPS groups. Compound **25** was synthesized via oxidative dehydrogenation on dihydro precursor **24**. At the same time, **27** was synthesized by treating its diketone intermediate **26** with TIPS acetylene, followed by $SnCl_2$-mediated reductive elimination (Scheme 1.5). The introduction of bulky aryl and TIPS groups ensures solubility and stability, which facilitated the investigation of these compounds. Theoretical and experimental investigations were conducted to determine the ground-state electronic structure of two isomers. The results showed that isomer **27** exhibited a greater degree of diradical character than isomer **25**. This difference in diradical character can be attributed to the fact that isomer **27** has five possible aromatic sextet rings, while isomer **27** accommodated only three aromatic π-sextet rings in their OS diradical forms, **27B** and **25B**, respectively. As a result, the OS form of isomer **27** was more stabilized than that of isomer **25** and exhibited y_0 = 0.57 and 0.30, respectively.

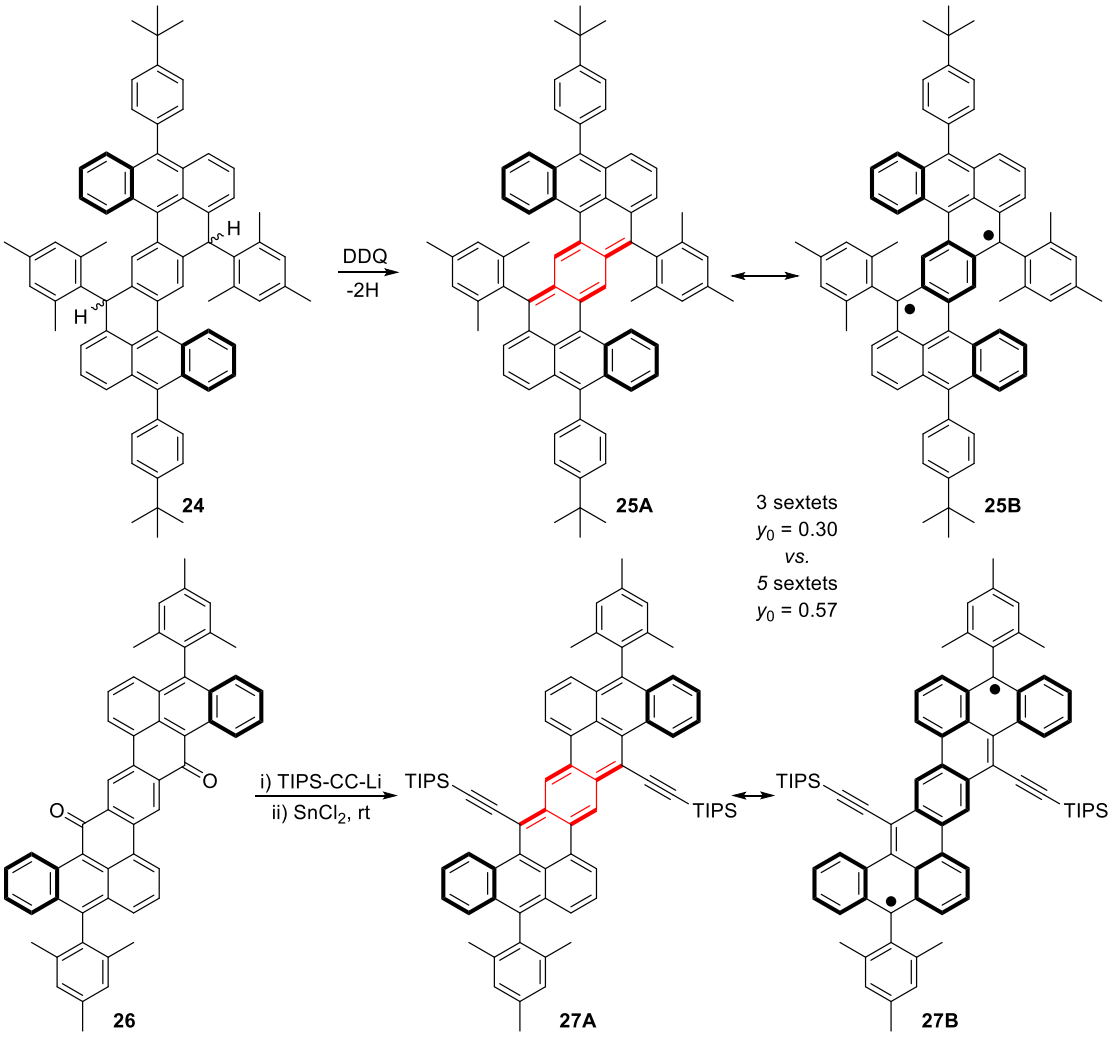

Scheme 1.5 Synthetic route for 1,2:9,10-DBHZ **25** and 5,6:13,14-DBHZ **27**.

The remaining two regioisomers are 2,3:10,11-DBHZ **22** and 4,5:12,13-DBHZ **23**. These two isomers have four aromatic Clar sextets in the CS forms, while only one additional π-sextet is recovered in the OS forms (Figure 1.5), in contrast to the anthracene-based DBHZ isomer. Therefore, the stabilization of CS resonance forms for phenanthrene-based DBHZ isomer, effectively reduces the diradical character to 0.11 for **22** and 0.13 for **23**,[29] which was even lower than that of parent heptazethrene **9.** Clar and co-workers first reported parent 4,5:12,13-DBHZ **23**. However, its ground-state properties were not studied due to its high reactivity.[30] Recently, Sun *et al.* documented the synthesis of kinetically protected 2,3:10,11-DBHZ **29** and 4,5:12,13-DBHZ **31** isomers from suitable diketones (**28** and **30**, respectively) as the intermediate.[29] The nucleophilic addition of TIPS lithium reagent followed by $SnCl_2$-mediated reductive elimination yielded compounds **29** and **31** as blue solids. The electronic ground states were investigated using various experimental and theoretical approaches. Moreover, they also demonstrated the utilization of these isomers as semiconductors for air-stable organic field-effect transistors (OFETs).

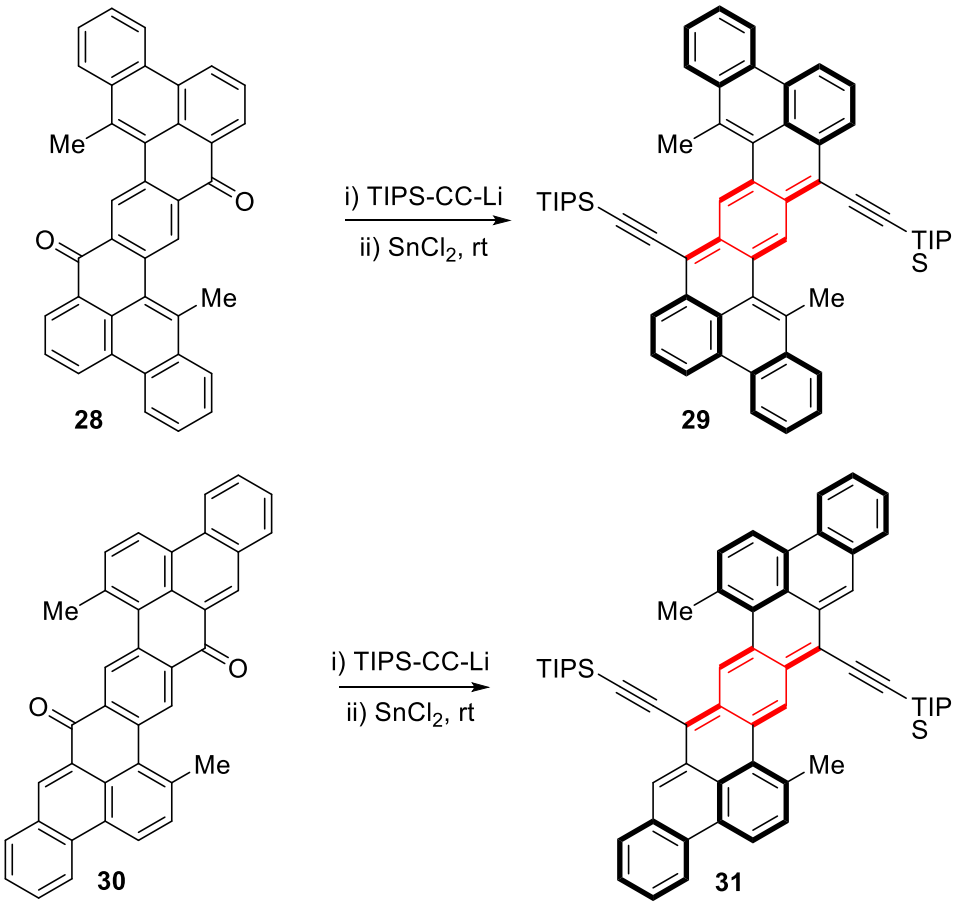

Scheme 1.6 Synthesis of 2,3:10,11-DBHZ **29** and 4,5:12,13-DBHZ **31.**

1.1.2 Indacene

Indacene is a formally antiaromatic PA with 12π-electrons in its periphery.[3b] *s*-Indacene and *as*-indacene are the structural isomers for indacene with linearly and angularly fused 5-6-5 rings, respectively. *s*-indacene contains a *p*-QDM subunit **32**, whereas *as*-indacene can be represented in two forms, containing *p*-QDM **33** or *o*-QDM **34** subunit in the tricyclic framework (shown in red, Figure 1.6). Due to the high reactivity of indacenes, only *s*-indacene was reported in 1963, whereas experimental synthesis of *as*-indacene is still unknown.[31] However, benzannulation to both ends of indacenes could stabilize the π-conjugated systems in the form of indenofluorene isomers (Figure 1.7).[14]

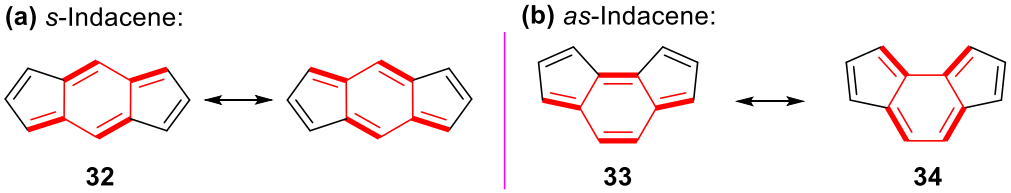

Figure 1.6 (a) *s*-Indacene **32** structures with *p*-QDM subunit; (b) *as*-Indacene resonance forms **33** and **34** with *p*-QDM and *ortho*-quinodimethane (*o*-QDM) subunits, respectively.

PAs and PHAs bearing indacene units in the π-backbone are attractive synthetic targets as they exhibit antiaromatic properties in their ground state.[32] Antiaromatic compounds display low HOMO–LUMO energy gap,[33] redox amphoteric character, and ambipolar charge-transport properties.[34] These attributes can hold enormous potential for a wide range of useful materials applications such as organic light-emitting diodes (OLEDs), field-effect transistors (OFETs), and photovoltaics (OPVs).

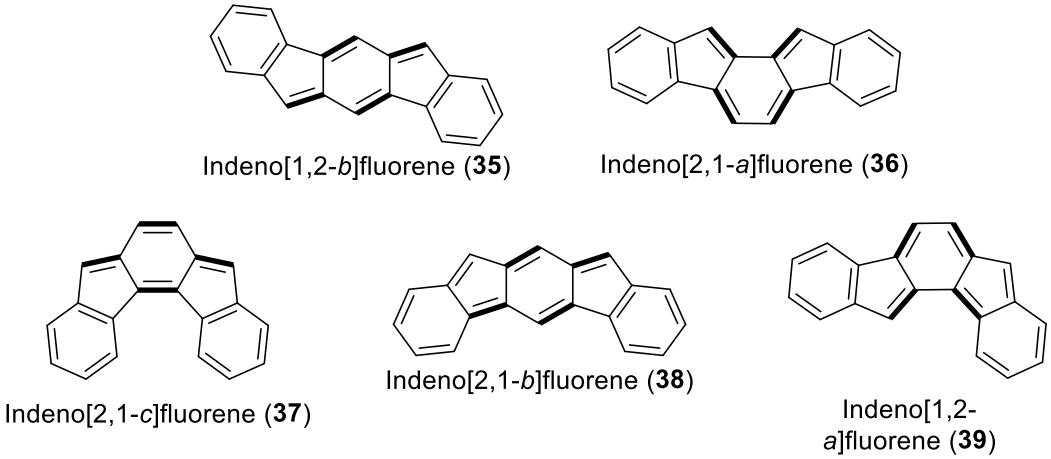

Figure 1.7 Indenofluorene isomers

Modulation of the antiaromatic character of the indacene subunit within its π-extended form is important to fine tune the HOMO–LUMO energy gap. The approach involves the fusion of arene or heteroarenes rings on the indacene core. For example, indenofluorenes (IF) are the dibenzo-fused indacenes and can be termed as non-alternant fully conjugated antiaromatic systems. Depending on the fusion pattern at the indacene unit and QDM type (*p*-, *o*-, *m*-QDM), there are five possible constitutional isomers of indenofluorene. These are indeno[1,2-*b*]fluorene **35**, indeno[2,1-*a*]fluorene **36**, indeno[2,1-*b*]fluorene **37**, indeno[2,1-*c*]fluorene **38**, and indeno[1,2-*a*]fluorene **39** as shown in Figure 1.7. [1,2-*b*]IF and [2,1-*b*]IF can be viewed as the dibenzo-fused *s*-indacenes, whereas [2,1-*a*]IF, [2,1-*c*]IF and [1,2-*a*]IF are regarded as *as*-indacene homologues.

Mainly, the groups of Haley[35,36,37] and Tobe[38,39] synthesized and intensively studied five fully conjugated IF isomers with apical carbons sterically protected bulkier aryl and ethynyl substituents. In addition to increasing solubility by disrupting the molecular aggregation, aryl or ethynyl substituents can help in kinetically blocking the potentially reactive radical sites to improve stability. Due to the presence of an *o*-QDM substructure in [2,1-*a*]IF, *p*-QDM substructure in [1,2-*b*]IF and [2,1-*c*]IF, and *m*-QDM substructure in [2,1-*b*]IF and [1,2-*a*]IF, it was highly anticipated that each IF isomer would exhibit distinct optical and electronic characteristics. The IF isomers with *o*-QDM and *p*-QDM substructures are widely studied as compared to *m*-QDM congeners.

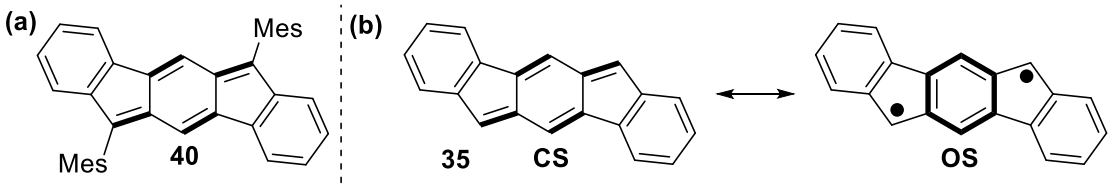

Figure 1.8 (a) Mesityl substituted [1,2-*b*]IF derivative (b) representative CS and OS resonance structure of parent [1,2-*b*]IF **35**.

In 2011, Haley and co-workers documented the synthesis and characterization of fully conjugated derivatives for [1,2-*b*]IF **35**.[35,40,41] Single crystal analysis of mesityl-disubstituted [1,2-*b*]IF **40** suggested large bond length alternation (BLA) for the *p*-QDM core, suggesting quinoidal contribution in the ground state. Furthermore, electrochemical and optical properties suggested that derivatives of **35** can be a promising semiconducting material. Later on, groups of Haley[41] and Yamashita[42] independently synthesized series 6,12-diaryl[1,2-*b*]IF. It has been found that the aryl

substituent had a significant impact on the molecule's stability, HOMO−LUMO energy level, and both optical and redox properties. In Yamashita's group they fabricated a FET device using vapor-deposited thin film, which revealed the ambipolar charge transport behavior of IFs with low mobilities. In parallel, microcrystals of [1,2-*b*] IF **35** derivatives were used as the active channel to fabricate the single crystal OFETs by Haley's group. The OFETs exhibited ambipolar charge transport with hole and electron mobilities of 7 x 10^{-4} and 3 x 10^{-3} $cm^2V^{-1}s^{-1}$, respectively.

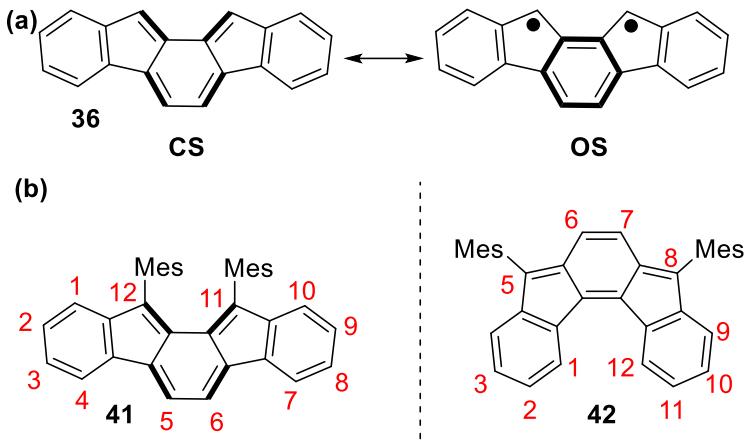

Figure 1.9 (a) CS and OS resonance structures of **36**. (b) Structure of 11,12-dimesityl[2,1-*a*]IF **41**. (c) 5,8-dimesityl[2,1-*c*]IF derivative **42**.

[2,1-*a*]IF **36** is an *as*-indacene-embedded IF regioisomer. The central benzenoid ring of [2,1-*a*]IF features a highly reactive *ortho*-quinoidimethane (*o*-QDM) arrangement (Figure 1.9). In 2011, Tobe *et al.* documented the synthesis and characterization of the stable 11,12-dimesityl[2,1-*a*]IF **41** having a CS ground state.[38] In 2013, Haley and co-workers reported the synthesis of another *as*-indacene congener called [2,1-*c*]IF derivative **42**.[36] The single-crystal x-ray diffractometry (SCXRD) analysis suggested its slightly helical backbone with large bond alternation for the *as*-indacene core, indicating a *para*-quinoidal arrangement. The UV-vis absorption spectra of the [2,1-*c*]IF derivatives displayed strong absorbance in the UV region, accompanied by broad, low-energy absorption bands that extended into the near-IR region. These broad low-energy absorption bands (550–800 nm) were analogous to those of 11,12-dimesityl[2,1-*a*]IF **41**, which shares the *as*-indacene core. Electrochemical analysis revealed that these derivatives accept up to two electrons and could be utilized as electron-accepting materials. Recently, our group has reported the ambipolar charge-transport properties of **42**, and unsymmetrical 5,8-disubstituted [2,1-*c*]IFs derivatives.[43] The SCXRD analysis indicated improved intermolecular π–π

interaction between the [2,1-*c*]IF units, which resulted in good charge transport properties (hole and electron mobilities up to 1.6 x 10^{-3} and 8.66 x 10^{-3} $cm^2V^{-1}s^{-1}$, respectively) under space-charge-limited current (SCLC) measurements.

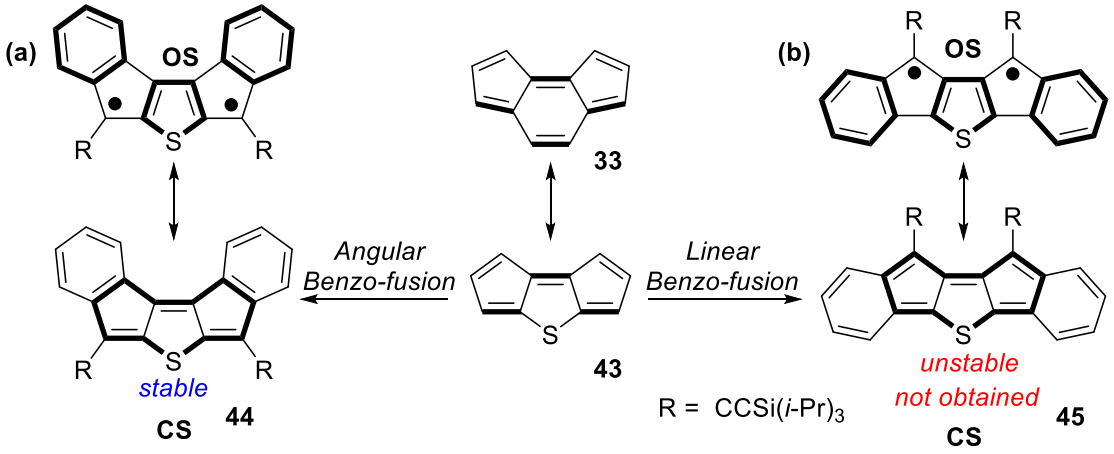

Figure 1.10 (a) Stable compound **44** as a derivative of angular dibenzo-fused dicyclopenta[*b*,*d*]thiophene, while (b) linear dibenzo-fused dicyclopenta[*b*,*d*]thiophene **45** was unstable.

As discussed above, *as*-indacene can be represented in two resonance forms containing *p*-QDM **33** or *o*-QDM **34** subunits. On replacing the bridging double bond of the central six-membered ring of **33** with isoelectronic heteroatom such as sulfur, dicyclopenta[*b*,*d*]thiophene (DCPT or heterocyclic *as*-indacene) **43** is obtained. Angular dibenzo-fusion of DCPT **43** resulted in heterocyclic [2,1-*c*]IF analogue **44** as a stable compound. The groups of Haley[44] and Chi[45] independently synthesized compound **44** via reductive dearomatization reaction using $SnCl_2$ in toluene. The experimental and theoretical studies indicated a closed-shell ground state for compound **44**. However, linear dibenzo-fusion of **43** doesn't afford a stable product **45**,[4] likely due to its high diradical character owing to the recovery of three local aromatic rings (two benzene and one thiophene) in its OS form (as shown in Figure 1.10) as it switches from non-aromatic CS form, which probably hindered the isolation of the 4nπ-system and thus the electronic ground state for **45** is still unknown.

In contrast to *as*-indacene, *s*-indacene congener with different arene and heteroarene rings fused at both ends, such as naphthalene **46-48**, phenanthrene **49**, anthracene **50**,[46] dibenzoheterole,[47] thiophene **51-52**,[48] and benzothiophene **53-54**[49] are widely investigated. Furthermore, unsymmetrical analogues **55-56**,[50] wherein one of the outer benzene rings is substituted with a thiophene ring, are also reported. The extensive studies carried out by Haley's group demonstrated that the strength of the

paratropic ring-current within the diaraeno-fused *s*-indacene core could be tuned by changing the bond order of the annulated outer aromatic rings.[46] The fusion of *s*-indacene at the 1,2-position of naphthalene with a bond-order (BO) of 1.66 gives rise to two *s*-indacenodinaphthalene (*s*-IDN) regioisomers **46** and **48** with enhanced paratropicity in comparison to [1,2-*b*]IF **35**. Similarly, *s*-indacene fusion at the 9,10-postion of the phenanthrene resulted in greater degree of paratropicity for the antiaromatic *s*-indacene core in **49**. In contrast, *s*-IDN **47** (BO = 1.33) and *s*-indacenodianthracene **50** (BO = 1.25) both have a similar 2,3-bond fusion mode, resulting in the central π-system displaying reduced paratropicity relative to IF **35**. Furthermore, this concept was also extended to indacenedithiophenes[48] and indacenodibenzothiophenes,[49] where outer benzene rings are replaced with thiophene and benzothiophene rings, respectively. Direct attachment of aromatic heterocycles to the *s*-indacene core can significantly enhance its paratropicity due to the lower aromaticity of the thiophene ring as compared to the benzene ring. This leads to a greater contribution of C-C double bonds towards forming the central antiaromatic *s*-indacene unit.

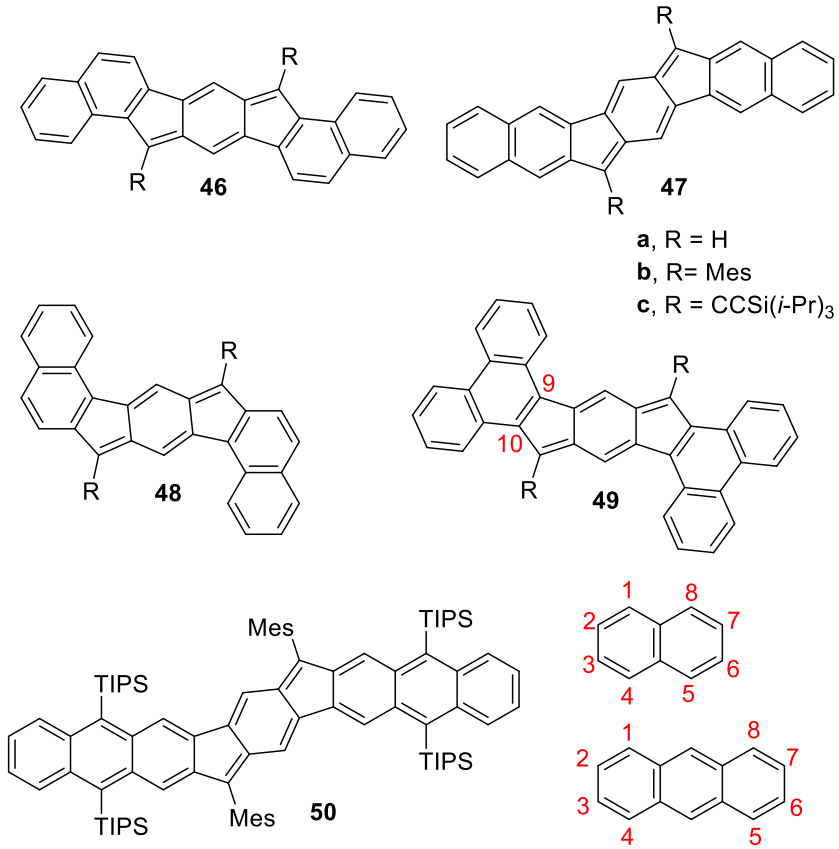

Figure 1.11 Molecular structures of various naphthalene (**46**-**48**), phenanthrene (**49**) and anthracene (**50**) fused *s*-indacene derivatives.

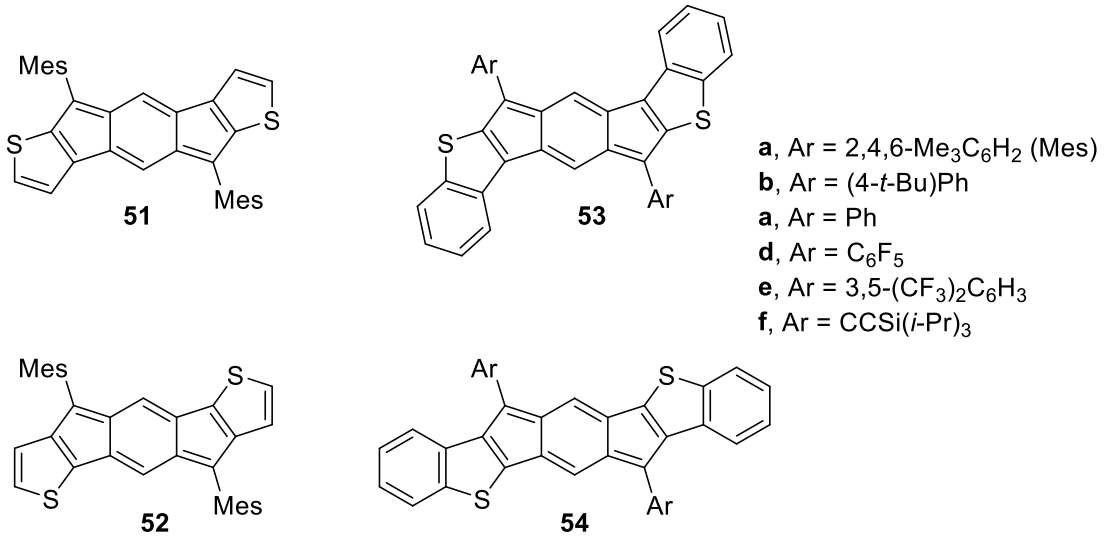

Figure 1.12 Chemical structures of indacenedithiophenes **51-52** and indacenodibenzothiophenes **53-54** derivatives.

Haley *et al.* reported the synthesis and characterization of *syn* and *anti*-isomer of fully conjugated indacenedithiophenes **51-52**[48] and indacenodibenzothiophenes **53-54**[49] (Figure 1.13). The fusion of a less aromatic thiophene core into the *s*-indacene core has effectively stabilized the HOMO–LUMO energy levels for **51-54** in comparison to their PA counterparts, as evidenced by both optical and electrochemical analyses which were consistent with DFT calculations. SCXRD analysis revealed short intermolecular distance which was due to interaction between LUMO rich region of thiophene units. Moreover, they demonstrated high hole mobilities for indacenodibenzothiophenes derivatives and compound **54** showed hole mobilities of 0.44 cm^2/Vs. Two unsymmetrical [1,2-*b*]IF analogues **55** and **56** were also synthesized by the same group utilizing Suzuki cross-coupling reactions.[50] Optical and electrochemical investigation revealed that the properties of these two compounds lie between those of all carbonaceous fully conjugated [1,2-*b*]IF and indacenodithiophenes.

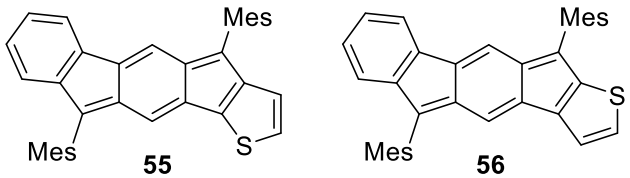

Figure 1.13 Chemical structures of unsymmetrical [1,2-*b*]IF analogues.

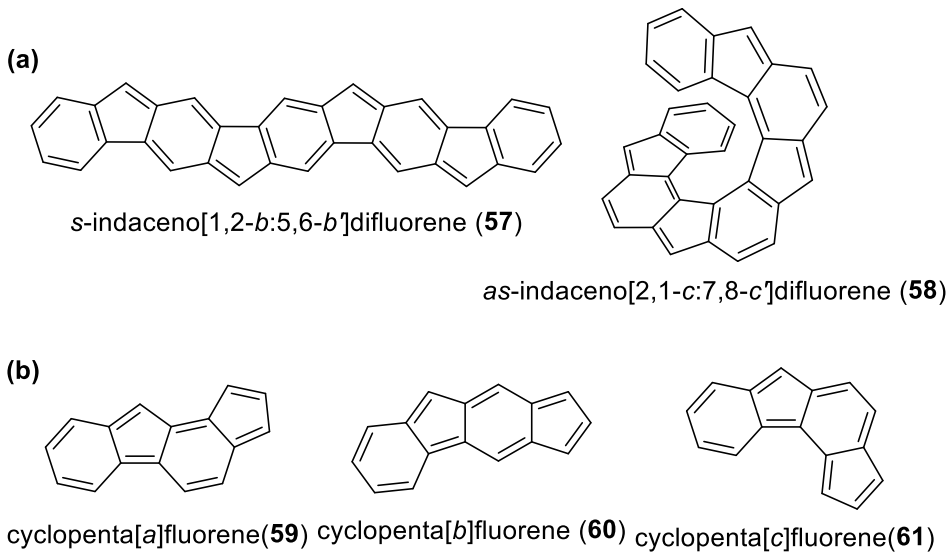

Figure 1.14 (a) Examples of indacenodifluorenes isomers (b) cyclopentafluorene subunits.

In 2014, Tobe presented the design of a new class of fully fused π-extended IF oligomers **57** and **58**.[51,52] These compounds consist of 6-5-6-5-6-5-6-5-6 fused polycycles and can be obtained by fusing cyclopentafluorene to the outer six-membered ring of the IF isomer. In 2020, our group classified these π-extended IF oligomers as indacenodifluorenes (IDF).[53] IDFs are 34π formally aromatic PAs that possess unique electronic and optical properties, making them of particular interest in the field of materials science. Among them, those based on *s*-indacene can be classified as *s*-indacenodifluorenes (*s*-IDFs), such as **57**, while *as*-indacene-based compounds, like **58**, may be termed as *as*-indacenodifluorenes (*as*-IDFs).

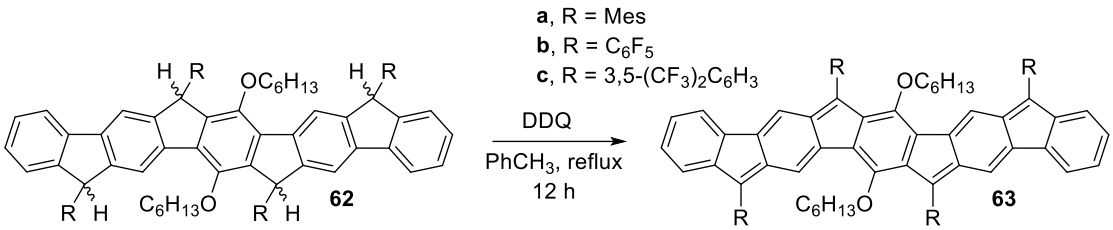

Scheme 1.7 Synthesis of *s*-indaceno[1,2-*b*:5,6-*b*′]difluorene derivatives **63**.

In 2016, Wu and co-worker successfully synthesized and characterized *s*-indaceno[1,2-*b*:5,6-*b*′]difluorene derivatives **63**.[54] This compound, which was cyclopenta[*b*]fluorene fused [1,2-*b*]IF, was obtained through $BF_3{\cdot}OEt_2$ promoted intramolecular cyclization of the corresponding diol, followed by oxidative dehydrogenation of its tetrahydro-precursor **62** using DDQ (Scheme 1.7). The electronic ground state of compound **63** had been thoroughly investigated using a range of experimental techniques, assisted by DFT calculations. Compound **63**

exhibited a CS ground state with a small diradical character of 0.038 and large ΔE_{S-T} = −8.4 kcal/mol. Similar to other antiaromatic compounds such as IFs, compound **63** exhibited a weak absorption tail reaching up to 1000 nm in the near-IR region and amphoteric redox behaviour. Our group recently reported the synthesis of the second isomer of the *s*-IDF series, mesityl substituted *s*-indaceno[2,1-*c*:6,5-*c*′]difluorene **65** which was also obtained using a similar synthetic approach that involved a DDQ-mediated oxidative dehydrogenation of a its tetrahydro-precursor **64**.[53]

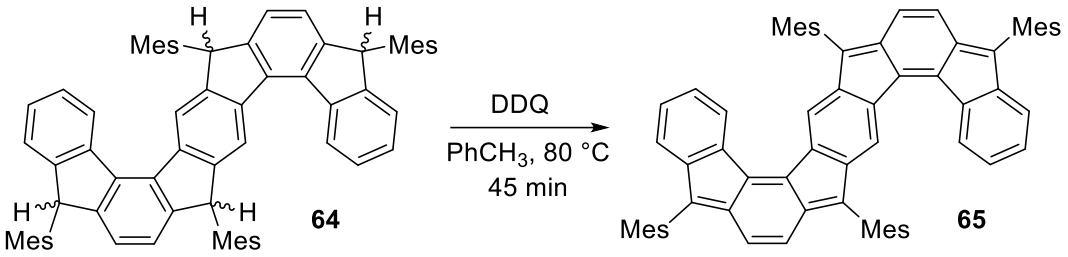

Scheme 1.8 Synthesis of *s*-indaceno[2,1-*c*:6,5-*c*′]difluorene **65.**

In contrast to *s*-IDF, the synthesis of *as*-IDF isomers still remains elusive. Though Tobe mentioned the design of first *as*-IDF isomer **58** in his personal account,[51] no further research has been conducted to date to investigate these types of PAs.

1.1.3 Azulene

The inclusion of non-hexagonal rings, such as pentagons and heptagons, within the hexagonal framework plays a crucial role in modulating their optical, electronic, and magnetic properties. They also exhibit unique intermolecular packing in the solid state. Azulene is a non-benzenoid aromatic 10π-electron system comprising fused five and seven-membered ring systems.[55] It is noteworthy that despite being an isomer of naphthalene, which is colorless (λ_{max} = 312 nm) and nonpolar, azulene shows a distinctive blue color with a maximum wavelength of 585 nm. It also exhibits an abnormal anti-Kasha emission, a small HOMO–LUMO energy gap, and displays a significant dipole moment of 1.08 D. The unique properties of azulene can be attributed to its zwitterionic resonance structure (Figure 1.15a), which comprises an electron-rich aromatic cyclopentadienide and electron-poor tropylium ions. This donor-acceptor-like structure of azulene results in an abnormal distribution of electron density between the HOMO and LUMO energy levels (Figure 1.15b), distinguishing it from typical fused benzenoid polycyclic aromatic hydrocarbons (PAHs). These unusual electronic and optical properties led to the development of azulene-embedded PAs for their applications in organic optoelectronics.[56] However, developing a

synthetic method that results in two different non-hexagonal rings in a single molecule remains a challenging task.[57] Typically, there are two ways to incorporate the azulene moiety within the π-backbone: starting from commercially available azulene derivatives to construct azulene-embedded PAs or by *in-situ* synthesis of azulene moiety from non-azulene substrates. The latter approach facilitates the incorporation of azulene moiety with diverse structural modifications using easily accessible and cost-effective non-azulene substrates.

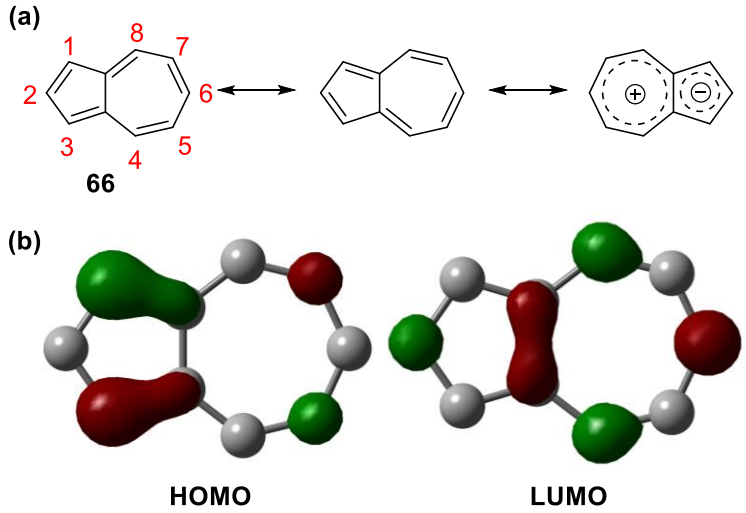

Figure 1.15 (a) Resonance structures (b) HOMO and LUMO profile of azulene **66**.

It is important to note that the fused azulene moiety in these π-systems may or may not exhibit pristine azulene-like electronic properties because the dominant aromaticity of the neighboring benzene rings or structural distortions can influence the electronic structure of the embedded azulene unit, which may diminish its azulene-like character and can be referred to as a "formal azulene" unit. Recently, a significant number of polycyclic aromatic hydrocarbons containing formal azulene (or 5/7-membered rings) have been synthesized and studied. These include acenes, 2D π-expanded, and helical PAs, which exhibit interesting (anti)aromatic properties, low energy absorptions, as well as diradical characters.[58]

The investigation of azulene-embedded PAs dates back to the early 20th century. *bis*-Periazulene, also known as cyclohepta[*def*]fluorene **69**, is a non-alternant isomer of pyrene with one azulene unit. It was first introduced in 1955 by Reid *et al.*, and it is a structural isomer of cyclohepta[*bc*]acenaphthylene **67** and cyclohepta[*klm*]benz[*e*]indene **68**.[59] Based on the resonance structures of cyclohepta[*bc*]acenaphthylene **67** and cyclohepta[*def*]fluorene **69**, they predicted that **68** would possess azulene-like characteristics, whereas **69** behaves as a typical

cyclopolyolefin. Reid and coworkers attempted to synthesize this isomer. However, due to its inherent instability, they were unable to isolate it. From the resonance analysis in Figure 1.16, as a result of double *peri*-benzannulation onto the azulene moiety, the six-membered rings within cyclohepta[*def*]fluorene **69** adopt an *o*-quinoidal arrangement with 14π-electrons in the periphery in its closed-shell Kekulé form **69A**. When the outer quinoidal hexagonal rings become aromatic, two additional resonance forms can be considered. One is the zwitterionic resonance structure **69C**, which displays a more localized charge distribution, unlike that of azulene. Another is an open-shell diradical form with an *m*-quinoidal arrangement **69D**. In contrast to previous theoretical calculations that predicted a triplet ground state for **69**,[60,61] triaryl-substituted *bis*-priazulene derivatives exhibit a singlet diradical ground state, as evidenced by the theoretical as well as experimental studies.[62]

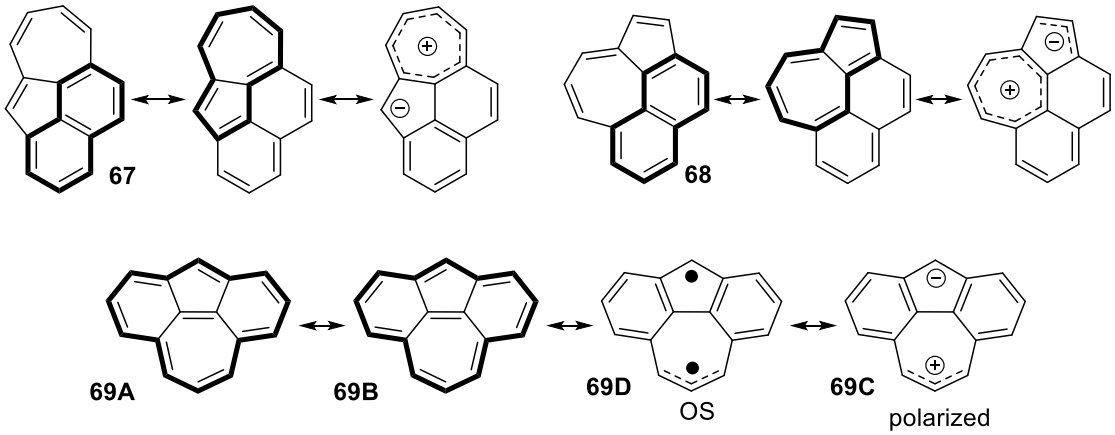

Figure 1.16 Resonance structures of cyclohepta[*bc*]acenaphthylene **67**, cyclohepta[*klm*]benz[*e*]indene **68** and cyclohepta[*def*]fluorene **69** (14π-electrons in the periphery indicated by bold lines).

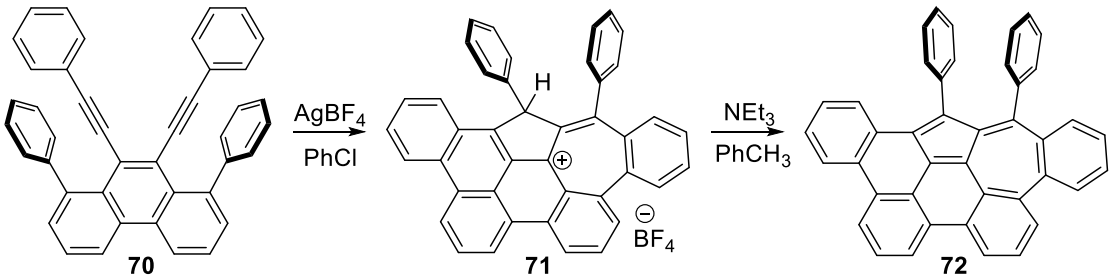

Scheme 1.9 Synthetic route to azulene embedded PA **72**.

In 2018, Yasuda and co-workers reported the synthesis of non-alternant isomer of tribenzo[*fg*,*ij*,*rst*]pentaphene via tandem oxidative transannulation reaction between aromatic and acetylene units of **70**, in the presence of the $AgBF_4$ as a one-electron

oxidant.[63] SCXRD analysis indicated that the main core of compound **72** adopted a slightly contorted π-backbone, resulting in a saddle-like structure with phenyl groups oriented orthogonal to the main core. Furthermore, the distortion around the bay-regions imparts a helical conformation. Bond length analysis suggested the greater contribution of the pentafulvene subunit in the molecular skeleton rather than an ideal azulene core. In contrast to its benzenoid isomer, compound **72** displays a broad and weak absorption band in the low-energy region, as well as amphoteric redox behaviour. These distinct electronic and structural features of compound **72** are attributed to its azulene core.

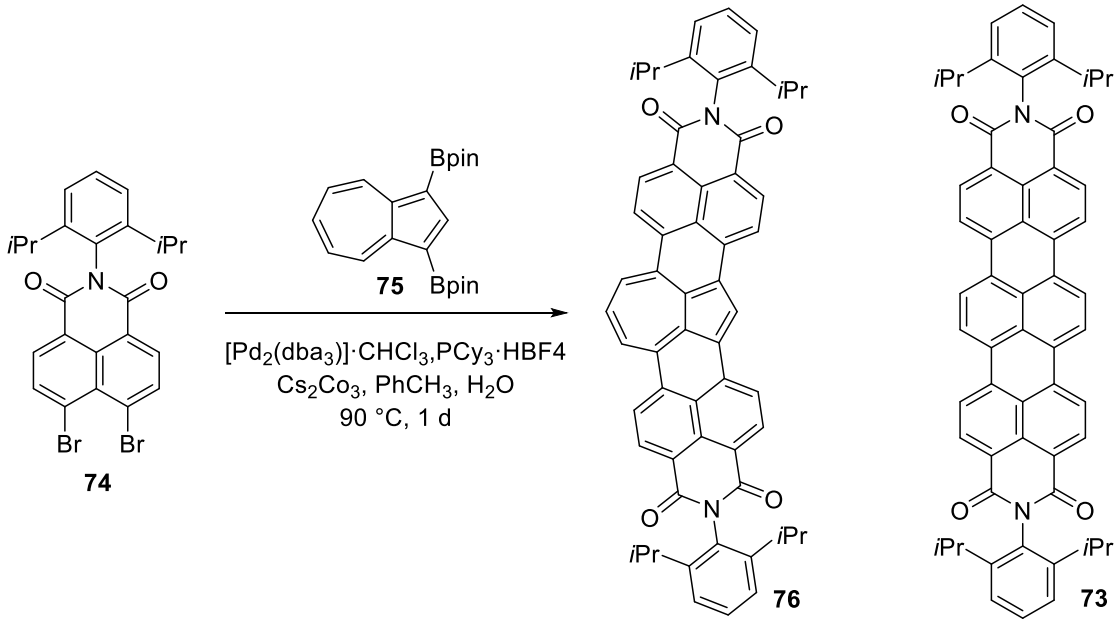

Scheme 1.10 Synthesis of non-alternat isomer of terrylene bisimide.

Würthner *et al.* envisioned that the azulene-like characteristics would be preserved if aromatic rings were fused at the 1,8 and 3,4 positions of the azulene unit. They reported the synthesis of a planar non-alternat isomer of terrylene bisimide, in which a Pd-catalyzed annulation reaction between azulene and naphthalimide provided the target compound **76**, as shown in Scheme 1.10.[64] Compound **76** can undergo further functionalization via selective bromination and nucleophilic substitution which was challenging for other azulene-embedded PAs. The bond length analysis and theoretical calculations revealed that the azulene unit in this molecule exhibited aromaticity similar to pristine azulene. The substitution of the central naphthalene ring with an azulene motif resulted in significant changes to the electronic properties of **73**. The UV-vis-IR absorption of compound **76** showed absorption

maxima at 1041 nm, which was strongly red-shifted in comparison to **73**, resulting in a narrow optical energy gap. This work demonstrated the complete retention of the azulene's electronic structure for compound **76** and its derivatives through the benzo-fusion onto the periphery of the azulene unit.

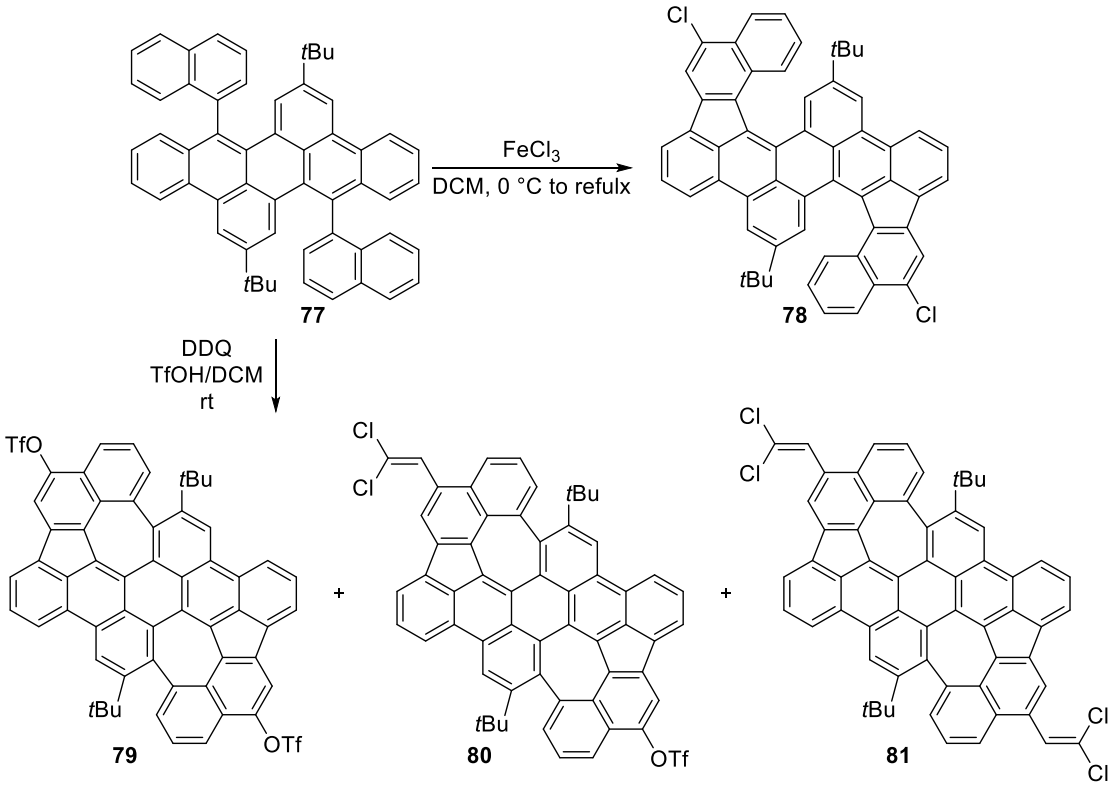

DDQ (8 eq),	14%	30%	9%
DDQ (10 eq)	25%	11%	2%

Scheme 1.11 Synthetic route for defective nanographenes embedded with two formal azulene units.

In 2019, Mastalerz and co-worker utilized the Scholl-type oxidative dehydrogenation reaction to synthesize a defective nanographene embedded with two formal azulene units.[65] The Scholl-type oxidation reaction is the most commonly used approach for synthesizing nanographenes, which typically results in the formation of hexagonal rings. Additionally, this reaction can be a powerful tool for the synthesis of contorted PAs. The Scholl reaction employs a combination of Lewis acid and oxidant. Some of the extensively used reagents include DDQ/methanesulfonic acid or trifluoromethanesulfonic acid and $FeCl_3/CH_3NO_2$. As shown in Scheme 1.11, in the presence of $FeCl_3/CH_3NO_2$ compound **77** exclusively provided the five-membered ring containing chlorinated product. On the other hand, the treatment of **77** with DDQ/TfOH, the reaction yielded three unexpected substitutional products, comprising

two formal azulene units. The amount of DDQ used directly impacted the yield of the respective products. Triflated product **79**, can be further utilized for the construction of larger PAs through Pd-catalysed reactions. Further they were able to grow single crystals of **81** for the SCXRD analysis, which confirmed contorted π-scaffold exhibiting negative curvature due to the presence of seven-membered rings. The azulene subunits of **81** showed large bond length alternation compared to pristine azulene unit, indicating reduced aromaticity, and thus may be considered as 'formal azulene' core. The UV-vis absorption and emission spectroscopy were employed to study the optical properties of these compounds. The low energy bands ranging from 625 to 645 nm can be attributed to the HOMO to LUMO transition due to extension in π-conjugation. These azuleno-PAs exhibited emission spectra close to NIR region ranging between 645 and 675 nm with a quantum yield of up to 27%.

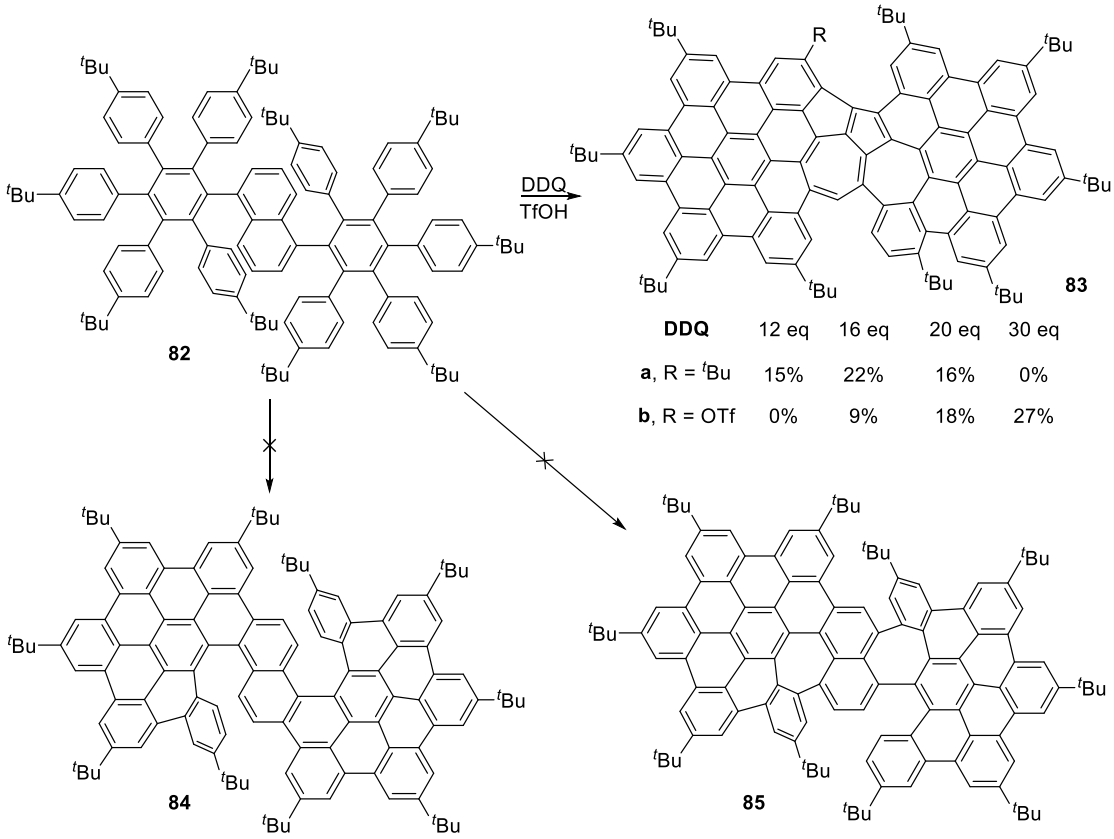

Scheme 1.12 Synthesis of defective nanographene **83** using Scholl reaction.

Although the Scholl reaction is a powerful tool for synthesizing nanographenes with odd-numbered rings, this reaction is still unpredictable. In 2020, Chi *et al.* reported the unusual naphthalene to azulene rearrangement during the Scholl reaction.[66] Their primary objective was to synthesize naphthalene-bridged helicene and heptagon-containing scaffold **84**, utilizing the Scholl reaction. To their surprise,

instead of the formation of **84** or **85**, the Scholl-type oxidative cyclization resulted in the formation of a fully fused contorted π-scaffold **83** bearing two formal azulene units, and its triflyloxylated derivative **83b** was obtained through the thermodynamically favorable naphthalene to azulene rearrangement. It has been found that the amount of DDQ used significantly affected the yield of these two products. For instance, increasing the amount of DDQ from 12 to 30 equivalents resulted in a change in the yields of **83a** and **83b**, ranging from 15% to 0% and 0% to 27%, respectively. As discussed above, the Mastalerz group also observed this regioselective triflation. Single crystal analysis of the **83b** confirmed the formation of fused 7/5/5/7 rings at the centre of the scaffold forming a pair of two azulene units. Additionally, the analysis revealed that one *tert*-butyl group has shifted to the bay region, and one of the *tert*-butyl groups has been replaced with a triflate group via the suggested arenium ion mechanism. The bond length analysis and the DFT studies showed that only one azulene moiety has an electronic structure similar to that of pristine azulene.

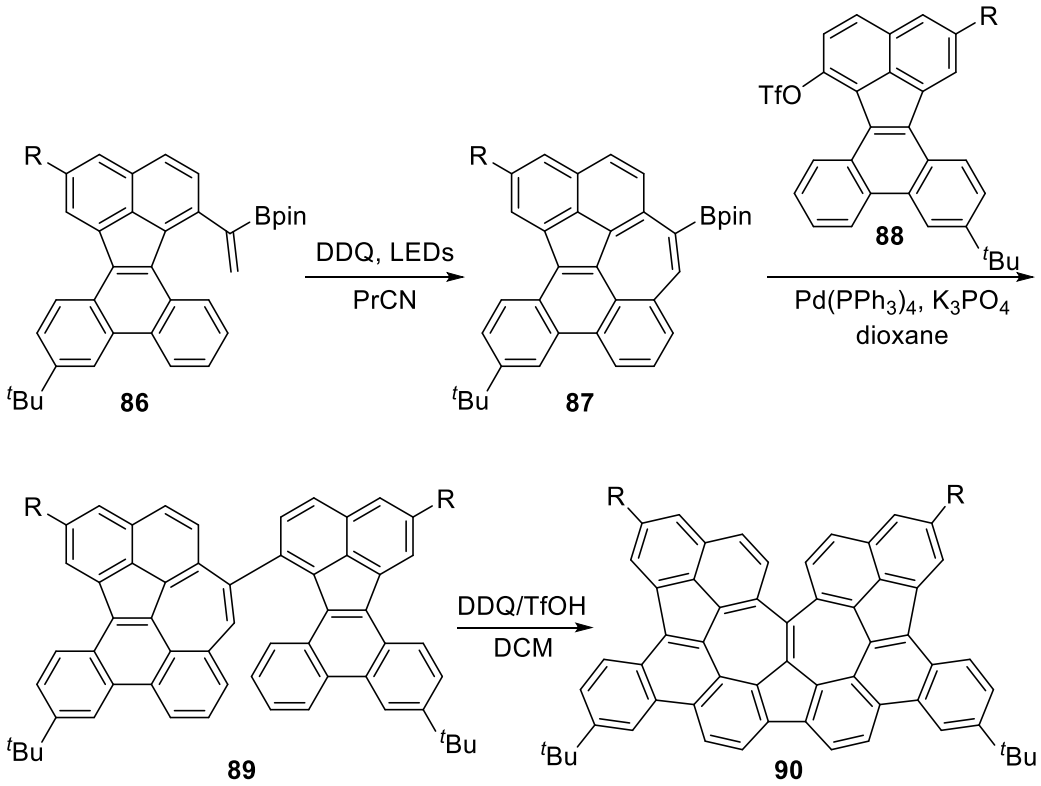

Scheme 1.13 Synthesis of helical nanographene **90** using Scholl reaction

In 2020, Yasuda *et al*. reported the synthesis of helical nanographene embedded with contiguous azulene units using the Scholl-type oxidative aromatic coupling reaction.[67] As illustrated in Scheme 1.13, compound **86** underwent a photoinduced 10π-electrocyclization, resulting in the formation of the key intermediate

87 containing a heptagon. Subsequent treatment of intermediate **87** under Pd-catalyzed Suzuki coupling reaction and Scholl-type reaction conditions provided the desired compound **90**. SCXRD analysis of **90** demonstrated that due to the steric congestion in the cove-like region, compound **90** exhibited a stable helical chirality, which is different from the normal cove regions.

1.2 Thesis outline

This thesis comprises five chapters, commencing with Chapter 1, which presents an introduction to the background of zethrene and its higher homologues, specifically heptazethrene. The subsequent discussion is related to indacene and azulene-embedded PHAs and PAs. Based on the aforementioned topics, a series of novel PAs and PHAs are designed, wherein the heptazethrene, indacene, and azulene core are incorporated into the π-backbone, as illustrated in Figure 1.17. The main aim of this study is to synthesize and comprehensively investigate the impact of structural modifications on the electronic ground state properties of newer arrays of π-conjugated systems, using computational and various analytical approaches.

As discussed earlier, higher-order zethrenes exhibit diradical character in the ground state, which can only be modulated by π-ring annulation whereas substitution does not affect the electronic ground state of the zethrene molecules. In Chapter 2, I have isolated dibenzoheptazethrene derivative in closed-shell ground state bearing push and pull substituents, which results in low-lying a zwitterionic form. In Chapter 3, attempts were made to isolate the highly reactive DCPT core through different fusion modes. As mentioned, DCPT is a heteroatom-modified *as*-indacene in which one of the $C_{sp}{}^2$–$C_{sp}{}^2$ double bonds is replaced with an isoelectronic sulfur atom. Extending this indacene chemistry to the 4th chapter, I reported a formally aromatic dicyclopenta[*c*]fluorenothiophene, which exhibits a dominant antiaromatic character *as*-indacene subunit due to the inclusion of thiophene unit in the π-backbone. Finally, in Chapter 5, a tribenzo-extended non-alternat isomer of *peri*-acenoacene is reported with a formal azulene unit embedded in the π-backbone. All the reported molecules exhibit remarkable photophysical properties, making them attractive candidates for a variety of applications, including organic light-emitting diodes (OLEDs), field-effect transistors (OFETs), and photovoltaics (OPVs).

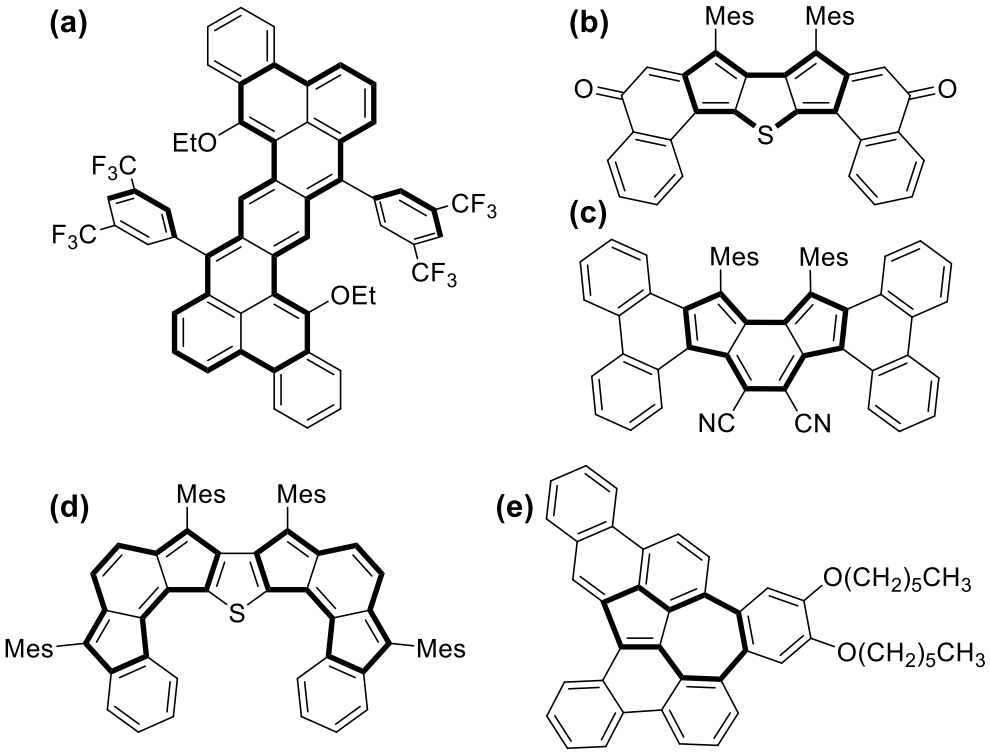

Figure 1.17 Structure of target compounds in this thesis.

1.3 References

1. (a) Hafner, K. August Kekulé─The Architect of Chemistry Commemorating the 150th Anniversary of His Birth. *Angew. Chem., Int. Ed.* **1979**, *18*, 641–651. (b) Martín, N.; Scott, L. T. Challenges in aromaticity: 150 years after Kekuleʹs benzene. *Chem. Soc. Rev.* **2015**, *44*, 6397−6400. (c) Watson, M. D.; Fechtenkötter, A.; Müllen, K. Big Is Beautiful- "Aromaticity" Revisited from the Viewpoint of Macromolecular and Supramolecular Benzene Chemistry. *Chem. Rev*. **2001**, *101*, 1267−1300.

2. (a) Harvey, R. G. Polycyclic Aromatic Hydrocarbons, *Wiley-VCH, Weinheim*, **1997**. (b) Fetzer, J. C. The Chemistry and Analysis of the Large Polycyclic Aromatic Hydrocarbons, *John Wiley, New York*, **2000**. (c) Polycyclic Arenes and Heteroarenes, ed. Q. Miao, *Wiley-VCH, Weinheim*, **2016**.

3. (a) Tobe, Y. Non-Alternant Non-Benzenoid Aromatic Compounds: Past, Present, and Future. *Chem. Rec.* **2015**, *15*, 86–96. (b) Tobe, Y. Quinodimethanes Incorporated in Non-Benzenoid Aromatic or Antiaromatic Frameworks. *Top. Curr. Chem*. **2018**, 376, 12.

4. Shi, X.; Chi, C. Heterocyclic Quinodimethanes. *Top. Curr. Chem*. **2017**, *375*, 68.

5. Clar, E. Polycyclic Hydrocarbons; *Springer Berlin Heidelberg*, **1964**; Vol. 2. (b) Clar, E. The Aromatic Sextet; *Wiley-VCH: London*, **1972**.

6. (a) Harvey, R. G. Polycyclic Aromatic Hydrocarbons; *Wiley-VCH: New York*, **1997**. (b) Haley, M. M.; Pak, J. J.; Brand, S. C. Carbon Rich Compounds II. *Topics, in: Current Chemistry*, **1999**, 201, 81–130. (c) Vikki, M.; Tsefrikas, V. M.; Scott, L. T. Geodesic Polyarenes by Flash Vacuum Pyrolysis. *Chem. Rev.* **2006**, *106*, 4868−4884. (d) Hagen, S.; Hopf, H. Modern Routes to Extended Aromatic Compounds. *Top. Curr. Chem.* **1998**, *196*, 45–89.

7. (a) Spitler, E. L.; Johnson, C. A.; Haley, M. M. Renaissance of Annulene Chemistry. *Chem. Rev*. **2006**, *106*, 5344−5386. (b) von Schleyer, P. Introduction: Aromaticity. *Chem. Rev.* **2001**, *101*, 1115–1118

8. (a) Gu, Y. W.; Qiu, Z. J.; Müllen, K. Nanographenes and Graphene Nanoribbons as Multitalents of Present and Future Materials Science. *J. Am. Chem. Soc*. **2022**, *144*, 11499–11524 (b) Islam, S. M.; Malone, R. J.; Yang, W.; George, S. P.; Gautam, R. P.; Chalifoux, W. A.; Barile, C. J. Nanographene Cathode Materials for Nonaqueous Zn-Ion Batteries. *J. Electrochem. Soc.* **2022**, *169*, 110517. (c) Avouris, P. Graphene:

Electronic and Photonic Properties and Devices. *Nano Lett*. **2010**, *10*, 4285−4294. (d) Meric, I.; Han, M. Y.; Young, A. F.; Ozyilmaz, B.; Kim, P.; Shepard, K. L. Current saturation in zero-bandgap, top-gated graphene field-effect transistors. *Nat. Nanotechnol.* **2008**, 3, 654−659.

9. (a) Wu, J.; Pisula, W.; Müllen, K. Graphenes as Potential Materials for Electronics. *Chem. Rev.* **2007**, *107*, 718−747. (b) Jiao, L.; Zhang, L.; Wang, X.; Diankov, G.; Dai, H. Narrow Graphene Nanoribbons from Carbon Nanotubes. *Nature* **2009**, *458*, 877–880. (c) Jiao, L.; Wang, X.; Diankov, G.; Wang, H.; Dai, H. Facile synthesis of high-quality graphene nanoribbons. *Nat. Nanotechnol*. **2010**, *5*, 321−325. (d) Chen, C.; Lin, Y.; Zhou, W.; Gong, M.; He, Z.; Shi, F.; Li, X.; Wu, J. Z.; Lam, K. T.; Wang, J. N.; Yang, F.; Zeng, Q.; Guo, J.; Gao, W.; Zuo, J.-M.; Liu, J.; Hong, G.; Antaris, A. L.; Lin, M.-C.; Mao, W. L.; Dai, H. Sub-10-nm graphene nanoribbons with atomically smooth edges from squashed carbon nanotubes. *Nat. Electron* **2021**, *4*, 653−663.

10 Anthony, J. E. The larger acenes: Versatile organic semiconductors. *Angew. Chem., Int. Ed.* **2008**, *47*, 452–483.

11 (a) Bunz, U. H. F. The Larger Linear N-Heteroacenes *Acc. Chem. Res*. **2015**, *48* 1676–1686. (b) Bunz, U. H. F.; Engelhart, J. U.; Lindner, B. D.; Schaffroth, M. Large N-Heteroacenes: New Tricks for Very Old Dogs?. *Angew. Chem., Int. Ed.* **2013**, *52*, 3810–3821.

12. Takimiya, K.; Osaka, I.; Mori, T.; Nakano, M. Organic Semiconductors Based on [1]Benzothieno[3,2-*b*][1]benzothiophene Substructure *Acc. Chem. Res*. **2014**, *47*, 1493–1502.

13. (a) Hu, P.; Wu, J. Modern Zethrene Chemistry. *Can. J. Chem.* **2017**, *95*, 223–233. (b) Sun, Z.; Wu, J. Zethrene and expanded zethrenes with tunable ground states and physical properties. *Pure and Applied Chemistry* **2014**, *86*, 529–537.

14. Fix, A. G.; Chase, D. T.; Haley, M. M. Indenofluorenes and Derivatives: Syntheses and Emerging Materials Applications. *Top. Curr. Chem.* **2012**, *349*, 159–195. (b) Shimizu, A.; Nobusue, S.; Miyoshi, H.; Tobe, Y. Indenofluorene congeners: Biradicaloids and beyond. *Pure Appl. Chem*. **2014**, *86*, 517– 528

15. Clar, E.; Lang, K. F.; Schulz-Kiesow, H. Aromatische Kohlenwasserstoffe, LXX. Mittei: Zethren (1.12;6.7-Di-benztetracen) *Chem. Ber*. **1955**, *88*, 1520–1527.

16. (a) Umeda, R.; Hibi, D.; Miki, K.; Tobe, Y. Tetradehydrodinaphtho[10]annulene: A Hitherto Unknown Dehydroannulene and a Viable Precursor to Stable Zethrene Derivatives *Org. Lett.* **2009**, *11*, 4104–4106. (b) Wu, T. C.; Chen, C. H.; Hibi, D.; Shimizu, A.; Tobe, Y.; Wu, Y. T. Synthesis, Structure, and Photophysical Properties of Dibenzo[*de,mn*]naphthacenes. *Angew. Chem., Int. Ed.* **2010**, *49*, 7059–7062 (c) Sun, Z.; Huang, K.-W.; Wu, J. Soluble and Stable Zethrenebis (dicarboximide) and Its Quinone *Org. Lett.* **2010**, *12*, 4690–4693. (d) Wu, T. C.; Chen, C. H.; Hibi, D.; Shimizu, A.; Tobe, Y.; Wu, Y. T. Synthesis, Structure, and Photophysical Properties of Dibenzo-[*de,mn*]naphthacenes. *Angew. Chem., Int. Ed*. **2010**, *49*, 7059−7062. (e) Shan, L.; Liang, Z.-X.; Xu, X.-M.; Tang, Q.; Miao, Q. Revisiting Zethrene: Synthesis, Reactivity and Semiconductor Property. *Chem. Sci.* **2013**, *4*, 3294–3297. (f) Sun, Z.; Wu, J. 7, 14-Diaryl-Substituted Zethrene Diimides as Stable Far-Red Dyes with Tunable Photophysical Properties. *J. Org. Chem.* **2013**, *78*, 9032–9040.

17. Ruiz-Morales, Y. HOMO–LUMO Gap As An Index Of Molecular Size and Structure for Polycyclic Aromatic Hydrocarbons (PAHs) and Asphaltenes: A Theoretical Study. I. *J. Phys. Chem. A* **2002**, *106*, 11283–11308.

18. Désilets, D.; Kazmaier, P. M.; Burt, R. A. Design and synthesis of near-infrared absorbing pigments. I. Use of Pariser–Parr–Pople molecular orbital calculations for the identification of near-infrared absorbing pigment candidates. *Can. J. Chem.* **1995**, *73*, 319–324.

19. Knežević, A.; Maksić, Z. B. The Absolute Proton Affinity and The Second Order Hyperpolarizability of Some Catacondensed Linear Polyacenes and Pericondensed Zethrenes. *New J. Chem*. **2006**, *30*, 215–222.

20. Clar, E.; Macpherson, I. A. The significance of Kekulé structures for the stability of aromatic systems—II *Tetrahedron* **1962**, *18*, 1411–1416.

21. Yamaguchi, K. The Electronic Structures of Biradicals in the Unrestricted Hartree-Fock Approximation. *Chem. Phys. Lett*. **1975**, *33*, 330–335.

22. Zeng, W.; Sun, Z.; Herng, T. S.; Gonçalves, T. P.; Gopalakrishna, T. Y.; Huang, K.-W.; Ding, J.; Wu, J. Super-heptazethrene. *Angew. Chem., Int. Ed.* **2016**, *55*, 8615–8619.

23. Sun, Z.; Huang, K. W.; Wu, J. Soluble and stable heptazethrenebis(dicarboximide) with a singlet open-shell ground state. *J. Am. Chem. Soc*. **2011**, *133*, 11896–11899.

24. Li, Y.; Heng, W. K.; Lee, B. S.; Aratani, N.; Zafra, J. L.; Bao, N.; Lee, R.; Sung, Y. M.; Sun, Z.; Huang, K. W.; Webster, R. D.; López Navarrete, J. T.; Kim, D.; Osuka, A.; Casado, J.; Ding, J.; Wu, J. Kinetically Blocked Stable Heptazethrene and Octazethrene: Closed-Shell or Open-Shell in the Ground State?. *J. Am. Chem. Soc*. **2012**, *134*, 14913–14922.

25. Tönshoff, C.; Bettinger, H. F. Pushing the Limits of Acene Chemistry: The Recent Surge of Large Acenes. *Chem. – Eur. J.* 2021, 27, 3193–3212.

26. Das, S.; Lee, S.; Son, M.; Zhu, X.; Zhang, W.; Zheng, B.; Hu, P.; Zeng, Z.; Sun, Z.; Zeng, W.; Li, R.-W.; Huang, K.-W.; Ding, J.; Kim, D.; Wu, J. Para-quinodimethane-bridged perylene dimers and pericondensed quaterrylenes: The effect of the fusion mode on the ground states and physical properties. *Chem. – Eur. J.* **2014**, *20*, 11410−11420.

27. Di Motta, S.; Negri, F.; Fazzi, D.; Castiglioni, C.; Canesi, E. V. Biradicaloid and Polyenic Character of Quinoidal Oligothiophenes Revealed by the Presence of a Low-Lying Double-Exciton State. *J. Phys. Chem. Lett*. **2010**, *1*, 3334–3339.

28. Sun, Z.; Lee, S.; Park, K. H.; Zhu, X.; Zhang, W.; Zheng, B.; Hu, P.; Zeng, Z.; Das, S.; Li, Y.; Chi, C.; Li, R. W.; Huang, K. W.; Ding, J.; Kim, D.; Wu, J. Dibenzoheptazethrene Isomers with Different Biradical Characters: An Exercise of Clar's Aromatic Sextet Rule in Singlet Biradicaloids. *J. Am. Chem. Soc*. **2013**, *135*, 18229–18236.

29. Zong, C.; Zhu, X.; Xu, Z.; Zhang, L.; Xu, J.; Guo, J.; Xiang, Q.; Zeng, Z.; Hu, W.; Wu, J.; Li, R.; Sun, Z. Isomeric Dibenzoheptazethrenes for air-stable organic field-effect transistors. *Angew. Chem., Int. Ed.* **2021**, *60*, 16230–16236.

30. Clar, E.; Fell, G. S.; Richmond, M. H. 4,5:12,13-dibenzoheptazethrene and 5,6:8,9:14,15:17,18-tetrabenzoheptacene. *Tetrahedron* **1960**, *9*, 96−105.

31 (a) Hafner, K. Structure and Aromatic Character of Non-benzenoid Cyclically Conjugated Systems *Angew. Chem. Int. Ed. Engl.* **1964**, *3*, 165–173, (b) Prinzbach, H.; Knothe, L. Multi-electron (12π-20π) pericyclic processes. *Pure Appl. Chem.* **1986**, *58*, 25–37.

32. (a) Tobe, Y. Quinodimethanes Incorporated in Non-Benzenoid Aromatic or Antiaromatic Frameworks. *Top. Curr. Chem. (Z)* **2018**, *376*, 12. (b) Frederickson, C. K.; Rose, B. D.; Haley, M. M. Explorations of the Indenofluorenes and Expanded

Quinoidal Analogues. *Acc. Chem. Res.* **2017**, *50*, 977–987. (c) Can, A.; Facchetti, A.; Usta, H. Indenofluorenes for organic optoelectronics: the dance of fused five- and six-membered rings enabling structural versatility. *J. Mater. Chem. C* **2022**, *10*, 8496–8535.

33. Warren, G. I.; Barker, J. E.; Zakharov, L. N.; Haley, M. M. Enhancing the Antiaromaticity of *s*-Indacene through Naphthothiophene Fusion. *Org. Lett.* **2021**, *23*, 5012–5017.

34. Higashino, T.; Mori, T. Small-molecule ambipolar transistors. *Phys. Chem. Chem. Phys.* **2022**, *24*, 9770–9806.

35. Chase, D. T.; Rose, B. D.; McClintock, S. P.; Zakharov, L. N.; Haley, M. M. Indeno[1,2-*b*]fluorenes: Fully Conjugated Antiaromatic Analogues of Acenes. *Angew. Chem., Int. Ed.* **2011**, *50*, 1127–1130.

36. Fix, A. G.; Deal, P. E.; Vonnegut, C. L.; Rose, B. D.; Zakharov, L. N.; Haley, M. M. Indeno[2,1-*c*]fluorene: A New Electron-Accepting Scaffold for Organic Electronics. *Org. Lett.* **2013**, *15*, 1362–1365.

37. Dressler, J. J.; Zhou, Z.; Marshall, J. L.; Kishi, R.; Takamuku, S.; Wei, Z.; Spisak, S. N.; Nakano, M.; Petrukhina, M. A.; Haley, M. M. Synthesis of the Unknown Indeno[1,2-*a*]fluorene Regioisomer: Crystallographic Characterization of Its Dianion. *Angew. Chem., Int. Ed.* **2017**, *56*, 15363–15367.

38. Shimizu, A.; Tobe, Y. Indeno[2,1-*a*]fluorene: An Air-Stable ortho-Quinodimethane Derivative. *Angew. Chem., Int. Ed.* **2011**, *50*, 6906–6910.

39. Shimizu, A.; Kishi, R.; Nakano, M.; Shiomi, D.; Sato, K.; Takui, T.; Hisaki, I.; Miyata, M.; Tobe, Y. Indeno [2,1-*b*] fluorene: A 20-π-Electron Hydrocarbon with Very Low-Energy Light Absorption. *Angew. Chem., Int. Ed.* **2013**, *52*, 6076–6079.

40. Chase, D. T.; Fix, A. G.; Rose, B. D.; Weber, C. D.; Nobusue, S.; Stockwell, C. E.; Zakharov, L. N.; Lonergan, M. C.; Haley, M. M. *Angew. Chem., Int. Ed.* **2011**, *50*, 11103–11106.

41. Chase, D. T.; Fix, A. G.; Kang, S. J.; Rose, B. D.; Weber, C. D.; Zhong, Y.; Zakharov, L. N.; Lonergan, M. C.; Nuckolls, C.; Haley, M. M. 6,12-Diarylindeno[1,2-*b*]Fluorenes: Syntheses, Photophysics, and Ambipolar OFETs. *J. Am. Chem. Soc.* **2012**, *134*, 10349–10352.

42. Nishida, J.-i.; Tsukaguchi, S.; Yamashita, Y. Synthesis, Crystal Structures, and Properties of 6,12-Diaryl-Substituted Indeno[1,2-*b*]fluorenes. *Chem. – Eur. J.* **2012**, *18*, 8964–8970.

43. Sharma, H.; Ankita, A.; Bhardwaj, P.; Pandey, U. K.; Das, S. Exploring Indeno[2,1-*c*]fluorene Antiaromatics with Unsymmetrical Disubstitution and Balanced Ambipolar Charge-Transport Properties. *Organic Materials* **2023**, *5*, 72–83.

44. Rudebusch, G. E.; Fix, A. G.; Henthorn, H. A.; Vonnegut, C. L.; Zakharov, L. N.; Haley, M. M. Quinoidal diindenothienoacenes: synthesis and properties of new functional organic materials. *Chem. Sci.* **2014**, *5*, 3627−3633.

45. Shi, X.; Burrezo, P. M.; Lee, S.; Zhang, W.; Zheng, B.; Dai, G.; Chang, J.; López Navarrete, J. T.; Huang, K.-W.; Kim, D.; Casado, J.; Chi, C. Antiaromatic bisindeno-[*n*]thienoacenes with small singlet biradical characters: syntheses, structures and chain length dependent physical properties. *Chem. Sci*. **2014**, *5*, 4490−4503.

46. Frederickson, C. K.; Zakharov, L. N.; Haley, M. M. Modulating Paratropicity Strength in Diareno-Fused Antiaromatics. *J. Am. Chem. Soc.* **2016**, *138*, 16827−16838.

47. (a) Saha, H. K.; Mallick, D.; Das, S. Unveiling two antiaromatic *s*-indacenodicarbazole isomers with tunable paratropicity. *Chem. Commun.* **2022**, *58*, 8492–8495 (b) Saha, H. K.; Mallick, D.; Das, S. Dibenzoheterole-Fused *s*-Indacenes *J. Org. Chem.* **2023**, 88, 16248–16258.

48. Young, B. S.; Chase, D. T.; Marshall, J. L.; Vonnegut, C. L.; Zakharov, L. N.; Haley, M. M. Synthesis and Properties of Fully Conjugated Indacenedithiophenes. *Chem. Sci.* **2014**, *5*, 1008−1014.

49. Marshall, J. L.; Uchida, K.; Frederickson, C. K.; Schütt, C.; Zeidell, A. M.; Goetz, K. P.; Finn, T. W.; Jarolimek, K.; Zakharov, L. N.; Risko, C.; Herges, R.; Jurchescu, O.; Haley, M. M. Indacenodibenzothiophenes: Synthesis, Optoelectronic Properties and Materials Applications of Molecules with Strong Antiaromatic Character. *Chem. Sci.* **2016**, *7*, 5547−5558.

50. Marshall, J. L.; O'Neal, N. J.; Zakharov, L. N.; Haley, M. M. Synthesis and Characterization of Two Unsymmetrical Indenofluorene Analogues: Benzo[5,6]-*s*-indaceno[1,2-*b*]thiophene and Benzo-[5,6]-*s*-indaceno[2,1-*b*]thiophene. *J. Org. Chem.* **2016**, *81*, 3674−3680.

51. Tobe, Y. Non-Alternant Non-Benzenoid Aromatic Compounds: Past, Present, and Future. *Chem. Rec.* **2015**, *15*, 86−96.

52. Shimizu, A.; Nobusue, S.; Miyoshi, H.; Tobe, Y. Indenofluorene congeners: Biradicaloids and beyond. *Pure Appl. Chem.* **2014**, *86*, 517−528.

53. Sharma, H.; Sharma, P. K.; Das, S. Revisiting indeno[2,1-*c*]fluorene synthesis while exploring the fully conjugated *s*-indaceno-[2,1-*c*:6,5-*c*′]difluorene. *Chem. Commun*. **2020**, *56*, 11319−11322.

54. Hu, P.; Lee, S.; Herng, T. S.; Aratani, N.; Gonçalves, T. P.; Qi, Q.; Shi, X.; Yamada, H.; Huang, K.-W.; Ding, J.; Kim, D.; Wu, J. Toward Tetraradicaloid: The Effect of Fusion Mode on Radical Character and Chemical Reactivity. *J. Am. Chem. Soc.* **2016**, *138*, 1065−1077.

55. (a) Wheland, G. W.; Mann, D. E. The Dipole Moments of Fulvene and Azulene. *J. Chem. Phys.* **1949**, *17*, 264–268. (b) Beer, M.; Longuet-Higgins, H. C. Anomalous Light Emission of Azulene. *J. Chem. Phys*. **1955**, *23*, 1390–1391. (c) Anderson, A. G.; Steckler, B. M. Azulene. VIII. A Study of the Visible Absorption Spectra and Dipole Moments of Some 1- and 1,3-Substituted Azulenes[1,2]. *J. Am. Chem. Soc.* **1959**, *81*, 4941– 4946.

56. (a) Yamaguchi, Y.; Ogawa, K.; Nakayama, K.; Ohba, Y.; Katagiri, H. Terazulene: a high-performance n-type organic field-effect transistor based on molecular orbital distribution control. *J. Am. Chem. Soc.* **2013**, *135*, 19095–19098, (b) Yamaguchi, Y.; Takubo, M.; Ogawa, K.; Nakayama, K.-I.; Koganezawa, T.; Katagiri, H. Terazulene isomers: polarity change of OFETs through molecular orbital distribution contrast. J. Am. Chem. Soc. 2016, 138, 11335–11343. (c) Xin, H.; Ge, C.; Yang, X.; Gao, H.; Yang, X.; Gao, X. Biazulene diimides: a new building block for organic electronic materials. *Chem. Sci.* **2016**, *7*, 6701–6705. (d) Xin, H.; Ge, C.; Jiao, X.; Yang, X.; Rundel, K.; McNeill, C. R.; Gao, X. Incorporation of 2,6-Connected Azulene Units into the Backbone of Conjugated Polymers: Towards High-Performance Organic Optoelectronic Materials. *Angew. Chem., Int. Ed.* **2018**, *57*, 1322–1326. (e) Cai, S.; Deng, W.; Huang, F.; Chen, L.; Tang, C.; He, W.; Long, S.; Li, R.; Tan, Z.; Liu, J.; Shi, J.; Liu, Z.; Xiao, Z.; Zhang, D.; Hong, W. Light-driven reversible intermolecular proton transfer at single-molecule junctions. *Angew. Chem., Int. Ed.* **2019**, *58*, 3829–3833. (f) Xin, H.; Gao, X. J. C. Application of azulene in constructing organic

optoelectronic materials: new tricks for an old dog. *ChemPlusChem* **2017**, *82*, 945−956.

57. (a) Baumgartner, P.; Weltin, E.; Wagnière, G.; Heilbronner, E. Ist Die Molekel Ein Biradikal?. *Helv. Chim. Acta* **1965**, *48*, 751–764. (b) Kurotobi, K.; Kim, K. S.; Noh, S. B.; Kim, D.; Osuka, A. A Quadruply Azulene-Fused Porphyrin with Intense Near-IR Absorption and a Large Two-Photon Absorption Cross Section. *Angew. Chem., Int. Ed.* **2006**, *45*, 3944–3947. (c) Das, S.; Wu, J. Toward Singlet–Triplet Bistable Nonalternant Kekulé Hydrocarbons: Azulene-to-Naphthalene Rearrangement. *Org. Lett.* **2015**, *17*, 5854–5857. (d) Yamamoto, K.; Ie, Y.; Tohnai, N.; Kakiuchi, F.; Aso, Y. Antiaromatic Character of Cycloheptatriene-Bis-Annelated Indenofluorene Framework Mainly Originated from Heptafulvene Segment. *Sci. Rep.* **2018**, *8*, 17663. (e) Jiang, Q.; Tao, T.; Phan, H.; Han, Y.; Gopalakrishna, T. Y.; Herng, T. S.; Li, G.; Yuan, L.; Ding, J.; Chi, C. Diazuleno-*s*-Indacene Diradicaloids: Syntheses, Properties, and Local (Anti)Aromaticity Shift from Neutral to Dicationic State. *Angew. Chem., Int. Ed.* **2018**, *57*, 16737–16741. (f) Liu, J.; Mishra, S.; Pignedoli, C. A.; Passerone, D.; Urgel, J. I.; Fabrizio, A.; Lohr, T. G.; Ma, J.; Komber, H.; Baumgarten, M.; Corminboeuf, C.; Berger, R.; Ruffieux, P.; Müllen, K.; Fasel, R.; Feng, X. Open-Shell Nonbenzenoid Nanographenes Containing Two Pairs of Pentagonal and Heptagonal Rings. *J. Am. Chem. Soc.* **2019**, *141*, 12011–12020. (g) Sasaki, Y.; Takase, M.; Okujima, T.; Mori, S.; Uno, H. Synthesis and Redox Properties of Pyrrole- and Azulene-Fused Azacoronene. *Org. Lett.* **2019**, *21*, 1900–1903. (h) Konishi, A.; Horii, K.; Shiomi, D.; Sato, K.; Takui, T.; Yasuda, M. Open-Shell and Antiaromatic Character Induced by the Highly Symmetric Geometry of the Planar Heptalene Structure: Synthesis and Characterization of a Nonalternant Isomer of Bisanthene. *J. Am. Chem. Soc.* **2019**, *141*, 10165–10170. (i) Yang, X.; Rominger, F.; Mastalerz, M. Contorted Polycyclic Aromatic Hydrocarbons with Two Embedded Azulene Units. *Angew. Chem., Int. Ed*. **2019**, *58*, 17577–17582. (j) Ma, J.; Fu, Y.; Dmitrieva, E.; Liu, F.; Komber, H.; Hennersdorf, F.; Popov, A. A.; Weigand, J. J.; Liu, J.; Feng, X. Helical Nanographenes Containing an Azulene Unit: Synthesis, Crystal Structures, and Properties. *Angew. Chem., Int. Ed.* **2020**, *59*, 5637–5642. (k) Zhang, X. S.; Huang, Y. Y.; Zhang, J.; Meng, W.; Peng, Q.; Kong, R.; Xiao, Z.; Liu, J.; Huang, M.; Yi, Y.; Chen, L.; Fan, Q.; Lin, G.; Liu, Z.; Zhang, G.; Jiang, L.; Zhang, D. Dicyclohepta[*ijkl,uvwx*]rubicene with Two

Pentagons and Two Heptagons as a Stable and Planar Non-benzenoid Nanographene. *Angew. Chem., Int. Ed.* **2020**, *59*, 3529–3533.

58 (a) Konishi, A.; Yasuda, M. Breathing New Life into Nonalternant Hydrocarbon Chemistry: Syntheses and Properties of Polycyclic Hydrocarbons Containing Azulene, Pentalene, and Heptalene Frameworks. *Chem. Lett.* **2021**, *50*, 195−212. (b) Fei, Y.; Liu, J. Synthesis of Defective Nanographenes Containing Joined Pentagons and Heptagons. *Adv. Sci.* **2022**, *9*, 2201000 (c) Konishi, A.; Horii, K.; Yasuda, M. The road to bis-periazulene (cyclohepta[*def*]fluorene): Realizing one of the longstanding dreams in nonalternant hydrocarbons. *J. Phys. Org. Chem.* **2023**, No. e4495.

59. Reid, D. H.; Stafford, W. H.; Ward, J. P. The Fine Structure of Azulene. Part I. CycloHepta[*bc*]Acenaphthylene and Cyclohepta[*def*]Fluorene. *J. Chem. Soc.* **1955**, *84*, 1193.

60. Baumgartner, P.; Weltin, E.; Wagnière, G.; Heilbronner, E. Ist Die Molekel Ein Biradikal?. *Helv. Chim. Acta* **1965**, *48*, 751–764.

61. Nendel, M.; Goldfuss, B.; Houk, K. N.; Grieser, U.; Hafner, K. Bis-Periazulene: A Simple Kekulé Biradical with a Triplet Ground State. Theor. *Chem. Acc.* **1999**, *102*, 397– 400.

62. Horii, K.; Kishi, R.; Nakano, M.; Shiomi, D.; Sato, K.; Takui, T.; Konishi, A.; Yasuda Bis-periazulene (Cyclohepta[*def*]fluorene) as a Nonalternant Isomer of Pyrene: Synthesis and Characterization of Its Triaryl Derivatives. *J. Am. Chem. Soc.* **2022**, *144*, 3370–3375.

63. Konishi, A.; Morinaga, A.; Yasuda, M. Construction of Polycyclic π-Conjugated Systems Incorporating an Azulene Unit Following the Oxidation of 1,8-Diphenyl-9,10-bis(phenylethynyl)- phenanthrene. *Chem. − Eur. J.* **2018**, *24*, 8548−8552.

64. Pigulski, B.; Shoyama, K.; Würthner, F. NIR-Absorbing π-Extended Azulene: Non-Alternant Isomer of Terrylene Bisimide. *Angew. Chem., Int. Ed.* **2020**, 59, 15908−15912.

65. Yang, X.; Rominger, F.; Mastalerz, M. Contorted Polycyclic Aromatic Hydrocarbons with Two Embedded Azulene Units. *Angew. Chem., Int. Ed.* **2019**, 58, 17577-17582.

66. Han, Y.; Xue, Z.; Li, G.; Gu, Y.; Ni, Y.; Dong, S.; Chi, C. Formation of Azulene-Embedded Nanographene: Naphthalene to Azulene Rearrangement During the Scholl Reaction. *Angew. Chem., Int. Ed*. **2020**, *59*, 9026−9031.
67. Ogawa, N.; Yamaoka, Y.; Takikawa, H.; Yamada, K.; Takasu, K. Helical Nanographenes Embedded with Contiguous Azulene Units. *J. Am. Chem. Soc.* **2020**, *142*, 13322−13327.

Chapter 2

Unveiling a Quinoidal 2,3:10,11-Dibenzoheptazethrene

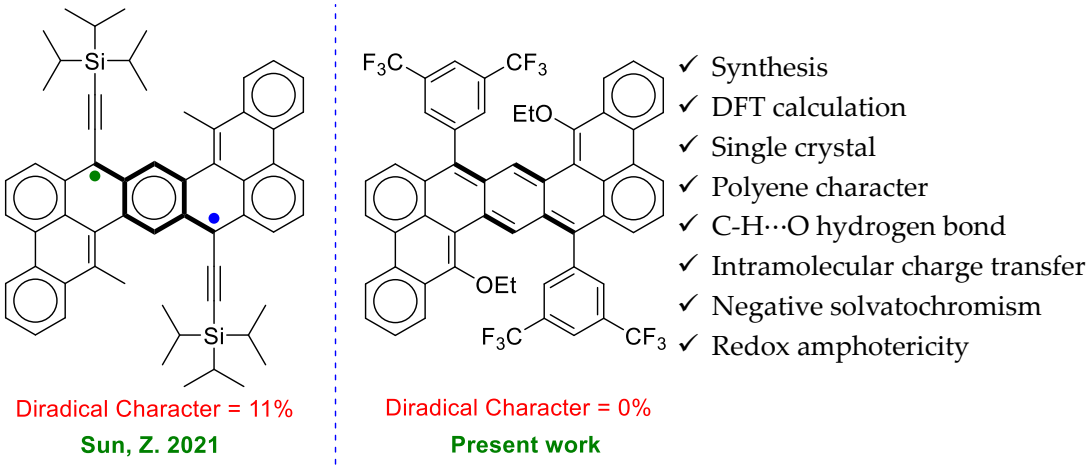

This work was published in *The Journal of Organic Chemistry* (an ACS journal). Please see the citation as: "Sharma, P. K., Das, S. Unveiling a Quinoidal 2,3:10,11-Dibenzoheptazethrene. *J. Org. Chem.* **2022**, *87*, 5430–5436."

2 Abstract

Parent 2,3:10,11-dibenzoheptazethrene is a singlet diradicaloid polycyclic hydrocarbon in the ground state that didn't change its diradical character upon substitution (methyl and triisopropylsilylethynyl). Described herein are the synthesis and characterization of an ethoxy/3,5-$(CF_3)_2C_6H_3$-substituted 2,3:10,11-dibenzoheptazethrene **3** that prefers to retain *para*-quinoidal core and shows *zero* diradical character, as determined by the single crystal analysis and density functional theory calculations. Negative solvatochromism, π-π interactions, C_{sp^2}–H···O hydrogen bonding, intramolecular charge transfer, redox amphotericity, and a narrow HOMO–LUMO energy gap make **3** a potential candidate for application in optoelectronics.

2.1 Introduction

As discussed in Chapter 1, heptazethrene (HZ) is an open-shell polycyclic hydrocarbon (PH) with 17% singlet diradical character in the ground state, and may be drawn in either Kekulé or diradical form.[1] The diradical ground state of core-modified HZ-bis(dicarboximide) was experimentally validated[2] and its further core-extension showed 46.5% diradical character with higher stability due to kinetic protection of the reactive radical sites.[3] Substituents such as methyl, alkoxy, triisopropylsilylethynyl (TIPSE), mesityl, and perfluorophenyl have negligible effect on the diradical character of HZ.[4] However, π-ring annulation (benzannulation) can markedly tune the singlet diradical character index (y_0) of HZ.[5]

Symmetrical *peri*-dibenzannulation at the peripheral naphthalene rings of HZ afforded closed-shell benzodipyrene,[6] whereas, symmetrical *cata*-dibenzannulation can afford up to four open-shell dibenzoheptazethrene (DBHZ) regioisomers, namely, 2,3:10,11-DBHZ **1** (Figure 2.1a),[5b] 4,5:12,13-DBHZ,[5b] 5,6:13,14-DBHZ,[5a] and 1,2:9,10-DBHZ,[5a] with different diradical characters. Among the four *cata*-fused regioisomers, parent 4,5:12,13-DBHZ was first synthesized by Clar,[7] and its electronic ground state was theoretically identified in 2021.[5b] Anthracene-based 5,6:13,14-DBHZ and 1,2:9,10-DBHZ were shown to have different y_0 values in the ground state, based on the recovery of number of Clar sextets.[5a] By applying same logic, phenanthrene-based 4,5:12,13-DBHZ and **1** were found to possess comparable y_0 values since both can recover only one Clar sextet in the diradical form,[5b] as represented in the form of **OS-I** for **1**. All DBHZ structural isomers are singlet diradicaloid with low-lying

thermally accessible triplet excited state, to date, and since they can recover benzene aromaticity in diradical forms, they are classified as pro-aromatic PHs.[8]

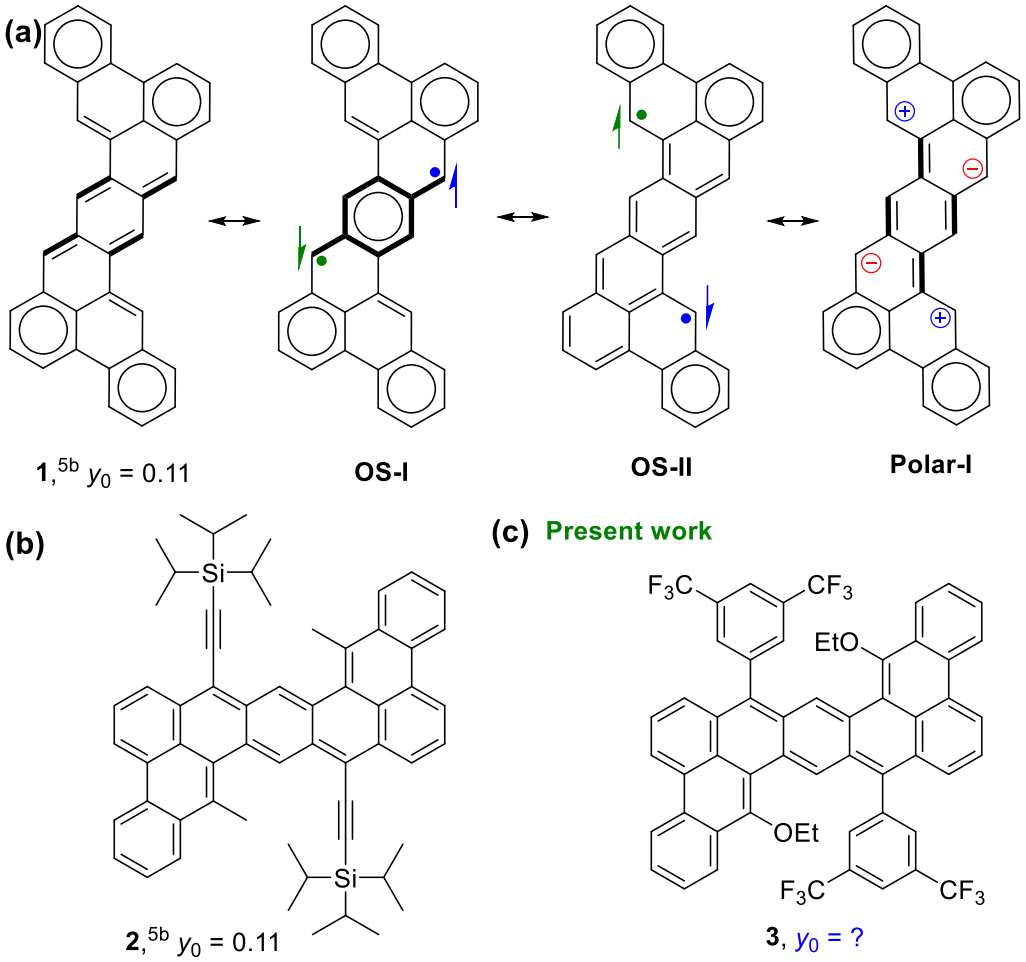

Figure 2.1 (a) Plausible Kekulé **1**, diradical (open-shell singlet), and zwitterionic resonance forms for the parent 2,3:10,11-DBHZ **1**. (b) Sun's 2,3:10,11-DBHZ derivative **2**. (c) Our target 2,3:10,11-DBHZ derivative **3**.

Compound **2**, a derivative of **1**, showed red-shifted absorption, small optical energy gap, and high hole mobility in comparison to the 4,5:12,13-DBHZ with same substituents (methyl, triisopropylsilylethynyl (TIPSE)). Interestingly, both **1** and **2** have the same y_0 value.[5b] It seems, TIPSE has no effect on the y_0 values for both the HZ and DBHZ derivatives.[5b,4a] The effect of different substituents on the ground state for HZ-based π-series are seldom studied.[9,4b] Kekulé structure **1** can be viewed further as another open-shell diradical form **OS-II** and a zwitterionic resonance form **Polar-I** (Figure 2.1a). We envisioned attaching proper substituents to **1** in order to stabilize the **Polar-I** form to afford a new 2,3:10,11-DBHZ derivative bearing donor/acceptor substituents,[10] that may show strong quinoidal character because the neutral form **1** and the zwitterionic **Polar-I** form have the same number of Clar sextets in the ground

state with *para*-quinoidal arrangement in the core. Thus, electron-acceptor 3,5-$(CF_3)_2C_6H_3$ and electron-donor ethoxy groups were chosen as the potentially polarizing substituents to design **3** (Figure 2.1c). Herein, apart from a new approach to synthesize **3** and its analytical characterizations, the ground state of **3** was studied by x-ray crystallographic analysis, and the experimental observations were supported by the density functional theory (DFT) calculations at the B3LYP/6-31G(d,p) level of theory.[11]

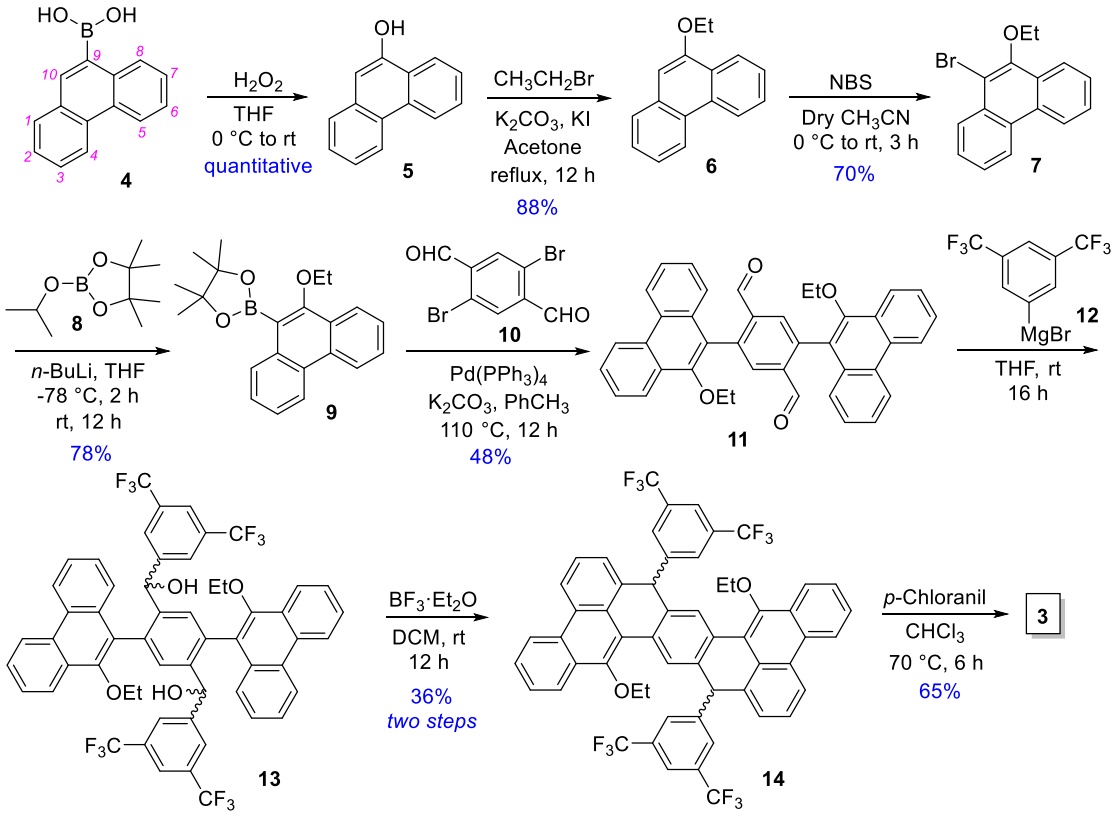

Scheme 2.1 Synthesis of **3**.

2.2 Results and Discussion

2.2.1 Syntheses. 9-Phenanthracenylboronic acid **4** was converted to **5** using hydrogen peroxide following the literature procedure (Scheme 2.1).[12] Crude **5** was converted to **6** in the presence of bromoethane using potassium iodide mediated nucleophilic substitution reaction, and the subsequent bromination using *N*-bromosuccinimide in dry acetonitrile afforded **7** in 70% yield. Compound **7** was treated with *n*-BuLi at −78 °C for 2 h, followed by quenching with **8** to afford **9**. A Pd^0-catalyzed Suzuki reaction between **10** and 3 equivalents of **9** afforded **11** in 48% yield. Nucleophilic addition of **12** to **11** afforded the dicarbinol **13**, which, without purification, was treated with $BF_3{\cdot}Et_2O$ to afford the dihydro precursor **14**. Compound

14, after passing through a short pad of silica gel, was treated with 2.1 equivalents of *p*-chloranil in dry chloroform at 70 °C for 6 h to afford **3** as blue-green solid after column chromatographic purification on silica gel. The structure of **3** was established by the 1D- and 2D-nuclear magnetic resonance (NMR) spectroscopy in benzene-d_6 (Figure 2.2, 2.3, and 2.4), and it was further unequivocally confirmed by the X-ray crystallographic analysis.

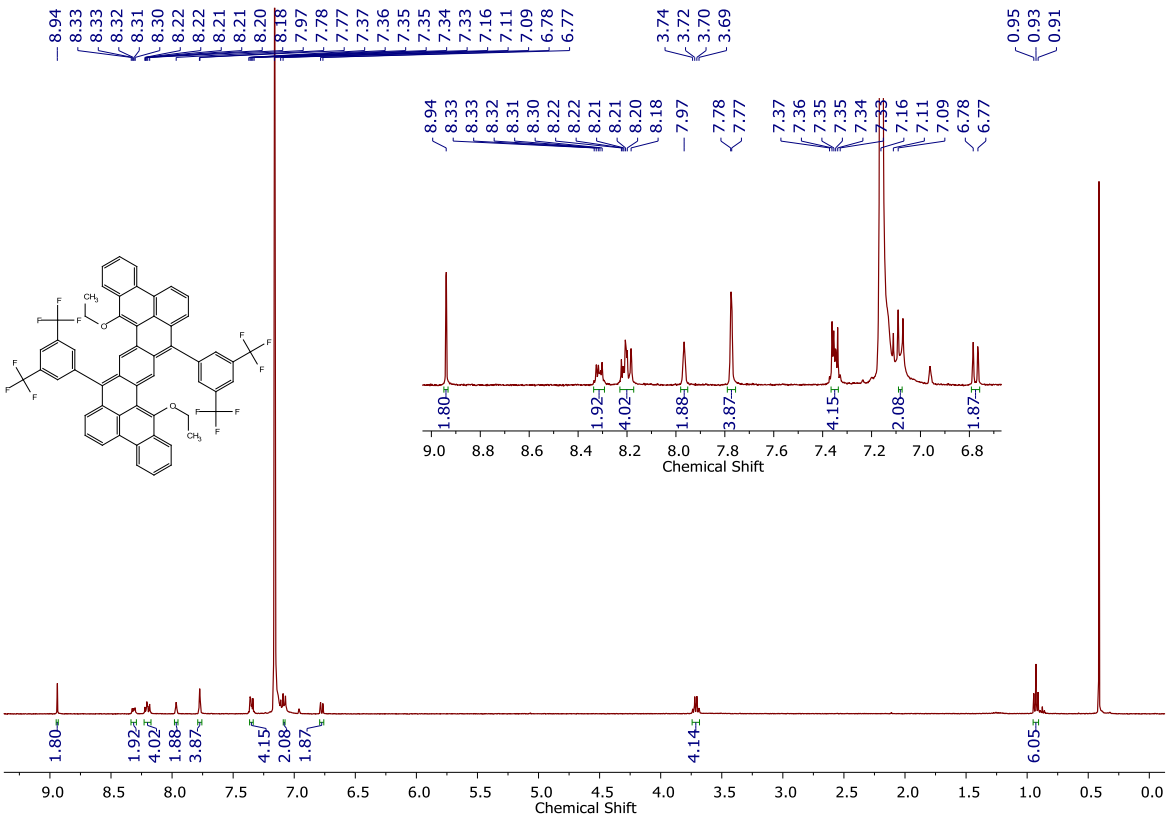

Figure 2.2 ^{1}H NMR spectrum of **3** (in C_6D_6, 400 MHz) at 298 K.

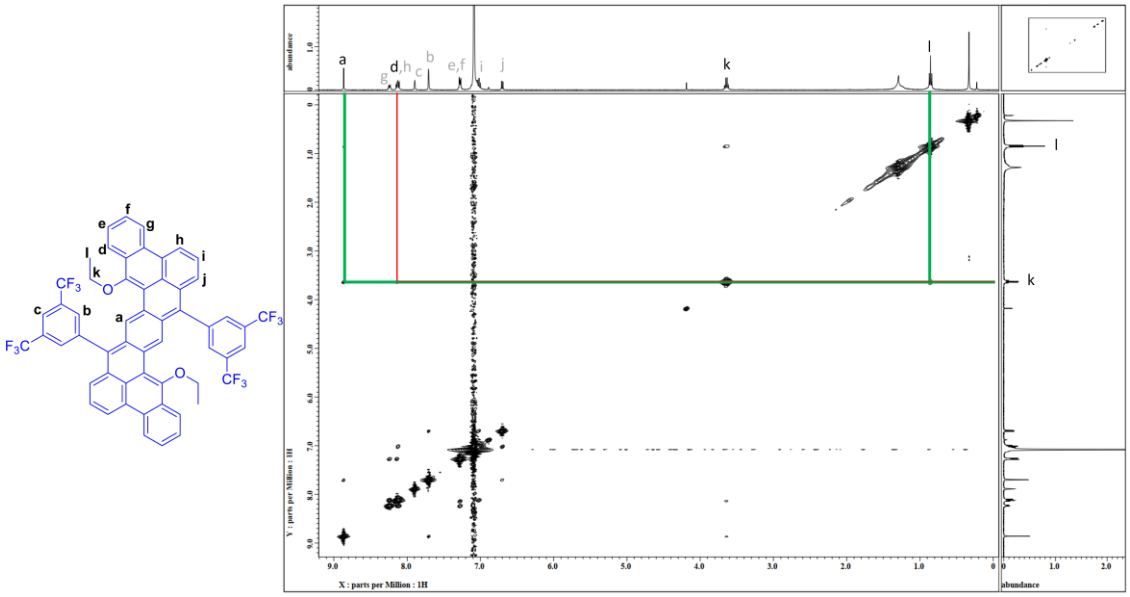

Figure 2.3 Full ^{1}H-^{1}H NOESY spectrum of **3** in C_6D_6.

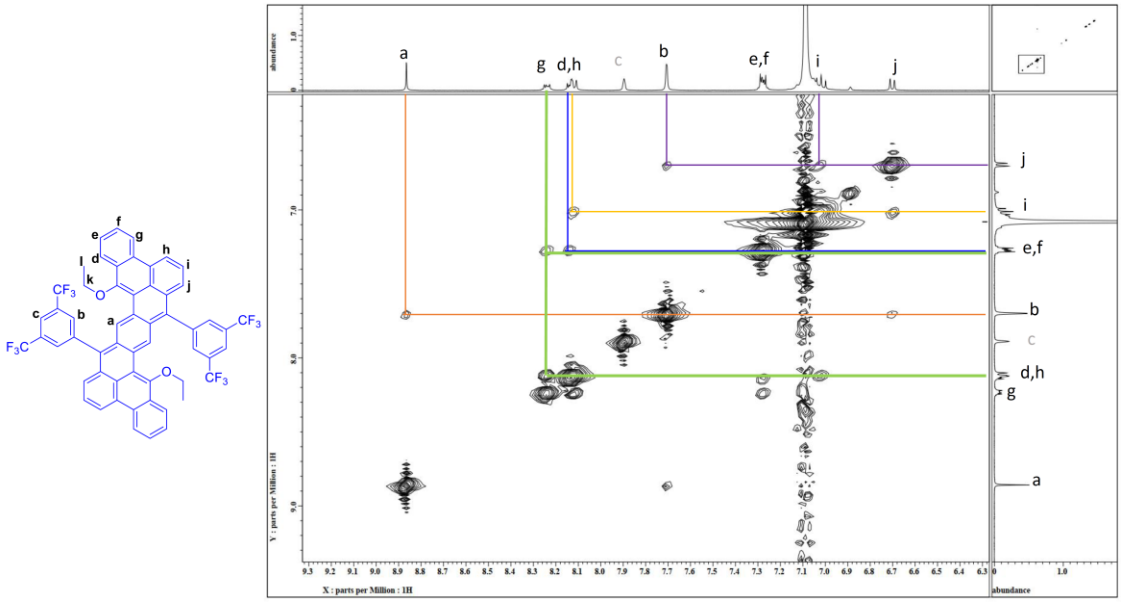

Figure 2.4 ^{1}H-^{1}H NOESY spectrum of **3** in C_6D_6 (aromatic region expansion).

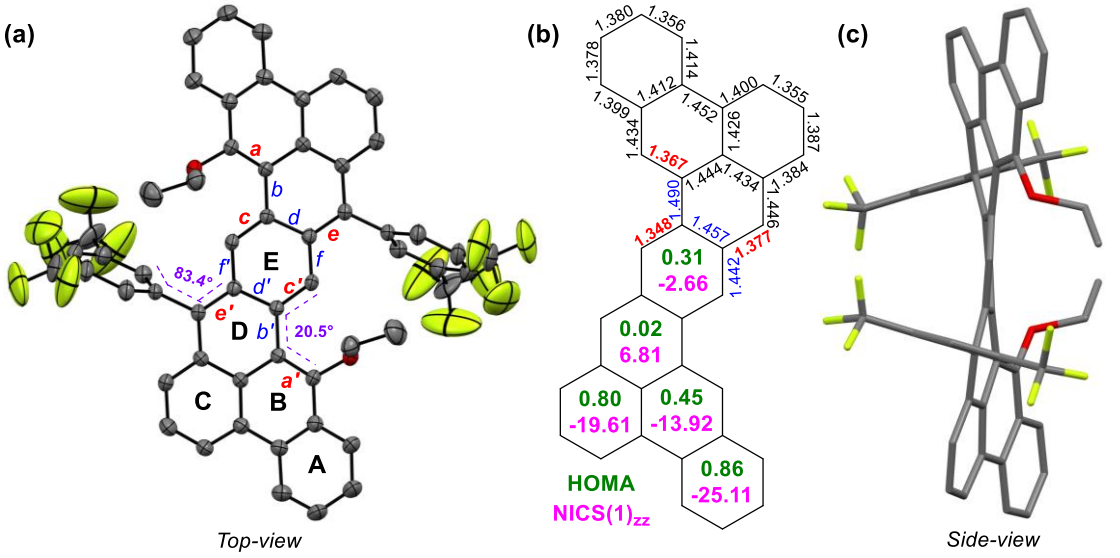

Figure 2.5 (a) ORTEP drawing of **3** at 30% probability level (hydrogens are omitted). (b) C–C bond lengths (in Å) for **3**, with HOMA and NICS(1)$_{zz}$ indices. (c) Side-view of **3**.

2.2.2 X-ray crystallography and aromaticity analyses. Single crystals of **3** for X-ray crystallographic analysis were grown by the slow evaporation from chloroform/toluene mixture at ambient temperature in the dark. The backbone of **3** is found to be non-planar, with the B rings are twisted by 20.5° torsion angle against the D/E π-rings at the bay-region, due to the steric effects (Figure 2.5a and 2.5c). The 3,5-$(CF_3)_2C_6H_3$ group is near orthogonally oriented (dihedral angle 83.4°) to the conjugated π-backbone. The ethoxy groups are projected to the same side, allowing

two molecules to stack co-facially with another molecule within the crystal lattice at the outer phenanthrene part (Figure 2.6a). The closest intermolecular C–C contact distance is 3.347 Å, which is larger than those of Kubo's bisphenalenyl systems[13] or diradicaloid 5,6:12,13-dibenzozethrene[14] where intermolecular spin-spin interactions dominate. Such a close intermolecular contact may suggest the existence of strong π-π interactions in **3**, which was not observed for **2**,[5b] enabling a wave-like packing arrangement for **3** (Figure 2.6a and 2.6b). Replacement of methyl with ethoxy in **3** has resulted not only in a reduced dihedral angle (20.5° for **3**, in comparison to 22.5° for **2**) at the bay region, but also in a weak intramolecular C_{sp^2}–H···O hydrogen bonding interaction (2.212 Å, $\angle C_{sp^2}$–H···O = 121.8°),[15] that might explain the downfield-shifted signal for the hydrogens on ring E (δ: 8.94 in benzene-d_6 for **3** (Figure 2.2), in comparison to 8.71 in chloroform-*d* or 8.46 in toluene-d_8 for **2**[5b]).

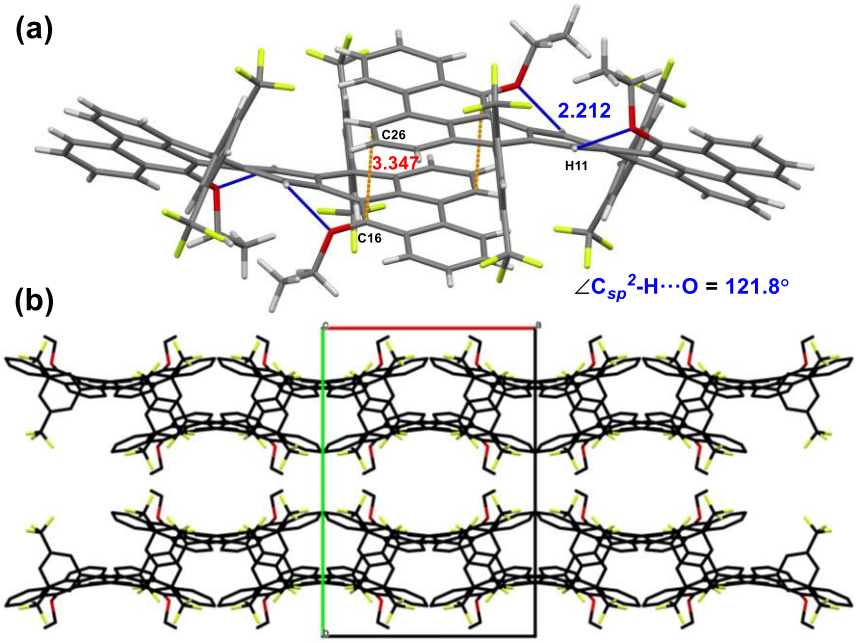

Figure 2.6 (a) Intermolecular C–C contact, and hydrogen bonding distances (Å) with angle. (b) Packing diagram of **3**.

Because compound **2** is a singlet diradical in the ground state at the expense of a double bond of *para*-quinomethane (*p*-QDM is shown in bold, Figure 2.1a) to gain a benzene aromaticity for the central benzenoid ring E, the bond lengths for **3** and **2**, which are important to determine the ground state electronic configuration, are summarized in Table 2.1 against the reported *p*-QDM bond lengths (*c/c'*, *d/d'*, *e/e'*, *f/f'*) for Thiele's hydrocarbon.[16] The bond length analysis of the *p*-QDM skeleton for **3** (Figure 2.5a and 2.5b) revealed the *c/c'* C_{sp^2}=C_{sp^2} bonds to be 1.348 Å long (close to

olefin double bond), whereas the *exo*-methylene *e/e'* C_{sp^2}=C_{sp^2} bonds are 1.377 Å long, which are similar to or shorter than that of the closed-shell Thiele's hydrocarbon, and are obviously shorter than that in **2**. The homogeneous distribution of bond lengths for ring A (avg. 1.389 Å) and ring C (avg. 1.397 Å) in **3** suggested localized aromaticity at the outer phenanthrene parts, similar to those of **2**. The observations certainly suggest compound **3** retains the *para*-quinoidal arrangement in the core, with strong C–C bond length alternations for *a/a'* and *b/b'* bonds, where the *a/a'* C_{sp^2}=C_{sp^2} bond is distinctly shorter for **3** in comparison to **2** (Table 2.1). Therefore, compound **3** is better viewed as a *p*-QDM-embedded DBHZ with strong polyene character in the ground state.

Table 2.1 Mean C–C bond lengths (in angstroms (Å)) for **2**, **3**, and Thiele's *p*-QDM skeleton from crystals.

C-C bonds	**2**	**3**	Thiele's *p*-QDM
a/a'	1.388	1.367	–
b/b'	1.479	1.490	–
c/c'	1.365	1.348	1.346
d/d'	1.456	1.457	1.449
e/e'	1.388	1.377	1.381
f/f'	1.431	1.442	1.449

DFT calculations for **2** showed the closed-shell state to be roughly 2 kcal/mol higher than the open-shell singlet ground state, with 9.3 kcal/mol gap between the open-shell singlet and triplet states, which was in agreement with the small diradical character.[5b] Our DFT calculations, by optimizing the crystal structure, found the molecule **3** to have a singlet closed-shell ground state and zero diradical character with the triplet state located 12.5 kcal/mol above the singlet state (Table 2.5). Both CASSCF and broken symmetry approach agree with the zero diradical character for **3**, whereas CASSCF calculation predicted **2** to have 15.3% diradical character. Additionally, DFT examination found 8.5% or 8.2% diradical character, respectively, for the derivatives of **1** with only 3,5-$(CF_3)_2C_6H_3$ or ethoxy substituents in the singlet ground state (Table 2.5). The results clearly indicate that substituents can strongly impact the electronic ground state for diradicaloid **1** with small gap between singlet open-shell and closed-shell states.

The harmonic oscillator model of aromaticity (HOMA)[17] values for ring E (0.31) and ring D (0.02) indicated large bond length alternations for **3** (Figure 2.5b), whereas localization of Clar sextets is suggested for ring A (0.86) and C (0.80). The aromaticity for ring B (0.45) is quite weak, signifying the dominance of phenanthrene substructure in the ground state. The nucleus independent chemical shift [NICS$(1)_{zz}$][18] indices are also in good agreement with the HOMA values, implying the central ring E to be essentially atropic (Figure 2.5b). Notably, according to the NICS and HOMA indices, the aromaticity of ring E has decreased for **3**, in comparison to that of **2**.[5b] These results are obviously suggest a closed-shell structure with *para*-quinoidal arrangement in the core is primarily contributing to the singlet ground state for **3**.

2.2.3 Optical and electrochemical properties. The toluene solution of **3** is blue, and shows a *p*-band in the visible region with the lowest energy absorption maximum at 629 nm (ε = 50,080 M^{-1} cm^{-1}) (Figure 2.7a), belonging to the HOMO→LUMO transition (Table 2.2, theoretical λ_{max} = 712 nm, oscillator strength (*f*) = 0.9291). It also displays two low-intense high energy absorption bands at λ_{max} = 376 nm (TDDFT: 387.3 nm, *f* = 0.3036) and λ_{max} = 340 nm (TDDFT: 341.5 nm, *f* = 0.5027). Interestingly, a negative solvatochromism is observed for **3** in tetrahydrofuran (THF), as the lowest energy absorption maximum appears at 621 nm (ε = 40,840 M^{-1} cm^{-1}), which is blue-shifted by 8 nm. Calculations show that the ground state of **3** is slightly polar (dipole moment (μ) = 2.91 D). The observation indicates that the neutral resonance structure **3** may contribute to the ground state in a non-polar solvent, while in relatively polar solvents, a dipolar resonance form may predominate.[19] The natural population analyses (NPA)[20] for **3** suggested that the carbon attached to the electron-releasing ethoxy group is positive (+0.368) due to strongly polarizing oxygen (−0.579), whereas the negative charge is dispersed *via* the π-backbone to the electron-withdrawing 3,5-$(CF_3)_2C_6H_3$, suggesting a moderate donor-acceptor type intramolecular charge transfer (ICT) interaction operating through the π-backbone spacer (D-π-A, Figure 2.7b and 2.7c). The results suggest that a dipolar zwitterionic form **3-Polar** (Figure 2.7c and 2.11) is stabilized in polar THF and causes blue-shift in absorption maximum.

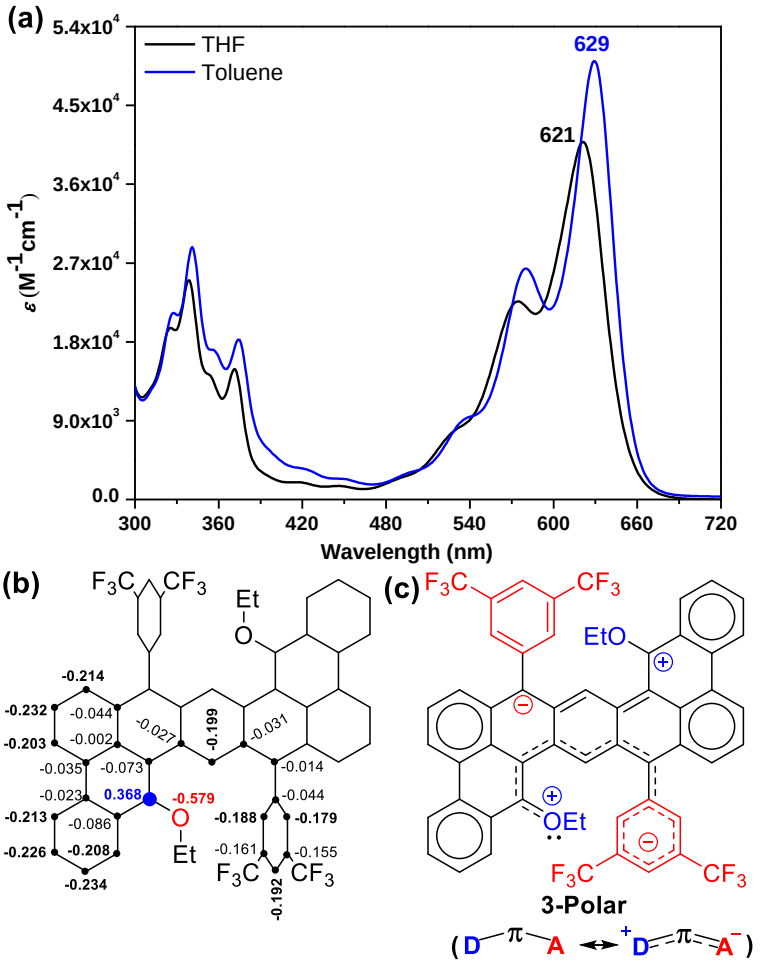

Figure 2.7 (a) UV-vis absorption spectra of **3** in toluene (blue) and THF (black). (b) NPA charges for **3** in gas phase. (c) The dipolar resonance form (**3-Polar**) for **3**, stabilized by the donor-acceptor charge transfer interaction through π-backbone.

Table 2.2 Calculated major electronic transitions for **3** in toluene.

Wavelength (nm)	Oscillator Strength	Major contributions
712	0.9291	HOMO->LUMO (101%)
523	0	H-1->LUMO (41%), HOMO->L+1 (58%)
479	0.0143	H-1->LUMO (52%), HOMO->L+1 (37%)
448	0.0079	HOMO->L+3 (92%)
446	0.0115	HOMO->L+2 (90%)
426	0.0384	H-2->LUMO (61%), HOMO->L+5 (30%)
416	0.0005	H-3->LUMO (20%), HOMO->L+4 (78%)
410	0.0586	HOMO->L+6 (90%)
408	0.0011	H-3->LUMO (44%), HOMO->L+4 (16%), HOMO->L+7 (37%)
387	0.3036	H-2->LUMO (30%), HOMO->L+5 (59%)
376	0.0071	H-4->LUMO (19%), H-3->LUMO (24%), HOMO->L+7 (50%)
363	0.002	H-4->LUMO (22%), HOMO->L+8 (70%)

347	0.0286	H-5->LUMO (68%), HOMO->L+9 (29%)
345	0.0006	H-4->LUMO (56%), HOMO->L+8 (27%)
341	0.5027	H-1->L+1 (91%)
328	0.0681	H-5->LUMO (25%), HOMO->L+9 (63%)
315	0.0449	H-1->L+2 (94%)
315	0.0002	H-1->L+3 (88%)
313	0.0245	H-7->LUMO (81%), H-6->LUMO (13%)
308	0.0053	H-2->L+1 (72%), H-1->L+5 (10%)

The experimental absorption trend with the variation of solvent polarity (toluene, chloroform, dichloromethane, THF) is also consistent with the TDDFT calculations (Table 2.3 and Figure 2.8). Compound **3** showed reasonable photostability under ambient light conditions, with a half-life time of 40 h in air-saturated toluene solution (Figure 2.9).[21,5b] Compound **3** also exhibited a small fluorescence quantum yield of 7.2% (with methylene blue[22] as a standard) with an emission maximum at 645 nm in toluene, including solvent-dependent solvatochromism behavior (Figure 2.8).

Table 2.3 HOMO → LUMO transition in different solvents by TDDFT calculations and experimental observations

Solvent	**λ (theory)**	**λ (experiment)**
Toluene	712 nm	629 nm
Chloroform	709 nm	626 nm
Dichloromethane	707 nm	623 nm
Tetrahydrofuran	705 nm	621 nm

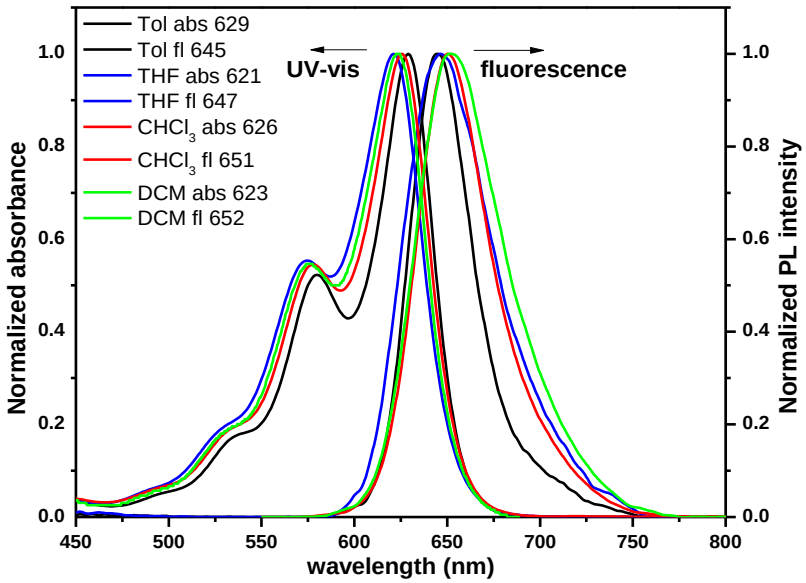

Figure 2.8 Normalized UV-vis absorption and fluorescence spectra in toluene, THF, $CHCl_3$, DCM.

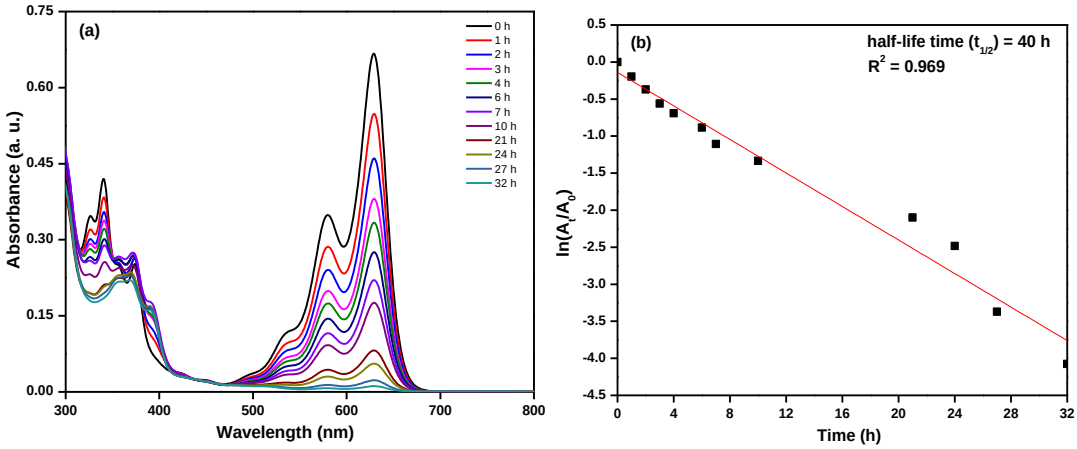

Figure 2.9 (a) Absorption spectral changes under ambient light for compound **3** in toluene. (b) Fitting with first order kinetics.

The DFT optimized HOMO and LUMO profiles for **3** show large amplitude on the bond *a* (C=C double bond character), suggesting anti-bonding interaction between the lone-pair on oxygen and the p orbital on carbon to which the ethoxy group is attached (Figure 2.10a), thereby destabilizing both the energy levels. Consequently, compound **3** was easily oxidized during cyclic voltammetry (CV) experiment in dichloromethane, displaying three reversible oxidation waves with the half-wave potentials at $E_{1/2}^{ox1} = -0.61$ V, $E_{1/2}^{ox2} = -0.07$ V and $E_{1/2}^{ox3} = 0.24$ V (*vs* ferrocene/ferrocenium (Fc/Fc^+)), respectively. The half-wave reduction potentials appeared at $E_{1/2}^{red1} = -1.31$ V and $E_{1/2}^{red2} = -1.88$ V (Figure 2.10b).

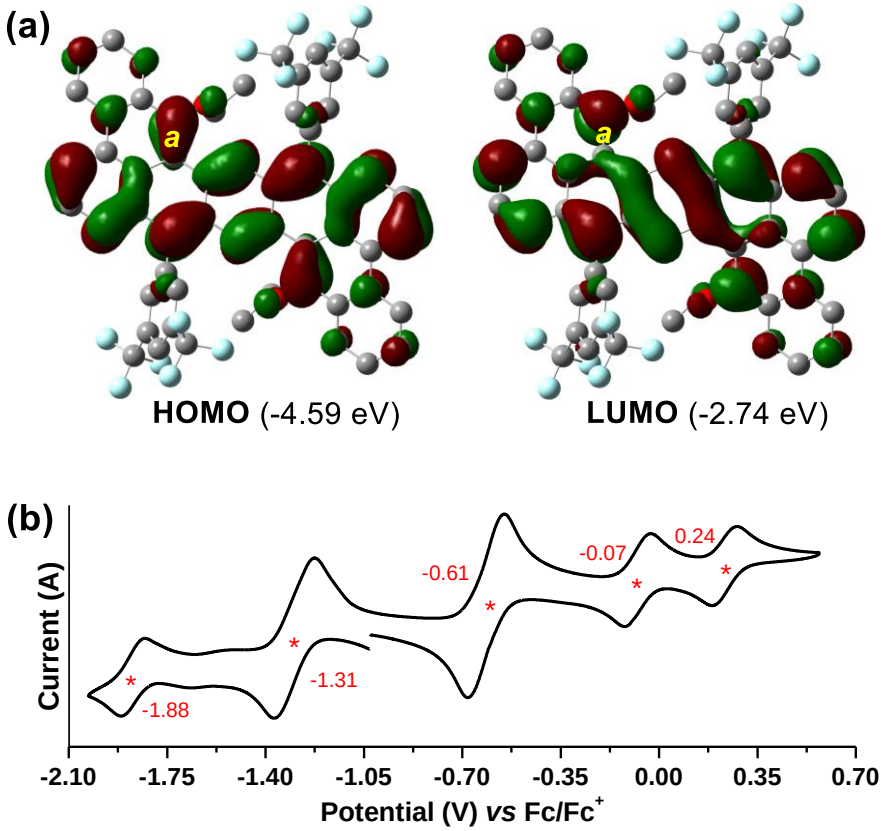

Figure 2.10 (a) The HOMO and LUMO profiles from DFT calculations. (b) Cyclic voltammogram of **3** in CH_2Cl_2/Bu_4NPF_6 solvent/electrolyte couple at 50 mV s^{-1} scan rate.

The larger first reduction and oxidation waves can be attributed to two-electron processes,[10b] due to the plausible formation of two carbocation and carbanion centres which are stabilized by electron-donation (OEt) and electron-withdrawing (3,5-$(CF_3)_2C_6H_3$)) effects, respectively (Figure 2.11). The dication formation for **3** is facilitated by a low-lying zwitterionic state (**3-Polar**), which is accessible due to the polarizing effects of the substituents. The ethoxy group stabilizes the carbocation centers mesomerically for $\mathbf{[3]^{+2}}$, while the carbanions are stabilized by the -I and resonance effects from the electron-accepting $(CF_3)_2C_6H_3$ substituent for $\mathbf{[3]^{-2}}$. Thus, the observed larger redox waves are attributed to two-electron transfer processes, supported by the readily accessible zwitterionic state of quinoidal **3** in the singlet ground state. The HOMO and LUMO energies for **3** can be estimated as −4.11 eV and −3.56 eV, from the onset potentials,[5b] affording a small electrochemical energy gap (E_g^{ec}) of 0.55 eV, likely hinting the contribution of a π-extended second resonance structure ($D^+{=}\pi{=}A^-$) over the neutral structure (D–π–A) (Figure 2.7c and Figure 2.11). The electrochemical energy gap is quite smaller than its optical energy gap

(E_g^{opt}), 1.84 eV, estimated from the lowest energy absorption onset (Figure 2.7a), and the E_g^{ec} of **2** is also noticeably (0.43 eV) smaller than its E_g^{opt}.[5b] It is worth mentioning that a recent report[23] has stressed that the electrochemical HOMO and LUMO energies should more accurately be defined as the ionization potential and electron affinity, respectively. In fact, the E_g^{opt} of **3** (1.84 eV) is consistent with the theoretical HOMO–LUMO energy gap value of 1.85 eV (Figure 2.10a).

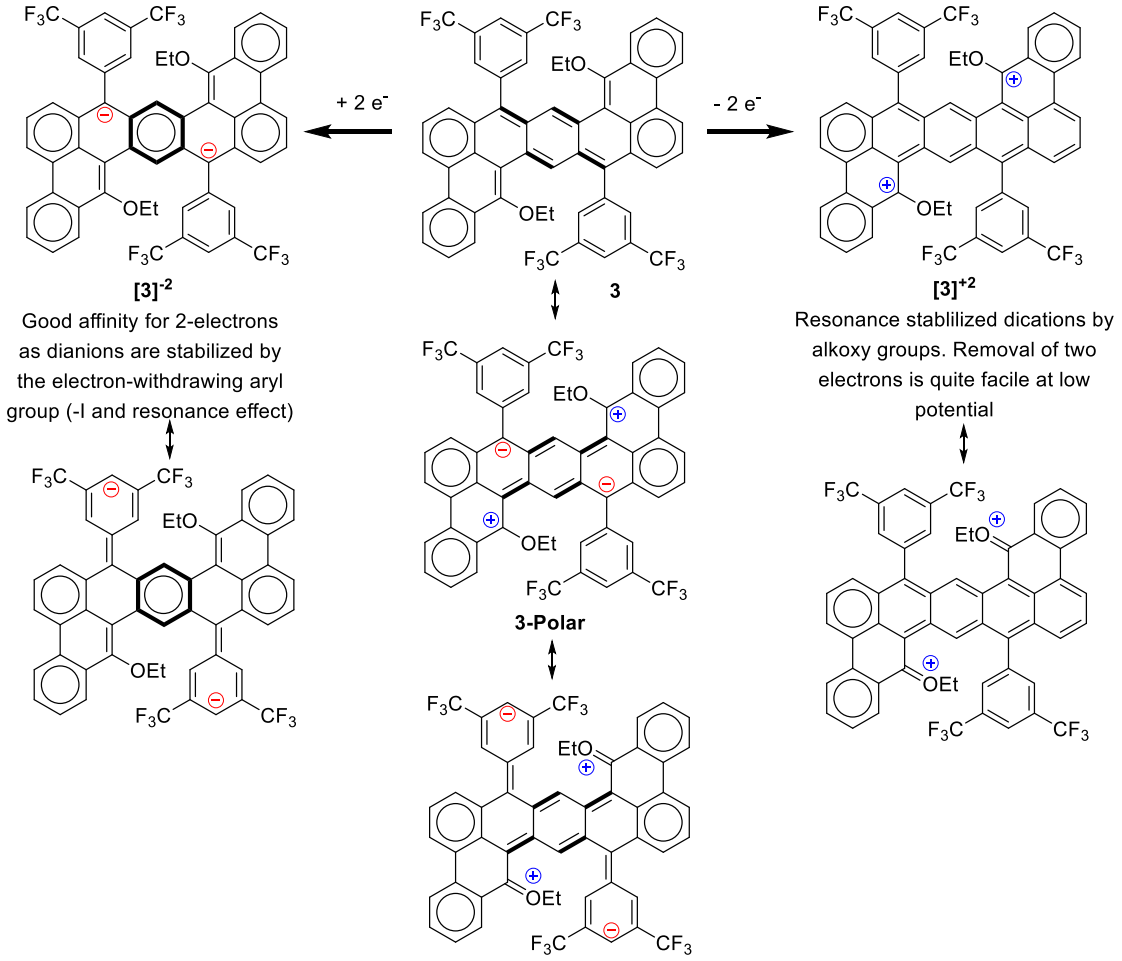

Figure 2.11 Plausible species after the first oxidation and reduction processes involving two-electrons for **3**, and the zwitterionic **3-Polar** resonance form in singlet ground state.

2.3 Conclusions

In conclusion, a 2,3:10,11-DBHZ derivative **3** was synthesized in quinoidal singlet ground state with strong polyene character. It showed blue-shifted UV-vis absorption in polar solvents, in comparison to toluene, suggesting dipolar structural contribution in the ground state with moderate ICT interaction. A very low oxidation potential and a

small electrochemical energy gap were found for **3**, which are the smallest values among the entire zethrene family, to date,[9,24] including the *p*-QDM bridged corannulene dimer bearing the 2,3:10,11-DBHZ fragment with methoxy substituent at same position.[24c] The negative solvatochromism and facile electrochemical oxidations of quinoidal **3** could be attributed to a readily accessible low-lying zwitterionic form **3-Polar** in the singlet ground state due to potentially polarizing substituents. Our work clearly indicates that substitution can play important role in tuning the ground state properties of pro-aromatic PHs, and may stimulate the exploration of donor/acceptor substituted π-conjugated diradicaloid PHs.[10,25]

2.4 Experimental section

2.4.1 General information: Chemicals and reagents were purchased from local and international commercial suppliers (Merck, GLR innovations, BLDpharm, Sainor lab) and used without further purification. Thin layer chromatography (TLC) was performed using pre-coated silica-plates purchased from Merck (silica gel 60 PF254, 0.25 mm). Column chromatography was performed using silica gel 100-200 mesh. NMR spectra were recorded in $CDCl_3$, DMSO-D_6, and C_6D_6 (Eurisotop) at room temperature, on JEOL JNM-ECS400 spectrometer at operating frequencies of 400 MHz (^{1}H) or 100 MHz (^{13}C) as indicated in the individual spectrum. Chemical shifts (δ) are given in ppm relative to residual solvent (chloroform δ = 7.26, dimethylsulfoxide δ = 2.50, and benzene δ = 7.16 for ^{1}H, and benzene δ = 128.06, chloroform δ = 77.16 for proton-decoupled ^{13}C NMR) and coupling constants (*J*) are expressed in Hz. Multiplicity is tabulated as s for singlet, d for doublet, dd for doublet of doublet, t for triplet, q for quartet and m for multiplet. Structural assignments were made with additional information from gCOSY, and gNOESY experiments. High resolution mass spectra (HRMS) were recorded using electron spray ionization (ESI) methods on Waters (XEVO G2-XS QTOF) mass spectrometer. UV-vis spectra were recorded in JASCO V-770 spectrophotometer. Fluorescence spectra were recorded on PerkinElmer LS55 fluorescence spectrophotometer. Cyclic voltammetry was performed on CHI-1110C instrument with a glassy carbon working electrode, Pt wire counter electrode, and Ag wire as pseudo-reference electrode in DCM/Bu_4NPF_6 solvent/electrolyte couple at room temperature using 50 mV s^{-1} scan rate. The potential was externally calibrated against the ferrocene/ferrocenium couple (0.43 V). Melting points were determined using BIBBY-SMP30 melting point analyzer.

2.4.2 Syntheses

9-ethoxyphenanthrene (6): To a suspension of **5** (1.2 g, 6.18 mmol), K_2CO_3 (1.28 g, 9.27 mmol) and KI (1.18 g, 7.10 mmol) in acetone was added ethyl bromide (0.80 mL, 10.50 mmol) and the mixture was heated at reflux for 12 h using an oil bath, under nitrogen atmosphere. After cooling down to room temperature, the volatiles were evaporated and the mixture was extracted with CH_2Cl_2 (50 mL x 4) and water (50 mL). The organic layer was dried over anhydrous sodium sulphate, and filtered. The filtrate was evaporated, and the residue was purified on a silica column using hexanes as eluent to give the title product as white solid (1.21 g, 88% yield): R_f = 0.30 (hexanes); mp 95–96 °C; ^{1}H NMR (400 MHz, $CDCl_3$) δ 8.66 (d, *J* = 8.1 Hz, 1H), 8.59 (d, *J* = 7.8 Hz, 1H), 8.42 (dd, *J* = 8.1, 1.3 Hz, 1H), 7.76 (dd, *J* = 7.5, 1.4 Hz, 1H), 7.71 – 7.61 (m, 2H), 7.57 – 7.47 (m, 2H), 6.97 (s, 1H), 4.31 (q, *J* = 7.0 Hz, 2H), 1.61 (t, *J* = 6.9 Hz, 3H); ^{13}C{^{1}H} NMR (100 MHz, $CDCl_3$) δ 152.9, 133.1, 131.3, 127.3, 127.1, 126.9, 126.8, 126.4 (2 C), 124.2, 122.7, 122.6, 102.6, 63.7, 14.9; NMR data are consistent with the literature report.[26] HRMS (ESI) *m/z*: $[M + H]^+$ Calcd for $C_{16}H_{15}O$ 223.1123, found 223.1112.

9-bromo-10-ethoxyphenanthrene (7): It is prepared by slightly modifying the literature procedure.[27] An oven-dried two-necked round bottom flask, equipped with a magnetic stir-bar, was charged with **6** (1.10 g, 4.95 mmol) dissolved in 20 mL of anhydrous acetonitrile. NBS (969 mg, 5.44 mmol) was added at 0 °C in one shot and the reaction mixture was warmed to room temperature and stirred well for 3 h. Reaction mixture was quenched with saturated solution of sodium thiosulphate, and the solvents were removed using a rotatory evaporator. The resulting mixture was then extracted with dichloromethane (50 mL x 3), dried over sodium sulphate, and filtered. The organic layer was evaporated, and the crude residue was purified by silica gel column chromatography (hexanes) to give the title product **7** as yellow solid (1.05 g, 70% yield): R_f = 0.36 (5% EtOAc in hexanes); mp 60–61 °C; ^{1}H NMR (400 MHz, $CDCl_3$) δ 8.70 – 8.64 (m, 2H), 8.40 (dd, *J* = 8.0, 1.5 Hz, 1H), 8.24 (dd, *J* = 8.1, 1.4 Hz, 1H), 7.74 – 7.62 (m, 4H), 4.24 (q, *J* = 7.0 Hz, 2H), 1.63 (t, *J* = 7.1 Hz, 3H); ^{13}C{^{1}H} NMR (100 MHz, $CDCl_3$) δ 151.4, 131.1, 131.0, 129.0, 128.6, 127.9, 127.8, 127.5, 127.3, 126.5, 123.2, 123.1, 122.7, 114.2, 69.9, 15.8; HRMS (ESI) *m/z*: $[M + H]^+$ Calcd for $C_{16}H_{14}BrO$ 301.0228, found 301.0239. The characterization data agree with the literature values.[27]

2-(10-ethoxyphenanthren-9-yl)-4,4,5,5-tetramethyl-1,3,2-dioxaborolane (9): A solution of *n*-butyllithium (1.7 mL, 2.66 mmol, 1.6 M in hexanes) was added dropwise into a solution of **7** (400 mg, 1.33 mmol) in 20 mL of anhydrous THF under nitrogen at −78 °C. It was stirred at -78 °C for 2 h, and then 2-isopropoxy-4,4,5,5-tetramethyl-1,3,2-dioxaborolane **8** (0.54 mL, 2.66 mmol) was added. The reaction mixture was stirred for 12 h at room temperature. The solution was quenched with saturated solution of NH_4Cl, and extracted with dichloromethane (100 mL x 5 times). The organic phases were washed with water (100 mL x 2) and brine (100 mL x 2), and dried over Na_2SO_4. After evaporation of the organic layer, the residue was purified by silica gel column chromatography (EtOAc:hexanes, 1:10) to afford **9** as yellow solid (364 mg, 78 % yield): R_f = 0.27 (5% EtOAc in hexanes); mp 112–113 °C; ^{1}H NMR (400 MHz, $CDCl_3$) δ 8.67 (d, *J* = 8.2 Hz, 1H), 8.65 – 8.60 (m, 1H), 8.20 (dd, *J* = 7.8, 1.4 Hz, 1H), 8.11 – 8.05 (m, 1H), 7.67 (ddd, *J* = 8.3, 7.0, 1.4 Hz, 1H), 7.61 (ddd, *J* = 7.9, 7.0, 1.1 Hz, 1H), 7.58 – 7.53 (m, 2H), 4.19 (q, *J* = 7.0 Hz, 2H), 1.56 (t, *J* = 7.1 Hz, 3H), 1.52 (s, 12H); ^{13}C{^{1}H} NMR (100 MHz, $CDCl_3$) δ 158.9, 134.8, 132.9, 128.1, 127.5, 127.5, 126.9, 126.5, 125.3, 123.2, 123.0, 122.8, 84.2, 71.6, 25.2, 15.8; HRMS (ESI) *m/z*: $[M + H]^+$ Calcd for $C_{22}H_{26}BO_3$ 349.1975, found 349.1979.

2,5-bis(10-ethoxyphenanthren-9-yl)terephthalaldehyde (11): An oven dried thick-walled glass tube was charged with **9** (358 mg, 1.03 mmol), 2,5-dibromoterephthalaldehyde (100 mg, 0.34 mmol), anhydrous K_2CO_3 (237 mg, 1.71 mmol), dry toluene and purged with nitrogen for 30 minutes. Catalyst $Pd(PPh_3)_4$ (33.6 mg, 10 mol%) was subsequently added under nitrogen, and the glass tube was sealed before being warmed to 110 °C using an oil bath. After 12 h, the flask was first cooled to room temp and the resulting suspension was filtered and the solid was washed successively with water (100 mL), MeOH (100 mL) and pentane (100 mL). The solid was dried to afford title product **11** (96 mg, 48%) as a light brown powder: R_f = 0.31 (10 % EtOAc in hexanes); mp 314–315 °C; ^{1}H NMR (400 MHz, DMSO-d_6) δ 9.86 (s, 2H), 9.01 (t, *J* = 9.0 Hz, 4H), 8.28 (dd, *J* = 8.0, 1.2 Hz, 2H), 8.18 (s, 2H), 7.89 – 7.79 (m, 4H), 7.77 – 7.65 (m, 6H), 3.86 (m, 2H), 3.66 (m, 2H), 1.14 (t, *J* = 7.0 Hz, 6H); HRMS (ESI) *m/z*: $[M + H]^+$ Calcd for $C_{40}H_{31}O_4$ 575.2222, found 575.2225. Poor solubility didn't allow us to record the ^{13}C NMR.

8,18-bis(3,5-bis(trifluoromethyl)phenyl)-10,20-diethoxy-8,18-dihydrobenzo[fg]naphtho[3,2,1-mn]hexaphene (14): 3,5-

Bis(trifluoromethyl)phenylmagnesium bromide **12** (0.5 M in THF, 3.13 mL, 1.57 mmol) was added to the dry THF (5 mL) solution of **11** (90 mg, 0.16 mmol) under nitrogen. The mixture was stirred at room temperature for 24 h and quenched with saturated aq. NH_4Cl solution (15 mL). The volatile organics were evaporated, and the mixture was extracted with DCM (3 x 15 mL). The organic layer was dried over anhydrous Na_2SO_4, filtered, and removed under reduced pressure to afford crude mixture containing intermediate compound **13** (437 mg). To the solution of crude **13** in anhydrous DCM (10 mL), $BF_3{\cdot}Et_2O$ (0.1 mL) was added dropwise under nitrogen and the reaction mixture was stirred for 10 h at room temperature. Once **13** was completely consumed, as monitored by TLC, saturated aqueous $NaHCO_3$ solution (20 mL) was added and the reaction mixture was extracted with DCM (3 x 10 mL). The organic layer was dried over anhydrous Na_2SO_4, filtered, and evaporated under reduced pressure. The residue was subjected to silica gel column chromatography (EtOAc:hexanes, 1:10) to give title product **14** as light brown solid (54 mg, 36% over two steps): R_f = 0.37 (5% EtOAc in hexanes); mp 319–320 °C; ^{1}H NMR (400 MHz, $CDCl_3$) δ 8.94 (s, 2H), 8.62 (dd, *J* = 6.4, 3.1 Hz, 2H), 8.56 (d, *J* = 7.9 Hz, 2H), 8.44 (dd, *J* = 6.6, 3.0 Hz, 2H), 7.71 – 7.65 (m, 6H), 7.64 – 7.58 (m, 6H), 7.50 (s, 2H), 5.79 (s, 2H), 4.40 (m, 2H), 4.09 (m, 2H), 1.57 (m, 6H, merged with residual water signal); HRMS (ESI) *m/z*: $[M + H]^+$ Calcd for $C_{56}H_{35}F_{12}O_2$ 967.2445, found 967.2440. Poor solubility didn't allow us to record the ^{13}C NMR.

8,18-bis(3,5-bis(trifluoromethyl)phenyl)-10,20-diethoxybenzo[fg]naphtho[3,2,1-mn]hexaphene (3): *p*-Chloranil (23 mg, 0.09 mmol, 2.1 equiv) was added to **14** (30 mg, 0.03 mmol) in dry chloroform (4 mL) under N_2, and the reaction mixture was warmed to 70 °C for 6 h in an oil bath. Once the starting material was consumed (monitored by TLC), the solvent was removed in vacuo and the crude was purified by silica gel column chromatography (hexanes:EtOAc, 99:1) to afford the product **3** as blue-green solid (15 mg, 65%): R_f = 0.33 (20% EtOAc in hexanes). Recrystallization of **3** from chloroform:toluene (1:1) mixture at ambient temperature in dark afforded single crystals suitable for X-ray crystallographic analysis: mp 245 °C (decomposed); ^{1}H NMR (400 MHz, C_6D_6) δ 8.94 (s, 2H), 8.33 – 8.29 (m, 2H), 8.23 – 8.17 (m, 4H), 7.97 (s, 2H), 7.78 (s, 4H), 7.45 – 7.30 (m, 4H), 7.09 (t, *J* = 7.8 Hz, 2H), 6.77 (d, *J* = 7.8 Hz, 2H), 3.71 (q, *J* = 7.1 Hz, 4H), 0.93 (t, *J* = 7.1 Hz, 6H); ^{13}C{^{1}H} NMR (100 MHz, C_6D_6) δ 168.8, 154.6, 141.9, 140.1, 133.9, 133.3, 132.9, 132.6, 132.3, 132.1, 131.6, 130.8, 129.6, 127.0, 126.4, 125.8, 125.3, 124.2, 123.3, 122.7, 122.6, 121.9,

119.6, 67.8, 15.7; HRMS (ESI) *m/z*: $[M]^+$ Calcd for $C_{56}H_{32}F_{12}O_2$ 964.2211, found 964.2220.

2.4.3 X-ray crystallographic analysis

A suitable single crystal of **3** was selected using paratone oil and mounted on glass fiber with the help of gum. The intensity data and geometric parameters of these crystals were garnered with the help of Bruker D8 Venture X-ray diffractometer having a micro-focus sealed X-ray tube Mo-Kα (λ = 0.71073 Å) source of X-rays along with a PHOTON 100 detector with inclining Phi and Omega (width of 0.5 for one frame) working at a scan speed of 10 s per frame. The crystal was kept at 298 K during data collection. Data acquisition as well as extraction of data was accomplished by utilizing Bruker Apex-3 and Bruker SAINT software packages using a narrow - frame algorithm.[28] By utilizing OLex2,[29] the crystal structure was solved with the help of olex2.solve[30] structure solution program by employing intrinsic Phasing methods and crystal structure refinement was done with the SHELXL[31] refinement package by putting into use Least Squares minimization. Refinement of all non-hydrogen atoms was completed with the help of anisotropic thermal parameters.

Table 2.4 Crystal data and structure refinement for **3**.

CCDC number	2141677
Empirical formula	$C_{56}H_{32}F_{12}O_2$
Formula weight	964.81
Temperature/K	298.00
Crystal system	monoclinic
Space group	C2/c
a/Å	14.736(3)
b/Å	19.866(5)
c/Å	18.418(5)
α/°	90
β/°	111.894(8)
γ/°	90
Volume/Å^3	5003(2)
Z	4
ρ_{calc}g/cm^3	1.281
μ/mm^{-1}	0.108
F(000)	1968.0
Crystal size/mm^3	0.569 × 0.189 × 0.109
Radiation	MoKα (λ = 0.71073)
2Θ range for data collection/°	3.616 to 50.148

Index ranges	$-17 \leq h \leq 17, -22 \leq k \leq 23, -21 \leq l \leq 19$
Reflections collected	22089
Independent reflections	4344 [R_{int} = 0.0962, R_{sigma} = 0.0838]
Data/restraints/parameters	4344/0/318
Goodness-of-fit on F^2	1.000
Final R indexes [I>=2σ (I)]	R_1 = 0.0789, wR_2 = 0.2133
Final R indexes [all data]	R_1 = 0.1309, wR_2 = 0.2475
Largest diff. peak/hole / e $Å^{-3}$	0.41/-0.31

2.4.4 DFT calculations

DFT calculations were performed with Gaussian 09 package using a high-performance computing cluster facility of IIT Ropar in gas phase using the B3LYP level of theory with basis set 6-31G(d,p).[11] Optimization of the molecular geometries for **2** and **3**, taken from X-ray crystallographic data, were done by restricted B3LYP and unrestricted B3LYP wave-functions using broke symmetry formalism.[32] Calculation of NOON (natural orbital occupation number) value was based on the broken symmetry UB3LYP method. The calculated NOON values for HOMO and LUMO levels were used to estimate the diradical character index (y_0) using Yamaguchi equation.[33] The y_0 is formally expressed as $y_0 = 1 - (2T/(1 + T^2))$, where T represents the HOMO/LUMO occupancies as: $T = (n\text{HOMO} - n\text{LUMO})/2$. The optimized molecular geometries for **2** and **3** were used for estimating their diradical characters by the CASSCF(2,2)/6-31G approach, which is based on the LUMO occupation numbers.[34] Natural bond orbital (NBO) calculations were performed at the same theory level. $NICS(1)_{zz}$ indices were estimated using the standard GIAO procedure. Excitation energy was computed using time dependent density functional theory (TDDFT) for the closed-shell optimized structure of **3**, using solvation (PCM) model. Molecular orbital contributions were determined using GaussSum 3.0 package.[35]

Table 2.5 Relative energies of optimized geometries of **3** and **2**.

Compounds	Optimization	Hartree	kcal/mol
3	Singlet closed-shell B3LYP/6-31G(d,p)	−3501.92096	−2197455.402
	Singlet open-shell UB3LYP/6-31G(d,p)	−3501.92096	−2197455.402
	Triplet open-shell UB3LYP/6-31G(d,p)	−3501.900982	−2197442.866
2	Singlet closed-shell B3LYP/6-31G(d,p)	−2904.06777	−1822302.531
	Singlet open-shell UB3LYP/6-31G(d,p)	−2904.06777	−1822302.531
	Triplet open-shell	−2904.05231	−1822292.825

UB3LYP/6-31G(d,p)

Compound 3: $\Delta E_{\text{Triplet-Singlet}}$ = 12.5 kcal/mol. Occupation numbers are found for HOMO (246) = 2.0 and LUMO (247) = 0, for the open-shell singlet state, affording *zero* diradical character (y_0 = 0) for **3**. CASSCF calculation also estimated zero singlet diradical character for **3**, based on the occupancy of LUMO (247) = 0.

Compound 2: $\Delta E_{\text{Triplet-Singlet}}$ = 9.7 kcal/mol. Occupation numbers are found for HOMO (226) = 1.99966 and LUMO (227) = 0.00034, for the singlet open-shell structure, affording negligible diradical character (y_0 = 5.78197 x 10^{-8}) for **2**. However, CASSCF calculation estimated 15.3% singlet diradical character for **2**, based on the occupancy of LUMO[34] [LUMO (227) = 0.15303 and HOMO (226) = 1.84697].

2.5 References

1. Zeng, W.; Sun, Z.; Herng, T. S.; Gonçalves, T. P.; Gopalakrishna, T. Y.; Huang, K.-W.; Ding, J.; Wu, J. Super-heptazethrene. *Angew. Chem., Int. Ed.* **2016**, *55*, 8615–8619.

2. Sun, Z.; Huang, K.-W.; Wu, J. Soluble and stable heptazethrenebis(dicarboximide) with a singlet open-shell ground state. *J. Am. Chem. Soc.* **2011**, *133*, 11896–11899.

3. Das, S.; Lee, S.; Son, M.; Zhu, X.; Zhang, W.; Zheng, B.; Hu, P.; Zeng, Z.; Sun, Z.; Zeng, W.; Li, R.-W.; Huang, K.-W.; Ding, J.; Kim, D.; Wu, J. Para-quinodimethane-bridged perylene dimers and pericondensed quaterrylenes: The effect of the fusion mode on the ground states and physical properties. *Chem. – Eur. J.* **2014**, *20*, 11410–11420.

4. (a) Li, Y.; Heng, W.-K.; Lee, B. S.; Aratani, N.; Zafra, J. L.; Bao, N.; Lee, R.; Sung, Y. M.; Sun, Z.; Huang, K.-W.; Webster, R. D.; López Navarrete, J. T.; Kim, D.; Osuka, A.; Casado, J.; Ding, J.; Wu, J. Kinetically blocked stable heptazethrene and octazethrene: Closed-shell or open-shell in the ground state?. *J. Am. Chem. Soc*. **2012**, *134*, 14913–14922. (b) Hu, P.; Lee, S.; Herng, T. S.; Aratani, N.; Gonçalves, T. P.; Qi, Q.; Shi, X.; Yamada, H.; Huang, K.-W.; Ding, J.; Kim, D.; Wu, J. Toward tetraradicaloid: The effect of fusion mode on radical character and chemical reactivity. *J. Am. Chem. Soc*. **2016**, *138*, 1065–1077.

5. (a) Sun, Z.; Lee, S.; Park, K. H.; Zhu, X.; Zhang, W.; Zheng, B.; Hu, P.; Zeng, Z.; Das, S.; Li, Y.; Chi, C.; Li, R.-W.; Huang, K.-W.; Ding, J.; Kim, D.; Wu, J. Dibenzoheptazethrene isomers with different biradical characters: An exercise of

Clar's aromatic sextet rule in singlet biradicaloids. *J. Am. Chem. Soc.* **2013**, *135*, 18229–18236. (b) Zong, C.; Zhu, X.; Xu, Z.; Zhang, L.; Xu, J.; Guo, J.; Xiang, Q.; Zeng, Z.; Hu, W.; Wu, J.; Li, R.; Sun, Z. Isomeric Dibenzoheptazethrenes for air-stable organic field-effect transistors. *Angew. Chem., Int. Ed.* **2021**, *60*, 16230–16236.

6. Yang, W.; Monteiro, J. H.; de Bettencourt-Dias, A.; Catalano, V. J.; Chalifoux, W. A. Synthesis, structure, photophysical properties, and photostability of Benzodipyrenes. *Chem. – Eur. J.* **2018**, *25*, 1441–1445.

7. Clar, E.; Fell, G. S.; Richmond, M. H. 4,5:12,13-dibenzoheptazethrene and 5,6:8,9:14,15:17,18-tetrabenzoheptacene. *Tetrahedron* **1960**, *9*, 96–105.

8. Zeng, Z.; Shi, X.; Chi, C.; López Navarrete, J. T.; Casado, J.; Wu, J. Pro-aromatic and anti-aromatic π-conjugated molecules: An irresistible wish to be diradicals. *Chem. Soc. Rev.* **2015**, *44*, 6578–6596.

9. (a) Sun, Z.; Zeng, Z.; Wu, J. Zethrenes, extended p-quinodimethanes, and periacenes with a singlet biradical ground state. *Acc. Chem. Res.* **2014**, *47*, 2582–2591. (b) Hu, P.; Wu, J. Modern Zethrene Chemistry. *Can. J. Chem.* **2017**, *95*, 223–233.

10. Hibi, D.; Kitabayashi, K.; Shimizu, A.; Umeda, R.; Tobe, Y. Synthesis and physical properties of zethrene derivatives bearing donor/acceptor substituents at 7,14-positions. *Org. Biomol. Chem.* **2013**, *11*, 8256–8261.

11. Gaussian 09, Revision B.01, Frisch, M. J.; Trucks, G. W.; Schlegel, H. B.; Scuseria, G. E.; Robb, M. A.; Cheeseman, J. R.; Scalmani, G.; Barone, V.; Mennucci, B.; Petersson, G. A.; Nakatsuji, H.; Caricato, M.; Li, X.; Hratchian, H. P.; Izmaylov, A. F.; Bloino, J.; Zheng, G.; Sonnenberg, J. L.; Hada, M.; Ehara, M.; Toyota, K.; Fukuda, R.; Hasegawa, J.; Ishida, M.; Nakajima, T.; Honda, Y.; Kitao, O.; Nakai, H.; Vreven, T.; Montgomery, J. A.; Jr., Peralta, J. E.; Ogliaro, F.; Bearpark, M.; Heyd, J. J.; Brothers, E.; Kudin, K. N.; Staroverov, V. N.; Keith, T.; Kobayashi, R.; Normand, J.; Raghavachari, K.; Rendell, A.; Burant, J. C.; Iyengar, S. S.; Tomasi, J.; Cossi, M.; Rega, N.; Millam, J. M.; Klene, M.; Knox, J. E.; Cross, J. B.; Bakken, V.; Adamo, C.; Jaramillo, J.; Gomperts, R.; Stratmann, R. E.; Yazyev, O.; Austin, A. J.; Cammi, R.; Pomelli, C.; Ochterski, J. W.; Martin, R. L.; Morokuma, K.; Zakrzewski, V. G.; Voth, G. A.; Salvador, P.; Dannenberg, J. J.; Dapprich, S.; Daniels, A. D.; Farkas, O.; Foresman, J. B.; Ortiz, J. V.; Cioslowski, J; Fox, D. J. Gaussian, Inc., Wallingford CT, **2010**.

12. Jin, M.; Ren, W.; Qian, D.-W.; Yang, S.-D. Direct allylic C(sp^3)-H alkylation with 2-naphthols via Cooperative Palladium and copper catalysis: Construction of Cyclohexadienones with Quaternary Carbon Centers. *Org. Lett.* **2018**, *20*, 7015–7019.

13. (a) Shimizu, A.; Kubo, T.; Uruichi, M.; Yakushi, K.; Nakano, M.; Shiomi, D.; Sato, K.; Takui, T.; Hirao, Y.; Matsumoto, K.; Kurata, H.; Morita, Y.; Nakasuji, K. Alternating covalent bonding interactions in a one-dimensional chain of a phenalenyl-based singlet Biradical molecule having Kekulé structures. *J. Am. Chem. Soc.* **2010**, *132*, 14421–14428. (b) Shimizu, A.; Hirao, Y.; Matsumoto, K.; Kurata, H.; Kubo, T.; Uruichi, M.; Yakushi, K. Aromaticity and π-bond covalency: Prominent intermolecular covalent bonding interaction of a kekulé hydrocarbon with very significant singlet biradical character. *Chem. Commun.* **2012**, *48*, 5629–5631.

14. Yadav, P.; Das, S.; Phan, H.; Herng, T. S.; Ding, J.; Wu, J. Kinetically blocked stable 5,6:12,13-dibenzozethrene: A laterally π-extended zethrene with enhanced diradical character. *Org. Lett.* **2016**, *18*, 2886–2889.

15. Desiraju, G. R. A Bond by Any Other Name. *Angew. Chem. Int. Ed.* **2011**, *50*, 52–59.

16. Montgomery, L. K.; Huffman, J. C.; Jurczak, E. A.; Grendze, M. P. The molecular structures of Thiele's and Chichibabin's hydrocarbons. *J. Am. Chem. Soc.* **1986**, *108*, 6004–6011.

17. Kruszewski, J.; Krygowski, T. M. Definition of aromaticity basing on the harmonic oscillator model. *Tetrahedron Lett.* **1972**, *13*, 3839–3842.

18. (a) Dobrowolski, J. C.; Lipinski, P. F. J. On Splitting of the NICS(1) Magnetic Aromaticity Index *RSC Adv.* **2016**, 6, 23900–23904. (b) Antić, M.; Furtula, B.; Radenković, S. Aromaticity of Nonplanar Fully Benzenoid Hydrocarbons. *J. Phys. Chem. A* **2017**, 121, 3616–3626.

19. (a) Kim, J. J.; Funabiki, K.; Muramatsu, H.; Shibata, K.; Matsui, M.; Kim, S. H.; Shiozaki, H.; Hartmann, H. Negative solvatochromism of azo dyes derived from (dialkylamino)thiazole dimers. *Chem. Commun.* **2000**, 753–754. (b) Zeng, W.; Wu, J. Push–pull type Quinoidal Perylene Showing Solvent Polarity Dependent Diradical Character and Negative Solvatochromism. *Mater. Chem. Front.* **2019**, 2668–2672.

20. Charge analysis was performed for the singlet closed-shell optimized structure of **3** using the natural population analysis (NPA) as implemented in G09.

21. Xu, T.; Han, Y.; Shen, Z.; Hou, X.; Jiang, Q.; Zeng, W.; Ng, P. W.; Chi, C. Antiaromatic Dicyclopenta[*b,g*]/[*a,f*]naphthalene isomers showing an open-shell singlet ground state with tunable diradical character. *J. Am. Chem. Soc*. **2021**, *143*, 20562–20568.

22. Taniguchi, M.; Lindsey. J. S. Database of Absorption and Fluorescence Spectra of >300 Common Compounds for use in PhotochemCAD. *Photochem. Photobiol.* **2018**, *94*, 290– 327

23. Bredas, J-. L. Mind the gap! *Mater. Horiz.*, **2014**, *1*, 17–19.

24. (a) Huang, R.; Phan, H.; Herng, T. S.; Hu, P.; Zeng, W.; Dong, S.-qiang; Das, S.; Shen, Y.; Ding, J.; Casanova, D.; Wu, J. Higher order π-conjugated polycyclic hydrocarbons with open-shell singlet ground state: Nonazethrene versus nonacene. *J. Am. Chem. Soc.* **2016**, *138*, 10323–10330. (b) Zeng, W.; Gopalakrishna, T. Y.; Phan, H.; Tanaka, T.; Herng, T. S.; Ding, J.; Osuka, A.; Wu, J. Superoctazethrene: An open-shell graphene-like molecule possessing large diradical character but still with reasonable stability. *J. Am. Chem. Soc*. **2018**, *140*, 14054–14058. (c) Wang, Q.; Hu, P.; Tanaka, T.; Gopalakrishna, T. Y.; Herng, T. S.; Phan, H.; Zeng, W.; Ding, J.; Osuka, A.; Chi, C.; Siegel, J.; Wu, J. Curved π-conjugated corannulene dimer diradicaloids. *Chem. Sci.* **2018**, *9*, 5100–5105.

25. Nakano, M.; Minami, T.; Yoneda, K.; Muhammad, S.; Kishi, R.; Shigeta, Y.; Kubo, T.; Rougier, L.; Champagne, B.; Kamada, K.; Ohta, K. Giant Enhancement of the Second Hyperpolarizabilities of Open-Shell Singlet Polyaromatic Diphenalenyl Diradicaloids by an External Electric Field and Donor–Acceptor Substitution. *J. Phys. Chem. Lett.* **2011**, *2*, 1094–1098.

26. Dreher, S. D.; Paruch, K.; Katz, T. J. Acidified Alcohols as Agents to Introduce and Exchange Alkoxyls on the Periphery of Helicenes. *J. Org. Chem.* **2000**, *65*, 806–814.

27. Mohammad-Pour, G. S.; Ly, R. T.; Fairchild, D. C.; Burnstine-Townley, A.; Vazquez-Molina, D. A.; Trieu, K. D.; Campiglia, A. D.; Harper, J. K.; Uribe-Romo, F. J. Modular design of fluorescent dibenzo- and Naphtho-Fluoranthenes: Structural rearrangements and electronic properties. *J. Org. Chem.* **2018**, *83*, 8036–8053.

28. Bruker, SAINT V8.38A, (Bruker AXS Inc., 2017).

29. Dolomanov, O. V.; Bourhis, L. J.; Gildea, R. J.; Howard, J. A.; Puschmann, H. Olex2: A complete structure solution, refinement and Analysis Program. *J. Appl. Crystallogr.* **2009**, *42*, 339–341.

30. Bourhis, L. J.; Dolomanov, O. V.; Gildea, R. J.; Howard, J. A.; Puschmann, H. The anatomy of a comprehensive constrained, restrained refinement program for the modern computing environment –olex2dissected. *Acta Crystallogr. A.* **2015**, *71*, 59–75.

31. Sheldrick, G. M. Crystal structure refinement with SHELXL. *Acta Crystallogr. C Struct. Chem.* **2015**, *71*, 3–8.

32. (a) Kubo, T. Recent Progress in Quinoidal Singlet Biradical Molecules. *Chem. Lett.* **2015**, *44*, 111–122. (b) Das, S.; Wu, J. Open-shell benzenoid polycyclic hydrocarbons, in: *Polycyclic arenes and heteroarenes: synthesis, properties, and applications*. Qian M, editor. John Wiley & Sons Inc., 2015, 3–36.

33. Yamaguchi, K. The electronic structures of biradicals in the unrestricted Hartree-Fock approximation. *Chem. Phys. Lett.* **1975**, *33*, 330–335.

34. (a) Konishi, A.; Hirao, Y.; Nakano, M.; Shimizu, A.; Botek, E.; Champagne, B.; Shiomi, D.; Sato, K.; Takui, T.; Matsumoto, K.; Kurata, H.; Kubo, T. Synthesis and Characterization of Teranthene: A Singlet Biradical Polycyclic Aromatic Hydrocarbon Having Kekulé Structures. *J. Am. Chem. Soc.* **2010**, *132*, 11021–11023. (b) Döhnert, D.; Koutecký, J. Occupation numbers of natural orbitals as a criterion for biradical character. Different kinds of biradicals. *J. Am. Chem. Soc.* **1980**, *102*, 1789–1796

35. O'Boyle, N. M.; Tenderholt, A. L.; Langner, K. M. cclib: A library for package-independent computational chemistry algorithms. *J. Comp. Chem.* **2008**, *29*, 839–845.

2.6 Appendix

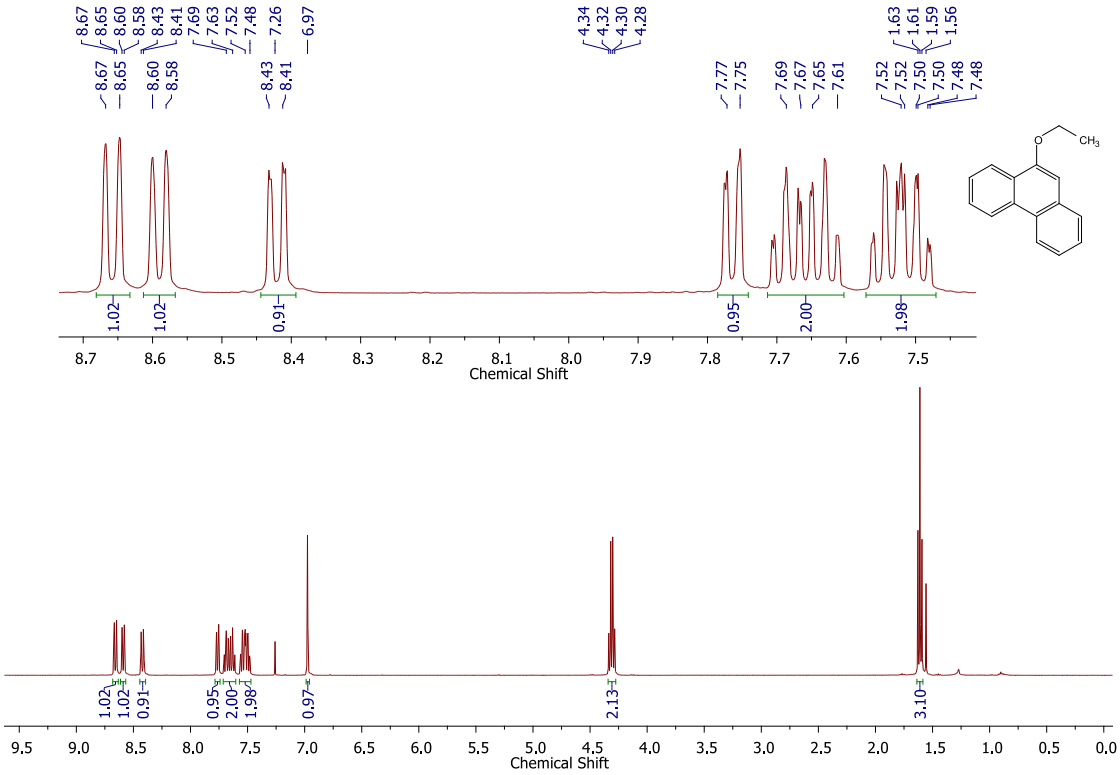

Figure 2.12 ^{1}H NMR spectrum of **6** (in $CDCl_3$, 400 MHz).

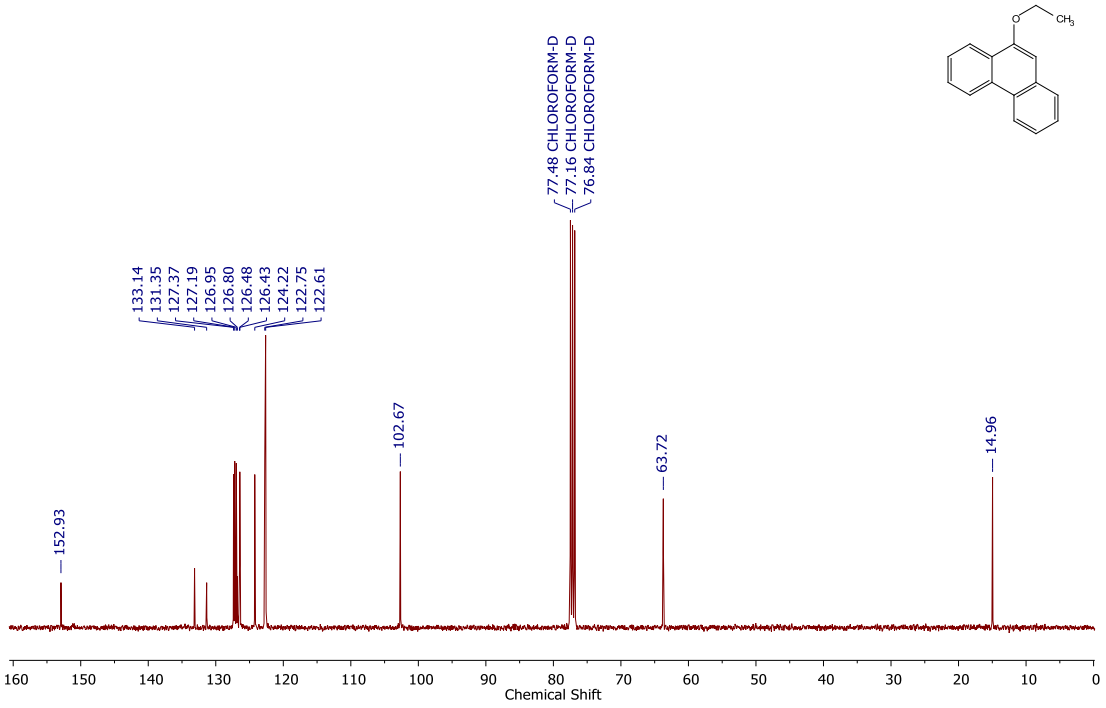

Figure 2.13 $^{13}C\{^{1}H\}$ NMR spectrum of **6** (in $CDCl_3$, 100 MHz).

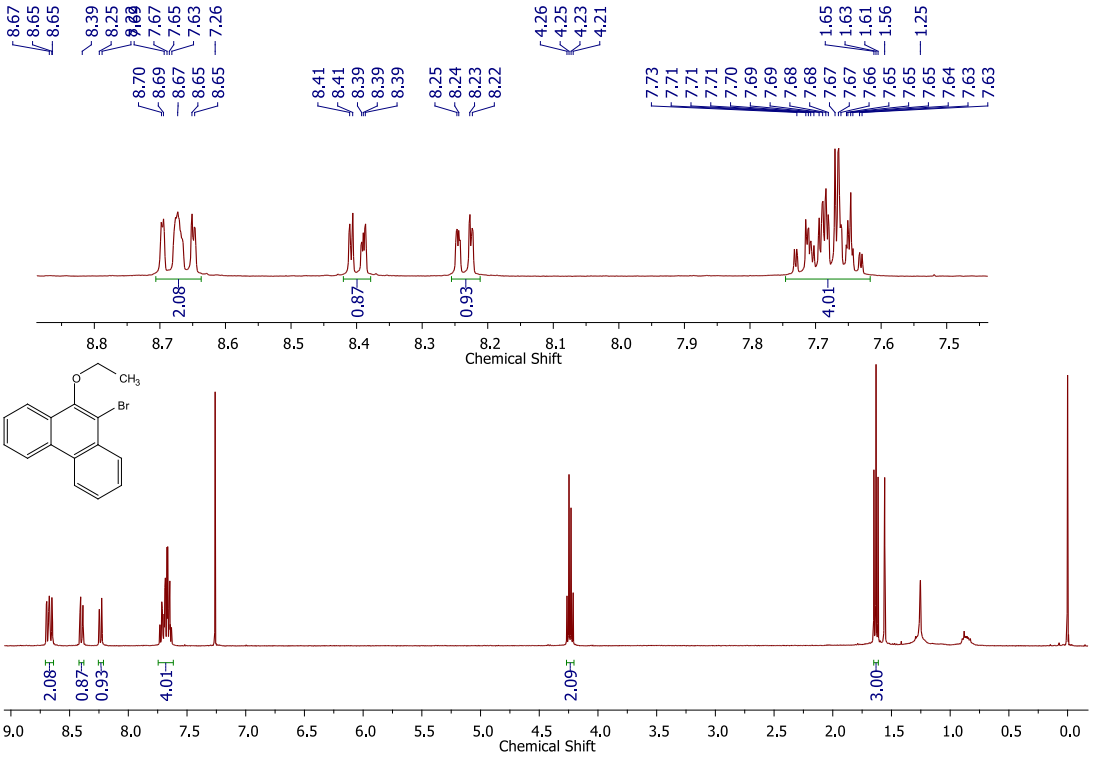

Figure 2.14 ^{1}H NMR spectrum of **7** (in $CDCl_3$, 400 MHz).

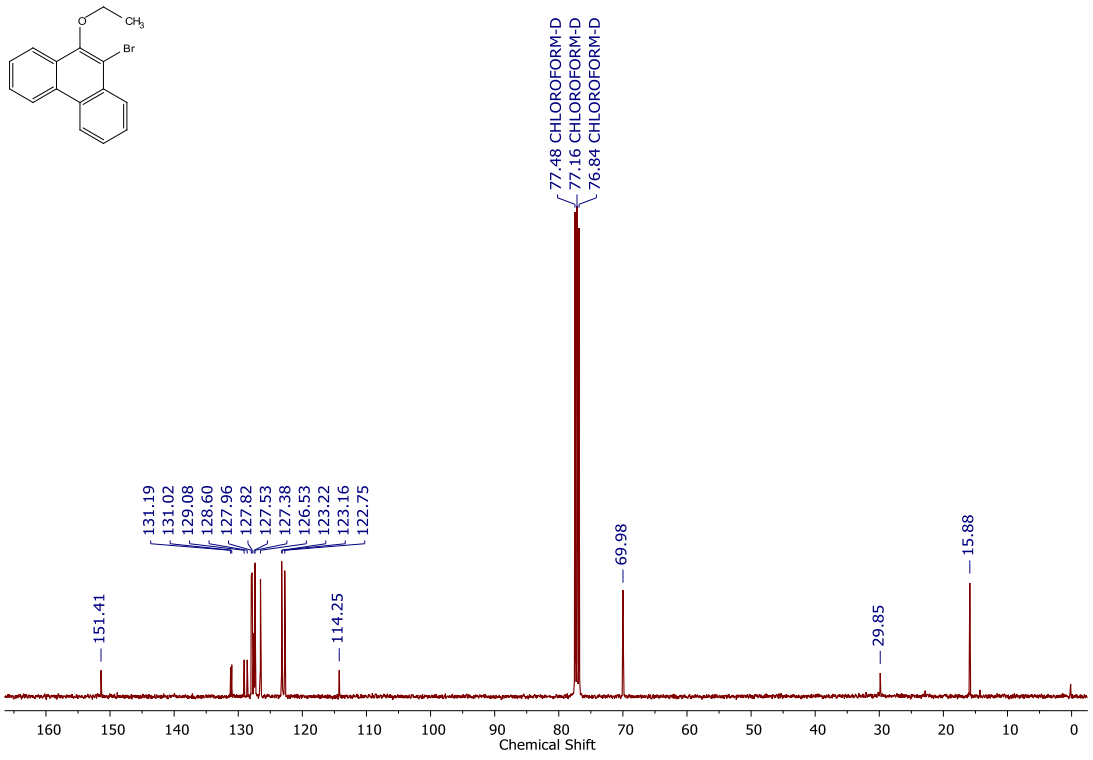

Figure 2.15 $^{13}C\{^{1}H\}$ NMR spectrum of **7** (in $CDCl_3$, 100 MHz) [grease at 29.8 ppm].

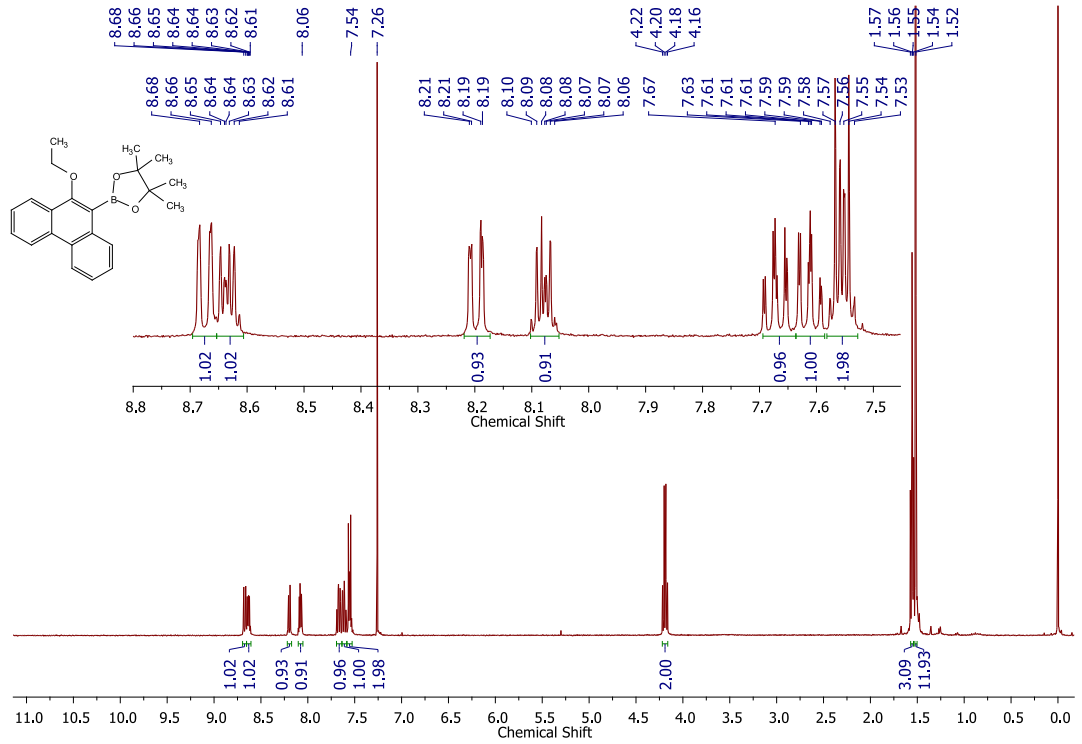

Figure 2.16 ^{1}H NMR spectrum of **9** (in $CDCl_3$, 400 MHz).

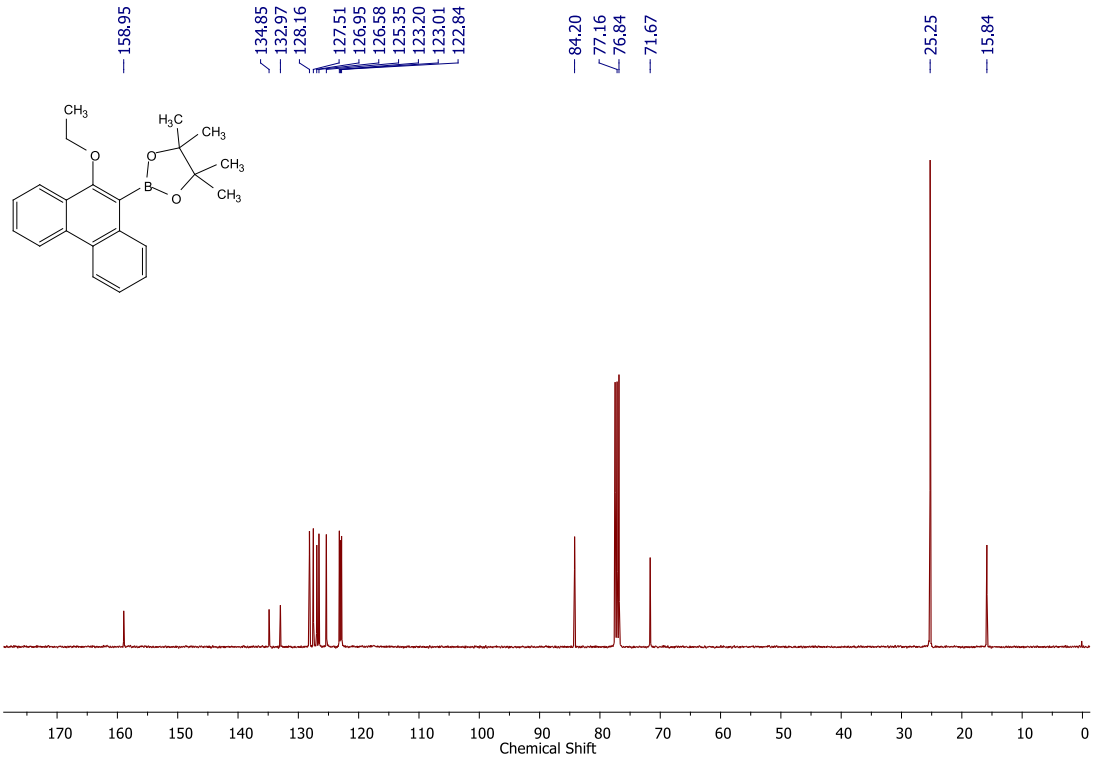

Figure 2.17 $^{13}C\{^{1}H\}$ NMR spectrum of **9** (in $CDCl_3$, 100 MHz).

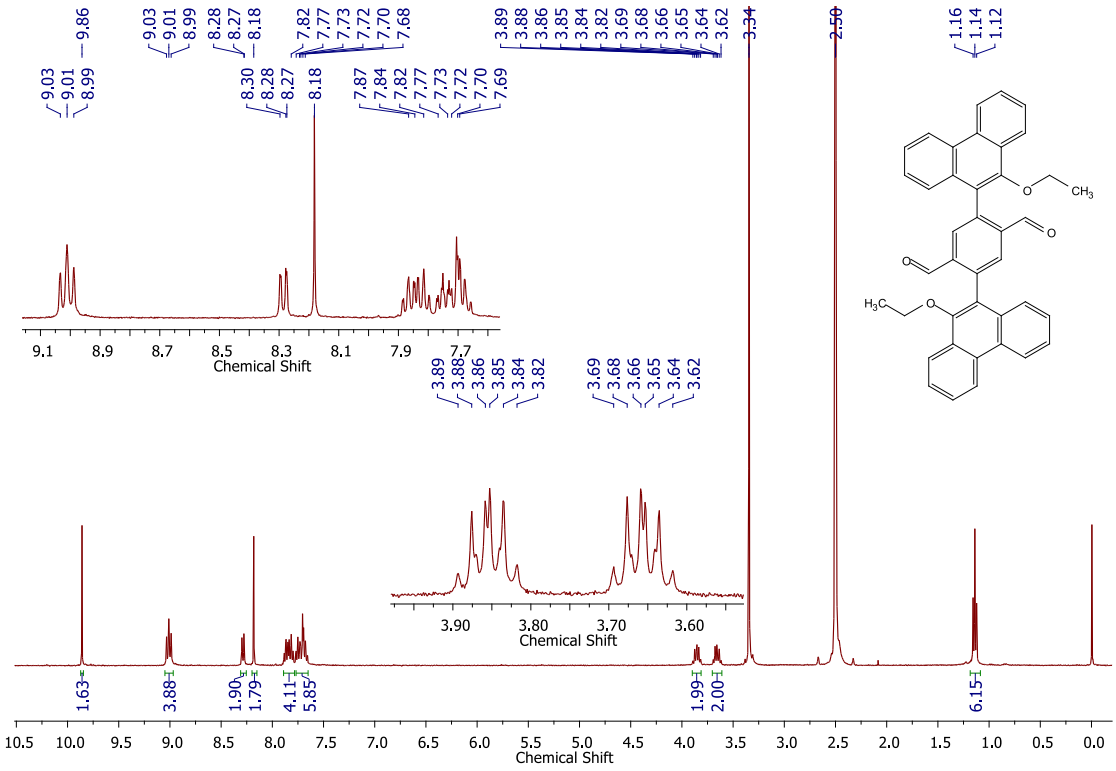

Figure 2.18 ^{1}H NMR spectrum of **11** (in CD_3SOCD_3, 400 MHz).

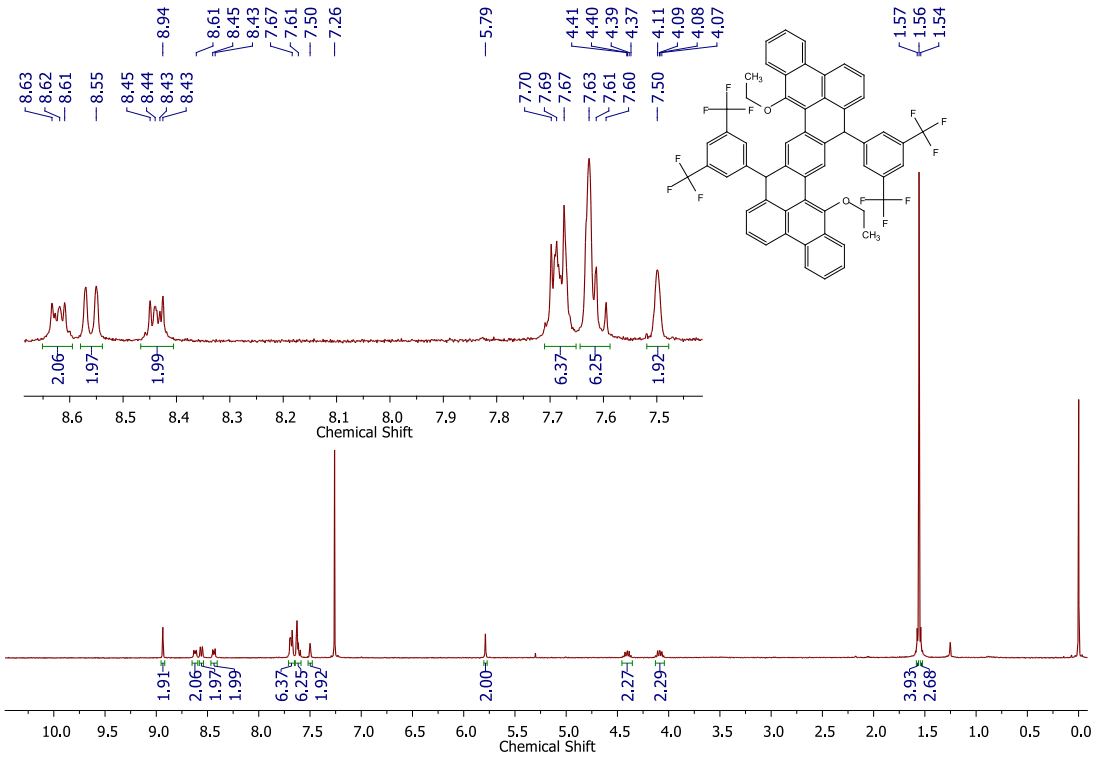

Figure 2.19 ^{1}H NMR spectrum of **14** (in $CDCl_3$, 400 MHz).

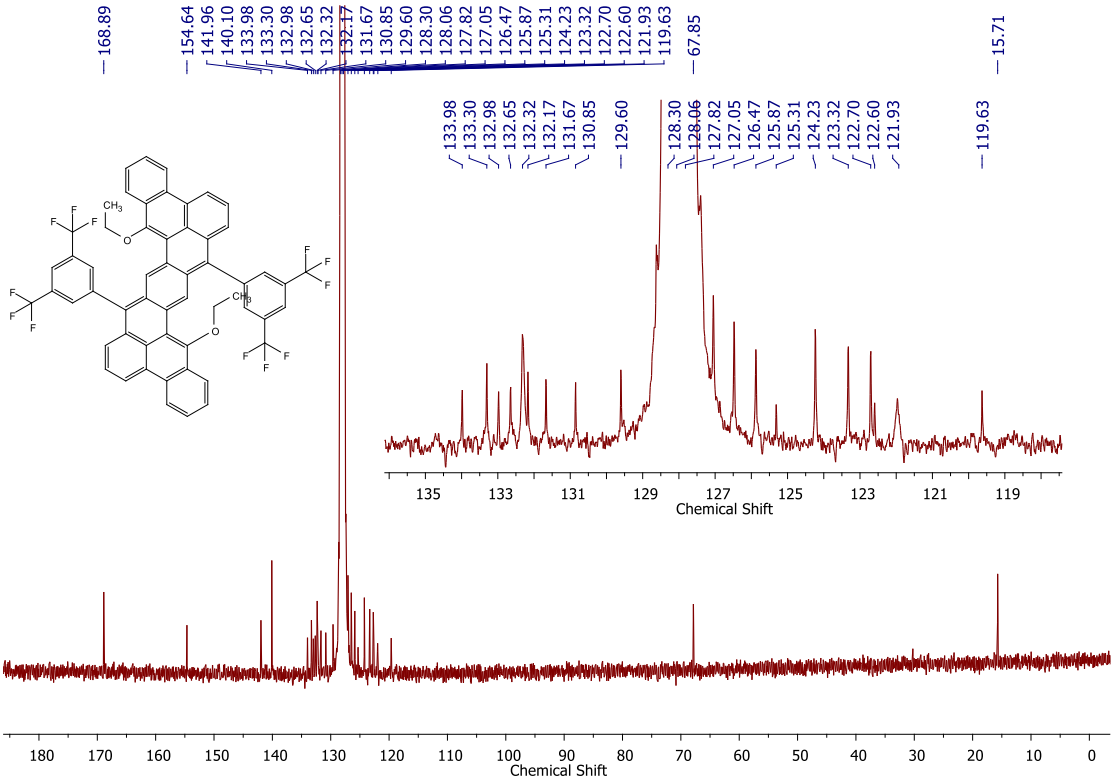

Figure 2.20 $^{13}C\{^{1}H\}$ NMR spectrum of **3** (in C_6D_6, 100 MHz) at 298 K.

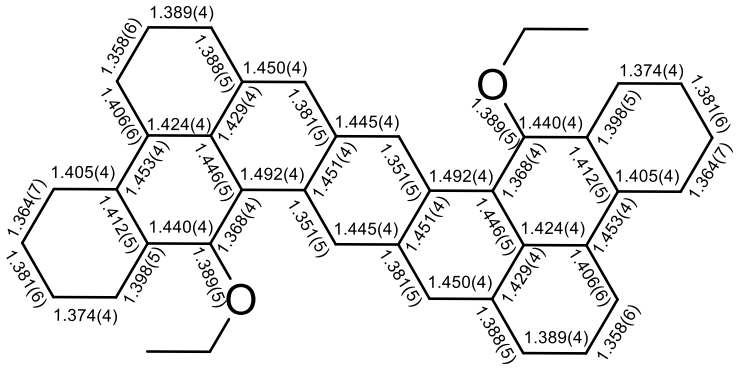

Figure 2.21 C_{sp^2}–C_{sp^2} bond-lengths (in Å) for **3**. with e.s.d values.

Chapter 3A

A Thiophenoradialene-Embedded Polycyclic Heteroterphenoquinone Exhibiting Dominant Antiaromatic Traits

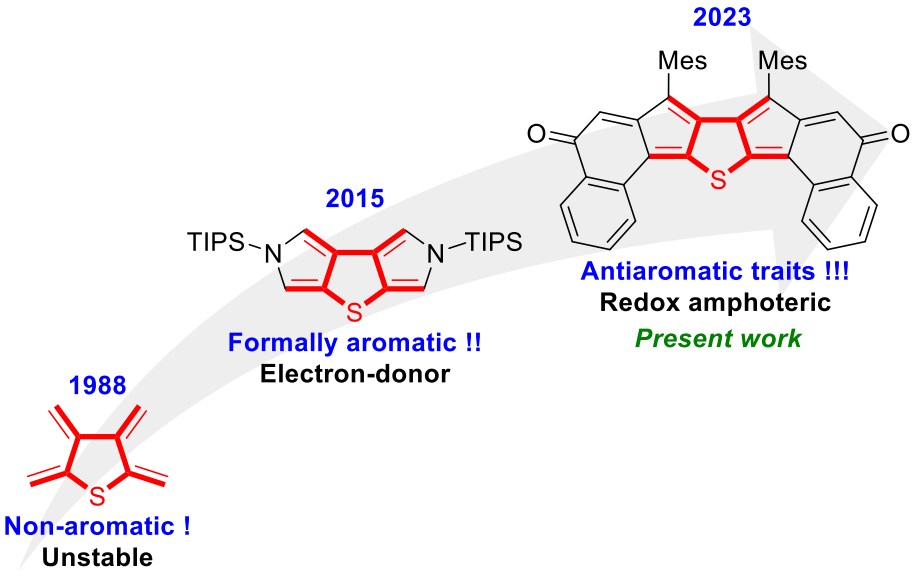

This work was published in *Organic Letters* (an ACS journal). Please see the citation as: "Sharma, P. K., Mallick, D., Das, S. A Thiophenoradialene-Embedded Polycyclic Heteroterphenoquinone Exhibiting Dominant Antiaromatic Traits. *Org. Lett.* **2023**, *25*, 5089–5093."

3A Abstract

In this Chapter, a thiophenoradialene-embedded polycyclic heteroterphenoquinone (PHTPQ) derivative, diindeno[1,2-*b*:2',1'-*d*]thiophene-2,8-dione, with antiaromatic characteristics, was synthesized by dehydrogenating its fluorescent dihydro PHTPQ precursor. The antiaromatic character was evidenced by the visible absorption band with a weakly intense tail extending to 800 nm in the near-infrared region (forbidden HOMO→LUMO transition) and non-emissive and amphoteric redox properties. Single crystal and (anti)aromaticity analyses found a non-aromatic thiophene core while suggesting antiaromaticity/paratropicity of the pentafulvene subunits dominating the overall ground-state properties.

3A.1 Introduction

Cross-conjugation was usually regarded as being less effective in promoting electron delocalization.[1] Improved conductance properties[2] and high-performance battery[3] applications of cross-conjugated molecules made them stimulating synthetic targets. Conventional [5]radialene[4] is a cross-conjugated π-system with five exocyclic $C(_{sp}{}^2)=C(_{sp}{}^2)$ double bonds (Figure 3A.1a), and belongs to the well-known [*n*]radialene family.[5] Studies on the hybrid [*n*]radialenes[6] with different heteroatoms (such as: O, P, S, As, Si) introduced into the radialene backbone (Figure 3A.1a) were relatively less explored.[7] Among them, the oxa-hybrid [5]radialene and thia-hybrid [5]radialene systems were first generated as cross-conjugated reactive furanoradialene **1a**[7a,b] and thiophenoradialene **1b**[7c] by the flash vacuum pyrolysis. Sulfur-centered dithienothiophene **2**[7j] or bispyrrolothiophene **3**[7h] bearing a thia-hybrid [5]radialene (or thiophenoradialene) unit was generated by attaching two aromatic heterocycles to the opposite sides of central thiophene ring with the outer heteroatoms (S or N) facing the opposite direction. Such ring-fusion arrangement for tricyclic **2** or **3** should better represent them as hybrid [5]radialene-like[8] molecules, considering aromatic 14π-electron perimeter.

As detailed in Chapter 1, an earlier attempt to isolate dicyclopenta[*b*,*d*]thiophene through linear dibenzo-extension failed[9] due to large singlet diradical character caused by the recovery of three local aromatic rings,[10] but no decomposition product was reported. We envisaged that dinaphtho-fusion could be viable approach for isolating dinaphtho-dicyclopenta[*b*,*d*]thiophene **5**, as two Clar sextets (shown in orange hexagon in Figure 3A.1b) would be retained for **5** while only

one weakly aromatic thiophene would be dearomatized; a successful approach was adopted by the groups of both Haley and Chi to synthesize the elusive antiaromatic heterocyclic indenofluorenes.[11] We adopted the oxidative dehydrogenation approach of dihydro precursor **4** to construct **5** (Figure 3A.1b),[12] but failed to synthesize it; instead, we isolated a fully fused polycyclic heteroterphenoquinone (PHTPQ) **6**.

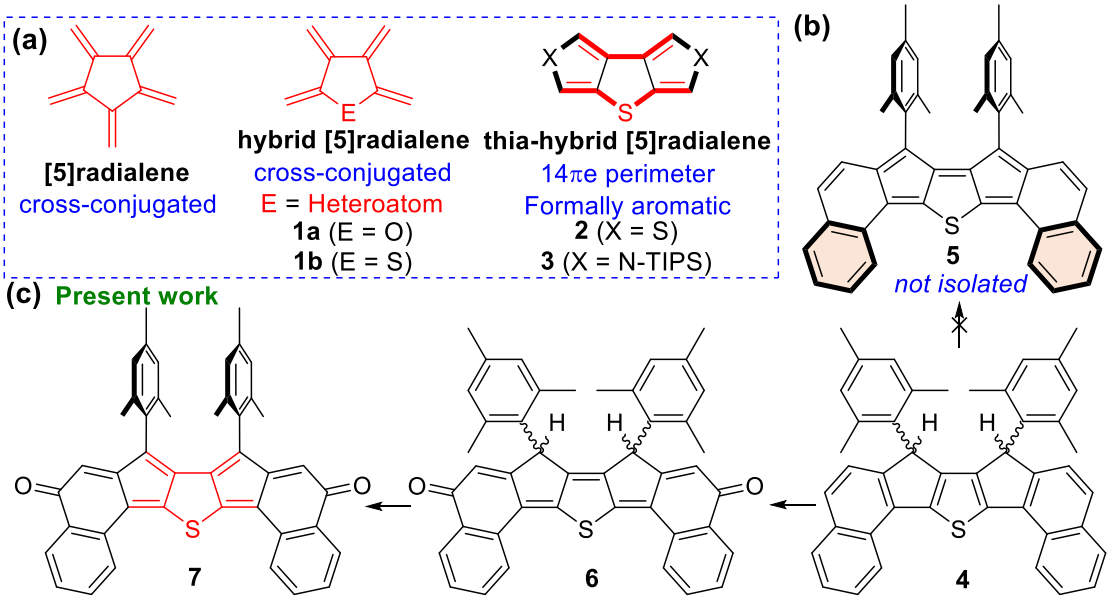

Figure 3A.1 (a) Structure of [5]radialene, furanoradialene **1a**, and thiophenoradialene **1b**. Formally aromatic thiophenoradialenes **2** and **3** with (4n + 2)π-electron in the outer conjugation circuit. (b) Structure of **5** which, could not be isolated from **4**. (c) Instead, **6** was isolated and dehydrogenated to target **7**.

Our observation was quite similar to literature reports in which π-extension of potential diradicaloid polycyclic hydrocarbons caused degradation and resulted in isolation of dione as decomposition products, but their properties remained unexciting.[13] Nevertheless, to the best of our knowledge, **6** is the only example of a fully fused PHTPQ congener of π-conjugated HTPQ in which the central benzo-unit was replaced by a heterocycle (thiophene for **6**).[14] Notably, *para*-terphenoquinone (*p*TPQ) analogue with a central dihydrothiophenediylidene unit could uniquely display intense absorption in the visible region (λ_{max} = 558 nm, log ε = 4.90),[14a] and three-stage[14a,b] or four-stage[15] amphoteric single-electron redox events, but no fluorescence for such quinones has been documented thus far. Herein, the quinone **6** was characterized to explore its ground state electronic properties, including the elusive fluorescence property.

Oxidative dehydrogenation of the through-conjugated[3] (or linearly conjugated) dihydro PHTPQ **6** was envisioned to afford a dibenzo-extended diindeno[1,2-*b*:2′,1′-*d*]thiophene2,8-dione derivative **7**, bearing a thiophenoradialene unit (Figure 3A.1c, shown in red). Notably, the carbonyl groups of both **6** and **7** are cross-conjugatively connected to sulfur,[16] but the carbonyl groups are through-conjugated with each other, with **7** containing one fewer π-electron pair than **6** in the conjugation path. Unlike the reported formally aromatic thia-hybrid [5]radialene with an obvious negative nucleus independent chemical shift (NICS) for the central thiophene unit of **3** of –5.16 ppm,[7h] the thiophene unit of **7** was expected to be dearomatized, making **7** a rare example of cross-conjugated thia-hybrid [5]radialene-embedded PHTPQ that may act as electron-accepting scaffold unlike **2** or **3** which are electron-donors. The properties of **7** were studied by single crystal X-ray diffractometry (SCXRD), ultraviolet-visible (UV-vis) absorption, cyclic voltammetry (CV), and density functional theory (DFT) approaches, while NICS(1)$_{zz}$,[17] HOMA (harmonic oscillator model of aromaticity)[18] and ACID (anisotropy of the induced current density)[19] calculations were performed to assess the ground-state (anti)aromaticity.

3A.2 Results and Discussion

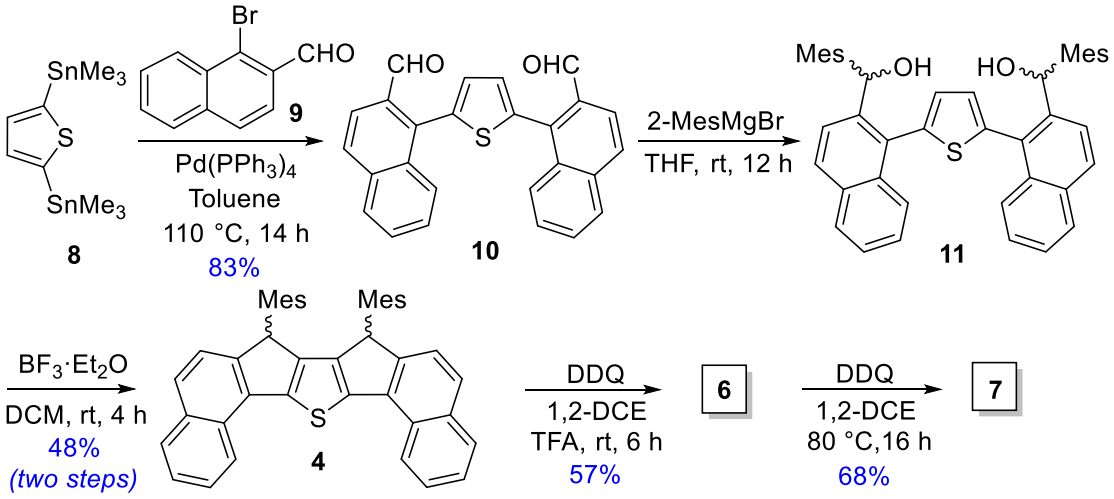

Scheme 3A.1 Syntheses of **6** and **7** (Mes = Mesityl).

3A.2.1 Synthesis. Stille reaction between presynthesized 2,5-bis(trimethylstannyl)thiophene[20] **8** and commercially available **9** in toluene afforded **10** in 83% yield (Scheme 3A.1). Nucleophilic addition of 2-mesitylmagnesium bromide to **10** gave diol **11**, which was subsequently treated with $BF_3{\cdot}Et_2O$ to afford **4** in 48% yield over two steps. The oxidative dehydrogenation of **4** with only 2,3-

dichloro-5,6-dicyano-1,4-benzoquinone (DDQ) did not work, but DDQ with trifluoroacetic acid (TFA) in 1,2-dichloroethane at room temperature afforded pink solution and disappearance of starting material **4**. Purification of the resulting reaction mixture through silica gel column chromatography afforded a purple-black powder in 57% yield. Unfortunately, after many attempts, we failed to grow a single crystal of the obtained purple-black solid. The high-resolution mass spectrometry (HRMS) and NMR analyses suggested the formation of PHTPQ **6**, instead of **5** (Figure 3A.1b), as it showed intense UV-vis absorption and fluorescence in the visible region (*vide infra*).[14a] It was quite unprecedented observation because quinones are mostly non-emissive,[21] especially HTPQ or *p*TPQ analogues.[14,15] Thus, to unambiguously confirm the structure of **6**, we aimed to oxidatively dehydrogenate **6** in the presence of DDQ to construct the first thiophenoradialene-embedded PHTPQ **7** in 68% yield. Structure of **7** was established by HRMS and one- and two-dimensional NMR analyses (Figure 3A.2, 3A.3 and 3A.4), while SCXRD analysis provided further unambiguous confirmation of its formation.

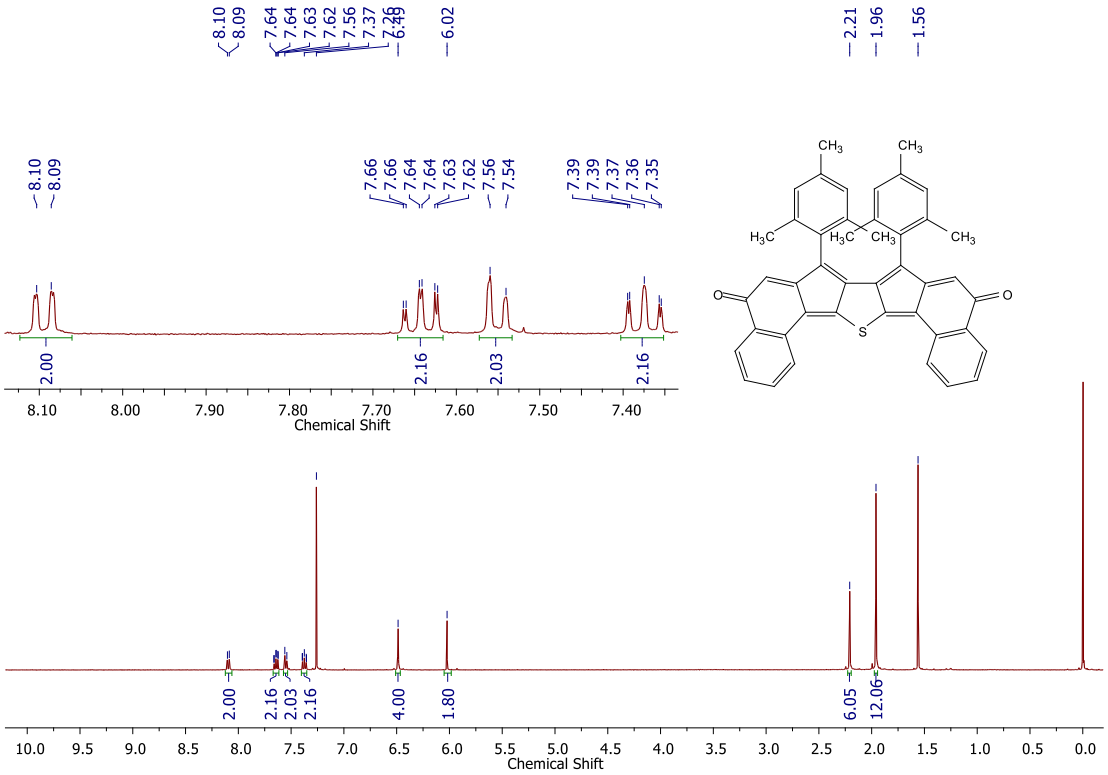

Figure 3A.2. ^{1}H NMR spectrum of **7** (in $CDCl_3$, 400 MHz, 298 K).

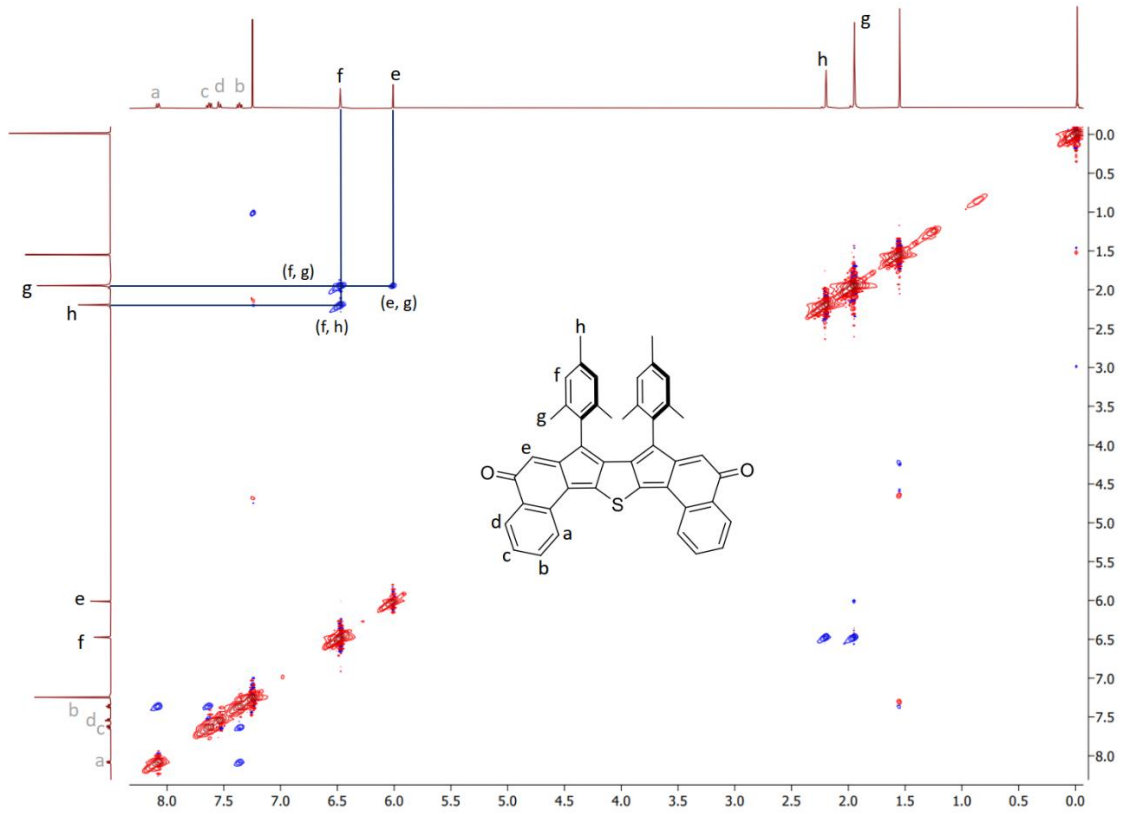

Figure 3A.3 ^{1}H-^{1}H NOESY spectrum of **7** in $CDCl_3$.

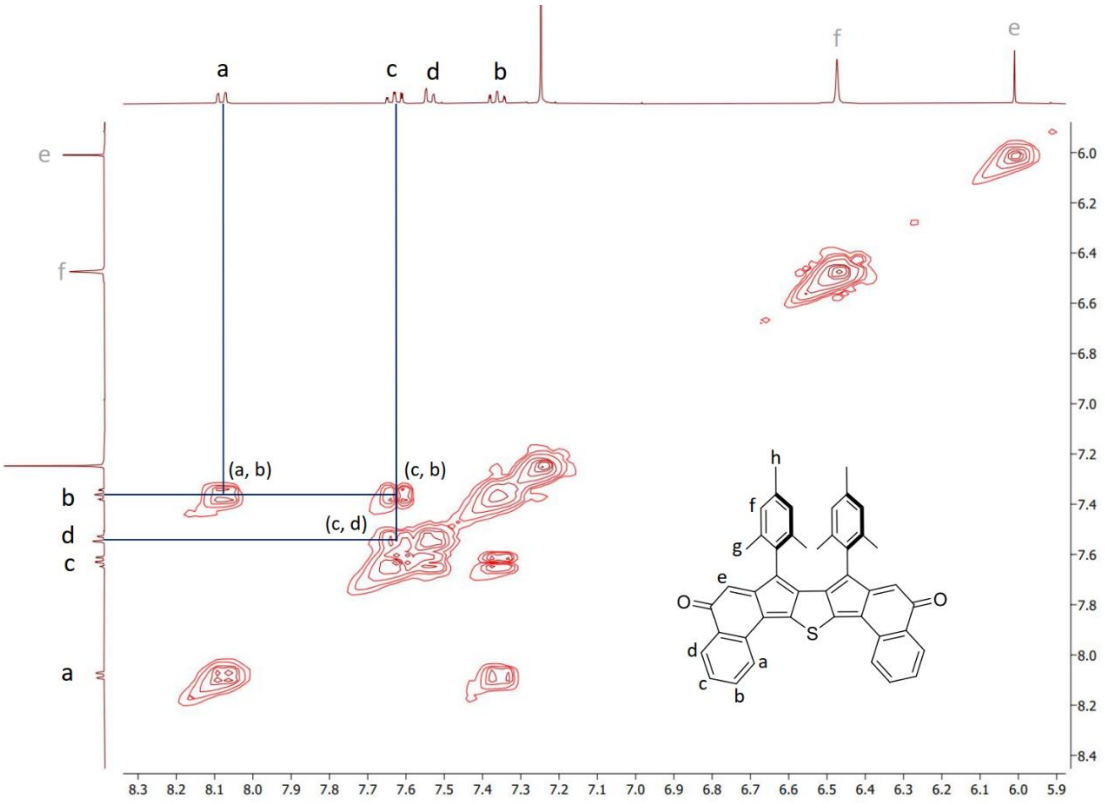

Figure 3A.4 ^{1}H-^{1}H COSY spectrum of **7** in $CDCl_3$ (aromatic region expansion).

3A.2.2 X-ray crystallography and antiaromaticity analyses. Single crystals of **7** (Figure 3A.5a) for SCXRD analysis were grown by diffusing methanol into the chloroform solution at ambient temperature. Compound **7** had a rigid and almost planar core structure (Figure 3A.5b) with the terminal benzene rings (A) slightly deviated by ~6.9° (average) in the cove-like region, as measured from the mean plane between central ring D and terminal rings A (rings are labeled in Figure 3A.5a). The mesityl groups are nearly orthogonal to the heptacyclic π-backbone, with an average torsional angle of 69.7°. The pentafulvene subunit of **7** exhibited significant C–C bond length alternation (BLA), as shown in Figure 3A.5a with C=C bonds *a*-*c* (see labeling in Figure 3A.5a) showing a greater double bond character compared to that of the other C_{sp}^2–C_{sp}^2 (*d*-*f*) bonds, thereby indicating an alternate double- and single-bond arrangement similar to that of unsubstituted pentafulvene.[22] The mean bond lengths for *g* (C–C) and *h* (S–C) of **7** are 1.433 and 1.738 Å, respectively, which apparently had significant single-bond character. Such bond length arrangements clearly indicated a non-aromatic thiophenoradialene motif for **7** with four exocyclic double bonds.[7g,h] On the contrary, BLA in the terminal six-membered rings (A) is less pronounced (average of 1.387 Å), suggesting benzene-like aromaticity.

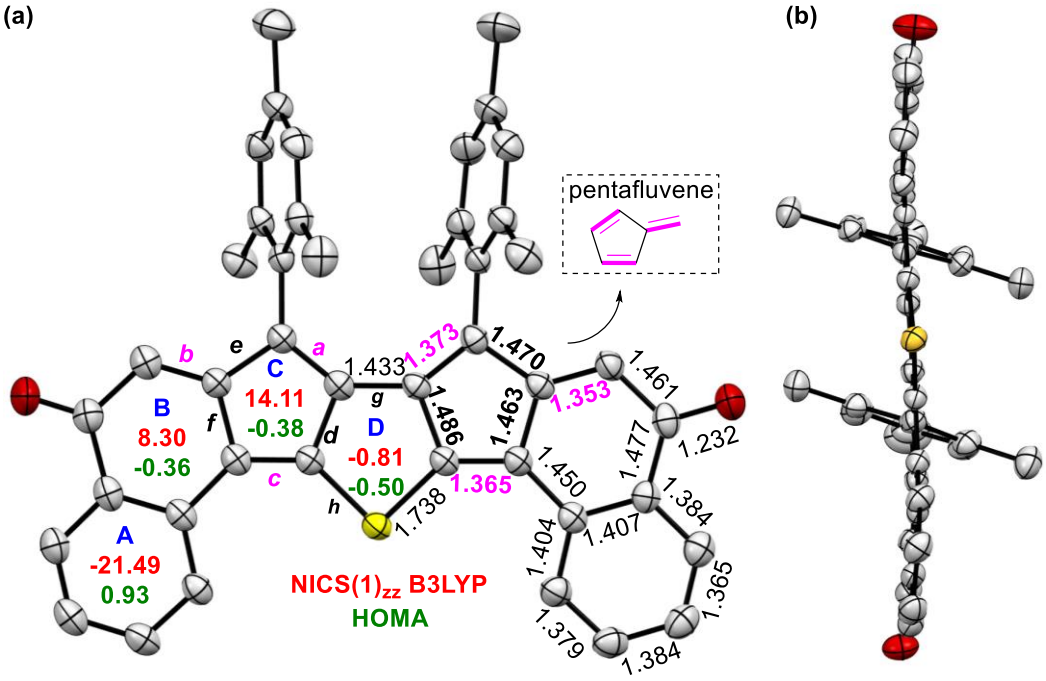

Figure 3A.5 (a) ORTEP drawing for the top-view of **7** with ellipsoids at the 30% probability level (hydrogens omitted), including mean bond lengths (angstroms (Å)), calculated NICS(1)$_{zz}$ (red) indices at the B3LYP/6-31G(d,p) level, and HOMA (green) values. (b) Side-view of **7**.

In the crystal lattice, **7** (Figure 3A.6a-c) packed in a three-dimensional arrangement owing to the short S···S interaction (k = 3.591 Å) and intermolecular π–π interaction measuring 3.33 Å (g = h) between a pair of **7** co-facially stacked at about a point of inversion, with another molecule parallel-displaced at 3.325 Å (i = j), in addition to a intermolecular C–H···π (l = 2.873 Å) and a C–H···O hydrogen bonding (HB) (m = 2.701 Å, 134.6°) interactions between two neighboring molecules. Compound **7** also displayed two intramolecular C–H···S (n = 2.853 Å, 130.8°; o = 2.839 Å, 131.0°) HB interactions.[23,24]

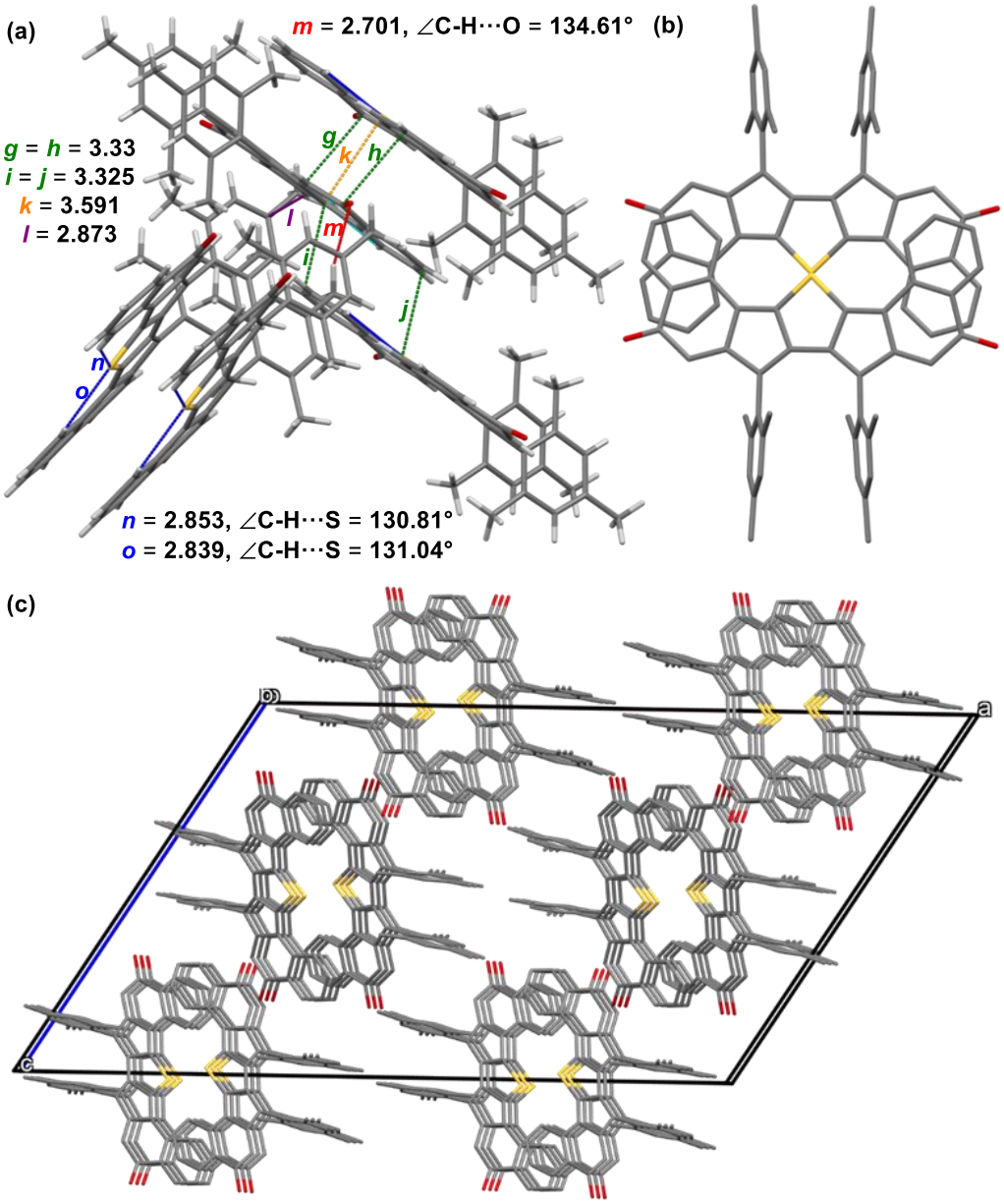

Figure 3A.6 (a) Non-covalent interactions (Å) are labeled for **7**. (b) Pair of molecules of **7**, cofacially π-stacked at about a point of inversion due to S···S interaction, forming a figure-eight like dimeric motif. (c) 3D-molecular packing of **7**.

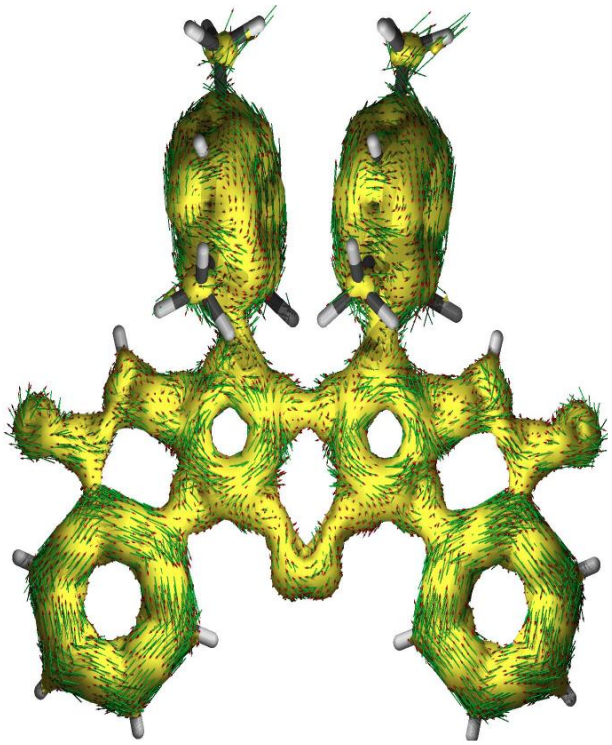

Figure 3A.7 Current–density vectors of **7** plotted onto the ACID isosurface of 0.02 at the B3LYP/6-31G(d,p) level of theory.

DFT optimization of **7** at the B3LYP/6-31G(d,p) level of theory suggested a singlet closed-shell ground state with large singlet-triplet energy gap (18.8 kcal/mol, Table 3A.5). The HOMA[18] analyses of the optimized closed-shell structure of **7** provided further support for the substantial BLA for rings C (−0.38) and B (−0.36), while insignificant BLA for terminal A rings (0.93) suggested its aromaticity. On the basis of the $NICS(1)_{zz}$[17] values of **7**, calculated using the same level of theory, ring A (−21.49) was found to be strongly aromatic while non-aromaticity for ring D (−0.81) and moderate to strong antiaromaticity for rings B (8.30) and C (14.11) were suggested. The ACID[19] plot of **7** corroborate with the $NICS(1)_{zz}$ values, showing counterclockwise ring-current over ring C, indicating significant paratropic nature of pentafulvene subunit, while rings B and D were essentially atropic (Figure 3A.7). A strong clockwise (diatropic) ring current observed over ring A was consistent with its large negative $NICS(1)_{zz}$ value. The strong antiaromaticity of the pentafulvene subunits could be attributed to the electron-withdrawing oxygen of carbonyl groups imposing positive charges on the attached carbons (Figure 3A.8), as analysed by natural population analyses (NPA charges, Figure 3A.9) in the ground state, which may delocalize to the pentafulvene subunit, forming the antiaromatic cyclopentadienyl cation with significant paratropic ring current.

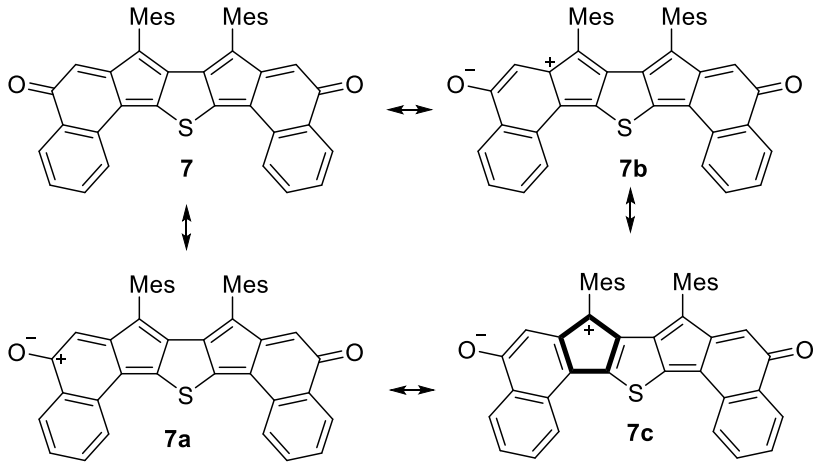

Figure 3A.8 Plausible resonance forms contributing to pentafulvene antiaromaticity

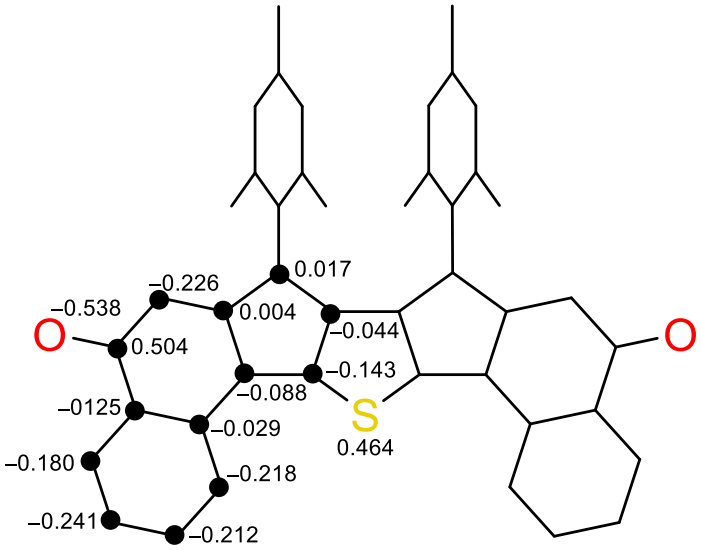

Figure 3A.9 Natural population analysis (NPA) charges of **7.**

3A.2.3 Optical and electrochemical properties. Compounds **6** and **7** were moderately soluble in common organic solvents, with **6** exhibiting pink color and **7** appearing to be dark yellow in dichloromethane (DCM, Figure 3A.10a and 3A.10b). The UV-vis absorption and fluorescence spectra of **6** in DCM are depicted in Figure 3A.10a. Compound **6** exhibited intense absorption in the visible region at λ_{max} = 557 nm (ε = 41730 M^{-1} cm^{-1}), which looks similar to HTPQ or *p*TPQ absorption bands,[14a] resulting from the allowed HOMO→LUMO transition (theoretical λ_{max} = 513 nm; oscillator strength (*f*) = 1.29, as shown in Table 3A.1 and Figure 3A.11 based on time-dependent DFT (TDDFT) calculations). Compound **7** showed an intense absorption in the visible region at λ_{max} = 504 nm (ε = 50150 M^{-1} cm^{-1} Figure 3A.10b) which is accompanied by a low energy shoulder at ~635 nm, despite shortening of the linear π-conjugation path in comparison to that of **6**. Such a weakly intense shoulder band with

its absorption tail extending to 800 nm (Figure 3A.10b, inset) is reminiscent of strong ground-state antiaromatic character,[23] which may be attributed to the dominant antiaromaticity of the pentafulvene subunit for **7**, as supported by NICS/ACID calculations. According to TDDFT, the absorption at 504 nm of **7** was an admixture of HOMO→LUMO+1, HOMO−1→LUMO and HOMO−5→LUMO (501 nm; f = 0.47) transitions, while the weakly intense absorption tail in the range of 535-800 nm resulted due to the combinations of several weak and apparently forbidden transitions (f < 0.021, Table 3A.2), including the forbidden HOMO→LUMO transition (TDDFT; 685 nm; f = 0.006), implying ground-state antiaromatic character. The optical HOMO–LUMO energy gaps for **6** and **7**, roughly estimated from the absorption onsets, were found to be 2.12 and 1.64 eV, respectively.

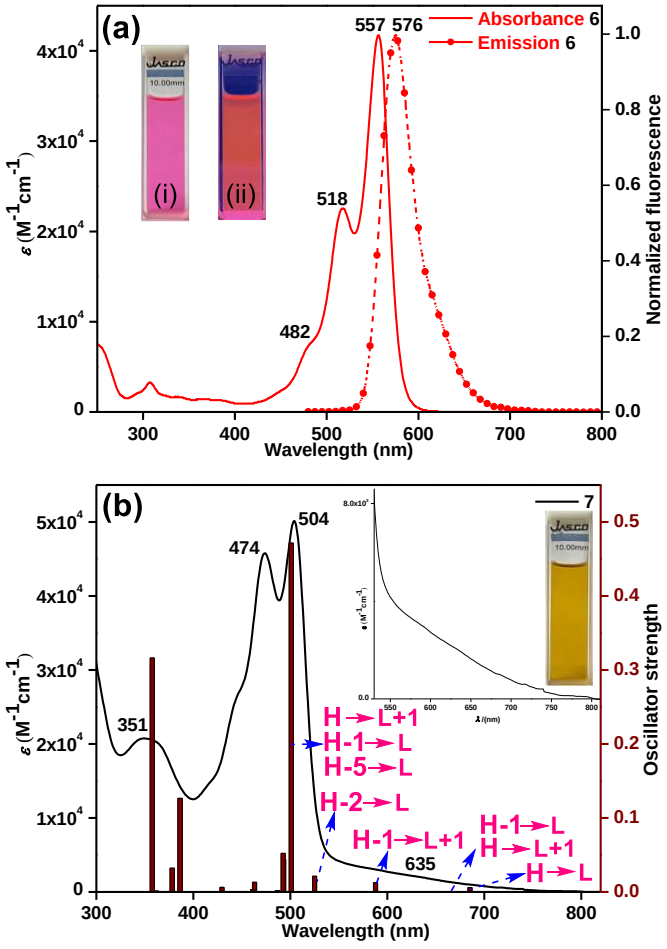

Figure 3A.10 (a) UV-vis absorption (solid line) and emission (dashed-dotted line) spectra of **6** with inset image under (i) visible (shows pink color as DCM solution) and (ii) 365 nm light irradiation; (b) UV-vis-NIR absorption of **7** (inset, 535-800 nm expansion and dark yellow color of **7** as the DCM solution) with TDDFT oscillator strengths as a bar diagram.

Usually, chalcogen-based HTPQ derivatives are non-emissive,[14] but PHTPQ **6** exhibited fluorescence with quantum yield (Φ) of 25% (with rhodamine B as a reference standard).[25] The emission maximum of **6** at 576 nm in DCM showed a small Stokes shift of 19 nm due to a planar and rigid backbone. Interestingly, the fluorescence disappeared upon oxidative dehydrogenation of **6** to **7**, which could likely be attributed to the dominant antiaromaticity of **7** opening the radiationless relaxation pathway due to conical intersection between the excited state and ground state potential energy surfaces.[26] Notably, formally aromatic thia-hybrid [5]radialenes[7h] are fluorescent.

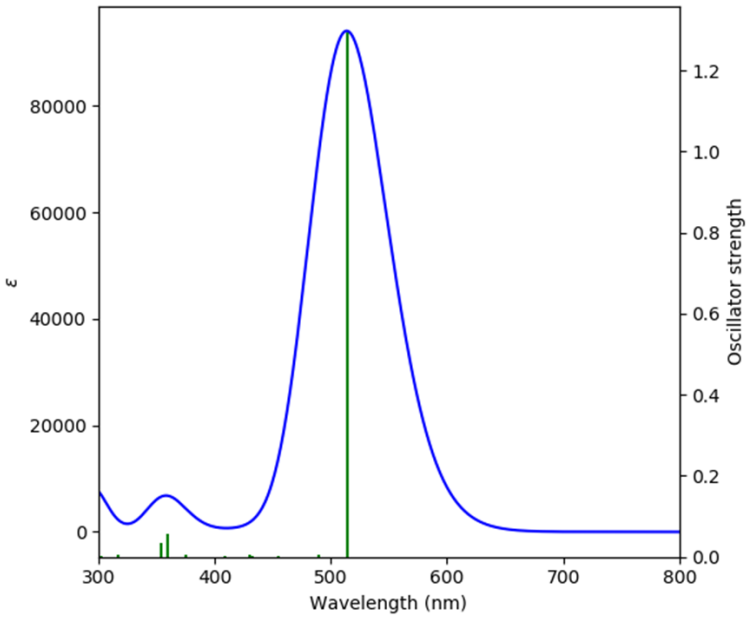

Figure 3A.11. Theoretical absorption of **6** in the gas-phase.

Table 3A.1. Summary of TDDFT calculation for **6**

Wavelength (nm)	**Oscillator Strength (*f*)**	**Major contributions**
513	1.2948	HOMO->LUMO (102%)
489	0.0046	H-4->LUMO (39%), H-3->LUMO (13%), H-1->LUMO (43%)
487	0.0001	H-5->LUMO (26%), H-2->LUMO (68%)
454	0.0017	H-4->LUMO (36%), H-1->LUMO (56%)
432	0.002	H-5->LUMO (57%), H-3->LUMO (11%), H-2->LUMO (26%)
430	0.0048	H-5->LUMO (12%), H-4->LUMO (16%), H-3->LUMO (68%)
408	0.0009	H-6->LUMO (99%)
385	0.0003	H-7->LUMO (40%), HOMO->L+1 (53%)
375	0.0067	H-10->LUMO (12%), H-8->LUMO (85%)

365	0	H-11->LUMO (34%), H-9->LUMO (47%), HOMO->L+1 (10%)
359	0.0578	H-11->LUMO (16%), H-9->LUMO (42%), H-7->LUMO (31%)
353	0.0335	H-10->LUMO (78%), H-8->LUMO (10%)
337	0.0002	H-12->LUMO (97%)
317	0.0063	HOMO->L+2 (87%)
310	0	H-11->LUMO (39%), H-7->LUMO (14%), HOMO->L+1 (24%)
302	0.0005	H-4->L+1 (33%), H-3->L+1 (11%), H-1->L+1 (29%)
302	0.0016	H-5->L+1 (21%), H-4->L+2 (10%), H-2->L+1 (52%)
295	0.102	HOMO->L+3 (80%)
288	0.0081	H-4->L+1 (23%), H-1->L+1 (64%)
283	0.0007	HOMO->L+4 (96%)

Table 3A.2 Summary of TTDFT calculation for **7**

Wavelength (nm)	**Oscillator Strength (*f*)**	**Major contributions**
685	0.006	HOMO->LUMO (90%)
671	0.0004	H-1->LUMO (81%), HOMO->L+1 (18%)
587	0.0126	H-1->L+1 (91%)
525	0.0213	H-2->LUMO (94%)
501	0.4717	H-5->LUMO (10%), H-1->LUMO (13%), HOMO->L+1 (62%)
493	0.0441	H-3->LUMO (86%)
492	0.0521	H-7->LUMO (37%), H-6->L+1 (21%), H-5->LUMO (17%)
486	0.002	H-7->L+1 (28%), H-6->LUMO (62%)
463	0.013	H-7->LUMO (19%), H-5->LUMO (29%), H-4->LUMO (31%), H-2->L+1 (11%)
461	0.0031	H-5->LUMO (24%), H-4->LUMO (61%)
429	0.0061	H-5->LUMO (17%), H-2->L+1 (81%)
412	0	H-3->L+1 (95%)
392	0.0001	H-5->L+1 (72%), H-4->L+1 (21%)
389	0.0001	H-5->L+1 (21%), H-4->L+1 (77%)
386	0.1265	H-8->LUMO (88%)
378	0.0322	H-9->LUMO (88%)
370	0.0001	H-7->LUMO (29%), H-6->L+1 (66%)
369	0.0005	H-7->L+1 (67%), H-6->LUMO (28%)
362	0.0014	H-11->LUMO (79%), H-8->L+1 (10%)
357	0.3161	H-10->LUMO (82%)

The cyclic voltammogram (CV) of **6** in DCM (Figure 3A.12a) exhibited a two-electron reduction wave with half-wave potential $E_{1/2}^{red} = -1.07$ V, and two irreversible oxidations at $E_{peak}^{ox1} = 0.83$ V and $E_{peak}^{ox2} = 1.02$ V. Compound **7** displayed redox amphotericity with two reversible reductions at half-wave potentials $E_{1/2}^{red1} = -1.02$ V and $E_{1/2}^{red2} = -1.40$ V and a quasi-reversible oxidation at $E_{peak}^{ox} = 1.05$ V. The reversible reduction events signify strong antiaromaticity of pentafulvene subunit of **7**, which resulted in facile electron injections to form of 4n + 2 cyclopentadienyl anion.[23,27] Notably, thia-hybrid [5]radialene **3** was reported to be an electron-donor[7h] and could not be reduced, while thia-hybrid [5]radialene-embedded **7** could act as both electron acceptor and donor. The electrochemical HOMO and LUMO energy levels of **6** were –5.52 eV and –3.82 eV, respectively, as estimated from the onset potentials, affording energy gap of 1.7 eV, while the electrochemical HOMO and LUMO levels for **7** were –5.68 eV and –3.86 eV, with energy gap 1.82 eV. The theoretical HOMO–LUMO energy gaps were found to be 2.20 eV and 2.30 eV for **6** and **7**, respectively (Figure 3A.12b).

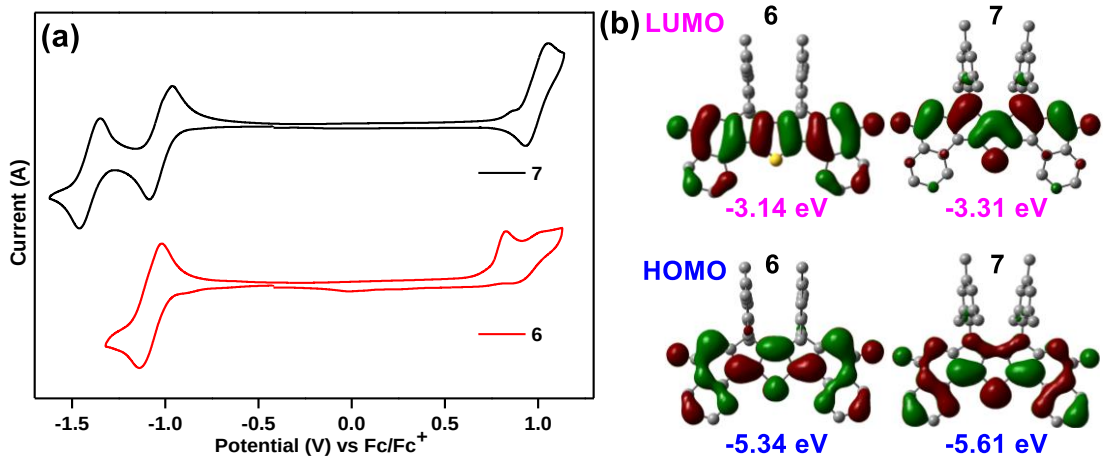

Figure 3A.12 (a) Cyclic voltammograms of **6** and **7**. (b) LUMO and HOMO profiles of **6** and **7**.

3A.3 Conclusions

In conclusion, a fluorescent PHTPQ **6** was synthesized and oxidized to thiophenoradialene containing PHTPQ **7**, which may be regarded as an underexplored thiaradialene[28]-based π-system. SCXRD and (anti)aromaticity analyses ($NICS(1)_{zz}$ and ACID) suggested large BLA and dominant antiaromatic character of the embedded pentafulvene subunits for **7**, as a result of the electron-withdrawing π-extended

carbonyl substituents *exo* to the five-membered ring.[29] The antiaromaticity was demonstrated experimentally by the weakly intense absorption band in 535-800 nm region owing to forbidden HOMO→LUMO transition, facile two-stage electron reductions with good reversibility, and non-emissive properties.[23,26,27] Our current synthetic approach has the potential to construct other heteroatom (i.e., selenium)[30] counterpart of **7** (and **6**) with tunable solid-state ordering and HOMO–LUMO energy gaps for potential application as ambipolar organic semiconductors.[31]

3A.4 Experimental section

3A.4.1 General information. Chemicals and reagents were purchased from local and international commercial suppliers (Merck, GLR innovations, BLDpharm, Spectrochem) and used without further purification. Compound **8** was synthesized according to known method, and the NMR data (shown below) are consistent with the literature.[20,32] Compound **9** (1-bromo-2-naphthaldehyde, CAS no: 3378-82-3) was purchased from BLDpharm. Thin layer chromatography (TLC) was performed using pre-coated silica-plates purchased from Merck (silica gel 60 PF254, 0.25 mm). Column chromatography was performed using silica gel 100-200 mesh. NMR spectra were recorded in $CDCl_3$ (Eurisotop) at room temperature, on JEOL JNM-ECS400 spectrometer at operating frequencies of 400 MHz (^1H) or 100 MHz (^{13}C) as indicated in the individual spectrum. Chemical shifts (δ) are given in ppm relative to residual solvent (chloroform δ = 7.26 for ^1H, and δ = 77.16 for proton-decoupled ^{13}C NMR), and coupling constants (*J*) are expressed in hertz (Hz). Multiplicity is tabulated as s for singlet, d for doublet, dd for doublet of doublet, t for triplet, q for quartet and m for multiplet. Structural assignments were made with additional information from gCOSY, and gNOESY experiments. High-resolution mass spectra (HRMS) were recorded using electronspray ionization (ESI) methods on Waters (XEVO G2-XS QTOF) mass spectrometer. UV-vis-NIR spectra were recorded in JASCO V-770 spectrophotometer. Fluorescence spectrum was recorded on a PerkinElmer LS55 fluorescence spectrophotometer. Cyclic voltammetry was performed using an Electrochemical Analyzer potentiostat model CHI-1110C from CH Instruments with a conventional three-electrode cell at room temperature under a nitrogen atmosphere at a scan rate of 50 mV s^{-1}. This electrochemical cell contains a glassy carbon (disc shaped with 3-mm diameter) as working electrode, Pt wire as counter electrode, and Ag wire as pseudo-reference electrode. The glassy carbon working electrode was polished with 1.0-

micron α-alumina polishing powder using a figure-eight motion. Electrolyte solution (0.1 M) was prepared from dichloromethane (DCM) and tetra-*n*-butylammonium hexafluorophosphate (Bu_4NPF_6). The DCM was degassed by nitrogen gas sparging for 10 minutes prior to measurements. The potential was externally calibrated against the ferrocene/ferrocenium couple (0.43 V). Melting points were determined using Cole-Parmer MP 250D-P melting point analyzer.

3A.4.2 Syntheses

1,1'-(thiophene-2,5-diyl)bis(2-naphthaldehyde) (10): An oven-dried thick-walled glass tube was charged with 2,5-bis(trimethylstannyl)thiophene **8** (500 mg, 1.22 mmol), 1-bromo-2-naphthaldehyde **9** (630 mg, 2.68 mmol), and dry toluene (10 mL) and the mixture was purged with nitrogen for 30 min. $Pd(PPh_3)_4$ (141 mg, 10 mol %) was subsequently added under nitrogen, and the glass vial was sealed before being warmed to 110 °C for 14 h using an oil bath. After cooling the reaction mixture to room temperature, toluene was evaporated under reduced pressure, water was added, and the reaction mixture was extracted with DCM. The organic layer was dried over sodium sulfate and then evaporated to dryness. The crude residue was subjected to silica gel column chromatography (hexanes/EtOAc, 97:3) to afford title product **10** as a yellow solid (400 mg, 83% yield): R_f = 0.15 (5% EtOAc/hexanes); mp 136–137 °C; ^{1}H NMR (400 MHz, $CDCl_3$) δ 10.32 (s, 2H), 8.11 (d, *J* = 8.6 Hz, 2H), 8.03 (d, *J* = 8.7 Hz, 4H), 7.97 (dd, *J* = 8.0, 1.3 Hz, 2H), 7.70 (ddd, *J* = 8.2, 6.9, 1.3 Hz, 2H), 7.64 (ddd, *J* = 8.2, 6.9, 1.4 Hz, 2H), 7.36 (s, 2H); ^{13}C{^{1}H} NMR (100 MHz, $CDCl_3$) δ 192.0, 137.6, 137.5, 136.1, 133.3, 132.9, 131.0, 130.0, 129.3, 128.5, 127.8, 127.1, 122.3; HRMS (ESI) *m/z*: $[M + H]^+$ calcd for $C_{26}H_{17}O_2S$ 393.0949, found 393.0921 (error: −7.1 ppm).

7,8-dimesityl-7,8-dihydrobenzo[6,7]indeno[1,2-*b*]benzo[6,7]indeno[2,1-*d*]thiophene (4): 2-mesitylmagnesium bromide (1.0 M in diethyl ether, 1.83 mL, 1.83 mmol) was added dropwise to the dry tetrahydrofuran (5 mL) solution of **10** (180 mg, 0.45 mmol) under nitrogen. The mixture was stirred at room temperature for 12 h, and the reaction was quenched with a saturated aqueous NH_4Cl solution. The volatile organics were evaporated, and the mixture was extracted with dichloromethane (3 x 30 mL). The organic layer was dried over anhydrous Na_2SO_4, filtered, and removed under reduced pressure to afford a crude mixture containing intermediate compound **11** (365 mg). To the solution of crude **11** in anhydrous DCM (6 mL) was added dropwise

$BF_3{\cdot}Et_2O$ (0.1 mL) under nitrogen, and the reaction mixture was stirred for 4 h at room temperature. Once **11** was completely consumed, as monitored by TLC, a saturated aqueous $NaHCO_3$ solution (10 mL) was added and the reaction mixture was extracted with DCM (3 × 10 mL). The organic layer was dried over anhydrous Na_2SO_4, filtered, and evaporated under reduced pressure. The residue was subjected to silica gel column chromatography (hexanes/EtOAc, 95:5) to give title product **4** as a light green solid (130 mg, 48% over two steps): R_f = 0.57 (5% EtOAc/hexanes); mp 286−287 °C; ^{1}H NMR (400 MHz, $CDCl_3$) δ 8.38 (d, *J* = 8.2 Hz, 2H), 7.93 (d, *J* = 8.1 Hz, 2H), 7.70 (t, *J* = 7.4 Hz, 2H), 7.63 (d, *J* = 8.0 Hz, 2H), 7.55 (t, *J* = 7.4 Hz, 2H), 7.24 (d, *J* = 8.6 Hz, 2H), 6.87 (s, 2H), 6.61 (s, 2H), 4.98 (s, 2H), 2.30 (s, 6H), 1.74 (s, 6H), 1.23 (s, 6H); ^{13}C{^{1}H} NMR (100 MHz, $CDCl_3$) 146.7, 145.7, 138.8, 138.1, 136.5, 135.6, 133.2, 131.4, 129.7, 129.1, 128.8, 126.4, 126.3, 125.6, 125.5, 124.9, 122.6, 122.5, 47.1, 21.0, 20.6, 17.8; HRMS (ESI) *m/z*: $[M + H]^+$ calcd for $C_{44}H_{36}S$ 596.2538, found 596.2543 (error: 0.8 ppm).

7,8-dimesityl-7,8-dihydrobenzo[6,7]indeno[1,2-*b*]benzo[6,7]indeno[2,1-*d*]thiophene-5,10-dione (6): To a solution of **4** (40 mg, 0.06 mmol) in 1,2-dichloroethane (1,2-DCE, 6 mL) was added trifluoroacetic acid (TFA, 1.6 mL) and then added 2,3-dichloro-5,6-dicyanobenzoquinone (DDQ, 60 mg, 0.26 mmol). The reaction mixture was left to stir for 6 h, quenched with a saturated aq. $NaHCO_3$ solution, and then extracted with dichloromethane (3 × 20 mL). The combined organic phase was dried over anhydrous sodium sulfate, and then the solvent was removed under reduced pressure. The residue was purified by silica gel column chromatography (hexanes/EtOAc, 90:10) to afford title product **6** as a purple-black solid (24 mg, 57% yield): R_f = 0.26 (15% EtOAc/hexanes); mp 240 °C dec; ^{1}H NMR (400 MHz, $CDCl_3$) δ 8.35 (d, *J* = 7.7 Hz, 2H), 7.94 (d, *J* = 7.7 Hz, 2H), 7.80 (t, *J* = 7.4 Hz, 2H), 7.64 (t, *J* = 7.5 Hz, 2H), 6.79 (s, 2H), 6.72 (s, 2H), 6.20 (s, 2H), 5.02 (s, 2H), 2.28 (s, 6H), 1.73 (s, 6H), 1.53 (s, 6H); ^{13}C{^{1}H} NMR (100 MHz, $CDCl_3$) δ 184.1, 163.7, 159.6, 147.4, 138.5, 137.7, 137.1, 132.0, 131.3, 131.0, 130.24, 130.21, 129.8, 129.7, 129.4, 127.8, 126.0, 119.4, 43.7, 20.9, 20.1, 19.3; HRMS (ESI) *m/z*: $[M + H]^+$ calcd for $C_{44}H_{35}O_2S$ 627.2358, found 627.2363 (error: 0.8 ppm).

7,8-dimesitylbenzo[6,7]indeno[1,2-*b*]benzo[6,7]indeno[2,1-*d*]thiophene-5,10-dione (7): DDQ (54 mg, 0.24 mmol) was added to pink colored solution of **6** (30 mg, 0.04 mmol) in 1,2-DCE (10 mL) under nitrogen, and the reaction mixture was warmed to 80 °C using an oil bath. The color of the solution turned dark brown as the reaction

progressed and the reaction mixture was stirred for 16 h. The progress of the reaction was monitored by TLC. Once the starting material was consumed, the 1,2-DCE was removed in vacuo and the crude material was purified by silica gel column chromatography (hexanes/EtOAc, 95:5) to afford the desired product **7** as brown solid (20 mg, 68% yield). Recrystallization of **7** from a chloroform/methanol (1:1) mixture at ambient temperature afforded single crystals suitable for X-ray crystallographic analysis: R_f = 0.19 (5% EtOAc/hexanes); mp 390 °C dec; ^{1}H NMR (400 MHz, $CDCl_3$) δ 8.09 (d, *J* = 7.0 Hz, 2H), 7.64 (dt, *J* = 7.6, 1.3 Hz, 2H), 7.55 (d, *J* = 7.6 Hz, 2H), 7.39 – 7.35 (m, 2H), 6.49 (s, 4H), 6.02 (s, 2H), 2.21 (s, 6H), 1.96 (s, 12H); The ^{13}C NMR spectrum with a good signal-to-noise ratio could not be obtained for spectroscopic analysis due to insufficient solubility; HRMS (ESI) *m/z*: $[M + H]^+$ calcd for $C_{44}H_{33}O_2S$ 625.2201, found 625.2207 (error: 1.0 ppm).

3A.4.3 X-ray crystallographic analysis

A suitable single crystal of **7** was selected using paratone oil and mounted on glass fiber with the help of gum. The intensity data and geometric parameters of these crystals were garnered with the help of Bruker D8 Venture X-ray diffractometer having a micro-focus sealed X-ray tube Mo-Kα (λ = 0.71073 Å) source of X-rays along with a PHOTON 100 detector with inclining Phi and Omega (width of 0.5 for one frame) working at a scan speed of 10 s per frame. The crystal was kept at 298 K during data collection. Data acquisition as well as extraction of data was accomplished by utilizing Bruker Apex-3 and Bruker SAINT software packages using a narrow-frame algorithm.[33] By utilizing OLex2,[34] the crystal structure was solved with the help of olex2.solve[35] structure solution program by employing intrinsic Phasing methods and crystal structure refinement was done with the SHELXL[36] refinement package by putting into use Least Squares minimization. Refinement of all non-hydrogen atoms was completed with the help of anisotropic thermal parameters.

Table 3A.3 X-ray crystallographic information of **7**

CCDC No.	2264335
Empirical formula	$C_{44}H_{32}O_2S$
Formula weight	624.75
Temperature/K	298.00
Crystal system	monoclinic
Space group	*C*2/*c*
a/Å	38.473(4)

b/Å	8.2936(8)
c/Å	23.865(3)
α/°	90
β/°	122.870(4)
γ/°	90
Volume/Å^3	6395.9(12)
Z	8
ρ_{calc}g/cm^3	1.298
μ/mm^{-1}	0.140
F(000)	2624.0
Crystal size/mm^3	0.506 × 0.098 × 0.078
Radiation	MoKα (λ = 0.71073)
2Θ range for data collection/°	4.438 to 51.32
Index ranges	$-46 \leq h \leq 46$, $-9 \leq k \leq 10$, $-29 \leq l \leq 29$
Reflections collected	27213
Independent reflections	5979 [R_{int} = 0.0900, R_{sigma} = 0.0732]
Data/restraints/parameters	5979/0/431
Goodness-of-fit on F^2	1.025
Final R indexes [I>=2σ (I)]	R_1 = 0.0608, wR_2 = 0.1561
Final R indexes [all data]	R_1 = 0.1120, wR_2 = 0.1927
Largest diff. peak/hole / e Å^{-3}	0.75/-0.34

3A.4.4 DFT calculations

DFT calculations, in gas phase, were performed with Gaussian 09 package using a high-performance computing cluster facility of IIT Ropar at the B3LYP level of theory with basis set 6-31G(d,p).[37] Optimization of the molecular geometries for **7**, taken from X-ray crystallographic data, and **6** were done by restricted B3LYP, and unrestricted B3LYP wave-functions. NICS(1)$_{zz}$ (standard GIAO method) and HOMA indices were calculated for the optimized closed-shell structure of **7**. Excitation energy of **6** and **7** were computed using time dependent density functional theory (TDDFT) for the closed-shell optimized structure in gas phase. Molecular orbital contributions of **6** and **7** were determined using GaussSum 3.0 package.[38]

Optimized closed-shell structure of 6 (*syn*-conformation)

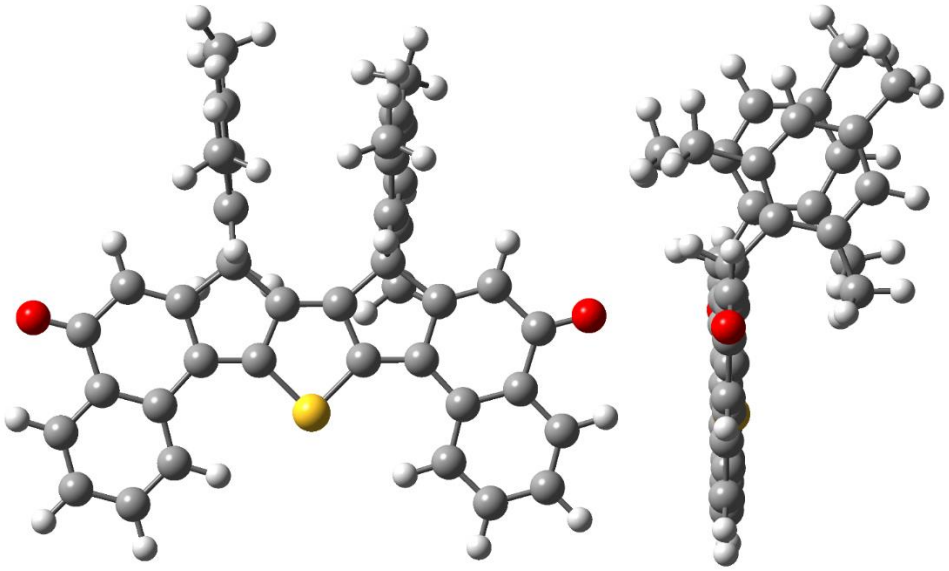

Figure 3A.13 Optimized structure of **6** (*syn*-conformation) top-view (left) and side-view (right).

Optimized closed-shell structure of 6 (*anti*-conformation)

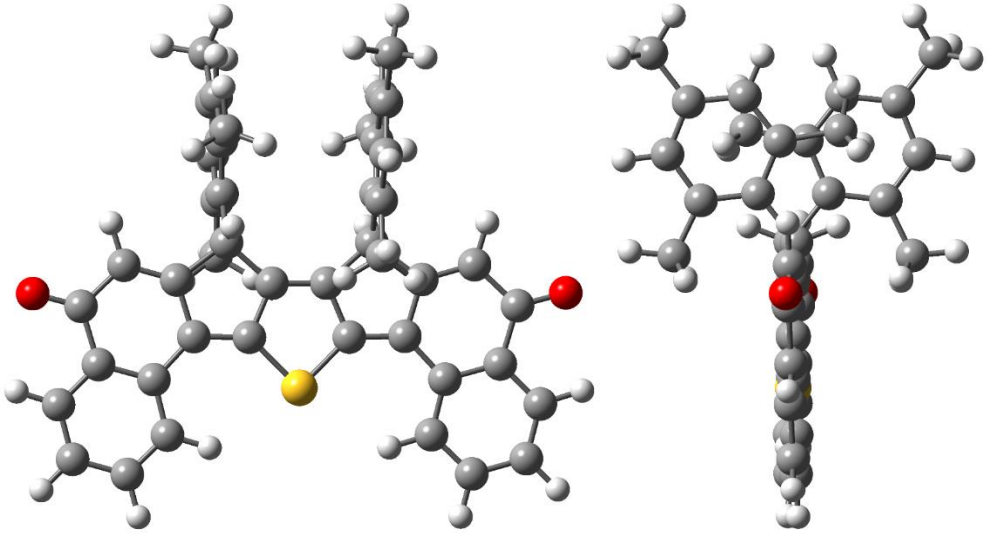

Figure 3A.14 Optimized structure of **6** (*anti*-conformation) top-view (left) and side-view (right).

Table 3A.4 Relative energies of **6** in *syn*- and *anti*-conformation.

Compound 6 (Conformation)	Hartree	kcal/mol
Syn	−2245.882714	−1409311.616
Anti	−2245.888517	−1409315.257

Compound 6: $\Delta E_{anti\text{-}syn}$ = −3.64 kcal/mol.

Table 3A.5 Relative energies of **6** and **7** in closed- and open-shell states.

Compounds	Optimization	Hartree	kcal/mol
6	Singlet closed-shell B3LYP/6-31G(d,p)	−2245.888517	−1409315.257
	Singlet open-shell UB3LYP/6-31G(d,p)	−2245.888517	−1409315.257
	Triplet open-shell UB3LYP/6-31G(d,p)	−2245.859131	−1409296.817
7	Singlet closed-shell B3LYP/6-31G(d,p)	−2244.657765	−1408542.949
	Singlet open-shell UB3LYP/6-31G(d,p)	−2244.657765	−1408542.949
	Triplet open-shell UB3LYP/6-31G(d,p)	−2244.627731	−1408524.103

Compound 6: $\Delta E_{\text{Triplet-Singlet}}$ = 18.4 kcal/mol.
Compound 7: $\Delta E_{\text{Triplet-Singlet}}$ = 18.8 kcal/mol.

3A.5 References

1. Limacher, P. A.; Lüthi, H. P. Cross-conjugation. *Wiley Interdiscip. Rev. Comput. Mol. Sci.* **2011**, *1*, 477−486.

2. Andrews, D. Q.; Solomon, G. C.; Van Duyne, R. P.; Ratner, M. A. Single Molecule Electronics: Increasing Dynamic Range and Switching Speed Using Cross-Conjugated Species. *J. Am. Chem. Soc.* **2008**, *130*, 17309–17319.

3. Jing, Y.; Liang, Y.; Gheytani, S.; Yao, Y. Cross-Conjugated Oligomeric Quinones for High Performance Organic Batteries. *Nano Energy* **2017**, *37*, 46–52.

4. (a) Matsuo, T.; Fure, H.; Sekiguchi, A. Isolation and characterization of the tetralithium salt of [5]radialene tetraanion stabilized by silyl groups. *Chem. Commun.* **1999**, 1981–1982. (b) Mackay, E. G.; Newton, C. G.; Toombs-Ruane, H.; Lindeboom, E. J.; Fallon, T.; Willis, A. C.; Paddon-Row, M. N.; Sherburn, M. S. [5]Radialene. *J. Am. Chem. Soc.* **2015**, *137*, 14653–14659.

5. G. Maas. Cross conjugation: Modern Dendralene, Radialene and Fulvene Chemistry (Eds.: H. Hopf, M. S. Sherburn). *Wiley-VCH, Weinheim* **2016**, 79–116.

6. Gholami, M.; Tykwinski, R. R. Oligomeric and Polymeric Systems with a Cross-conjugeated π-Framework. *Chem. Rev.* **2006**, *106*, 4997–5027.

7. (a) Jullien, J.; Pechine, J. M.; Perez, F.; Piade, J. J. Preparation and characterization of "furanoradialene" (tetramethylene-tetrahydrofuran) *Tetrahedron Lett.* **1980**, *21*,

611–612. (b) Trahanovsky, W. S.; Cassady, T. J. Preparation of furanoradialene by the flash vacuum pyrolysis of diesters of 3,4-bis(hydroxymethyl)-2,5-dimethylfuran. *J. Am. Chem. Soc.* **1984**, *106*, 8197–8201. (c) Münzel, N.; Kesper, K.; Schweig, A.; Specht, H. Detection of 2,5-dimethylene-2,5-dihydrothiophene and thiophenoradialene. *Tetrahedron Lett.* **1988**, *29*, 6239–6242. (d) Miyahara, I.; Hayashi, A.; Hirotsu, K.; Yoshifuji, M.; Yoshimura, H.; Toyota, K. The first x-ray analysis of a phospha[3]radialene *Polyhedron* **1992**, *11*, 385–387. (e) Mahieu, A.; Miquel, Y.; Igau, A.; Donnadieu, B.; Majoral, J.-P. Versatile Behavior of a New Class of Bicyclic Compounds: Zirconacyclopentadiene Phosphiranes *Organometallics* **1997**, *16*, 3086–3088. (f) Komen, C. M.; Horan, C. J.; Krill, S.; Gray, G. M.; Lutz, M.; Spek, A. L.; Ehlers, A. W.; Lammertsma, K. Phospha[3]radialenes. Syntheses, Structures, Strain Energies, and Reactions *J. Am. Chem. Soc.* **2000**, *122*, 12507−12516. (g) Urushizaki, A.; Yumura, T.; Kitagawa, Y.; Hasegawa, Y.; Imoto, H.; Naka, K. Dithieno[3,4-*b*:3′,4′-*d*]arsole: A Novel Class of Hetero[5]radialenes. *Eur. J. Org. Chem.* **2020**, *2020*, 3965–3970. (h) Higashino, T.; Imahori, H. Hybrid [5]Radialenes with Bispyrroloheteroles: New Electron-Donating Units. *Chem. – Eur. J.* **2015**, *21*, 13375−13381. (i) Janssen, M. J.; De Jong, F. Synthesis, Oxidation, and Electronic Spectra of Four Dithienothiophenes. *J. Org. Chem.* **1971**, *36*, 1645–1648. (j) Iyoda, M.; Miura, M. I.; Sasaki, S.; Kabir, S. M. H.; Kuwatani, Y.; Yoshida, M. Synthesis of dithienothiophenes, cyclopentadithiophene and silacyclopentadithiophenes using palladium-catalyzed cyclization *Tetrahedron Lett.***1997**, *38*, 4581−4582. (k) Brieden, W.; Kellersohn, T. Synthesis and Crystal Structure of the First “1,2-Diphospha[4]radialene. *Chem. Ber*. **1993**, *126*, 845–847.

8. Berionni, G.; Wu, J. I. C.; Schleyer, P. v. R. Aromaticity Evaluations of Planar [6]Radialenes. *Org. Lett.* **2014**, *16*, 6116–6119.

9. Shi, X., Chi, C., Heterocyclic Quinodimethanes. *Top. Curr. Chem.* **2017**, *375*, 68.

10. Zeng, Z.; Shi, X.; Chi, C.; Lopez Navarrete, J. T.; Casado, J.; Wu, J. Pro-aromatic and anti-aromatic π-conjugated molecules: an irresistible wish to be diradicals. *Chem. Soc. Rev.* **2015**, *44*, 6578–6596.

11. (a) Rudebusch, G. E.; Fix, A. G.; Henthorn, H. A.; Vonnegut, C. L.; Zakharov, L. N.; Haley, M. M., Quinoidal diindenothienoacenes: synthesis and properties of new functional organic materials *Chem. Sci*. **2014**, *5*, 3627–3633. (b) Shi, X.; Burrezo, P.

M.; Lee, S.; Zhang, W.; Zheng, B.; Dai, G.; Chang, J.; López Navarrete, J. T.; Huang, K.-W.; Kim, D.; Casado, J.; Chi, C, Antiaromatic bisindeno-[*n*]thienoacenes with small singlet biradical characters: syntheses, structures and chain length dependent physical properties *Chem. Sci*. **2014**, *5*, 4490–4503.

12. Marshall, J. L.; Lehnherr, D.; Lindner, B. D.; Tykwinski, R. R. Reductive Aromatization/Dearomatizationand Elimination Reactions to Access Conjugated Polycyclic Hydrocarbons, Heteroacenes, and Cumulenes. *ChemPlusChem* **2017**, *82*, 967–1001.

13. (a) Hu, P.; Lee, S.; Park, K. H.; Das, S.; Herng, T. S.; Gonçalves, T. P.; Huang, K.-W.; Ding, J.; Kim, D.; Wu, J. Octazethrene and Its Isomer with Different Diradical Characters and Chemical Reactivity: The Role of the Bridge Structure. *J. Org. Chem.***2016**, *81*, 2911–2919. (b) Hayashi, H.; Barker, J. E.; Cárdenas Valdivia, A.; Kishi, R.; MacMillan, S. N.; Gómez-García, C. J.; Miyauchi, H.; Nakamura, Y.; Nakano, M.; Kato, S.; Haley, M. M.; Casado, J. Monoradicals and Diradicals of Dibenzofluoreno[3,2-*b*]Fluorene Isomers: Mechanisms of Electronic Delocalization. *J. Am. Chem. Soc.* **2020**, *142*, 20444–20455.

14. (a) Takahashi, K.; Suzuki, T.; Akiyama, K.; Ikegami, Y.; Fukazawa, Y. Synthesis and characterization of novel *p*-terphenoquinone analogs involving a central dihydrothiophenediylidene structure. *J. Am. Chem. Soc.* **1991**, *113*, 4576–4583. (b) Takahashi, K.; Suzuki, T. *p*-Diphenoquinone analogs extended by dihydrothiophenediylidene insertion. A novel amphoteric multistage redox system *J. Am. Chem. Soc.* **1989**, *111*, 5483–5485. (c) Kazuko, T.; Atsushi, G.; Kimio,A. Novel Amphoteric 2,5-Furoquinonoid-Containing *p*-Terphenoquinone Analogues Giving Both a Stable Radical Anion and a Stable Radical Cation *Chem. Lett.* **1994**, *23*, 863–866.

15. Kazuko, T.; Sakai, T. Substituent Effects on Redox Potentials of Novel Amphoteric Terphenoquinone Analogues. Unsymmetrically Substituted 2,5-Bis(4-oxo-2,5-cyclohexadien-1-ylidene)-2,5-dihydrothiophenes. *Chem. Lett.* **1993**, *22*, 157–160.

16. Phelan, N. F.; Orchin, M. Cross conjugation. *J. Chem. Educ.* **1968**, *45*, 633–637.

17. Fallah-Bagher-Shaidaei, H.; Wannere, C. S.; Corminboeuf, C.; Puchta, R.; Schleyer, P. v. R., Which NICS aromaticity index for planar π rings is best? *Org. Lett.* **2006**, *8*, 863–866.

18. Lu, T.; Chen F., Multiwfn: A multifunctional wavefunction analyzer. *J. Comput. Chem.* **2012**, *33*, 580–592.

19. Geuenich, D.; Hess, K.; Köhler, F.; Herges, R. Anisotropy of the Induced Current Density (ACID), a General Method To Quantify and Visualize Electronic Delocalization. *Chem. Rev.* **2005**, *105*, 3758–3772.

20. van Pham, C.; Macomber, R. S.; Mark, H. B., Jr.; Zimmer, H. Lithiation reaction of 2, 5-dibromothiophene. 13C NMR spectra of 3-substituted derivatives. *J. Org. Chem.* **1984**, *49*, 5250–5253.

21. Casado, J.; Ponce Ortiz, R. P.; Lopez Navarrete, J. T. Quinoidal oligothiophenes: new properties behind an unconventional electronic structure. *Chem. Soc. Rev.* **2012**, *41*, 5672–5686.

22. Baron, P. A.; Brown, R. D.; Burden, F. R.; Domaille, P. J.; Kent, J. E. The microwave spectrum and structure of fulvene *J. Mol. Spectrosc.* **1972**, *43*, 401–410.

23. Sharma, P. K.; Mallick, D.; Sharma, H.; Das, S. Dominating Antiaromatic Character of *as*-Indacene Decides Overall Properties of a Formally Aromatic Dicyclopenta[*c*]fluorenothiophene *Org. Lett.* **2023**, *25*, 2201–2206.

24. Fargher, H. A.; Sherbow, T. J.; Haley, M. M.; Johnson, D. W.; Pluth, M. D. C–H··· S hydrogen bonding interactions *Chem. Soc. Rev.* **2022**, *51*, 1454–1469.

25. Taniguchi, M.; Lindsey, J. S. Database of Absorption and Fluorescence Spectra of > 300 Common Compounds for use in PhotochemCAD, *Photochem. Photobiol.* **2018**, *94*, 290–327.

26. (a) Rosenberg, M.; Dahlstrand, C.; Kilså, K.; Ottosson, H. Excited State Aromaticity and Antiaromaticity: Opportunities for Photophysical and Photochemical Rationalizations. *Chem. Rev.* **2014**, *114*, 5379–5425. (b) Grzybowski, M.; Morawski, O.; Nowak, K.; Garbacz, P. Fluorene analogues of xanthenes–low molecular weight near-infrared dyes *Chem. Commun.* **2022**, *58*, 5455–5458.

27. Chase, D. T.; Fix, A. G.; Rose, B. D.; Weber, C. D.; Nobusue, S.; Stockwell, C. E.; Zakharov, L. N.; Lonergan, M. C.; Haley, M. M. Electron-Accepting 6,12-Diethynylindeno[1,2-*b*]fluorenes: Synthesis, Crystal Structures, and Photophysical Properties *Angew. Chem. Int. Ed.* **2011**, *50*, 11103–11106.

28. Gleiter, R.; Röckel, H.; Irngartinger, H.; Oeser, T. Efficient Synthesis of Heteroradialenes by SN′ Reaction *Angew. Chem., Int. Ed. Engl.* **1994**, *33*, 1270–1272.

29. (a) Krygowski, T. M.; Oziminski, W. P.; Palusiak, M.; Fowler, P. W.; McKenzie, A. D. Aromaticity of substituted fulvene derivatives: substituent-dependent ring currents *Phys. Chem. Chem. Phys.* **2010**, *12*, 10740−10745. (b) Preethalayam, P.; Krishnan, K. S.; Thulasi, S.; Chand, S. S.; Joseph, J.; Nair, V.; Jaroschik, F.; Radhakrishnan, K. V. Recent advances in the chemistry of pentafulvenes, *Chem. Rev.* **2017**, *117*, 3930–3989.

30. Patra, A.; Bendikov, M. Polyselenophenes *J. Mater. Chem.* **2010**, *20*, 422–433.

31. (a) Higashino, T.; Mori, T. Small-molecule ambipolar transistors *Phys. Chem. Chem. Phys.* **2022**, *24*, 9770–9806. (b) Sharma, H.; Ankita, A.; Bhardwaj, P.; Pandey, U. K.; Das, S. Exploring Indeno[2,1-*c*]fluorene Antiaromatics with Unsymmetrical Disubstitution and Balanced Ambipolar Charge-Transport Properties. *Organic Materials*, **2023**, *5*, 72–83.

32. Chen, C. -H.; Hsieh, C. -H.; Dubosc, M.; Cheng, Y. -J.; Hsu, C. -S. Synthesis and Characterization of Bridged Bithiophene-Based Conjugated Polymers for Photovoltaic Applications: Acceptor Strength and Ternary Blends. *Macromolecules*, **2010**, *43*, 697–708.

33. Bruker, SAINT V8.38A, (Bruker AXS Inc., **2017**).

34. Dolomanov, O. V.; Bourhis, L. J.; Gildea, R. J.; Howard, J. A.; Puschmann, H. Olex2: A complete structure solution, refinement and Analysis Program. *J. Appl. Crystallogr.* **2009**, *42*, 339–341.

35. Bourhis, L. J.; Dolomanov, O. V.; Gildea, R. J.; Howard, J. A.; Puschmann, H. The anatomy of a comprehensive constrained, restrained refinement program for the modern computing environment –olex2dissected. *Acta Crystallogr. A.* **2015**, *71*, 59–75.

36. Sheldrick, G. M. Crystal structure refinement with SHELXL, *Acta Crystallogr. C Struct. Chem.* **2015**, *71*, 3–8.

37. Gaussian 09, *Revision B.01*, Frisch, M. J.; Trucks, G. W.; Schlegel, H. B.; Scuseria, G. E.; Robb, M. A.; Cheeseman, J. R.; Scalmani, G.; Barone, V.; Mennucci, B.; Petersson, G. A.; Nakatsuji, H.; Caricato, M.; Li, X.; Hratchian, H. P.; Izmaylov, A. F.; Bloino, J.; Zheng, G.; Sonnenberg, J. L.; Hada, M.; Ehara, M.; Toyota, K.; Fukuda, R.; Hasegawa, J.; Ishida, M.; Nakajima, T.; Honda, Y.; Kitao, O.; Nakai, H.; Vreven, T.; Montgomery, J. A.; Jr., Peralta, J. E.; Ogliaro, F.; Bearpark, M.; Heyd, J. J.; Brothers, E.; Kudin, K. N.; Staroverov, V. N.; Keith, T.; Kobayashi, R.; Normand, J.;

Raghavachari, K.; Rendell, A.; Burant, J. C.; Iyengar, S. S.; Tomasi, J.; Cossi, M.; Rega, N.; Millam, J. M.; Klene, M.; Knox, J. E.; Cross, J. B.; Bakken, V.; Adamo, C.; Jaramillo, J.; Gomperts, R.; Stratmann, R. E.; Yazyev, O.; Austin, A. J.; Cammi, R.; Pomelli, C.; Ochterski, J. W.; Martin, R. L.; Morokuma, K.; Zakrzewski, V. G.; Voth, G. A.; Salvador, P.; Dannenberg, J. J.; Dapprich, S.; Daniels, A. D.; Farkas, O.; Foresman, J. B.; Ortiz, J. V.; Cioslowski, J; Fox, D. J. Gaussian, Inc., Wallingford CT, **2010**.

38. O'boyle, N. M.; Tenderholt, A. L.; Langner, K. M. cclib: A library for package-independent computational chemistry algorithms. *J. Comput. Chem*. **2008**, *29*, 839–845.

3A.6 Appendix

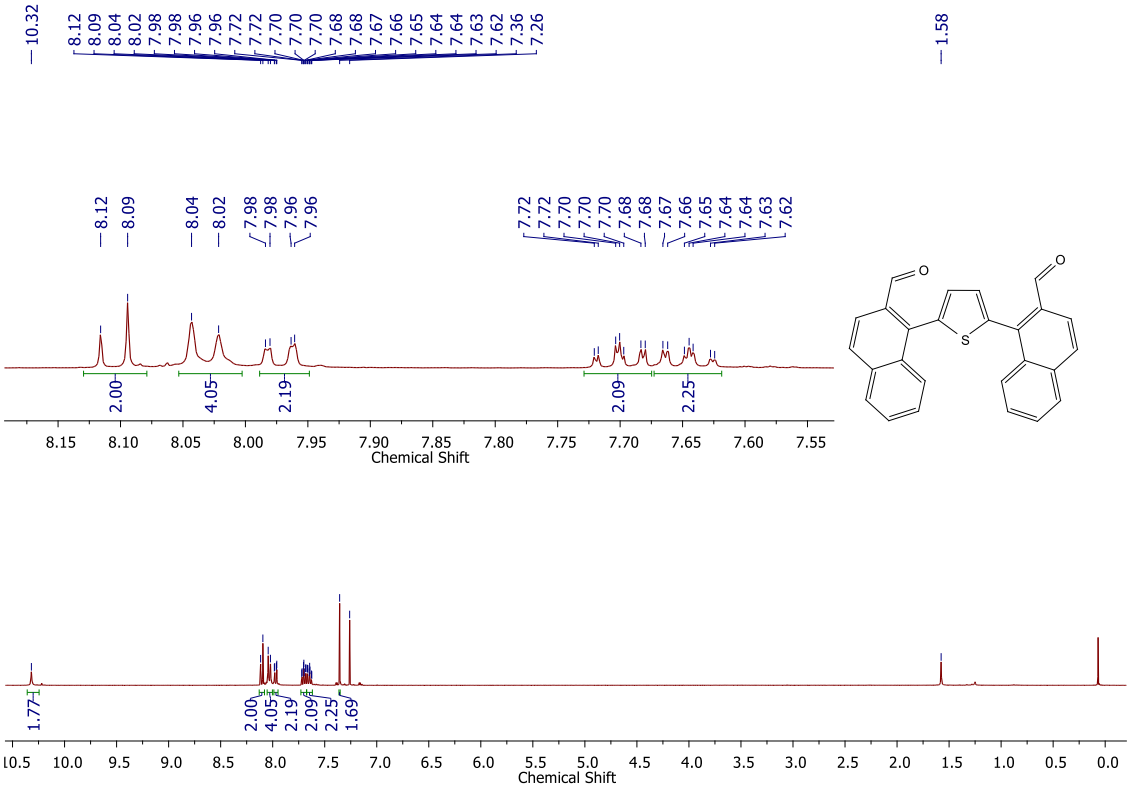

Figure 3A.15 ^{1}H NMR spectrum of **10** (in $CDCl_3$, 400 MHz, 298 K).

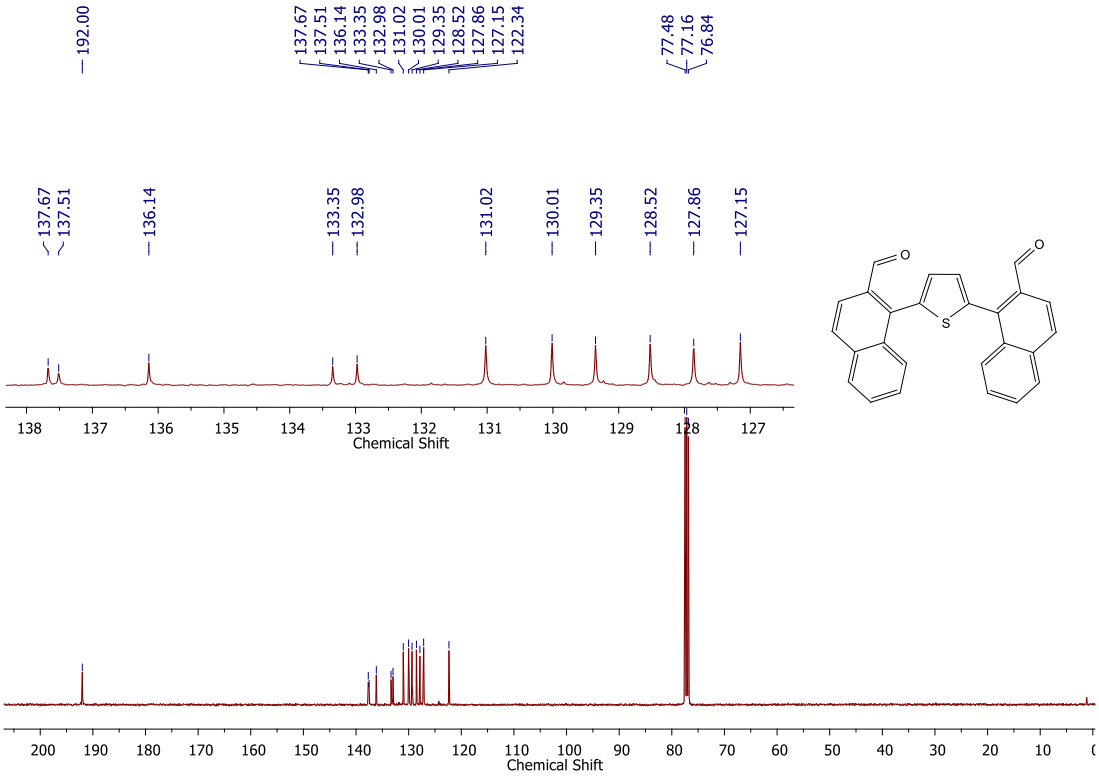

Figure 3A.16 $^{13}C\{^{1}H\}$ NMR spectrum of **10** (in $CDCl_3$, 100 MHz, 298 K).

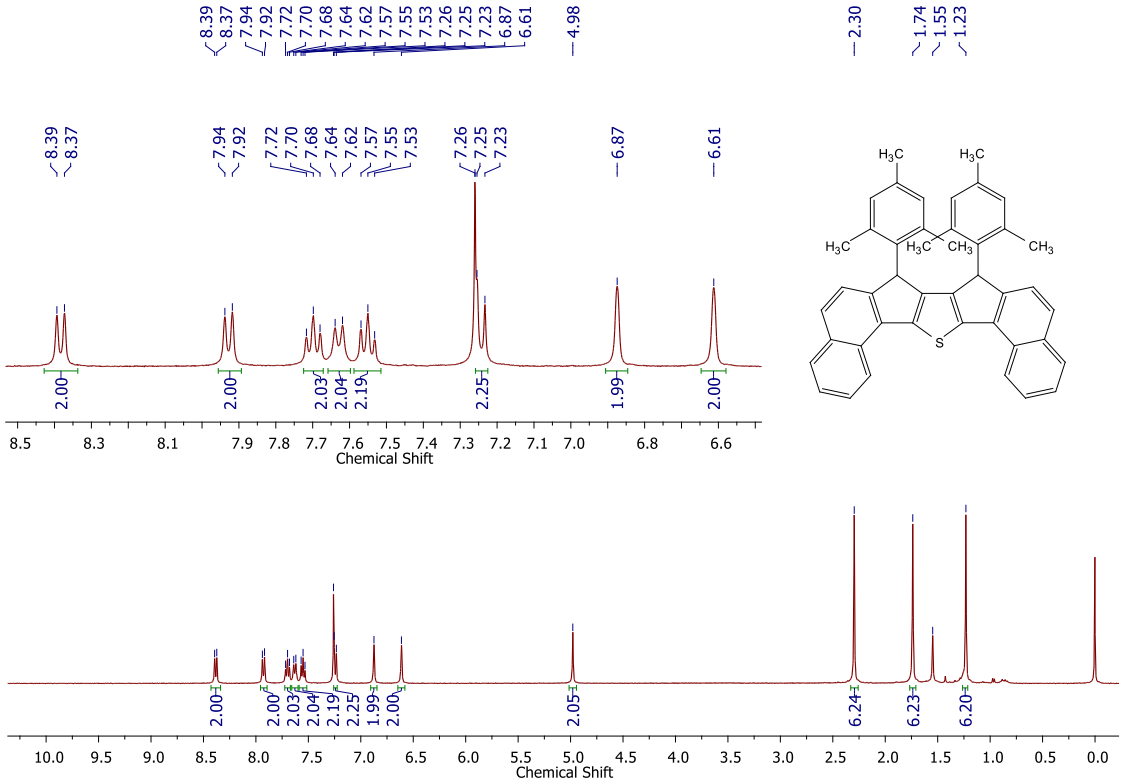

Figure 3A.17 ^{1}H NMR spectrum of **4** (in $CDCl_3$, 400 MHz, 298 K).

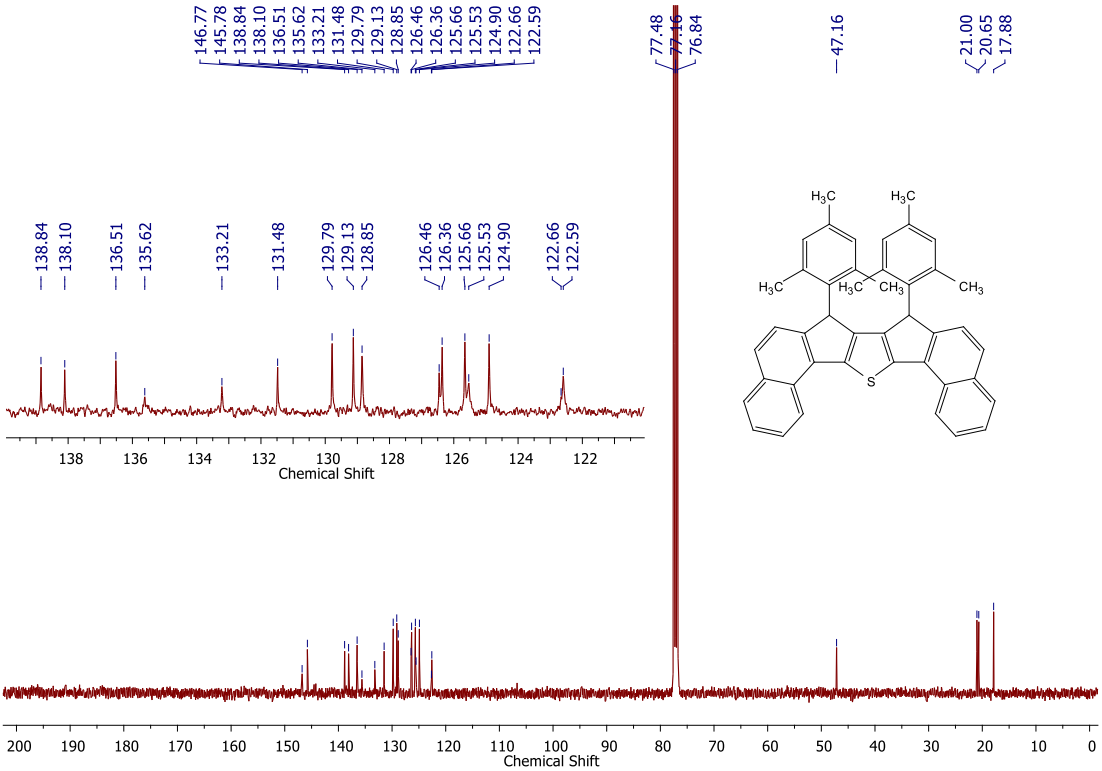

Figure 3A.18 $^{13}C\{^{1}H\}$ NMR spectrum of **4** (in $CDCl_3$, 100 MHz, 298 K).

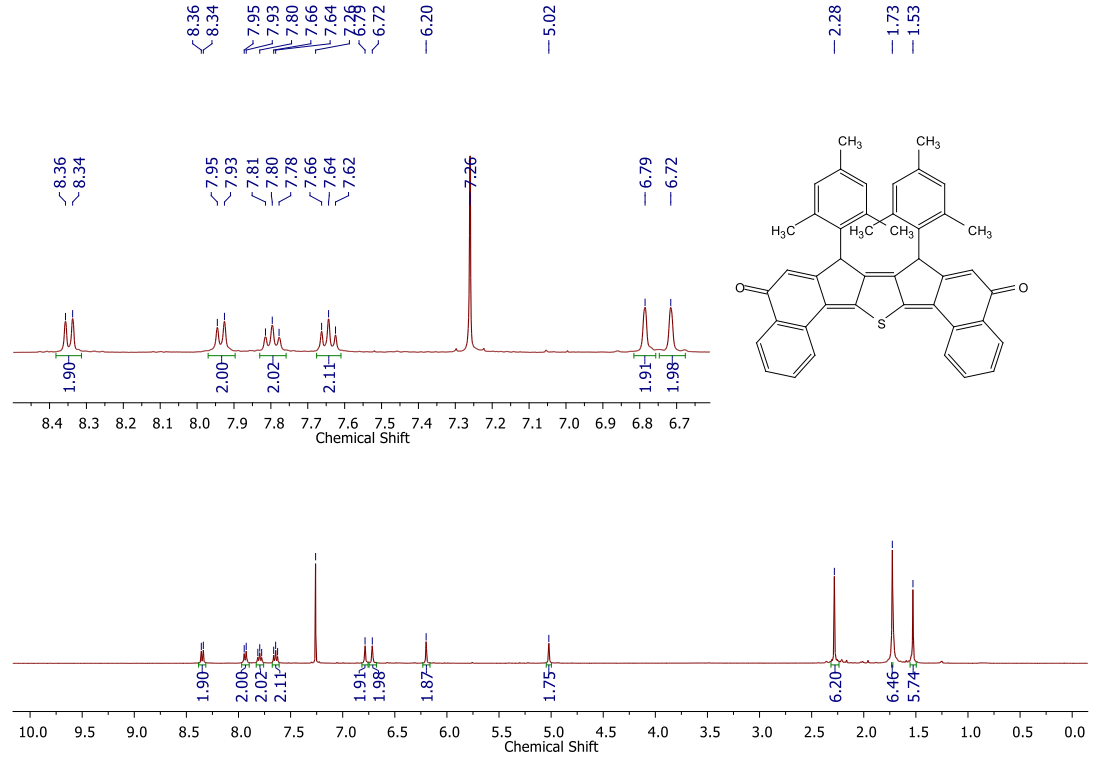

Figure 3A.19 ^{1}H NMR spectrum of **6** (in $CDCl_3$, 400 MHz, 298 K).

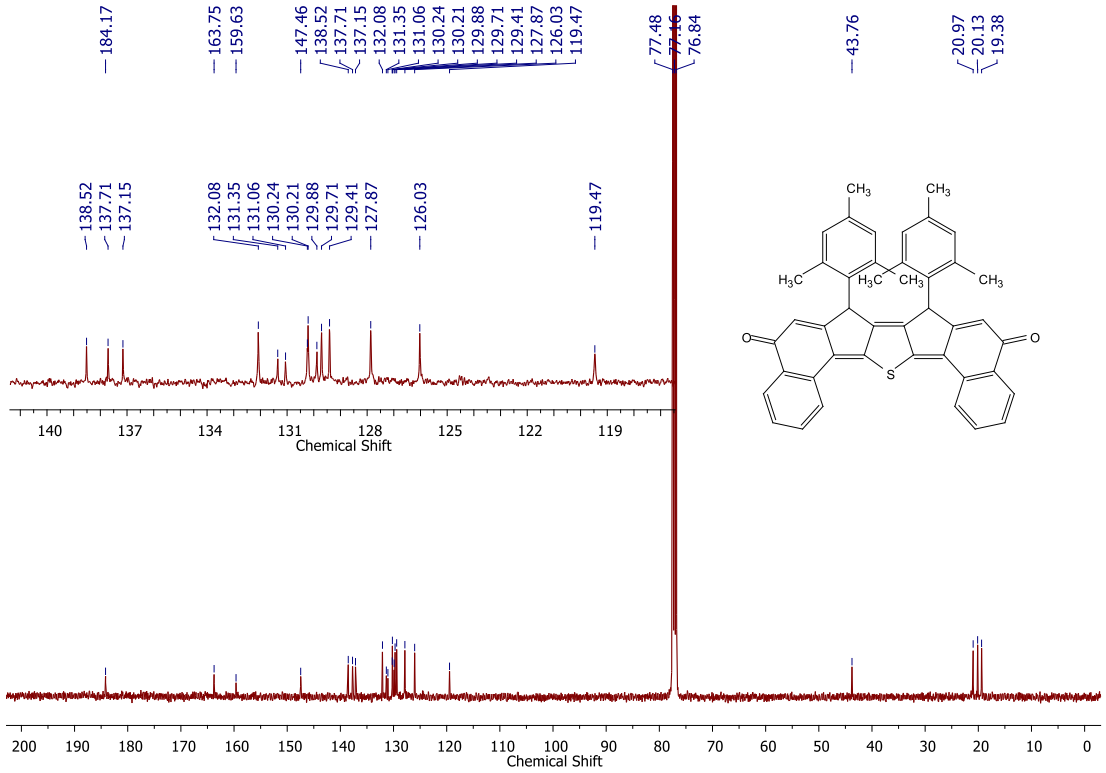

Figure 3A.20 $^{13}C\{^{1}H\}$ NMR spectrum of **6** (in $CDCl_3$, 100 MHz, 298 K).

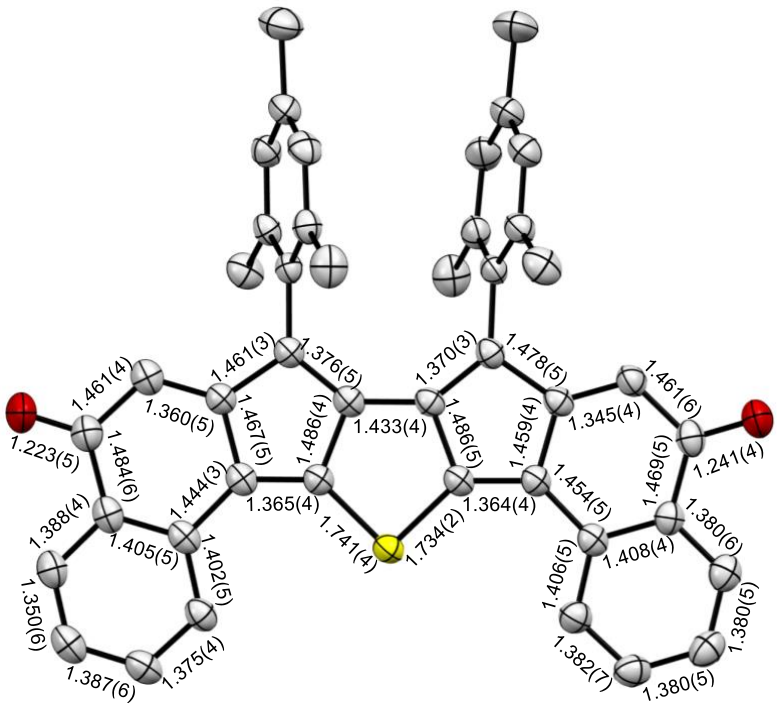

Figure 3A.21 ORTEP drawing of **7** with thermal ellipsoids at 30% probability level, showing the core bond lengths with e.s.d values.

Chapter 3B

Cyano Disubstituted Tetrabenzoindeno[2,1-*a*]fluorene: Open-shell or Closed-shell?

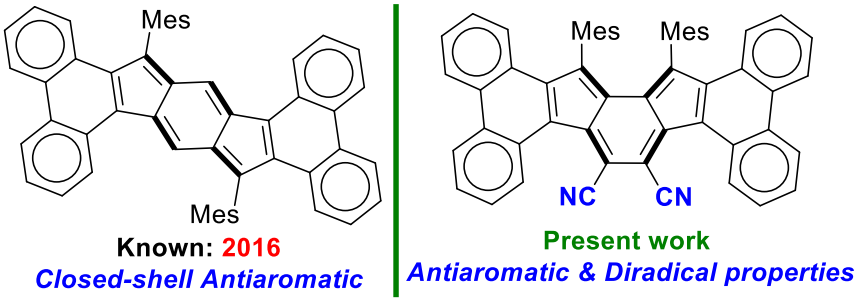

This work was published in *Chemical Communications* (an RSC journal). Please see the citation as: "Sharma, P. K., Jana P., Bandyopadhyay, S., Das, S. Cyano Disubstituted Tetrabenzoindeno[2,1-*a*]fluorene: Open-shell or Closed-shell?. *Chem. Commun.* **2024,** *60*, 7319–7322."

3B Abstract

Organic diradicaloids have lately emerged as potential spintronic materials. We report the unprecedented synthesis of a near-IR absorbing indeno[2,1-*a*]fluorene derivative that displayed remarkably low LUMO (–4.15 eV) and a small HOMO–LUMO energy gap (0.85 eV). NMR/EPR studies indicated its open-shell diradical property, which was supported by DFT calculations while suggesting a 30% diradical character and a small singlet (S)-triplet (T) gap (–2.52 kcal/mol). A large bond length alternation of the *as*-indacene core for its single-crystals indicated a quinoidal contribution with greater antiaromaticity, which is in line with the small diradical character despite showing a small S-T gap.

3B.1 Introduction

Exploration of polycyclic hydrocarbons (PHs) with antiaromatic and diradical properties has attracted immense interest in recent years,[1] as tuning such properties may provide paths toward new organic semiconductor materials with tunable band gaps. As mentioned in Chapter 1, formally antiaromatic indeno[1,2-*b*]fluorene[2] **1** and indeno[2,1-*a*]fluorene[3] **2** regioisomers are stable closed-shell (CS) molecules that displayed moderate antiaromaticity for the central *s*-indacene and *as*-indacene units,[4] respectively (Figure 3B.1a). Unsymmetrical disubstitution of [2,1-*a*]IF also resulted in a stable CS molecule **3**,[5] but benzo-extension of the central *as*-indacene unit of [2,1-*a*]IF afforded an open-shell (OS) molecule **benzo-2** with large diradical character index (y_0 = 0.63), likely causing instability (half-life 77 min) and 8% synthetic yield.[6]

In continuation of efforts[7] to synthesize the elusive arene-fused dicyclopenta[*b*,*d*]thiophene (DCPT),[7a,7b] a diphenanthro-DCPT (**DPDCPT**) derivative was targeted (Figure 3B.1b). While attempting its synthesis by a DDQ (2,3-dichloro-5,6-dicyano-1,4-benzoquinone) mediated dehydrogenation from dihydro precursor **2H-DPDCPT**, we failed to isolate it presumably due to the high reactivity (electron-rich, large y_0 = 0.51, and a small singlet-triplet energy gap ($\Delta E_{S\text{-}T}$) = –0.64 kcal/mol; Table 3B.4), as analysed by density functional theory (DFT) calculation. Instead, we isolated a cyano disubstituted tetrabenzoindeno[2,1-*a*]fluorene **6** (Figure 3B.1b) as a degradation product, and it was confirmed by the single-crystal X-ray diffraction (SCXRD) analysis (*vide infra*). Isolation of **6** was interesting since there is no straightforward synthetic approach known thus far to construct **5**, which is a

constitutional isomer of known tetrabenzoindeno[1,2-*b*]fluorene **4**,[8] that displays a greater degree of antiaromaticity for the *s*-indacene unit than that of **1**. Our DFT optimization of **5** indicated its CS ground state, like **4**, and its OS singlet state was found to be isoenergetic with the CS state with a small $\Delta E_{S\text{-}T}$ = –3.46 kcal/mol (Table 3B.4). A lowering of triplet state for **5**, despite showing a negligible diradical character (y_0 = 0.01), is in line with a recent report[9] by Ottosson and Solà *et al*. explaining diphenanthro-fused antiaromatics (pentalene, *s*-indacene) may display low-lying triplet states. Despite the lowering of the triplet excited state, **5** didn't show an OS ground state, theoretically.

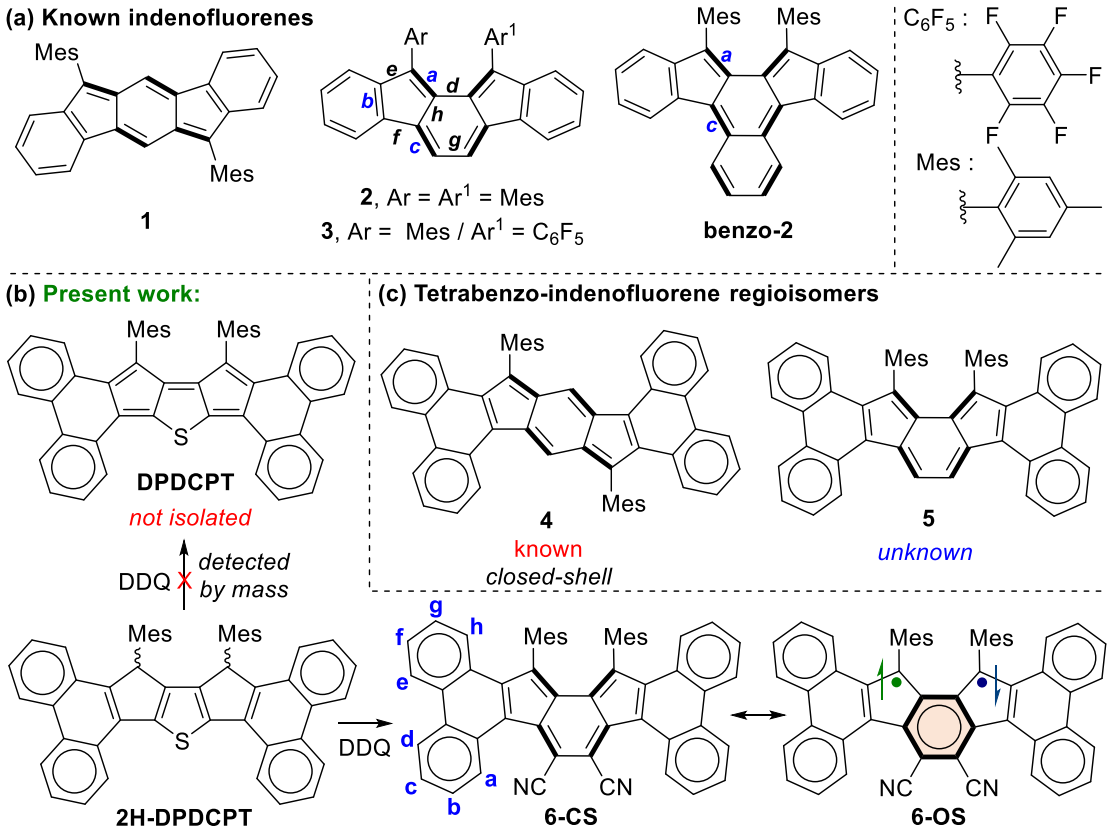

Figure 3B.1 (a) Indeno[1,2-*b*]fluorene **1**, indeno[2,1-*a*]fluorenes **2** & **3**, benzo-fused [2,1-*a*]IF **benzo-2**; (b) Targeted diphenanthro-DCPT, and the synthesized tetrabenzoindeno[2,1-*a*]fluorene **6** and its resonance forms; (c) tetrabenzoindeno[1,2-*b*]fluorene and tetrabenzoindeno[2,1-*a*]fluorene regioisomers.

We envisaged that the cyano (-CN) substituents for **6** may result in a smaller HOMO−LUMO energy spacing than that of **5**, seemingly due to the greater stabilization effect exerted by electron-withdrawing -CN groups (negative resonance effect) which are attached to *as*-indacene carbons containing large LUMO coefficients (Figure 3B.2).[10] A small HOMO–LUMO energy gap is crucial to show an OS ground

state, as evident from CS heptazethrene-triisopropylsilylethynyl (**HZ-TIPS**)[11] *vs* OS heptazethrene-dicarboximide (**HZ-DI**),[12] though the number of Clar sextet recoveries remains the same for them. Therefore, in this work, compound **6** was thoroughly studied by various analytical techniques and DFT calculations to conclude its electronic ground state, while reporting its unprecedented synthesis.

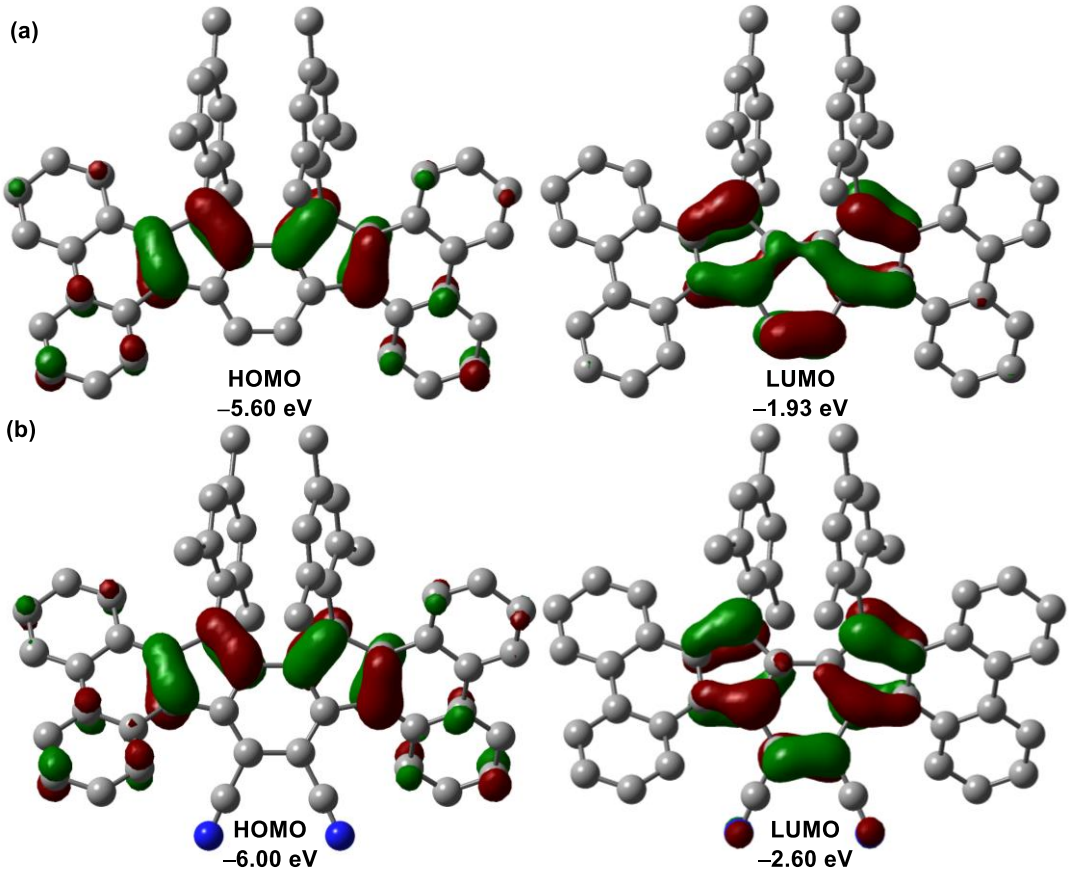

Figure 3B.2 Highest occupied and lowest unoccupied molecular orbital (HOMO and LUMO) profiles (isovalue 0.04) of (a) **5** and (b) **6**, calculated at BHandHLYP/6-31G(d).

3B.2 Results and Discussion

3B.2.1 Syntheses. Suzuki coupling between commercially available **7** and 2,5-dibromothiophene-3,4-dicarbaldehyde **8**,[13] as depicted in Scheme 3B.1, afforded dialdehyde derivative **9**. Treatment of **9** with 2-mesitylmagnesium bromide afforded a diol intermediate, which was subsequently treated with $BF_3{\cdot}Et_2O$ to give **2H-DPDCPT**, which is the dihydro precursor of **DPDCPT**. DDQ-mediated oxidative dehydrogenation of **2H-DPDCPT** in dichloromethane (DCM) remained partially complete, even after refluxing or increasing the reaction time, as monitored by thin

layer chromatography. To ensure complete conversion, 4 equiv. DDQ was added, and the reactant was consumed within 30 minutes at room temperature (rt). The formation of targeted **DPDCPT** could be detected from crude reaction mixture by direct mass spectrometric (MS) analysis (Figure 3B.21), but unfortunately, no desired product traces was obtained after traditional silica gel column chromatography; instead, **DPDCPT-DDQ** was isolated as a 10+2 cycloaddition adduct,[14] likely due to the reaction of **DPDCPT** and DDQ on silica surface (Scheme 3B.2). The **DPDCPT-DDQ** adduct was successfully characterized using ^{1}H NMR, ^{13}C NMR, (Figure 3B.3 and 3B.4) and HRMS analysis (Figure 3B.22). However, the **DPDCPT-DDQ** adduct was unstable and had low solubility.

Treatment of silica gel with triethylamine, prior to loading the slurry of crude reaction mixture containing DDQ, afforded a deep purple solid in 42% yield. However, the high-resolution mass (*m/z* = 739.3099) didn't match the desired mass of **DPDCPT**. It was found to be an unexpected product **6** after SCXRD analysis of the purple solid (Figure 3B.5), plausibly formed by the loss of sulfur atom and O=C=C(Cl)C(Cl)=C=O unit from the **DPDCPT-DDQ** adduct on neutral silica gel or alumina column (Scheme 3B.2).[14b,14c] Nonetheless, **6** is the first diphenanthro-*as*-indacene derivative with *ortho*-quinoidal backbone, which is a structural isomer of **4**.

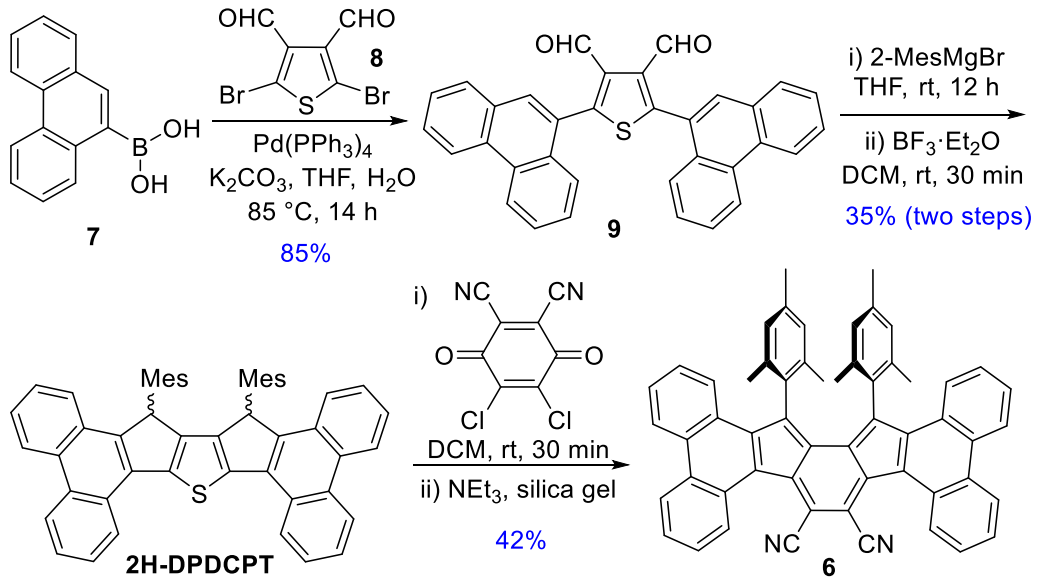

Scheme 3B.1 Synthesis of **6**.

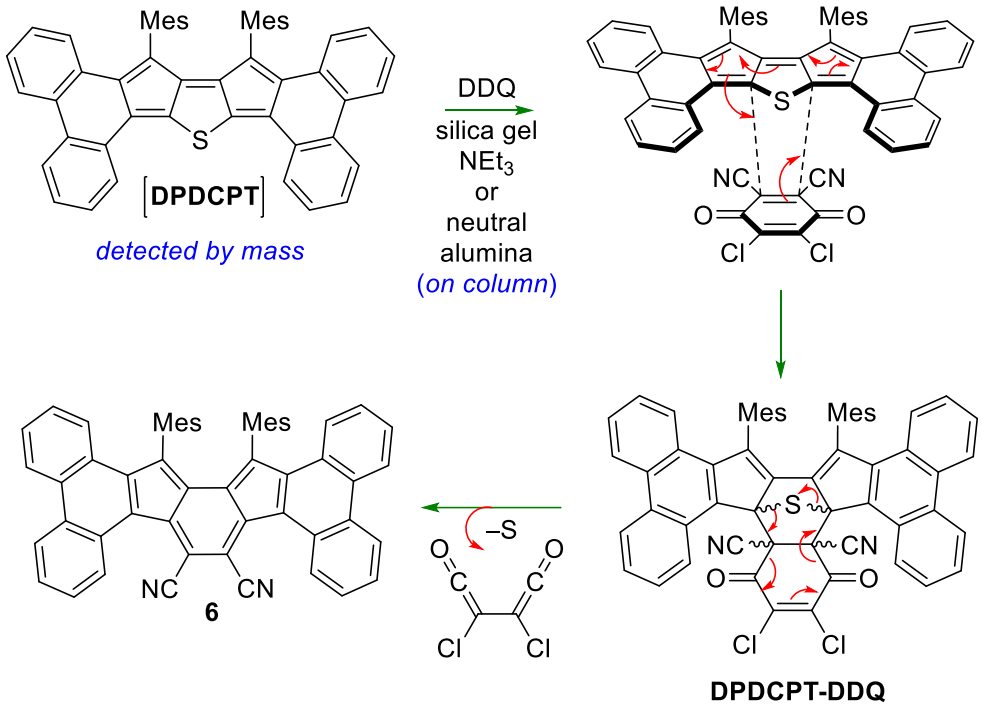

Scheme 3B.2 Plausible mechanism for the conversion of intermediate **DPDCPT** to **6** via an intermediate 10+2 cycloadduct **DPDCPT-DDQ** during column chromatographic purification using triethylamine treated silica or neutral alumina stationary phase.

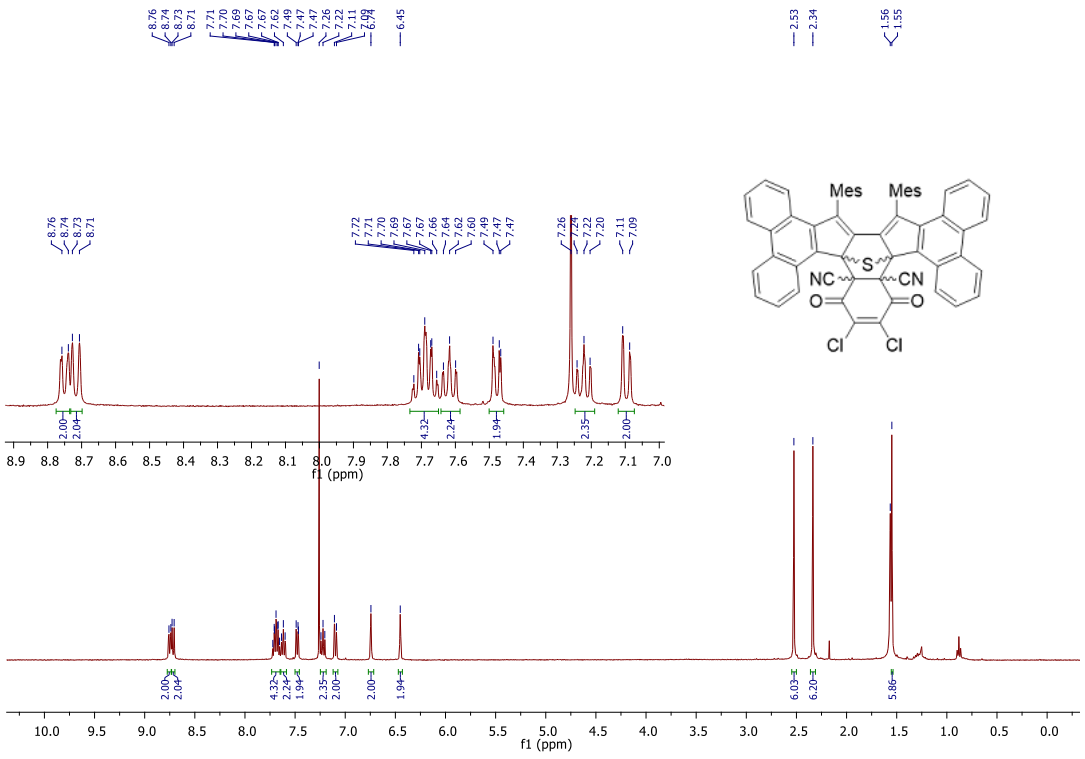

Figure 3B.3 ^{1}H NMR spectrum of **DPDCPT-DDQ** ($CDCl_3$, 400 MHz, 298 K).

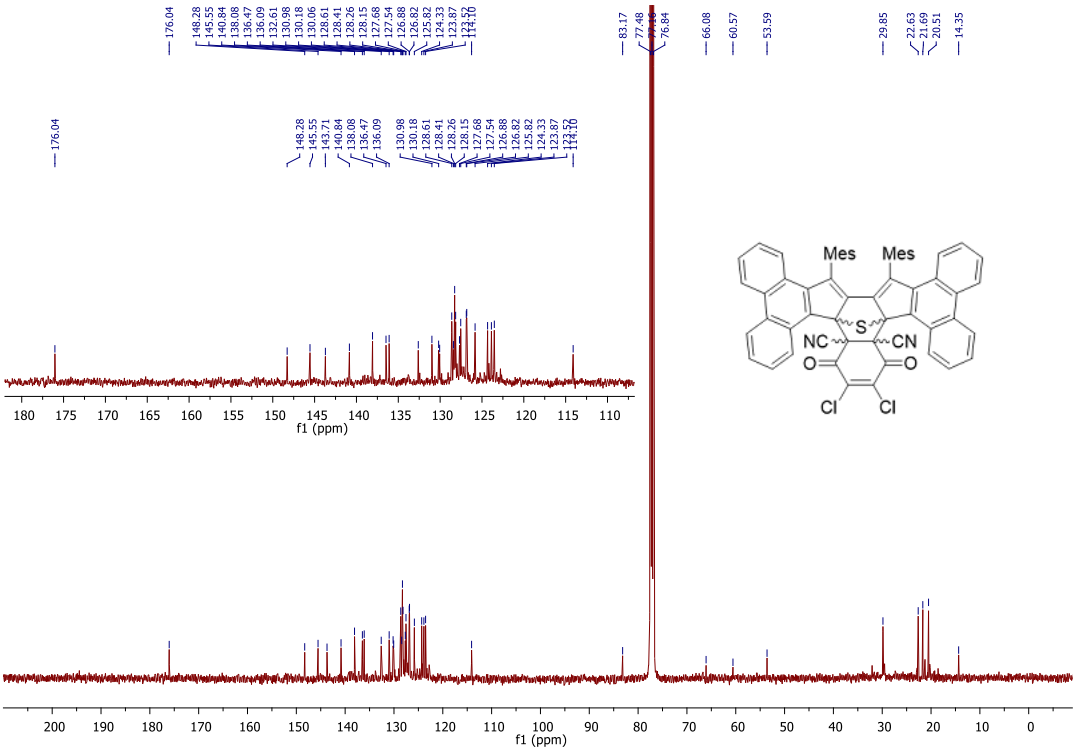

Figure 3B.4 $^{13}C\{^{1}H\}$ NMR of **DPDCPT-DDQ** ($CDCl_3$, 100 MHz, 298 K) (residual hexanes: 14.35, 29.85).

3B.2.2 X-ray crystallography and (anti)aromaticity analyses. The single crystals of **6** were grown in a DCM/acetonitrile mixture (Figure 3B.5a). SCXRD analysis of **6** revealed a contorted π- backbone (Figure 3B.5b) due to the steric congestion between the -CN group and ring-C hydrogen in the cove region and repulsive interaction between bulky mesityl groups, which are orthogonal to the IF backbone. The terminal phenanthrene units were twisted by an avg. torsional angle of 30.1°, as measured from the mean planes between central ring E and outer phenanthrene units. The C–C double bond *b* linking *as*-indacene and phenanthrene unit and the *exo*-methylene bond *a* for **6** are 0.032 Å and 0.016 Å, respectively, shorter than those of **2** (Figure 3B.5a and Table 3B.1). The C–C single bonds *d*-*h* for **6** possess more single bond character (1.455 to 1.491 Å), with *e* and *g* bonds 0.016 and 0.037 Å longer than those of **2**. The degree of bond length alternation (BLA) in the *as*-indacene unit has significantly enhanced for **6** in comparison to **2**, suggesting a reduced extent of π-delocalization for the *as*-indacene core in **6**, indicating a greater degree of antiaromaticity for **6** than that of **2**. On the other hand, homogeneous bond length distribution for rings A (avg. 1.394 Å) and C (avg. 1.393 Å) in **6** suggested a greater degree of benzene-like aromaticity than that of ring B (avg. 1.425 Å).

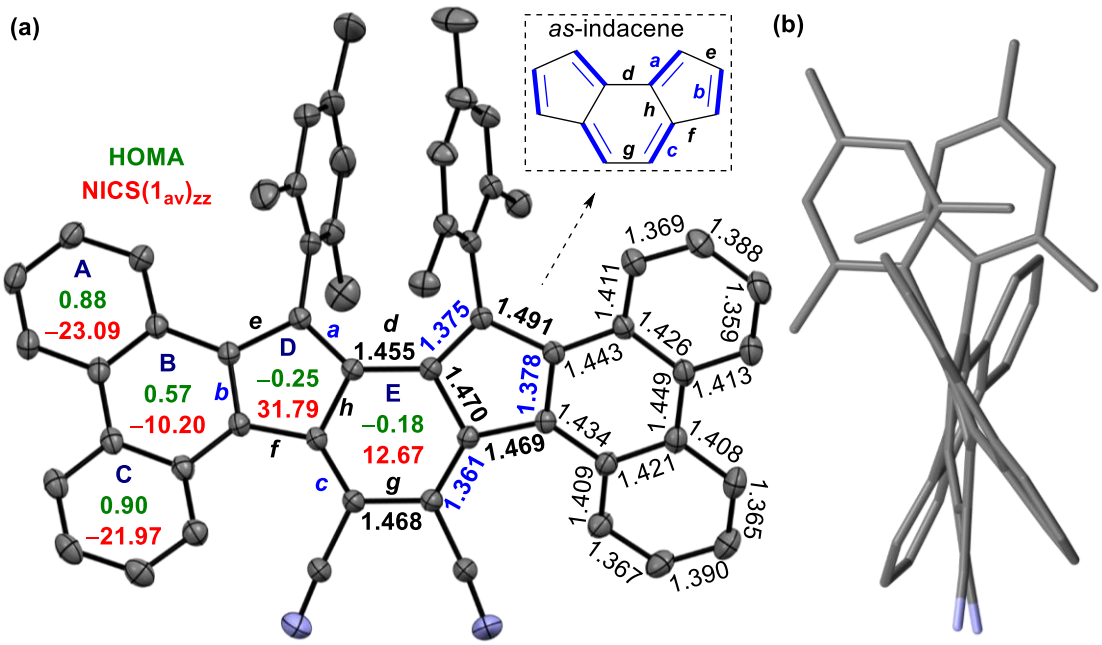

Figure 3B.5 (a) ORTEP drawing of **6** with thermal ellipsoids at the 30% probability level (hydrogens and disordered solvent omitted), including the mean bond lengths (in angstroms), NICS(1)$_{zz}$ (red) and HOMA (green) indices; (b) Side view of **6** showing non-planar backbone.

Table 3B.1 Mean $C_{sp}{}^2$–$C_{sp}{}^2$ bond lengths (*a*-*h*, in Å) of **6** *vs* **2**, for *as*-indacene unit.

Compd.	*a*	*b*	*c*	*d*	*e*	*f*	*g*	*h*
6	1.375	1.378	1.361	1.455	1.491	1.469	1.468	1.470
2	1.391	1.410	1.359	1.454	1.475	1.463	1.431	1.480

The harmonic oscillator model of aromaticity (HOMA)[15] analyses of the optimized structure **6** (at BHandHLYP/6-31G(d)) supported the large BLA for rings D (−0.25) and E (−0.18), whereas small (A = 0.88, C = 0.90) to moderate (B = 0.57) BLA for phenanthrene indicated its aromaticity (Figure 3B.5a). Nuclear independent chemical shift (NICS)[16] calculation showed larger positive NICS(1)$_{zz}$ values for rings D (31.79) and E (12.67) for **6** than those of **2**, suggesting enhanced antiaromaticity of *as*-indacene unit for **6**. The negative NICS values of rings A (−23.09), B (−10.20), and C (−21.97) for **6** are in line with HOMA values, supporting phenanthrene ring aromaticity.

3B.2.3 Analysis of open-shell diradicaloid ground state. The observation of proton NMR (nuclear magnetic resonance) line broadening for **6** at rt (Figure 3B.6) prompted us to study its variable temperature (VT) NMR behaviour. In $CDCl_3$, **6** exhibited broad NMR signals for some of the aromatic protons (d, c, b protons in Figure 3B.7, see

Figure 3B.1b for proton labels) at rt, while other ring protons were also broadened upon heating (Figure 3B.8). These broad NMR signals became sharper upon gradual cooling and became reasonably sharper at −60 °C (213 K). This is a typical observation for OS diradicaloid PHs with small $\Delta E_{S\text{-}T}$,[11,17] due to which the excited triplet state can be thermally populated at rt or by slight heating. The observation was also supported by VT-EPR (electron paramagnetic resonance), exhibiting a featureless broad signal (g_e = 2.0041) at rt, while the signal intensity decreased as the temperature was lowered from 260 K to 150 K (Figure 3B.7b), which is a consequence of reduced population of magnetically active triplet species at lower temperatures.[18] A careful fitting of the VT-EPR data using the Bleaney-Bowers equation[19] gave a $\Delta E_{S\text{-}T}$ = −0.97 kcal/mol for **6** (Figure 3B.9a), suggesting singlet OS ground state, which is in line with VT-EPR in solution ($\Delta E_{S\text{-}T}$ = −1.73 kcal/mol, Figure 3B.9b and 3B.9c).

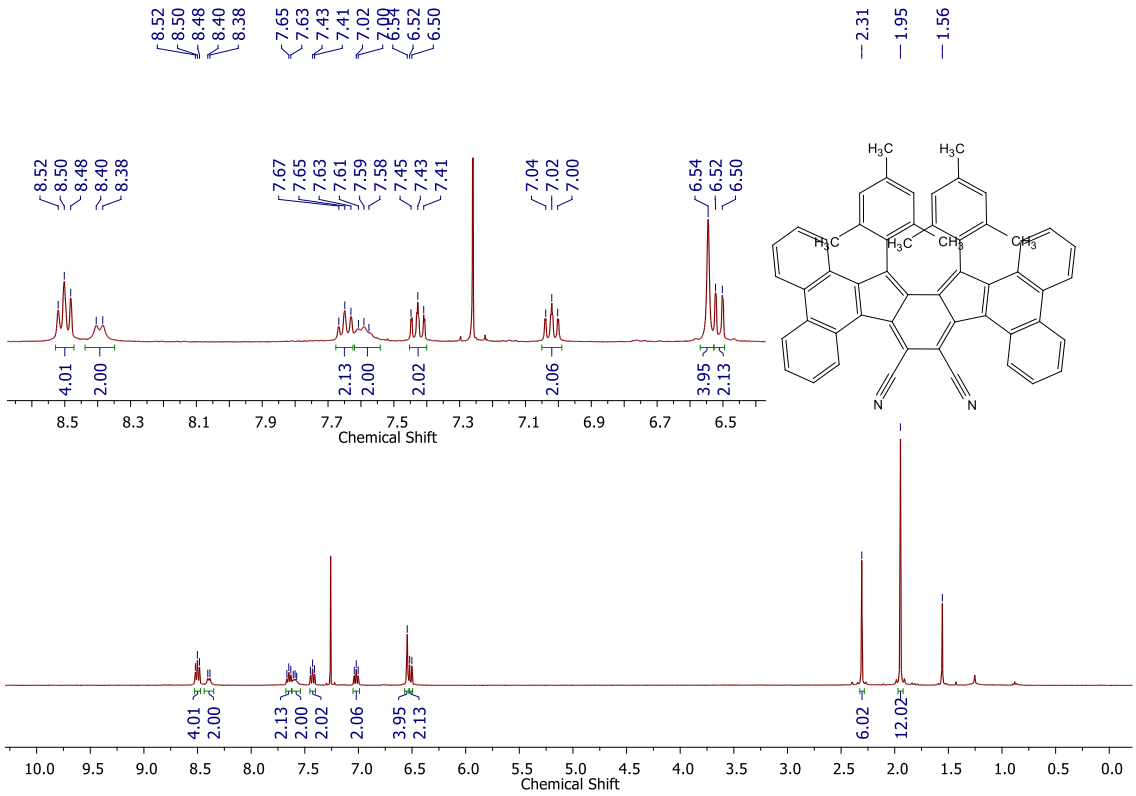

Figure 3B.6 ^{1}H NMR spectrum of **6** (in $CDCl_3$, 400 MHz, 298 K).

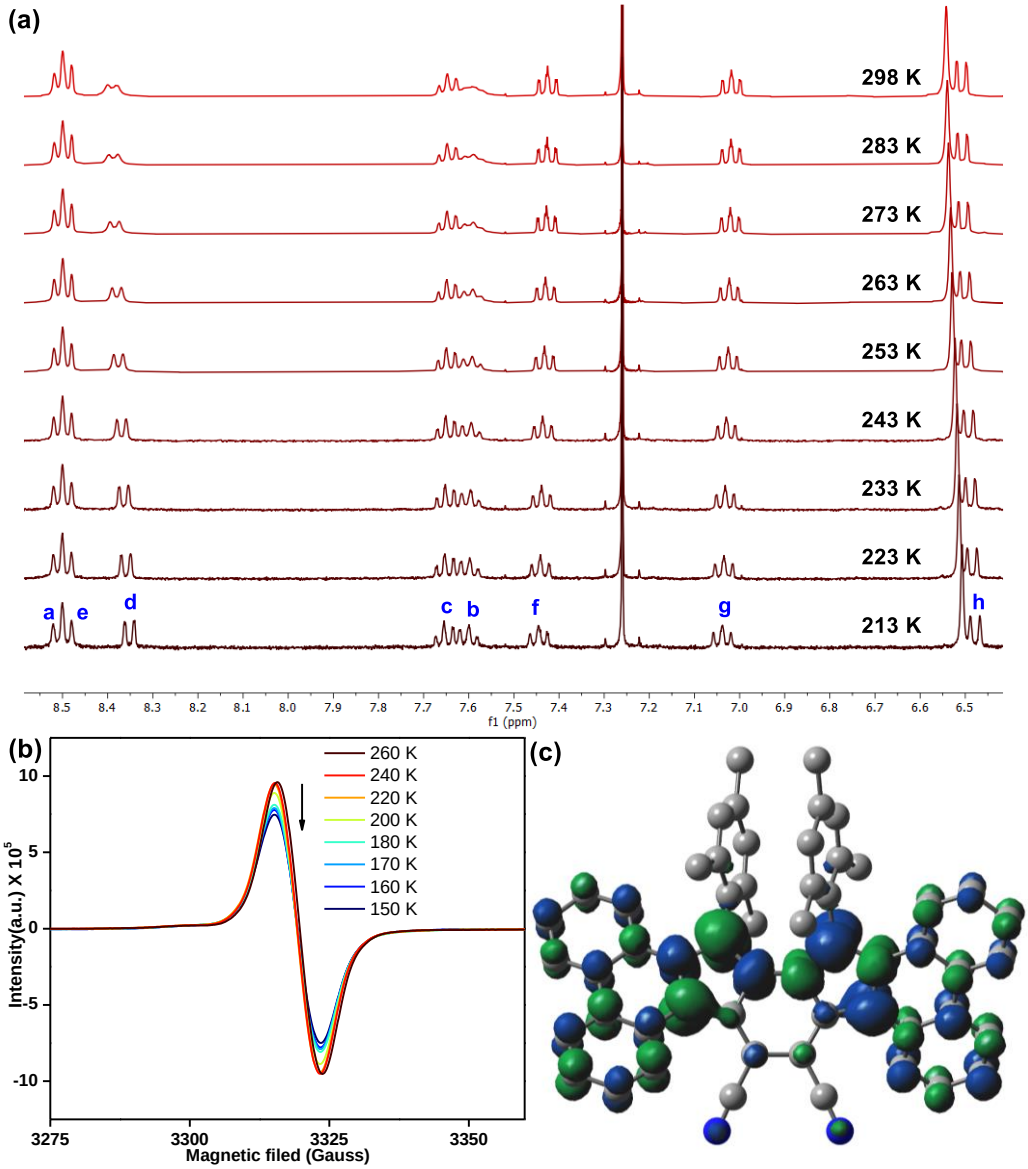

Figure 3B.7 (a) Partial VT-NMR of **6** in $CDCl_3$ showing aromatic protons (see Figure 3B.1b for proton labels); (b) VT-EPR spectra of solid sample **6**; (c) Spin density distribution of singlet OS **6**.

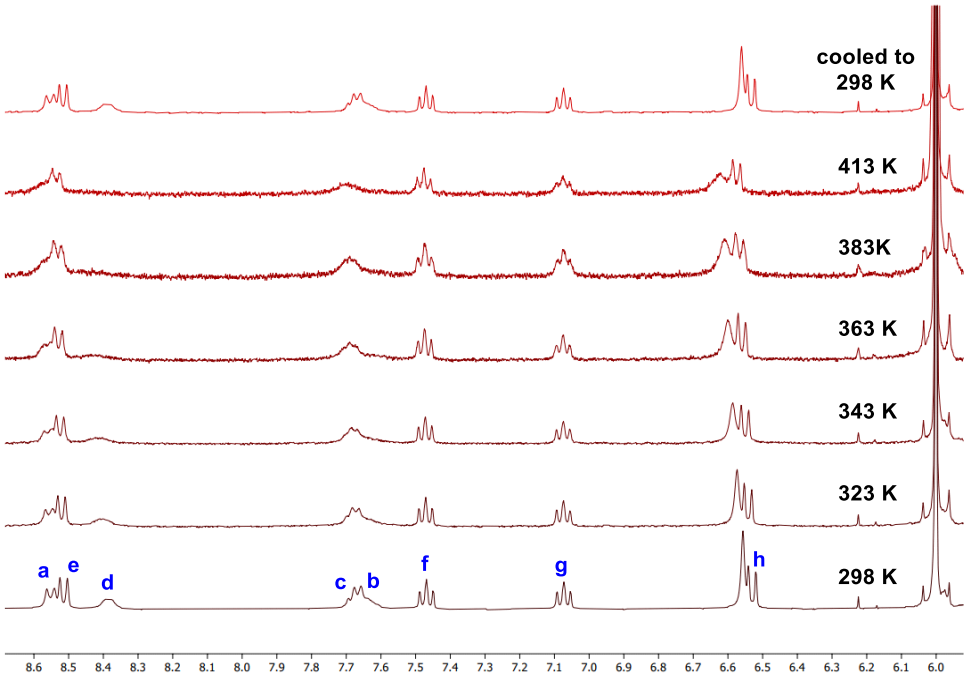

Figure 3B.8 Variable temperature (VT) ^{1}H NMR spectra for **6** in $C_2D_2Cl_4$ showing the aromatic phenanthrene proton signals were broadened upon heating (up to 413 K), and when cooled back to 298 K, the original spectrum could be recovered.

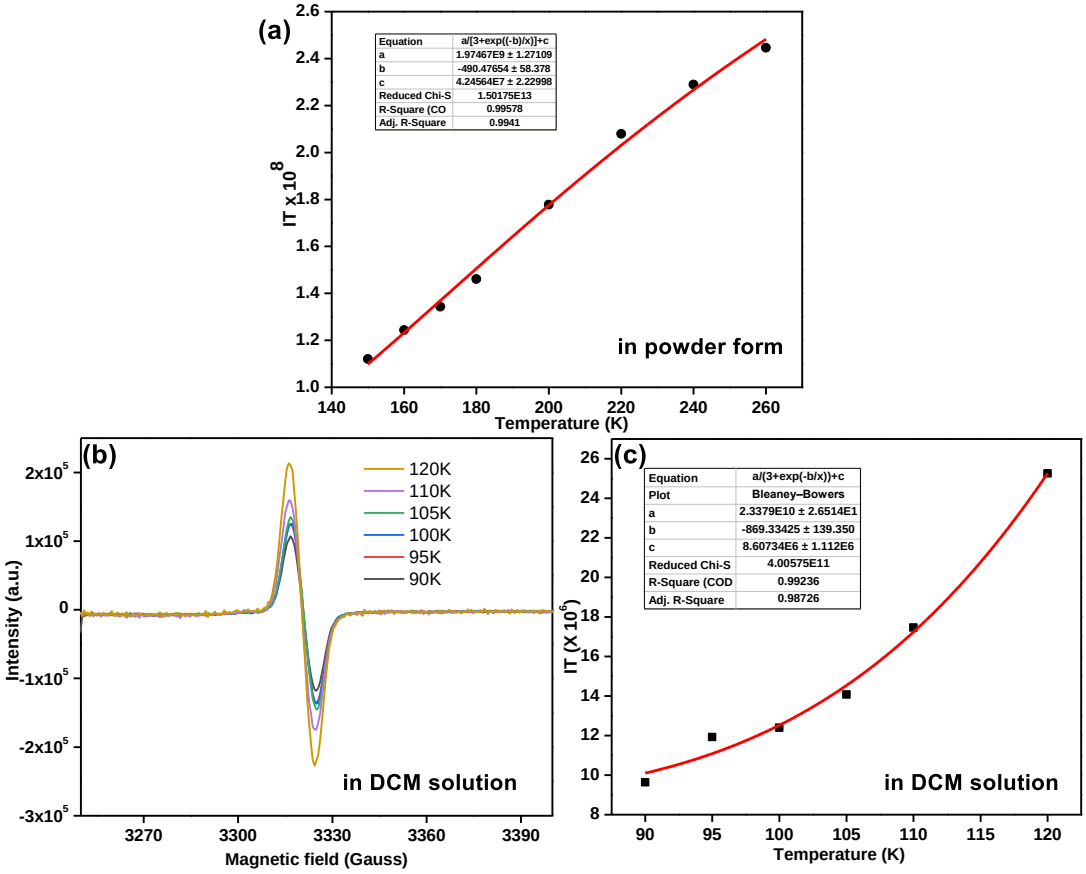

Figure 3B.9 (a) The Bleaney-Bowers plot for solid sample **6**. (b) VT-EPR spectra and (c) The Bleaney-Bowers plot of **6** in DCM solution.

DFT calculation of **6** at the BHandHLYP/6-31G(d) level of theory[20] confirmed that the energy of an OS singlet state was 1.96 kcal/mol and 2.52 kcal/mol lower than the energy of the CS singlet (quinoidal) and triplet (biradical) states, respectively (Table 3B.4). The y_0 for **6** was estimated to be 0.30, based on the natural orbital occupation numbers using broken symmetry formalism. The frontier molecular orbital profiles for α- and β- spins (Figure 3B.10) displayed the characteristic disjointed nature in the ground state singlet diradical form. The spin densities were observed to be uniformly dispersed across the entire π-conjugated framework (Figure 3B.7c), giving thermodynamic stability.

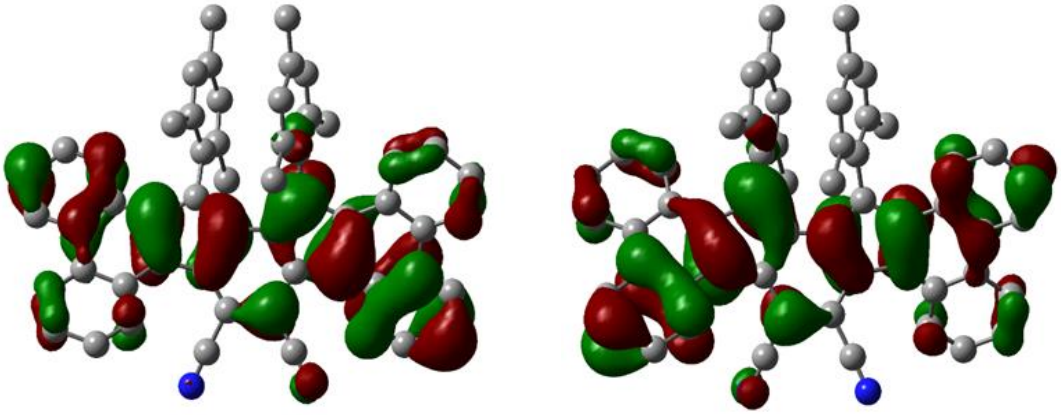

Figure 3B.10 Calculated (UBHandHLYP/6-31G(d)) frontier molecular orbital (FMO) profiles for the α-spin and β-spin of **6** (isovalue of 0.02).

3B.2.4 Optical and electrochemical properties. UV-vis-NIR (UV-visible-near infrared) spectrum (Figure 3B.11) of **6** exhibited intense absorption peaks at λ_{max} = 312 nm (ε = 30000 $M^{-1}cm^{-1}$) and λ_{max} = 365 nm (ε = 19000 M^{-1} cm^{-1}) in the UV region and a moderate absorption in the visible region λ_{max} = 554 nm (ε = 11000 M^{-1} cm^{-1}), which is associated with a weak absorption band in the lowest energy region stretching from 750 to 1500 nm in the NIR region with absorption maximum at λ_{max} = 1000 nm (ε = 650 M^{-1} cm^{-1}). Time dependent-DFT (TD-DFT) calculations of **6** in toluene suggested that the absorption in the visible region is dominated by the HOMO−1→LUMO transition (λ_{max} = 476 nm, oscillator strength (*f*) = 0.55, Table 3B.2), while the weaker lowest energy absorption tail has originated from a forbidden HOMO→LUMO transition (λ_{max} = 877 nm, *f* = 0.028). Such a long wavelength absorption tail could originate due to the admixing of doubly excited electronic configuration (H,H→L,L) for **6** owing to its OS ground state, as observed for Kubo's diphenaleno-DCPT.[14a]

Compound **6** displayed a very small optical HOMO−LUMO energy gap of 0.85 eV, as roughly estimated from the lowest energy absorption onset ($1240/\lambda_{onset}$); yet, a good photostability under ambient conditions with a half-life of 9 days was observed for **6** (Figure 3B.12).

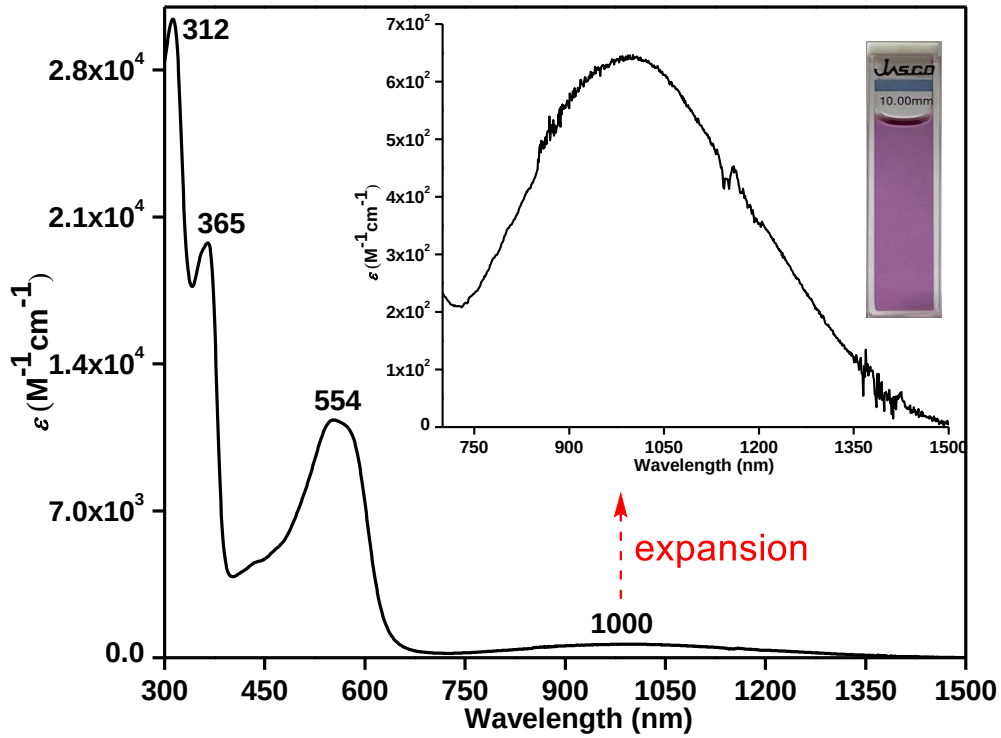

Figure 3B.11 UV-vis-NIR absorption spectrum of **6** in toluene (715−1500 nm expansion shown in inset).

Table 3B.2 Summary of TDDFT calculation for **6**

Wavelength (nm)	Oscillator Strength (*f*)	Major contributions
877	0.0281	HOMO->LUMO (96%)
499	0.0571	H-2->LUMO (85%)
476	0.5599	H-1->LUMO (89%)
424	0.0278	H-4->LUMO (90%)
396	0.0006	H-3->LUMO (88%)
384	0.0086	H-5->LUMO (86%)
367	0	H-6->LUMO (98%)
353	0.0245	H-8->LUMO (72%), H-7->LUMO (21%)
353	0.0071	HOMO->L+1 (85%)
343	0.0051	H-8->LUMO (21%), H-7->LUMO (77%)
297	0.1029	H-10->LUMO (66%)
297	0.0725	H-9->LUMO (84%)
291	0.5117	H-11->LUMO (10%), H-2->L+3 (11%), HOMO->L+2 (57%)

285	0.0117	H-1->L+1 (42%), HOMO->L+3 (24%)
278	0.2266	H-11->LUMO (12%), H-10->LUMO (22%), H-2->L+1 (42%), HOMO->L+4 (10%)
272	0.1661	H-5->L+1 (13%), H-1->L+1 (38%), HOMO->L+3 (28%)
271	0.1689	H-11->LUMO (60%), H-2->L+1 (16%)
268	0.1295	H-14->LUMO (35%), H-12->LUMO (35%)
257	0.5147	H-3->L+1 (20%), HOMO->L+5 (52%)
254	0.002	H-2->L+1 (22%), HOMO->L+4 (53%)
254	0.0139	H-14->LUMO (12%), H-1->L+3 (10%), HOMO->L+6 (39%)
249	0.1024	H-14->LUMO (32%), H-12->LUMO (51%)
246	0.0158	H-4->L+1 (91%)
246	0.0551	H-3->L+1 (53%), HOMO->L+5 (17%)
243	0.0122	H-13->LUMO (83%)
242	0.0946	H-5->L+1 (59%), HOMO->L+3 (14%)
236	0.5504	H-3->L+3 (22%), H-1->L+2 (39%), HOMO->L+4 (14%)
233	1.4557	H-3->L+2 (17%), H-1->L+3 (21%), HOMO->L+6 (36%)
229	0.0634	H-15->LUMO (21%), HOMO->L+7 (24%)
229	0.0018	H-6->L+1 (96%)

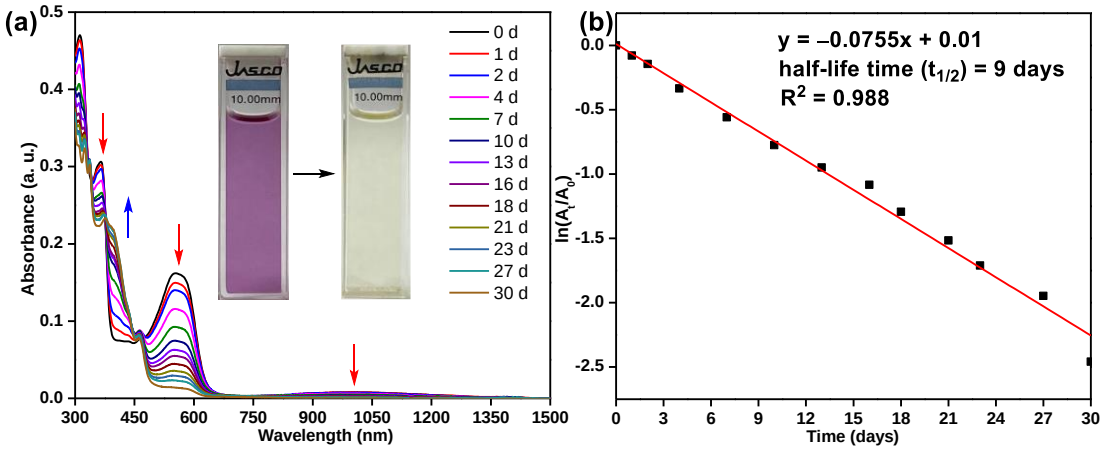

Figure 3B.12 (a) Absorption spectral changes under ambient light conditions for compound **6** in toluene (0 days to 30 days). (b) Fitting with first-order kinetics.

The half-life ($t_{1/2}$) of **6** was determined according to the following equation:

$$t_{1/2} = \frac{\ln 2}{0.0755} = 9.18 \text{ days}$$

Cyclic voltammetry (CV) and differential pulse voltammetry (DPV) analyses in DCM (Figure 3B.13) suggested that **6** could be easily reversibly reduced at $E_{1/2}^{red1}$ = −0.73 V and at $E_{1/2}^{red2}$ = −1.16 V (*vs* ferrocene/ferrocenium (Fc/Fc^+) couple). It can also be oxidized to its radical cation and dication species at E_{peak}^{ox1} = 0.68 V and E_{peak}^{ox2} =

0.93 V, respectively. The HOMO and LUMO energy levels were −5.40 eV and −4.15 eV, as estimated from the onset potentials of oxidation and reduction waves, respectively, giving a small electrochemical energy gap of 1.25 eV. The LUMO energy level of **6** is remarkably stabilized (low-lying) due to the electron-withdrawing cyano substituent, as hypothesized.

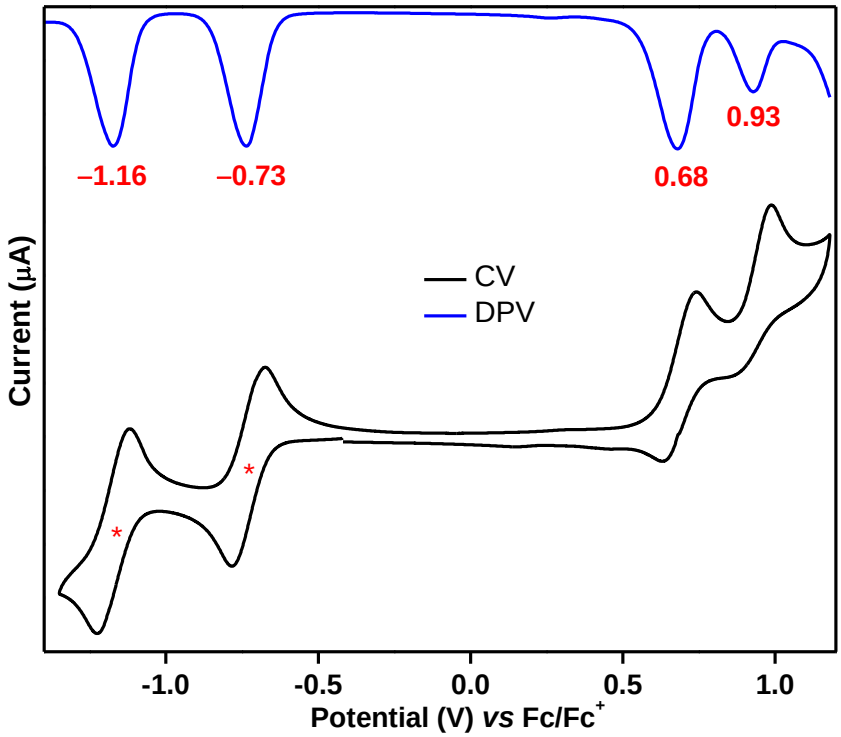

Figure 3B.13 CV and DPV of **6** in DCM/Bu_4NPF_6 solvent/electrolyte couple at 50 mV s^{-1} scan rate

The greater stabilization of LUMO basically reduced the HOMO–LUMO energy gap, and the observation is comparable to **HZ-TIPS** *vs* **HZ-DI**, where **HZ-DI** with small HOMO-LUMO gap displayed an OS diradicaloid ground state despite one Clar sextet could be recovered for both molecules in their OS forms.[11,12] The smaller $\Delta E_{S\text{-}T}$ for **6** than that of **5** could be caused by the narrower HOMO–LUMO gap of **6** pushing its triplet excited state to locate closer to the singlet ground state.[21] As a result, the excited triplet state could be easily thermally populated at rt or by slight heating, despite a small y_0. Usually, the greater the y_0, the smaller the $\Delta E_{S\text{-}T}$;[22] with a few noteworthy exceptions[23] (including **benzo-2**)[6] showing a larger $\Delta E_{S\text{-}T}$ although exhibiting a larger y_0. To the best of our knowledge, compound **6** is a unique example that exhibits a small y_0 despite showing a small $\Delta E_{S\text{-}T}$.

Typically, an OS PH with large y_0 displays a large energy difference between its CS singlet and OS singlet states, and a small energy difference between its OS singlet state and first excited triplet state.[24] Our experimental and theoretical studies confirmed that **6** exists as an OS diradicaloid in the singlet ground state with its CS quinoidal state lying in between the OS ground state and triplet excited state, which is unlike the known diradicaloid PHs[17,24] with large y_0 displaying CS quinoidal states lying vertically at much higher energy level above the triplet state. A significant BLA for the central *as*-indacene unit of **6** in its crystalline form indicates a dominant quinoidal structure presumably due to rt accessible low-lying CS state, which is in line with the small y_0. This observation suggested that both CS and OS resonance forms for **6** may contribute to the singlet ground state.

3B.3 Conclusions

In summary, a formally antiaromatic diphenanthro-*as*-indacene derivative **6** was synthesized, that exhibits diradical-like and antiaromatic properties in its OS singlet ground state as a result of a low-lying CS state. Though the formation of **6** was unexpected, its detailed characterization gave newer insights in diradical chemistry as our study suggested that substitution driven HOMO–LUMO energy gap modulation can affect ground state properties for antiaromatic PHs. The small y_0 (30%) for **6** could likely be attributed to the dominant *as*-indacene antiaromaticity owing to the low-lying quinoidal CS form, as supported by SCXRD analysis and NICS(1)$_{zz}$ calculation. The VT-NMR and VT-EPR experiments indicated its singlet diradicaloid nature in the singlet ground state, which is the consequence of a small HOMO–LUMO energy gap. Qualitative correlations between the structural features and the properties of different diradicaloid systems usually indicate an increased y_0 as the energy separation between the singlet and triplet states decreased. However, compound **6** is an example of a rare diradicaloid exhibiting a small y_0 despite showing a small $\Delta E_{S\text{-}T}$, implying potential for applications in organic spintronics and photonics (non-linear optics and singlet-fission).[25]

3B.4 Experimental section

3B.4.1 General information. Chemicals and reagents were purchased from local and international commercial suppliers (Merck, GLR innovations, BLDpharm, Spectrochem) and used without further purification. Thin layer chromatography (TLC)

was performed using pre-coated silica-plates purchased from Merck (silica gel 60 PF254, 0.25 mm). Column chromatography was performed using silica gel 100-200 mesh. NMR spectra were recorded in $CDCl_3$ (Eurisotop, on JEOL JNM-ECS400 spectrometer at operating frequencies of 400 MHz (^1H) or 100 MHz (^{13}C) as indicated in the individual spectrum. Chemical shifts (δ) are given in ppm relative to residual solvent (chloroform δ = 7.26 for ^1H, and δ = 77.16 for proton-decoupled ^{13}C NMR), and coupling constants (*J*) are expressed in hertz (Hz). Multiplicity is tabulated as s for singlet, d for doublet, dd for doublet of doublet, t for triplet, q for quartet, and m for multiplet. Structural assignments were made with additional information from gCOSY, and gNOESY experiments. High-resolution mass spectra (HRMS) were recorded using electronspray ionization (ESI) methods on Waters (XEVO G2-XS QTOF) mass spectrometer. UV-vis-NIR spectra were recorded in JASCO V-770 spectrophotometer. Cyclic voltammetry was performed using an Electrochemical Analyzer potentiostat model CHI-1110C from CH Instruments with a conventional three-electrode cell at room temperature under a nitrogen atmosphere at a scan rate of 50 mV s^{-1}. This electrochemical cell contains a glassy carbon (disc-shaped with 3-mm diameter) as a working electrode, Pt wire as a counter electrode, and Ag wire as a pseudo-reference electrode. The glassy carbon working electrode was polished with 1.0-micron α-alumina polishing powder using a figure-eight motion. Electrolyte solution (0.1 M) was prepared from dichloromethane (DCM) and tetra-*n*-butylammonium hexafluorophosphate (Bu_4NPF_6). The DCM was degassed by nitrogen gas sparging for 15 minutes prior to measurements. The potential was externally calibrated against the ferrocene/ferrocenium couple (0.43 V). Melting points were determined using a Cole-Parmer MP 250D-P melting point analyzer. X-band electron paramagnetic resonance (EPR) spectra were recorded using an EMX MICRO X Bruker EPR instrument.

3B.4.2 Syntheses

2,5-di(phenanthren-9-yl)thiophene-3,4-dicarbaldehyde (9): An oven-dried thick-walled glass tube was charged with **7** (715.45 mg, 3.22 mmol), **8** (300 mg, 1.01 mmol), K_2CO_3 (696 mg, 5.03 mmol), THF (12 mL) and water (2.4 mL), and the mixture was purged with nitrogen for 30 mins. Catalyst $Pd(PPh_3)_4$ (100 mg, 10 mol %) was subsequently added under nitrogen, and the glass tube was sealed before being warmed to 85 °C using an oil bath. After 14 h, the flask was cooled to room temperature, and THF was evaporated under reduced pressure. Water was added, and

the reaction mixture was extracted with EtOAc (5 x 30 mL). The organic layer was dried over anhydrous Na_2SO_4, filtered, and removed under reduced pressure. The residue was purified by silica gel column chromatography (hexanes:EtOAc, 94:6) to afford the title product **9** (420 mg, 85% yield) as light brown solid: R_f = 0.19 (5% EtOAc/hexanes); mp 280−281 °C; ^{1}H NMR (400 MHz, $CDCl_3$) δ 10.21 (s, 2H), 8.81 (d, *J* = 8.2 Hz, 2H), 8.76 (d, *J* = 8.2 Hz, 2H), 8.00 – 7.90 (m, 6H), 7.80 – 7.73 (m, 4H), 7.72 – 7.65 (m, 4H). ^{13}C{^{1}H} NMR (100 MHz, $CDCl_3$) δ 186.9, 152.3, 137.1, 131.0 (2 C), 130.7 (2 C), 130.5, 129.2, 128.2, 127.5, 127.4, 127.2, 126.1, 123.3, 122.9; HRMS (ESI) *m/z*: $[M + H]^+$ calcd for $C_{34}H_{21}O_2S$ 493.1262, found 493.1262 (error: 0.0 ppm).

18,19-dimesityl-18,19-dihydrodibenzo[4,5:6,7]indeno[1,2-*b*]dibenzo[4,5:6,7]indeno[2,1-*d*]thiophene (2H-DPDCPT): 2-Mesitylmagnesium bromide (1.0 M in diethyl ether, 1.62 mL, 1.62 mmol) was added dropwise to the dry tetrahydrofuran (5 mL) solution of **9** (180 mg, 0.45 mmol) under nitrogen. The mixture was stirred at room temperature for 12 h, and the reaction was quenched with a saturated aqueous NH_4Cl solution. The volatile organics were evaporated under reduced pressure, and the mixture was extracted with dichloromethane (3 x 30 mL). The organic layer was dried over anhydrous Na_2SO_4, filtered, and removed under reduced pressure to afford a crude mixture containing intermediate diol (320 mg) compound. In the next step, $BF_3{\cdot}Et_2O$ (0.1 mL) was added to the solution of crude diol in anhydrous DCM (5 mL) under nitrogen, and the reaction mixture was stirred for 30 min at room temperature. Once diol was completely consumed, as monitored by TLC, a saturated aqueous $NaHCO_3$ solution (12 mL) was added and the reaction mixture was extracted with DCM (3 × 30 mL). The organic layer was dried over anhydrous Na_2SO_4, filtered, and evaporated under reduced pressure. The residue was subjected to silica gel column chromatography (hexanes/DCM, 90:10) to give title product **2H-DPDCPT** as a light yellow solid (100 mg, 35% over two steps): R_f = 0.27 (5% DCM/hexanes); mp 387 °C dec; ^{1}H NMR (400 MHz, $CDCl_3$) δ 8.81 (d, *J* = 8.3 Hz, 2H), 8.70 (d, *J* = 8.2 Hz, 2H), 8.57 (d, *J* = 7.9 Hz, 2H), 7.87 (t, *J* = 7.5 Hz, 2H), 7.80 – 7.73 (m, 2H), 7.50 – 7.44 (m, 4H), 7.34 – 7.28 (m, 2H), 7.00 (s, 2H), 6.60 (s, 2H), 5.29 (s, 2H), 2.33 (s, 6H), 1.80 (s, 6H), 1.32 (s, 6H); ^{13}C{^{1}H} NMR (100 MHz, $CDCl_3$) δ 145.2, 144.2, 142.2, 138.4, 138.3, 136.7, 134.5, 133.4, 130.7, 130.3, 130.1, 130.0, 129.4, 127.1, 126.5, 126.4, 125.4, 125.2, 123.6, 123.5, 123.5, 48.2, 21.2, 21.0, 17.6; HRMS (ESI) *m/z*: $[M]^+$ calcd for $C_{52}H_{40}S$ 696.2851, found 696.2858 (error: 1.0 ppm).

19,20-dimesityl-as-indaceno[2,3-l:6,7-l']diphenanthrene-9,10-dicarbonitrile (6): DDQ (68 mg, 0.30 mmol) was added to the solution of **2H-DPDCPT** (52 mg, 0.074 mmol) in dry DCM (5 mL) under nitrogen, and the reaction mixture was stirred at room temperature for 30 min. Once the starting material was consumed (as monitored by TLC), the DCM was removed *in vacuo*, and the crude was purified by silica gel column chromatography (silica gel was treated with triethylamine; hexanes:DCM, 70:30) to afford target compound **6** as dark-purple solid (23 mg, 42% yield over three steps): R_f = 0.15 (5% EtOAc/hexanes). Recrystallization of **6** from a dichloromethane/acetonitrile (1:1) mixture, by solvent diffusion method, at ambient temperature in the dark afforded single crystals suitable for x-ray crystallographic analysis: mp 325−326 °C; ^{1}H NMR (400 MHz, $CDCl_3$): δ 8.50 (t, *J* = 7.6 Hz, 4H), 8.39 (d, *J* = 7.9 Hz, 2H), 7.65 (t, *J* = 7.4 Hz, 2H), 7.62 – 7.55 (m, 2H), 7.46 – 7.39 (m, 2H), 7.02 (t, *J* = 7.3 Hz, 2H), δ 6.54 (s, 4H), 6.51 (d, J = 8.3 Hz, 2H), 2.31 (s, 6H), 1.95 (s, 12H); ^{13}C{^{1}H} NMR (100 MHz, $CDCl_3$) δ 158.0, 137.6, 135.4, 133.5, 131.1, 128.6, 128.1, 127.7, 127.5, 127.4, 126.7, 123.8, 123.5, 123.4, 116.0, 107.4, 21.4, 21.12 [Likely the population of triplet species at 25 °C resulting in weaker intensity for aromatic signals for the π-backbone]; HRMS (ESI) *m/z*: $[M + H]^+$ calcd for $C_{56}H_{39}N_2$ 739.3113, found 739.3099 (error: −1.9 ppm). **NOTE:** A DDQ-adduct (**DPDCPT-DDQ**) could be isolated when a crude reaction mixture was subjected to silica gel (not treated with NEt_3) column chromatography under nitrogen.

Characterization data of **DPDCPT-DDQ**: ^{1}H NMR (400 MHz, $CDCl_3$) δ 8.75 (d, *J* = 7.6 Hz, 2H), 8.72 (d, *J* = 8.3 Hz, 2H), 7.73 – 7.65 (m, 4H), 7.62 (t, *J* = 7.2 Hz, 2H), 7.49 – 7.46 (m, 2H), 7.22 (t, *J* = 7.7 Hz, 2H), 7.10 (d, *J* = 8.2 Hz, 2H), 6.74 (s, 2H), 6.45 (s, 2H), 2.53 (s, 6H), 2.34 (s, 6H), 1.55 (s, 6H). ^{13}C{^{1}H} NMR (100 MHz, $CDCl_3$) δ 176.0, 148.2, 145.5, 143.7, 140.8, 138.0, 136.4, 136.0, 132.6, 130.9, 130.1, 130.0, 128.6, 128.4, 128.2, 128.1, 127.6, 127.5, 126.8 (2), 125.8, 124.3, 123.8, 123.5, 114.1, 83.1, 66.0, 60.5, 53.5, 22.6, 21.6, 20.5. HRMS (ESI) *m/z*: $[M + Na]^+$ calcd for $C_{60}H_{38}N_2O_2NaSCl_2$ 943.1929, found 943.1907 (error: −2.3 ppm).

3B.4.3 Variable temperature (VT) ESR measurement.

To get the ground sate spin multiplicity and the energy separation between the singlet and triplet state, VT-EPR experiment were carried out using solid sample of **6**, and VT-EPR of **6** in DCM solution was also recorded. The EPR spectra were recorded in a X band EPR instrument (EMX MICRO X, Bruker EPR instrument).

EPR experimental parameters:

Frequency: 9.31 GHz; Power: 8.47 mW; Modulation frequency: 100 KHz; Modulation amplitude: 10G

Conversion time: 120 msec, Time constant: 328 msec.

The modified Bleaney-Bowers equation were used to fit the IT against the T data points to get the energy separation between the singlet and triplet spin state of the diradical species.

$$IT = \frac{2\rho N_A g^2 \beta^2}{k_b} * \frac{1}{3 + \exp\left(-\frac{2J}{k_b T}\right)} + \frac{(1-\rho) N_A g^2 \beta^2}{2k_b}$$

Here, '*I*' is the EPR intensity, 'T' is the temperature in Kelvin scale, *g* is the g factor, N_A is the Avogadro constant, β is the Bohr magneton, k_b is the Boltzmann constant, and ρ is the paramagnetic purity

The *IT* vs. *T* data set was fitted according to the below equation using Origin 2021 software package.

$$IT = \frac{a}{3 + \exp\left(-\frac{b}{T}\right)} + c$$

$$a = \frac{2\rho N_A g^2 \beta^2}{k_b}\ ; = \frac{2J}{k_b}\ ; \text{c} \quad \text{M} = \frac{(1-\rho) N_A g^2 \beta^2}{2k_b}$$

a = 1.97467e9; *b* = –490.47654; *c* = 4.24564e7

The singlet-triplet energy gap ($\Delta E_{S\text{-}T}$) as solid = 2J = –490.47*0.0019872 kcal/mol = –0.97 kcal/mol

VT-EPR in DCM solution:

$\Delta E_{S\text{-}T}$ in solution = −869.3342*0.0019872 = −1.73 kcal/mol.

3B.4.4 X-ray crystallographic analysis

A suitable single crystal of **6** was selected using paratone oil and mounted on glass fiber with the help of gum. The intensity data and geometric parameters of these crystals were garnered with the help of Bruker D8 Venture X-ray diffractometer having a micro-focus sealed X-ray tube Mo-Kα (λ = 0.71073 Å) source of X-rays along with a PHOTON 100 detector with inclining Phi and Omega (width of 0.5 for one frame) working at a scan speed of 10 s per frame. The crystal was kept at 298 K during data collection. Data acquisition, as well as extraction of data, was accomplished by utilizing Bruker Apex-3 and Bruker SAINT software packages using a narrow-frame algorithm.[26] By utilizing OLex2[27] the crystal structure was solved with

the help of olex2.solve[28] structure solution program by employing intrinsic Phasing methods, and crystal structure refinement was done with the SHELXL[29] refinement package by putting into use Least Squares minimization. Refinement of all non-hydrogen atoms was completed with the help of anisotropic thermal parameters.

Table 3B.3 X-ray crystallographic information of **6**

CCDC No.	2309430
Empirical formula (including disordered acetonitrile)	$C_{58}H_{41}N_3$
Formula weight	779.94
Temperature/K	298
Crystal system	orthorhombic
Space group	$P2_12_12_1$
a/Å	12.7061(5)
b/Å	14.0855(4)
c/Å	23.6488(10)
α/°	90
β/°	90
γ/°	90
Volume/Å^3	4232.5(3)
Z	4
ρ_{calc}g/cm^3	1.224
μ/mm^{-1}	0.071
F(000)	1640.0
Crystal size/mm^3	0.231 × 0.214 × 0.123
Radiation	MoKα (λ = 0.71073)
2Θ range for data collection/°	4.498 to 52.9
Index ranges	$-15 \leq h \leq 15$, $-15 \leq k \leq 17$, $-25 \leq l \leq 29$
Reflections collected	48088
Independent reflections	8683 [R_{int} = 0.0441, R_{sigma} = 0.0299]
Data/restraints/parameters	8683/0/557
Goodness-of-fit on F^2	1.041
Final R indexes [I>=2σ (I)]	R_1 = 0.0384, wR_2 = 0.0921
Final R indexes [all data]	R_1 = 0.0447, wR_2 = 0.0961
Largest diff. peak/hole / e Å^{-3}	0.14/-0.16
Flack parameter	0.1(10)

3B.4.5 DFT calculations

Gas-phase DFT calculations were performed with Gaussian 09 package using a high-performance computing cluster facility of IIT Ropar at the BHandHLYP level of

theory with basis set 6-31G(d).[30] X-ray crystallographic structure of **6** was used for DFT-optimization. The calculated NOON (natural orbital occupation number) value for **DPDCPT**, **4**, **5** and **6** was based on the broken symmetry formalism.[31] NICS (standard GIAO method)[16] and HOMA[15] indices were calculated for the optimized closed-shell structure for **6**. The reported $NICS(1)_{zz}$ indices were the average of two positions (above and below the plane) for non-planar **6**. Excitation energy was computed using time-dependent density functional theory (TD-DFT) for the optimized closed-shell structure of **6** in toluene. Molecular orbital contributions were determined using the GaussSum 3.0 package.[32]

Table 3B.4 Relative electronic energies of optimized geometries for **DPDCPT**, **4**, **5** and **6**.

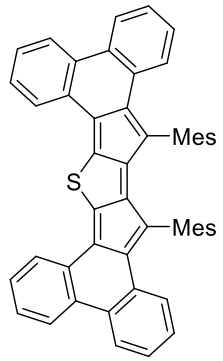

DPDCPT

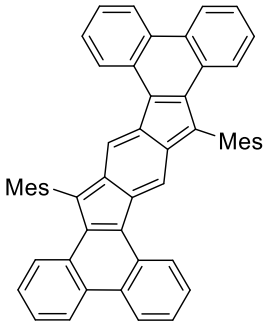

4

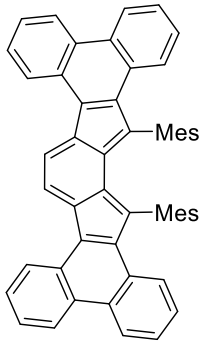

5

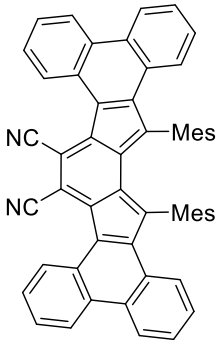

6

Compounds	Optimization	hartree	kcal/mol	% diradical character
DPDCPT	Singlet closed-shell BHandHLYP /6-31G(d)	–2401.384192	–1506890.193	51
	Singlet open-shell UBHandHLYP /6-31G(d)	–2401.404936	–1506903.21	
	Triplet open-shell UBHandHLYP /6-31G(d)	–2401.403911	–1506902.567	
4	Singlet closed-shell BHandHLYP /6-31G(d)	–2080.649108	–1305626.041	0
	Singlet open-shell UBHandHLYP /6-31G(d)	–2080.649108	–1305626.041	
	Triplet open-shell UBHandHLYP /6-31G(d)	–2080.638009	–1305619.076	
5	Singlet closed-shell BHandHLYP /6-31G(d)	–2080.623976	–1305610.271	1
	Singlet open-shell UBHandHLYP /6-31G(d)	–2080.623976	–1305610.271	
	Triplet open-shell UBHandHLYP /6-31G(d)	–2080.618459	–1305606.809	
6	Singlet closed-shell	–2264.984351	–1421298.065	30

BHandHLYP /6-31G(d)		
Singlet open-shell UBHandHLYP /6-31G(d)	–2264.987479	–1421300.028
Triplet open-shell UBHandHLYP /6-31G(d)	–2264.98346	–1421297.506

DPDCPT: $\Delta E_{\text{Singlet(OS)-Triplet(OS)}}$ = –0.64 kcal/mol; $\Delta E_{\text{OS-CS}}$ = –13.01 kcal/mol; $\Delta E_{\text{CS-T}}$ = 12.37 kcal/mol. Occupation number calculation of the open-shell singlet **DPDCPT** for HOMO = 1.26 and LUMO = 0.74 affords a 51% diradical character (singlet diradical character index (y_0) = 0.51).

Compound 4: $\Delta E_{\text{Singlet(OS)-Triplet(OS)}}$ = –6.96 kcal/mol; $\Delta E_{\text{OS-CS}}$ = 0 kcal/mol; $\Delta E_{\text{CS-T}}$ = –6.96 kcal/mol. Occupation number calculation of the open-shell singlet **5** for HOMO = 2.00 and LUMO = 0.00 affords a 0% diradical character (singlet diradical character index (y_0) = 0)

Compound 5: $\Delta E_{\text{Singlet(OS)-Triplet(OS)}}$ = –3.46 kcal/mol; $\Delta E_{\text{OS-CS}}$ = 0 kcal/mol; $\Delta E_{\text{CS-T}}$ = –3.46 kcal/mol. Occupation number calculation of the open-shell singlet **5** for HOMO = 1.89 and LUMO = 0.11 affords a 0.7% diradical character (singlet diradical character index (y_0) = 0.01)

Compound 6: $\Delta E_{\text{Singlet(OS)-Triplet(OS)}}$ = –2.52 kcal/mol; $\Delta E_{\text{OS-CS}}$ = –1.96 kcal/mol; $\Delta E_{\text{CS-T}}$ = –0.56 kcal/mol. Occupation number calculation of the open-shell singlet **6** for HOMO = 1.41 and LUMO = 0.59 affords a 30% diradical character (singlet diradical character index (y_0) = 0.301713).

3B.5 References

1. (a) Konishi, A.; Okada, Y.; Nakano, M.; Sugisaki, K.; Sato, K.; Takui, T.; Yasuda, M. Synthesis and Characterization of Dibenzo[*a*,*f*]Pentalene: Harmonization of the Antiaromatic and Singlet Biradical Character. *J. Am. Chem. Soc.* **2017**, *139*, 15284–15287. (b) Xu, T.; Hou, X.; Han, Y.; Wei, H.; Li, Z.; Chi, C. Fused Indacene Dimers. *Angew. Chem., Int. Ed.* **2023**, *62*, e202304937.

2. Chase, D. T.; Fix, A. G.; Kang, S. J.; Rose, B. D.; Weber, C. D.; Zhong, Y.; Zakharov, L. N.; Lonergan, M. C.; Nuckolls, C.; Haley, M. M. 6,12-Diarylindeno[1,2-*b*]fluorenes: Syntheses, Photophysics, and Ambipolar OFETs. *J. Am. Chem. Soc.* **2012**, *134*, 10349–10352.

3. Shimizu, A.; Tobe, Y. Indeno[2,1-*a*]fluorene: An Air-Stable *ortho*-Quinodimethane Derivative. *Angew. Chem., Int. Ed.* **2011**, *50*, 6906–6910.

4. Tobe, Y. Quinodimethanes Incorporated in Non-Benzenoid Aromatic or Antiaromatic Frameworks. *Top. Curr. Chem. (Z)* **2018**, *376*, 12.

5. Sharma, H.; Bhardwaj, N.; Das, S. Revisiting indeno[1,2-*b*]fluorene by steric promoted synthesis while isolating the second stable 4nπ indeno[2,1-*a*]fluorene. *Org. Biomol. Chem.* **2022**, *20*, 8071–8077.

6. Miyoshi, H.; Nobusue, S.; Shimizu, A.; Hisaki, I.; Miyata, M.; Tobe, Y. Benz[*c*]indeno[2,1-*a*]fluorene: a 2,3-naphthoquinodimethane incorporated into an indenofluorene frame. *Chem. Sci.* **2014**, *5*, 163–168.

7. (a) Shi, X.; Chi, C. Heterocyclic Quinodimethanes. *Top. Curr. Chem.* **2017**, *375*, 68. (b) Sharma, P. K.; Mallick, D.; Das, S. A Thiophenoradialene-Embedded Polycyclic Heteroterphenoquinone Exhibiting Dominant Antiaromatic Traits. *Org. Lett.* **2023**, *25*, 5089–5093. (c) Shi, X.; Burrezo, P. M.; Lee, S.; Zhang, W.; Zheng, B.; Dai, G.; Chang, J.; López Navarrete, J. T.; Huang, K.-W.; Kim, D.; Casado, J.; Chi, C. Antiaromatic bisindeno-[*n*]thienoacenes with small singlet biradical characters: syntheses, structures and chain length dependent physical properties. *Chem. Sci.* **2014**, *5*, 4490–4503. (d) Rudebusch, G. E.; Fix, A. G.; Henthorn, H. A.; Vonnegut, C. L.; Zakharov, L. N.; Haley, M. M. Quinoidal diindenothienoacenes: synthesis and properties of new functional organic materials. *Chem. Sci.* **2014**, *5*, 3627–3633.

8. Frederickson, C. K.; Zakharov, L. N.; Haley, M. M. Modulating Paratropicity Strength in Diareno-Fused Antiaromatics. *J. Am. Chem. Soc.* **2016**, *138*, 16827–16838.

9. Ayub, R.; El Bakouri, O.; Jorner, K.; Solà, M.; Ottosson, H. Can Baird's and Clar's Rules Combined Explain Triplet State Energies of Polycyclic Conjugated Hydrocarbons with Fused 4nπ- and (4n + 2)π-Rings?. *J. Org. Chem.* **2017**, *82*, 6327–6340.

10. Casey, A.; Dimitrov, S. D.; Shakya-Tuladhar, P.; Fei, Z.; Nguyen, M.; Han, Y.; Anthopoulos, T. D.; Durrant, J. R.; Heeney, M. Effect of Systematically Tuning Conjugated Donor Polymer Lowest Unoccupied Molecular Orbital Levels via Cyano Substitution on Organic Photovoltaic Device Performance. *Chem. Mater.* **2016**, *28*, 5110–5120.

11. Li, Y.; Heng, W.-K.; Lee, B. S.; Aratani, N.; Zafra, J. L.; Bao, N.; Lee, R.; Sung, Y. M.; Sun, Z.; Huang, K.-W.; Webster, R. D.; López Navarrete, J. T.; Kim, D.; Osuka, A.; Casado, J.; Ding, J.; Wu, J. Kinetically blocked stable heptazethrene and octazethrene: Closed-shell or open-shell in the ground state?. *J. Am. Chem. Soc.* **2012**, *134*, 14913–14922.

12. Sun, Z.; Huang, K.-W.; Wu, J. Soluble and stable heptazethrenebis(dicarboximide) with a singlet open-shell ground state. *J. Am. Chem. Soc.* **2011**, *133*, 11896–11899.

13. Sharma, P. K.; Mallick, D.; Sharma, H.; Das, S. Dominating Antiaromatic Character of *as*-Indacene Decides Overall Properties of a Formally Aromatic Dicyclopenta[*c*]fluorenothiophene. *Org. Lett.* **2023**, *25*, 2201–2206

14. (a) Kubo, T.; Sakamoto, M.; Akabane, M.; Fujiwara, Y.; Yamamoto, K.; Akita, M.; Inoue, K.; Takui, T.; Nakasuji, K. Four-Stage Amphoteric Redox Properties and Biradicaloid Character of Tetra-*tert*-butyldicyclopenta[*b*;*d*]thieno[1,2,3-*cd*;5,6,7-*c'd'*]diphenalene. *Angew. Chem., Int. Ed.* **2004**, *43*, 6474–6479. (b) Wang, Z.-L.; Li, H.-L.; Ge, L.-S.; An, X.-L.; Zhang, Z.-G.; Luo, X.; Fossey, J. S.; Deng, W.-P. DDQ-Mediated Oxidative Coupling: An Approach to 2,3-Dicyanofuran (Thiophene). *J. Org. Chem.* **2014**, *79*, 1156–1165. (c) Li, J.-S.; Xue, Y.; Li, Z.-W.; Liu, W.-D.; Lu, C.-H.; Zhao, P.-X. An Efficient Access to Fluorescent 2,3,4-Tricyanofurans from α-Cyano Ketones Using DDQ as Maleonitrile Building Block. *Synlett* **2013**, *24*, 2003–2005.

15. (a) Lu, T.; Chen, F. Multiwfn: A multifunctional wavefunction analyzer. *J. Comput. Chem.* **2012**, *33*, 580–592. (b) Krygowski, T. M.; Cyrański, M. K. Structural Aspects of Aromaticity. *Chem. Rev.* **2001**, *101*, 1385–1420.

16. (a) Fallah-Bagher-Shaidaei, H.; Wannere, C. S.; Corminboeuf, C.; Puchta, R.; Schleyer, P. v. Which NICS Aromaticity Index for Planar π Rings Is Best?. *Org. Lett.* **2006**, *8*, 863–866. (b) Dobrowolski, J. C.; Lipinski, P. F. J. On Splitting of the NICS(1) Magnetic Aromaticity Index. *RSC Adv.* **2016**, *6*, 23900−23904. (c) Chen, Z.; Wannere, C. S.; Corminboeuf, C.; Puchta, R.; von Ragué Schleyer, P. v. Nucleus-Independent Chemical Shifts (NICS) as an Aromaticity Criterion *Chem. Rev*. **2005**, *105*, 3842–3888.

17. (a) Das, S.; Lee, S.; Son, M.; Zhu, X.; Zhang, W.; Zheng, B.; Hu, P.; Zeng, Z.; Sun, Z.; Zeng, W.; Li, R.-W.; Huang, K.-W.; Ding, J.; Kim, D.; Wu, J. *para*-Quinodimethane-Bridged Perylene Dimers and Pericondensed Quaterrylenes: The Effect of the Fusion Mode on the Ground States and Physical Properties. *Chem. – Eur. J.* **2014**, *20*, 11410–11420. (b) Yadav, P.; Das, S.; Phan, H.; Herng, T. S.; Ding, J.; Wu, J. Kinetically Blocked Stable 5,6:12,13-Dibenzozethrene: A Laterally π-Extended Zethrene with Enhanced Diradical Character. *Org. Lett.* **2016**, *18*, 2886–2889.

18. Jana, P.; Koppayithodi, S.; Mahato, S.; Molla, S.; Bandyopadhyay, S. Stable Diradical on the Dimethyldihydropyrene Scaffold. *J. Phys. Chem. Lett.* **2023**, *14*, 7433–7439.

19. Bleaney, B.; Bowers, K. D. Anomalous paramagnetism of copper acetate. *Proc. R. Soc. London, Ser. A* **1952**, *214*, 451–465

20. Lehtola, S.; Dimitrova, M.; Fliegl, H.; Sundholm, D. Benchmarking Magnetizabilities with Recent Density Functionals. *J. Chem. Theory Comput.* **2021**, *17*, 1457–1468.

21. Zeng, W.; Qi, Q.; Wu, J. Toward Long Rylene Ribbons and Quinoidal Rylene Diradicaloids. *Eur. J. Org. Chem.* **2018**, *2018*, 7–17.

22. Dressler, J. E.; Haley, M. M. Learning how to fine-tune diradical properties by structure refinement. *J. Phys. Org. Chem.* **2020**, *33*, e4114.

23. (a) Dressler, J. J.; Teraoka, M.; Espejo, G. L.; Kishi, R.; Takamuku, S.; Gómez-García, C. J.; Zakharov, L. N.; Nakano, M.; Casado, J.; Haley, M. M. Thiophene and Its Sulfur Inhibit Indenoindenodibenzothiophene Diradicals from Low-energy Lying Thermal Trip. *Nat. Chem.* **2018**, *10*, 1134–1140. (b) Barker, J. E.; Dressler, J. J.; Cárdenas Valdivia, A.; Kishi, R.; Strand, E. T.; Zakharov, L. N.; MacMillan, S. N.; Gómez-García, C. J.; Nakano, M.; Casado, J.; Haley, M. M. Molecule Isomerism Modulates the Diradical Properties of Stable Singlet Diradicaloids. *J. Am. Chem. Soc.* **2020**, *142*, 1548–1555.

24. Boominathan, S. S. K.; Chang, K.-H.; Liu, Y.-C.; Wang, C.-S.; Wu, C.-F.; Chiang, M.-H.; Chou, P.-T.; Yao-Ting Wu, Y.-T. Diindeno-Fused Dibenzo[*a*,*h*]anthracene and Dibenzo[*c*,*l*]chrysene: Syntheses, Structural Analyses, and Properties. *Chem. – Eur. J.* **2019**, *25*, 7280−7284.

25. (a) Datta, S.; Cai, Y.; Yudhistira, I.; Zeng, Z.; Zhang, Y.; Zhang, H.; Adam, S.; Wu, J.; Loh, K. P. Tuning magnetoresistance in molybdenum disulphide and graphene using a molecular spin transition. *Nat. Commun.* **2017**, *8*, 1–8. (b) Nakano, M. Open-Shell-Character-Based Molecular Design Principles: Applications to Nonlinear Optics and Singlet Fission. *Chem. Rec.* **2017**, *17*, 27–62.

26. Bruker, SAINT V8.38A, (Bruker AXS Inc., **2017**).

27. Dolomanov, O. V.; Bourhis, L. J.; Gildea, R. J.; Howard, J. A.; Puschmann, H. Olex2: A complete structure solution, refinement and Analysis Program. *J. Appl. Crystallogr.* **2009**, *42*, 339–341.

28. Bourhis, L. J.; Dolomanov, O. V.; Gildea, R. J.; Howard, J. A.; Puschmann, H. The anatomy of a comprehensive constrained, restrained refinement program for the modern computing environment –olex2dissected. *Acta Crystallogr. A.* **2015**, *71*, 59–75.

29. Sheldrick, G. M. Crystal structure refinement with SHELXL. *Acta Crystallogr. C Struct. Chem.* **2015**, *71*, 3–8.

30. Gaussian 09, *Revision B.01*, M. J. Frisch, G. W. Trucks, H. B. Schlegel, G. E. Scuseria, M. A. Robb, J. R. Cheeseman, G. Scalmani, V. Barone, B. Mennucci, G. A. Petersson, H. Nakatsuji, M. Caricato, X. Li, H. P. Hratchian, A. F. Izmaylov, J. Bloino, G. Zheng, J. L. Sonnenberg, M. Hada, M. Ehara, K. Toyota, R. Fukuda, J. Hasegawa, M. Ishida, T. Nakajima, Y. Honda, O. Kitao, H. Nakai, T. Vreven, J. A. Montgomery, J. E. Jr., Peralta, F. Ogliaro, M. Bearpark, J. J. Heyd, E. Brothers, K. N. Kudin, V. N. Staroverov, T. Keith, R. Kobayashi, J. Normand, K. Raghavachari, A. Rendell, J. C. Burant, S. S. Iyengar, J. Tomasi, M. Cossi, N. Rega, J. M. Millam, M. Klene, J. E. Knox, J. B. Cross, V. Bakken, C. Adamo, J. Jaramillo, R. Gomperts, R. E. Stratmann, O. Yazyev, A. J. Austin, R. Cammi, C. Pomelli, J. W. Ochterski, R. L. Martin, K. Morokuma, V. G. Zakrzewski, G. A. Voth, P. Salvador, J. J. Dannenberg, S. Dapprich, A. D. Daniels, O. Farkas, J. B. Foresman, J. V. Ortiz, J Cioslowski, D. J. Fox, Gaussian, Inc., Wallingford CT, **2010**.

31. (a) Kubo, T. Recent Progress in Quinoidal Singlet Biradical Molecules. *Chem. Lett.* **2015**, *44*, 111–122. (b) Das, S.; Wu, J. Open-shell benzenoid polycyclic hydrocarbons, in: Polycyclic arenes and heteroarenes: synthesis, properties, and applications. Qian M, editor. *John Wiley & Sons Inc.*, **2015**, 3–36.

32. O'Boyle, N. M.; Tenderholt, A. L.; Langner, K. M. cclib: A library for package-independent computational chemistry algorithms. *J. Comp. Chem.* **2008**, *29*, 839–845.

3B.6 Appendix

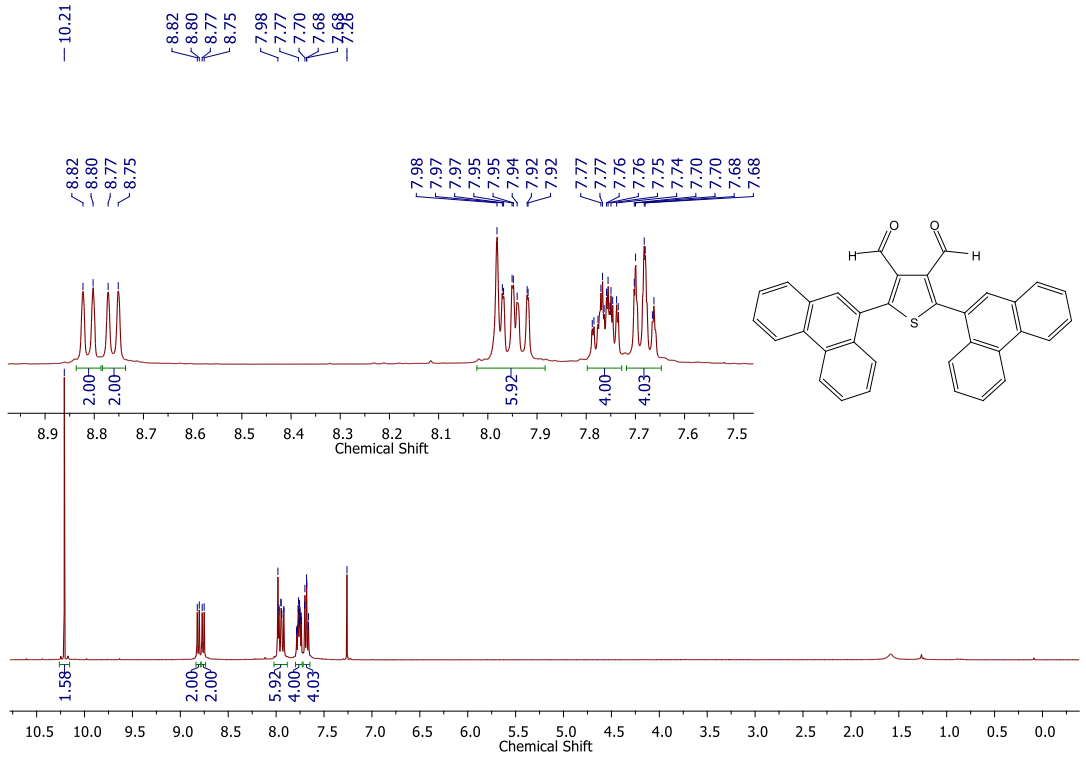

Figure 3B.13 ^{1}H NMR spectrum of **9** (in $CDCl_3$, 400 MHz, 298 K).

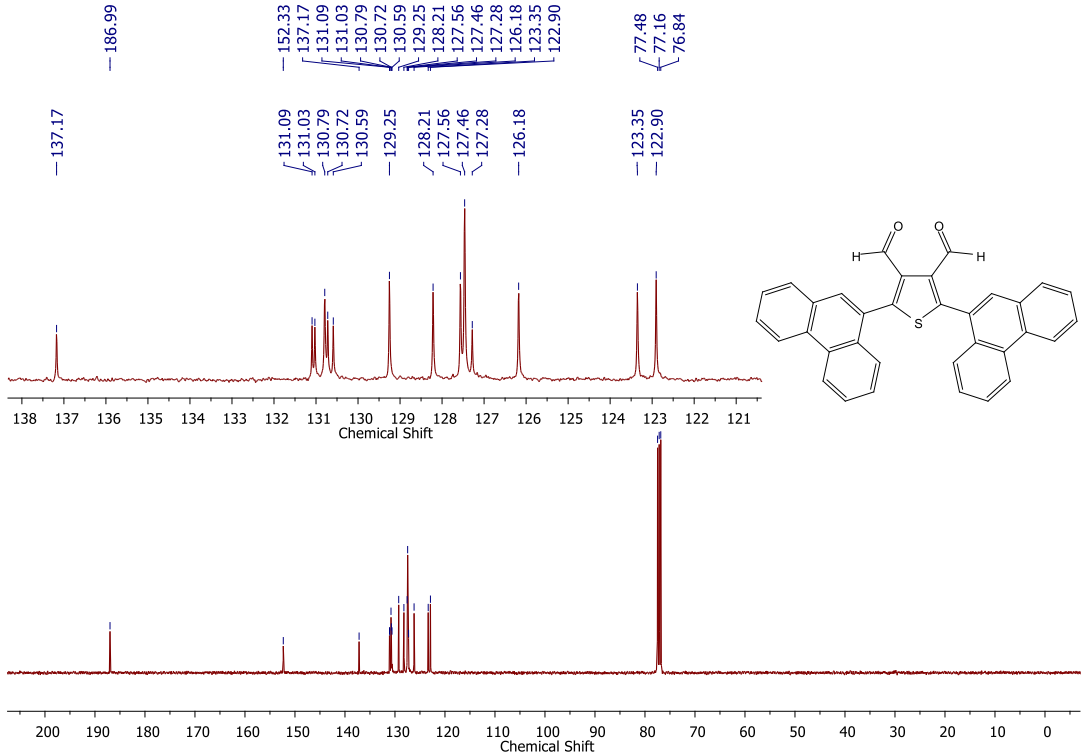

Figure 3B.14 $^{13}C\{^{1}H\}$ NMR spectrum of **9** (in $CDCl_3$, 100 MHz, 298 K).

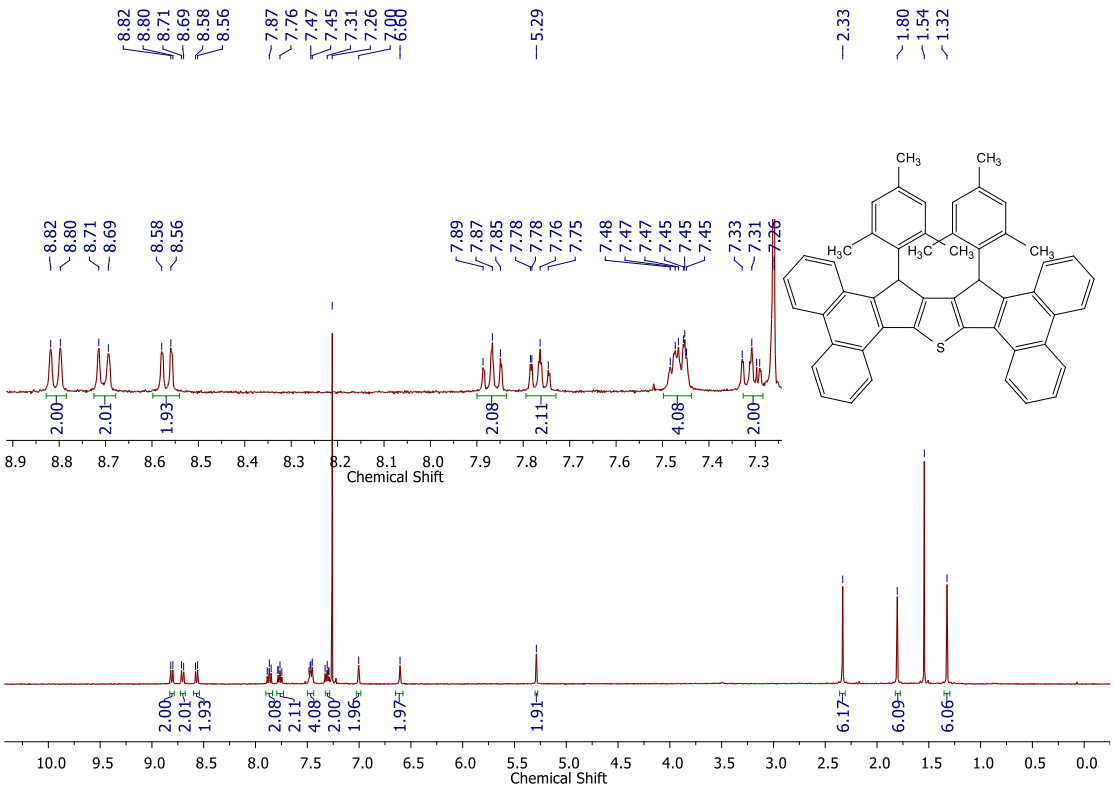

Figure 3B.15 ^{1}H NMR spectrum of **2H-DPDCPT** (in $CDCl_3$, 400 MHz, 298 K).

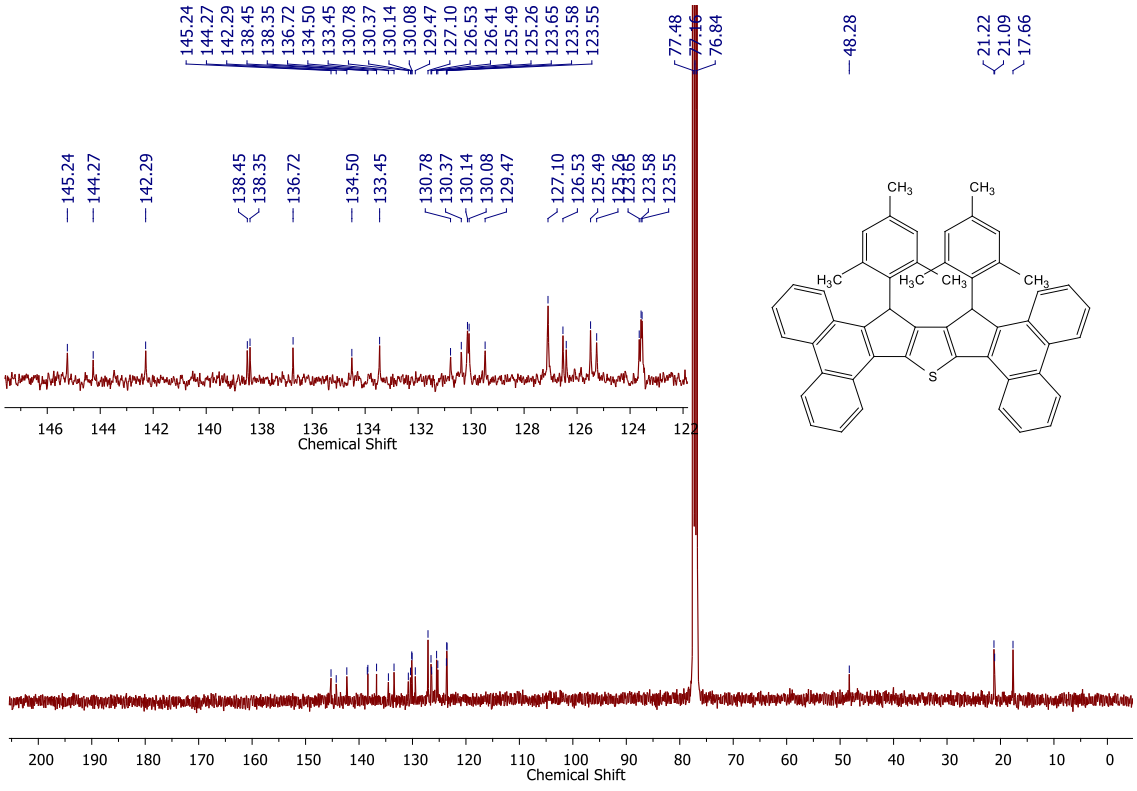

Figure 3B.16 ^{13}C{^{1}H} NMR spectrum of **2H-DPDCPT** (in $CDCl_3$, 100 MHz, 298 K).

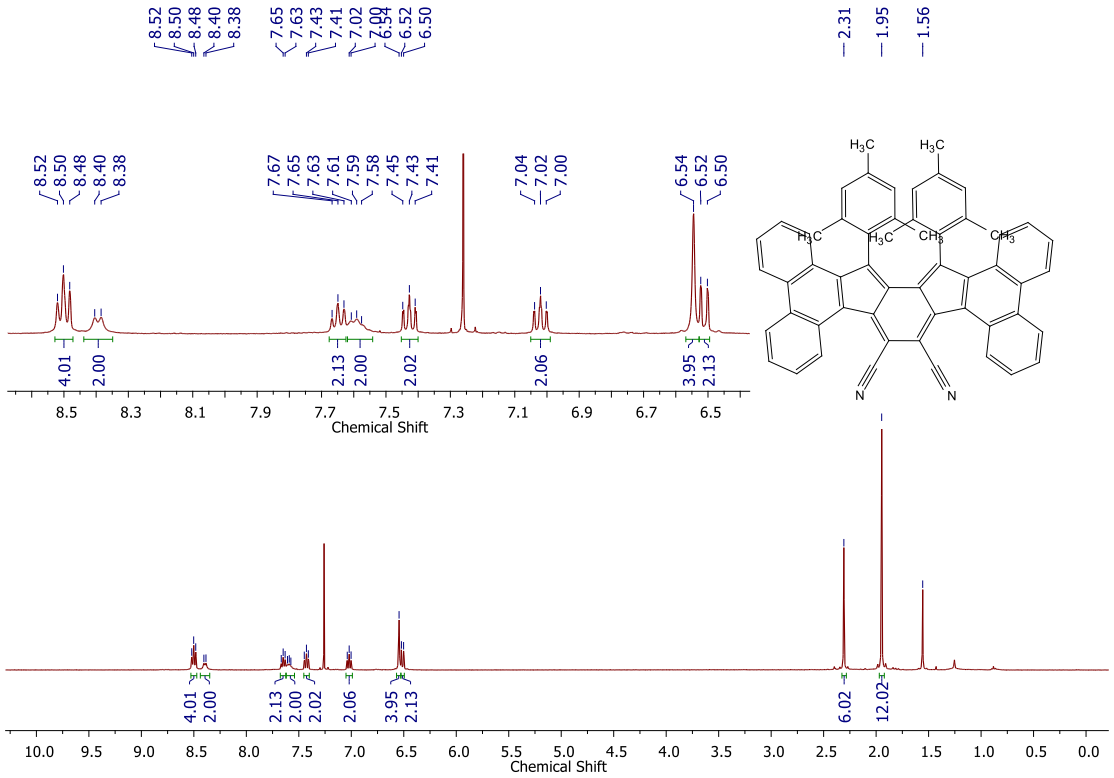

Figure 3B.17 ^{1}H NMR spectrum of **6** (in $CDCl_3$, 400 MHz, 298 K).

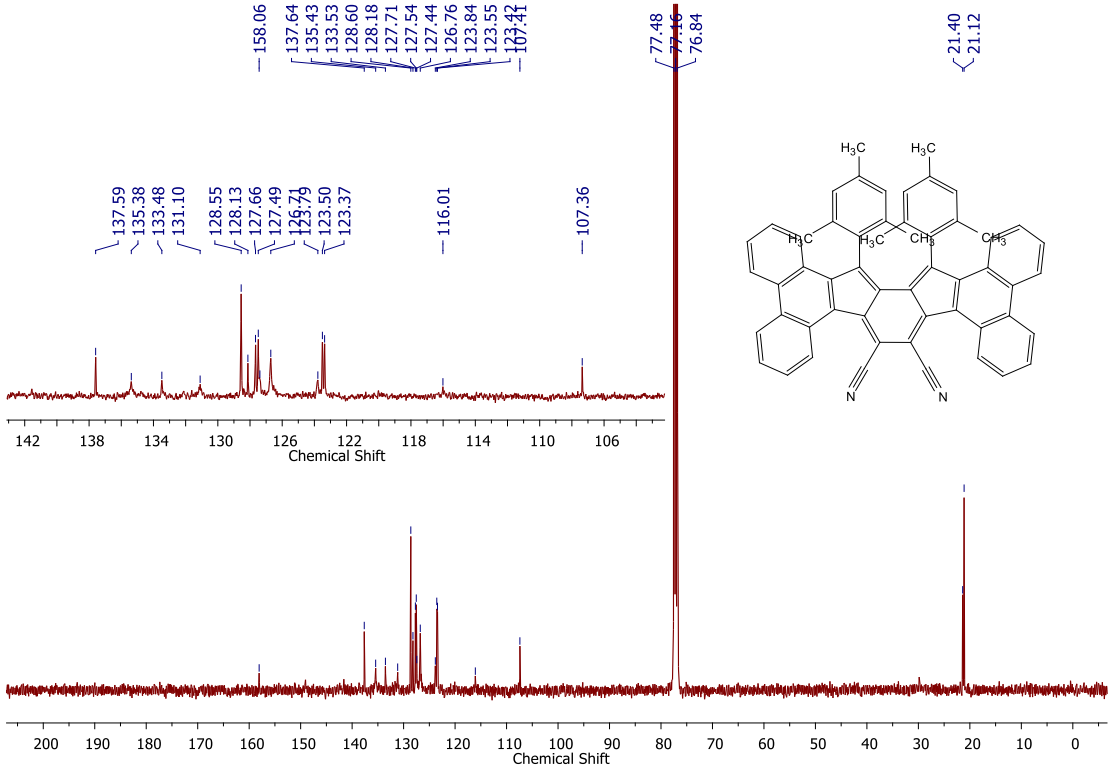

Figure 3B.18 $^{13}C\{^{1}H\}$ NMR spectrum of **6** (in $CDCl_3$, 100 MHz, 298 K).

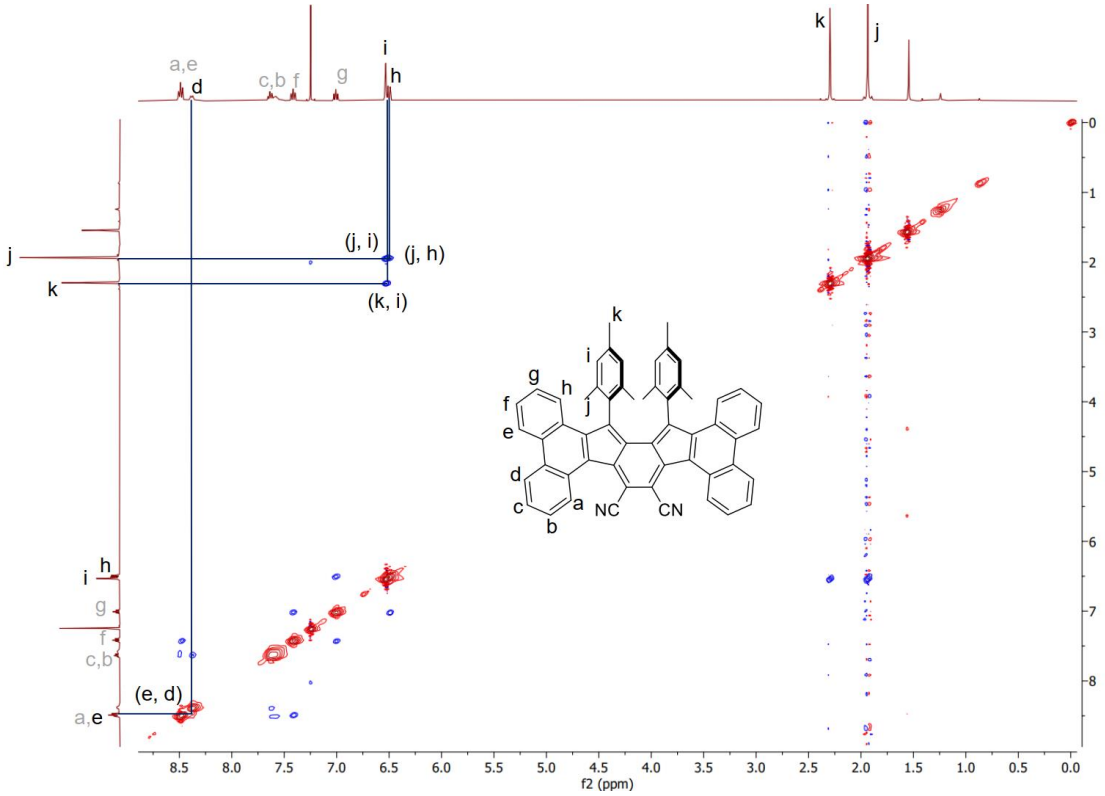

Figure 3B.19 ^{1}H-^{1}H NOESY spectrum of **6** (in $CDCl_3$, 298 K)

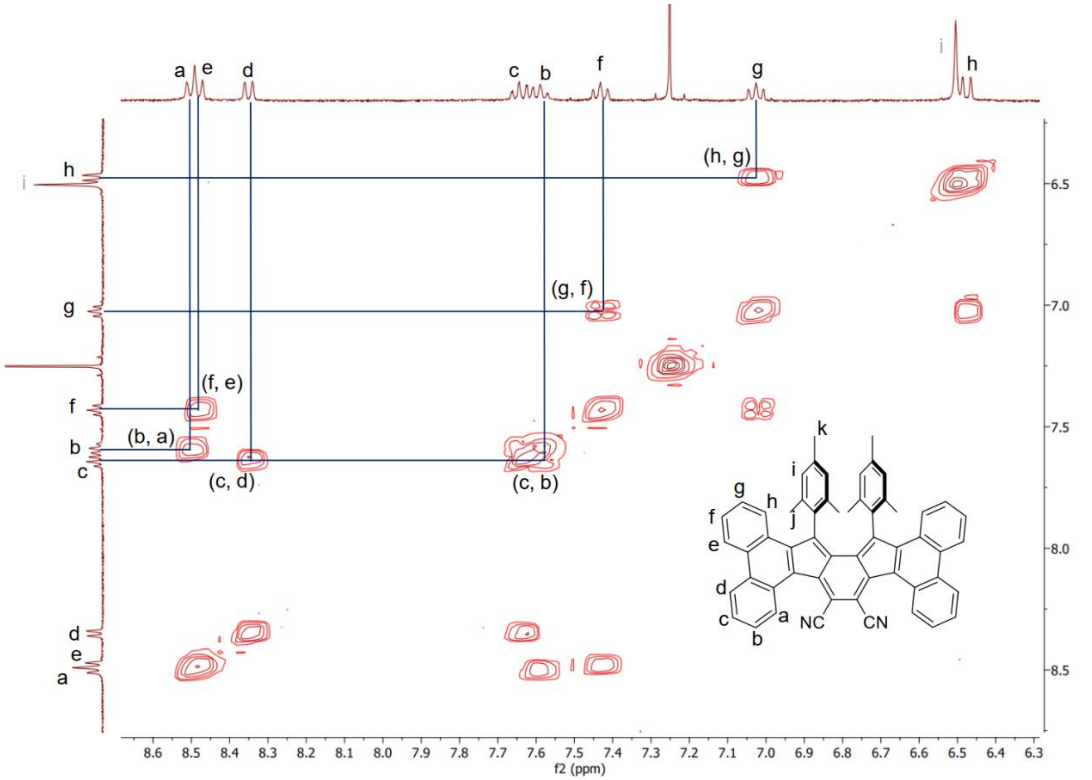

Figure 3B.20 ^{1}H-^{1}H COSY spectrum of **6** (in $CDCl_3$, 233 K, aromatic region expansion).

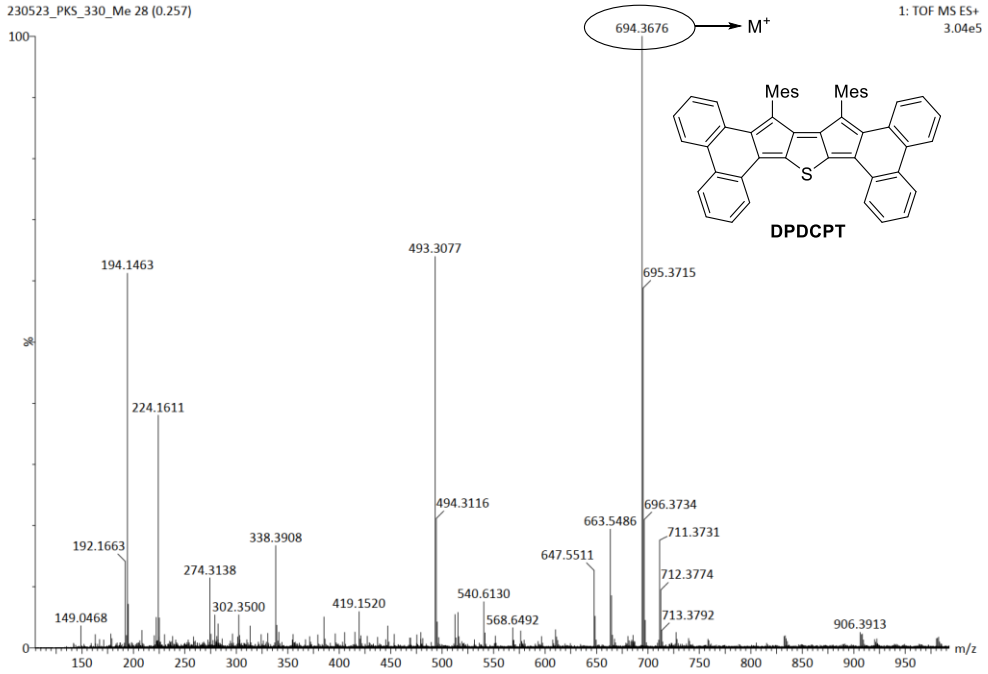

Figure 3B.21 Compound **DPDCPT** was detected by direct mass spectrometric analysis ((ESI) *m/z*: $[M]^+$ (z = 1) value of 694.3 (calcd 694.3) from the crude reaction mixture.

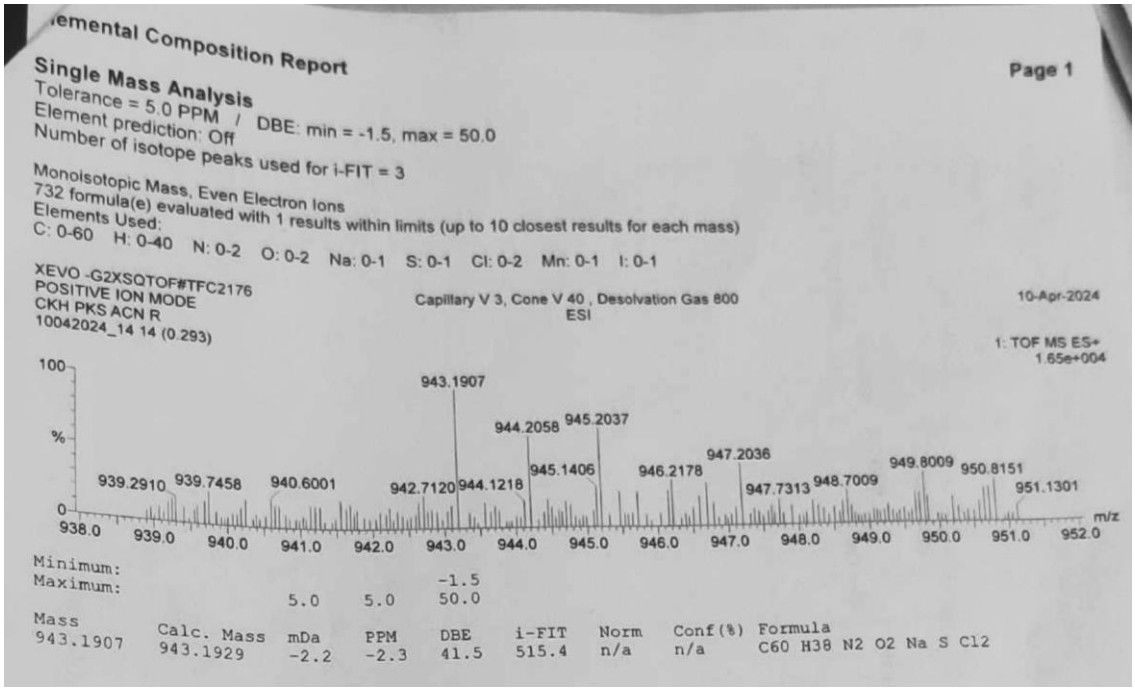

Figure 3B.22 HRMS spectrum of **DPDCPT-DDQ**. HRMS (ESI) *m/z*: $[M + Na]^+$ calcd for $C_{60}H_{38}N_2O_2NaSCl_2$ 943.1929, found 943.1907 (error: −2.3 ppm).

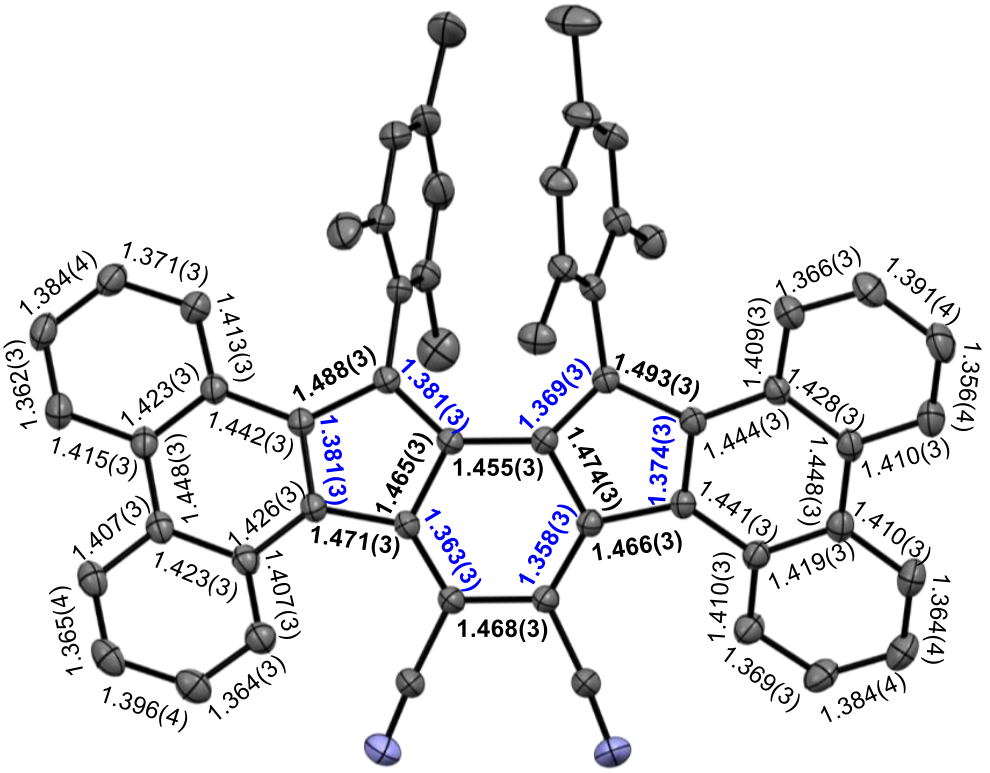

Figure 3B.23 ORTEP drawing of **6** with thermal ellipsoids at 30% probability level, showing the core bond lengths with e.s.d values (hydrogens, and acetonitrile solvent disorder omitted).

Reason for [$\pi^{10}_S + \pi^2_S$] thermally forbidden cycloaddition reaction:

Generally, [$\pi^{10}_S + \pi^2_S$] cycloaddition reactions are thermally forbidden and photochemically allowed. Interestingly, in this case, the reaction proceeds under thermal conditions. DFT calculations at BHandHLYP/6-31G(d) level suggest an open-shell singlet ground state with 51% diradical character, and it can be represented in two resonance forms: closed-shell and open-shell form, as shown in Figure 3B.24. In such open-shell diradical systems, the traditional concepts of symmetry-allowed or forbidden reactions become invalid. Furthermore, this double excitation configuration lowers the symmetry-imposed activation energy, which may facilitate the reaction under thermal conditions.[14a]

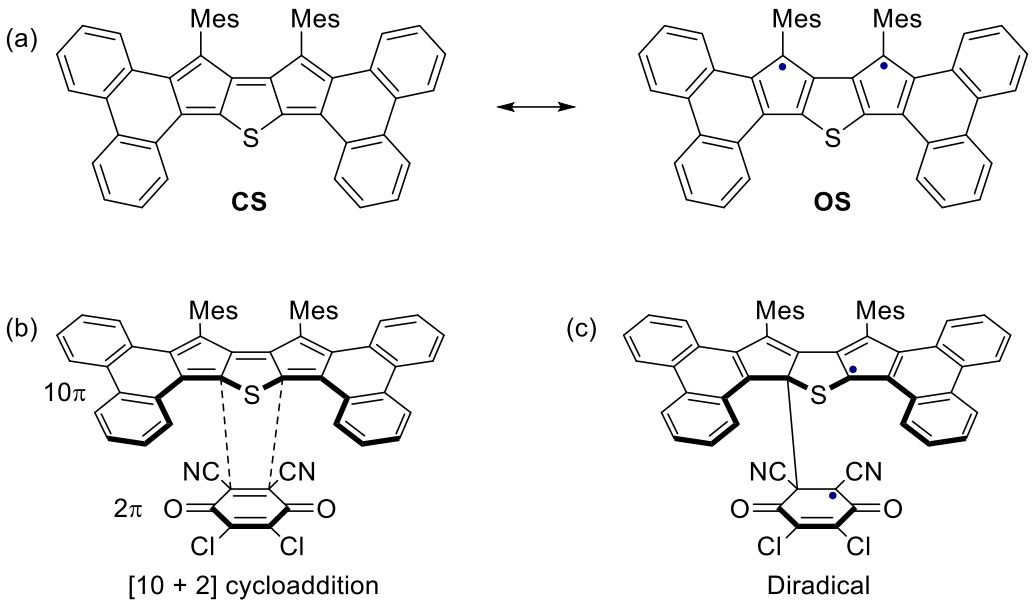

Figure 3B.24 (a) Representative closed-shell (CS) and open-shell (OS) diradical resonance forms of DPDCPT. Adducts through cycloaddition (b) and diradical (c) pathways are shown.

Chapter 4

Dominating Antiaromatic Character of *as*-Indacene Decides Overall Properties of a Formally Aromatic Dicyclopenta[*c*]fluorenothiophene

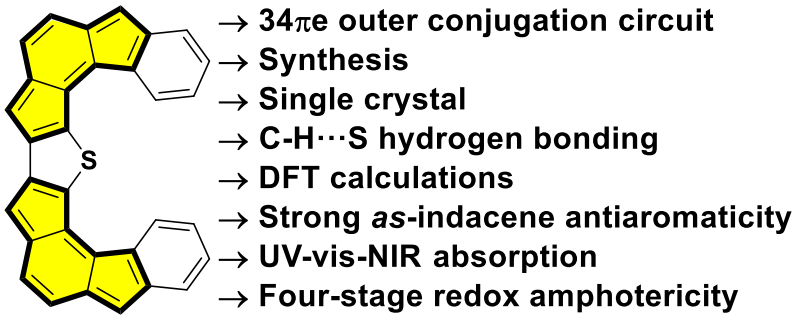

This work was published in *Organic Letters* (an ACS journal). Please see the citation as: "Sharma, P. K., Mallick, D., Sharma, H., Das, S. Dominating Antiaromatic Character of *as*-Indacene Decides Overall Properties of a Formally Aromatic Dicyclopenta[*c*]fluorenothiophene. *Org. Lett.* **2023**, *25*, 2201–2206."

4 Abstract

Dicyclopenta[*c*]fluorenothiophene **5** was synthesized as the isoelectronic polycyclic heteroarene analogue of an *as*-indacenodifluorene with a (4n + 2)π-electron perimeter. Single-crystal and ^{1}H NMR analyses indicated a quinoidal ground state for **5**, which was supported by theoretical calculations while suggesting a degree of antiaromaticity of the *as*-indacene subunit greater than that for *s*-indacenodifluorene **3**. The dominant antiaromaticity for **5** was evidenced by the broad weakly intense absorption tail reaching the near-IR region, four-stage redox amphotericity, and small HOMO−LUMO energy gap.

4.1 Introduction

Poly(indenoindene) or PININ is a fully conjugated ladder polymer based on π-extended antiaromatic indenofluorene (Figure 4.1a).[1] Theoretical studies of the structural isomers of Müllen's PININ revealed their small band gap and high spin ground states.[2] As highlighted in Chapter 1, after the reports of formally antiaromatic indeno[1,2-*b*]fluorene[3] and indeno[2,1-*c*]fluorene[4] regioisomers, Tobe reported the designs of the parent *s*-indaceno[1,2-*b*:5,6-*b′*]difluorene (Figure 4.1b) and π-extended [1,2-*b*:5,6-*b′*]*s*-IDF (Figure 4.1c) as non-benzenoid polycyclic arenes (PAs) based on *s*-indacene unit (shown in blue color).[5] In 2015, Tobe proposed an *as*-indacene-embedded (shown in red color, Figure 4.1d) helical *as*-indacenodifluorene **1** (*as*-IDF), but its synthesis and ground-state properties were unknown at that time.[6]

A helical fragment of **1** with seven alternatingly fused 6-5-6-5-6-5-6 rings in doublet ground state was reported.[7] It was Wu's group that synthesized a stable closed-shell *s*-indacenodifluorene (*s*-IDF) **2** (Figure 4.1e),[8] which was based on Tobe's [1,2-*b*:5,6-*b′*]*s*-IDF scaffold (Figure 4.1b).[5] *s*-IDF **2** is a fragment of the fully conjugated ladder oligo(ININ) [or OININ] which was lately investigated by on-surface synthesis.[9] Computational studies found small multiple diradical characters of these quasi-one-dimensional OININs made of *s*-indacene repeating units, with potential for nonlinear optics applications.[10] Our group reported **3** (Figure 4.1f) as the *as*-indacene containing second structural isomer of *s*-IDF series using a synthetic route that allowed us to synthesize [2,1-*c*]IF, too, without applying harsh conditions.[11a]

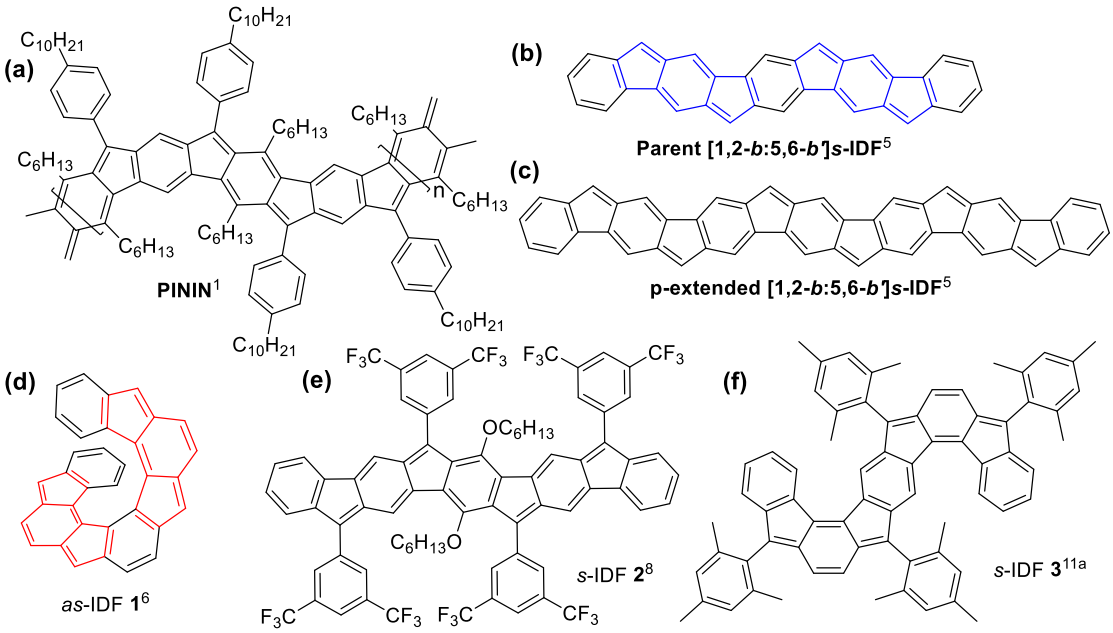

Figure 4.1. (a) Müllen's PININ. Tobe's (b) *s*-indaceno[1,2-*b*:5,6-*b'*]difluorene, and (c) π-extended [1,2-*b*:5,6-*b'*]*s*-IDF. (d) Helical *as*-indaceno[2,1-*c*:7,8-*c*']difluorene **1**. (e) Wu's *s*-IDF **2**. (f) Das's *s*-IDF **3**.

s-IDF **3** showed a HOMO–LUMO energy gap smaller than that of **2**, a red-shifted absorption in the NIR region, and a smaller singlet-triplet (S-T) energy gap that resulted in ^{1}H-NMR line broadening at higher temperature,[11a] whereas a dibenzo-extended derivative of *s*-IDF **3** bearing a 2,6-dichlorophenyl substituent in place of mesityl was reported to show an open-shell ground state.[11b] *as*-Indacene-embedded IFs usually showed smaller HOMO–LUMO and S-T energy gaps in comparison to *s*-indacene based PAs,[3,4,12] and thus the smaller electronic gaps for **3** than **2** could be attributed to the presence of *as*-indacene in the π-backbone. Though diareno-[13] or diheteroareno[14]-annulated *s*-indacenes with 4nπ-electron perimeter were known to have tunable antiaromaticity, reports on *as*-indacene-embedded polycyclic heteroarenes (PHAs) with (4n + 2)π-electron perimeter and the consequences of *as*-indacene antiaromatic character in the ground state electronic properties received hardly any attention.

Parent *as*-indaceno[2,3-*c*:7,6-*c*']difluorene **4** (Figure 4.2a) can be regarded as a constitutional isomer of *as*-IDF **1**; however, none of the two fully conjugated *as*-IDF regioisomers was synthesized to date. We envisaged replacing the bridging sp^2 carbon unit (shown in magenta color, Figure 4.2a) of the central benzene ring of **4** with an isoelectronic sulfur atom to design a new PHA **5**, which could be considered as an isoelectronic PHA analogue of *as*-IDF. It was anticipated that the incorporation of a

thiophene unit could significantly enhance the ground-state antiaromaticity of two *as*-indacene units, resulting in interesting optoelectronic properties. Our design of **5** was motivated from the recent works by Haley[14a,14b,14f] on modulation of *s*-indacene antiaromaticity by fusing aromatic heterocycles; however, per our knowledge, heterocycle-fused *as*-indacene displaying dominant ground-state antiaromaticity is rare.

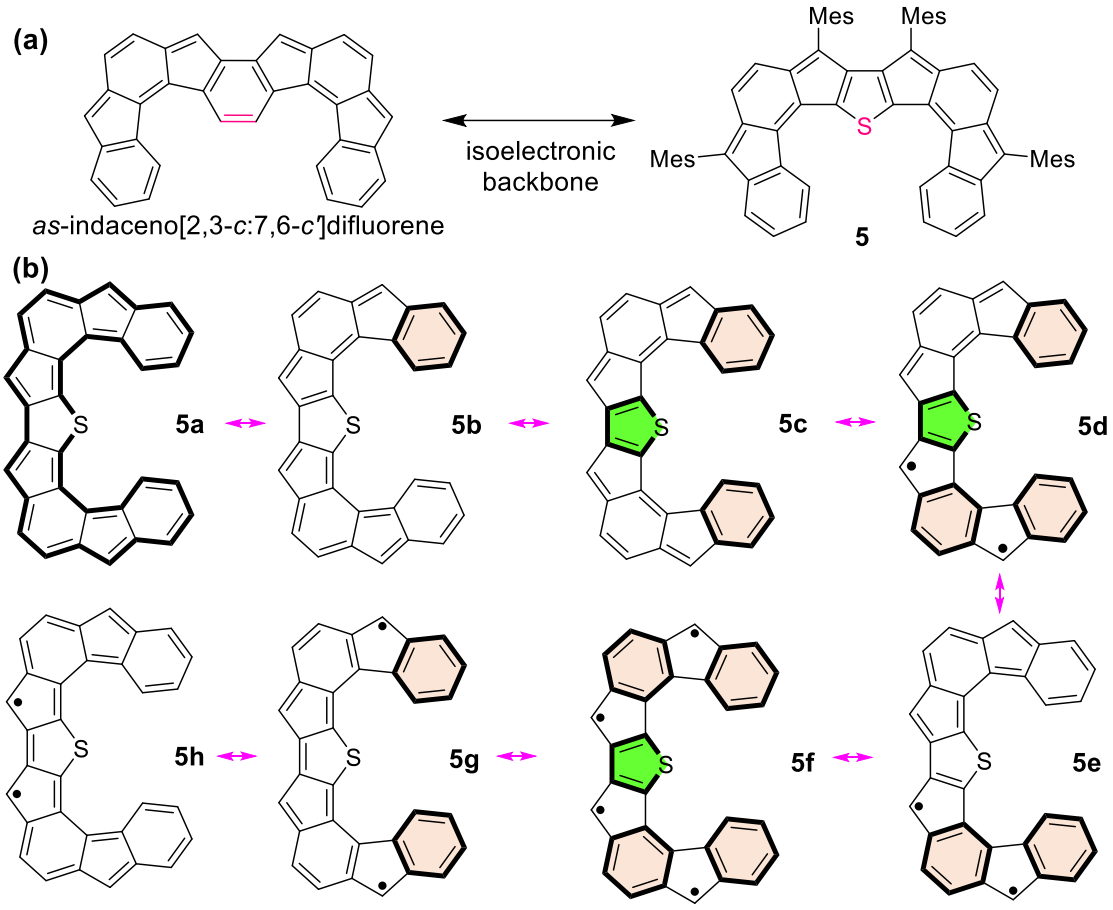

Figure 4.2 (a) Target **5** as isoelectronic analog of [2,3-*c*:7,6-*c*']*as*-IDF **4**. (b) Representative resonance forms of parent **5** (benzene and thiophene aromaticity are shaded with orange and green color, respectively).

Targeted PHA **5** can be viewed as a formally aromatic compound considering 34π-electrons in the outer conjugation circuit, as shown for parent structure **5a** (Figure 4.2b). It may also be represented as two more closed-shell forms, **5b** and **5c**, and as a potential diradical-like[10,11b] form **5d**, while other representative open-shell forms **5h**-**5e** are quite unlikely. Herein, we report the synthesis of *as*-indacene-embedded (4n + 2)π dicyclopenta[*c*]fluorenothiophene **5**, and its ground-state characteristics were experimentally analyzed by nuclear magnetic resonance (NMR), single crystal X-ray

diffractometry (SCXRD), UV-vis-NIR absorption, and cyclic voltammetry (CV) studies. The experimental findings were supported by density functional theory (DFT) calculations.

4.2 Results and Discussion

4.2.1 Synthesis. The synthetic route to **5** started by esterification of thiophene-3,4-dicarboxylic acid **6** with ethanol/sulfuric acid to afford diester **7**, which was subsequently brominated to **8** (Scheme 4.1).[15] Diisobutylaluminium hydride (DIBAL-H) reduction of the diester **8** to diol, followed by oxidation of the crude diol using pyridinium chlorochromate (PCC), afforded dialdehyde **9** in 55% yield. Compound **9** underwent Suzuki coupling with pincaolboronate **10** to afford **11**, following our reported method.[11a] Treatment of **11** with 2-mesitylmagnesium bromide (2-MesMgBr) in ambient condition gave alcohol **12**, which, without purification, was treated with methanesulfonic acid at room temperature to afford dihydro precursor **13**. Oxidative dehydrogenation of **13** using 2,3-dichloro-5,6-dicyano-1,4-benzoquinone (DDQ) in dry toluene gave **5** as dark-purple solid in 22% yield over three steps, after column chromatographic purification. The structure of **5** was established by 1D and 2D NMR spectroscopy (Figure 4.4 and 4.5), which showed an upfield shift for the two *as*-indacene hydrogens of **5** (5.79 and 5.65 ppm) than those of **3** (6.16 and 6.06 ppm) in $CDCl_3$ (Figure 4.3 and Figure 4.6).

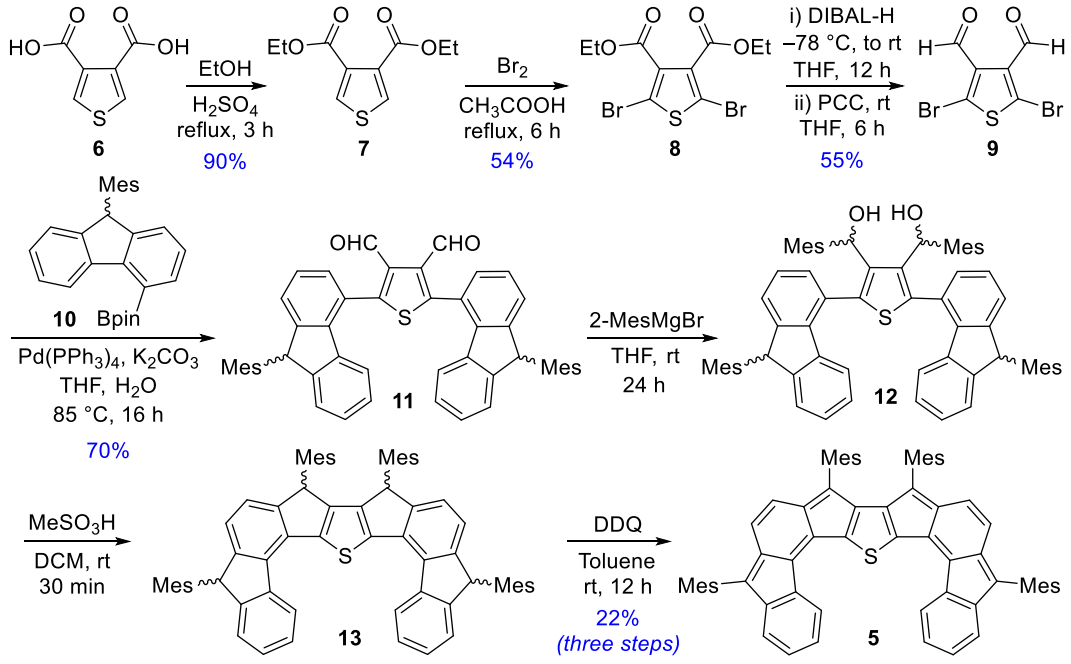

Scheme 4.1 Synthesis of **5** (Mes = Mesityl).

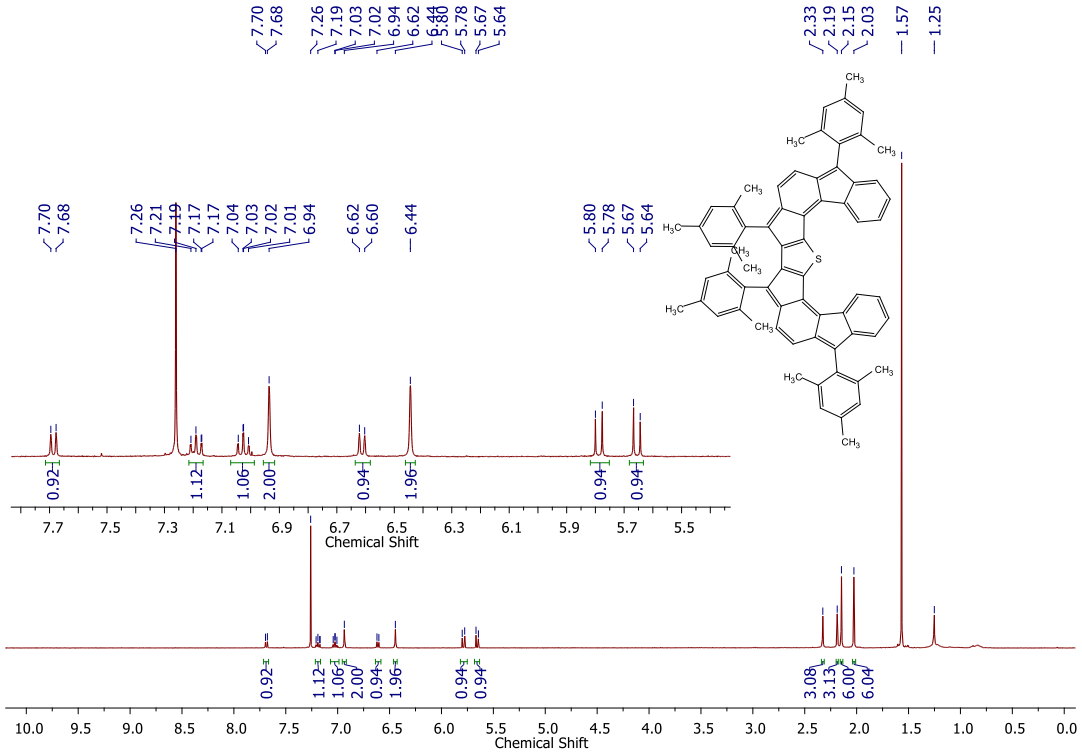

Figure 4.3 ^{1}H NMR spectrum of **5** (in $CDCl_3$, 400 MHz, 298 K).

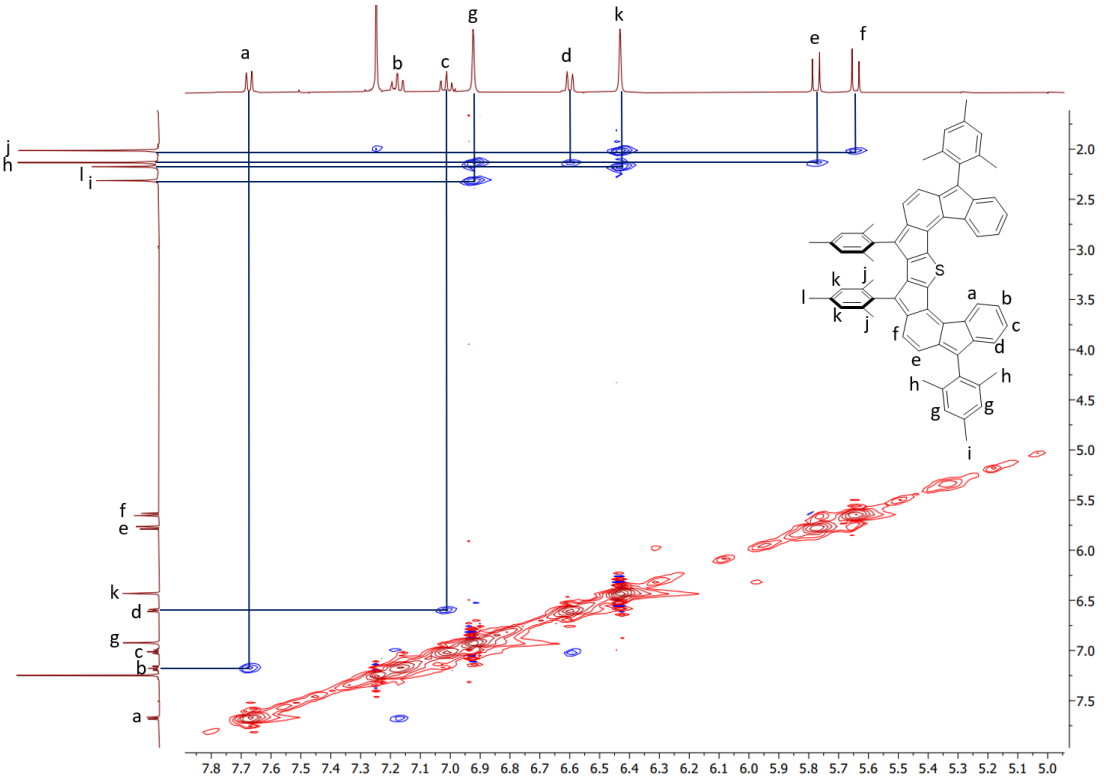

Figure 4.4 Full ^{1}H-^{1}H NOESY spectrum of **5** in $CDCl_3$.

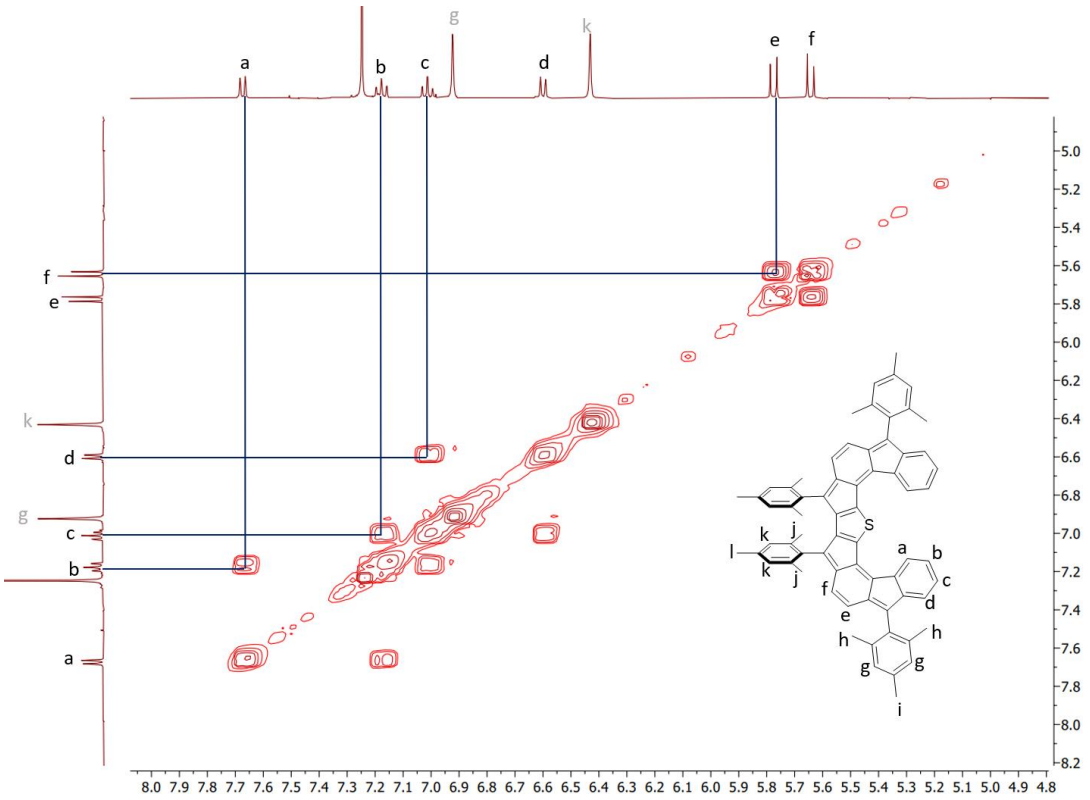

Figure 4.5 ^{1}H-^{1}H COSY spectrum of **5** in $CDCl_3$ (aromatic region expansion).

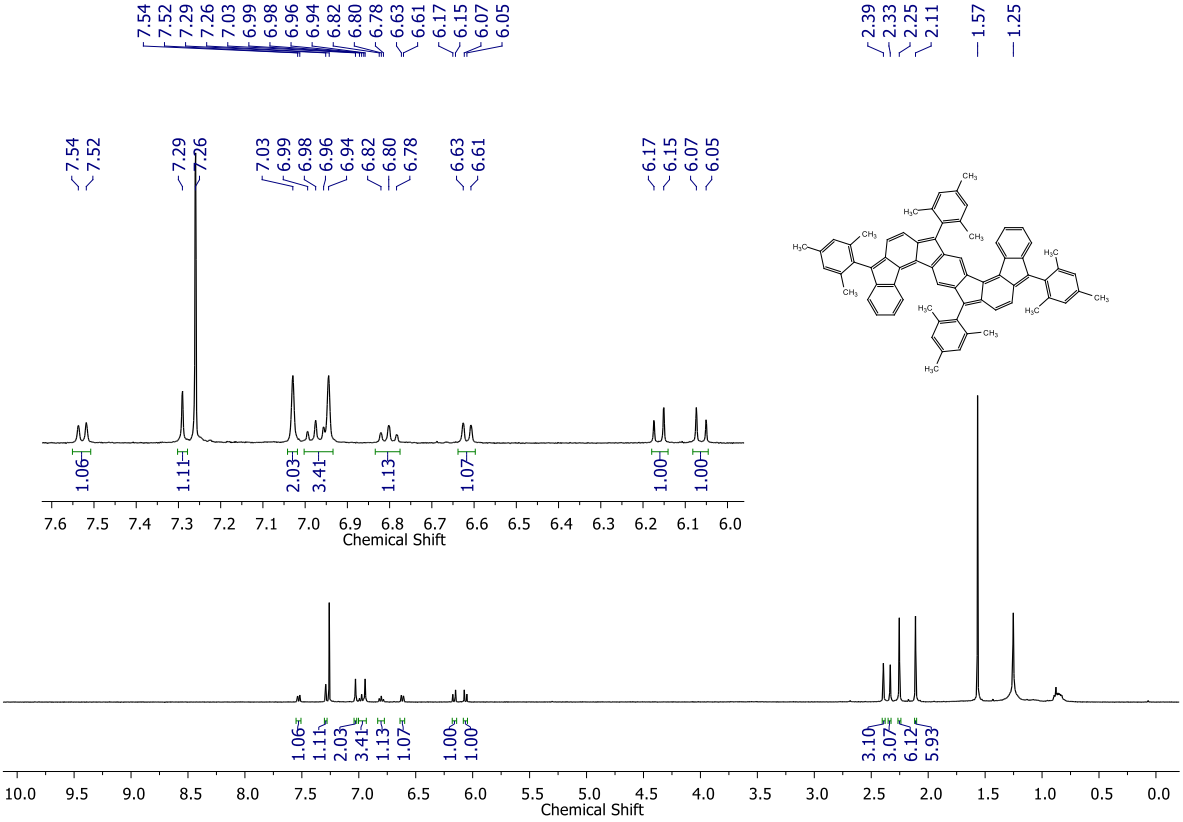

Figure 4.6 ^{1}H NMR spectrum of *s*-IDF **3**[11a] (400 MHz, 298 K, moisture at 1.57 ppm and residual hexane at 1.25, 0.88 ppm), recorded in $CDCl_3$ to compare the shifts of *as*-indacene protons with **5** (Figure 4.3).

4.2.2 X-ray crystallography and antiaromaticity analyses. Single crystals of **5** (Figure 4.7a) for SCXRD analysis were obtained by diffusing methanol to the dichloromethane (DCM) solution at ambient temperature. Compound **5** has a rigid and quasi-planar backbone with terminal benzene rings (A) twisted by ~8.3° (average) in the cove-like region, as measured from the mean planes between ring E and rings A (Figure 4.7b). The near orthogonally deviated mesityl groups likely prevented aggregation, and thus **5** was moderately soluble in common organic solvents. The *as*-indacene subunit of **5** showed large C_{sp}^2–C_{sp}^2 bond length alternation (BLA), as shown in Figure 4.7a, with C=C bonds (*a*-*f*, see labeling in Figure 4.7a) having greater double bond character than rest of the C_{sp}^2–C_{sp}^2 bonds (*g*-*l*), demonstrating an alternate double bond and single bond character. To compare BLA, *as*-indacene embedded *s*-IDF **3** and **5** were chosen (Table 4.1), which clearly revealed that C=C bond *a* linking cyclopenta[*c*]fluorene and thiophene for **5** is 0.016 Å shorter than that of *a* for **3** bearing benzene,[11a] while the other C=C bond lengths were identical. Shortening of the bond *a* for **5**, due to increased double-bond character of less aromatic thiophene,[14f] implies larger BLA for *as*-indacene than for **3**, hinting significant *para*-quinoidal contribution in the form of **5c** (Figure 4.2b) to the ground-state **5**.

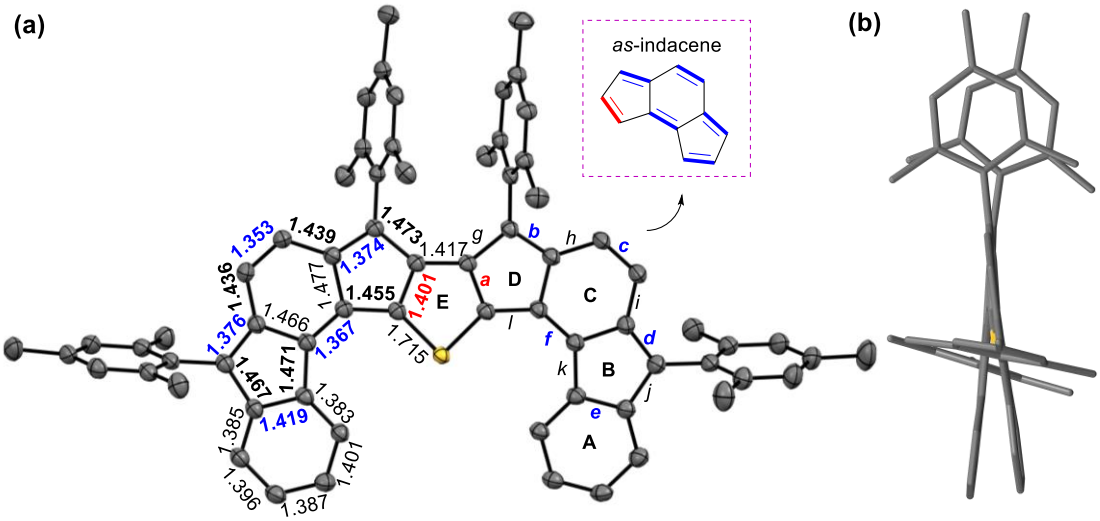

Figure 4.7 (a) ORTEP drawing of **5** with ellipsoids at the 50% probability level (hydrogens omitted), including average bond lengths (Å). (b) Side view of **5**.

Table 4.1 Mean C_{sp}^2=C_{sp}^2 bond lengths (in Å) of **5** and **3**, for *as*-Indacene.

Compound	*a*	*b*	*c*	*d*	*e*	*f*
3	1.417	1.373	1.351	1.372	1.420	1.365
5	1.401	1.374	1.353	1.376	1.419	1.367

The herringbone packing motif (Figure 4.8a) for the crystal of **5** was formed by several short contacts, listed in Figure 4.8b. The short intermolecular C−H···π interactions (*o* = 2.899 Å, *p* = 2.882 Å) between neighbouring molecules enabled the T-like arrangement, and another set of intermolecular C−H···π interaction (*n* = 2.861 Å) with a C−H···S hydrogen bonding (HB) interaction (*m* = 2.778 Å, 168.1°) enabled slipped π-stacks forming an overall two-dimensional herringbone-like arrangement. Compound **5** displayed two intramolecular C−H···S (*q* = 2.701 Å, 147.0; *r* = 2.675 Å, 147.4°) HB interactions, an underappreciated non-covalent interaction,[16] which likely shifted the hydrogen-bonded ring A protons toward downfield region in ^{1}H-NMR (7.69 ppm for **5**) than **3** (7.53 ppm, Figure 4.6).

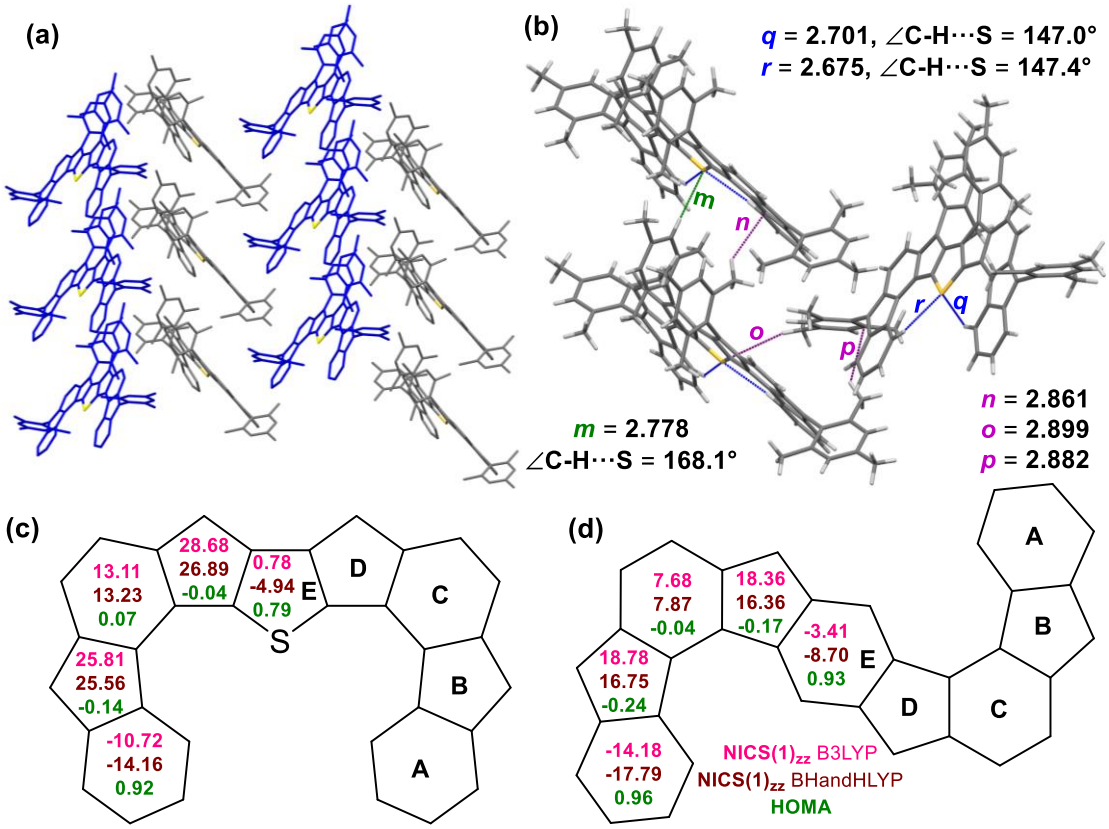

Figure 4.8 (a) Short contacts (Å) are labelled for **5**. (b) Two-dimensional herringbone packing arrangement of **5**. HOMA values, and NICS(1)$_{zz}$ indices for the π-backbone of (c) **5** and (d) **3**,[11a] respectively, using B3LYP/6-31G(d) (pink) and BHandHLYP/6-31G(d) (brown) functionals.

DFT optimization at B3LYP/6-31G(d) level of theory suggested that **5** has a singlet closed-shell ground state with large S-T gap (10.1 kcal mol^{-1}, zero diradical character, Table 4.4), which corresponds with the *para*-quinoidal *as*-indacene subunit. The harmonic oscillator model for aromaticity (HOMA) analysis of optimized

structure **5** indicated not so large BLA for ring A (0.92) and E (0.79),[17] while the rings B (–0.14), C (0.07), D (–0.04) showed significant BLA (Figure 4.8c). The nucleus independent chemical shift ($NICS(1)_{zz}$)[18] indices of **5** at the same level of theory agree with the aromaticity of ring A (–10.72), while non-aromaticity for ring E (0.78) and strong antiaromaticity for B (25.81), C (13.11), and D (28.68) rings were suggested, respectively (Figure 4.8c). Considering B3LYP may not accurately estimate (anti)aromaticity,[19] as we examined for **3** to get more reliable results (Figure 4.8d), BHandHLYP functional was used to quantify the aromaticity of **5**. The $NICS(1)_{zz}$ indices obtained at BHandHLYP level for **5** (A = –14.16, B = 25.56, C = 13.23, D = 26.89, E = –4.94; Figure 4.8c) are identical to those found for B3LYP level, except for the thiophene (ring E) which is found to be weakly aromatic and in line with HOMA value. The anisotropy of the induced current density (ACID)[20] plot of **5** (Figure 4.9) is in line with the NICS indices (Figure 4.8c), exhibiting counter-clockwise semiglobal ring-current spread over rings B, C and D with considerable localization of counterclockwise ring currents over B and D rings, which clearly suggested the significant paratropic nature of *as*-indacene subunit. The strong clockwise ring currents for aromatic ring A agree with the large negative NICS value, while observation of diatropic ring currents over ring E (Figure 4.9) is consistent with its weak aromatic character.

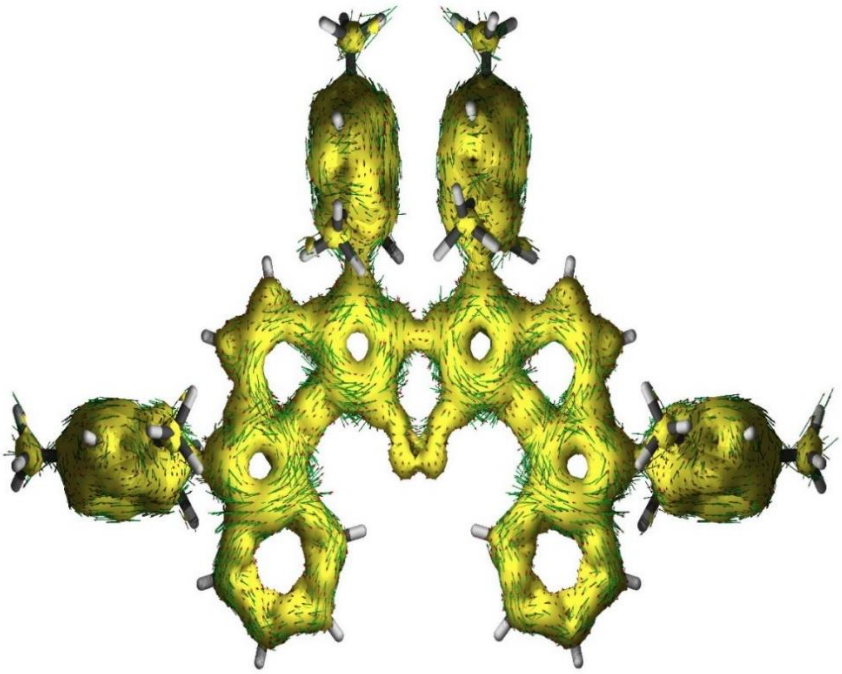

Figure 4.9 Current-density vectors for **5** are plotted onto the ACID isosurface of 0.02 at BHandHLYP /6-31G(d) level of theory.

4.2.3 Optical and electrochemical properties. The UV-vis-NIR absorption spectrum of **5** in DCM depicted in Figure 4.10a exhibited intense absorption in the UV region (λ_{max} = 342 nm, ε = 43945 M^{-1} cm^{-1}), with absorption in the visible region at λ_{max} = 557 nm (ε = 31940 M^{-1} cm^{-1}) which is accompanied by a weak shoulder roughly at λ_{max} = 616 nm (ε = 22065 M^{-1} cm^{-1}). Similar to the axosymmetric (4n + 2)π benzo-fused bispentalene[21] with strong antiaromaticity, the axosymmetric **5** displayed a long absorption tail from 680-1100 nm in the near-IR region with weak intensity. According to time dependent DFT (TDDFT) calculations, the absorptions at 557 and 616 nm could be attributed to the HOMO−2 → LUMO (554 nm, oscillator strength (*f*) = 0.40) transition and admixing of HOMO−1→ LUMO and HOMO → LUMO+1 (680 nm, *f* = 0.35) transitions, respectively (Table 4.2). The weak absorption band having long tail from 680 nm to1100 nm is assignable to an admixture of several weak, seemingly forbidden (*f* < 0.02), transitions (Table 4.2) including the forbidden HOMO→LUMO transition (796 nm; TDDFT: 779 nm, *f* = 0.004; Figure 4.10c) which is one of the typical traits of strong antiaromaticity.[14a,21,22] The optical HOMO–LUMO energy gap, roughly measured from the absorption onset, was 1.24 eV (1000 nm) for **5**, while the theoretical HOMO–LUMO gap was 1.90 eV. Curiously, the HOMO–LUMO energy gap has increased from **3**[11a] to **5**, despite enhancement of antiaromaticity of *as*-indacene.

The electrochemical behavior of **5** was studied by CV and differential pulse voltammetry (DPV) in DCM, displaying amphoteric redox behavior (Figure 4.10b). Two reversible reduction waves with half-wave potentials at $E_{1/2}^{red1}$ = −1.37 V and $E_{1/2}^{red2}$ = −1.65 V and two reversible oxidation waves with half-wave potentials at $E_{1/2}^{ox1}$ = 0.36 V and $E_{1/2}^{ox2}$ = 0.70 V (*vs* ferrocene/ferrocenium (Fc/Fc^+) were observed. Due to a stronger *as*-indacene antiaromaticity, electron injection in **5** was relatively facile than in **3**,[11a] while higher oxidation potential suggested that dominant antiaromatic character could resist electron extraction from **5**. The observation is comparable to *s*-indacene-based IFs with a greater degree of antiaromaticity.[12b,13] The HOMO and LUMO energy levels of **5** were −5.10 eV and −3.56 eV, as measured from the onset oxidation and reduction potentials, respectively, giving energy gap of 1.54 eV.

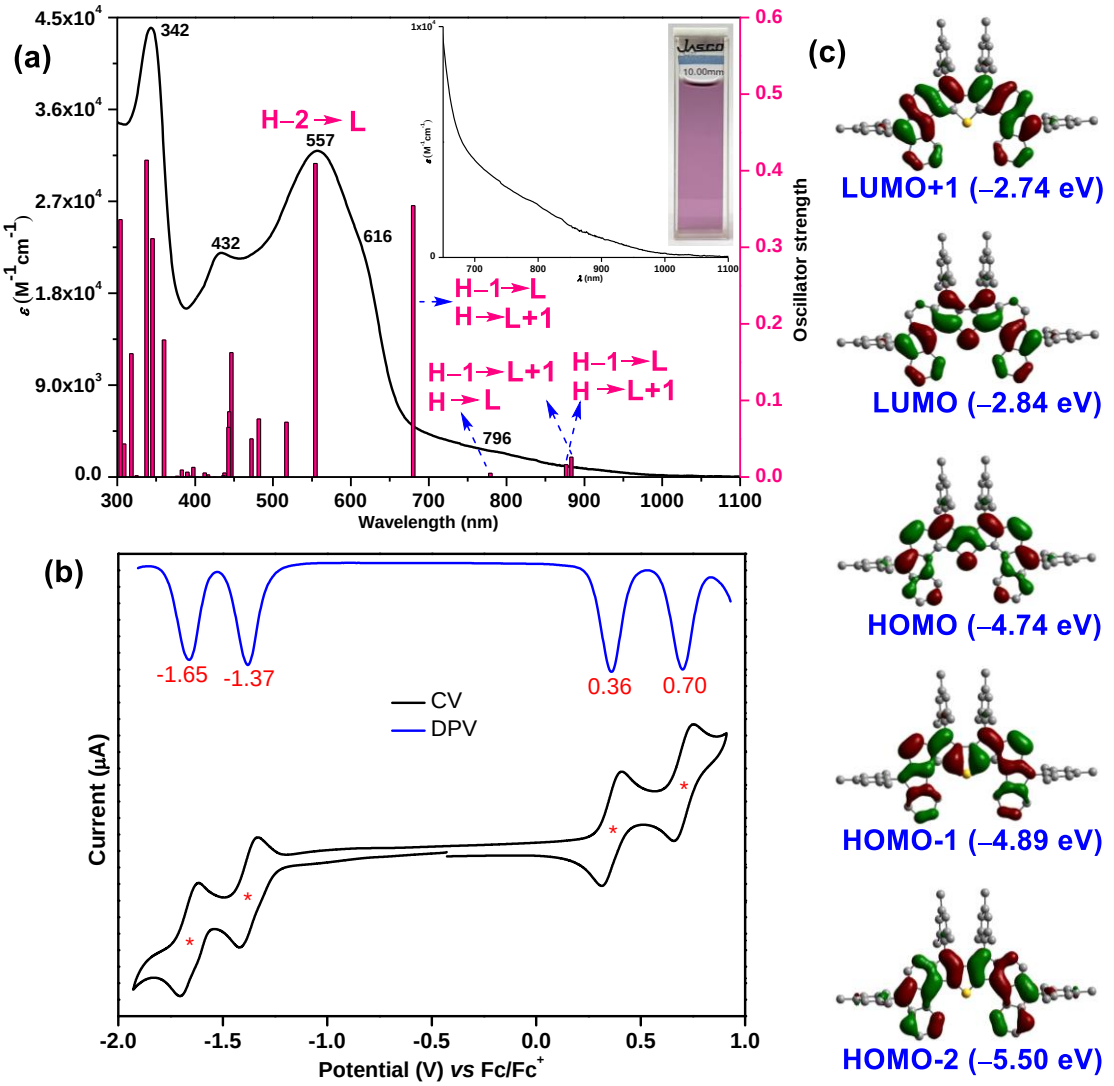

Figure 4.10 (a) UV-vis-NIR spectrum for **5** (600-1100 nm expansion in inset, and the DCM solution showing purple color) with TDDFT oscillator strengths as bar plot. (b) CV and DPV of **5**. (c) Frontier molecular orbitals of **5**.

Table 4.2 Summary of TDDFT calculation for **5**

Wavelength (nm)	Oscillator Strength (*f*)	Major contributions
883	0.0258	H-1->L+1 (32%), HOMO->LUMO (64%)
876	0.016	H-1->LUMO (63%), HOMO->L+1 (35%)
779	0.0049	H-1->L+1 (67%), HOMO->LUMO (33%)
680	0.3544	H-1->LUMO (35%), HOMO->L+1 (58%)
554	0.4095	H-2->LUMO (84%)
517	0.0716	H-5->LUMO (16%), H-3->LUMO (11%), H-2->L+1 (66%)
481	0.0757	H-3->LUMO (84%)
472	0.0499	H-3->L+1 (85%)

446	0.1625	H-5->L+1 (38%), H-4->LUMO (38%)
443	0.0853	H-5->L+1 (23%), H-4->LUMO (57%)
443	0.0648	H-5->LUMO (63%), H-2->L+1 (15%)
437	0.0054	H-8->L+1 (28%), H-7->LUMO (46%), H-6->LUMO (14%)
436	0.0017	H-8->LUMO (47%), H-7->L+1 (27%)
433	0	H-9->LUMO (21%), H-4->L+1 (76%)
425	0.0001	H-7->LUMO (11%), H-6->LUMO (55%), H-5->L+1 (16%)
416	0.0029	H-6->L+1 (70%)
414	0.0014	H-11->L+1 (32%), H-10->LUMO (65%)
414	0.0004	H-11->LUMO (65%), H-10->L+1 (33%)
412	0.0051	H-9->LUMO (74%), H-4->L+1 (19%)
402	0.0001	H-9->L+1 (95%)
397	0.0127	H-12->LUMO (82%), H-5->L+1 (10%)
391	0.0025	H-12->L+1 (42%), H-8->LUMO (13%), H-7->L+1 (24%)
389	0.0062	H-8->L+1 (51%), H-7->LUMO (22%)
388	0.0004	H-12->L+1 (35%), H-8->LUMO (18%), H-7->L+1 (31%)
382	0.0091	H-13->LUMO (63%), H-12->L+1 (12%)
376	0.0011	H-11->LUMO (32%), H-10->L+1 (65%)
376	0.0001	H-11->L+1 (62%), H-10->LUMO (32%)
360	0.1791	H-13->L+1 (75%), H-1->L+2 (10%)
345	0.3112	HOMO->L+2 (71%)
337	0.4137	H-13->L+1 (10%), H-1->L+2 (74%)
324	0.0017	HOMO->L+3 (84%)
317	0.161	H-14->LUMO (87%)
308	0.043	H-14->L+1 (44%), H-1->L+3 (39%)
304	0.3362	H-14->L+1 (39%), H-1->L+3 (40%)
298	0.0044	HOMO->L+4 (79%)

4.3 Conclusions

In conclusion, antiaromatic unit embedded PAs bearing (4n + 2)π-electron perimeter with dominant contribution from its antiaromatic subunit are underexplored, with limited examples of quinoidal dicyclopenta[*a*,*e*]pentalene,[23] bispentalenes,[21] *s*-IDFs,[8,11a] phenylene-based acenes;[24] while pentalenodifluorene,[25] dibenzo-*s*-IDF[11b] and diindenobiphenylene[26] displayed open-shell ground state instead of antiaromaticity. Therefore, (4n + 2)π-systems made of antiaromatic subunits are of special interest, but their heteroaromatic analogues are unknown. Synthesis and characterization of a formally aromatic axosymmetric PHA **5**, which is unlike centrosymmetric PA analogues,[8,11a] showed enhanced *as*-indacene antiaromaticity as

analysed by NICS/ACID calculations. The enhanced antiaromaticity for **5** was also evidenced by the weakly intense absorption bands extending to 1100 nm with a small HOMO–LUMO gap of 1.24 eV, higher oxidation and lower reduction potentials with good reversibility, and an upfield NMR shift for the *as*-indacene protons compared to that with **3**.[11a] Thiophene-fused pentalenes[27] and indacenes[28] gained attention due to strong antiaromaticity. Inclusion of thiophene can be an effective strategy to enhance *as*-indacene antiaromaticity for (4n + 2)π-systems, which may find future applications in optoelectronics[29] as stable alternatives of isoelectronic acenes.[30]

4.4 Experimental section

4.4.1 General information. Chemicals and reagents were purchased from local and international commercial suppliers (Merck, GLR innovations, and BLDpharm) and used without further purification. Compound **8** was synthesized and fully characterized, since its synthetic details from **6**, and characterizations were not reported.[15,31] Compound **10** was synthesized according to our reported procedure.[11a] Thin layer chromatography (TLC) was performed using pre-coated silica-plates purchased from Merck (silica gel 60 PF254, 0.25 mm). Column chromatography was performed using silica gel 100-200 mesh. NMR spectra were recorded in $CDCl_3$ (Eurisotop) at room temperature, on JEOL JNM-ECS400 spectrometer at operating frequencies of 400 MHz (^1H) or 100 MHz (^{13}C) as indicated in the individual spectrum. Chemical shifts (δ) are given in ppm relative to residual solvent (chloroform δ = 7.26 for ^1H, and δ = 77.16 for proton-decoupled ^{13}C NMR) and coupling constants (*J*) are expressed in Hz. Multiplicity is tabulated as s for singlet, d for doublet, dd for doublet of doublet, t for triplet, q for quartet and m for multiplet. Structural assignments were made with additional information from gCOSY, and gNOESY experiments. High resolution mass spectra (HRMS) were recorded using electron spray ionization (ESI) methods on Waters (XEVO G2-XS QTOF) mass spectrometer. UV-vis spectra were recorded in JASCO V-770 spectrophotometer. Cyclic voltammetry was performed using an Electrochemical Analyzer potentiostat model CHI1110C from CH Instruments with a conventional three-electrode cell at room temperature under a nitrogen atmosphere at a scan rate of 50 mVs^{-1}. This electrochemical cell contains a glassy carbon (disc shaped with 3-mm diameter) as working electrode, Pt wire as counter electrode, and Ag wire as pseudo-reference electrode. The glassy carbon working electrode was polished with 1.0 micron α-

alumina polishing powder using a figure-eight motion. Electrolyte solution (0.1 M) was prepared from DCM and tetra-*n*-butylammonium hexafluorophosphate (Bu_4NPF_6). The DCM was degassed by nitrogen gas sparging for 10 minutes prior to measurements. The potential was externally calibrated against the ferrocene/ferrocenium couple (0.43 V). Melting points were determined using BIBBY-SMP30 melting point analyzer.

4.4.2 Syntheses.

Diethyl thiophene-3,4-dicarboxylate (7): To the suspension of thiophene-3,4-dicarboxylic acid **5** (1 g, 5.8 mmol) in ethanol (10 mL) was added conc. sulphuric acid (1 mL) dropwise and the mixture was refluxed using an oil bath. Progress of the reaction was monitored by TLC. After completion of the reaction, the mixture was cooled to room temperature and neutralized with aq. K_2CO_3. The volatiles were evaporated and the mixture was extracted with CH_2Cl_2 (3 x 50 mL). The organic layer was dried over anhydrous sodium sulfate and filtered. The crude mixture was purified on a short pad of silica gel (heaxnes:EtOAc, 95:5) to afford title product **7** (1.2 g, 90% yield) as white solid: R_f = 0.3 (10% EtOAc/ hexanes); mp 52−53 °C; ^{1}H NMR (400 MHz, $CDCl_3$) δ 7.84 (s, 2H), 4.34 (q, *J* = 7.2 Hz, 4H), 1.36 (t, *J* = 7.1 Hz, 6H); $^{13}C\{^1H\}$ NMR (100 MHz, $CDCl_3$) δ 163.2, 133.7, 131.6, 61.4, 14.2; HRMS (ESI) *m/z*: $[M + H]^+$ calcd for $C_{10}H_{13}O_4S$ 229.0535, found 229.0528 (error: −3.1 ppm).

Diethyl 2,5-dibromothiophene-3,4-dicarboxylate (8): Bromine (3 mL) was added dropwise to a solution of **7** (1.1 g, 4.8 mmol) in 15 mL of acetic acid at room temperature. After addition, the mixture was refluxed using oil bath for 6 h. The reaction mixture was then neutralized with saturated solution of sodium bicarbonate and extracted with dichloromethane. The organic layer was washed with water and brine and dried over sodium sulfate. After evaporation of the organic layer, the residue was purified by silica gel column chromatography (hexanes:EtOAc, 95:5) to afford **8** as yellow solid (1 g, 54% yield): R_f = 0.42 (5% EtOAc/hexanes); mp 95–96 °C; ^{1}H NMR (400 MHz, $CDCl_3$) δ 4.35 (q, *J* = 7.1 Hz, 4H), 1.36 (t, *J* = 7.2 Hz, 6H); $^{13}C\{^1H\}$ NMR (100 MHz, $CDCl_3$) δ 161.6, 133.8, 115.8, 62.1, 14.1; HRMS (ESI) *m/z*: $[M + H]^+$ calcd for $C_{10}H_{11}Br_2O_4S$ 384.8745, found 384.8745 (error: 0.0 ppm).

2,5-dibromothiophene-3,4-dicarbaldehyde (9): To a solution of **8** (900 mg, 2.33 mmol) in dry dichloromethane (12 mL) at −78 °C in was slowly added diisobutylaluminium hydride (9.33 mL, 9.33 mmol, 1.0 M solution in toluene),

dropwise. The reaction mixture was stirred at −78 °C for 2 h, and then allowed to come to room temperature and stirred for 12 h. The reaction was quenched with saturated solution of ammonium chloride at 0 °C. The reaction mixture was diluted with diethyl ether (15 mL), which was filtered through celite, and the volatiles were evaporated to get the crude product which was used further without purification.

The crude product was dissolved in dichloromethane (8 mL) and cooled to 0 °C. Pyridinium chlorochromate (1.64 g, 7.64 mmol) was added in portions and the mixture was allowed to warm to room temperature and stirred for 3 h, and then filtered through celite. The organic solvent was removed under reduced pressure and the residue was purified by silica gel chromatography (hexanes:EtOAc, 98:2) to afford the title product **9** (380 mg, 55%) as white solid: R_f = 0.25 (5% EtOAc/hexanes); mp 118–119 °C; ^{1}H NMR δ 10.18 (s, 2H); ^{13}C{^{1}H} NMR (100 MHz, $CDCl_3$): δ 184.9, 136.7, 123.7; HRMS (ESI) *m/z*: $[M + H]^+$ calcd for $C_6H_3Br_2O_2S$ 296.8221, found 296.8219 (error: −0.7 ppm).

2,5-bis(9-mesityl-9H-fluoren-4-yl)thiophene-3,4-dicarbaldehyde (11): An oven-dried thick-walled glass tube was charged with **9** (165 mg, 0.55 mmol), **10** (705 mg, 1.72 mmol), anhydrous K_2CO_3 (383 mg, 2.77 mmol), THF (6 mL) and water (1.2 mL), and the mixture was purged with nitrogen for 30 mins. Catalyst $Pd(PPh_3)_4$ (64 mg, 10 mol %) was subsequently added under nitrogen, and the glass tube was sealed before being warmed to 85 °C using an oil bath. After 12 h, the flask was cooled to room temperature, and THF was evaporated under reduced pressure. Water was added, and the mixture was extracted with EtOAc (3 x 30 mL). The organic layer was dried over anhydrous Na_2SO_4, filtered and removed under vacuum. The residue was purified by silica gel column chromatography (hexanes:EtOAc, 98:2) to afford the title product **11** (275 mg, 70% yield) as light brown solid: R_f = 0.29 (10% EtOAc/hexanes); mp 169−170 °C; ^{1}H NMR (400 MHz, $CDCl_3$) δ 10.26 – 10.13 (m, 2H), 7.54 – 7.40 (m, 4H), 7.40 – 7.34 (m, 4H), 7.35 – 7.27 (m, 4H), 7.26 – 7.23 (m, 2H), 7.05 (s, 2H), 6.75 – 6.64 (m, 2H), 5.63 – 5.53 (m, 2H), 2.71 (d, *J* = 5.2 Hz, 6H), 2.30 (d, *J* = 6.9 Hz, 6H), 1.24 (d, *J* = 8.1 Hz, 3H), 1.09 (d, *J* = 5.1 Hz, 3H). ^{13}C{^{1}H} NMR (100 MHz, $CDCl_3$) δ 187.0, 186.7, 153.0, 148.5, 148.3, 148.1, 139.8, 139.6, 138.0, 137.8, 136.7, 136.7, 136.5, 133.4, 130.9, 130.7, 130.1, 129.9, 129.1, 129.0, 128.0, 127.1, 127.0, 126.9, 125.7, 125.2, 124.6, 124.5, 122.2 (2 C), 122.1, 49.7 (2 C), 21.9, 21.0, 18.8.; HRMS (ESI) *m/z*: $[M + H]^+$ calcd for $C_{50}H_{41}O_2S$ 705.2827, found 705.2831 (error: 0.6 ppm).

5,8,9,12-tetramesitylbenzo[7,8]-*as*-indaceno[1,2-*b*]benzo[7,8]-*as*-indaceno[2,1-*d*]thiophene (5): 2-mesitylmagnesium bromide (1.0 M in diethyl ether, 1.53 mL, 1.53 mmol) was added dropwise to the dry THF (5 mL) solution of **11** (180 mg, 0.25 mmol) under nitrogen. The mixture was stirred at room temperature for 12 h, and the reaction was quenched with a saturated aqueous NH_4Cl solution. The volatile organics were evaporated, and the mixture was extracted with dichloromethane (3 x 30 mL). The organic layer was dried over anhydrous Na_2SO_4, filtered, and removed under reduced pressure to afford a crude mixture containing intermediate compound **12** (310 mg). To the solution of crude **12** in anhydrous DCM (10 mL) was added dropwise methanesulfonic acid (0.1 mL) under nitrogen, and the reaction mixture was stirred for 10 mins at room temperature. Once **12** was consumed, as monitored by TLC, saturated NH_4Cl solution was added and the reaction mixture was extracted with DCM (3 x 30 mL). The organic layer was dried over anhydrous Na_2SO_4 and concentrated under reduced pressure. The residue was passed through a short pad of silica gel (hexanes:EtOAc = 95:5) to afford dihydro precursor **13** (93 mg, pink solid). DDQ (59 mg, 0.24 mmol) was added to the solution of **13** (55 mg, 0.6 mmol) in dry toluene (3 mL) under nitrogen, and the reaction mixture was stirred at room temperature for 12 h. Once the stating material was consumed (as monitored by TLC), the toluene was removed *in vacuo* and the crude was purified by silica gel column chromatography (hexanes:DCM, 90:5) to afford target compound **5** as dark-purple solid (20 mg, 22% yield over three steps): R_f = 0.38 (5% EtOAc/hexanes). Recrystallization of **5** from a dichloromethane/methanol (1:1) mixture, by solvent diffusion method, at ambient temperature in the dark afforded single crystals suitable for X-ray crystallographic analysis: mp 337 °C dec; ^{1}H NMR (400 MHz, $CDCl_3$): δ 7.69 (d, *J* = 7.3 Hz, 2H), 7.18 (dd, *J* = 7.6, 0.8 Hz, 2H), 7.03 (dd, *J* = 7.4, 0.8 Hz, 2H), 6.94 (s, 4H), 6.61 (d, *J* = 7.3 Hz, 2H), 6.44 (s, 4H), 5.79 (d, *J* = 9.5 Hz, 2H), 5.65 (d, *J* = 9.3 Hz, 2H), 2.33 (s, 6H), 2.19 (s, 6H), 2.15 (s, 12H), 2.03 (s, 12H); ^{13}C{^{1}H} NMR (100 MHz, $CDCl_3$) δ 146.5, 146.0, 145.4, 139.8, 138.9, 138.8, 137.5, 136.9, 136.6 (2 C), 136.2, 136.0, 135.8, 132.3, 130.0, 129.8, 129.4, 128.2, 127.4 (2 C), 124.4, 122.2, 122.0, 118.7, 29.8, 21.3, 21.2, 20.9, 20.4; HRMS (ESI) *m/z*: $[M]^+$ calcd for $C_{68}H_{56}S$ 904.4103, found 904.4108 (error: 0.6 ppm).

4.4.3 X-ray crystallographic analysis

Single crystal of **5** was mounted on Hampton cyoloops. The intensity data and geometric parameters of these crystals were garnered with the help of Rigaku XtaLAB Synergy-I, Dualflex, HyPix3000 X-ray diffractometer having a micro-focus sealed X-ray tube Cu-Kα (λ =1.54184 Å) source of X-rays. The crystal was kept at 100 K during data collection. By utilizing OLex2,[32] the crystal structure was solved with the help of olex2.solve[33] structure solution program by employing direct methods and crystal structure refinement was done with the SHELXL refinement package by putting into use Least Squares minimization.[34] Refinement of all non-hydrogen atoms was completed with the help of anisotropic thermal parameters.

Table 4.3 X-ray crystallographic information of **5**.

CCDC No.	2238024
Empirical formula	$C_{68}H_{56}S$
Formula weight	905.18
Temperature/ K	100(2)
Wavelength	1.54178 Å
Crystal system	Monoclinic
Space group	*P*21/*c*
a/Å	29.4354(4)
b/Å	9.66160(10)
c/Å	19.2010(3)
α/°	90
β/°	103.0500(10)
γ/°	90
Volume/ $Å^3$	5319.60(12)
Z	4
ρ_{calc}g/cm^3	1.130
μ/mm^{-1}	0.836
F(000)	1920
Crystal size/mm^3	0.250 x 0.090 x 0.075
2*Θ* range for data collection/°	3.082 to 68.261
Index ranges	$-34 \leq h \leq 35$, $-11 \leq k \leq 10$, $-23 \leq l \leq 22$
Reflections collected	41875
Independent reflections	9663 [R_{int} = 0.0496]
Completeness to theta = 67.679°	99.5 %
Absorption correction	Semi-empirical from equivalents
Max. and min. transmission	0.939 and 0.914
Refinement method	Full-matrix least-squares on F^2
Data / restraints / parameters	9663 / 0 / 634
Goodness-of-fit on F^2	1.029
Final R indexes [I>=2σ (I)]	R_1 = 0.0513, wR_2 = 0.1362
R indices (all data)	R_1 = 0.0573, wR_2 = 0.1417

Extinction coefficient	n/a
Largest diff. peak and hole / e $Å^{-3}$	1.984 and -0.286

4.4.4 DFT calculations

DFT calculations were performed with Gaussian 09 package using a high-performance computing cluster facility of IIT Ropar in gas phase using the B3LYP level of theory with basis set 6-31G(d).[35] Optimization of the molecular geometries for **5**, taken from X-ray crystallographic data, were done by restricted B3LYP, and unrestricted B3LYP wave-functions using broke symmetry formalism.[36] NOON (natural orbital occupation number) value was based on the broken symmetry UB3LYP method. NICS (standard GIAO method)[37] and HOMA[38] indices were calculated for the optimized closed-shell structure. The reported $NICS(1)_{zz}$ indices were the average of two positions (above and below the plane) for **5**. Excitation energy was computed using time dependent density functional theory (TDDFT) for the closed-shell optimized structure of **5**, in gas phase. Molecular orbital contributions were determined using GaussSum 3.0 package.[39]

Table 4.4. Relative electronic energies of optimized geometries for **5**.

Compound	Optimization	hartree	kcal/mol
5	Singlet closed-shell B3LYP/6-31G(d)	–3023.205309	–1897061.331
	Singlet open-shell UB3LYP/6-31G(d)	–3023.205309	–1897061.331
	Triplet open-shell UB3LYP/6-31G(d)	–3023.189185	–1897078.422

Compound 5: $\Delta E_{\text{Triplet-Singlet}}$ = 10.1 kcal/mol. Occupation numbers are found for HOMO (240) = 0 and LUMO (240) = 0, for the open-shell singlet structure, affording *zero* diradical character ($y_0 = 0$)[40] for **5**.

4.5 References

1. Scherf, U.; Müllen, K. Polyarylenes and poly(arylenevinylene)s: 8. The first soluble ladder polymer with 1,4-benzoquinone-bismethide subunits. *Polymer* **1992**, *33*, 2443–2446.

2. Kertesz, M. Structure and Electronic Structure of Low-Band-Gap Ladder Polymers. *Macromolecules* **1995**, *28*, 1475–1480.

3. Chase, D. T.; Rose, B. D.; McClintock, S. P.; Zakharov, L. N.; Haley, M. M. Indeno[1,2-*b*]fluorenes: Fully Conjugated Antiaromatic Analogues of Acenes. *Angew. Chem., Int. Ed*. **2010**, *50*, 1127–1130.

4. Fix, A. G.; Deal, P. E.; Vonnegut, C. L.; Rose, B. D.; Zakharov, L. N.; Haley, M. M. Indeno[2,1-*c*]fluorene: A New Electron-Accepting Scaffold for Organic Electronics. *Org. Lett.* **2013**, *15*, 1362–1365.

5. Shimizu, A.; Nobusue, S.; Miyoshi, H.; Tobe, Y. Indenofluorene congeners: Biradicaloids and beyond. *Pure Appl. Chem.* **2014**, *86*, 517–528.

6. Tobe, Y. Non-Alternant Non-Benzenoid Aromatic Compounds: Past, Present, and Future. *Chem. Rec.* **2015**, *15*, 86–96.

7. Herzog, S.; Hinz, A.; Breher, F.; Podlech, J. Cyclopenta-fused polyaromatic hydrocarbons: synthesis and characterisation of a stable, carbon-centred helical radical. *Org. Biomol. Chem.* **2022**, *20*, 2873–2880.

8. Hu, P.; Lee, S.; Herng, T. S.; Aratani, N.; Gonçalves, T. P.; Qi, Q.; Shi, X.; Yamada, H.; Huang, K.-W.; Ding, J.; Kim, D.; Wu, J. Toward Tetraradicaloid: The Effect of Fusion Mode on Radical Character and Chemical Reactivity. *J. Am. Chem. Soc.* **2016**, *138*, 1065–1077.

9. Di Giovannantonio, M.; Chen, Q.; Urgel, J. I.; Ruffieux, P.; Pignedoli, C. A.; Müllen, K.; Narita, A.; Fasel, R. On-Surface Synthesis of Oligo(indenoindene). *J. Am. Chem. Soc.* **2020**, *142*, 12925–12929.

10. Fukuda, K.; Fujiyoshi, J.-ya; Matsui, H.; Nagami, T.; Takamuku, S.; Kitagawa, Y.; Champagne, B.; Nakano, M. A theoretical study on quasi-one-dimensional open-shell singlet ladder oligomers: multi-radical nature, aromaticity and second hyperpolarizability. *Org. Chem. Front*. **2017**, *4*, 779–789.

11. (a) Sharma, H.; Sharma, P. K.; Das, S. Revisiting indeno[2,1-*c*]fluorene synthesis while exploring the fully conjugated *s*-indaceno[2,1-*c*:6,5-*c*′]difluorene. *Chem. Commun.* **2020**, *56*, 11319–11322. (b) Jiang, Q.; Han, Y.; Zou, Y.; Phan, H.; Yuan, L.; Herng, T. S.; Ding, J.; Chi, C. S-shaped *para*-quinodimethane-Embedded Double [6]Helicene and Its Charged Species Showing Open-Shell Diradical Character. *Chem. – Eur. J*. **2020**, *26*, 15613–15622.

12. (a) Tobe, Y. Quinodimethanes Incorporated in Non-Benzenoid Aromatic or Antiaromatic Frameworks. *Top. Curr. Chem*. *(Chem)* **2018**, *376*, 12. (b) Sharma, H.;

Bhardwaj, N.; Das, S. Revisiting indeno[1,2-*b*]fluorene by steric promoted synthesis while isolating the second stable 4nπ indeno[2,1-*a*]fluorene. *Org. Biomol. Chem.* **2022**, *20*, 8071–8077. (c) Shimizu, A.; Tobe, Y. Indeno[2,1-*a*]fluorene: An Air-Stable ortho-Quinodimethane Derivative. *Angew. Chem., Int. Ed*. **2011**, *50*, 6906–6910.

13. Frederickson, C. K.; Zakharov, L. N.; Haley, M. M. Modulating Paratropicity Strength in Diareno-Fused Antiaromatics. *J. Am. Chem. Soc*. **2016**, *138*, 16827–16838.

14. (a) Warren, G. I.; Barker, J. E.; Zakharov, L. N.; Haley, M. M. Enhancing the Antiaromaticity of *s*-Indacene through Naphthothiophene Fusion. *Org. Lett*. **2021**, *23*, 5012–5017. (b) Barker, J. E.; Price, T. W.; Karas, L. J.; Kishi, R.; MacMillan, S. N.; Zakharov, L. N.; Gómez-García, C. J.; Wu, J. I.; Nakano, M.; Haley, M. M. A Tale of Two Isomers: Enhanced Antiaromaticity/Diradical Character versus Deleterious Ring-Opening of Benzofuran-fused *s*-Indacenes and Dicyclopenta[*b*,*g*]naphthalenes. *Angew. Chem., Int. Ed.* **2021**, *60*, 22385–22392. (c) Barker, J. E.; Dressler, J. J.; Cárdenas Valdivia, A.; Kishi, R.; Strand, E. T.; Zakharov, L. N.; MacMillan, S. N.; Gómez-García, C. J.; Nakano, M.; Casado, J.; Haley, M. M. Molecule Isomerism Modulates the Diradical Properties of Stable Singlet Diradicaloids. *J. Am. Chem. Soc*. **2020**, *142*, 1548–1555. (d) Dressler, J. J.; Barker, J. E.; Karas, L. J.; Hashimoto, H. E.; Kishi, R.; Zakharov, L. N.; MacMillan, S. N.; Gomez-Garcia, C. J.; Nakano, M.; Wu, J. I.; Haley, M. M. Late-Stage Modification of Electronic Properties of Antiaromatic and Diradicaloid Indeno[1,2-*b*]fluorene Analogues via Sulfur Oxidation. *J. Org. Chem.* **2020**, *85*, 10846–10857. (e) Saha, H. K.; Mallick, D.; Das, S. Unveiling two antiaromatic *s*-indacenodicarbazole isomers with tunable paratropicity *Chem. Commun.* **2022**, *58*, 8492–8495. (f) Marshall, J. L.; Uchida, K.; Frederickson, C. K.; Schutt, C.; Zeidell, A. M.; Goetz, K. P.; Finn, T. W.; Jarolimek, K.; Zakharov, L. N.; Risko, C.; Herges, R.; Jurchescu, O. D.; Haley, M. M. Indacenodibenzothiophenes: Synthesis, Optoelectronic Properties and Materials Applications of Molecules with Strong Antiaromatic Character. *Chem. Sci.* **2016**, *7*, 5547–5558.

15. Lim, C. J.; Li, L.; Lei, Y.; Zhou, F.; Wu, B.; Liu, X.; Zhu, F.; Ong, B. S.; Hu, X.; Su, H.; Ng, S.-C. Synthesis and characterization of three thienopyridazine-based copolymers and their application in OFET. *Tetrahedron Lett.* **2016**, *57*, 1523–1527.

16. Fargher, H. A.; Sherbow, T. J.; Haley, M. M.; Johnson, D. W.; Pluth, M. D. C–H···S Hydrogen Bonding Interactions. *Chem. Soc. Rev*. **2022**, *51*, 1454–1469.

17. (a) Krygowski, T. M.; Cyrański, M. K. Structural Aspects of Aromaticity. *Chem. Rev.* **2001**, *101*, 1385–1420. (b) Najmidin, K.; Kerim, A.; Abdirishit, P.; Kalam, H.; Tawar, T. A comparative study of the aromaticity of pyrrole, furan, thiophene, and their aza-derivatives. *J. Mol. Model.* **2013**, *19*, 3529–3535.

18. Fallah-Bagher-Shaidaei, H.; Wannere, C. S.; Corminboeuf, C.; Puchta, R.; Schleyer, P. v. Which NICS Aromaticity Index for Planar π Rings Is Best?. *Org. Lett*. **2006**, *8*, 863–866.

19. (a) Valiev, R. R.; Fliegl, H.; Sundholm, D. Closed-Shell Paramagnetic Porphyrinoids. *Chem. Commun*. **2017**, *53*, 9866–9869. (b) Lehtola, S.; Dimitrova, M.; Fliegl, H.; Sundholm, D. Benchmarking Magnetizabilities with Recent Density Functionals. *J. Chem. Theory Comput*. **2021**, *17*, 1457–1468.

20. Geuenich, D.; Hess, K.; Köhler, F.; Herges, R. Anisotropy of the Induced Current Density (ACID), a General Method to Quantify and Visualize Electronic Delocalization. *Chem. Rev*. **2005**, *105*, 3758–3772.

21. Cao, J.; London, G.; Dumele, O.; von Wantoch Rekowski, M.; Trapp, N.; Ruhlmann, L.; Boudon, C.; Stanger, A.; Diederich, F. The Impact of Antiaromatic Subunits in (4*n* + 2) π-Systems: Bispentalenes with (4n + 2) π-Electron Perimeters and Antiaromatic Character. *J. Am. Chem. Soc*. **2015**, *137*, 7178–7188.

22. (a) Oshima, H.; Fukazawa, A.; Yamaguchi, S. Facile Synthesis of Polycyclic Pentalenes with Enhanced Hückel Antiaromaticity. *Angew. Chem. Int. Ed.* **2017**, *56*, 3270–3274. (b) Konishi, A.; Okada, Y.; Kishi, R.; Nakano, M.; Yasuda, M. Enhancement of Antiaromatic Character via Additional Benzoannulation into Dibenzo[*a*,*f*]pentalene: Syntheses and Properties of Benzo[*a*]naphtho[2,1-*f*]pentalene and Dinaphtho[2,1-*a*,*f*]pentalene. *J. Am. Chem. Soc.* **2019**, *141*, 560–571. (c) Xu, T.; Han, Y.; Shen, Z.; Hou, X.; Jiang, Q.; Zeng, W.; Ng, P. W.; Chi, C. Antiaromatic Dicyclopenta[*b*,*g*]/[*a*,*f*]naphthalene Isomers Showing an Open-Shell Singlet Ground State with Tunable Diradical Character *J. Am. Chem. Soc.* **2021**, *143*, 20562–20568. (d) Wang, J.; Gámez, F. G.; Marín-Beloqui, J.; Diaz-Andres, A.; Miao, X.; Casanova, D.; Casado, J.; Liu, J. Synthesis of a Dicyclohepta[*a*,*g*]heptalene-Containing Polycyclic Conjugated Hydrocarbon and the Impact of Non-Alternant Topologies *Angew. Chem., Int. Ed.* **2023**, e202217124.

23. Stowasser, B.; Hafner, K. Synthesis of a Dicyclopenta[*a,e*]pentalene by [6 + 2]-Cycloaddition of 1,3-Di-tert-butyl-5-vinylidenecyclopentadiene and Consecutive 8π-Electrocyclic Reaction. *Angew. Chem., Int. Ed. Engl*. **1986**, *25*, 466–468.

24. Parkhurst, R. R.; Swager, T. M. Synthesis and Optical Properties of Phenylene-Containing Oligoacenes. *J. Am. Chem. Soc.* **2012**, *134*, 15351–15356.

25. Maekawa, T.; Ueno, H.; Segawa, Y.; Haley, M. M.; Itami, K. Synthesis of Open-Shell Ladder π-systems by Catalytic C–H Annulation of Diarylacetylenes. *Chem. Sci*. **2016**, *7*, 650–654.

26. Chen, P.-Y.; Liu, Y.-C.; Hung, H.-Y.; Pan, M.-L.; Wei, Y.-C.; Kuo, T.-C.; Cheng, M.-J.; Chou, P.-T.; Chiang, M.-H.; Wu, Y.-T. Diindeno[2,1-*b*:2′,1′-*h*]biphenylenes: Syntheses, Structural Analyses, and Properties. *Org. Lett.* **2021**, *23*, 8794–8798.

27. Usuba, J.; Hayakawa, M.; Yamaguchi, S.; Fukazawa, A. Dithieno[*a,e*]pentalenes: Highly Antiaromatic Yet Stable π-Electron Systems without Bulky Substituents. *Chem. – Eur. J*. **2021**, *27*, 1638–1647.

28. Marshall, J. L.; O'Neal, N. J.; Zakharov, L. N.; Haley, M. M. Synthesis and Characterization of Two Unsymmetrical Indenofluorene Analogues: Benzo[5,6]-*s*-indaceno[1,2-*b*]thiophene and Benzo[5,6]-*s*-indaceno[2,1-*b*]thiophene. *J. Org. Chem*. **2016**, *81*, 3674–3680.

29. (a) Higashino. T.; Mori, T. Small-molecule ambipolar transistors. *Phys. Chem. Chem. Phys.*, **2022**, *24*, 9770–9806. (b) Sharma, H.; A, Ankita.; Bhardwaj, P.; Pandey, U. K.; Das, S. *Organic Materials*, **2023**, *5*, 72-83.

30 Tönshoff, C.; Bettinger, H. F. Photogeneration of Octacene and Nonacene. *Angew. Chem., Int. Ed.*, **2010**, *49*, 4125–4128.

31. Asil, D.; Cihaner, A.; Önal, M. A. A glow in the dark: synthesis and electropolymerization of a novel chemiluminescent terthienyl system. *Chem. Commun.*, **2009**, 307–309.

32. Dolomanov, O. V.; Bourhis, L. J.; Gildea, R. J.; Howard, J. A.; Puschmann, H. Olex2: A complete structure solution, refinement and Analysis Program. *J. Appl. Crystallogr.* **2009**, *42*, 339–341.

33. Bourhis, L. J.; Dolomanov, O. V.; Gildea, R. J.; Howard, J. A.; Puschmann, H. The anatomy of a comprehensive constrained, restrained refinement program for the

modern computing environment –olex2dissected. *Acta Crystallogr. A*. **2015**, *71*, 59–75.

34. Sheldrick, G. M. Crystal structure refinement with SHELXL, *Acta Crystallogr. C Struct. Chem*. **2015**, *71*, 3–8.

35. Gaussian 09, *Revision B.01*, Frisch, M. J.; Trucks, G. W.; Schlegel, H. B.; Scuseria, G. E.; Robb, M. A.; Cheeseman, J. R.; Scalmani, G.; Barone, V.; Mennucci, B.; Petersson, G. A.; Nakatsuji, H.; Caricato, M.; Li, X.; Hratchian, H. P.; Izmaylov, A. F.; Bloino, J.; Zheng, G.; Sonnenberg, J. L.; Hada, M.; Ehara, M.; Toyota, K.; Fukuda, R.; Hasegawa, J.; Ishida, M.; Nakajima, T.; Honda, Y.; Kitao, O.; Nakai, H.; Vreven, T.; Montgomery, J. A.; Jr., Peralta, J. E.; Ogliaro, F.; Bearpark, M.; Heyd, J. J.; Brothers, E.; Kudin, K. N.; Staroverov, V. N.; Keith, T.; Kobayashi, R.; Normand, J.; Raghavachari, K.; Rendell, A.; Burant, J. C.; Iyengar, S. S.; Tomasi, J.; Cossi, M.; Rega, N.; Millam, J. M.; Klene, M.; Knox, J. E.; Cross, J. B.; Bakken, V.; Adamo, C.; Jaramillo, J.; Gomperts, R.; Stratmann, R. E.; Yazyev, O.; Austin, A. J.; Cammi, R.; Pomelli, C.; Ochterski, J. W.; Martin, R. L.; Morokuma, K.; Zakrzewski, V. G.; Voth, G. A.; Salvador, P.; Dannenberg, J. J.; Dapprich, S.; Daniels, A. D.; Farkas, O.; Foresman, J. B.; Ortiz, J. V.; Cioslowski, J; Fox, D. J. Gaussian, Inc., Wallingford CT, **2010**.

36. (a) Kubo, T. Recent Progress in Quinoidal Singlet Biradical Molecules. *Chem. Lett.* **2015**, *44*, 111–122. b) Das, S.; Wu, J. Open-shell benzenoid polycyclic hydrocarbons, in: Polycyclic arenes and heteroarenes: synthesis, properties, and applications. Qian M, editor. *John Wiley & Sons Inc*., **2015**, 3.

37. Chen, Z.; Wannere, C. S.; Corminboeuf, C.; Puchta, R.; Schleyer, P. v. R. Nucleus-Independent Chemical Shifts (NICS) as an Aromaticity Criterion. *Chem. Rev*. **2005**, *105*, 3842–3888.

38. (a) Lu, T.; Chen, F. Multiwfn: A multifunctional wavefunction analyser. *J. Comput. Chem*. **2011**, *33*, 580. b) Kruszewski, J.; Krygowski, T. M. Definition of Aromaticity Basing on the Harmonic Oscillator Model. *Tetrahedron Lett*. **1972**, *13*, 3839–3842.

39. O'boyle, N. M.; Tenderholt, A. L.; Langner, K. M. cclib: A library for package-independent computational chemistry algorithms. *J. Comput. Chem*. **2008**, *29*, 839–845.

40. Yamaguchi, K. The electronic structures of biradicals in the unrestricted Hartree-Fock approximation. *Chem. Phys. Lett.* **1975**, *33*, 330–335.

4.6 Appendix

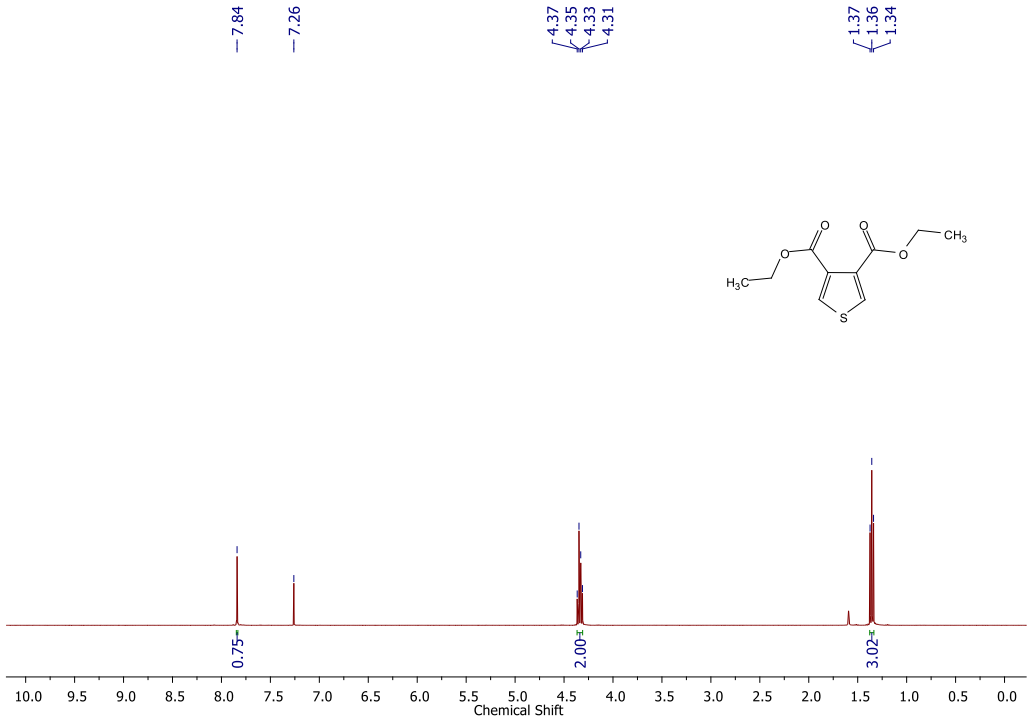

Figure 4.11 ^{1}H NMR spectrum of **7** (in $CDCl_3$, 400 MHz, 298 K).

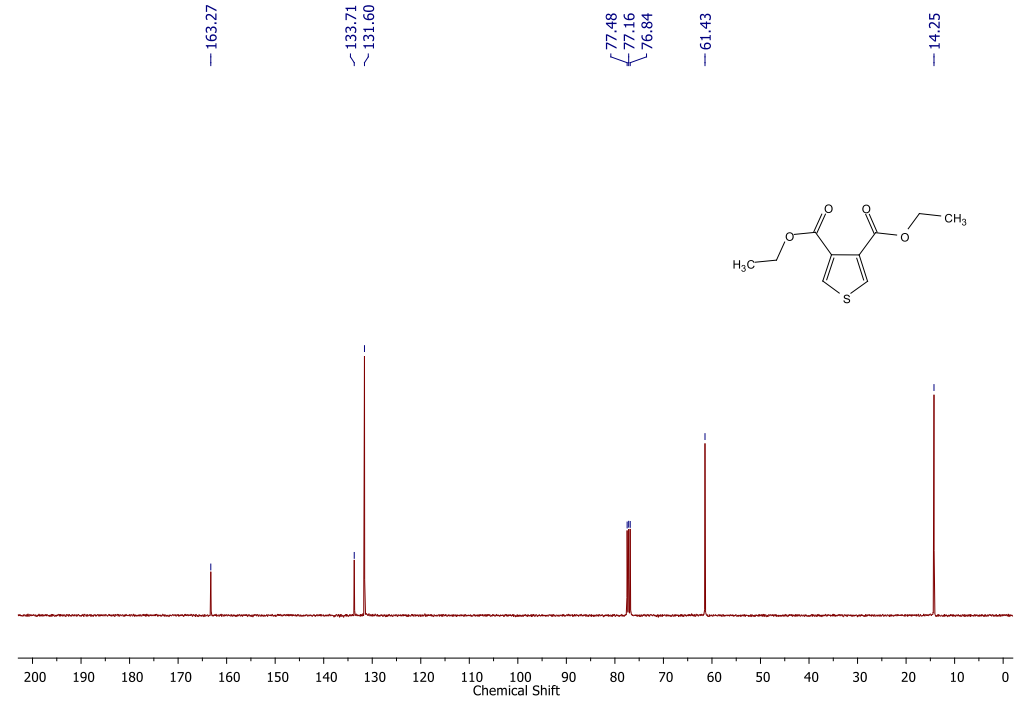

Figure 4.12 $^{13}C\{^{1}H\}$ NMR spectrum of **7** (in $CDCl_3$, 100 MHz, 298 K).

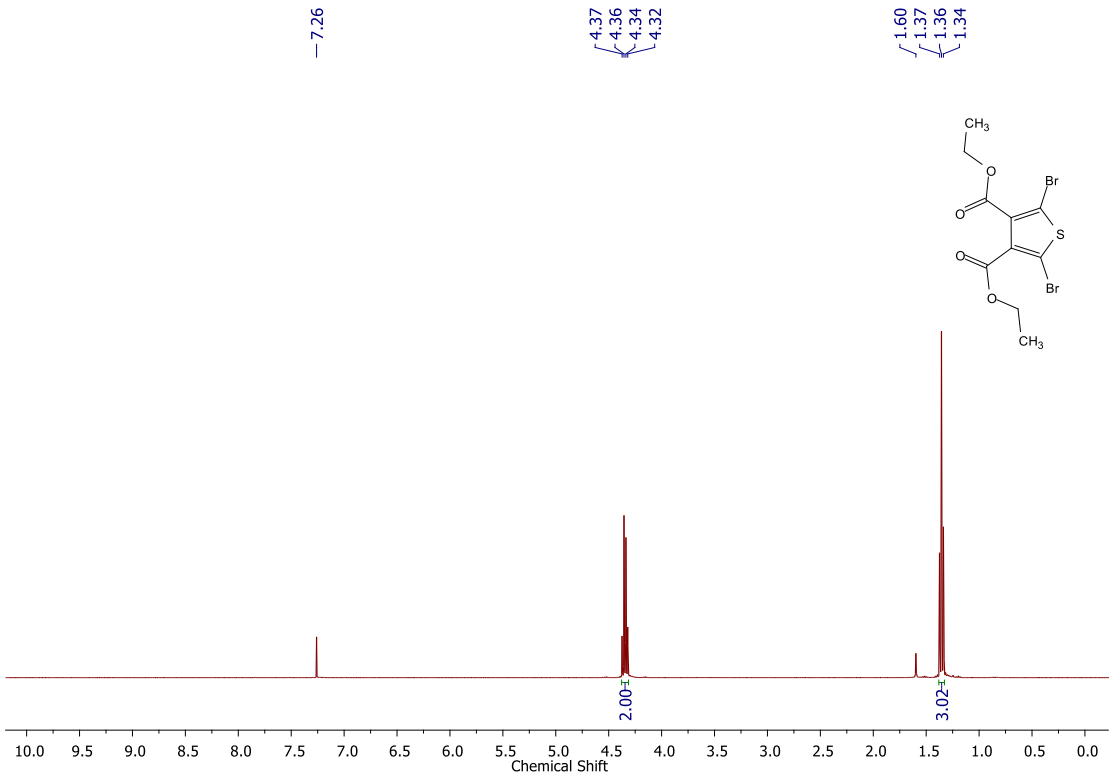

Figure 4.13 ^{1}H NMR spectrum of **8** (in $CDCl_3$, 400 MHz, 298 K).

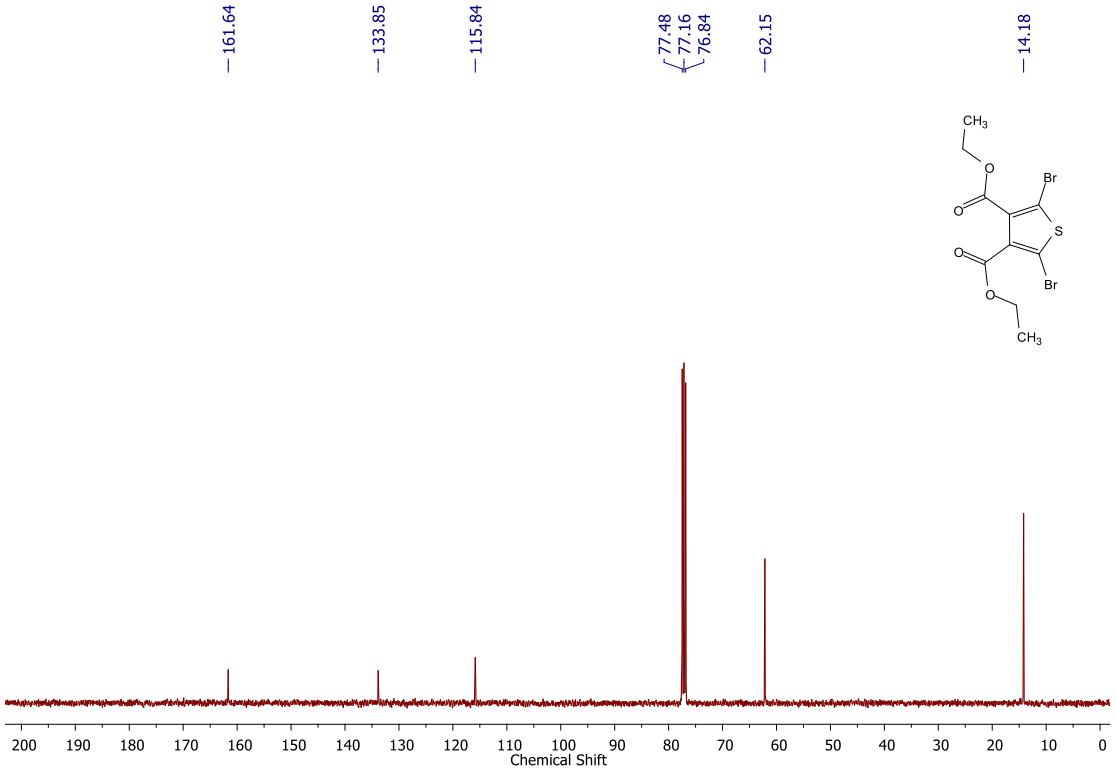

Figure 4.14 $^{13}C\{^{1}H\}$ NMR spectrum of **8** (in $CDCl_3$, 100 MHz, 298 K).

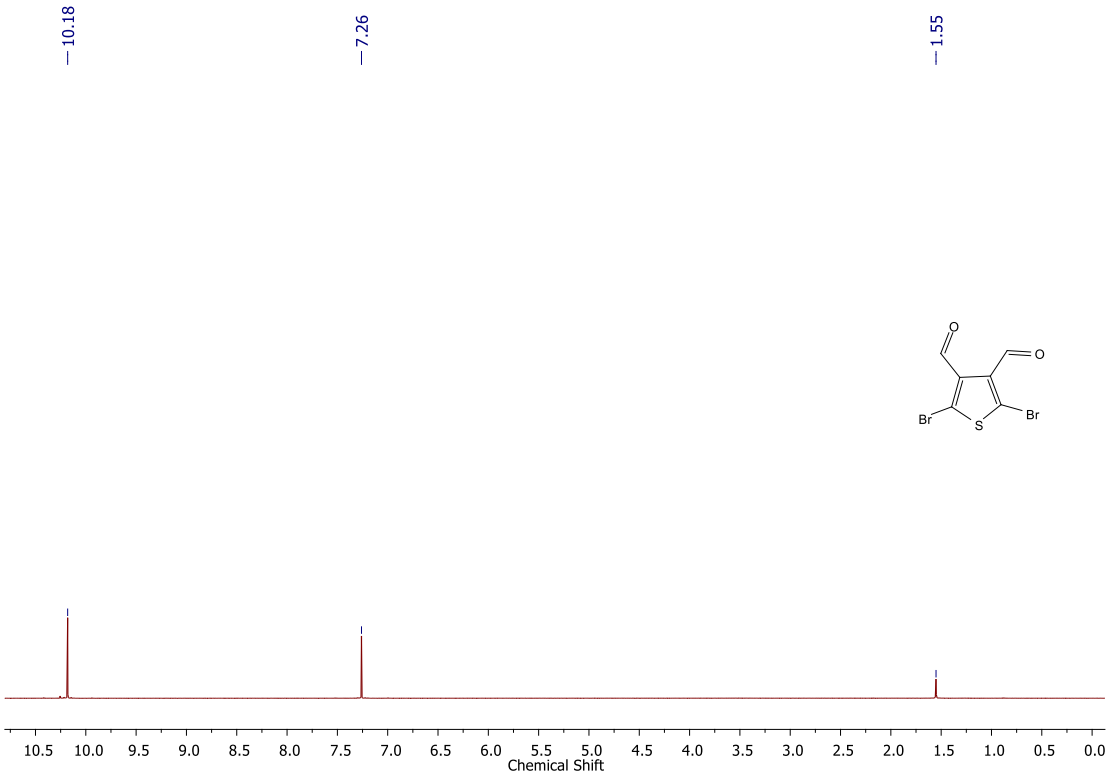

Figure 4.15 ^{1}H NMR spectrum of **9** (in $CDCl_3$, 400 MHz, 298 K).

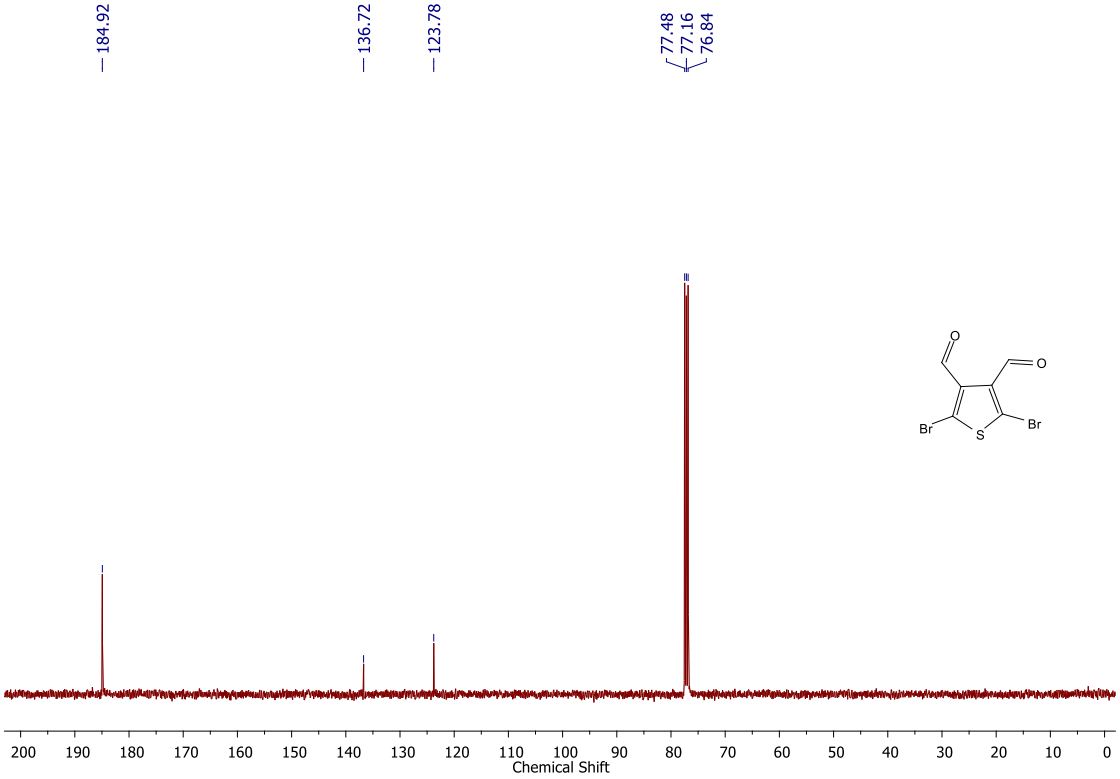

Figure 4.16 $^{13}C\{^{1}H\}$ NMR spectrum of **9** (in $CDCl_3$, 100 MHz, 298 K).

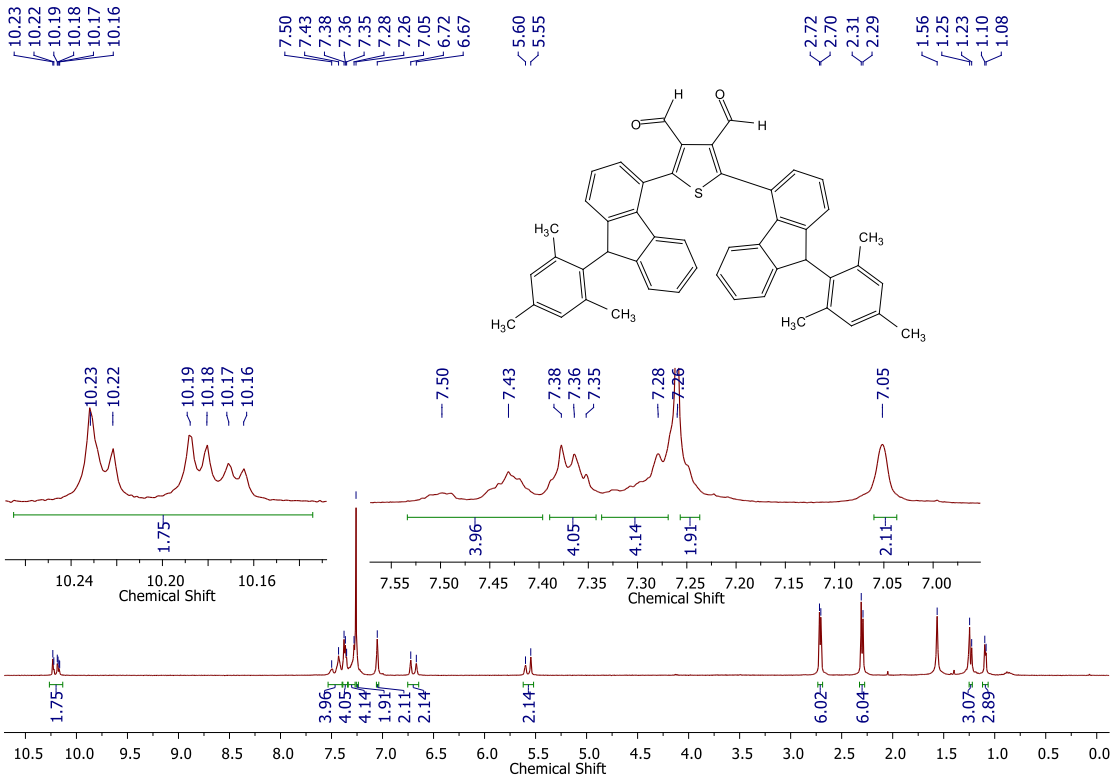

Figure 4.17 ^{1}H NMR spectrum of **11** (in $CDCl_3$, 400 MHz, 298 K).

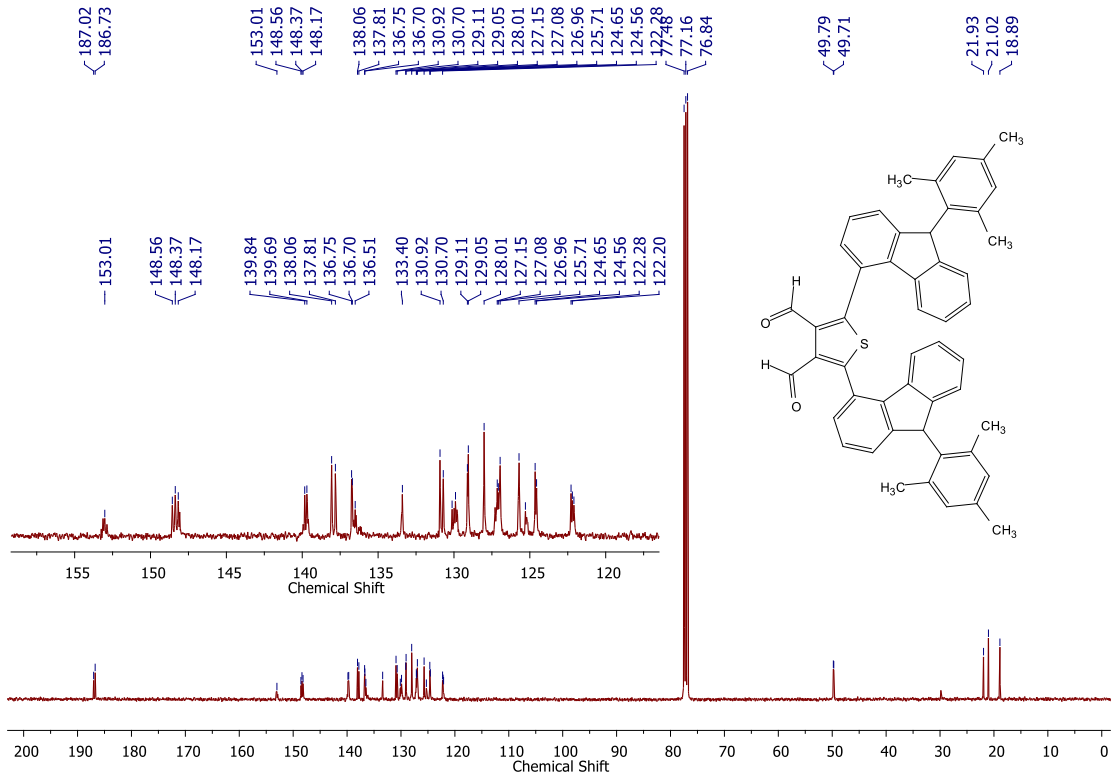

Figure 4.18 $^{13}C\{^{1}H\}$ NMR spectrum of **11** (in $CDCl_3$, 100 MHz, 298 K).

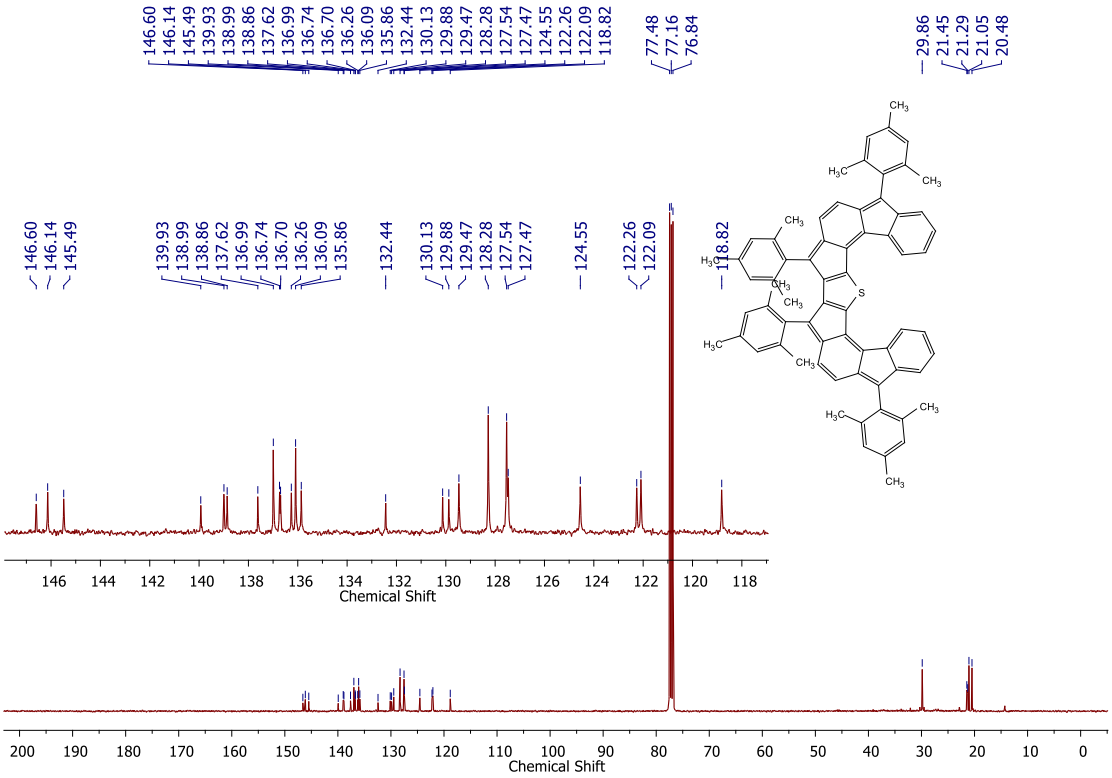

Figure 4.19 $^{13}C\{^{1}H\}$ NMR spectrum of **5** (in $CDCl_3$, 100 MHz, 298 K).

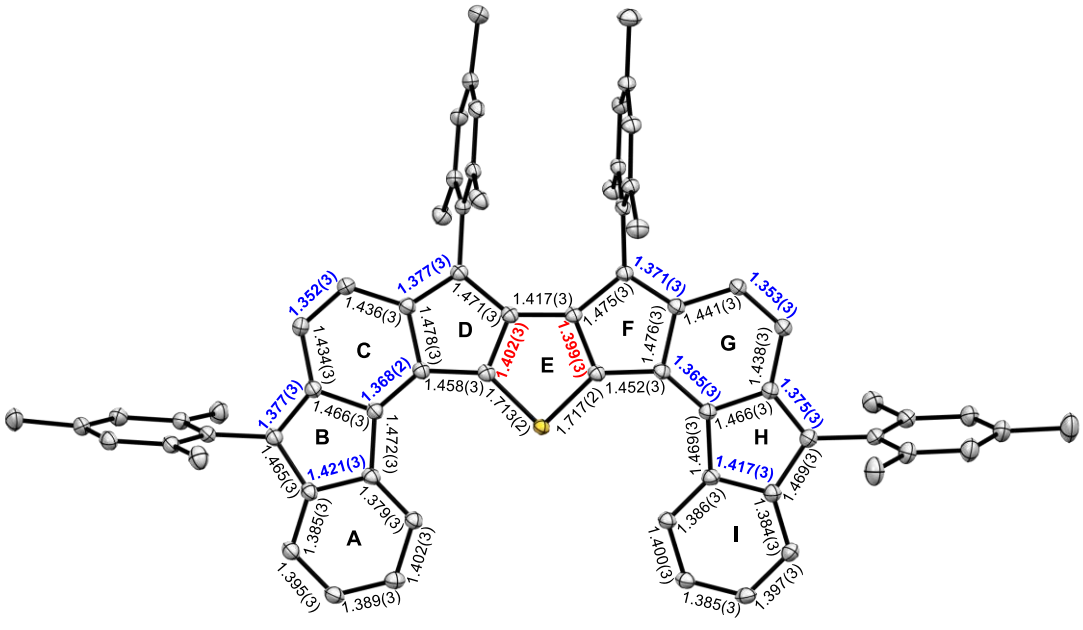

Figure 4.20 ORTEP drawing for **5** with thermal ellipsoids at 30% probability level, showing the core bond lengths with e.s.d values

Chapter 5

Constructing 1-Ethoxyphenanthro[9,10-*e*]acephenanthrylene for the Synthesis of a Polyaromatic Hydrocarbon Containing Formal Azulene Unit

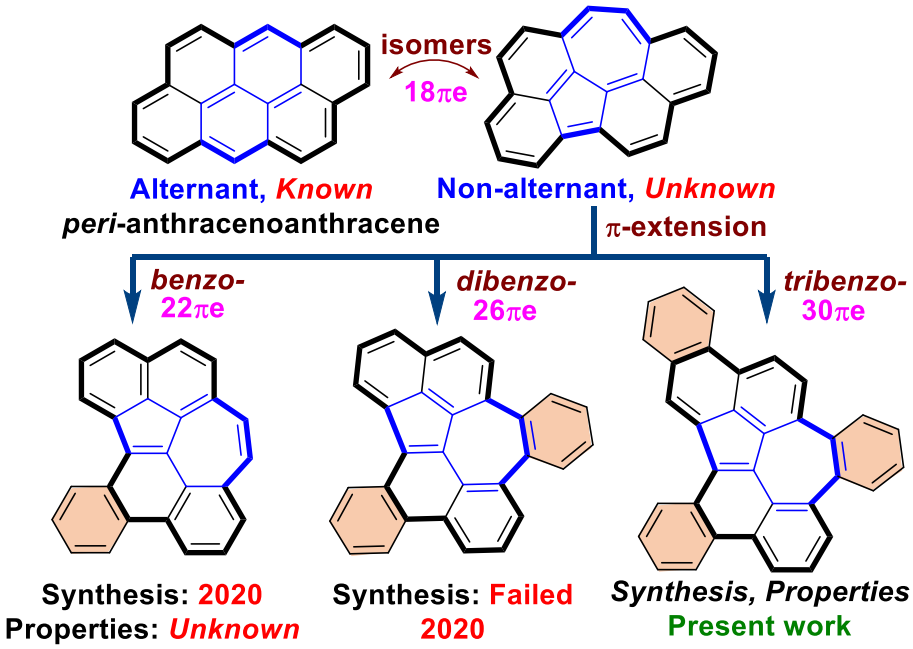

This work was published in *The Journal of Organic Chemistry* (an ACS journal). Please see the citation as: "Sharma, P. K., Babbar, A., Mallick, D., Das, S. Constructing 1-Ethoxyphenanthro[9,10-*e*]Acephenanthrylene for the Synthesis of a Polyaromatic Hydrocarbon Containing a Formal Azulene Unit. *J. Org. Chem.* **2023**, *88*, 5473–5482."

5 Abstract

peri-Acenoacenes are attractive synthetic targets, but their non-benzenoid isomeric counterparts were unnoticed. 1-Ethoxyphenanthro[9,10-*e*]acephenanthrylene **8** was synthesized and converted to azulene-embedded **9**, which is a tribenzo-fused non-alternant isomeric motif of *peri*-anthracenoanthracene. Aromaticity and single-crystal analyses suggested a formal azulene core for **9**, which showed a smaller energy gap between highest occupied and lowest unoccupied molecular orbitals with a charge-transfer absorption band and brighter fluorescence than **8** (quantum yield (Φ): **9** = 41.8%, **8** = 8.9%). The reduction potentials of **8** and **9** were nearly identical, and the observations were further supported by density functional theory (DFT) calculations.

5.1 Introduction

In continuation with the discussion initiated in Chapter 1, the construction of azulene-embedded π-extended polyaromatic hydrocarbons (PAHs, with a central azulene unit)[1] has recently gained increasing attention from several research groups.[2] Because the azulene-like structural defects are often observed in graphene networks, the synthesis of atomically precise 5-7 (pentagon-heptagon) ring-fused defective nanographene is much desired to understand the structure-property relationships.[3] Theoretical studies of graphene monolayers containing azulene-like defects attracted considerable attention in this regard for a long time,[4] however, embedding 5-7 fused rings in place of 6-6 (hexagon-hexagon) rings in a polyarene skeleton, synthetically,[5] is a challenging task to achieve.[1,3]

Construction of the central azulene unit for an azulene-embedded PAH is recommended at the late stage,[6] instead of using azulene motif as a starting material, to avoid unusual rearrangements leading to unexpected product formation.[7] For example, the formation of an azulene unit of singlet diradicaloid **2**,[6] a *peri*-dibenzo-fused derivative of benzo[*f*]azulene[8] (azulene fragment is shown in blue color, Figure 5.1a), was achieved at the late stage using a synthetic protocol that was applicable to construct two additional azulene-embedded diradicaloids with an extremely small singlet-triplet energy gap. As discussed in Chapter 1, compound **2** is a benzo-extended cyclohepta[*def*]fluorene (benzo-CHF),[9] which was long theoretically predicted to possess a singlet-triplet bistable ground state;[10] though, lately it was established as a singlet diradicaloid in the ground state.[11] Notably, in Feng's report,[6] additional two

benzannulation (shown in bold hexagons, Figure 5.1b) of benzo-CHF **2** afforded **Dibenzo-2** with a singlet diradicaloid ground state.

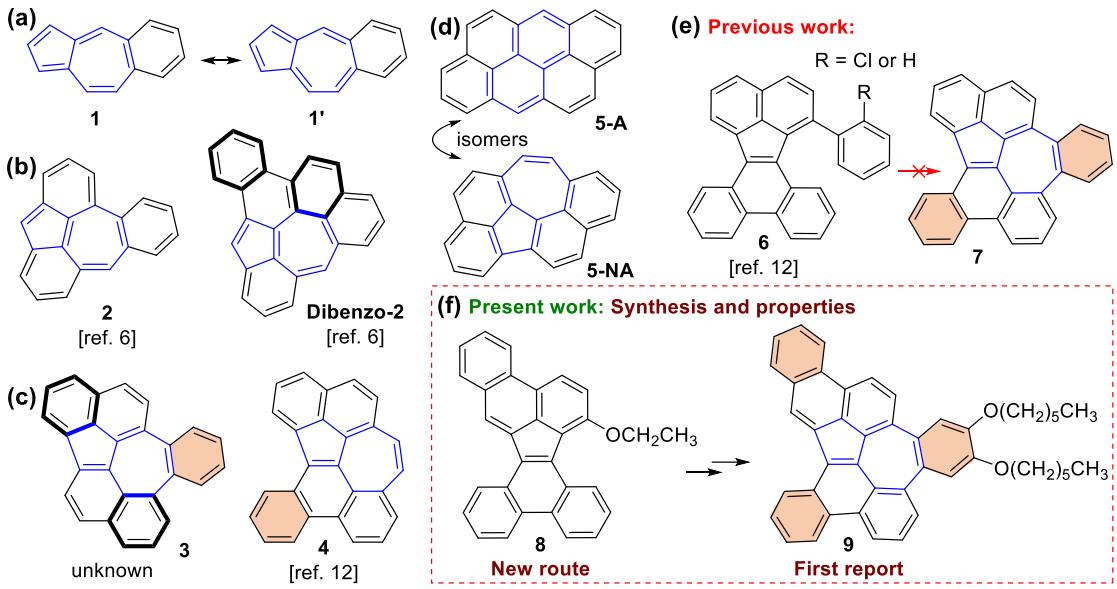

Figure 5.1 (a) Resonance forms **1** and **1'** for benzo[*f*]azulene. (b) Feng's benzo-extended cyclohepta[*def*]fluorene **2** and its dibenzannulated derivative **Dibenzo-2**. (c) Structures **3** and **4** are the constitutional isomers of **Dibenzo-2**. (d) Isomeric **5-NA** is the non-alternant isoelectronic (18πe) motif of alternant *peri*-acenoacene **5-A**. (e) Unsuccessful attempts to synthesize **7** from **6** bearing different substituents. (f) Target phenanthroacephenanthrylene isomer **8**, which was used to construct non-benzenoid PAH **9** in multi-steps.

We envisioned that annulation of the two benzene rings at *peri*-positions of **2** may afford **3**, which is a structural isomer of **Dibenzo-2** and is still unknown (Figure 5.1c). However, compound **4**, a constitutional isomer of **3**, was lately synthesized by Takasu *et al.* by a photoinduced 10π-electrocyclization approach but its electronic properties were not studied.[12] Isomers **3** and **4** may be viewed as benzo-extended **5-NA** (benzene ring is shown by orange hexagon, Figure 5.1c), which can be considered as the non-alternant isomeric motif of alternant *peri*-anthracenoanthracene **5-A** (Figure 5.1d).[13] To our knowledge, non-alternant isomeric *peri*-acenoacene scaffold **5-NA** is overlooked in the literature, and attempts to synthesize **7**, a dibenzo-fused **5-NA**, from **6** were unsuccessful.[12] Stimulated by the recent studies of alternant *peri*-acenoacenes[14] from theoretical[15] and experimental[13,16,17,18] viewpoints, including the non-availability of non-alternant *peri*-acenoacene and the renaissance of azulene-embedded PAHs,[1,3,19] we envisaged to construct the heptagon unit by a Scholl-type oxidative aromatic

coupling[20] using a phenanthroacephenanthrylene (PAP) **8** instead of dibenzofluoroanthene **6**. It is worth mentioning that one can draw seven regioisomers of PAP π-system (Figure 5.2) including parent **8** (phenanthro[9,10-*e*]acephenanthrylene or [9,10-*e*]PAP), but they received seldom attention due to the lack of suitable synthetic strategies.[21]

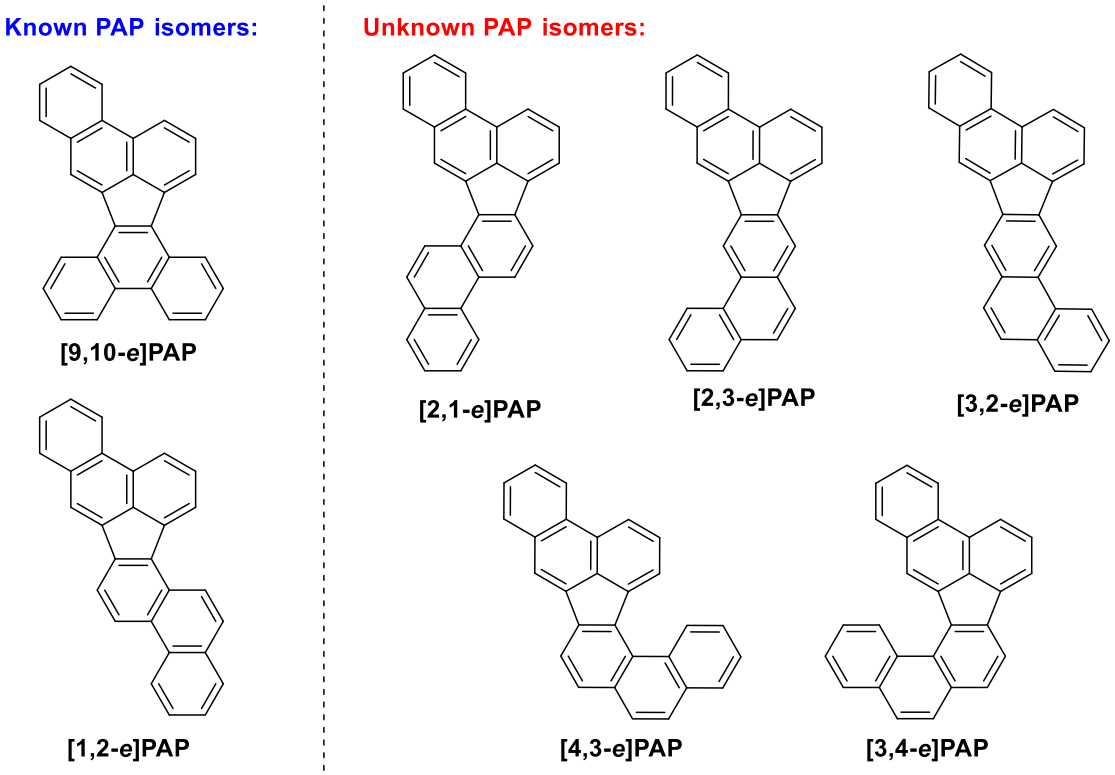

Figure 5.2 Seven possible PAP isomers, and five of them are still unknown. Parent [1,2-*e*]PAP was reported in 1970.[22]

5.2 Results and Discussion

5.2.1 Syntheses. Synthesis of unsubstituted[21] and 8-substituted[23] [9,10-*e*]PAPs were known. PAP is a phenanthrene-fused acephenanthrylene (AP), which is a cyclopentannulated-PAH (CP-PAH),[24] and parent AP was known since 1985.[25] Despite various synthetic approaches for substituted AP motifs,[26,27,28,29] herein we adopted an oxidative aromatic coupling[30] route to synthesize 1-ethoxy[9,10-*e*]PAP **8** in order to use it to construct the diphenanthro-benzo[*f*]azulene **9** with [30]π-electrons in the periphery, which may be viewed as a tribenzo-fused **5-NA**. The ground-state electronic properties of **9** were studied by both experimental and computational approaches.

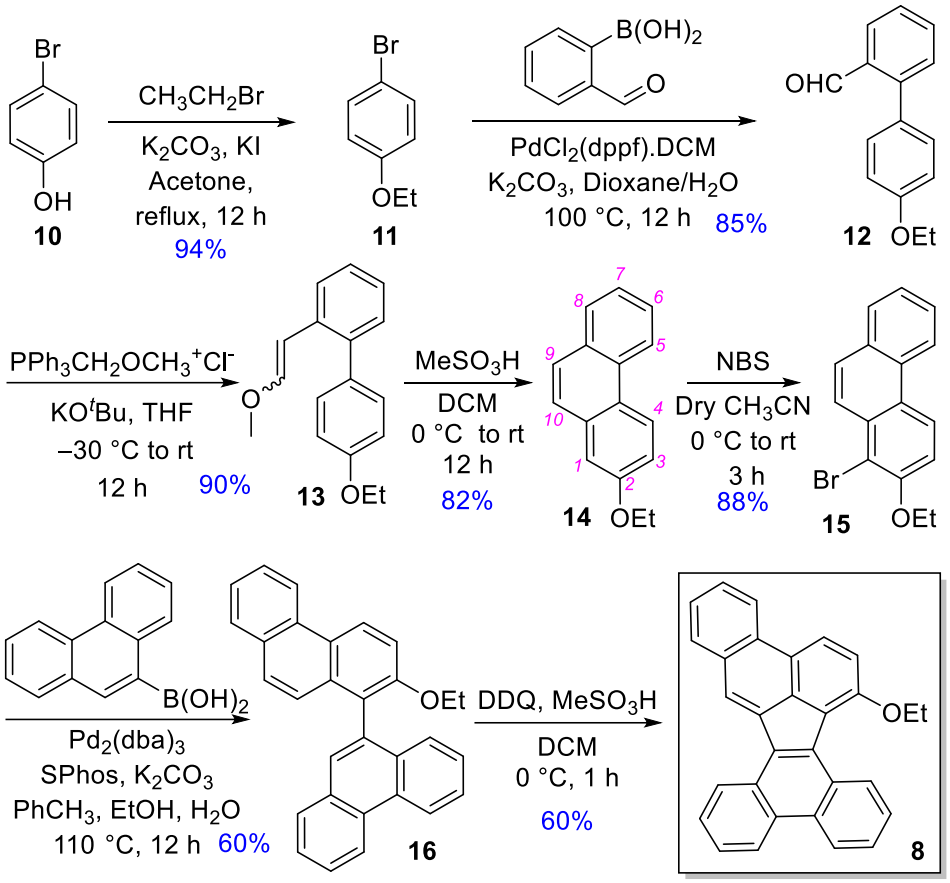

Scheme 5.1 Synthesis of **8**.

Commercially available bromophenol **10** was first converted to **11**, which was subjected to Pd-catalyzed Suzuki reaction with (2-formylphenyl)boronic acid to afford **12** in 85% yield (Scheme 5.1). Compound **12** was subsequently converted to **13** by (methoxymethyl)triphenylphosphonium chloride, and then **13** was treated with methanesulfonic acid to give **14**. Compound **14** could be regioselectively brominated with *N*-bromosuccinimide to afford **15** in 88% yield. Pd^0-catalyzed Suzuki reaction between **15** and 9-phenanthracenylboronic acid gave **16**, which underwent intramolecular oxidative coupling[20] in dry dichloromethane (DCM) at 0 °C with 2,3-dichloro-5,6-dicyano-1,4-benzoquinone (DDQ)[30b] and $MeSO_3H$ to form 1-ethoxy-[9,10-*e*]PAP **8**. Formation of CP-PAH **8** seems reasonable since five-membered ring formation is thermodynamically more favorable over a six-membered ring, and the central ring of phenanthrene bearing strong olefinic C–C double bond character is also usually more reactive toward aromatic electrophilic substitutions. Furthermore, we envisaged that replacing 1-ethoxy group of **8** with electron-rich 3,4-dialkoxyphenyl group,[31] and treating the resulting phenyl derivative under Scholl reaction[30] conditions may afford desired product **9**, as 1-position of 2-ethoxyphenanthrene is reactive

toward aromatic electrophilic substitution, which is evident from the conversion of **14** to **15** (Scheme 5.1).

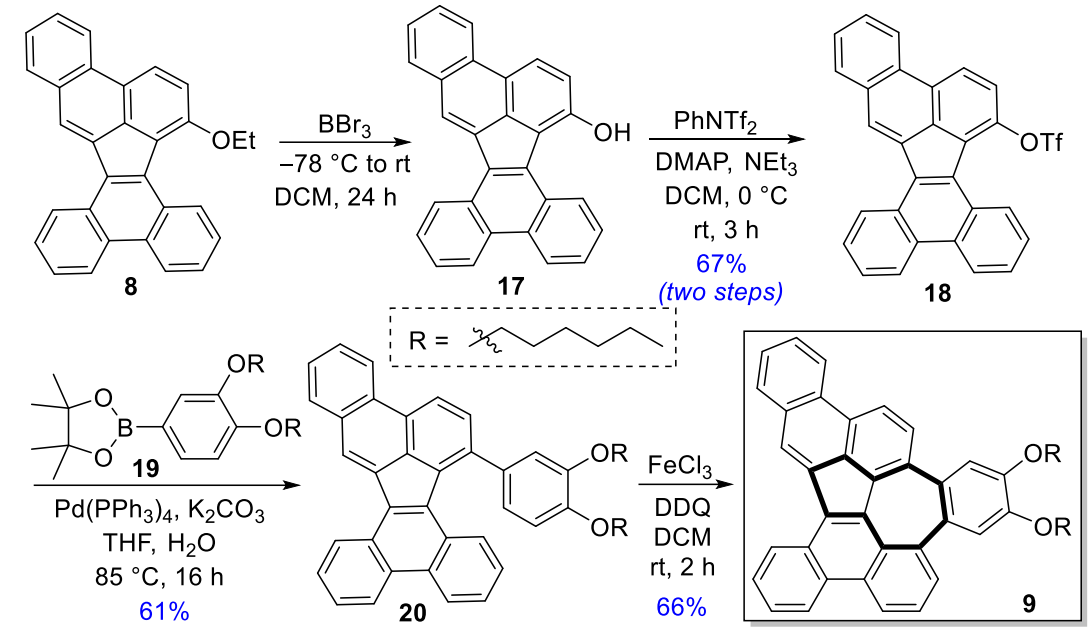

Scheme 5.2 Synthesis of **9**.

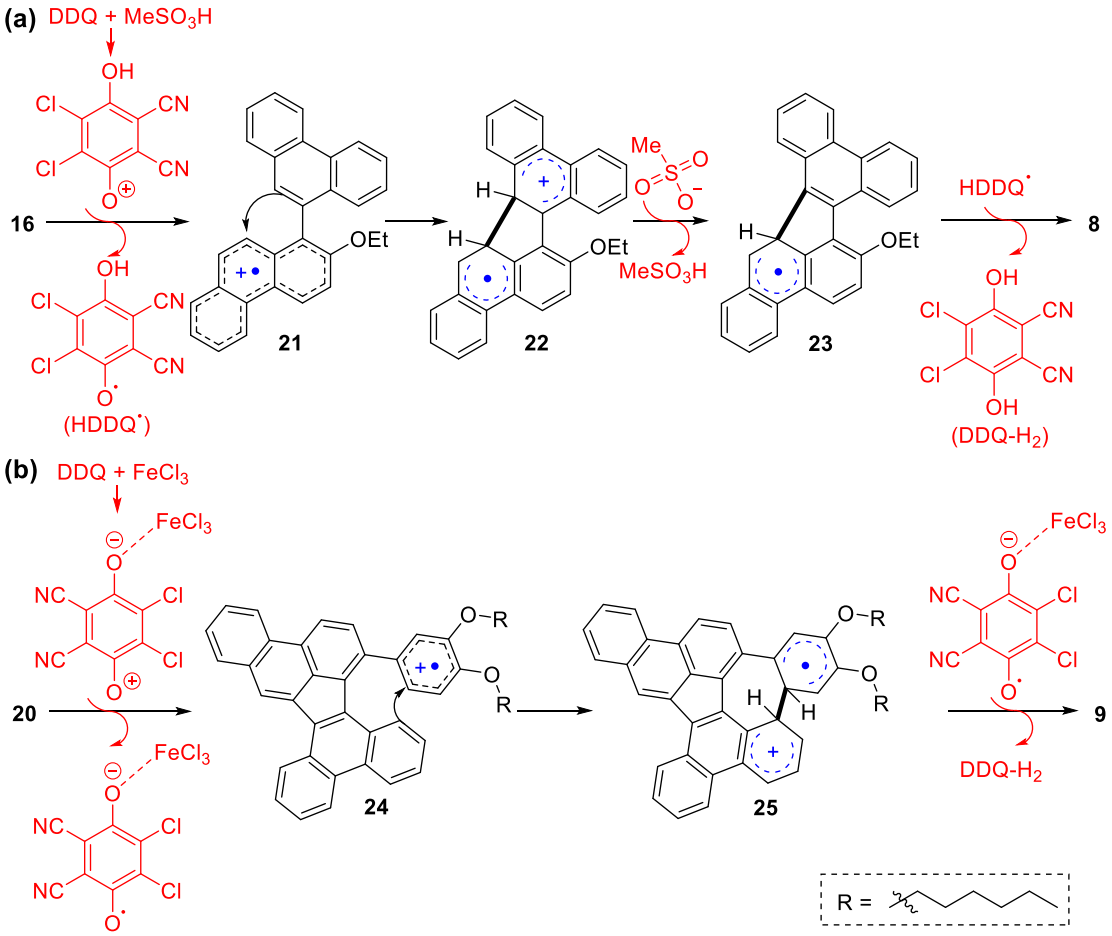

Scheme 5.3 Plausible aryl radical mechanistic pathway for the conversion of **20** to **9**, by DDQ/$FeCl_3$.

Boron tribromide (BBr_3)-mediated dealkylation of **8** in dry DCM afforded **17**, which was converted to triflate **18** in 67% yield over two steps (Scheme 5.2). The Suzuki reaction between triflate **18** and pinacolboronate **19** with two hexyloxy substituents afforded **20** in 61% yield. The Scholl-type oxidative dehydrogenative aromatic coupling[20] of precursor **20** with anhydrous $FeCl_3$/DDQ[21,32] resulted in formation of desired product **9** in 66% yield with no significant byproducts, which was unambiguously confirmed by single-crystal X-ray diffraction (SCXRD) analyses. Based on the literature reports on Scholl-type oxidative aromatic coupling using DDQ,[33] the radical cation pathway could plausibly contribute to the formation of both products **8** and **9**, as proposed in Scheme 5.3. Noticeably, when compared to Takasu's approach,[12] installation of alkoxy chains on the benzene ring was found to be quite essential to promote the Scholl cyclization-induced heptagon ring formation, which is in line with Miao's approach.[31b]

5.2.2 X-ray crystallography and aromaticity analyses. Single crystals of **9**, suitable for SCXRD analysis, were obtained by slow evaporation of tetrahydrofuran/toluene at ambient conditions. The benzene ring F of **9** was twisted from planarity by 21.5° and 37.0° dihedral angle at the bay-II and bay-III regions, respectively, due to steric congestions among C-E-F and I-E-F π-rings, thus resulting in a saddle-like structure (Figure 5.3a and 5.3b). While the dihedral angle at bay-I (0.36°) region suggests insignificant twist, the bay-IV region is twisted by 20.4°, as measured from the torsional angle of H-G-I rings. The cove region involving B-D-G-H rings with a dihedral angle of 9.9°, including the significant twists at the bay-II to IV regions, induced sufficient strain in the azulene unit that resulted in significant bond-length alternation (BLA), ranging from 1.378(5) to 1.507(6) Å (Figure 5.5b), compared to pristine azulene.[34] Furthermore, the twisted backbone forms triple helical substructures for **9** bearing *P,M,P*- and *M,P,M*-configurations in the crystal packing (Figure 5.4). As shown in Figure 5.3c, molecules of **9** were stacked cofacially within the crystal lattice with several short C–C contacts ranging from 3.249 to 3.381 Å, implying strong intermolecular π-π interactions. The C–H···π (2.879 Å) and intermolecular hydrogen bonding interactions (2.699−2.701 Å) between the alkoxy side chains and conjugated skeleton, including the strong intermolecular π-π interactions, enabled a one-dimensional columnar stack for **9** forming herringbone packing motifs (Figure 5.3d).

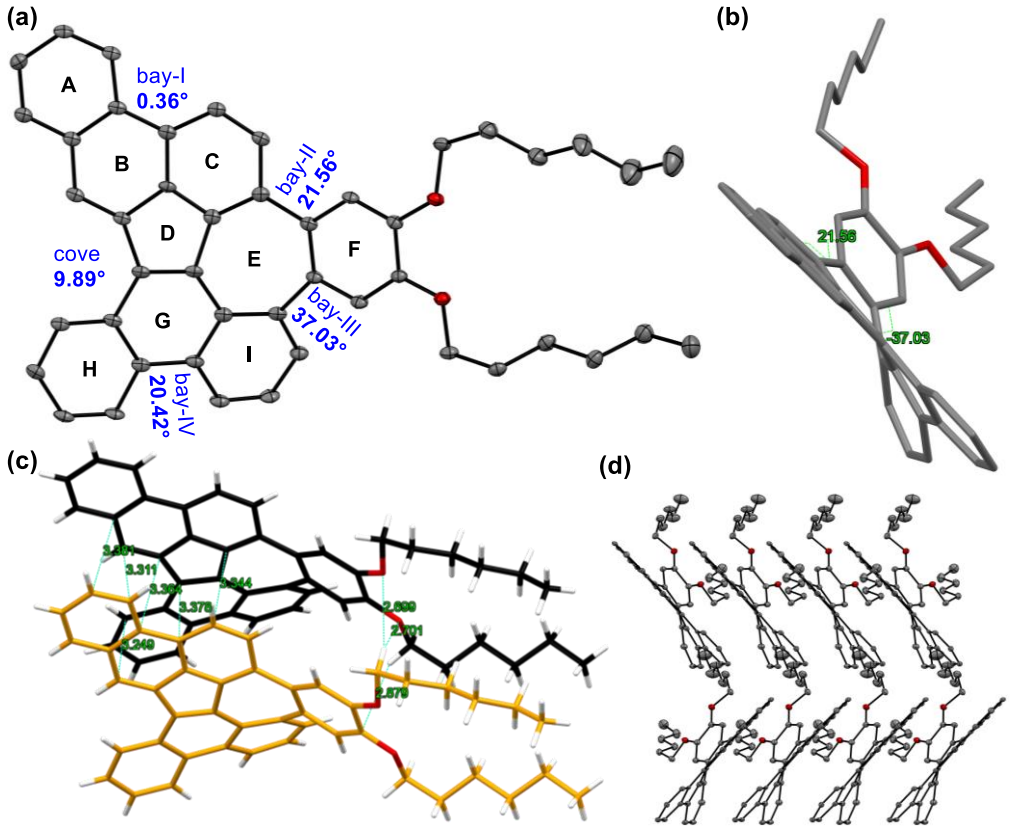

Figure 5.3 (a) ORTEP drawing of **9** at 30% probability of ellipsoids (hydrogens omitted). (b) Side-view of **9** showing saddle-like structure. (c) Intermolecular close C–C contacts, and hydrogen bonding distance (in Å) for **9**. (d) Herringbone packing arrangement of **9** showing columnar 1D-stacks.

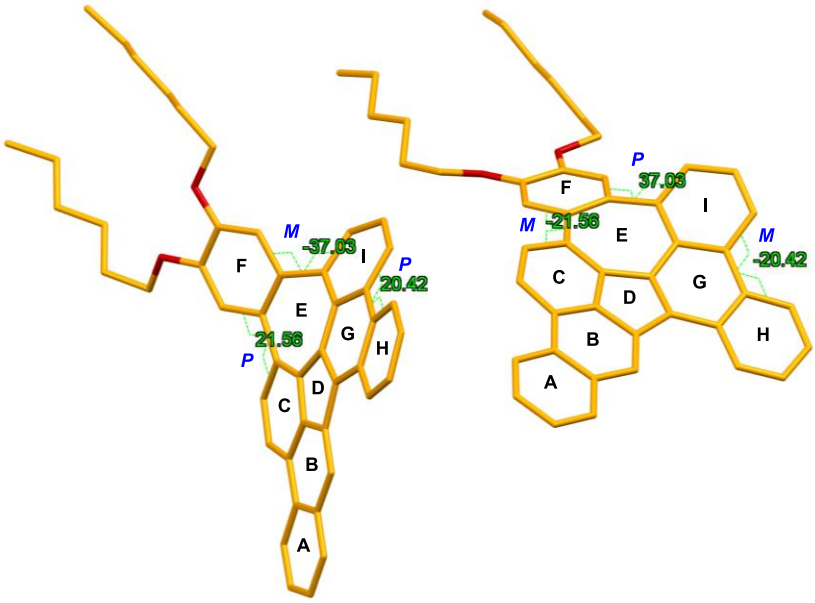

Figure 5.4 Crystal structure of **9** showing a pair of enantiomers with triple helical *P,M,P*- and *M,P,M*-configurations. Hydrogens are omitted for clarity.

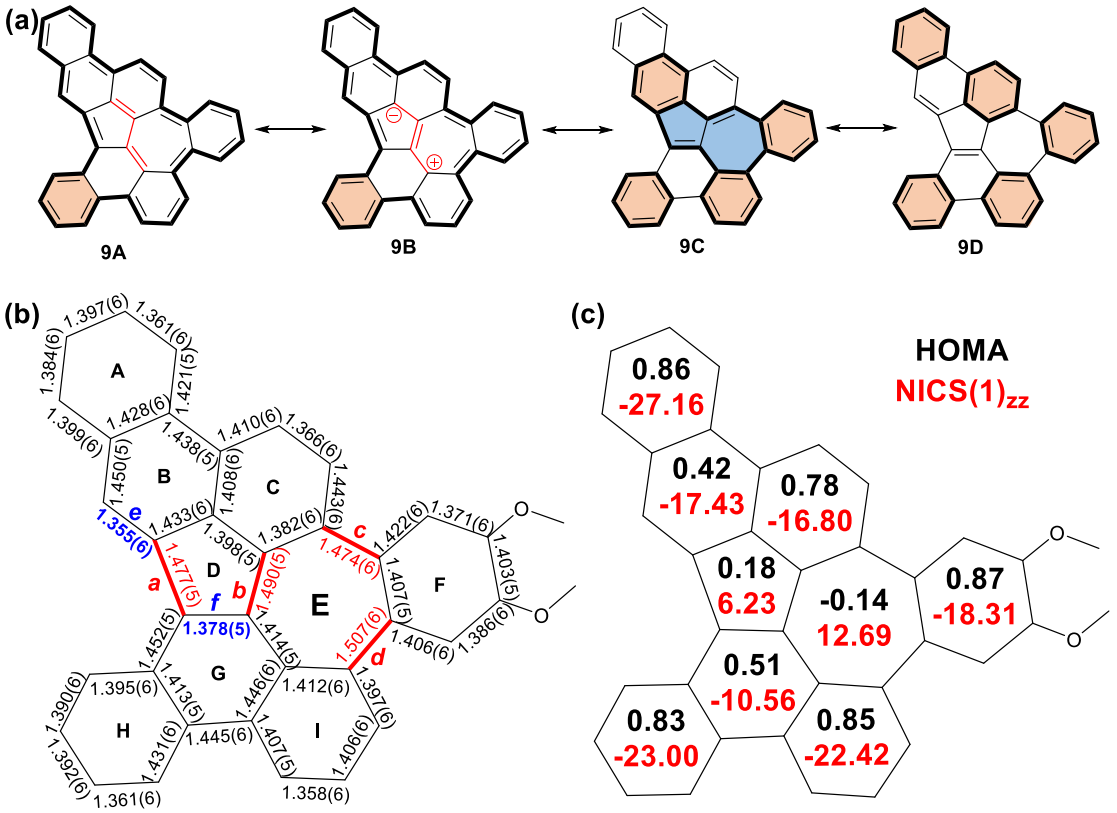

Figure 5.5 (a) Representative canonical forms of **9**. (b) C_{sp^2}–C_{sp^2} bond-lengths (in Å) for **9** with *a*, *b*, *c*, *d* bonds suggesting weak π-bond character while *e* and *f* bonds suggested strong *trans*-diene character. (c) NICS(1)$_{zz}$ and HOMA indices of **9**.

Compound **9** may be viewed in four different Kekulé forms **9A-9D**, and regarded as a formally 30π-aromatic system **9A** with central *trans*-diene arrangement (Figure 5.5a). A zwitterionic azulene in the form of **9B** with one Clar sextet[35] (shown in orange hexagon, Figure 5.5a), and another neutral form **9C** with four Clar sextets and one azulene-like C_{sp^2}–C_{sp^2} alternate double/single bond arrangement for the central 5-7 π-rings (shaded in blue color) can be drawn. Additionally, the **9D** form can be drawn with five Clar sextets and a *trans*-diene arrangement at the cove region which misses the azulene-like C_{sp^2}-C_{sp^2} bond-length arrangement in central 5-7 fused rings. Crystal structure analyses suggested that the central azulene unit did not show near equal bond-length distributions (1.378(5)−1.507(6) Å) for C_{sp^2}–C_{sp^2} bonds, like the typical parent azulene bond-length distributions (1.387−1.404 Å),[34] whereas homogeneous bond-length distributions for five outer six-membered rings A (avg. 1.398 Å), C (avg. 1.401 Å), F (avg. 1.399 Å), I (avg. 1.404 Å), and H (avg. 1.397 Å) suggested localization of benzene aromaticity (Figure 5.5b). The observation was further supported by harmonic oscillator model of aromaticity (HOMA) analyses for

the DFT optimized closed-shell ground state structure of **9**,[36] implying A (0.86), C (0.78), F (0.87), I (0.85) and H (0.83) rings to be aromatic with non-significant BLA, while B and G rings are weakly aromatic (Figure 5.5c).[37] The small HOMA values of the D (0.18) and E (–0.14) rings suggested large BLA, indicating non-aromaticity of the azulene unit, though a negative HOMA value[38] of ring E prompted us to calculate the nucleus independent chemical shift [NICS(1)$_{zz}$ values][39] for **9** to confirm whether the heptagon E would show antiaromaticity!

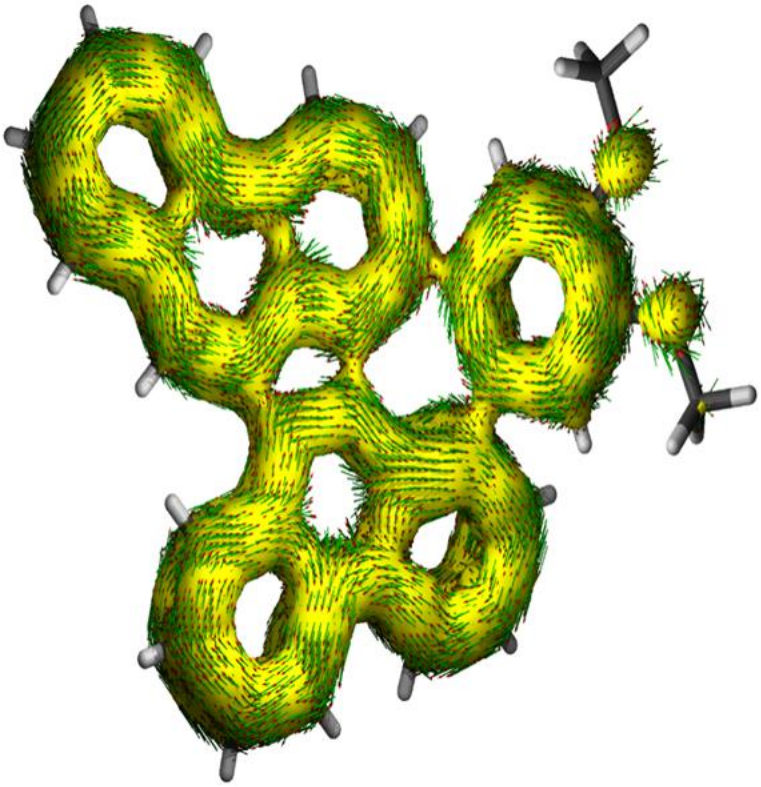

Figure 5.6 ACID isosurface (0.02) of **9** showing π-contribution including the current density vectors (clock-wise currents are diatropic).

NICS(1)$_{zz}$ indices for the ground state of **9** were found to be consistent with the aromatic nature of rings A (–27.16), C (–16.80), F (–18.31), I (–22.42) and H (–23.00) rings, showing large negative NICS(1)$_{zz}$ indices (Figure 5.5c). However, positive NICS(1)$_{zz}$ indices of rings D (6.23) and E (12.69) of **9** stimulated us to study the ring-currents by anisotropy of the induced current density (ACID) calculations.[40] Strong diatropic ring currents for A-B-C and H-G-I phenanthrene substructures with some localization of diatropic ring currents for A, F, I and H benzenoid rings (Figure 5.6) were observed. The large C_{sp^2}–C_{sp^2} bond lengths for *a* (1.477(5) Å), *b* (1.490(5) Å), *c* (1.474(6) Å), *d* (1.507(6) Å) bonds of **9** suggested weak C–C π-bond character, which

is in line with the absence of any ring currents above those bonds, clearly confirming D and E rings to be non-aromatic (i.e. formal azulene unit[2d,2a]). The small positive $NICS(1)_{zz}$ values over the formal azulene unit could be a result of the diatropic ring currents of surrounding phenanthrene/benzene rings inducing some paratropic effect.[41,2e] Our results clearly indicated that resonance form **9D** with the five Clar sextets and a *trans*-diene (C=C bonds *e*: 1.355(6) Å, and *f*: 1.378(5) Å) arrangement in the cove region should majorly contribute to the ground state of **9** with diminished zwitterionic contribution of the true azulene unit.

5.2.3 Optical and electrochemical properties. The UV-vis absorption spectra were measured in DCM at room temperature to study the optical properties of **8** and **9** (Figure 5.7a). Compound **8** displayed high energy absorption bands in the UV region[21] (absorption maxima: λ_{max} = 241 nm, ε = 49620 M^{-1} cm^{-1}; λ_{max} = 261 nm, ε = 63400 M^{-1} cm^{-1}; λ_{max} = 330 nm, ε = 23980 M^{-1} cm^{-1}; λ_{max} = 346 nm ε = 21830 M^{-1} cm^{-1}) and low energy band (λ_{max} = 382 nm, ε = 11730 M^{-1} cm^{-1}; λ_{max} = 406 nm, ε = 8540 M^{-1} cm^{-1}) with a weak band at 446 nm due to HOMO→LUMO transition (theoretical λ_{max} = 452 nm, oscillator strength (*f*) = 0.0772, according to TDDFT calculations shown in Table 5.1), which was extended to 500 nm in the visible region. The absorption profile of compound **9** was red-shifted in comparison to **8**, with intense bands in the higher energy region (λ_{max} = 248 nm, ε = 74100 M^{-1} cm^{-1}; λ_{max} = 280 nm, ε = 73150 M^{-1} cm^{-1}) and low intense bands in the lower energy regions with absorption maxima λ_{max} = 358 nm (ε = 21500 M^{-1} cm^{-1}) and 470 nm (ε = 10300 M^{-1} cm^{-1}), accompanied with a shoulder band at λ_{max} = 500 nm (ε = 6350 M^{-1} cm^{-1}) extending till 540 nm due to extension of π-conjugation. While the lowest energy absorption of **9** at 470 nm may be attributed to the HOMO→LUMO transition, according to TDDFT calculations (theoretical λ_{max} = 489 nm, *f* = 0.1559, Table 5.2), the shoulder band red-shifted on changing solvent polarity from non-polar hexane to DCM to more polar dimethyl sulfoxide (Figure 5.7b), suggesting that the lowest energy transition may have weak charge-transfer (CT) character.

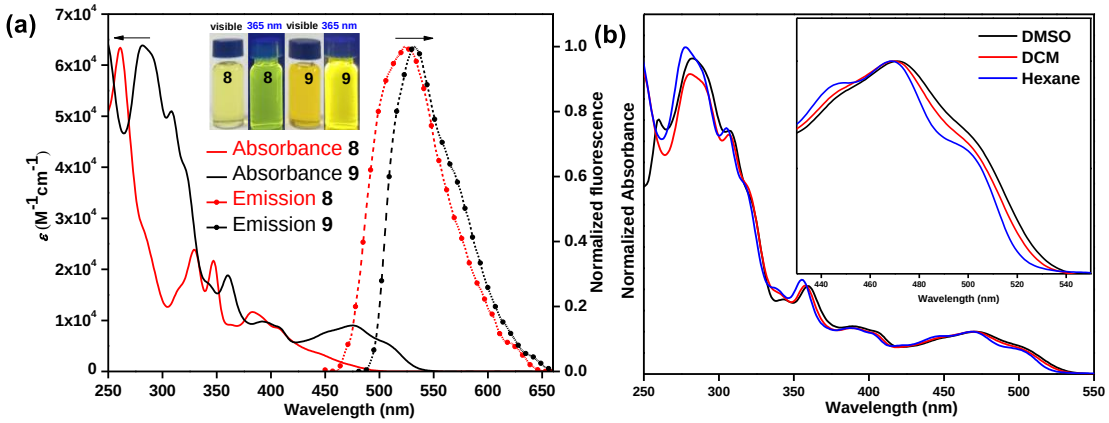

Figure 5.7 (a) UV-vis absorption (straight line) and emission (dash-dotted line) spectra of **8** and **9**, with inset picture under visible and 365 nm light irradiation. (b) Normalized UV-vis absorption spectra in DMSO, DCM, hexane for **9**, with expansion. The shoulder at long wavelength absorption maxima exhibited positive solvatochromic shift of ~8 nm.

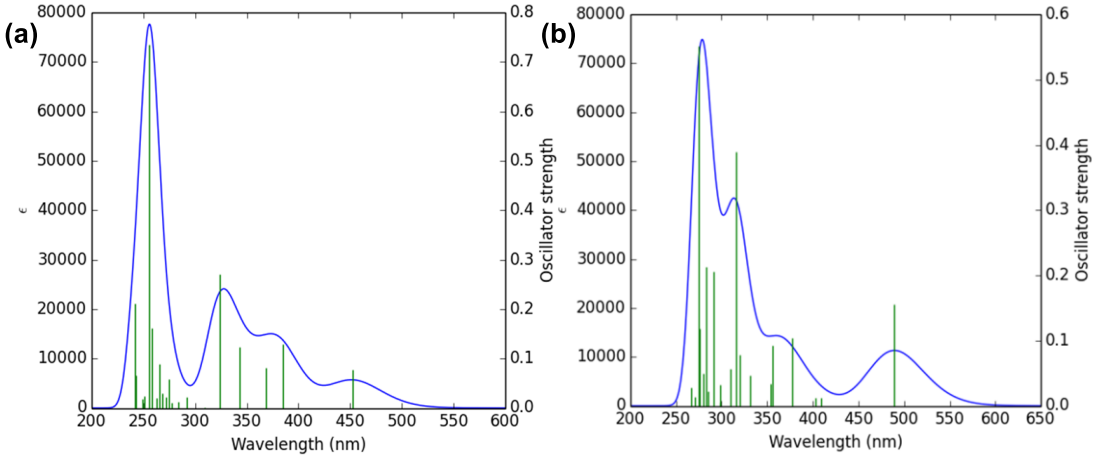

Figure 5.8 (a) Theoretical absorption of **8** in the gas-phase. (b) Theoretical absorption of **9** in the gas-phase**.**

Table 5.1 Summary of TDDFT calculation for **8**.

Wavelength (nm)	**Oscillator Strength (*f*)**	**Major contributions**
452	0.0772	HOMO->LUMO (92%)
385	0.1293	H-1->LUMO (84%)
368	0.0821	H-2->LUMO (84%)
343	0.1235	H-3->LUMO (86%)
323	0.2707	HOMO->L+1 (85%)
309	0.0015	HOMO->L+2 (85%)
292	0.0218	H-1->L+1 (35%), HOMO->L+3 (54%)
284	0.0133	H-4->LUMO (73%)

278	0.0107	H-2->L+1 (17%), H-1->L+1 (31%), H-1->L+2 (11%), HOMO->L+3 (18%)
274	0.0583	H-5->LUMO (14%), H-2->L+1 (29%), H-1->L+1 (14%), H-1->L+2 (10%), HOMO->L+4 (19%)
271	0.0226	H-5->LUMO (33%), H-4->LUMO (10%), H-2->L+1 (19%), H-1->L+2 (16%)
268	0.0292	H-5->LUMO (24%), H-3->L+1 (29%), H-1->L+2 (23%)
265	0.0893	H-6->LUMO (32%), H-3->L+1 (10%), H-2->L+2 (11%), HOMO->L+4 (17%)
262	0.0206	H-6->LUMO (38%), H-2->L+2 (40%), H-1->L+3 (12%)
258	0.1611	H-6->LUMO (10%), H-3->L+1 (28%), H-2->L+3 (14%)
255	0.7357	H-2->L+1 (11%), H-2->L+2 (15%), HOMO->L+4 (44%)
251	0.0248	H-2->L+2 (13%), H-1->L+3 (40%), HOMO->L+5 (26%)
249	0.0191	H-7->LUMO (43%), H-3->L+2 (34%)
242	0.0653	H-7->LUMO (15%), H-3->L+2 (28%), H-2->L+3 (26%), HOMO->L+5 (12%)
241	0.2116	H-3->L+1 (14%), H-3->L+2 (10%), H-2->L+3 (11%), H-1->L+4 (49%)

Table 5.2 Summary of TDDFT calculation for **9**.

Wavelength (nm)	**Oscillator Strength (*f*)**	**Major contributions**
489	0.1559	HOMO->LUMO (95%)
409	0.0128	H-1->LUMO (87%)
402	0.0129	HOMO->L+1 (93%)
377	0.1046	H-2->LUMO (70%), HOMO->L+2 (17%)
355	0.0928	H-2->LUMO (12%), HOMO->L+2 (59%)
353	0.0336	H-3->LUMO (80%)
331	0.0461	H-4->LUMO (69%), HOMO->L+2 (12%)
319	0.0788	H-4->LUMO (13%), H-1->L+1 (16%), HOMO->L+3 (53%)
315	0.3888	H-2->L+1 (11%), H-1->L+1 (47%), HOMO->L+3 (17%)
309	0.0562	H-5->LUMO (31%), H-2->L+1 (45%)
298	0.0326	H-1->L+2 (74%)
298	0.0052	H-5->LUMO (43%), H-2->L+1 (21%), HOMO->L+4 (14%)
291	0.2054	H-5->LUMO (11%), H-3->L+1 (40%), HOMO->L+4 (20%)
285	0.0217	H-2->L+2 (64%), HOMO->L+5 (10%)
282	0.2123	H-4->L+1 (15%), H-3->L+1 (18%), HOMO->L+4 (21%), HOMO->L+5 (29%)
280	0.0495	H-6->LUMO (47%), H-4->L+1 (15%), HOMO->L+5 (13%)
276	0.1182	H-6->LUMO (31%), H-4->L+1 (14%), H-2->L+2 (14%), HOMO->L+5 (10%)
275	0.5515	H-4->L+1 (24%), H-3->L+1 (14%), HOMO->L+4

		(24%), HOMO->L+5 (19%)
271	0.0142	H-7->LUMO (13%), H-4->L+1 (19%), H-1->L+3 (45%)
267	0.0284	H-7->LUMO (15%), H-3->L+2 (61%)

The optical HOMO–LUMO energy gaps, measured from the absorption onsets, were found to be 2.54 eV and 2.33 eV for **8** and **9**, respectively (Figure 5.7a). Compound **8** and **9** displayed fluorescence in DCM solution, with an emission maximum of **8** at λ_{max} = 523 nm (excited at 430 nm), and for **9**, the emission maximum was observed at λ_{max} = 532 nm (excited at 510 nm, Figure 5.7a). The fluorescence quantum yields (Φ) for **8** and **9** in DCM solution were 8.9% and 41.8%, respectively (with fluorescein and rhodamine 6G as standards[42] for **8** and **9**, in 1 μM ethanol, respectively).

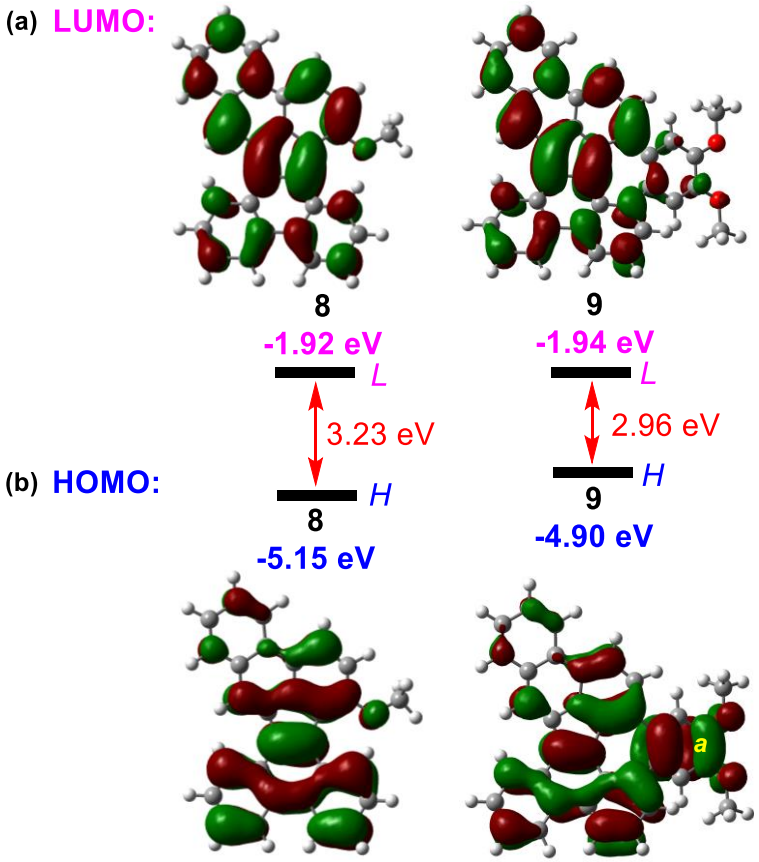

Figure 5.9 DFT optimized (a) LUMO and (b) HOMO profiles of **8** and **9**.

The molecular orbital profiles of **9** (Figure 5.9a and 5.9b) suggested that the orbital coefficients are majorly distributed over the PAP unit, suggesting fluoroanthene[24b] subunit of **9** as the main contributor to the observed optoelectronic properties and not the azulene subunit, which is unlike other azulene-containing PAHs

with greater azulene-like character[2b,5a,6,11a,12] and consistent with the SCXRD/aromaticity analyses (Figure 5.5b, 5.5c and Figure 5.6).

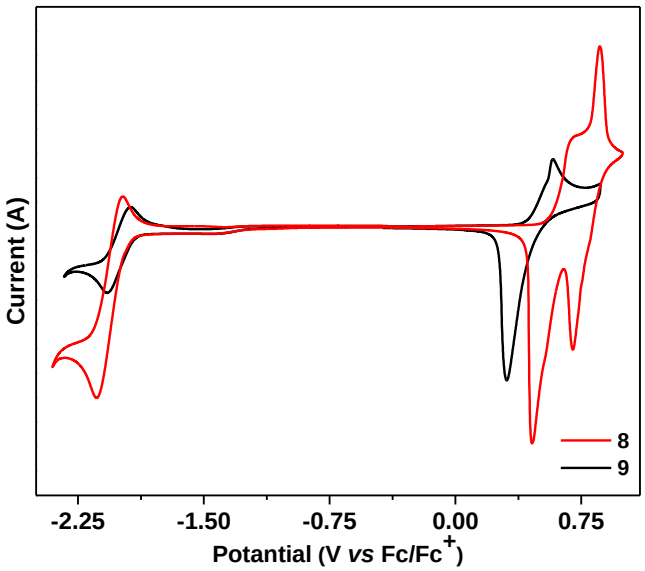

Figure 5.10 Cyclic voltammograms for **8** and **9**.

Cyclic voltammograms of **8** and **9** in DCM solution displayed reversible reduction waves with nearly identical half-wave potentials at $E_{1/2}^{red}$ = –2.05 V and –2.00 V (vs Fc/Fc^{+}), respectively, while **8** exhibited quasi-reversible oxidation wave at E_{peak}^{ox1} = 0.70 V (appearing at a lower oxidation potential than unsubstituted **8**),[21] and **9** appeared at a relatively lower oxidation potential E_{peak}^{ox1} = 0.58 V than **8** (Figure 5.10). However, the reason of such peculiar shapes of the oxidation events are unclear, and they are similar to the unsubstituted **8**.[21] The electrochemical energy gaps, estimated from the first onset redox potentials, of **8** and **9** were 2.55 eV (HOMO: –5.38 eV, LUMO: –2.83 eV) and 2.34 eV (HOMO: –5.20 eV, LUMO: –2.86 eV), respectively. The nearly unaffected reversible reduction potentials for **8** and **9** could be explained by their respective frontier molecular orbital (FMO) profiles, showing that the distribution of LUMO coefficients of **9** remained almost similar to that of the PAP **8** (Figure 5.9a). It was suggested that electron density was mostly distributed over the PAP backbone of **9** and thus, the reduction potentials of **8** and **9** were nearly identical, in line with the calculated LUMO of **9** (–1.94 eV), which is only marginally stabilized compared to that of **8** (–1.92 eV, Figure 5.9a).

The FMO profiles of **Parent-9** (Figure 5.11) suggested that two *ortho*-dialkoxy substituents for **9** may destabilize the HOMO more than the two *para*-alkoxy substituents (**9-Para**, Figure 5.11), and thus could result in a smaller HOMO–LUMO

gap for **9**. Accordingly, the theoretical HOMO of **9** increased to –4.90 eV, in comparison to **8** (–5.15 eV), and the large orbital amplitudes on ring F carbons of **9** (C=C bond with large amplitude is labelled as *a* for **9**, Figure 5.9b) attached to two hexyloxy groups suggested its electron-donating ability to the PAP core of **9** with the electron-accepting[43] CP-PAH subunit with appreciable LUMO coefficients, likely explaining the CT absorption band at ~500 nm (Figure 5.11 and Figure 5.7a). Hence, **9** was relatively easily oxidized at a lower potential than **8**, but their reduction potentials remained identical. The theoretical HOMO–LUMO energy gap of **9** was found to be 0.27 eV smaller than that of **8**, which is similar to the decreasing trend observed for optical and electrochemical energy gaps of **8** and **9**.

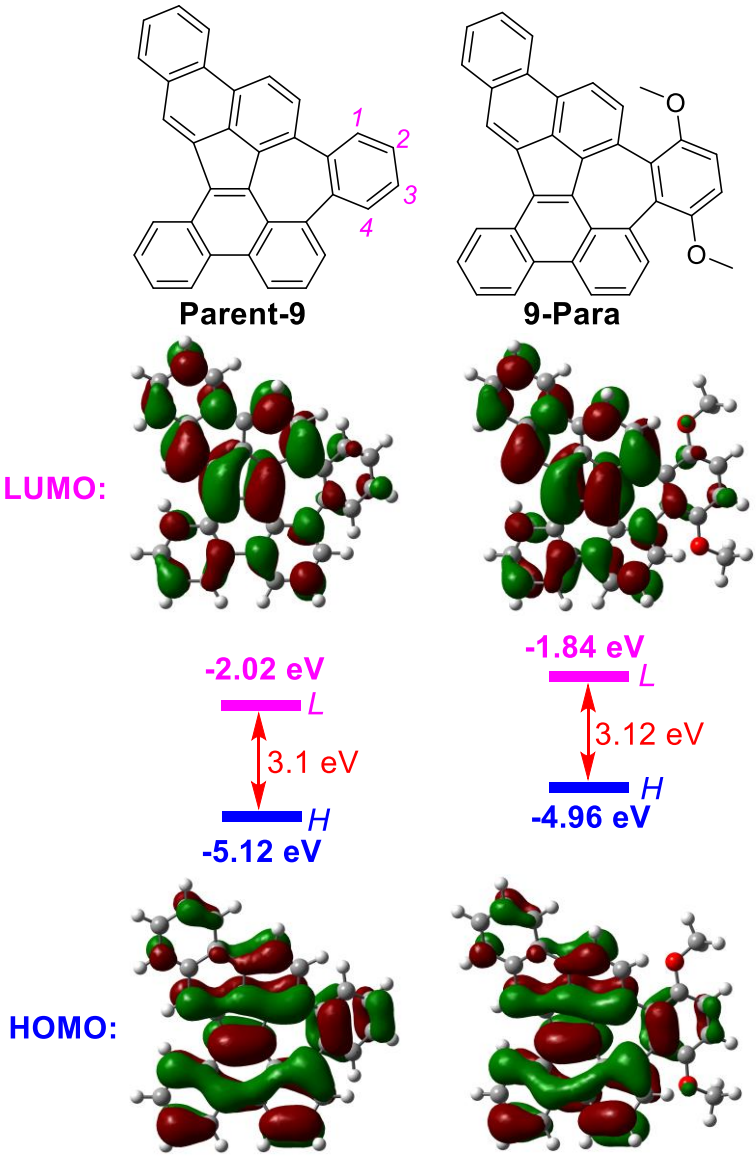

Figure 5.11 Calculated (B3LYP/6-31G(d)) frontier molecular orbital profiles of **Parent-9 and 9-Para**.

5.3 Conclusions

In summary, a new synthetic approach for 1-substituted PAP isomer **8** and its conversion to a fully conjugated PAH **9** bearing fused 5-7-membered rings was described utilizing Scholl-type oxidation, which was seldom applied to construct 7-membered ring containing PAHs.[1,2a,2c,2d,44] The synthetic approach has potential to synthesize some of the hitherto unknown structural isomers of PAP. Single-crystal analyses, HOMA, NICS and ACID calculations suggested localization of Clar sextets in the π-backbone of **9**, which resulted in non-aromaticity of the central azulene unit. The UV-vis absorption profile of **9** was red-shifted in comparison to **8**, suggesting extension of π-conjugation with weak intramolecular CT character. CV analyses suggested that the smaller HOMO–LUMO energy gap of **9** than that of **8** could be due to the destabilization of HOMO energy level, while the LUMO level remained nearly unaffected, which was supported by their identical reduction potentials, and the experimental results were in line with DFT calculations.

5.4 Experimental section

5.4.1 General information. Chemicals and reagents were purchased from local and international commercial suppliers (Merck, GLR innovations, BLDpharm) and used without further purification. Compound **19**, 2-(3,4-bis(hexyloxy)phenyl)-4,4,5,5-tetramethyl-1,3,2-dioxaborolane, was synthesized according to the reported procedure.[45] Thin layer chromatography (TLC) was performed using pre-coated silica-plates purchased from Merck (silica gel 60 PF254, 0.25 mm). Column chromatography was performed using silica gel 100-200 mesh. NMR spectra were recorded in $CDCl_3$ (Eurisotop) at room temperature, on JEOL JNM-ECS400 spectrometer at operating frequencies of 400 MHz (^1H) or 100 MHz (^{13}C) as indicated in the individual spectrum. Chemical shifts (δ) are given in ppm relative to residual solvent (chloroform δ = 7.26 for ^1H, and, δ = 77.16 for proton-decoupled ^{13}C NMR) and coupling constants (*J*) are expressed in Hz. Multiplicity is tabulated as s for singlet, d for doublet, dd for doublet of doublet, t for triplet, q for quartet and m for multiplet. Structural assignments were made with additional information from gCOSY and gNOESY experiments. High resolution mass spectra (HRMS) were recorded using electron spray ionization (ESI) and atmospheric pressure chemical ionization (APCI) methods on Waters (XEVO G2-XS QTOF) mass spectrometer. UV-vis spectra were recorded in JASCO V-770 spectrophotometer. Fluorescence spectra were recorded on

PerkinElmer LS55 fluorescence spectrophotometer. Cyclic voltammetry was performed on CHI-1110C instrument with a glassy carbon working electrode, Pt wire counter electrode, and Ag wire as pseudo-reference electrode in DCM/Bu_4NPF_6 solvent/electrolyte couple at room temperature using a scan rate of 50 mV s^{-1}. The potential was externally calibrated against the ferrocene/ferrocenium couple (0.43 V). Melting points were determined using BIBBY-SMP30 melting point analyzer.

5.4.2 Syntheses.

1-Bromo-4-ethoxybenzene (11). To a suspension of 4-bromophenol **10** (2 g, 11.6 mmol), K_2CO_3 (2.4 g, 17.3 mmol), and KI (2.2 g, 13.3 mmol) in acetone was added bromoethane (1.4 mL, 18.5 mmol), and the mixture was heated at reflux for 12 h using oil bath, under nitrogen atmosphere. After being cooled to room temperature, volatile organics were removed under reduced pressure and water was added. The mixture extracted with EtOAc (3 x 30 mL), dried over anhydrous Na_2SO_4, and filtered. The organic layer was removed under reduced pressure, and crude product was purified by silica gel column chromatography with hexane as eluent to obtain **11** as colourless viscous oil (2.18 g, 94%): R_f = 0.38 (hexanes); ^{1}H NMR (400 MHz, $CDCl_3$) δ 7.38 – 7.34 (m, 2H), 6.79 – 6.74 (m, 2H), 3.99 (q, *J* = 7.0 Hz, 2H), 1.40 (t, *J* = 7.1 Hz, 3H); $^{13}C\{^1H\}$ NMR (100 MHz, $CDCl_3$) δ 158.1, 132.3, 116.3, 112.74, 63.8, 14.8; HRMS (APCI) *m/z*: M^+ Calcd for C_9H_9BrO 199.9837, found 199.9837.

4'-Ethoxy-[1,1'-biphenyl]-2-carbaldehyde (12). An oven-dried thick waled glass tube was charged with **11** (1 g, 4.97 mmol), 2-formylphenylboronic acid (895 mg, 5.97 mmol), K_2CO_3 (3.44 g, 24.8 mmol), 1,4-dioxane (6 mL) and water (0.6 mL), and purged with nitrogen for 30 mins. Catalyst $PdCl_2$(dppf).DCM complex (82 mg, 2 mol%, DCM = dichloromethane) was added. After sealing the glass vial, the reaction mixture was warmed to 100 °C using an oil bath. After 12 h, the flask was cooled to room temperature, volatile organics were removed under reduced pressure, water was added, and the resulting mixture was extracted with EtOAc (3 x 50 mL). The organic layer was dried over Na_2SO_4, filtered, and evaporated under reduced pressure to afford a crude residue which was purified by silica gel column chromatography (hexanes) to give compound **12** as brown solid (960 mg, 85% yield): R_f = 0.59 (hexanes); mp 66–67 °C; ^{1}H NMR (400 MHz, $CDCl_3$) δ 10.00 (s, 1H), 8.00 (dd, *J* = 7.8, 1.1 Hz, 1H), 7.62 (td, *J* = 7.5, 1.5 Hz, 1H), 7.49 – 7.41 (m, 2H), 7.32 – 7.27 (m, 2H), 7.01 – 6.97 (m, 2H), 4.10 (q, *J* = 6.9 Hz, 3H), 1.46 (t, *J* = 7.0 Hz, 4H); $^{13}C\{^1H\}$ NMR (100 MHz,

$CDCl_3$) δ 192.9, 159.1, 145.8, 133.8, 133.6, 131.4, 130.9, 129.9, 127.7, 127.4, 114.5, 63.7, 14.9; HRMS (ESI) *m/z*:$[M + H]^+$ Calcd for $C_{15}H_{15}O_2$ 227.1072, found 227.1063.

2-Ethoxyphenanthrene (14). A solution of *t*-BuOK (1.4 g, 12.4 mmol) in dry THF (12 mL) was added dropwise to a solution of (methoxymethyl)triphenylphosphonium chloride (3.18 g, 9.3 mmol) in 15 mL of anhydrous THF under nitrogen at −30 °C. The mixture was stirred at −30 °C for 2 h, and then a solution of **12** in dry THF (10 mL) was added dropwise. The reaction mixture was stirred for 12 h at room temperature, and then quenched with a saturated solution of NH_4Cl. The volatile organics were evaporated, and the mixture was extracted with DCM (3 x 50 mL). The organic layer was dried over anhydrous Na_2SO_4 and the solvent was subsequently removed under reduced pressure. The residue was passed through a pad of silica gel (hexanes:EtOAc, 95:5) to give a mixture of the *E*- and *Z*-isomers of **13** as viscous yellow oil (1.42 g, 90%), and it was used directly in the next step.

To a solution of **13** (775 mg, 3.05 mmol) in dry DCM (10 mL) was added methanesulfonic acid (0.2 mL) under nitrogen at 0 °C, and the solution was stirred for 3 h at room temperature. Progress of the reaction was monitored by TLC. As the starting material was consumed, a saturated solution of $NaHCO_3$ (10 mL) was added, and stirring was continued for 10 min and the reaction mixture was extracted with DCM (3 x 30 mL). The organic layer was dried over anhydrous Na_2SO_4, filtered, and evaporated under reduced pressure. The residue was subjected to silica gel column chromatography (hexanes:EtOAc, 98:2) to give title product **14** as a white solid (560 mg, 82%): R_f = 0.48 (5% EtOAc/hexanes); mp 103–104 °C; ^{1}H NMR (400 MHz, $CDCl_3$) δ 8.59 (d, *J* = 8.8 Hz, 2H), 7.86 (dd, *J* = 8.0, 0.9 Hz, 1H), 7.72 (d, *J* = 8.9 Hz, 1H), 7.65 (d, *J* = 9.1 Hz, 1H), 7.63 – 7.60 (m, 1H), 7.56 – 7.50 (m, 1H), 7.29 (dd, *J* = 9.0, 2.7 Hz, 1H), 7.25 (d, 1H), 4.21 (q, *J* = 7.0 Hz, 2H), 1.51 (t, *J* = 7.0 Hz, 3H); $^{13}C\{^1H\}$ NMR (100 MHz, $CDCl_3$) δ 157.7, 133.5, 131.1, 130.5, 128.6, 127.5, 126.7, 126.6, 125.6, 124.6, 124.3, 122.2, 117.5, 109.4, 63.7, 15.0; HRMS (ESI) *m/z*: M^+ Calcd for $C_{16}H_{15}O$ 223.1123, found 223.1118.

1-Bromo-2-ethoxyphenanthrene (15). To a suspension of **14** (550 mg, 2.5 mmol) in dry acetonitrile (20 mL) was added NBS (530 mg, 3 mmol) at 0 °C, and the reaction mixture was stirred for 3 h at room temperature. The progress of the reaction was monitored by TLC, and once the reactant was consumed, the reaction mixture was quenched by saturated solution of sodium thiosulfate. The volatile organics were

removed using a rotatory evaporator, and the resulting mixture was extracted with dichloromethane (3 x 30 mL), dried over sodium sulfate and filtered. The organic layer was evaporated, and the crude residue was purified by silica gel column chromatography (hexanes) to give the title product **15** as yellow solid (660 mg, 88% yield): R_f = 0.4 (5% EtOAc/hexanes); mp 140–141 °C; ^{1}H NMR (400 MHz, $CDCl_3$) δ 8.63 (d, *J* = 8.9 Hz, 1H), 8.59 (d, *J* = 8.2 Hz, 1H), 8.24 (d, *J* = 9.2 Hz, 1H), 7.89 (dd, *J* = 7.8, 1.2 Hz, 1H), 7.82 (d, *J* = 9.2 Hz, 1H), 7.65 (ddd, *J* = 8.4, 7.1, 1.5 Hz, 1H), 7.60 – 7.55 (m, 1H), 7.34 (d, *J* = 9.1 Hz, 1H), 4.30 (q, *J* = 7.0 Hz, 2H), 1.56 (t, *J* = 7.0 Hz, 3H); ^{13}C{^{1}H} NMR (100 MHz, $CDCl_3$) δ 154.1, 132.2, 130.9, 130.2, 129.0, 128.7, 127.2, 126.4, 126.0, 125.3, 123.2, 122.4, 113.8, 111.3, 65.7, 15.1; HRMS (ESI) *m/z*: $[M + H]^+$ Calcd for $C_{16}H_{14}OBr$ 301.0228, found 301.0210.

2-Ethoxy-1,9'-biphenanthrene (16): An oven-dried thick-walled glass tube was charged with phenanthren-9-ylboronic acid (445 mg, 2 mmol), 1-bromo-2-ethoxyphenanthrene **15** (500 mg, 1.66 mmol), K_2CO_3 (1.15 g, 8.30 mmol), toluene (8 mL), ethanol (1.5 mL), and water (1.5 mL), and the mixture was purged with nitrogen for 30 min. $Pd_2(dba)_3$ (75 mg, 5 mol%) and SPhos (136 mg, 20 mol%) were added subsequently under nitrogen, and the glass vial was sealed before being warmed to 110 °C for 12 h using an oil bath. After cooling the reaction mixture to room temperature, toluene was evaporated under reduced pressure, water was added, and the reaction mixture was extracted with DCM. The organic layer was dried over sodium sulfate and then evaporated to dryness. The crude mixture was subjected to silica gel column chromatography (hexanes:EtOAc, 95:5) to afford the title product **16** as white solid (400 mg, 60% yield): R_f = 0.33 (5% EtOAc/hexanes); mp 186–187 °C; ^{1}H NMR (400 MHz, $CDCl_3$) δ 8.85 – 8.80 (m, 3H), 8.71 (d, *J* = 8.4 Hz, 1H), 7.92 (d, *J* = 7.9 Hz, 1H), 7.79 (d, *J* = 7.8 Hz, 1H), 7.74 – 7.70 (m, 2H), 7.65 (dt, *J* = 5.8, 4.5 Hz, 3H), 7.54 (dd, *J* = 10.5, 5.0 Hz, 2H), 7.46 (d, *J* = 9.2 Hz, 1H), 7.43 – 7.35 (m, 2H), 7.24 (d, 1H), 4.18 – 4.04 (m, 2H), 1.07 (t, *J* = 7.1 Hz, 3H); ^{13}C{^{1}H} NMR (100 MHz, $CDCl_3$) δ 155.3, 133.7, 133.0, 132.3, 132.0, 130.9, 130.5, 130.4, 129.2, 128.8, 128.6, 127.5, 127.0, 126.8, 126.7, 126.6, 126.4, 125.9, 125.5, 125.0, 124.8, 124.0, 122.8, 122.7, 122.4, 114.0, 65.0, 14.9; HRMS (APCI) *m/z*: M^+ Calcd for $C_{30}H_{23}O$ 399.1749, found 399.1735.

1-Ethoxyphenanthro[9,10-*e*]acephenanthrylene (8). To a solution of **16** (200 mg, 0.5 mmol) in dry DCM (10 mL) was added methanesulfonic acid (1 mL) at 0 °C and then added 2,3-dichloro-5,6-dicyanobenzoquinone (DDQ) (340 mg, 1.5 mmol). The

reaction mixture was left to stir for 30 min at 0 °C and quenched with saturated aq. $NaHCO_3$ solution and then extracted with dichloromethane (3 x 20 mL). The combine organic phase was dried over anhydrous sodium sulfate, and then solvent was removed under reduced pressure. The residue was purified by silica gel column chromatography (hexanes:EtOAc, 98:2) to afford the tile product as yellow solid **8** (120 mg, 60% yield): R_f = 0.33 (5% EtOAc/hexanes); mp 235–236 °C; ^{1}H NMR (400 MHz, $CDCl_3$) δ 10.01 – 9.91 (m, 1H), 9.04 (d, *J* = 8.1 Hz, 1H), 8.92 (s, 1H), 8.79 (t, *J* = 8.2 Hz, 2H), 8.61 (d, *J* = 8.1 Hz, 1H), 8.50 (d, *J* = 8.8 Hz, 1H), 8.13 (d, *J* = 7.8 Hz, 1H), 7.80 – 7.74 (m, 1H), 7.73 – 7.60 (m, 5H), 7.44 (d, *J* = 8.8 Hz, 1H), 4.43 (q, *J* = 7.0 Hz, 2H), 1.70 (t, *J* = 6.9 Hz, 3H); ^{13}C{^{1}H} NMR (100 MHz, $CDCl_3$) δ 153.8, 138.1, 135.5, 133.6, 132.8, 131.3, 131.2, 131.0, 130.5, 130.3, 130.0, 129.8, 129.3, 127.5, 127.2, 127.2, 126.5, 126.0, 125.9, 125.9, 125.1, 125.0, 123.0, 122.4, 121.8, 116.5, 65.9, 15.1; HRMS (APCI) *m/z*: M^+ Calcd for $C_{30}H_{21}O$ 397.1592, found 397.1585.

Phenanthro[9,10-*e*]acephenanthrylen-1-yl trifluoromethanesulfonate (18). To a solution of **8** (93 mg, 0.23 mmol) in anhydrous DCM (6 mL) was added BBr_3 (1.0 M in DCM, 0.93 mL, 0.93 mmol) at −78 °C and the reaction mixture was stirred at room temperature for 12 h. After cooling the reaction mixture to 0 °C, water was added, and then it was extracted with dichloromethane (3 x 30 mL). The combined organic layer was dried over anhydrous sodium sulfate and concentrated to afford a residue containing intermediate **17** (295 mg, yellow solid) which was used for the next step without purification.

To a solution of crude **17** in anhydrous DCM (10 mL) was added 4-dimethylaminopyridine (8.8 mg, 10 mol%) and triethyl amine (0.2 mL, 1.44 mmol), and the reaction mixture was stirred for 30 min at 0 °C, followed by addition of *N*-phenyl-bis(trifluoromethanesulfonimide) (283 mg, 0.8 mmol). Then the reaction mixture was stirred for 3 h at room temperature, before adding water and following extraction with DCM (3 x 20 mL). The combined organic phase was dried over anhydrous sodium sulfate and the solvent was removed under reduced pressure. The residue was purified by column chromatography on silica gel (hexanes:DCM, 99:1) to afford **18** as yellow solid (79 mg, 67% yield over two steps): R_f = 0.22 (5% EtOAc/hexanes); mp 208–209 °C; ^{1}H NMR (400 MHz, $CDCl_3$) δ 8.93 (ddd, *J* = 6.1, 4.2, 2.7 Hz, 2H), 8.85 (s, 1H), 8.77 (dd, *J* = 11.9, 4.7 Hz, 2H), 8.61 (d, *J* = 8.1 Hz, 1H), 8.53 (d, *J* = 8.9 Hz, 1H), 8.14 – 8.08 (m, 1H), 7.79 – 7.66 (m, 7H); ^{13}C{^{1}H} NMR (100 MHz, $CDCl_3$) δ 141.9, 135.4, 134.9, 134.0, 134.0, 133.9, 131.8, 131.2, 130.8,

129.9, 129.0, 128.7, 128.6, 128.4, 127.8, 127.7, 127.5, 127.5, 127.1, 127.1, 127.0, 126.2, 125.0, 124.5, 123.7, 123.5, 123.1, 122.6; HRMS (ESI) *m/z*: M^+ Calcd for $C_{29}H_{15}F_3O_3S$ 500.0694, found 500.0691.

1-(3,4-Bis(hexyloxy)phenyl)phenanthro[9,10-*e*]acephenanthrylene (20). An oven dried glass tube was charged with **18** (80 mg, 0.16 mmol), 2-(3,4-bis(hexyloxy)phenyl)-4,4,5,5-tetramethyl-1,3,2-dioxaborolane **19** (72 mg, 0.18 mmol), K_2CO_3 (111 mg, 0.8 mmol), THF (3 mL) and water (0.6 mL), and the mixture was purged with nitrogen for 30 mins. Catalyst $Pd(PPh_3)_4$ (18 mg, 10 mol%) was subsequently added under nitrogen, and the glass tube was sealed before being warmed to 85 °C using an oil bath. After 16 h, the reaction mixture was cooled to room temperature, and THF was evaporated under reduced pressure. Water was added to the reaction mixture, and then it was extracted with dichloromethane (3 x 30 mL). The organic layer was dried over anhydrous sodium sulfate, filtered, and evaporated under reduced pressure to afford a solid residue which was subjected to silica gel column chromatography (hexanes:DCM, 95:5) to give **20** as yellow solid. (62 mg, 61% yield): R_f = 0.37 (5% EtOAc/hexanes); mp 161–162 °C; ^{1}H NMR (400 MHz, $CDCl_3$) δ 9.03 (d, *J* = 8.1 Hz, 1H), 8.88 (s, 1H), 8.76 (d, *J* = 8.2 Hz, 1H), 8.70 (d, *J* = 7.8 Hz, 1H), 8.62 (d, *J* = 8.5 Hz, 1H), 8.53 (d, *J* = 8.5 Hz, 1H), 8.16 (d, *J* = 7.5 Hz, 1H), 7.86 (d, *J* = 8.3 Hz, 1H), 7.80 (t, *J* = 7.5 Hz, 1H), 7.74 (t, *J* = 6.9 Hz, 1H), 7.68 (q, *J* = 7.2 Hz, 2H), 7.57 (d, *J* = 8.1 Hz, 1H), 7.43 (t, *J* = 7.6 Hz, 1H), 7.18 (dd, *J* = 8.2, 1.9 Hz, 1H), 7.07 – 6.91 (m, 3H), 4.13 – 4.00 (m, 2H), 3.70 (s, 1H), 3.49 (s, 1H), 1.86 (dd, *J* = 13.8, 7.1 Hz, 2H), 1.52 (s, 2H), 1.37 (dt, *J* = 13.7, 5.0 Hz, 4H), 1.32 – 1.09 (m, 8H), 0.94 (t, *J* = 7.0 Hz, 3H), 0.83 (t, *J* = 7.1 Hz, 3H); ^{13}C{^{1}H} NMR (100 MHz, $CDCl_3$) δ 149.4, 148.9, 138.4, 137.9, 135.9, 135.7, 134.6, 133.9, 133.4, 132.8, 132.0, 131.5, 131.2, 130.6, 129.9, 128.6, 127.8, 127.7, 127.4, 126.8, 126.7, 126.2, 126.1, 125.5, 125.2, 125.1, 123.7, 123.0, 122.8, 122.2, 122.1, 116.6, 114.6, 69.6, 69.1, 31.8, 31.5, 29.3, 28.9, 25.8, 25.6, 22.8, 22.7, 14.2, 14.1; HRMS (APCI) *m/z*: M^+ Calcd for $C_{46}H_{45}O_2$ 629.3420, found 629.3423.

2,3-bis(hexyloxy)benzo[*g*]diphenanthro[9,10,1-*cde*:2',1',10'-*ija*]azulene (9). To a solution of **20** (55 mg, 0.09 mmol) in dry DCM (10 mL) was added DDQ (80 mg, 0.35 mmol), resulting in a colour change from yellow to dark green, and then anhydrous $FeCl_3$ (142 mg, 0.9 mmol) added to the reaction mixture. The colour of the solution turned dark brown as the reaction progressed and the reaction mixture was stirred for 2 h. The progress of the reaction was monitored by TLC. Thereafter, the reaction

mixture was quenched with saturated aq. $NaHCO_3$ solution and then extracted with dichloromethane (3 x 30 mL). The organic layer was dried over anhydrous sodium sulfate, filtered, and removed under reduced pressure to afford crude residue **9**, which was further subjected to silica gel column chromatography (hexanes:DCM, 90:10) to afford pure title product **9** as orange solid (37 mg, 66% yield) [R_f = 0.31 (5% EtOAc/hexanes)]. Recrystallization of **9** from a tetrahydrofuran/toluene (1:1) mixture at ambient temperature afforded single crystal suitable for X-ray crystallographic analysis: mp 178–179 °C; ^{1}H NMR (400 MHz, $CDCl_3$) δ 8.91 (d, *J* = 8.0 Hz, 1H), 8.86 (s, 1H), 8.72 (d, *J* = 8.2 Hz, 2H), 8.63 (d, *J* = 8.0 Hz, 1H), 8.56 (d, *J* = 8.7 Hz, 1H), 8.23 (d, *J* = 8.7 Hz, 1H), 8.19 (d, *J* = 7.5 Hz, 1H), 7.95 (d, *J* = 7.5 Hz, 1H), 7.82 – 7.73 (m, 2H), 7.68 (dd, *J* = 15.9, 8.0 Hz, 3H), 7.61 (s, 1H), 7.25 (s, 1H), 4.21 (t, *J* = 6.6 Hz, 2H), 4.15 (t, *J* = 6.6 Hz, 2H), 1.61 – 1.54 (m, 3H), 1.44 – 1.36 (m, 8H), 0.94 (q, *J* = 7.1 Hz, 6H); ^{13}C NMR spectrum with good signal-to-noise ratio could not be obtained for spectroscopic analysis due to insufficient solubility; HRMS (ESI) *m/z*: M^+ Calcd for $C_{46}H_{42}O_2$ 626.3185, found 626.3185.

5.4.3 X-ray crystallographic analysis

Single crystal of **9** was mounted on Hampton cyoloops. The intensity data and geometric parameters of these crystals were garnered with the help of Rigaku XtaLAB Synergy-I, Dualflex, HyPix3000 X-ray diffractometer having a micro-focus sealed X-ray tube Cu-Kα (λ =1.54184 Å) source of X-rays. The crystal was kept at 100 K during data collection. By utilizing OLex2,[46] the crystal structure was solved with the help of olex2.solve[47] structure solution program by employing direct methods and crystal structure refinement was done with the SHELXL refinement package by putting into use Least Squares minimization.[48] Refinement of all non-hydrogen atoms was completed with the help of anisotropic thermal parameters.

Table 5.3 X-ray crystallographic information of **9**

CCDC No.	2220621
Empirical formula	$C_{46}H_{42}O_2$
Formula weight	626.79
Temperature/K	100
Crystal system	monoclinic
Space group	*P*2/*c*
a/Å	38.2962(8)
b/Å	4.59680(10)

c/Å	18.6932(4)
α/°	90
β/°	95.237(2)
γ/°	90
Volume/Å^3	3277.01(12)
Z	4
ρ_{calc}g/cm^3	1.270
μ/mm^{-1}	0.582
F(000)	1336.0
Crystal size/mm^3	0.5 × 0.2 × 0.1
Radiation	CuKα (λ = 1.54184)
2*Θ* range for data collection/°	4.634 to 134.202
Index ranges	$-45 \leq h \leq 45$, $-3 \leq k \leq 5$, $-22 \leq l \leq 22$
Reflections collected	23842
Independent reflections	5848 [R_{int} = 0.0678, R_{sigma} = 0.0498]
Data/restraints/parameters	5848/0/435
Goodness-of-fit on F^2	1.084
Final R indexes [I>=2σ (I)]	R_1 = 0.1024, wR_2 = 0.2736
Final R indexes [all data]	R_1 = 0.1143, wR_2 = 0.2806
Largest diff. peak/hole / e Å^{-3}	0.54/-0.40

5.4.4 DFT calculations

DFT calculations were performed using the Gaussian 09 Rev. B.01 package at B3LYP/6-31G(d) level of theory in the gas phase. During optimization, the ethyl and hexyl chains of **8** and **9** were replaced by methyl group. HOMA values of **9** were calculated using Multiwfn package for the optimized singlet closed-shell ground state structure.[38] NICS values of ground state structure **9** were estimated at the same level of theory using the standard GIAO procedure, and the reported $NICS(1)_{zz}$ indices were averaged by the two positions (above and below the plane).[39] ACID plot (π-only) was calculated following Herges's method.[40] Excitation energies of **8** and **9** were computed using time-dependent DFT (TDDFT) for the singlet closed-shell structures in the gas phase. Molecular orbital contributions of **8** and **9** were determined using GaussSum 3.0 package.[49]

Table 5.4 Relative energies of **9** in closed- and open-shell states

Compound	Optimization	Hartree	kcal/mol
9	Singlet closed-shell B3LYP/6-31G(d,p)	−1535.571178	−963570.9143
	Singlet open-shell UB3LYP/6-31G(d,p)	−1535.571178	−963570.9143

	Triplet open-shell UB3LYP/6-31G(d,p)	−1535.510926	−963533.1058

Singlet-Triplet energy gap = 37.80 kcal mol^{-1}

5.5 References

1. (a) Konishi, A.; Yasuda, M. Breathing New Life into Nonalternant Hydrocarbon Chemistry: Syntheses and Properties of Polycyclic Hydrocarbons Containing Azulene, Pentalene, and Heptalene Frameworks. *Chem. Lett*. **2021**, *50*, 195–212. (b) Chaolumen; Stepek, I. A.; Yamada, K. E.; Ito, H.; Itami, K. Construction of Heptagon-Containing Molecular Nanocarbons. *Angew. Chem., Int. Ed.* **2021**, *60*, 23508–23532.

2. (a) Yang, X.; Rominger, F.; and Mastalerz, M. Contorted Polycyclic Aromatic Hydrocarbons with Two Embedded Azulene Units. *Angew. Chem., Int. Ed.* **2019**, *58*, 17577–17582. (b) Zhang, X. S.; Huang, Y. Y.; Zhang, J.; Meng, W.; Peng, Q.; Kong, R.; Xiao, Z.; Liu, J.; Huang, M.; Yi, Y.; Chen, L.; Fan, Q.; Lin, G.; Liu, Z.; Zhang, G.; Jiang L.; Zhang, D. Dicyclohepta[*ijkl*,*uvwx*]rubicene with Two Pentagons and Two Heptagons as a Stable and Planar Non-benzenoid Nanographene. *Angew. Chem., Int. Ed.* **2020**, *59*, 3529–3533. (c) Ma, J.; Fu, Y.; Dmitrieva, E.; Liu, F.; Komber, H.; Hennersdorf, F.; Popov, A. A.; Weigand, J. J.; Liu, J.; Feng, X. Helical Nanographenes Containing an Azulene Unit: Synthesis, Crystal Structures, and Properties. *Angew. Chem., Int. Ed.* **2020**, *59*, 5637–5642. (d) Han, Y.; Xue, Z.; Li, G.; Gu, Y.; Ni, Y.; Dong, S.; Chi, C. Formation of Azulene-Embedded Nanographene: Naphthalene to Azulene Rearrangement During the Scholl Reaction. *Angew. Chem., Int. Ed.* **2020**, *59*, 9026–9031. (e) Uehara, K.; Mei, P.; Murayama, T.; Tani, F.; Hayashi, H.; Suzuki, M.; Aratani, N.; Yamada, H. An Anomalous Antiaromaticity That Arises from the Cycloheptatrienyl Anion Equivalent. *Eur. J. Org. Chem.* **2018**, 4508–4511. (f) Liu, J.; Mishra, S.; Pignedoli, C. A.; Passerone, D.; Urgel, J. I.; Fabrizio, A.; Lohr, T. G.; Ma, J.; Komber, H.; Baumgarten, M.; Corminboeuf, C.; Berger, R.; Ruffieux, P.; Müllen, K.; Fasel, R.; Feng, X. Open-Shell Nonbenzenoid Nanographenes Containing Two Pairs of Pentagonal and Heptagonal Rings. *J. Am. Chem. Soc.* **2019**, *141*, 12011–12020. (g) Pigulski, B.; Shoyama, K.; Würthner, F. NIR-Absorbing π-Extended Azulene: Non-Alternant Isomer of Terrylene Bisimide. *Angew. Chem., Int. Ed.* **2020**, *59*, 15908–15912. (h) Mathey, P.; Lirette, F.; Fernández, I.; Renn, L.; Thomas, R. W., Morin, J.-F. Annulated Azuleno[2,1,8-*ija*]azulenes: Synthesis and Properties. *Angew.*

Chem. Int. Ed. **2023**, *62*, e202216281. (i) Wang, J.; Gámez, F. G.; Marín-Beloqui, J.; Diaz-Andres, A.; Miao, X.; Casanova, D.; Casado, J.; Liu, J. Synthesis of a Dicyclohepta[*a*,*g*]heptalene-Containing Polycyclic Conjugated Hydrocarbon and the Impact of Non-Alternant Topologies. *Angew. Chem., Int. Ed.* **2023**, *62*, e202217124.

3. (a) Fei, Y.; Liu, J. Synthesis of Defective Nanographenes Containing Joined Pentagons and Heptagons. *Adv. Sci.* **2022**, *9*, 2201000. (b) Ahmed, J.; Mandal, S. K. Phenalenyl Radical: Smallest Polycyclic Odd Alternant Hydrocarbon Present in the Graphene Sheet. *Chem. Rev.* **2022**, *122*, 11369–11431. (c) Fei, Y.; Fu, Y.; Bai, X.; Du, L.; Li, Z.; Komber, H.; Low, K.-H.; Zhou, S.; Phillips, D. L.; Feng, X.; Liu, J. Defective Nanographenes Containing Seven-Five-Seven (7–5–7)-Membered Rings. *J. Am. Chem. Soc.* **2021**, *143*, 2353–2360.

4. (a) Yazyev, O. V.; Louie, S. G. Topological defects in graphene: Dislocations and grain boundaries. *Phys. Rev. B: Condens. Matter Mater. Phys.* **2010**, *81*, 195420. (b) Vicarelli, L.; Heerema, S. J.; Dekker, C.; Zandbergen, H. W. Controlling Defects in Graphene for Optimizing the Electrical Properties of Graphene Nanodevices. *ACS Nano* **2015**, *9*, 3428–3435. (c) Banhart, F.; Kotakoski, J.; Krasheninnikov, A. V. Structural Defects in Graphene. *ACS Nano* **2011**, *5*, 26–41. (d) Lu, J.; Bao, Y.; Su, C. L.; Loh, K. P. Properties of Strained Structures and Topological Defects in Graphene. *ACS Nano* **2013**, *7*, 8350–8357. (e) Costa, A.; López-Castillo, A. Prediction of azulene-based nanographene-like materials. *Diamond Relat. Mater.* **2021**, *112*, 108235. (f) Huang, P. Y.; Ruiz-Vargas, C. S.; van der Zande, A. M.; Whitney, W. S.; Levendorf, M. P.; Kevek, J. W.; Garg, S.; Alden, J. S.; Hustedt, C. J.; Zhu, Y.; Park, J.; McEuen, P. L.; Muller, D. A. Grains and grain boundaries in single-layer graphene atomic patchwork quilts. *Nature* **2011**, *469*, 389–392.

5. (a) Konishi, A.; Morinaga, A.; Yasuda, M. Construction of Polycyclic π-Conjugated Systems Incorporating an Azulene Unit Following the Oxidation of 1,8-Diphenyl-9,10-bis(phenylethynyl)phenanthrene. *Chem. – Eur. J.* **2018**, *24*, 8548–8552. (b) Wang, S.; Tang, M.; Wu, L.; Bian, L.; Jiang, L.; Liu, J.; Tang, Z.-B.; Liang, Y.; Liu, Z. Linear Nonalternant Isomers of Acenes Fusing Multiple Azulene Units. *Angew. Chem. Int. Ed.* 2022, **61**, e202205658. (c) Ong, A.; Tao, T.; Jiang, Q.; Han, Y.; Ou, Y.; Huang, K.-W.; Chi, C. Azulene-Fused Acenes. *Angew. Chem. Int. Ed.* **2022**, *61*, e202209286.

6. Wu, F.; Ma, J.; Lombardi, F.; Fu, Y.; Liu, F.; Huang, Z.; Liu, R.; Komber, H.; Alexandropoulos, D. I.; Dmitrieva, E.; Lohr, T. G.; Israel, N.; Popov, A. A.; Liu, J.; Bogani, L.; Feng, X. Benzo-Extended Cyclohepta[*def*]fluorene Derivatives with Very Low-Lying Triplet States. *Angew. Chem., Int. Ed.* **2022**, *61*, e202202170.

7. (a) Das, S.; Wu, J. Toward Singlet–Triplet Bistable Nonalternant Kekulé Hydrocarbons: Azulene-to-Naphthalene Rearrangement. *Org. Lett.* **2015**, *17*, 5854–5857. (b) Ponugoti, N.; Parthasarathy, V. Rearrangements in Scholl Reaction. *Chem. Eur. J.* **2022**, *28*, e202103530.

8. Jutz, C.; Schweiger, E. Darstellung von Benzazulenen aus Azulenderivaten. *Chem. Ber.* **1974**, *107*, 2383–2396.

9. Munday, R.; Sutherland, I. O. Synthesis of compounds related to cyclohepta[*def*]fluorine. *J. Chem. Soc. C.* **1969**, 1427.

10. (a) Baumgartner, P.; Weltin, E.; Wagnière, G.; Heilbronner, E. Ist die Molekel ein Biradikal?. *Helv. Chim. Acta*. **1965**, *48*, 751–764. (b) Nendel, M.; Goldfuss, B.; Houk, K. N.; Grieser, U.; Hafner, K. Bis-periazulene: a simple Kekulé biradical with a triplet ground state. *Theor. Chem. Acc.* **1999**, *102*, 397–400.

11. (a) Horii, K.; Kishi, R.; Nakano, M.; Shiomi, D.; Sato, K.; Takui, T.; Konishi, A.; Yasuda. Bis-periazulene (Cyclohepta[*def*]fluorene) as a Nonalternant Isomer of Pyrene: Synthesis and Characterization of Its Triaryl Derivatives. *J. Am. Chem. Soc.* **2022**, *144*, 3370–3375. (b) Konishi, A.; Horii, K.; Yasuda, M. The road to bis-periazulene (cyclohepta[*def*]fluorene): Realizing one of the long-standing dreams in nonalternant hydrocarbons. *J. Phys. Org. Chem.* **2023**, e4495.

12. Ogawa, N.; Yamaoka, Y.; Takikawa, H.; Yamada, K; Takasu, K. Helical Nanographenes Embedded with Contiguous Azulene Units. *J. Am. Chem. Soc.* **2020**, *142*, 13322–13327.

13. (a) Zhang, L.; Walker, B.; Liu, F.; Colella, N. S.; Mannsfeld, S. C.; Watkins, J. J.; Nguyen, T.-Q.; Briseno, A. L. Triisopropylsilylethynyl-functionalized dibenzo[*def,mno*]chrysene: a solution-processed small molecule for bulk heterojunction solar cells. *J. Mater. Chem.* **2012**, *22*, 4266–4268. (b) Desroches, M.; Morin, J.-F. Wurster-Type Nanographenes as Stable Diradical Dications. *Chem. – Eur. J.* **2018**, *24*, 2858–2862.

14. Gu, Y.; Wu, X.; Gopalakrishna, T. Y.; Phan, H.; Wu, J. Graphene-like Molecules with Four Zigzag Edge. *Angew. Chem., Int. Ed.* **2018**, *57*, 6541–6545.

15. Omist, A.; Ricci, G.; Derradji, A.; Pérez-Jiménez, A. J.; San-Fabián, E.; Olivier, Y.; Sancho-García, J. C. *peri*-Acenoacene molecules: tuning of the singlet and triplet excitation energies by modifying their radical character. *Phys. Chem. Chem. Phys.* **2021**, *23*, 24016–24028.

16. Gu, Y.; Tullimilli, Y. G.; Feng, J.; Phan, H.; Zeng, W.; Wu, J. Wu, *peri*-Acenoacenes. *Chem. Commun.* **2019**, *55*, 5567–5570.

17. Gu, Y.; Muñoz-Mármol, R.; Fan, W.; Han, Y.; Wu, S.; Li, Z.; Bonal, V.; Villalvilla, J. M.; Quintana, J. A.; Boj, P. G.; Díaz-García, M. A.; Wu, J. *peri*-Acenoacene for Solution Processed Distributed Feedback Laser: The Effect of 1,2-Oxaborine Doping. *Adv. Opt. Mater.* **2022**, *10*, 2102782.

18. Jousselin-Oba, T.; Mamada, M.; Wright, K.; Marrot, J.; Adachi, C.; Yassar, A.; Frigoli, M. Synthesis, Aromaticity, and Application of *peri*-Pentacenopentacene: Localized Representation of Benzenoid Aromatic Compounds. *Angew. Chem., Int. Ed.* **2021**, *61*, e202112794.

19. Liu, T.; Qi, C.; Zhou, Q.; Dai, W.; Lan, Y.; Xu, L.; Ren, J.; Pan, Y.; Yang, L.; Ge, Y.; Qu, Y.-K.; Li, W.; Li, H.; Xiao, S. Divergent Synthesis of Contorted Polycyclic Aromatics Containing Pentagons, Heptagon, and/or Azulene. *Org. Lett.* **2022**, *24*, 472–477.

20. Grzybowski, M.; Skonieczny, K.; Butenschön, H.; Gryko, D. T. Comparison of Oxidative Aromatic Coupling and the Scholl Reaction. *Angew. Chem., Int. Ed.* **2013**, *52*, 9900–9930.

21. Liu, E.-C.; Chen, M.-K.; Li, J.-Y.; Wu, Y.-T. Palladium-Catalyzed Annulation of 9-Halophenanthrenes with Alkynes: Synthesis, Structural Analysis, and Properties of Acephenanthrylene-Based Derivatives. *Chem. - Eur. J.* **2015**, *21*, 4755–4761.

22. Crawford, M.; Supanekar, V. R. Synthesis of benzo[*b*]naphtho[2,1-*j*]fluoranthene, benzo[*a*]naphtho[2,3-*j*]fluoranthene and other related benzo[*j*]fluoranthene derivatives. *J. Chem. Soc. C*, **1970**, 1832–1835.

23. Ogawa, N.; Yamaoka, Y.; Yamada, K; Takasu, K. Synthesis of π-Extended Fluoranthenes via a KHMDS-Promoted Anionic-Radical Reaction Cascade. *Org. Lett.* **2017**, *19*, 3327–3330.

24. (a) Liu, Y.-H.; Perepichka, D. F. Acenaphthylene as a building block for π-electron functional materials. *J. Mater. Chem. C*. **2021**, *9*, 12448–12461. (b) Wegner, H. A.; Scott, L. T.; Meijere, A. A New Suzuki−Heck-Type Coupling Cascade: Indeno[1,2,3]-Annelation of Polycyclic Aromatic Hydrocarbons. *J. Org. Chem.* **2003**, *68*, 883–887.

25. (a) Scott, L. T.; Reinhardt, G.; Roelofs, N. H. Acephenanthrylene. *J. Org. Chem*. **1985**, *50*, 5886–5887. (b) Sing, Y. L.; Lee, L. F. Lee, Condensation with trifluoroacetonitrile: a simple one step synthesis of 5-cyano-6-(trifluoromethyl) uracil. *J. Org. Chem*. **1985**, *50*, 4642– 4646.

26. Anthony, J. E.; Scott, J. L.; Parkin, S. R. Radical-Induced Cycloaromatization: Routes to Fluoranthenes and Acephenanthrylenes. *Synlett*. **2004**, 161–164.

27. (a) Ma, J.; Fu, Y.; Liu, J.; Feng, X. One-pot synthesis of dicyclopenta-fused peropyrene via a fourfold alkyne annulation. *Beilstein J. Org. Chem.* **2020**, *16*, 791–797. (b) Dang, H.; Garcia-Garibay, M. A. Palladium-Catalyzed Formation of Aceanthrylenes: A Simple Method for Peri-Cyclopentenelation of Aromatic Compounds. *J. Am. Chem. Soc.* **2001**, *123*, 355–356.

28. Ackermann, M.; Freudenberg, J.; Jänsch, D.; Rominger, F.; Bunz, U. H.; Müllen, K. Palladium-Catalyzed Dimerization of Bis(2-biphenylyl)acetylene toward Sterically Hindered Acephenanthrylene. *Org. Lett.* **2018**, *20*, 3758–3761.

29. Chen, P.-T.; Yu, C.-L.; Shen, M.-H.; Cheng, M.-J.; Wu, Y.-T.; Hsu, H.-F. Highly Substituted Acephenanthrylenes and Their π-Extended Derivatives: Syntheses, Structural Analyses, and Properties. *Org. Lett.* **2022**, *24*, 4778–4782.

30. (a) Zhai, L.; Shukla, R.; Wadumethrige, S. H.; Rathore, R. Probing the Arenium-Ion (Proton Transfer) versus the Cation-Radical (Electron Transfer) Mechanism of Scholl Reaction Using DDQ as Oxidant. *J. Org. Chem.* **2010**, *75*, 4748–4760. (b) Zhai, L.; Shukla, R.; Rathore, R. Oxidative C−C Bond Formation (Scholl Reaction) with DDQ as an Efficient and Easily Recyclable Oxidant. *Org. Lett.* **2009**, *11*, 3474–3477. (c) Wadumethrige, S. H.; Rathore, R. A Facile Synthesis of Elusive Alkoxy-Substituted Hexa-*peri*-hexabenzocoronene. *Org. Lett.* **2008**, *10*, 5139–5142.

31. (a) Zhang, Y.; Pun, S. H.; Miao, Q. The Scholl Reaction as a Powerful Tool for Synthesis of Curved Polycyclic Aromatics. *Chem. Rev.* **2022**, *122*, 14554–14593. (b) Pun, S. H.; Cheung, K. M.; Yang, D.; Chen, H.; Wang, Y.; Kershaw, S. V.; Miao, Q. A Near-Infrared Absorbing and Emissive Quadruple Helicene Enabled by the Scholl

Reaction of Perylene. *Angew. Chem., Int. Ed.* **2022**, *61*, e202113203. (c) Yang, Y.; Yuan, L.; Shan, B.; Liu, Z.; Miao, Q. Twisted polycyclic arenes from tetranaphthyldiphenylbenzenes by controlling the Scholl reaction with substituents. *Chem. - Eur. J.* **2016**, *22*, 18620−18627.

32. (a) Ma, Y.; Zhang, D.; Yan, Z.; Wang, M.; Bian, C.; Gao, X.; Bunel, E. E.; Lei, A. Iron-Catalyzed Oxidative C–H/C–H Cross-Coupling between Electron-Rich Arenes and Alkenes. *Org. Lett.* **2015**, *17*, 2174–2177. (b) Jang, S. S.; Youn, S. W. The cooperative FeCl3/DDQ system for the regioselective synthesis of 3-arylindoles from β-monosubstituted 2-alkenylanilines. *Org. Biomol. Chem.* **2016**, *14*, 2200–2204.

33. (a) Jassas, R. S.; Mughal, E. U.; Sadiq, A.; Alsantali, R. I.; Al-Rooqi, M. M.; Naeem, N.; Moussa, Z.; Ahmed, S. A. Scholl reaction as a powerful tool for the synthesis of nanographenes: a systematic review. *RSC Adv.* **2021**, *11*, 32158–32202. (b) Alsharif, M. A.; Raja, Q. A.; Majeed, N. A.; Jassas, R. S.; Alsimaree, A. A.; Sadiq, A.; Naeem, N.; Mughal, E. U.; Alsantali, R. I.; Moussa, Z.; Ahmed, S. A. DDQ as a versatile and easily recyclable oxidant: a systematic review. *RSC Adv.* **2021**, *11*, 29826–29858.

34. Hanson, A. W. The crystal structure of the azulene, s-trinitrobenzene complex. *Acta Crystallogr.* **1965**, *19*, 19–26.

35. Solà, M. Forty years of Clar's aromatic π-sextet rule. *Front. Chem.* **2013**, *1*, 22.

36. DFT optimization at B3LYP/6-31G(d) showed ground state of **9** to be singlet closed-shell with a large singlet-triplet energy gap (37.8 kcal mol^{-1}, Table 5.4).

37. (a) Kruszewski, J.; Krygowski, T. M. Definition of aromaticity basing on the harmonic oscillator model. *Tetrahedron Lett.* **1972**, *13*, 3839-3842. (b) Krygowski, T. M.; Bankiewicz, B.; Czarnocki, Z.; Palusiak, M. Aromaticity: what does it mean?. *ChemTexts* **2015**, *1*, 12. (c) Sharma, P. K.; Das, S. Unveiling a Quinoidal 2,3:10,11-Dibenzoheptazethrene. *J. Org. Chem.* **2022**, *87*, 5430–5436.

38. (a) Dominikowska, J.; Palusiak, M. EL: the new aromaticity measure based on one-electron density function. *Struct. Chem.* **2012**, *23*, 1173–1183. (b) Sharma, H.; Bhardwaj, N.; Das, S. Revisiting indeno[1,2-*b*]fluorene by steric promoted synthesis while isolating the second stable 4nπ indeno[2,1-*a*]fluorine. *Org. Biomol. Chem.* **2022**, *20*, 8071–8077.

39. (a) Fallah-Bagher-Shaidaei, H.; Wannere, C. S.; Corminboeuf, C.; Puchta, R.; Schleyer, P. v. Which NICS Aromaticity Index for Planar π Rings Is Best?. *Org. Lett.* **2006**, *8*, 863–866. (b) Dobrowolski, J. C.; Lipiński, P. F. On splitting of the NICS(1) magnetic aromaticity index. *RSC Adv.* **2016**, *6*, 23900–23904. (c) Antić, M.; Furtula, B.; Radenković, S. Aromaticity of Nonplanar Fully Benzenoid Hydrocarbons. *J. Phys. Chem. A.* **2017**, *121*, 3616–3626.

40. Geuenich, D.; Hess, K.; Köhler, F.; Herges, R. Anisotropy of the Induced Current Density (ACID), a General Method To Quantify and Visualize Electronic Delocalization. *Chem. Rev.* **2005**, *105*, 3758–3772.

41. (a) Stanger, A. The Seven-Membered Ring in Bis-Azuleno-Naphthalene is Non-Aromatic. *Eur. J. Org. Chem.* **2019**, 857–859. (b) Stanger, A. NICS – Past and Present. *Eur. J. Org. Chem.* **2020**, 3120–3127. (c) Uehara, K.; Mei, P.; Murayama, T.; Tani, F.; Hayashi, H.; Suzuki, M.; Aratani, N.; Yamada, H. An Anomalous Antiaromaticity That Arises from the Cycloheptatrienyl Anion Equivalent. *Eur. J. Org. Chem.* **2018**, *2018*, 4508–4511. (d) Uehara, K.; Mei, P.; Murayama, T.; Tani, F.; Hayashi, H.; Suzuki, M.; Aratani, N.; Yamada, H. *Eur. J. Org. Chem.* **2019**, *2019*, 860–861.

42. (a) Taniguchi, M.; Lindsey, J. S. Database of Absorption and Fluorescence Spectra of >300 Common Compounds for use in PhotochemCAD. *Photochem. Photobiol.* **2018**, *94*, 290– 327. (b) Kubin, R. F.; Fletcher, A. N. Fluorescence quantum yields of some rhodamine dyes. *J. Lumin.* **1982**, *27*, 455–462. (c) Kellogg, R. E.; Bennett, R. G. Radiationless Intermolecular Energy Transfer. III. Determination of Phosphorescence Efficiencies. *J. Chem. Phys.* **1964**, *41*, 3042–3045.

43. Wood, J. D.; Jellison, J. L.; Finke, A. D.; Wang, L.; Plunkett, K. N. Electron Acceptors Based on Functionalizable Cyclopenta[*hi*]Aceanthrylenes and Dicyclopenta[*de*,*mn*]Tetracenes. *J. Am. Chem. Soc.* **2012**, *134*, 15783–15789.

44. (a) Kawasumi, K.; Zhang, Q.; Segawa, Y.; Scott, L. T.; Itami, K. A grossly warped nanographene and the consequences of multiple odd-membered-ring defects. *Nat. Chem.* **2013**, *5*, 739–744. (b) Fernández-García, J. M.; Evans, P. J.; Medina Rivero, S.; Fernández, I.; García-Fresnadillo, D.; Perles, J.; Casado, J.; Martín, N. π-Extended Corannulene-Based Nanographenes: Selective Formation of Negative Curvature. *J. Am. Chem. Soc.* **2018**, *140*, 17188–17196. (c) Nobusue, S.; Fujita, K.; Tobe, Y.

Skeletal Rearrangement of Twisted Polycyclic Aromatic Hydrocarbons under Scholl Reaction Conditions. *Org. Lett.* **2017**, *19*, 3227–3230.

45. Zhao, B.; Liu, B.; Png, R. Q.; Zhang, K.; Lim, K. A.; Luo, J.; Shao, J.; Ho, P. K. H.; Chi C.; Wu, J. New Discotic Mesogens Based on Triphenylene-Fused Triazatruxenes: Synthesis, Physical Properties, and Self-Assembly. *Chem. Mater.* **2009**, *22*, 435–449.

46. Dolomanov, O. V.; Bourhis, L. J.; Gildea, R. J.; Howard, J. A.; Puschmann, H. Olex2: A complete structure solution, refinement and Analysis Program. *J. Appl. Crystallogr.* **2009**, *42*, 339–341.

47. Bourhis, L. J.; Dolomanov, O. V.; Gildea, R. J.; Howard, J. A.; Puschmann, H. The anatomy of a comprehensive constrained, restrained refinement program for the modern computing environment –olex2dissected. *Acta Crystallogr. A.* **2015**, *71*, 59–75.

48. Sheldrick, G. M. Crystal structure refinement with SHELXL, *Acta Crystallogr. C Struct. Chem*. **2015**, *71*, 3–8.

49. O'boyle, N. M.; Tenderholt, A. L.; Langner, K. M. cclib: A library for package independent computational chemistry algorithms. *J. Comput. Chem.* **2008**, *29*, 839–845.

5.6 Appendix

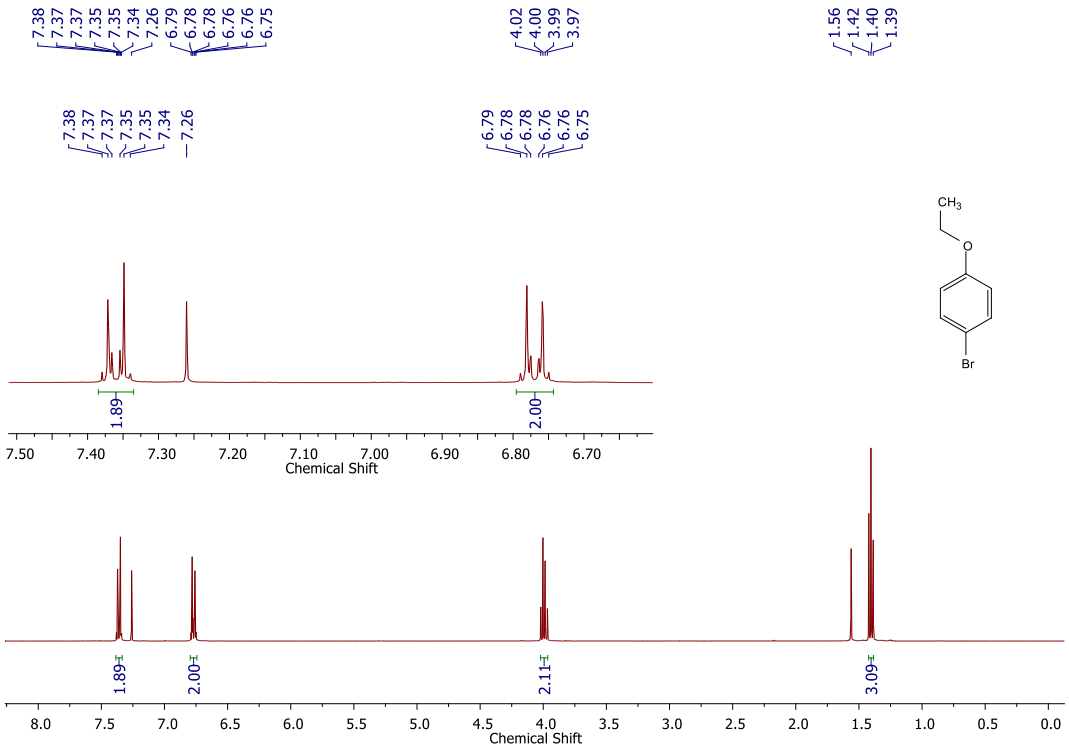

Figure 5.12 ^{1}H NMR spectrum of **11** (in $CDCl_3$, 400 MHz, 298 K).

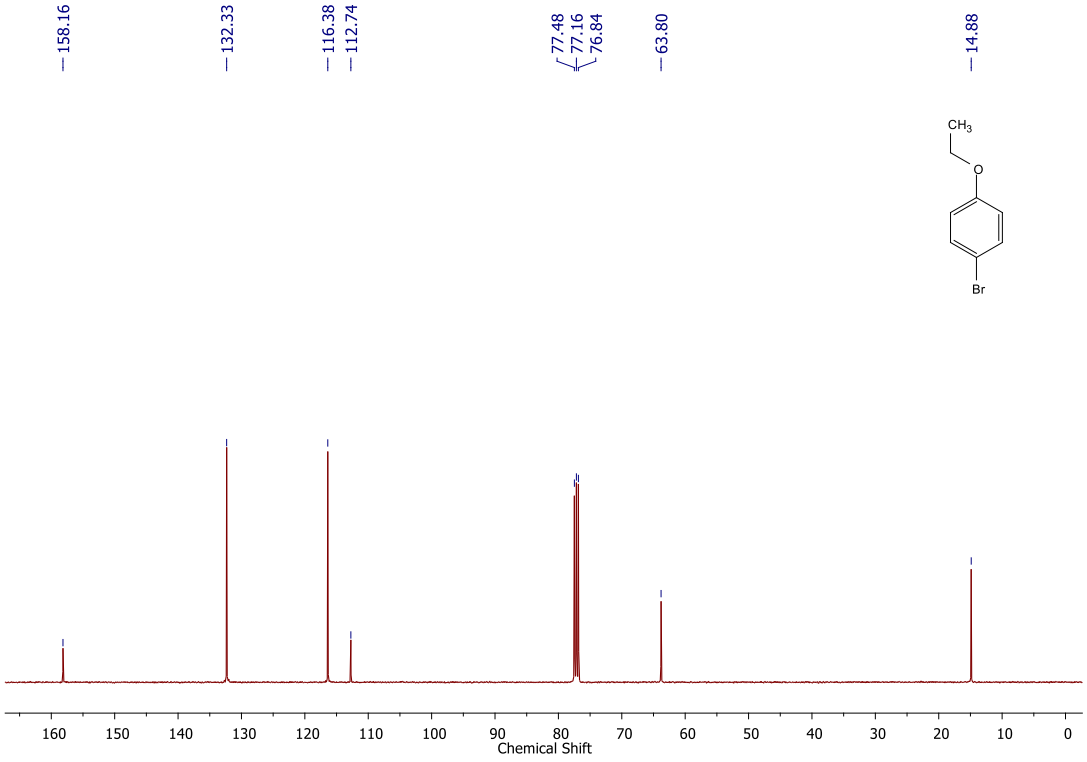

Figure 5.13 ^{13}C{^{1}H} NMR spectrum of **11** (in $CDCl_3$, 100 MHz, 298 K).

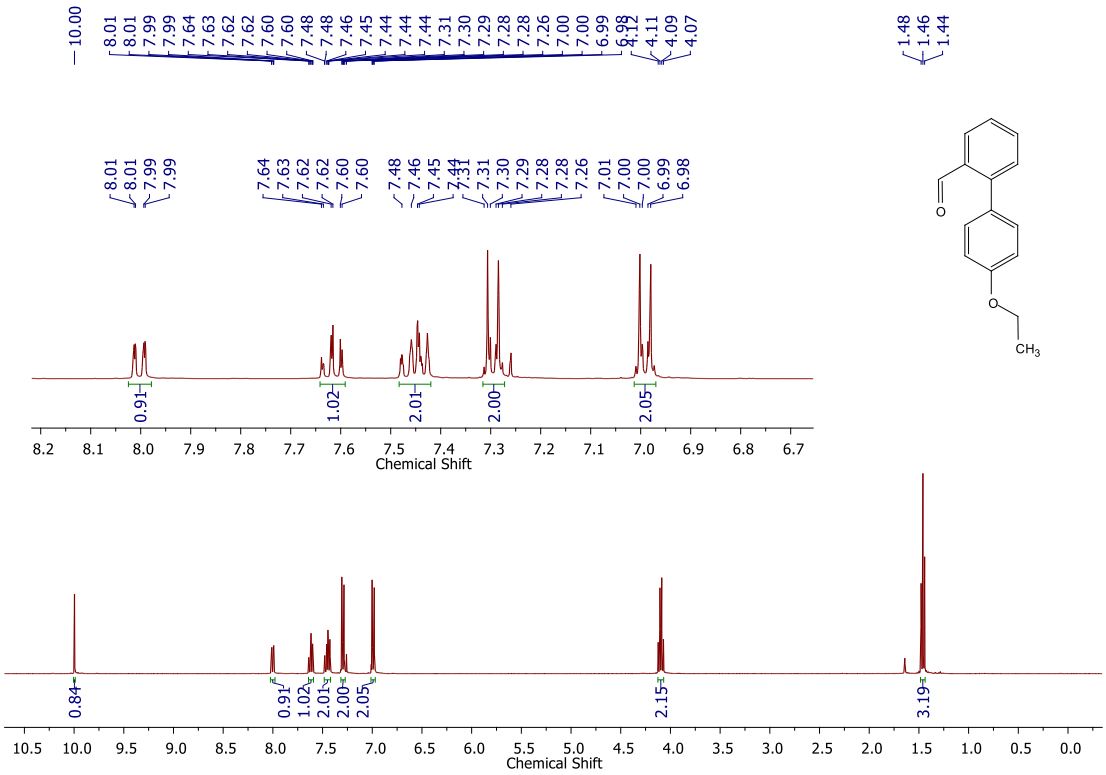

Figure 5.14 ^{1}H NMR spectrum of **12** (in $CDCl_3$, 400 MHz, 298 K).

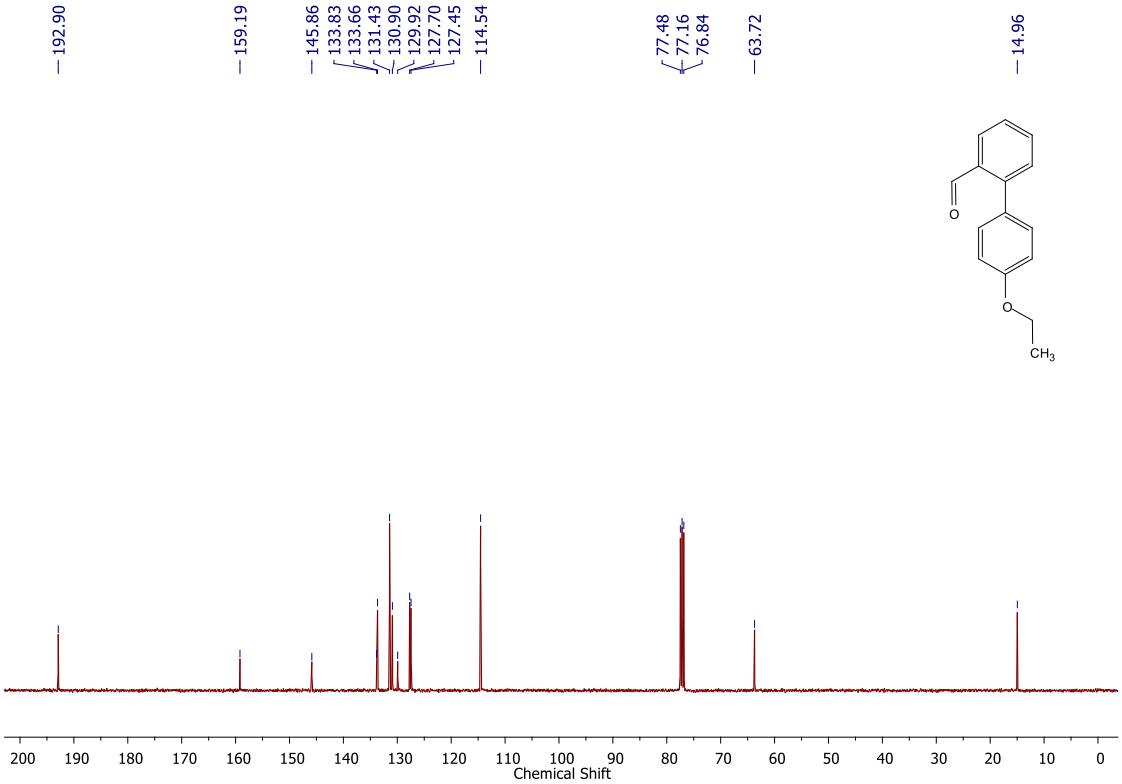

Figure 5.15 $^{13}C\{^{1}H\}$ NMR spectrum of **12** (in $CDCl_3$, 100 MHz, 298 K).

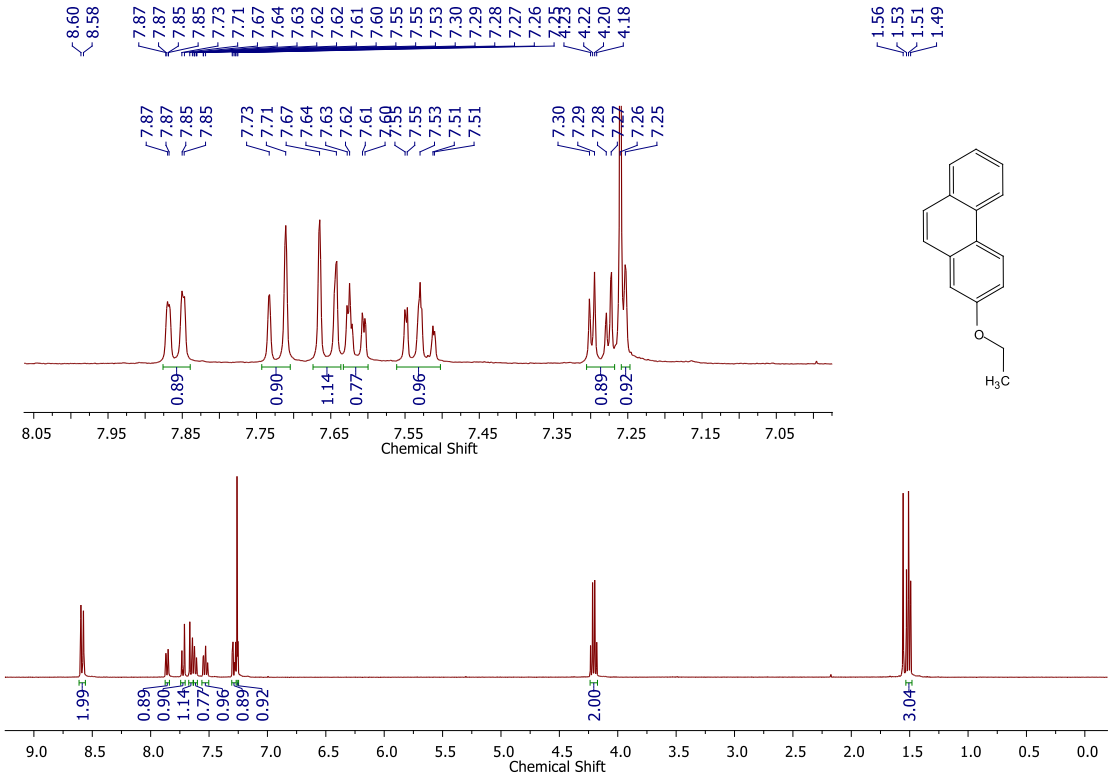

Figure 5.16 ^{1}H NMR spectrum of **14** (in $CDCl_3$, 400 MHz, 298 K).

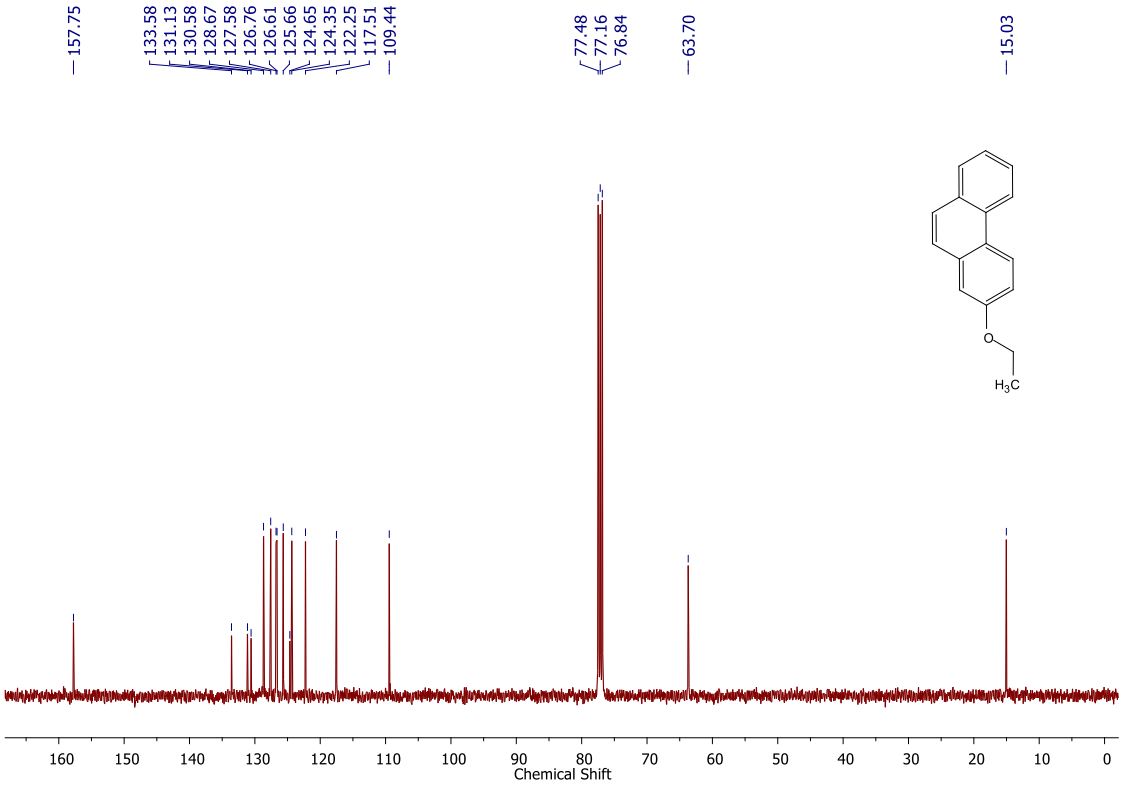

Figure 5.17 $^{13}C\{^{1}H\}$ NMR spectrum of **14** (in $CDCl_3$, 100 MHz, 298 K).

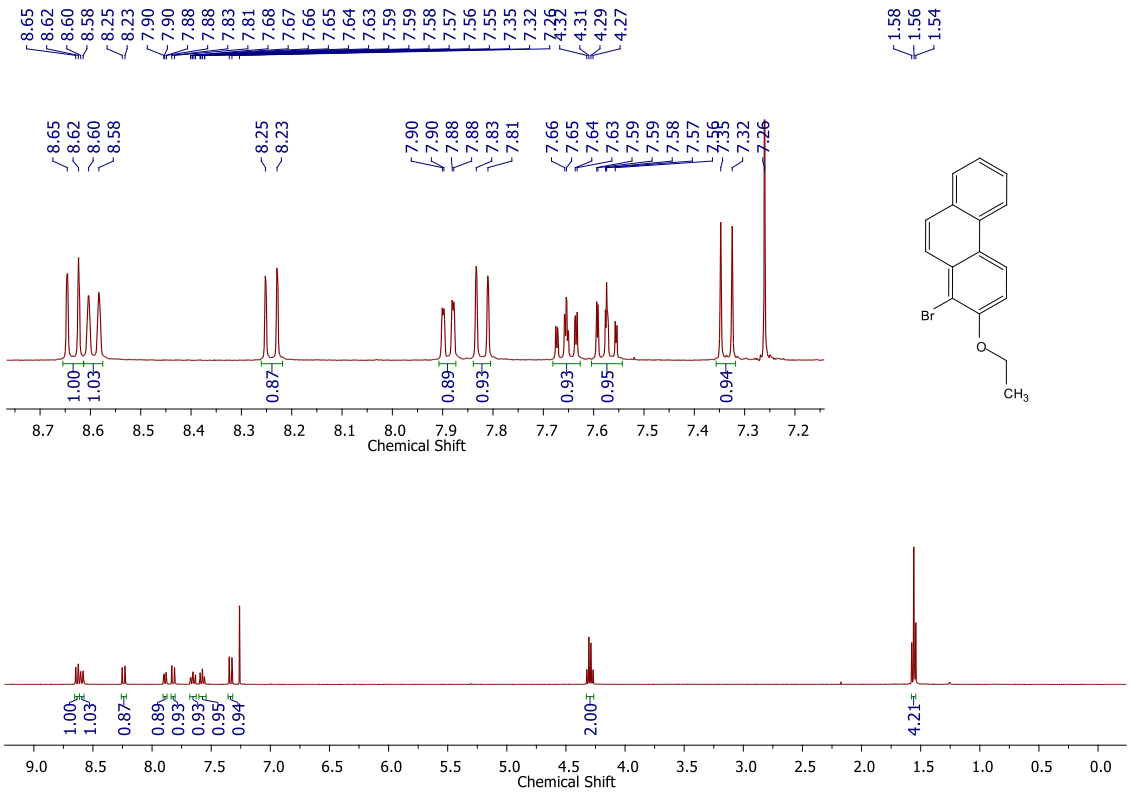

Figure 5.18 ^{1}H NMR spectrum of **15** (in $CDCl_3$, 400 MHz, 298 K).

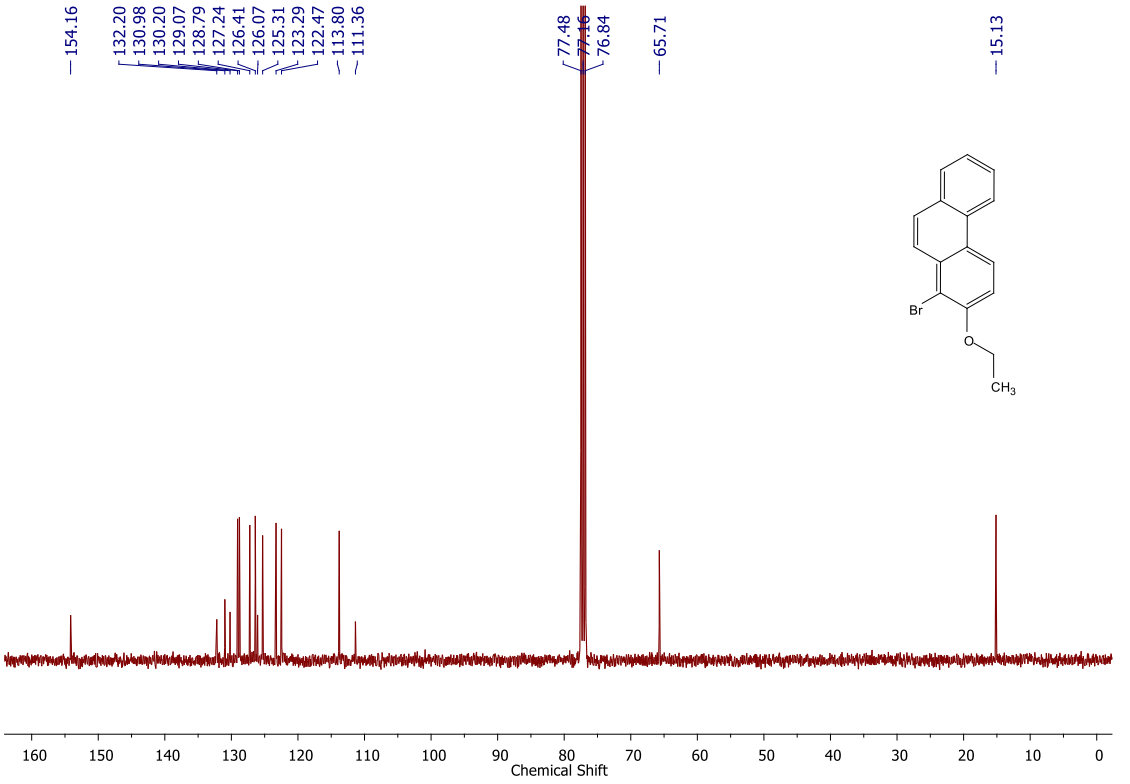

Figure 5.19 ^{13}C{^{1}H} NMR spectrum of **15** (in $CDCl_3$, 100 MHz, 298 K).

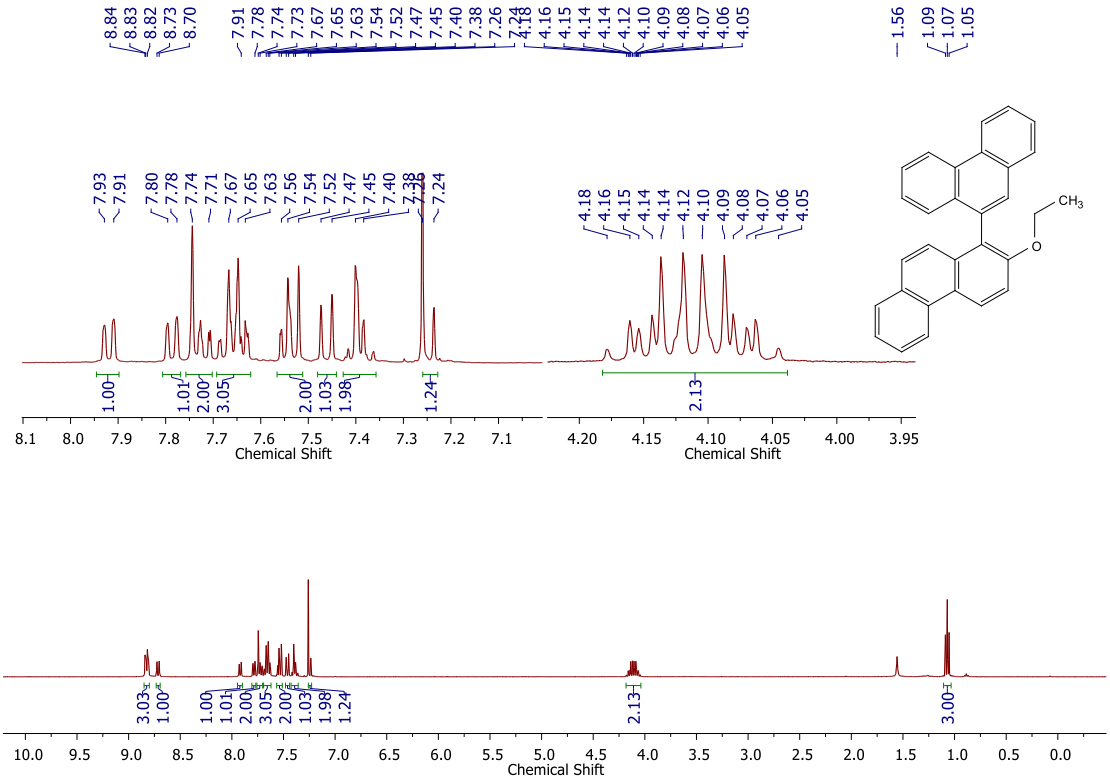

Figure 5.20 ^{1}H NMR spectrum of **16** (in $CDCl_3$, 400 MHz, 298 K).

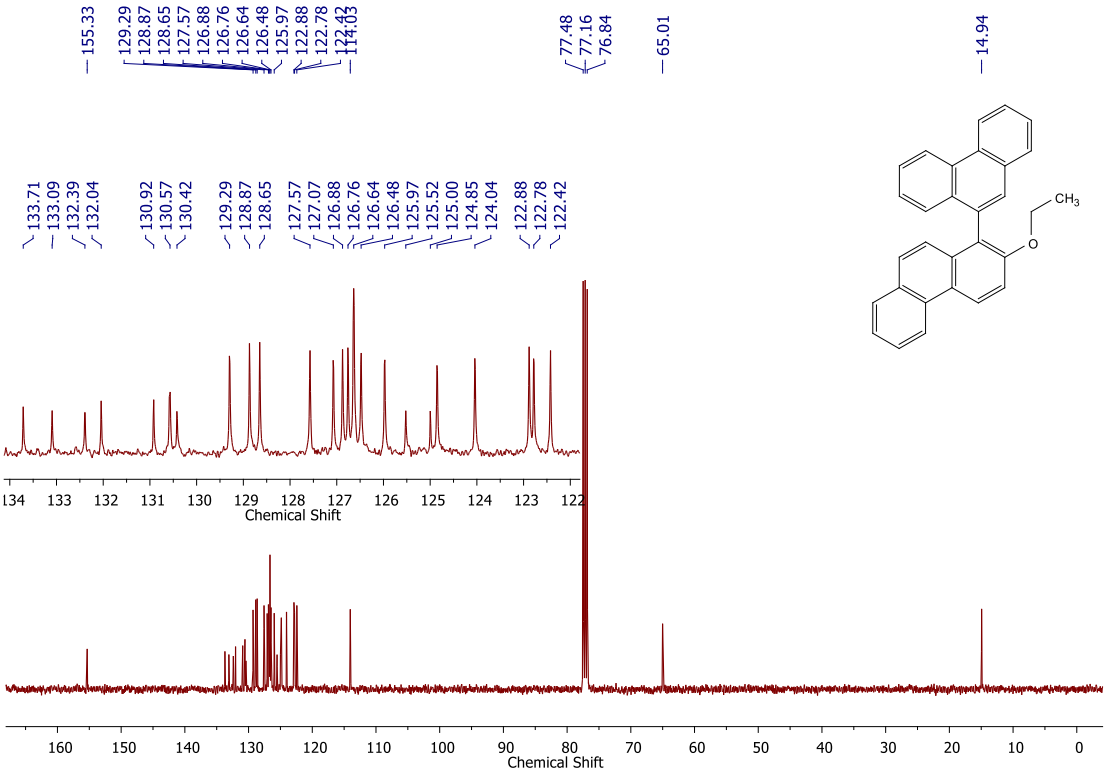

Figure 5.21 $^{13}C\{^{1}H\}$ NMR spectrum of **16** (in $CDCl_3$, 100 MHz, 298 K).

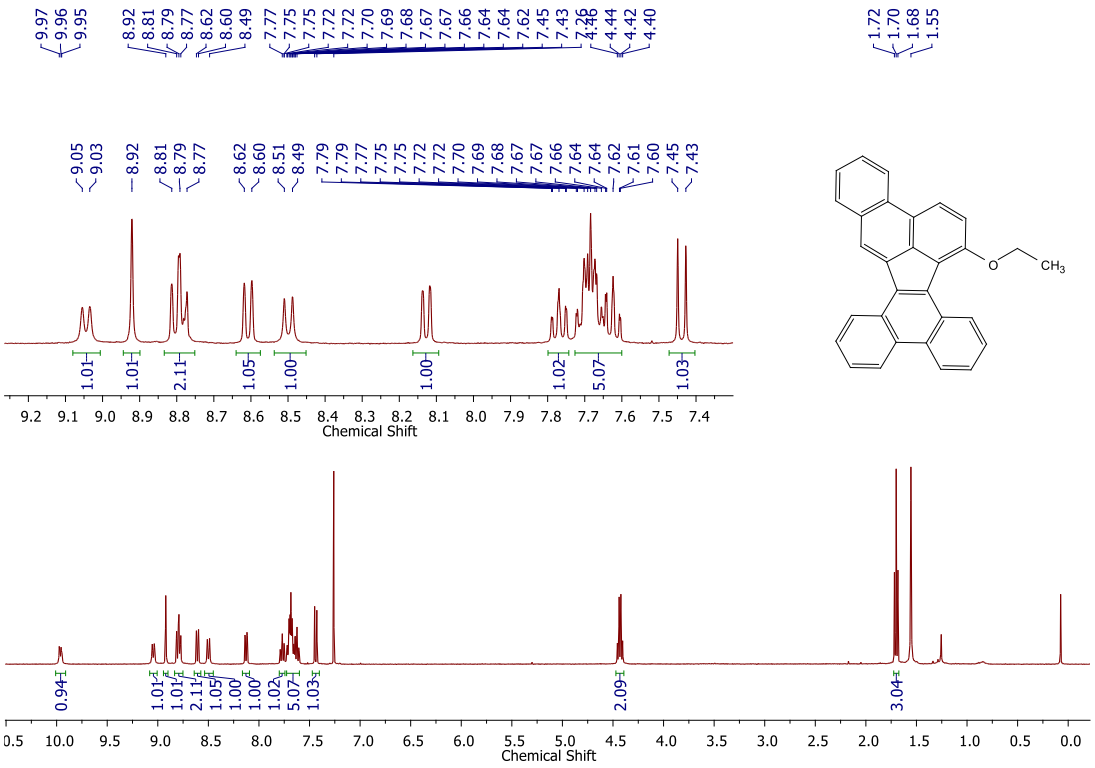

Figure 5.22 ^{1}H NMR spectrum of **8** (in $CDCl_3$, 400 MHz, 298 K).

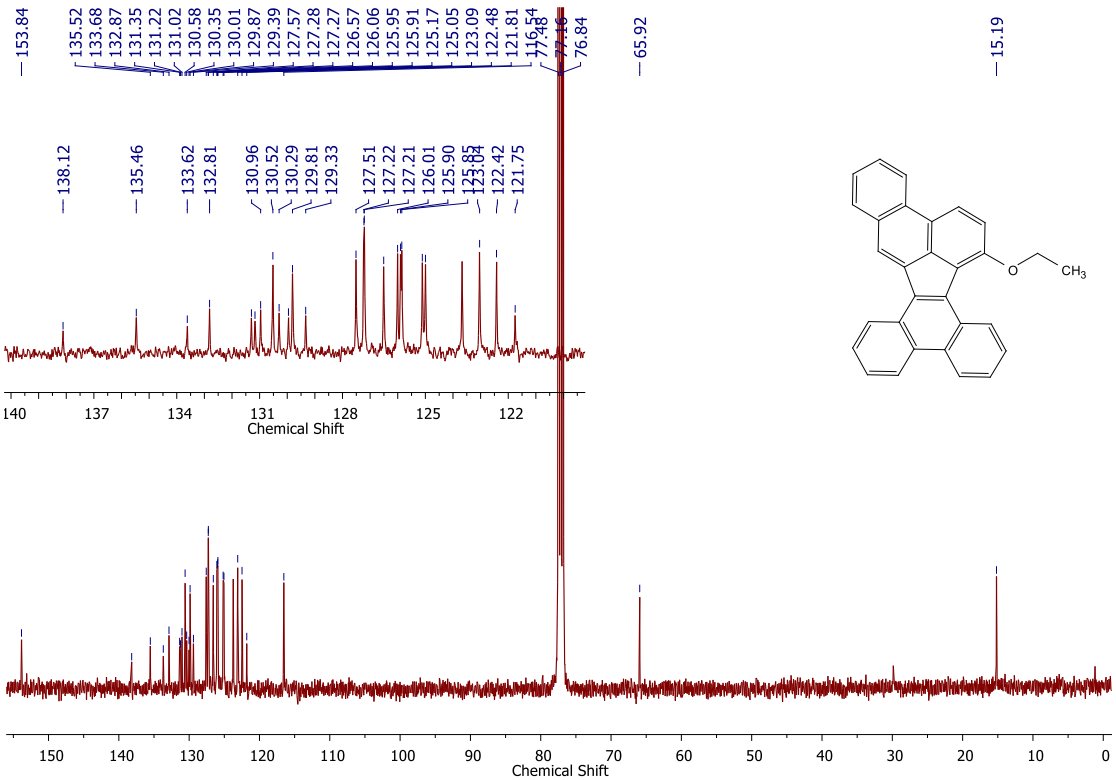

Figure 5.23 $^{13}C\{^{1}H\}$ NMR spectrum of **8** (in $CDCl_3$, 100 MHz, 298 K).

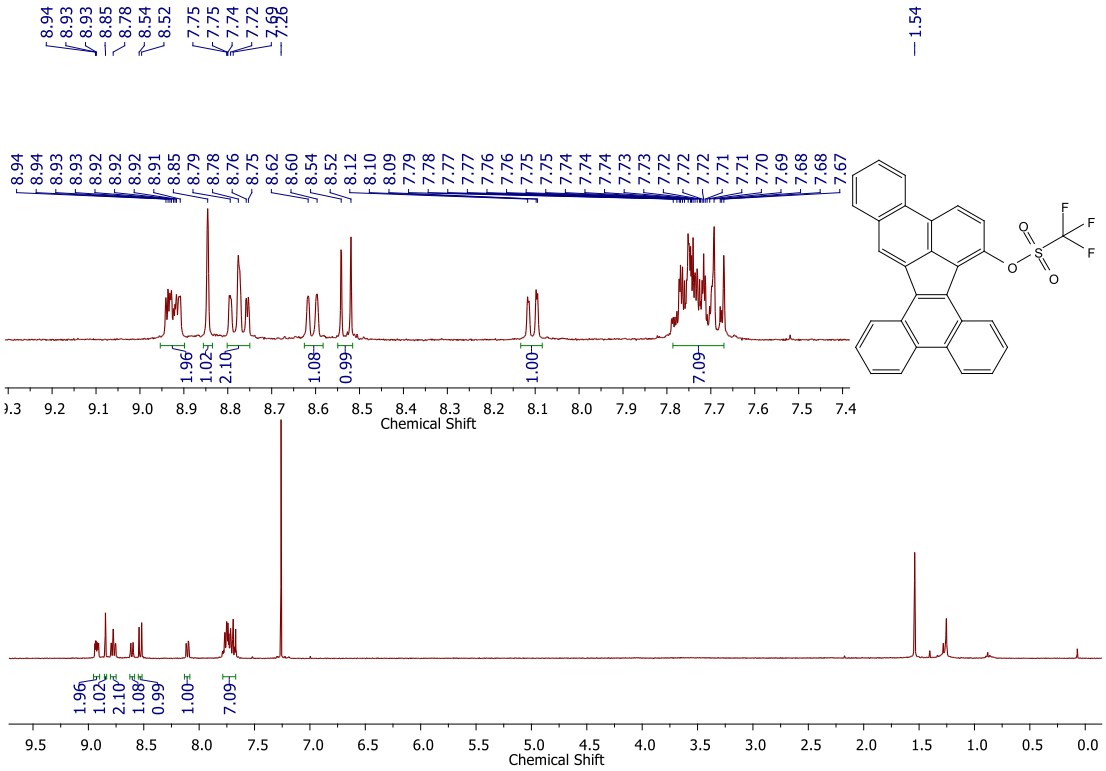

Figure 5.24 ^{1}H NMR spectrum of **18** (in $CDCl_3$, 400 MHz, 298 K).

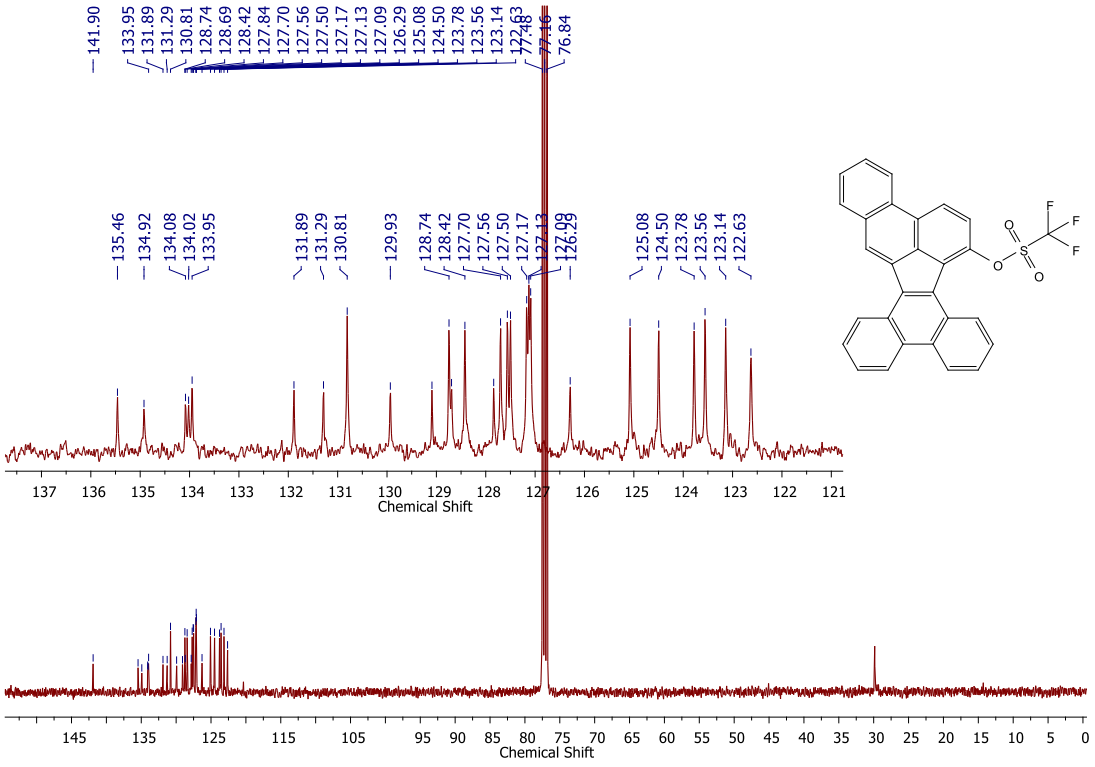

Figure 5.25 $^{13}C\{^{1}H\}$ NMR spectrum of **18** (in $CDCl_3$, 100 MHz, 298 K).

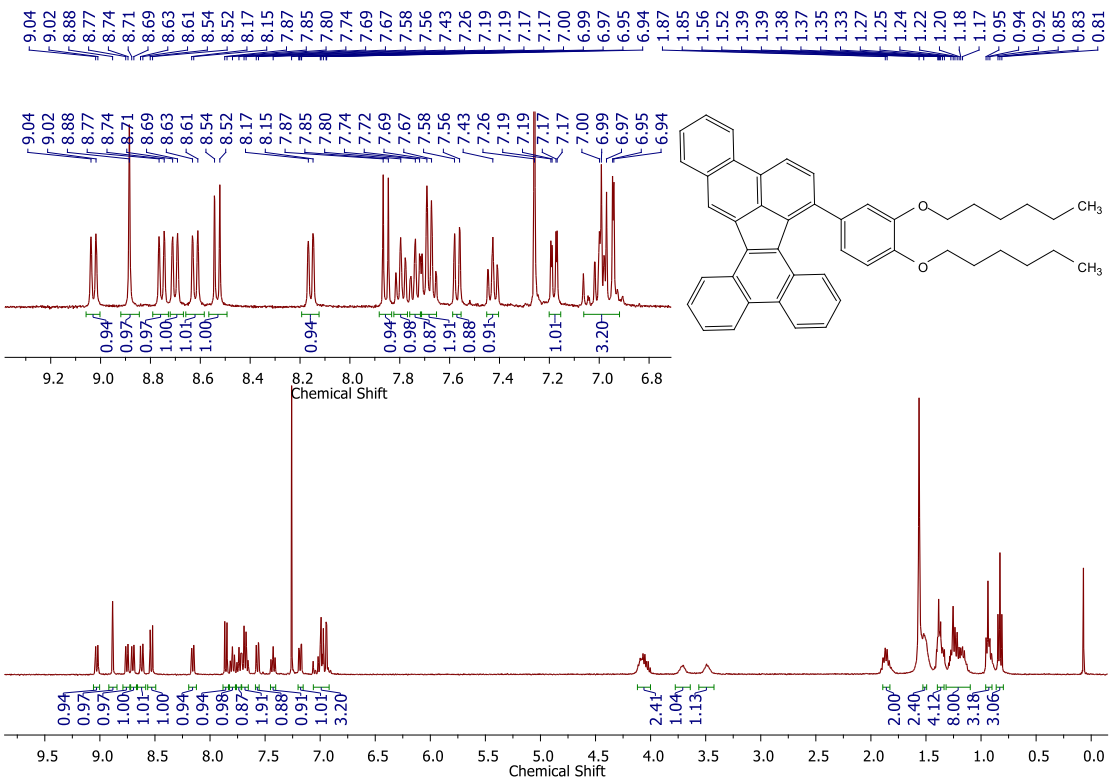

Figure 5.26 ^{1}H NMR spectrum of **20** (in $CDCl_3$, 400 MHz, 298 K).

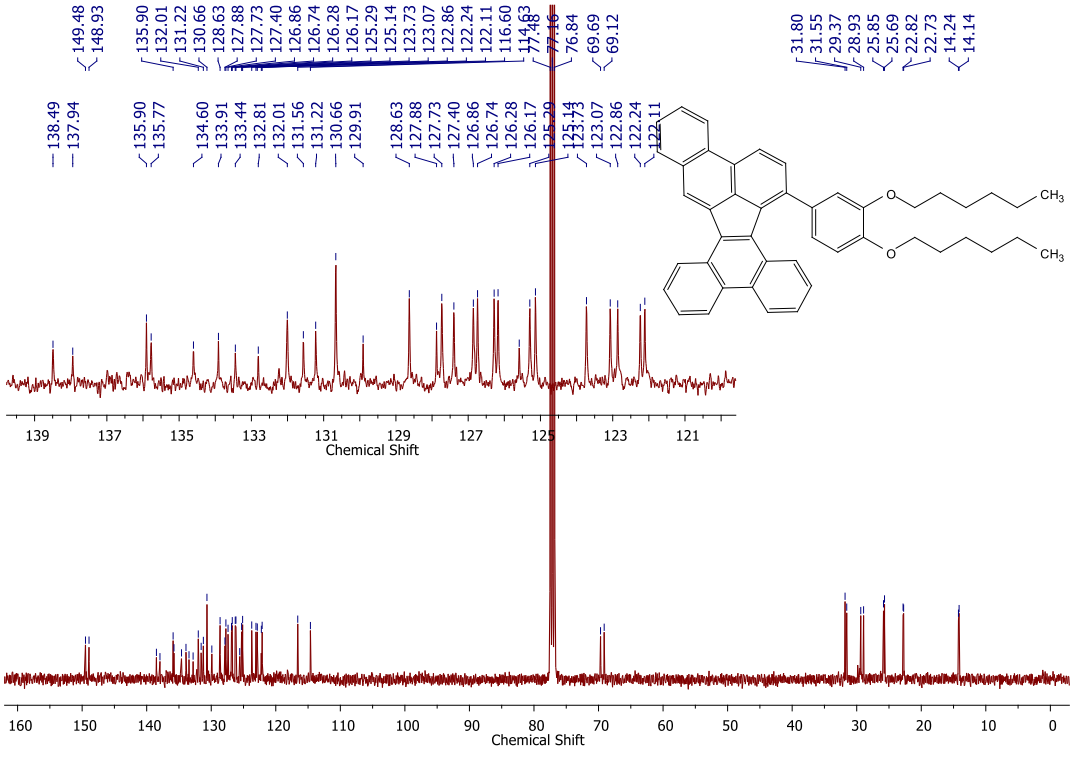

Figure 5.27 $^{13}C\{^{1}H\}$ NMR spectrum of **20** (in $CDCl_3$, 100 MHz, 298 K).

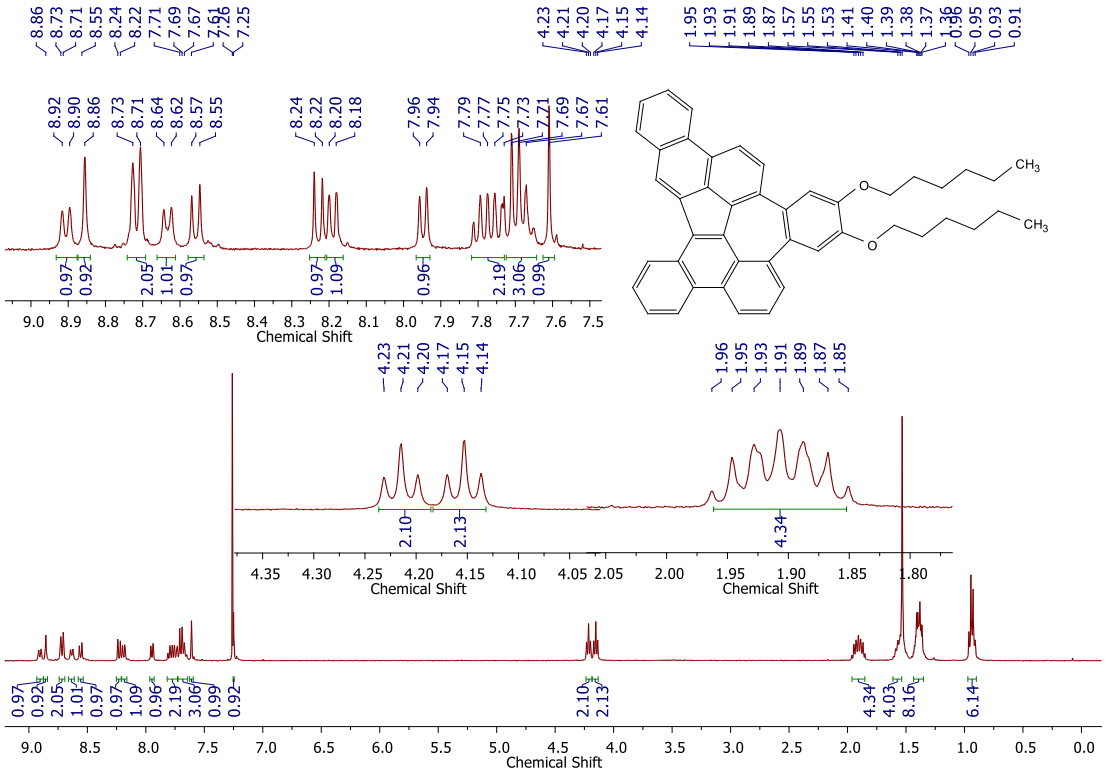

Figure 5.28 ^{1}H NMR spectrum of **9** (in $CDCl_3$, 400 MHz, 298 K).

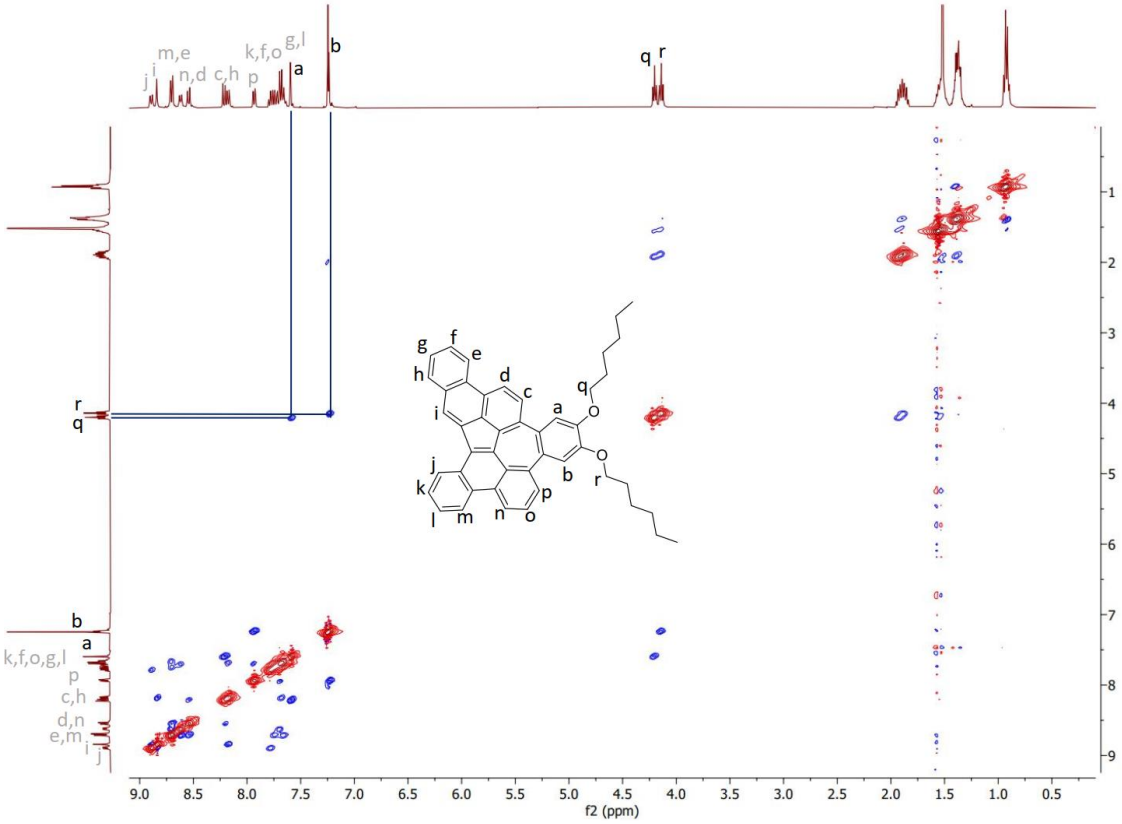

Figure 5.29 Full ^{1}H-^{1}H NOESY spectrum of **9** in $CDCl_3$.

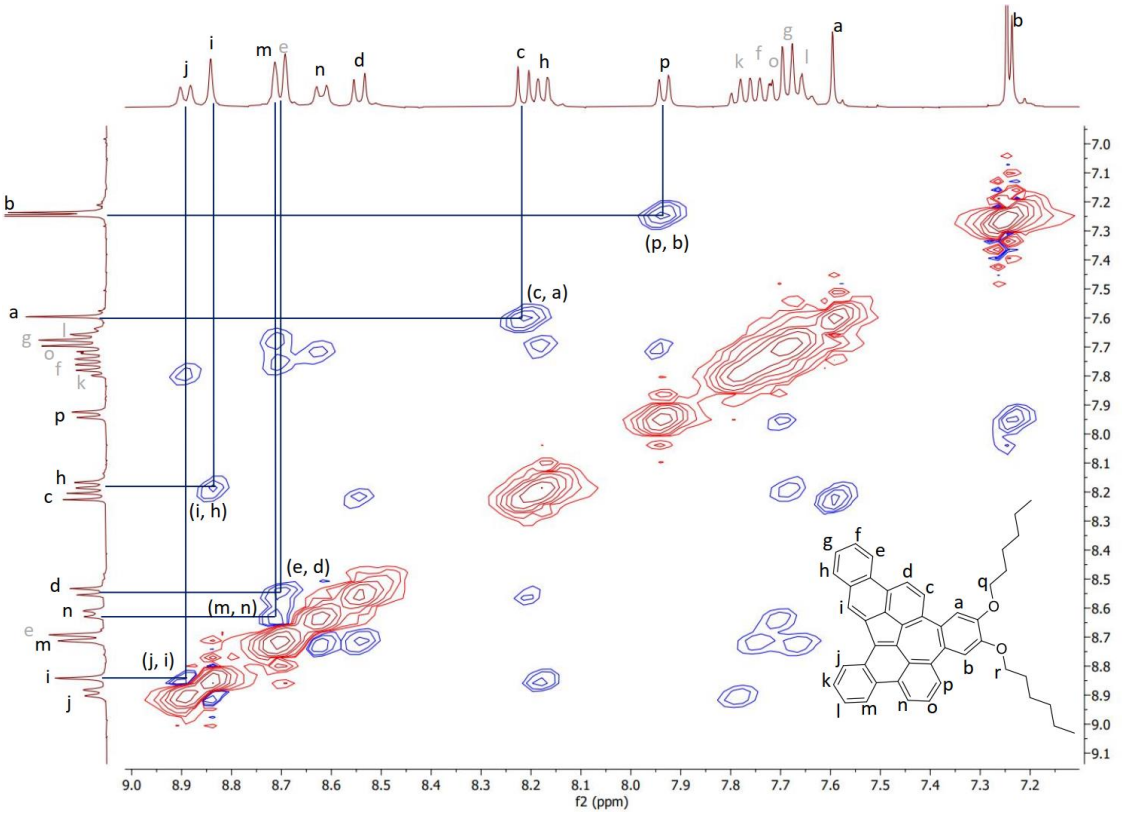

Figure 5.30 ^{1}H-^{1}H NOESY spectrum of **9** in $CDCl_3$ (aromatic region expansion).

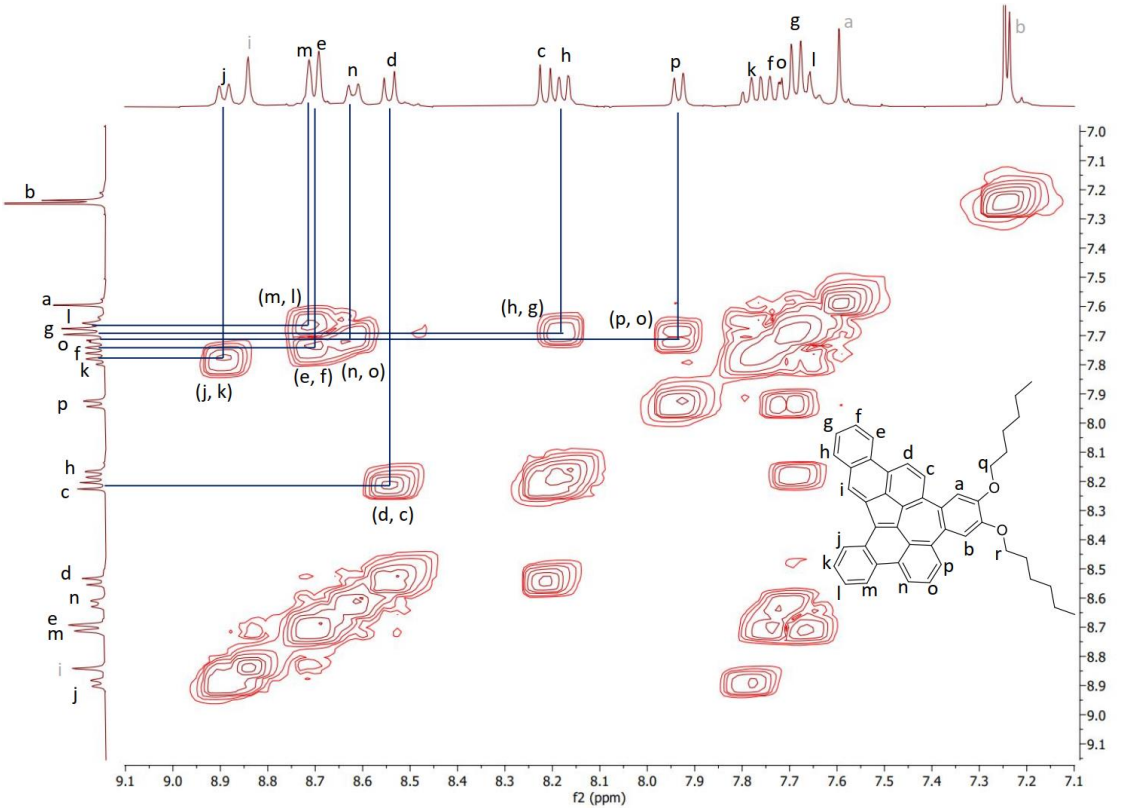

Figure 5.31 ^{1}H-^{1}H COSY spectrum of **9** in $CDCl_3$ (aromatic region expansion).

6.1 Conclusion

My thesis, titled "**Syntheses and Properties of Conjugated Polycyclic Molecules Containing Heptazethrene, Indacene, and Azulene Cores**," comprises five chapters. **Chapter 1** presents an introduction to the background of zethrene and its higher homologues, specifically heptazethrene. The subsequent discussion relates to indacene- and azulene-embedded polycyclic heteroarenes (PHAs) and polycyclic arenes (PAs). Based on these topics, a series of novel PAs and PHAs are designed, wherein the heptazethrene, indacene, and azulene cores are incorporated into the π-backbone, as shown in Figure 6.1

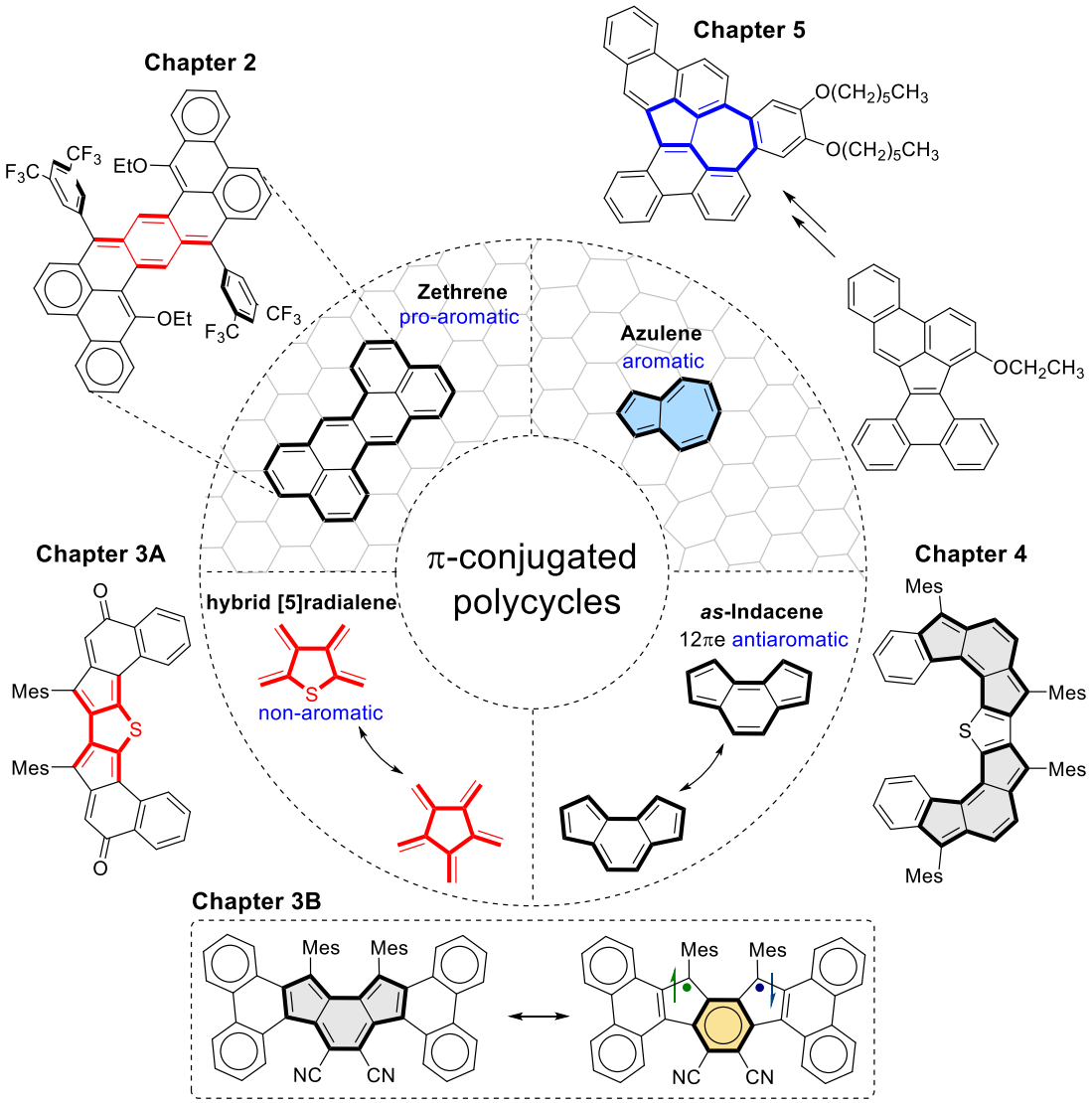

Figure 6.1 Structure of the target compounds shown chapter-wise.

In summary, we have synthesized and characterized heptazethrene-, indacene-, and azulene-embedded polycyclic arenes and heteroarenes. In **Chapter 2**, we isolated a dibenzoheptazethrene derivative in the closed-shell ground state, bearing push-pull substituents. This compound retains a *para*-quinoidal core and shows zero diradical character, as determined by single crystal analysis and density functional theory (DFT) calculations. Negative solvatochromism, π-π interactions, C_{sp}^2–H···O hydrogen bonding, intramolecular charge transfer, redox amphotericity, and a narrow HOMO–LUMO energy gap make this compound a potential candidate for application in organic optoelectronics.

Chapter 3 is divided into two sub-chapters, as two separate attempts were made to isolate a highly reactive dicyclopenta[*b*,*d*]thiophene core by dinaphtho-fusion approach in **Chapter 3A**, and diphenanthro-fusion in **Chapter 3B**. However, unexpected decomposition products were obtained. In **Chapter 3A**, we isolated a thiophenoradialene-embedded polycyclic heteroterphenoquinone (PHTPQ) derivative with antiaromatic characteristics. The antiaromatic character of this compound was evidenced by a visible absorption band with a weakly intense tail extending to 800 nm in the near-infrared region (forbidden HOMO→LUMO transition), and non-emissive and amphoteric redox properties. Single crystal and (anti)aromaticity analyses found a non-aromatic thiophene core, while suggesting the antiaromaticity/paratropicity of the pentafulvene subunits dominated the overall ground-state properties.

In **Chapter 3B**, we isolated a π-extended indeno[2,1-*a*]fluorene derivative, which was an antiaromatic diradicaloid with a small diradical character despite a small singlet-triplet energy gap. This compound displayed a remarkably low LUMO and a small HOMO–LUMO energy gap. NMR and EPR studies indicated its open-shell diradical property, supported by DFT calculations suggesting a 30% diradical character and a small singlet (S)-triplet (T) gap (−2.52 kcal/mol). However, a large bond length alternation of the *as*-indacene core in its single crystals indicated a quinoidal contribution with greater antiaromaticity, aligning with the small diradical character despite the small S-T gap.

In **Chapter 4**, I discussed the synthesis of a formally aromatic dicyclopenta[*c*]fluorenothiophene that exhibits a dominant antiaromatic character in the *as*-indacene subunit due to the inclusion of a thiophene unit in the π-backbone. Single crystal and ^{1}H NMR analyses indicated a quinoidal ground state for this

compound, supported by theoretical calculations suggesting a degree of antiaromaticity of the *as*-indacene subunit greater than that for *s*-indacenodifluorene. The dominant antiaromaticity was evidenced by a broad weakly intense absorption tail reaching the near-IR region, four-stage redox amphotericity, and a small HOMO−LUMO energy gap.

Finally, in **Chapter 5**, we reported a tribenzo-extended non-alternant isomer of *peri*-acenoacene with a formal azulene unit embedded in the polycyclic backbone, making it the newest non-hexagonal nanographene accessed through a Scholl-type oxidation approach. Aromaticity and single crystal analyses suggested a formal azulene core for this compound, which showed a smaller HOMO–LUMO energy gap with a charge-transfer absorption band and brighter fluorescence than phenanthroacephenanthrylene isomer (quantum yield (Φ): 41.8% vs. 8.9%). The reduction potentials of both compounds were nearly identical, and the observation is further supported by DFT calculations.

JOC The Journal of Organic Chemistry

pubs.acs.org/joc

Note

Unveiling a Quinoidal 2,3:10,11-Dibenzoheptazethrene

Priyank Kumar Sharma and Soumyajit Das*

Cite This: J. Org. Chem. 2022, 87, 5430−5436

Read Online

ACCESS | Metrics & More | Article Recommendations | Supporting Information

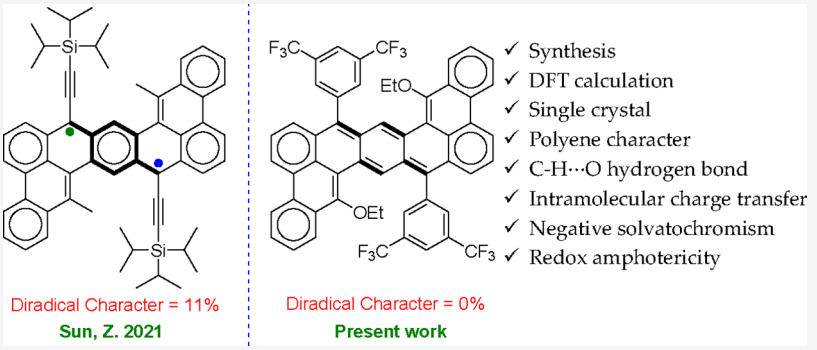

ABSTRACT: Parent 2,3:10,11-dibenzoheptazethrene is a singlet diradicaloid polycyclic hydrocarbon in the ground state that did not change its diradical character upon substitution (methyl and triisopropylsilylethynyl). Described herein are the synthesis and characterization of an ethoxy/3,5-$(CF_3)_2C_6H_3$-substituted 2,3:10,11-dibenzoheptazethrene **3** that prefers to retain its *p*-quinoidal core and shows zero diradical character, as determined by single-crystal analysis and density functional theory calculations. Negative solvatochromism, $\pi-\pi$ interactions, $C_{sp^2}-H\cdots O$ hydrogen bonding, intramolecular charge transfer, redox amphotericity, and a narrow HOMO−LUMO energy gap make **3** a potential candidate for application in optoelectronics.

Heptazethrene (HZ) is an open-shell polycyclic hydrocarbon (PH) with 17% singlet diradical character in the ground state and may be drawn in either Kekulé or diradical form.[1] The diradical ground state of core-modified HZ-bis(dicarboximide) was experimentally validated,[2] and its further core extension showed 46.5% diradical character with higher stability due to kinetic protection of the reactive radical sites.[3] Substituents such as methyl, alkoxy, triisopropylsilylethynyl (TIPSE), mesityl, and perfluorophenyl have a negligible effect on the diradical character of HZ.[4] However, π-ring annulation (benzannulation) can markedly tune the singlet diradical character index (y_0) of HZ.[5] Symmetrical *peri*-dibenzannulation at the peripheral naphthalene rings of HZ afforded closed-shell benzodipyrene,[6] whereas symmetrical *cata*-dibenzannulation can afford up to four open-shell dibenzoheptazethrene (DBHZ) regioisomers, namely, 2,3:10,11-DBHZ [**1** (Figure 1a)],[5b] 4,5:12,13-DBHZ,[5b] 5,6:13,14-DBHZ,[5a] and 1,2:9,10-DBHZ,[5a] with different diradical characters. Among the four *cata*-fused regioisomers, parent 4,5:12,13-DBHZ was first synthesized by Clar,[7] and its electronic ground state was theoretically identified in 2021.[5b] Anthracene-based 5,6:13,14-DBHZ and 1,2:9,10-DBHZ were shown to have different y_0 values in the ground state, based on the recovery of a number of Clar sextets.[5a] Using the same logic, phenanthrene-based 4,5:12,13-DBHZ and **1** were found to possess comparable y_0 values because both can recover only one Clar sextet in the diradical form **OS-I**.[5b] All DBHZ structural isomers, to date, are singlet diradicaloid with a low-lying thermally accessible triplet excited state, and because they can recover benzene aromaticity in diradical forms, they are classified as pro-aromatic PHs.[8]

Compound **2**, a derivative of **1**, showed red-shifted absorption, a small optical energy gap, and high hole mobility in comparison to those of 4,5:12,13-DBHZ with the same substituents [methyl and triisopropylsilylethynyl (TIPSE)]. Interestingly, both **1** and **2** have the same y_0 value.[5b] It seems that TIPSE has no effect on the y_0 values of the HZ or DBHZ derivative.[4a,5b] The effects of different substituents on the ground state for HZ-based π-series are seldom studied.[4b,9] Kekulé structure **1** can be viewed further as another open-shell diradical form **OS-II** and a zwitterionic resonance form **Polar-I** (Figure 1a). We envisioned the attachment of proper substituents to **1** to stabilize **Polar-I** to afford a new 2,3:10,11-DBHZ derivative bearing donor/acceptor substituents,[10] which could show strong quinoidal character because neutral form **1** and zwitterionic form **Polar-I** have the same number of Clar sextets in the ground state with a *p*-quinoidal

Received: January 14, 2022
Published: April 5, 2022

https://doi.org/10.1021/acs.joc.2c00089
J. Org. Chem. 2022, 87, 5430−5436

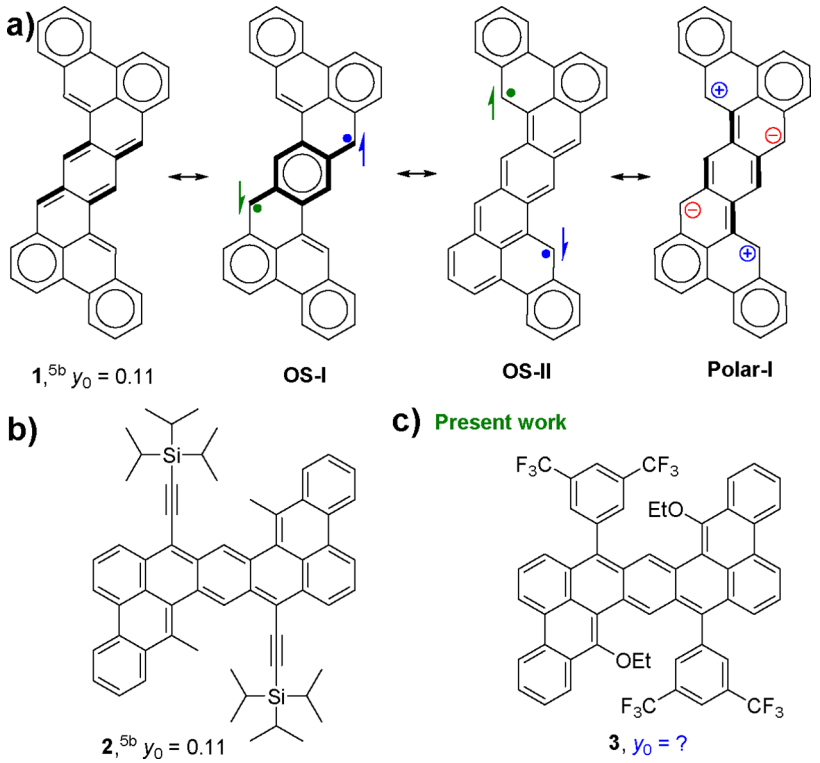

Figure 1. (a) Plausible Kekulé **1**, diradical (open-shell singlet), and zwitterionic resonance forms for the parent 2,3:10,11-DBHZ **1**. (b) Sun's 2,3:10,11-DBHZ derivative **2**. (c) Our target 2,3:10,11-DBHZ derivative **3**.

Scheme 1. Synthesis of 3

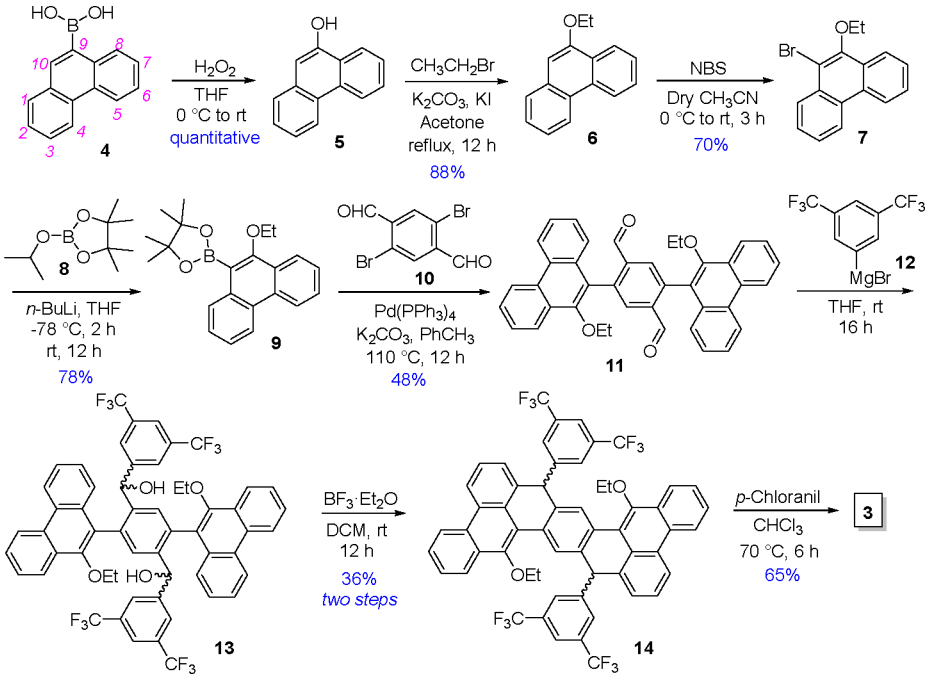

arrangement in the core. Thus, electron-accepting 3,5-$(CF_3)_2C_6H_3$ and electron-donating ethoxy groups were chosen as the potentially polarizing substituents to design **3** (Figure 1c). Herein, apart from a new approach for synthesizing **3** and its analytical characterizations, the ground state of **3** was studied by X-ray crystallographic analysis, and the experimental observations were supported by density functional theory (DFT) calculations at the B3LYP/6-31G(d,p) level of theory.[11]

9-Phenanthracenylboronic acid **4** was converted to **5** using hydrogen peroxide following the literature procedure (Scheme 1).[12] Crude **5** was converted to **6** in the presence of bromoethane using a potassium iodide-mediated nucleophilic substitution reaction, and the subsequent bromination using *N*-bromosuccinimide in dry acetonitrile afforded **7** in 70%

https://doi.org/10.1021/acs.joc.2c00089
J. Org. Chem. 2022, 87, 5430−5436

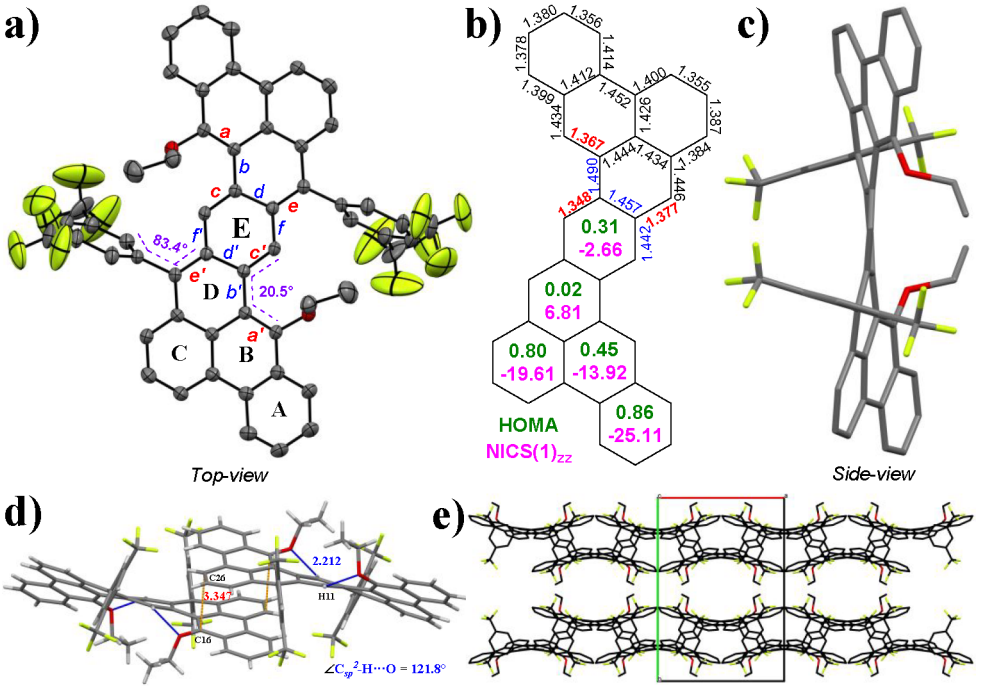

Figure 2. (a) ORTEP drawing of **3** at the 30% probability level (hydrogens omitted). (b) C−C bond lengths (in angstroms) for **3**, with HOMA and NICS(1)$_{zz}$ indices. (c) Side view of **3**. (d) Intermolecular C−C contact and hydrogen bonding distances with angles. (e) Packing diagram of **3**.

yield. Compound **7** was treated with *n*-BuLi at −78 °C for 2 h, followed by quenching with **8** to afford **9**. A Pd^0-catalyzed Suzuki reaction between **10** and 3 equiv of **9** afforded **11** in 48% yield. Nucleophilic addition of **12** to **11** afforded dicarbinol **13**, which, without purification, was treated with $BF_3{\cdot}Et_2O$ to afford dihydro precursor **14**. Compound **14**, after passing through a short pad of silica gel, was treated with 2.1 equiv of *p*-chloranil in dry chloroform at 70 °C for 6 h to afford **3** as a blue-green solid after column chromatographic purification on silica gel. The structure of **3** was established by one- and two-dimensional nuclear magnetic resonance (NMR) spectroscopy in benzene-d_6 (see the Supporting Information), and it was further unequivocally confirmed by X-ray crystallographic analysis.

Single crystals of **3** for X-ray crystallographic analysis were grown by slow evaporation from a chloroform/toluene mixture at ambient temperature in the dark. The backbone of **3** is found to be nonplanar, with the B rings twisted by a 20.5° torsion angle against the D/E π-rings in the bay region, due to steric effects (Figure 2a). The 3,5-$(CF_3)_2C_6H_3$ group is nearly orthogonally oriented (dihedral angle of 83.4°) with respect to the conjugated π-backbone. The ethoxy groups are projected to the same side, allowing two molecules to stack cofacially with another molecule within the crystal lattice in the outer phenanthrene part (Figure 2d). The shortest intermolecular C−C contact distance is 3.347 Å, which is longer than those of Kubo's bisphenalenyl systems[13] or diradicaloid 5,6:12,13-dibenzozethrene,[14] in which intermolecular spin−spin interactions dominate. Such a close intermolecular contact may suggest the existence of strong π−π interactions in **3**, which was not observed for **2**,[5b] enabling a wave-like packing arrangement for **3** (Figure 2d,e). Replacement of methyl with ethoxy in **3** has resulted in not only a smaller dihedral angle (20.5° for **3**, in comparison to 22.5° for **2**) in the bay region but also a weak intramolecular C_{sp^2}−H···O hydrogen bonding interaction (2.212 Å, $\angle C_{sp^2}$−H···O = 121.8°),[15] which might explain the downfield-shifted signal for the hydrogens on ring E [δ 8.94 in benzene-d_6 for **3** (Figure S9), in comparison to δ 8.71 in chloroform-*d* or δ 8.46 in toluene-d_8 for **2**[5b]].

Because compound **2** is a singlet diradical in the ground state at the expense of a double bond of *p*-quinomethane [*p*-QDM in bold (Figure 1a)] to gain benzene aromaticity for the central benzenoid ring E, the bond lengths for **3** and **2**, which are important for determining the ground state electronic configuration, are summarized in Table 1 along with the reported *p*-QDM bond lengths (*c*−*c*′, *d*−*d*′, *e*−*e*′, and *f*−*f*′) for Thiele's hydrocarbon.[16] The bond length analysis of the *p*-QDM skeleton for **3** (Figure 2a,b) revealed the *c*−*c*′ C_{sp^2}=C_{sp^2} bonds to be 1.348 Å long (close to the olefin double bond), whereas the *exo*-methylene *e*−*e*′ C_{sp^2}=C_{sp^2} bonds are 1.377 Å long, which are similar to or shorter than that of the closed-shell Thiele's hydrocarbon, and are obviously shorter than that in **2**. The homogeneous distribution of bond lengths for ring A (average of 1.389 Å) and ring C (average of 1.397 Å) in **3** suggested localized aromaticity in the outer phenanthrene parts, similar to those of **2**. The observations certainly suggest compound **3** retains the *p*-quinoidal arrangement in the core, with strong C−C bond length alternations for *a*−*a*′ and *b*−*b*′ bonds, where the *a*−*a*′ C_{sp^2}=C_{sp^2} bond is distinctly shorter for **3** than for **2** (Table 1). Therefore, compound **3** is better

Table 1. Mean C−C Bond Lengths (in angstroms) for 2, 3, and Thiele's *p*-QDM Skeleton from Crystals

C−C bond	2	3	Thiele's *p*-QDM
a−*a*′	1.388	1.367	–
b−*b*′	1.479	1.490	–
c−*c*′	1.365	1.348	1.346
d−*d*′	1.456	1.457	1.449
e−*e*′	1.388	1.377	1.381
f−*f*′	1.431	1.442	1.449

https://doi.org/10.1021/acs.joc.2c00089
J. Org. Chem. 2022, 87, 5430−5436

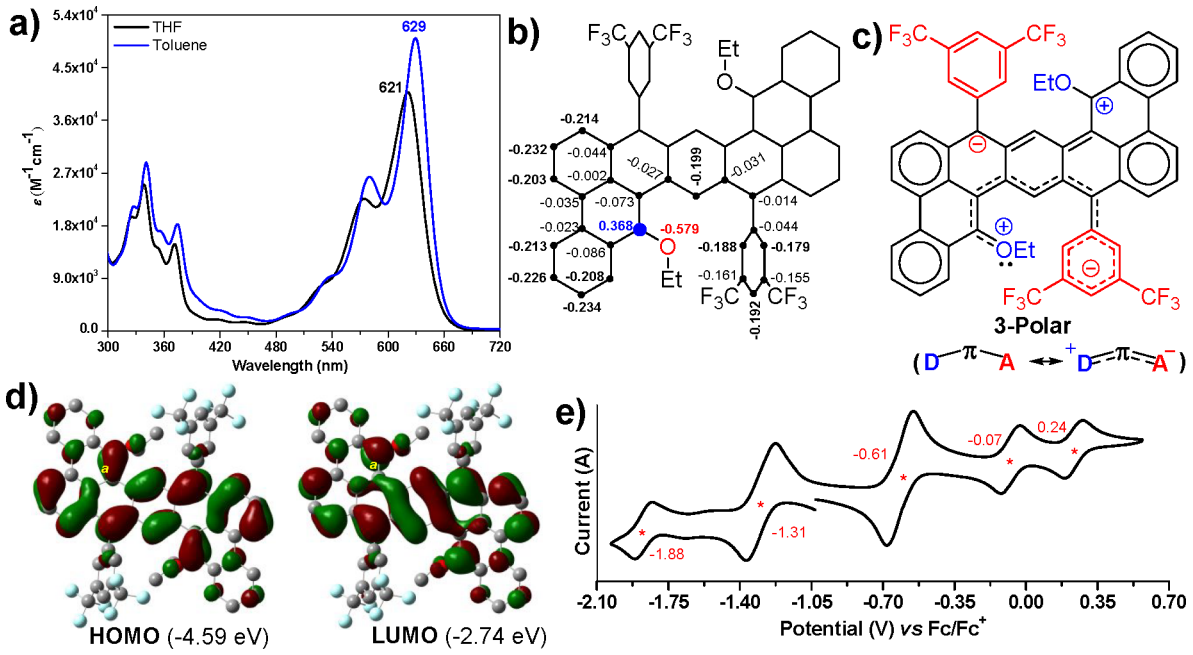

Figure 3. (a) UV−vis absorption spectra of **3** in toluene (blue) and THF (black). (b) NPA charges for **3** in the gas phase. (c) Dipolar resonance form (**3-Polar**) for **3**, stabilized by the donor−acceptor charge transfer interaction through the π-backbone. (d) HOMO and LUMO profiles from DFT calculations. (e) Cyclic voltammogram of **3** in the CH_2Cl_2/Bu_4NPF_6 solvent/electrolyte couple at a scan rate of 50 mV s^{-1}.

viewed as a *p*-QDM-embedded DBHZ with strong polyene character in the ground state.

DFT calculations for **2** showed the closed-shell state to be roughly 2 kcal/mol higher than the open-shell singlet ground state, with a 9.3 kcal/mol gap between the open-shell singlet and triplet states, which was in agreement with the small diradical character.[5b] Our DFT calculations, by optimizing the crystal structure, found molecule **3** to have a singlet closed-shell ground state and zero diradical character with the triplet state located 12.5 kcal/mol above the singlet state (Table S5). Both CASSCF and the broken symmetry approach agree with the zero diradical character for **3**, whereas CASSCF calculation predicted **2** to have 15.3% diradical character (see the Supporting Information). Additionally, DFT examination found 8.5% or 8.2% diradical character for the derivative of **1** with only a 3,5-$(CF_3)_2C_6H_3$ or an ethoxy substituent, respectively, in the singlet ground state (Table S14). The results clearly indicate that substituents can strongly impact the electronic ground state for diradicaloid **1** with a small gap between singlet open-shell and closed-shell states. The harmonic oscillator model of aromaticity (HOMA)[17] values for ring E (0.31) and ring D (0.02) indicated large bond length alternations for **3** (Figure 2b), whereas localization of Clar sextets is suggested for rings A (0.86) and C (0.80). The aromaticity for ring B (0.45) is quite weak, signifying the dominance of the phenanthrene substructure in the ground state. The nucleus-independent chemical shift [$NICS(1)_{zz}$][18] indices are also in good agreement with the HOMA values, implying that central ring E is essentially atropic (Figure 2b). Notably, according to the NICS and HOMA indices, the aromaticity of ring E has decreased for **3**, in comparison to that of **2**.[5b] These results obviously suggest a closed-shell structure with a *p*-quinoidal arrangement in the core is primarily contributing to the singlet ground state for **3**.

The toluene solution of **3** is blue and shows a *p*-band in the visible region with the lowest-energy absorption maximum at 629 nm (ε = 50080 M^{-1} cm^{-1}) (Figure 3a), belonging to the HOMO → LUMO transition (Table S8). Interestingly, a negative solvatochromism is observed for **3** in tetrahydrofuran (THF), as the absorption maximum appears at 621 nm (ε = 40840 M^{-1} cm^{-1}), which is blue-shifted by 8 nm. Calculations show that the ground state of **3** is slightly polar [dipole moment (μ) = 2.91 D]. This observation indicates that the neutral resonance structure **3** may contribute to the ground state in a nonpolar solvent, while in relatively polar solvents, a dipolar resonance form may predominate.[19] Natural population analyses (NPA)[20] for **3** suggested that the carbon attached to the electron-releasing ethoxy group is positive (+0.368) due to a strongly polarizing oxygen (−0.579), whereas the negative charge is dispersed via the π-backbone to the electron-withdrawing 3,5-$(CF_3)_2C_6H_3$, suggesting a moderate donor−acceptor type intramolecular charge transfer (ICT) interaction operating through the π-backbone spacer [D−π−A (Figure 3b,c)]. The results suggest that a dipolar zwitterionic form **3-Polar** (Figure 3c and Figure S16) is stabilized in polar THF and causes a blue shift in the absorption maximum. The experimental absorption trend with the variation of solvent polarity (toluene, chloroform, dichloromethane, and THF) is also consistent with the TDDFT calculations (Table S7 and Figure S15). Compound **3** showed reasonable photostability under ambient light conditions, with a half-life time of 40 h in an air-saturated toluene solution (Figure S14).[5b,21] Compound **3** also exhibited a small fluorescence quantum yield of 7.2% (with methylene blue[22] as a standard) with an emission maximum at 645 nm in toluene, including solvent-dependent solvatochromism behavior (Figure S15).

The DFT-optimized HOMO and LUMO profiles for **3** show large amplitudes on bond *a* (C=C bond character), suggesting antibonding interaction between the lone pair on oxygen and the p orbital on carbon to which the ethoxy group is attached (Figure 3d), thereby destabilizing both energy levels. Consequently, compound **3** was easily oxidized during

https://doi.org/10.1021/acs.joc.2c00089
J. Org. Chem. 2022, 87, 5430−5436

the cyclic voltammetry (CV) experiment in dichloromethane, displaying three reversible oxidation waves with the following half-wave potentials: $E_{1/2}^{ox1} = -0.61$ V, $E_{1/2}^{ox2} = -0.07$ V, and $E_{1/2}^{ox3} = 0.24$ V [vs ferrocene/ferrocenium (Fc/Fc^+)]. The half-wave reduction potentials appeared at $E_{1/2}^{red1} = -1.31$ V and $E_{1/2}^{red1} = -1.88$ V (Figure 3e). The larger first reduction and oxidation waves can be attributed to two-electron processes,[10] due to the plausible formation of two carbocation and carbanion centers that are stabilized by electron-donating (OEt) and electron-withdrawing [3,5-$(CF_3)_2C_6H_3$)] effects, respectively (Figure S16). The HOMO and LUMO energies for **3** can be estimated to be −4.11 and −3.56 eV, respectively, from the onset potentials,[5b] affording a small electrochemical energy gap (E_g^{ec}) of 0.55 eV, likely hinting at the contribution of a π-extended second resonance structure ($D^+{=}\pi{=}A^-$) over the neutral structure ($D{-}\pi{-}A$) (Figure 3c and Figure S16). The electrochemical energy gap is much smaller than its optical energy gap (E_g^{opt}), 1.84 eV, estimated from the lowest-energy absorption onset (Figure 3a), and the E_g^{ec} of **2** is also noticeably (0.43 eV) smaller than its E_g^{opt}.[5b] It is worth mentioning that a recent report[23] has stressed that the electrochemical HOMO and LUMO energies should more accurately be defined as the ionization potential and electron affinity, respectively. In fact, the E_g^{opt} of **3** (1.84 eV) is consistent with the theoretical HOMO−LUMO energy gap value of 1.85 eV (Figure 3d).

In conclusion, a 2,3:10,11-DBHZ derivative **3** was synthesized in a quinoidal singlet ground state with strong polyene character. It showed blue-shifted UV−vis absorption in polar solvents, in comparison to that in toluene, suggesting a dipolar structural contribution in the ground state with moderate ICT interaction. A very low oxidation potential and a small electrochemical energy gap were found for **3**, which are the smallest values among the entire zethrene family, to date,[9,24] including the *p*-QDM-bridged corannulene dimer bearing the 2,3:10,11-DBHZ fragment with a methoxy substituent at the same position.[24c] The negative solvatochromism and facile electrochemical oxidations of quinoidal **3** could be attributed to a readily accessible low-lying zwitterionic form **3-Polar** in the singlet ground state due to potentially polarizing substituents. Our work clearly indicates that substitution can play an important role in tuning the ground state properties of pro-aromatic PHs and may stimulate the exploration of donor/acceptor-substituted π-conjugated diradicaloid PHs.[10,25]

EXPERIMENTAL SECTION

General Information. Chemicals and reagents were purchased from local and international commercial suppliers (Merck, GLR innovations, BLDpharm, and Sainor lab) and used without further purification. Thin layer chromatography (TLC) was performed using precoated silica plates purchased from Merck (silica gel 60 PF254, 0.25 mm). Column chromatography was performed using silica gel 100−200 mesh. NMR spectra were recorded in $CDCl_3$, DMSO-d_6, and C_6D_6 (Eurisotop) at room temperature on a JEOL JNM-ECS400 spectrometer at operating frequencies of 400 MHz (^{1}H) and 100 MHz (^{13}C) as indicated in the individual spectrum. Chemical shifts (δ) are given in parts per million relative to the residual solvent (chloroform δ 7.26, dimethyl sulfoxide δ 2.50, and benzene δ 7.16 for ^{1}H NMR and benzene δ 128.06 and chloroform δ 77.16 for proton-decoupled ^{13}C NMR), and coupling constants (J) are expressed in hertz. Multiplicity is tabulated as follows: s for singlet, d for doublet, dd for doublet of doublets, t for triplet, q for quartet, and m for multiplet. Structural assignments were made with additional information from gCOSY and gNOESY experiments. High-resolution mass spectra (HRMS) were recorded using electrospray ionization (ESI) methods on a Waters (XEVO G2-XS QTOF) mass spectrometer. UV−vis spectra were recorded with a JASCO V-770 spectrophotometer. Fluorescence spectra were recorded on a PerkinElmer LS55 fluorescence spectrophotometer. Cyclic voltammetry was performed on a model CHI-1110C instrument with a glassy carbon working electrode, a Pt wire counter electrode, and a Ag wire pseudoreference electrode in a DCM/Bu_4NPF_6 solvent/electrolyte couple at room temperature using a scan rate of 50 mV s^{-1}. The potential was externally calibrated against the ferrocene/ferrocenium couple (0.43 V). Melting points were determined using a model BIBBY-SMP30 melting point analyzer.

9-Ethoxyphenanthrene (6). To a suspension of **5** (1.2 g, 6.18 mmol), K_2CO_3 (1.28 g, 9.27 mmol), and KI (1.18 g, 7.10 mmol) in acetone was added ethyl bromide (0.80 mL, 10.50 mmol), and the mixture was heated at reflux for 12 h using an oil bath, under a nitrogen atmosphere. After the mixture had cooled to room temperature, the volatiles were evaporated and the mixture was extracted with CH_2Cl_2 (4 × 50 mL) and water (50 mL). The organic layer was dried over anhydrous sodium sulfate and filtered. The filtrate was evaporated, and the residue was purified on a silica column using hexanes as the eluent to give the title product as a white solid (1.21 g, 88% yield): R_f = 0.30 (hexanes); mp 95−96 °C; ^{1}H NMR (400 MHz, $CDCl_3$) δ 8.66 (d, J = 8.1 Hz, 1H), 8.59 (d, J = 7.8 Hz, 1H), 8.42 (dd, J = 8.1, 1.3 Hz, 1H), 7.76 (dd, J = 7.5, 1.4 Hz, 1H), 7.71−7.61 (m, 2H), 7.57−7.47 (m, 2H), 6.97 (s, 1H), 4.31 (q, J = 7.0 Hz, 2H), 1.61 (t, J = 6.9 Hz, 3H); ^{13}C{^{1}H} NMR (100 MHz, $CDCl_3$) δ 152.9, 133.1, 131.3, 127.3, 127.1, 126.9, 126.8, 126.4 (2 C), 124.2, 122.7, 122.6, 102.6, 63.7, 14.9 (NMR data are consistent with ref 26); HRMS (ESI) m/z [M + H]$^+$ calcd for $C_{16}H_{15}O$ 223.1123, found 223.1112.

9-Bromo-10-ethoxyphenanthrene (7). The title compound was prepared by slightly modifying the literature procedure.[27] An oven-dried two-neck round-bottom flask, equipped with a magnetic stir bar, was charged with **6** (1.10 g, 4.95 mmol) dissolved in 20 mL of anhydrous acetonitrile. NBS (969 mg, 5.44 mmol) was added at 0 °C in one shot, and the reaction mixture was warmed to room temperature and stirred well for 3 h. The reaction was quenched with a saturated solution of sodium thiosulfate, and the solvents were removed using a rotatory evaporator. The resulting mixture was then extracted with dichloromethane (3 × 50 mL), dried over sodium sulfate, and filtered. The organic layer was evaporated, and the crude residue was purified by silica gel column chromatography (hexanes) to give title product **7** as a yellow solid (1.05 g, 70% yield): R_f = 0.36 (5% EtOAc in hexanes); mp 60−61 °C; ^{1}H NMR (400 MHz, $CDCl_3$) δ 8.70−8.64 (m, 2H), 8.40 (dd, J = 8.0, 1.5 Hz, 1H), 8.24 (dd, J = 8.1, 1.4 Hz, 1H), 7.74−7.62 (m, 4H), 4.24 (q, J = 7.0 Hz, 2H), 1.63 (t, J = 7.1 Hz, 3H); ^{13}C{^{1}H} NMR (100 MHz, $CDCl_3$) δ 151.4, 131.1, 131.0, 129.0, 128.6, 127.9, 127.8, 127.5, 127.3, 126.5, 123.2, 123.1, 122.7, 114.2, 69.9, 15.8; HRMS (ESI) m/z [M + H]$^+$ calcd for $C_{16}H_{14}BrO$ 301.0228, found 301.0239. The characterization data agree with ref 27.

2-(10-Ethoxyphenanthren-9-yl)-4,4,5,5-tetramethyl-1,3,2-dioxaborolane (9). A solution of *n*-butyllithium (1.7 mL, 2.66 mmol, 1.6 M in hexanes) was added dropwise to a solution of **7** (400 mg, 1.33 mmol) in 20 mL of anhydrous THF under nitrogen at −78 °C. The mixture was stirred at −78 °C for 2 h, and then 2-isopropoxy-4,4,5,5-tetramethyl-1,3,2-dioxaborolane **8** (0.54 mL, 2.66 mmol) was added. The reaction mixture was stirred for 12 h at room temperature. The reaction was quenched with a saturated solution of NH_4Cl, and the mixture extracted with dichloromethane (5 × 100 mL). The organic phases were washed with water (2 × 100 mL) and brine (2 × 100 mL) and dried over Na_2SO_4. After evaporation of the organic layer, the residue was purified by silica gel column chromatography (1:10 EtOAc/hexanes) to afford **9** as yellow solid (364 mg, 78% yield): R_f = 0.27 (5% EtOAc in hexanes); mp 112−113 °C; ^{1}H NMR (400 MHz, $CDCl_3$) δ 8.67 (d, J = 8.2 Hz, 1H), 8.65−8.60 (m, 1H), 8.20 (dd, J = 7.8, 1.4 Hz, 1H), 8.11−8.05 (m, 1H), 7.67 (ddd, J = 8.3, 7.0, 1.4 Hz, 1H), 7.61 (ddd, J = 7.9, 7.0, 1.1 Hz, 1H), 7.58−7.53 (m, 2H), 4.19 (q, J = 7.0 Hz, 2H), 1.56 (t, J = 7.1 Hz, 3H), 1.52 (s, 12H);

https://doi.org/10.1021/acs.joc.2c00089
J. Org. Chem. 2022, 87, 5430−5436

$^{13}C\{^1H\}$ NMR (100 MHz, $CDCl_3$) δ 158.9, 134.8, 132.9, 128.1, 127.5, 127.5, 126.9, 126.5, 125.3, 123.2, 123.0, 122.8, 84.2, 71.6, 25.2, 15.8; HRMS (ESI) m/z $[M + H]^+$ calcd for $C_{22}H_{26}BO_3$ 349.1975, found 349.1979.

2,5-Bis(10-ethoxyphenanthren-9-yl)terephthalaldehyde (11). An oven-dried thick-walled glass tube was charged with **9** (358 mg, 1.03 mmol), 2,5-dibromoterephthalaldehyde (100 mg, 0.34 mmol), anhydrous K_2CO_3 (237 mg, 1.71 mmol), and dry toluene and purged with nitrogen for 30 min. Catalyst $Pd(PPh_3)_4$ (33.6 mg, 10 mol %) was subsequently added under nitrogen, and the glass tube was sealed before being warmed to 110 °C using an oil bath. After 12 h, the flask was cooled to room temperature, the resulting suspension was filtered, and the solid was washed successively with water (100 mL), MeOH (100 mL), and pentane (100 mL). The solid was dried to afford title product **11** (96 mg, 48%) as a light brown powder: R_f = 0.31 (10% EtOAc in hexanes); mp 314−315 °C; ^1H NMR (400 MHz, DMSO-d_6) δ 9.86 (s, 2H), 9.01 (t, J = 9.0 Hz, 4H), 8.28 (dd, J = 8.0, 1.2 Hz, 2H), 8.18 (s, 2H), 7.89−7.79 (m, 4H), 7.77−7.65 (m, 6H), 3.86 (m, 2H), 3.66 (m, 2H), 1.14 (t, J = 7.0 Hz, 6H); HRMS (ESI) m/z $[M + H]^+$ calcd for $C_{40}H_{31}O_4$ 575.2222, found 575.2225. Poor solubility did not allow us to record the ^{13}C NMR data.

8,18-Bis[3,5-bis(trifluoromethyl)phenyl]-10,20-diethoxy-8,18-dihydrobenzo[*fg*]naphtho[3,2,1-*mn*]hexaphene (14). 3,5-Bis(trifluoromethyl)phenylmagnesium bromide **12** (0.5 M in THF, 3.13 mL, 1.57 mmol) was added to the dry THF (5 mL) solution of **11** (90 mg, 0.16 mmol) under nitrogen. The mixture was stirred at room temperature for 24 h, and the reaction quenched with a saturated aqueous NH_4Cl solution (15 mL). The volatile organics were evaporated, and the mixture was extracted with DCM (3 × 15 mL). The organic layer was dried over anhydrous Na_2SO_4, filtered, and removed under reduced pressure to afford a crude mixture containing intermediate compound **13** (437 mg). To the solution of crude **13** in anhydrous DCM (10 mL) was added dropwise $BF_3{\cdot}Et_2O$ (0.1 mL) under nitrogen, and the reaction mixture was stirred for 10 h at room temperature. Once **13** was completely consumed, as monitored by TLC, a saturated aqueous $NaHCO_3$ solution (20 mL) was added and the reaction mixture was extracted with DCM (3 × 10 mL). The organic layer was dried over anhydrous Na_2SO_4, filtered, and evaporated under reduced pressure. The residue was subjected to silica gel column chromatography (1:10 EtOAc/hexanes) to give title product **14** as a light brown solid (54 mg, 36% over two steps): R_f = 0.37 (5% EtOAc in hexanes); mp 319−320 °C; ^1H NMR (400 MHz, $CDCl_3$) δ 8.94 (s, 2H), 8.62 (dd, J = 6.4, 3.1 Hz, 2H), 8.56 (d, J = 7.9 Hz, 2H), 8.44 (dd, J = 6.6, 3.0 Hz, 2H), 7.71−7.65 (m, 6H), 7.64−7.58 (m, 6H), 7.50 (s, 2H), 5.79 (s, 2H), 4.40 (m, 2H), 4.09 (m, 2H), 1.57 (m, 6H, merged with residual water signal); HRMS (ESI) m/z $[M + H]^+$ calcd for $C_{56}H_{35}F_{12}O_2$ 967.2445, found 967.2440. Poor solubility did not allow us to record the ^{13}C NMR data.

8,18-Bis[3,5-bis(trifluoromethyl)phenyl]-10,20-diethoxybenzo[*fg*]naphtho[3,2,1-*mn*]hexaphene (3). *p*-Chloranil (23 mg, 0.09 mmol, 3 equiv) was added to **14** (30 mg, 0.03 mmol) in dry chloroform (4 mL) under N_2, and the reaction mixture was warmed to 70 °C for 5 h in an oil bath. Once the starting material was consumed (monitored by TLC), the solvent was removed in vacuo and the crude was purified by silica gel column chromatography (99:1 hexanes/EtOAc) to afford product **3** as a blue-green solid (15 mg, 65%) [R_f = 0.33 (20% EtOAc in hexanes)]. Recrystallization of **3** from a chloroform/toluene (1:1) mixture at ambient temperature in the dark afforded single crystals suitable for X-ray crystallographic analysis: mp 245 °C dec; ^1H NMR (400 MHz, C_6D_6) δ 8.94 (s, 2H), 8.33−8.29 (m, 2H), 8.23−8.17 (m, 4H), 7.97 (s, 2H), 7.78 (s, 4H), 7.45−7.30 (m, 4H), 7.09 (t, J = 7.8 Hz, 2H), 6.77 (d, J = 7.8 Hz, 2H), 3.71 (q, J = 7.1 Hz, 4H), 0.93 (t, J = 7.1 Hz, 6H); $^{13}C\{^1H\}$ NMR (100 MHz, C_6D_6) δ 168.8, 154.6, 141.9, 140.1, 133.9, 133.3, 132.9, 132.6, 132.3, 132.1, 131.6, 130.8, 129.6, 127.0, 126.4, 125.8, 125.3, 124.2, 123.3, 122.7, 122.6, 121.9, 119.6, 67.8, 15.7; HRMS (ESI) m/z $[M]^+$ calcd for $C_{56}H_{32}F_{12}O_2$ 964.2211, found 964.2220.

■ ASSOCIATED CONTENT

Supporting Information

The Supporting Information is available free of charge at https://pubs.acs.org/doi/10.1021/acs.joc.2c00089.

NMR spectra, photostability test, fluorescence spectra, X-ray crystallographic data, and details of DFT calculations (PDF)

Accession Codes

CCDC 2141677 contains the supplementary crystallographic data for this paper. These data can be obtained free of charge via www.ccdc.cam.ac.uk/data_request/cif, or by emailing data_request@ccdc.cam.ac.uk, or by contacting The Cambridge Crystallographic Data Centre, 12 Union Road, Cambridge CB2 1EZ, UK; fax: +44 1223 336033.

■ AUTHOR INFORMATION

Corresponding Author

Soumyajit Das − *Department of Chemistry, Indian Institute of Technology Ropar, Rupnagar, Punjab 140001, India;* orcid.org/0000-0003-0964-1958; Phone: (+91)1881-232067; Email: chmsdas@iitrpr.ac.in

Author

Priyank Kumar Sharma − *Department of Chemistry, Indian Institute of Technology Ropar, Rupnagar, Punjab 140001, India*

Complete contact information is available at: https://pubs.acs.org/10.1021/acs.joc.2c00089

Notes

The authors declare no competing financial interest.

■ ACKNOWLEDGMENTS

The authors gratefully acknowledge the financial support from SERB-DST India (SRG/2019/000401) and IIT Ropar (ISIRD grant). The authors thank Mr. Kamlesh Satpute for the single-crystal analysis. P.K.S. thanks CSIR for a research fellowship.

■ REFERENCES

(1) Zeng, W.; Sun, Z.; Herng, T. S.; Gonçalves, T. P.; Gopalakrishna, T. Y.; Huang, K.-W.; Ding, J.; Wu, J. Super-heptazethrene. *Angew. Chem., Int. Ed.* **2016**, *55*, 8615−8619.

(2) Sun, Z.; Huang, K.-W.; Wu, J. Soluble and stable heptazethrenebis(dicarboximide) with a singlet open-shell ground state. *J. Am. Chem. Soc.* **2011**, *133*, 11896−11899.

(3) Das, S.; Lee, S.; Son, M.; Zhu, X.; Zhang, W.; Zheng, B.; Hu, P.; Zeng, Z.; Sun, Z.; Zeng, W.; Li, R.-W.; Huang, K.-W.; Ding, J.; Kim, D.; Wu, J. Para-quinodimethane-bridged perylene dimers and pericondensed quaterrylenes: The effect of the fusion mode on the ground states and physical properties. *Chem. - Eur. J.* **2014**, *20*, 11410−11420.

(4) (a) Li, Y.; Heng, W.-K.; Lee, B. S.; Aratani, N.; Zafra, J. L.; Bao, N.; Lee, R.; Sung, Y. M.; Sun, Z.; Huang, K.-W.; Webster, R. D.; López Navarrete, J. T.; Kim, D.; Osuka, A.; Casado, J.; Ding, J.; Wu, J. Kinetically blocked stable heptazethrene and octazethrene: Closed-shell or open-shell in the ground state? *J. Am. Chem. Soc.* **2012**, *134*, 14913−14922. (b) Hu, P.; Lee, S.; Herng, T. S.; Aratani, N.; Gonçalves, T. P.; Qi, Q.; Shi, X.; Yamada, H.; Huang, K.-W.; Ding, J.; Kim, D.; Wu, J. Toward tetraradicaloid: The effect of fusion mode on radical character and chemical reactivity. *J. Am. Chem. Soc.* **2016**, *138*, 1065−1077.

(5) (a) Sun, Z.; Lee, S.; Park, K. H.; Zhu, X.; Zhang, W.; Zheng, B.; Hu, P.; Zeng, Z.; Das, S.; Li, Y.; Chi, C.; Li, R.-W.; Huang, K.-W.; Ding, J.; Kim, D.; Wu, J. Dibenzoheptazethrene isomers with different

biradical characters: An exercise of Clar's aromatic sextet rule in singlet biradicaloids. *J. Am. Chem. Soc.* **2013**, *135*, 18229−18236. (b) Zong, C.; Zhu, X.; Xu, Z.; Zhang, L.; Xu, J.; Guo, J.; Xiang, Q.; Zeng, Z.; Hu, W.; Wu, J.; Li, R.; Sun, Z. Isomeric Dibenzoheptazethrenes for air-stable organic field-effect transistors. *Angew. Chem., Int. Ed.* **2021**, *60*, 16230−16236.

(6) Yang, W.; Monteiro, J. H.; de Bettencourt-Dias, A.; Catalano, V. J.; Chalifoux, W. A. Synthesis, structure, photophysical properties, and photostability of Benzodipyrenes. *Chem. - Eur. J.* **2019**, *25*, 1441−1445.

(7) Clar, E.; Fell, G. S.; Richmond, M. H. 4,5:12,13-dibenzoheptazethrene and 5,6:8,9:14,15:17,18-tetrabenzoheptacene. *Tetrahedron* **1960**, *9*, 96−105.

(8) Zeng, Z.; Shi, X.; Chi, C.; López Navarrete, J. T.; Casado, J.; Wu, J. Pro-aromatic and anti-aromatic π-conjugated molecules: An irresistible wish to be diradicals. *Chem. Soc. Rev.* **2015**, *44*, 6578−6596.

(9) (a) Sun, Z.; Zeng, Z.; Wu, J. Zethrenes, extended p-quinodimethanes, and periacenes with a singlet biradical ground state. *Acc. Chem. Res.* **2014**, *47*, 2582−2591. (b) Hu, P.; Wu, J. Modern Zethrene Chemistry. *Can. J. Chem.* **2017**, *95*, 223−233.

(10) Hibi, D.; Kitabayashi, K.; Shimizu, A.; Umeda, R.; Tobe, Y. Synthesis and physical properties of zethrene derivatives bearing donor/acceptor substituents at 7,14-positions. *Org. Biomol. Chem.* **2013**, *11*, 8256−8261.

(11) Frisch, M. J.; et al. *Gaussian 09*, rev. B.01 (see the Supporting Information for the full reference).

(12) Jin, M.; Ren, W.; Qian, D.-W.; Yang, S.-D. Direct allylic C(sp3)-H alkylation with 2-naphthols via Cooperative Palladium and copper catalysis: Construction of Cyclohexadienones with Quaternary Carbon Centers. *Org. Lett.* **2018**, *20*, 7015−7019.

(13) (a) Shimizu, A.; Kubo, T.; Uruichi, M.; Yakushi, K.; Nakano, M.; Shiomi, D.; Sato, K.; Takui, T.; Hirao, Y.; Matsumoto, K.; Kurata, H.; Morita, Y.; Nakasuji, K. Alternating covalent bonding interactions in a one-dimensional chain of a phenalenyl-based singlet Biradical molecule having Kekulé structures. *J. Am. Chem. Soc.* **2010**, *132*, 14421−14428. (b) Shimizu, A.; Hirao, Y.; Matsumoto, K.; Kurata, H.; Kubo, T.; Uruichi, M.; Yakushi, K. Aromaticity and π-bond covalency: Prominent intermolecular covalent bonding interaction of a kekulé hydrocarbon with very significant singlet biradical character. *Chem. Commun.* **2012**, *48*, 5629.

(14) Yadav, P.; Das, S.; Phan, H.; Herng, T. S.; Ding, J.; Wu, J. Kinetically blocked stable 5,6:12,13-dibenzozethrene: A laterally π-extended zethrene with enhanced diradical character. *Org. Lett.* **2016**, *18*, 2886−2889.

(15) Desiraju, G. R. A Bond by Any Other Name. *Angew. Chem., Int. Ed.* **2011**, *50*, 52.

(16) Montgomery, L. K.; Huffman, J. C.; Jurczak, E. A.; Grendze, M. P. The molecular structures of Thiele's and Chichibabin's hydrocarbons. *J. Am. Chem. Soc.* **1986**, *108*, 6004−6011.

(17) Kruszewski, J.; Krygowski, T. M. Definition of aromaticity basing on the harmonic oscillator model. *Tetrahedron Lett.* **1972**, *13*, 3839−3842.

(18) (a) Dobrowolski, J. C.; Lipinski, P. F. J. On Splitting of the NICS(1) Magnetic Aromaticity Index. *RSC Adv.* **2016**, *6*, 23900−23904. (b) Antić, M.; Furtula, B.; Radenković, S. Aromaticity of Nonplanar Fully Benzenoid Hydrocarbons. *J. Phys. Chem. A* **2017**, *121*, 3616−3626.

(19) (a) Kim, J. J.; Funabiki, K.; Muramatsu, H.; Shibata, K.; Matsui, M.; Kim, S. H.; Shiozaki, H.; Hartmann, H. Negative solvatochromism of azo dyes derived from (dialkylamino)thiazole dimers. *Chem. Commun.* **2000**, 753−754. (b) Zeng, W.; Wu, J. Push−pull type Quinoidal Perylene Showing Solvent Polarity Dependent Diradical Character and Negative Solvatochromism. *Mater. Chem. Front.* **2019**, *3*, 2668−2672.

(20) Charge analysis was performed for the singlet closed-shell optimized structure of **3** using natural population analysis (NPA) as implemented in G09.

(21) Xu, T.; Han, Y.; Shen, Z.; Hou, X.; Jiang, Q.; Zeng, W.; Ng, P. W.; Chi, C. Antiaromatic Dicyclopenta[*b,g*]/[*a,f*]naphthalene isomers showing an open-shell singlet ground state with tunable diradical character. *J. Am. Chem. Soc.* **2021**, *143*, 20562−20568.

(22) Taniguchi, M.; Lindsey, J. S. Database of Absorption and Fluorescence Spectra of > 300 Common Compounds for use in PhotochemCAD. *Photochem. Photobiol.* **2018**, *94*, 290−327.

(23) Bredas, J.-L. Mind the gap! *Mater. Horiz.* **2014**, *1*, 17−19.

(24) (a) Huang, R.; Phan, H.; Herng, T. S.; Hu, P.; Zeng, W.; Dong, S.-q.; Das, S.; Shen, Y.; Ding, J.; Casanova, D.; Wu, J. Higher order π-conjugated polycyclic hydrocarbons with open-shell singlet ground state: Nonazethrene versus nonacene. *J. Am. Chem. Soc.* **2016**, *138*, 10323−10330. (b) Zeng, W.; Gopalakrishna, T. Y.; Phan, H.; Tanaka, T.; Herng, T. S.; Ding, J.; Osuka, A.; Wu, J. Superoctazethrene: An open-shell graphene-like molecule possessing large diradical character but still with reasonable stability. *J. Am. Chem. Soc.* **2018**, *140*, 14054−14058. (c) Wang, Q.; Hu, P.; Tanaka, T.; Gopalakrishna, T. Y.; Herng, T. S.; Phan, H.; Zeng, W.; Ding, J.; Osuka, A.; Chi, C.; Siegel, J.; Wu, J. Curved π-conjugated corannulene dimer diradicaloids. *Chem. Sci.* **2018**, *9*, 5100−5105.

(25) Nakano, M.; Minami, T.; Yoneda, K.; Muhammad, S.; Kishi, R.; Shigeta, Y.; Kubo, T.; Rougier, L.; Champagne, B.; Kamada, K.; Ohta, K. Giant Enhancement of the Second Hyperpolarizabilities of Open-Shell Singlet Polyaromatic Diphenalenyl Diradicaloids by an External Electric Field and Donor−Acceptor Substitution. *J. Phys. Chem. Lett.* **2011**, *2*, 1094−1098.

(26) Dreher, S. D.; Paruch, K.; Katz, T. J. Acidified Alcohols as Agents to Introduce and Exchange Alkoxyls on the Periphery of Helicenes. *J. Org. Chem.* **2000**, *65*, 806−814.

(27) Mohammad-Pour, G. S.; Ly, R. T.; Fairchild, D. C.; Burnstine-Townley, A.; Vazquez-Molina, D. A.; Trieu, K. D.; Campiglia, A. D.; Harper, J. K.; Uribe-Romo, F. J. Modular design of fluorescent dibenzo- and Naphtho-Fluoranthenes: Structural rearrangements and electronic properties. *J. Org. Chem.* **2018**, *83*, 8036−8053.

https://doi.org/10.1021/acs.joc.2c00089
J. Org. Chem. 2022, 87, 5430−5436

OL Organic Letters

pubs.acs.org/OrgLett Letter

Dominating Antiaromatic Character of *as*-Indacene Decides Overall Properties of a Formally Aromatic Dicyclopenta[*c*]fluorenothiophene

Priyank Kumar Sharma, Dibyendu Mallick, Himanshu Sharma, and Soumyajit Das*

Cite This: *Org. Lett.* 2023, 25, 2201−2206 Read Online

ACCESS | Metrics & More | Article Recommendations | Supporting Information

ABSTRACT: Dicyclopenta[*c*]fluorenothiophene **5** was synthesized as the isoelectronic polycyclic heteroarene analogue of an *as*-indacenodifluorene with a $(4n + 2)\pi$-electron perimeter. Single-crystal and ^{1}H NMR analyses indicated a quinoidal ground state for **5**, which was supported by theoretical calculations while suggesting a degree of antiaromaticity of the *as*-indacene subunit greater than that for *s*-indacenodifluorene **3**. The dominant antiaromaticity for **5** was evidenced by the broad weakly intense absorption tail reaching the near-IR region, four-stage redox amphotericity, and small HOMO−LUMO energy gap.

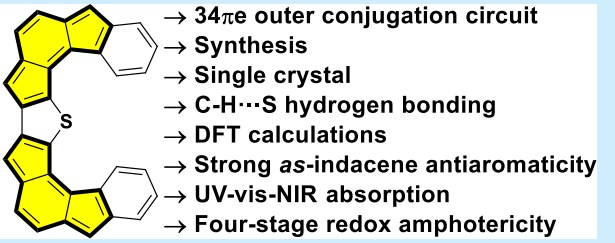

Poly(indenoindene) or PININ is a fully conjugated ladder polymer based on π-extended antiaromatic indenofluorene (Figure 1a).[1] Theoretical studies of the structural isomers

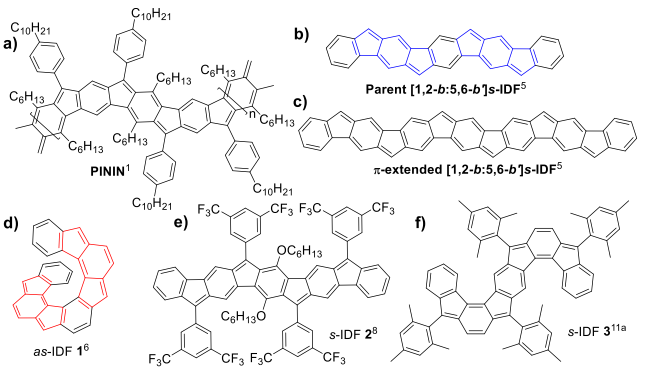

Figure 1. (a) Müllen's PININ. Tobe's (b) *s*-indaceno[1,2-*b*:5,6-*b*′]difluorene, and (c) π-extended [1,2-*b*:5,6-*b*′]*s*-IDF. (d) Helical *as*-indaceno[2,1-*c*:7,8-*c*′]difluorene **1**. (e) Wu's *s*-IDF **2**. (f) Our *s*-IDF **3**.

of Müllen's PININ revealed their small band gap and high spin ground states.[2] After the reports of formally antiaromatic indeno[1,2-*b*]fluorene[3] and indeno[2,1-*c*]fluorene[4] regioisomers, Tobe reported the designs of the parent *s*-indaceno[1,2-*b*:5,6-*b*′]difluorene (Figure 1b) and π-extended [1,2-*b*:5,6-*b*′]*s*-IDF (Figure 1c) as non-benzenoid polycyclic arenes (PAs) based on the *s*-indacene unit (shown in blue).[5] In 2015, Tobe proposed an *as*-indacene-embedded (shown in red, Figure 1d) helical *as*-indacenodifluorene **1** (*as*-IDF), but its synthesis and ground-state properties were unknown at that time.[6]

A helical fragment of **1** with seven alternatingly fused 6−5−6−5−6−5−6 rings in a doublet ground state was reported.[7] It was Wu's group that synthesized a stable closed-shell *s*-indacenodifluorene (*s*-IDF) **2** (Figure 1e),[8] which was based on Tobe's [1,2-*b*:5,6-*b*′]*s*-IDF scaffold (Figure 1b).[5] *s*-IDF **2** is a fragment of the fully conjugated ladder oligo(ININ) [or OININ] which was recently investigated by on-surface synthesis.[9] Computational studies found small multiple diradical characters of these quasi-one-dimensional OININs made of *s*-indacene repeating units, with potential for nonlinear optics applications.[10] We reported **3** (Figure 1f) as the *as*-indacene containing second structural isomer of the *s*-IDF series using a synthetic route that allowed us to synthesize [2,1-*c*]IF, too, without applying harsh conditions.[11a]

s-IDF **3** showed a HOMO−LUMO energy gap smaller than that of **2**, a red-shifted absorption in the NIR region, and a smaller singlet−triplet (S_0-T_1) energy gap that resulted in ^{1}H NMR line broadening at higher temperature,[11a] whereas a dibenzo-extended derivative of *s*-IDF **3** bearing a 2,6-dichlorophenyl substituent in place of mesityl was reported to show an open-shell ground state.[11b] *as*-Indacene-embedded IFs usually showed HOMO−LUMO and S_0-T_1 energy gaps smaller in comparison to those of *s*-indacene-based PAs,[3,4,12] and thus the smaller electronic gaps for **3** than for **2** could be attributed to the presence of *as*-indacene in the π-backbone.

Received: January 25, 2023
Published: March 29, 2023

https://doi.org/10.1021/acs.orglett.3c00261
Org. Lett. 2023, 25, 2201−2206

Though diareno-[13] or diheteroareno[14]-annulated *s*-indacenes with a 4nπ-electron perimeter were known to have tunable antiaromaticity, reports on *as*-indacene-embedded polycyclic heteroarenes (PHAs) with a $(4n + 2)\pi$-electron perimeter and the consequences of *as*-indacene antiaromatic character in the ground-state electronic properties have received hardly any attention.

Parent *as*-indaceno[2,3-*c*:7,6-*c*′]difluorene **4** (Figure 2a) can be regarded as a constitutional isomer of *as*-IDF **1**; however,

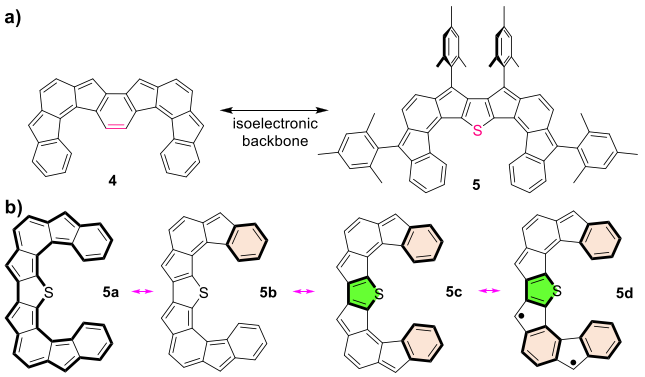

Figure 2. (a) Target **5** as isoelectronic analogue of parent [2,3-*c*:7,6-*c*′]*as*-IDF **4**. (b) Representative resonance forms of parent **5** (benzene and thiophene aromaticity are shaded with orange and green, respectively).

none of the two fully conjugated *as*-IDF regioisomers was synthesized to date. We envisaged replacing the bridging sp^2 carbon unit (shown in magenta color, Figure 2a) of the central benzene ring of **4** with an isoelectronic sulfur atom to design a new PHA **5**, which could be considered as an isoelectronic PHA analogue of *as*-IDF. It was anticipated that the incorporation of a thiophene unit could significantly enhance the ground-state antiaromaticity of two *as*-indacene units, resulting in interesting optoelectronic properties. Our design of **5** was motivated from the recent works by Haley[14a,b,f] on modulation of *s*-indacene antiaromaticity by fusing aromatic heterocycles; however, per our knowledge, heterocycle-fused *as*-indacene displaying dominant ground-state antiaromaticity is rare.

Targeted PHA **5** can be viewed as a formally aromatic compound considering 34π-electrons in the outer conjugation circuit, as shown for parent structure **5a** (Figure 2b). It may also be represented as two more closed-shell forms, **5b** and **5c**, and as a potential diradical-like[10,11b] form **5d**, while other representative open-shell forms are quite unlikely (Figure S18). Herein, we report the synthesis of *as*-indacene-embedded $(4n + 2)\pi$ dicyclopenta[*c*]fluorenothiophene **5**, and its ground-state characteristics were experimentally analyzed by nuclear magnetic resonance (NMR), single-crystal X-ray diffractometry (SCXRD), UV−vis−NIR absorption, and cyclic voltammetry (CV) studies. The experimental findings were supported by density functional theory (DFT) calculations.

The synthetic route to **5** started by esterification of thiophene-3,4-dicarboxylic acid **6** with ethanol/sulfuric acid to afford diester **7**, which was subsequently brominated to **8** (Scheme 1).[15] Diisobutylaluminum hydride (DIBAL-H) reduction of the diester **8** to diol, followed by oxidation of the crude diol using pyridinium chlorochromate (PCC), afforded dialdehyde **9** in 55% yield. Compound **9** underwent Suzuki coupling with pincaolboronate **10** to afford **11**,

Scheme 1. Synthesis of 5 (Mes = Mesityl)

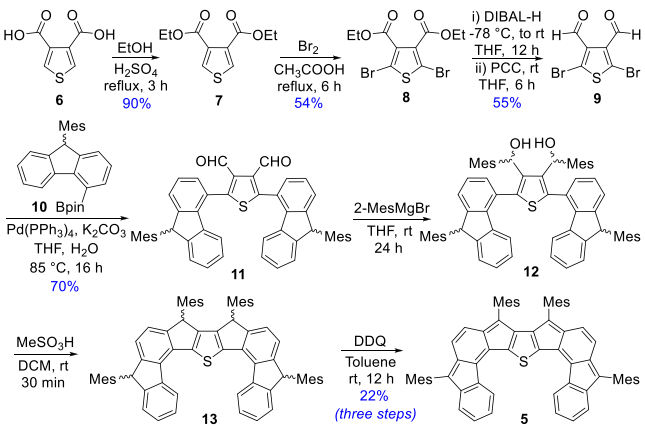

following our reported method.[11a] Treatment of **11** with 2-mesitylmagnesium bromide (2-MesMgBr) in ambient conditions gave alcohol **12**, which, without purification, was treated with methanesulfonic acid at room temperature to afford dihydro precursor **13**. Oxidative dehydrogenation of **13** using 2,3-dichloro-5,6-dicyano-1,4-benzoquinone (DDQ) in dry toluene gave **5** as dark-purple solid in 22% yield over three steps after column chromatographic purification. The structure of **5** was established by 1D and 2D NMR spectroscopy, which showed an upfield shift for the two *as*-indacene hydrogens of **5** (5.79 and 5.65 ppm) compared to those of **3** (6.16 and 6.06 ppm) in $CDCl_3$ (see Supporting Information).

Single crystals of **5** (Figure 3a) for SCXRD analysis were obtained by diffusing methanol to the dichloromethane (DCM) solution at ambient temperature. Compound **5** has a rigid and quasi-planar backbone with terminal benzene rings (A) twisted by ∼8.3° (average) in the cove-like region, as

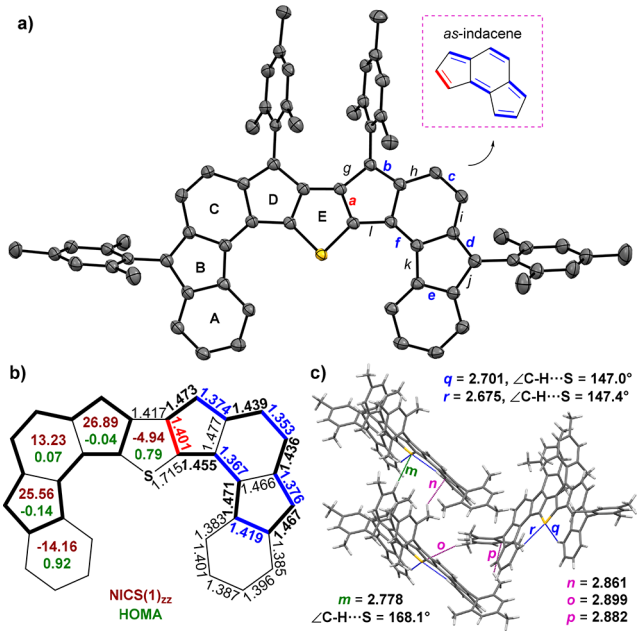

Figure 3. (a) ORTEP drawing of **5** with ellipsoids at the 50% probability level (hydrogens omitted). (b) Average bond lengths (Å) for axosymmetric **5**; calculated $NICS(1)_{zz}$ (brown, BHLYP) and HOMA (green) values for optimized structure **5**. (c) Short contacts (Å) are labeled for **5**.

https://doi.org/10.1021/acs.orglett.3c00261
Org. Lett. 2023, 25, 2201−2206

measured from the mean planes between ring E and rings A, while DFT optimization found it to be planar (Figure S15). The near orthogonally deviated mesityl groups likely prevented aggregation, and thus **5** was moderately soluble in common organic solvents. The *as*-indacene subunit of **5** showed large C_{sp}^2–C_{sp}^2 bond length alternation (BLA), as shown in Figure 3a,b (full bond length analyses with estimated standard deviation values are shown in Figure S14a), with C=C bonds (*a*–*f*; see labeling in Figure 3a) having greater double bond character than the rest of the C_{sp}^2–C_{sp}^2 bonds (*g*–*l*), demonstrating an alternate double bond and single bond character. To compare BLA, *as*-indacene-embedded *s*-IDF **3** and **5** were chosen (Table 1), which clearly revealed that C=

Table 1. Mean C_{sp}^2=C_{sp}^2 Bond Lengths (in Å) of 5 and 3 for *as*-Indacene

compound	*a*	*b*	*c*	*d*	*e*	*f*
3	1.417	1.373	1.351	1.372	1.420	1.365
5	1.401	1.374	1.353	1.376	1.419	1.367

C bond *a* linking cyclopenta[*c*]fluorene and thiophene for **5** is 0.016 Å shorter than that of *a* for **3** bearing benzene,[11a] while the other C=C bond lengths were identical. Shortening of the bond *a* for **5**, due to increased double-bond character of less aromatic thiophene,[14f] implies larger BLA for *as*-indacene than for **3**, hinting significant *para*-quinoidal contribution in the form of **5c** to the ground-state **5**.

The herringbone packing motif (Figure S14c) for the crystal of **5** was formed by several short contacts, listed in Figure 3c. The short intermolecular C–H···π interactions (*o* = 2.899 Å, *p* = 2.882 Å) between neighboring molecules enabled the T-like arrangement, and another set of intermolecular C–H···π interactions (*n* = 2.861 Å) with a C–H···S hydrogen bonding (HB) interaction (*m* = 2.778 Å, 168.1°) enabled slipped π-stacks forming an overall two-dimensional herringbone-like arrangement. Compound **5** displayed two intramolecular C–H···S (*q* = 2.701 Å, 147.0; *r* = 2.675 Å, 147.4°) HB interactions, an underappreciated noncovalent interaction,[16] which likely shifted the hydrogen-bonded ring A protons toward the downfield region in the ^{1}H NMR (7.69 ppm for **5**) compared to that with **3** (7.53 ppm, Figure S13).

DFT optimization at the B3LYP/6-31G(d) level of theory suggested that **5** has a singlet closed-shell ground state with large S_0–T_1 gap (10.1 kcal mol^{-1}, zero diradical character, Table S2), which corresponds with the *para*-quinoidal *as*-indacene subunit. The harmonic oscillator model for aromaticity (HOMA) analysis of optimized structure **5** indicated not so large BLA for ring A (0.92) and E (0.79),[17] while rings B (−0.14), C (0.07), and D (−0.04) showed significant BLA (Figure 3b). The nucleus independent chemical shift (NICS(1)$_{zz}$)[18] indices of **5** at the same level of theory agree with the aromaticity of ring A (−10.72), while nonaromaticity for ring E (0.78) and strong antiaromaticity for B (25.81), C (13.11), and D (28.68) rings were suggested, respectively (Figure S16a). Considering that B3LYP may not accurately estimate (anti)aromaticity,[19] as we examined for **3** to get more reliable results (Figure S16b), the BHLYP functional was used to quantify the aromaticity of **5**. The NICS(1)$_{zz}$ indices obtained at the BHLYP level for **5** (A = −14.16, B = 25.56, C = 13.23, D = 26.89, E = −4.94; Figure 3b) are identical to those found at the B3LYP level, except for the thiophene (ring E), which is found to be weakly aromatic and in line with the HOMA value. The anisotropy of the induced current density (ACID)[20] plot of **5** (Figure 4) is in

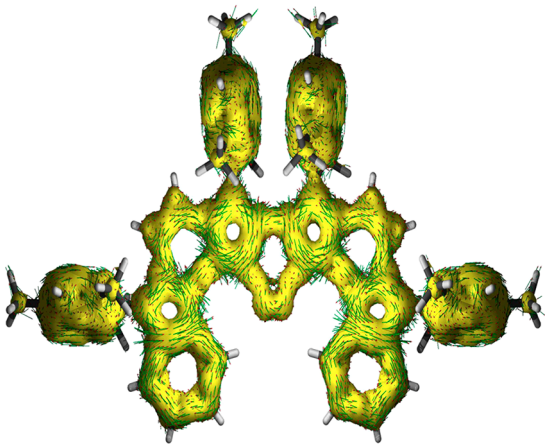

Figure 4. Current–density vectors for **5** are plotted onto the ACID isosurface of 0.02 at the BHLYP/6-31G(d) level of theory.

line with the NICS indices (Figure 3b), exhibiting counterclockwise semiglobal ring-current spread over rings B, C, and D with considerable localization of counterclockwise ring currents over B and D rings, which clearly suggested the significant paratropic nature of the *as*-indacene subunit. The strong clockwise ring currents for aromatic ring A agree with the large negative NICS value, while observation of diatropic ring currents over ring E (Figure 4) is consistent with its weak aromatic character. The high-resolution ACID plots at B3LYP and BHLYP levels are supplied in Figure S17.

The UV–vis–NIR absorption spectra of **5** in DCM depicted in Figure 5a exhibited intense absorption in the UV region (λ_{max} = 342 nm, ε = 43945 M^{-1} cm^{-1}), with absorption in the visible region at λ_{max} = 557 nm (ε = 31940 M^{-1} cm^{-1}), which

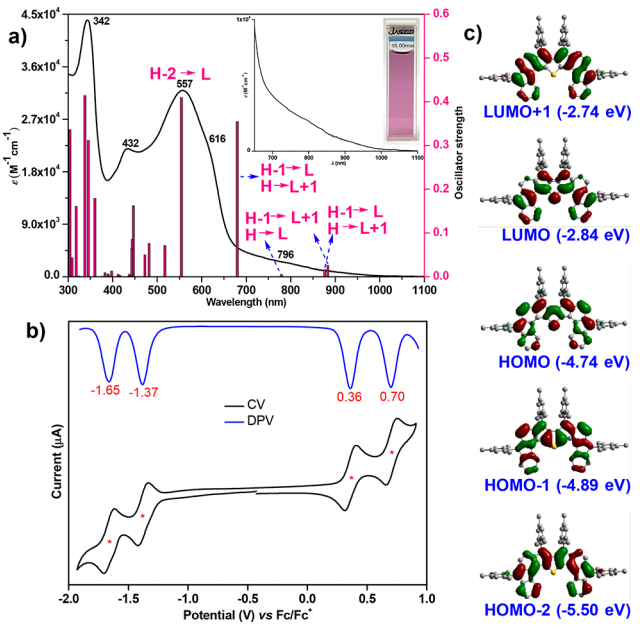

Figure 5. (a) UV–vis–NIR spectrum for **5** (600–1100 nm expansion in inset, and the DCM solution shown in purple) with time-dependent DFT oscillator strengths as a bar plot. (b) CV and DPV of **5**. (c) Frontier molecular orbitals of **5**.

https://doi.org/10.1021/acs.orglett.3c00261
Org. Lett. 2023, 25, 2201–2206

is accompanied by a weak shoulder roughly at λ_{max} = 616 nm (ε = 22065 M^{-1} cm^{-1}). Similar to the axosymmetric $(4n + 2)\pi$ benzo-fused bispentalene[21] with strong antiaromaticity, the axosymmetric **5** displayed a long absorption tail from 680 to 1100 nm in the near-IR region with weak intensity. According to time-dependent DFT (TDDFT) calculations, the absorptions at 557 and 616 nm could be attributed to the HOMO−2 → LUMO (554 nm, oscillator strength (f) = 0.40) transition and admixing of HOMO−1 → LUMO and HOMO → LUMO+1 (680 nm, f = 0.35) transitions, respectively (Table S3). The weak absorption band having a long tail from 680 to 1100 nm is assignable to an admixture of several weak, seemingly forbidden (f < 0.02), transitions (Table S3) including the forbidden HOMO → LUMO transition (796 nm; TDDFT: 779 nm, f = 0.004; Figure 5c) which is one of the typical traits of strong antiaromaticity.[14a,21,22] The optical HOMO−LUMO energy gap, roughly measured from the absorption onset, was 1.24 eV (1000 nm) for **5**, while the theoretical HOMO−LUMO gap was 1.90 eV. Curiously, the HOMO−LUMO energy gap increased from **3**[11a] to **5**, despite the enhancement of antiaromaticity of *as*-indacene.

The electrochemical behavior of **5** was studied by CV and differential pulse voltammetry (DPV) in DCM, displaying amphoteric redox behavior (Figure 5b). Two reversible reduction waves with half-wave potentials at $E_{1/2}^{red1}$ = −1.37 V and $E_{1/2}^{red2}$ = −1.65 V and two reversible oxidation waves with half-wave potentials at $E_{1/2}^{ox1}$ = 0.36 V and $E_{1/2}^{ox2}$ = 0.70 V (vs ferrocene/ferrocenium (Fc/Fc^+)) were observed. Due to a stronger *as*-indacene antiaromaticity, electron injection in **5** was relatively facile compared to that in **3**,[11a] while higher oxidation potential suggested that the dominant antiaromatic character could resist electron extraction from **5**. The observation is comparable to *s*-indacene-based IFs with a greater degree of antiaromaticity.[12b,13] The HOMO and LUMO energy levels of **5** were −5.10 and −3.56 eV, as measured from the onset oxidation and reduction potentials, respectively, giving an energy gap of 1.54 eV.

In conclusion, antiaromatic unit-embedded PAs bearing a $(4n + 2)\pi$-electron perimeter with dominant contribution from its antiaromatic subunit are underexplored, with limited examples of quinoidal dicyclopenta[*a*,*e*]pentalene,[23] bispentalenes,[21] *s*-IDFs,[8,11a] and phenylene-based acenes,[24] while pentalenodifluorene,[25] dibenzo-*s*-IDF,[11b] and diindenobiphenylene[26] displayed open-shell ground state instead of antiaromaticity. Therefore, $(4n + 2)\pi$-systems made of antiaromatic subunits are of special interest, but their heteroaromatic analogues are unknown. Synthesis and characterization of a formally aromatic axosymmetric PHA **5**, which is unlike centrosymmetric PA analogues,[8,11a] showed enhanced *as*-indacene antiaromaticity as analyzed by NICS/ACID calculations. The enhanced antiaromaticity for **5** was also evidenced by the weakly intense absorption bands extending to 1100 nm, higher oxidation and lower reduction potentials with good reversibility, and an upfield NMR shift for the *as*-indacene protons compared to that with **3**.[11a] Thiophene-fused pentalenes[27] and indacenes[28] gained attention due to strong antiaromaticity. Inclusion of thiophene can be an effective strategy to enhance *as*-indacene antiaromaticity for $(4n + 2)\pi$-systems, which may find future applications in optoelectronics[29] as stable alternatives of isoelectronic acenes.[30]

■ ASSOCIATED CONTENT

Data Availability Statement

The data underlying this study are available in the published article and its Supporting Information.

Supporting Information

The Supporting Information is available free of charge at https://pubs.acs.org/doi/10.1021/acs.orglett.3c00261.

General information, synthesis, and characterization of new compounds; DFT calculations; X-ray crystallographic data (PDF)

Accession Codes

CCDC 2238024 contains the supplementary crystallographic data for this paper. These data can be obtained free of charge via www.ccdc.cam.ac.uk/data_request/cif, or by emailing data_request@ccdc.cam.ac.uk, or by contacting The Cambridge Crystallographic Data Centre, 12 Union Road, Cambridge CB2 1EZ, UK; fax: +44 1223 336033.

■ AUTHOR INFORMATION

Corresponding Author

Soumyajit Das − *Department of Chemistry, Indian Institute of Technology Ropar, Rupnagar 140001 Punjab, India;* orcid.org/0000-0003-0964-1958; Email: chmsdas@iitrpr.ac.in

Authors

Priyank Kumar Sharma − *Department of Chemistry, Indian Institute of Technology Ropar, Rupnagar 140001 Punjab, India;* orcid.org/0000-0003-4360-2696

Dibyendu Mallick − *Department of Chemistry, Presidency University, Kolkata 700073 West Bengal, India;* orcid.org/0000-0002-0650-1872

Himanshu Sharma − *Department of Chemistry, Indian Institute of Technology Ropar, Rupnagar 140001 Punjab, India;* orcid.org/0000-0002-3910-9754

Complete contact information is available at: https://pubs.acs.org/10.1021/acs.orglett.3c00261

Author Contributions

P.K.S. performed the synthesis and characterization of all new compounds. S.D. and P.K.S. performed DFT calculations. D.M. performed ACID calculations. H.S. synthesized and characterized some intermediate molecules. S.D. conceived the idea, supervised the project, secured funding, and prepared the manuscript together with P.K.S. All authors have given approval to the final version of the manuscript.

Notes

The authors declare no competing financial interest.

■ ACKNOWLEDGMENTS

S.D. gratefully acknowledges the financial support from SERB (CRG/2022/003012), India. D.M. thanks National Supercomputing Mission (DST/NSM/R&D_HPC_Applications/2021/08) for computing resources of "PARAM Shakti" at IIT Kharagpur and "PARAM Brahma" at IISER Pune, implemented by C-DAC and supported by the Ministry of Electronics and Information Technology (MeitY) and DST, India. D.M. also thanks SERB (SRG/2019/001461) for funding. We thank Mr. Devendra Mayurdhwaj Sanke (IISER

Kolkata) for the low-temperature single-crystal data, and Dr. Tullimilli Y. Gopalakrishna (HPCL, India) for analyses. P.K.S. and H.S. thank CSIR and IIT Ropar, respectively, for senior research fellowships.

REFERENCES

(1) Scherf, U.; Müllen, K. Polyarylenes and poly(arylenevinylene)s: 8. The first soluble ladder polymer with 1,4-benzoquinone-bismethide subunits. *Polymer* **1992**, *33*, 2443−2446.
(2) Kertesz, M. Structure and Electronic Structure of Low-Band-Gap Ladder Polymers. *Macromolecules* **1995**, *28*, 1475−1480.
(3) Chase, D. T.; Rose, B. D.; McClintock, S. P.; Zakharov, L. N.; Haley, M. M. Indeno[1,2-*b*]fluorenes: Fully Conjugated Antiaromatic Analogues of Acenes. *Angew. Chem., Int. Ed.* **2011**, *50*, 1127−1130.
(4) Fix, A. G.; Deal, P. E.; Vonnegut, C. L.; Rose, B. D.; Zakharov, L. N.; Haley, M. M. Indeno[2,1-*c*]fluorene: A New Electron-Accepting Scaffold for Organic Electronics. *Org. Lett.* **2013**, *15*, 1362−1365.
(5) Shimizu, A.; Nobusue, S.; Miyoshi, H.; Tobe, Y. Indenofluorene congeners: Biradicaloids and beyond. *Pure Appl. Chem.* **2014**, *86*, 517−528.
(6) Tobe, Y. Non-Alternant Non-Benzenoid Aromatic Compounds: Past, Present, and Future. *Chem. Rec.* **2015**, *15*, 86−96.
(7) Herzog, S.; Hinz, A.; Breher, F.; Podlech, J. Cyclopenta-fused polyaromatic hydrocarbons: synthesis and characterisation of a stable, carbon-centred helical radical. *Org. Biomol. Chem.* **2022**, *20*, 2873−2880.
(8) Hu, P.; Lee, S.; Herng, T. S.; Aratani, N.; Gonçalves, T. P.; Qi, Q.; Shi, X.; Yamada, H.; Huang, K.-W.; Ding, J.; Kim, D.; Wu, J. Toward Tetraradicaloid: The Effect of Fusion Mode on Radical Character and Chemical Reactivity. *J. Am. Chem. Soc.* **2016**, *138*, 1065−1077.
(9) Di Giovannantonio, M.; Chen, Q.; Urgel, J. I.; Ruffieux, P.; Pignedoli, C. A.; Müllen, K.; Narita, A.; Fasel, R. On-Surface Synthesis of Oligo(indenoindene). *J. Am. Chem. Soc.* **2020**, *142*, 12925−12929.
(10) Fukuda, K.; Fujiyoshi, J.-ya; Matsui, H.; Nagami, T.; Takamuku, S.; Kitagawa, Y.; Champagne, B.; Nakano, M. A theoretical study on quasi-one-dimensional open-shell singlet ladder oligomers: multi-radical nature, aromaticity and second hyperpolarizability. *Org. Chem. Front.* **2017**, *4*, 779−789.
(11) (a) Sharma, H.; Sharma, P. K.; Das, S. Revisiting indeno[2,1-*c*]fluorene synthesis while exploring the fully conjugated *s*-indaceno-[2,1-*c*:6,5-*c*′]difluorene. *Chem. Commun.* **2020**, *56*, 11319−11322. (b) Jiang, Q.; Han, Y.; Zou, Y.; Phan, H.; Yuan, L.; Herng, T. S.; Ding, J.; Chi, C. S-shaped *para*-quinodimethane-Embedded Double [6]Helicene and Its Charged Species Showing Open-Shell Diradical Character. *Chem.—Eur. J.* **2020**, *26*, 15613−15622.
(12) (a) Tobe, Y. Quinodimethanes Incorporated in Non-Benzenoid Aromatic or Antiaromatic Frameworks. *Top. Curr. Chem. (Z)* **2018**, *376*, 12. (b) Sharma, H.; Bhardwaj, N.; Das, S. Revisiting indeno[1,2-*b*]fluorene by steric promoted synthesis while isolating the second stable 4nπ indeno[2,1-*a*]fluorene. *Org. Biomol. Chem.* **2022**, *20*, 8071−8077. (c) Shimizu, A.; Tobe, Y. Indeno[2,1-*a*]fluorene: An Air-Stable *ortho*-Quinodimethane Derivative. *Angew. Chem., Int. Ed.* **2011**, *50*, 6906−6910.
(13) Frederickson, C. K.; Zakharov, L. N.; Haley, M. M. Modulating Paratropicity Strength in Diareno-Fused Antiaromatics. *J. Am. Chem. Soc.* **2016**, *138*, 16827−16838.
(14) (a) Warren, G. I.; Barker, J. E.; Zakharov, L. N.; Haley, M. M. Enhancing the Antiaromaticity of *s*-Indacene through Naphthothiophene Fusion. *Org. Lett.* **2021**, *23*, 5012−5017. (b) Barker, J. E.; Price, T. W.; Karas, L. J.; Kishi, R.; MacMillan, S. N.; Zakharov, L. N.; Gómez-García, C. J.; Wu, J. I.; Nakano, M.; Haley, M. M. A Tale of Two Isomers: Enhanced Antiaromaticity/Diradical Character versus Deleterious Ring-Opening of Benzofuran-fused *s*-Indacenes and Dicyclopenta[*b*,g]naphthalenes. *Angew. Chem., Int. Ed.* **2021**, *60*, 22385−22392. (c) Barker, J. E.; Dressler, J. J.; Cárdenas Valdivia, A.; Kishi, R.; Strand, E. T.; Zakharov, L. N.; MacMillan, S. N.; Gómez-García, C. J.; Nakano, M.; Casado, J.; Haley, M. M. Molecule Isomerism Modulates the Diradical Properties of Stable Singlet Diradicaloids. *J. Am. Chem. Soc.* **2020**, *142*, 1548−1555. (d) Dressler, J. J.; Barker, J. E.; Karas, L. J.; Hashimoto, H. E.; Kishi, R.; Zakharov, L. N.; MacMillan, S. N.; Gomez-Garcia, C. J.; Nakano, M.; Wu, J. I.; Haley, M. M. Late-Stage Modification of Electronic Properties of Antiaromatic and Diradicaloid Indeno[1,2-*b*]fluorene Analogues via Sulfur Oxidation. *J. Org. Chem.* **2020**, *85*, 10846−10857. (e) Saha, H. K.; Mallick, D.; Das, S. Unveiling two antiaromatic *s*-indacenodicarbazole isomers with tunable paratropicity. *Chem. Commun.* **2022**, *58*, 8492−8495. (f) Marshall, J. L.; Uchida, K.; Frederickson, C. K.; Schutt, C.; Zeidell, A. M.; Goetz, K. P.; Finn, T. W.; Jarolimek, K.; Zakharov, L. N.; Risko, C.; Herges, R.; Jurchescu, O. D.; Haley, M. M. Indacenodibenzothiophenes: Synthesis, Optoelectronic Properties and Materials Applications of Molecules with Strong Antiaromatic Character. *Chem. Sci.* **2016**, *7*, 5547−5558.
(15) Lim, C. J.; Li, L.; Lei, Y.; Zhou, F.; Wu, B.; Liu, X.; Zhu, F.; Ong, B. S.; Hu, X.; Su, H.; Ng, S.-C. Synthesis and characterization of three thienopyridazine-based copolymers and their application in OFET. *Tetrahedron Lett.* **2016**, *57*, 1523−1527.
(16) Fargher, H. A.; Sherbow, T. J.; Haley, M. M.; Johnson, D. W.; Pluth, M. D. C−H···S Hydrogen Bonding Interactions. *Chem. Soc. Rev.* **2022**, *51*, 1454−1469.
(17) (a) Krygowski, T. M.; Cyrański, M. K. Structural Aspects of Aromaticity. *Chem. Rev.* **2001**, *101*, 1385−1420. (b) Najmidin, K.; Kerim, A.; Abdirishit, P.; Kalam, H.; Tawar, T. A comparative study of the aromaticity of pyrrole, furan, thiophene, and their aza-derivatives. *J. Mol. Model.* **2013**, *19*, 3529−3535.
(18) Fallah-Bagher-Shaidaei, H.; Wannere, C. S.; Corminboeuf, C.; Puchta, R.; Schleyer, P. v. Which NICS Aromaticity Index for Planar π Rings Is Best? *Org. Lett.* **2006**, *8*, 863−866.
(19) (a) Valiev, R. R.; Fliegl, H.; Sundholm, D. Closed-Shell Paramagnetic Porphyrinoids. *Chem. Commun.* **2017**, *53*, 9866−9869. (b) Lehtola, S.; Dimitrova, M.; Fliegl, H.; Sundholm, D. Benchmarking Magnetizabilities with Recent Density Functionals. *J. Chem. Theory Comput.* **2021**, *17*, 1457−1468.
(20) Geuenich, D.; Hess, K.; Köhler, F.; Herges, R. Anisotropy of the Induced Current Density (ACID), a General Method to Quantify and Visualize Electronic Delocalization. *Chem. Rev.* **2005**, *105*, 3758−3772.
(21) Cao, J.; London, G.; Dumele, O.; von Wantoch Rekowski, M.; Trapp, N.; Ruhlmann, L.; Boudon, C.; Stanger, A.; Diederich, F. The Impact of Antiaromatic Subunits in [4*n*+2] π-Systems: Bispentalenes with [4*n*+2] π-Electron Perimeters and Antiaromatic Character. *J. Am. Chem. Soc.* **2015**, *137*, 7178−7188.
(22) (a) Oshima, H.; Fukazawa, A.; Yamaguchi, S. Facile Synthesis of Polycyclic Pentalenes with Enhanced Hückel Antiaromaticity. *Angew. Chem., Int. Ed.* **2017**, *56*, 3270−3274. (b) Konishi, A.; Okada, Y.; Kishi, R.; Nakano, M.; Yasuda, M. Enhancement of Antiaromatic Character via Additional Benzoannulation into Dibenzo[*a*,*f*]-pentalene: Syntheses and Properties of Benzo[*a*]naphtho[2,1-*f*]-pentalene and Dinaphtho[2,1-*a*,*f*]pentalene. *J. Am. Chem. Soc.* **2019**, *141*, 560−571. (c) Xu, T.; Han, Y.; Shen, Z.; Hou, X.; Jiang, Q.; Zeng, W.; Ng, P. W.; Chi, C. Antiaromatic Dicyclopenta[*b*,g]/[*a*,*f*]-naphthalene Isomers Showing an Open-Shell Singlet Ground State with Tunable Diradical Character. *J. Am. Chem. Soc.* **2021**, *143*, 20562−20568. (d) Wang, J.; Gámez, F. G.; Marín-Beloqui, J.; Diaz-Andres, A.; Miao, X.; Casanova, D.; Casado, J.; Liu, J. Synthesis of a Dicyclohepta[*a*,g]heptalene-Containing Polycyclic Conjugated Hydrocarbon and the Impact of Non-Alternant Topologies. *Angew. Chem., Int. Ed.* **2023**, *62*, e202217124.
(23) Stowasser, B.; Hafner, K. Synthesis of a Dicyclopenta[*a*,*e*]-pentalene by [6 + 2]-Cycloaddition of 1,3-Di-tert-butyl-5-vinylidenecyclopentadiene and Consecutive 8π-Electrocyclic Reaction. *Angew. Chem., Int. Ed. Engl.* **1986**, *25*, 466−468.
(24) Parkhurst, R. R.; Swager, T. M. Synthesis and Optical Properties of Phenylene-Containing Oligoacenes. *J. Am. Chem. Soc.* **2012**, *134*, 15351−15356.

https://doi.org/10.1021/acs.orglett.3c00261
Org. Lett. 2023, 25, 2201−2206

(25) Maekawa, T.; Ueno, H.; Segawa, Y.; Haley, M. M.; Itami, K. Synthesis of Open-Shell Ladder π-systems by Catalytic C−H Annulation of Diarylacetylenes. *Chem. Sci.* **2016**, *7*, 650−654.
(26) Chen, P.-Y.; Liu, Y.-C.; Hung, H.-Y.; Pan, M.-L.; Wei, Y.-C.; Kuo, T.-C.; Cheng, M.-J.; Chou, P.-T.; Chiang, M.-H.; Wu, Y.-T. Diindeno[2,1-*b*:2′,1′-*h*]biphenylenes: Syntheses, Structural Analyses, and Properties. *Org. Lett.* **2021**, *23*, 8794−8798.
(27) Usuba, J.; Hayakawa, M.; Yamaguchi, S.; Fukazawa, A. Dithieno[*a*,*e*]pentalenes: Highly Antiaromatic Yet Stable π-Electron Systems without Bulky Substituents. *Chem.—Eur. J.* **2021**, *27*, 1638−1647.
(28) Marshall, J. L.; O'Neal, N. J.; Zakharov, L. N.; Haley, M. M. Synthesis and Characterization of Two Unsymmetrical Indenofluorene Analogues: Benzo[5,6]-*s*-indaceno[1,2-*b*]thiophene and Benzo[5,6]-*s*-indaceno[2,1-*b*]thiophene. *J. Org. Chem.* **2016**, *81*, 3674−3680.
(29) (a) Higashino, T.; Mori, T. Small-molecule ambipolar transistors. *Phys. Chem. Chem. Phys.* **2022**, *24*, 9770−9806. (b) Sharma, H.; Ankita, A.; Bhardwaj, P.; Pandey, U. K.; Das, S. Exploring Indeno[2,1-*c*]fluorene Antiaromatics with Unsymmetrical Disubstitution and Balanced Ambipolar Charge-Transport Properties. *Organic Materials* **2023**, *5*, 72−83.
(30) Tönshoff, C.; Bettinger, H. F. Photogeneration of Octacene and Nonacene. *Angew. Chem., Int. Ed.* **2010**, *49*, 4125−4128.

https://doi.org/10.1021/acs.orglett.3c00261
Org. Lett. 2023, 25, 2201−2206

JOC The Journal of Organic Chemistry

pubs.acs.org/joc Article

Constructing 1-Ethoxyphenanthro[9,10-*e*]acephenanthrylene for the Synthesis of a Polyaromatic Hydrocarbon Containing a Formal Azulene Unit

Priyank Kumar Sharma, Akanksha Babbar, Dibyendu Mallick, and Soumyajit Das*

Cite This: *J. Org. Chem.* 2023, 88, 5473−5482 Read Online

ACCESS | Metrics & More | Article Recommendations | Supporting Information

ABSTRACT: *peri*-Acenoacenes are attractive synthetic targets, but their non-benzenoid isomeric counterparts were unnoticed. 1-Ethoxyphenanthro[9,10-*e*]acephenanthrylene **8** was synthesized and converted to azulene-embedded **9**, which is a tribenzo-fused non-alternant isomeric motif of *peri*-anthracenoanthracene. Aromaticity and single-crystal analyses suggested a formal azulene core for **9**, which showed a smaller highest occupied molecular orbital (HOMO)−lowest unoccupied molecular orbital (LUMO) energy gap with a charge-transfer absorption band and brighter fluorescence than **8** (quantum yield (Φ): **9** = 41.8%, **8** = 8.9%). The reduction potentials of **8** and **9** were nearly identical, and the observations were further supported by density functional theory (DFT) calculations.

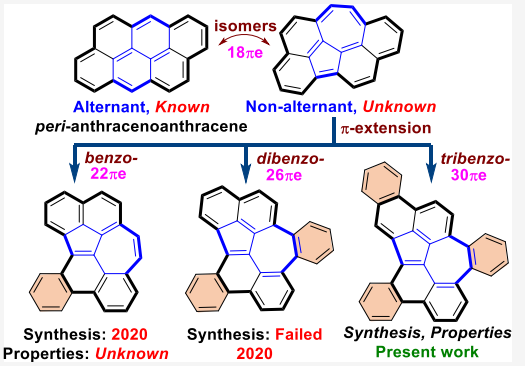

1. INTRODUCTION

Construction of azulene-embedded π-extended polyaromatic hydrocarbons (PAHs, with a central azulene unit)[1] has recently gained increasing attention from several research groups,[2] as the synthesis of atomically precise 5−7 (pentagon−heptagon) ring-fused defective nanographene is much desired to understand the structure−property relationships because azulene-like structural defects are often observed in graphene networks.[3] Theoretical studies of graphene monolayers containing azulene-like defects attracted considerable attention in this regard for a long time;[4] however, embedding 5−7 fused rings in place of 6−6 (hexagon−hexagon) rings in a polyarene skeleton, synthetically,[5] is a challenging task to achieve.[1,3]

Construction of the central azulene unit for an azulene-embedded PAH is recommended at the late stage,[6] instead of using the azulene motif as a starting material, to avoid unusual rearrangements, leading to unexpected product formation.[7] For example, the formation of an azulene unit of singlet diradicaloid **2**,[6] a *peri*-dibenzo-fused derivative of benzo[*f*]-azulene[8] (azulene fragment is shown in blue color, Figure 1a), was achieved at the late stage using a synthetic protocol that was applicable to construct two additional azulene-embedded diradicaloids with an extremely small singlet−triplet energy gap. Compound **2** is a benzo-extended cyclohepta[*def*]-fluorene (benzo-CHF),[9] which was long theoretically predicted to possess a singlet−triplet bistable ground state;[10] though lately it was established as a singlet diradicaloid in the ground state.[11] Notably, in Feng's report,[6] additional two benzannulation (shown in bold hexagons, Figure 1b) of benzo-CHF **2** afforded **Dibenzo-2** with a singlet diradicaloid ground state. We envisioned that annulation of the two benzene rings at *peri*-positions of **2** may afford **3**, which is a structural isomer of **Dibenzo-2** and is still unknown (Figure 1c). However, compound **4**, a constitutional isomer of **3**, was lately synthesized by Takasu et al. by a photoinduced 10π-electrocyclization approach, but its electronic properties were not studied.[12] Isomers **3** and **4** may be viewed as benzo-extended **5-NA** (benzene ring is shown by orange hexagon, Figure 1c), which can be considered as the non-alternant isomeric motif of alternant *peri*-anthracenoanthracene **5-A** (Figure 1d).[13] To our knowledge, non-alternant isomeric *peri*-acenoacene scaffold **5-NA** is overlooked in the literature, and attempts to synthesize **7**, a dibenzo-fused **5-NA**, from **6** were unsuccessful.[12] Stimulated by the recent studies of alternant *peri*-acenoacenes[14] from theoretical[15] and experimental[13,16−18] viewpoints, including the non-availability of non-alternant *peri*-acenoacene and the renaissance of azulene-embedded PAHs,[1,3,19] we envisaged to construct the heptagon unit by a Scholl-type oxidative aromatic coupling[20] using phenanthroacephenanthrylene (PAP) **8** instead of dibenzofluoroanthene **6**. It is worth mentioning that one can draw seven regioisomers of the PAP π-system (Figure S27) including parent **8**, but they

Received: December 31, 2022
Published: April 11, 2023

https://doi.org/10.1021/acs.joc.2c03103
J. Org. Chem. 2023, 88, 5473−5482

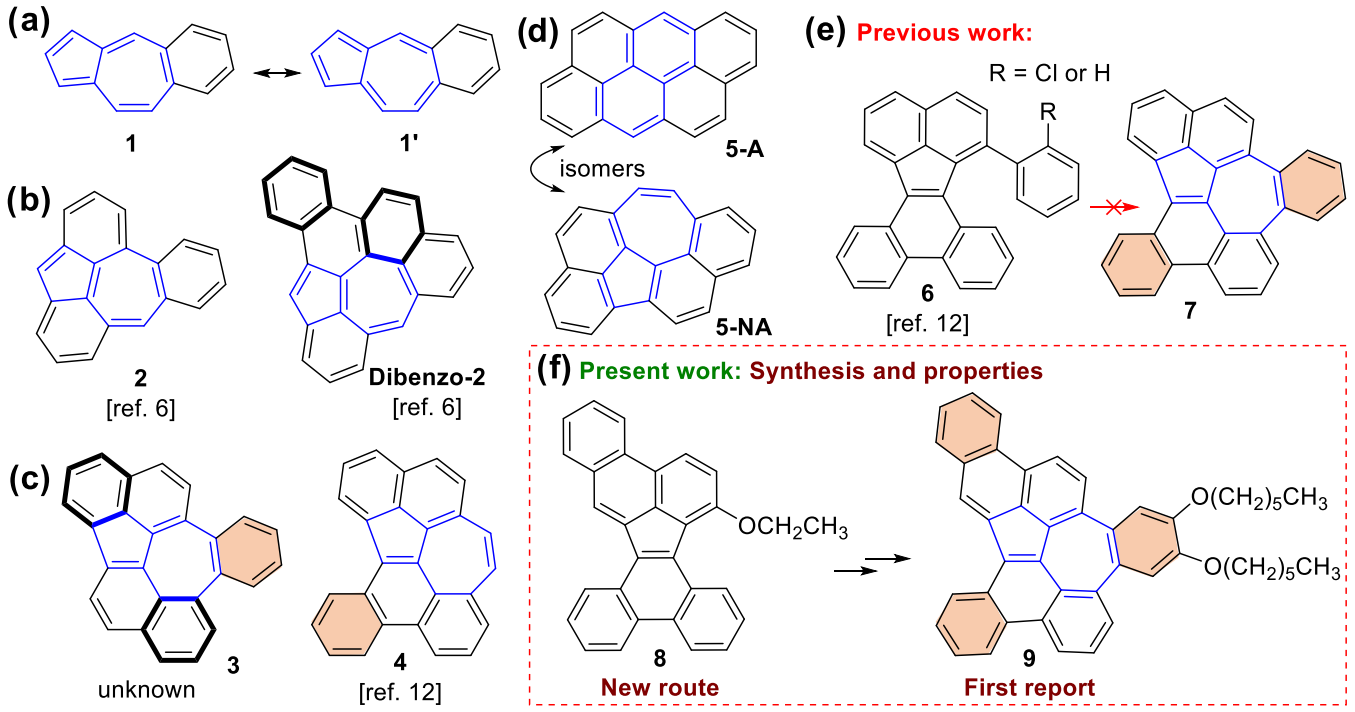

Figure 1. (a) Resonance forms **1** and **1′** for benzo[*f*]azulene. (b) Feng's benzo-extended cyclohepta[*def*]fluorene **2** and its dibenzannulated derivative **Dibenzo-2**. (c) Structures **3** and **4** are the constitutional isomers of **Dibenzo-2**. (d) Isomeric **5-NA** is the non-alternant isoelectronic (18πe) motif of alternant *peri*-acenoacene **5-A**. (e) Unsuccessful attempts to synthesize **7** from **6** bearing different substituents. (f) Target phenanthroacephenanthrylene isomer **8**, which was used to construct non-benzenoid PAH **9** in multisteps.

Scheme 1. Synthesis of 8

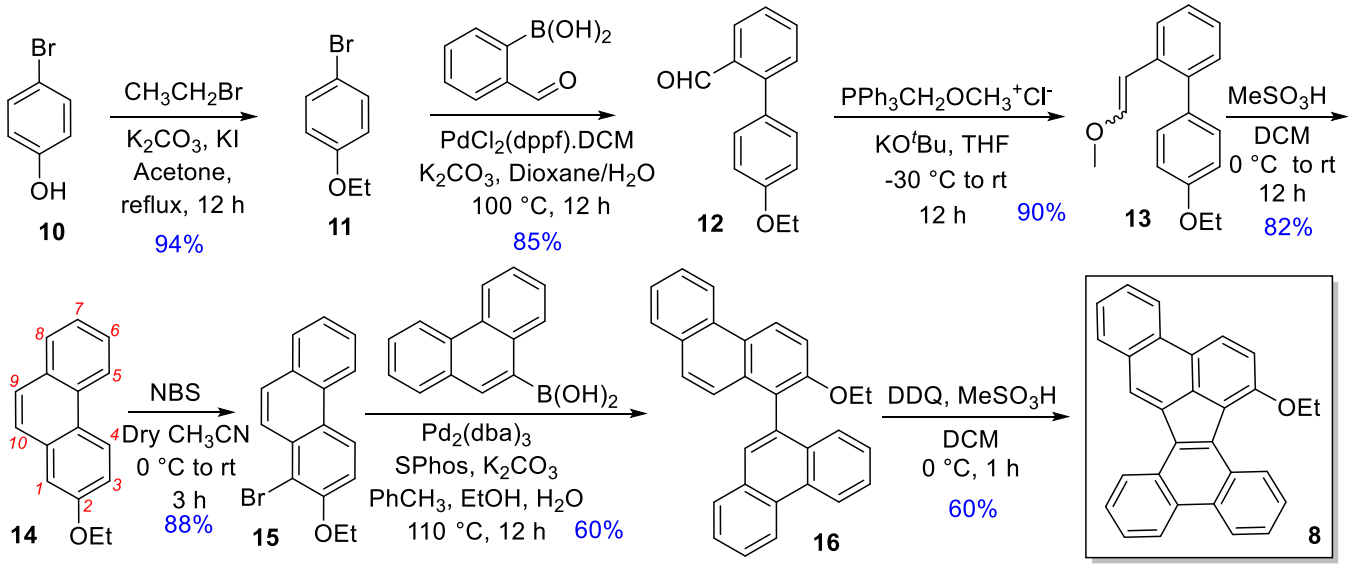

received seldom attention due to the lack of suitable synthetic strategies.[21]

2. RESULTS AND DISCUSSION

2.1. Syntheses. Synthesis of unsubstituted[21] and 8-substituted[22] phenanthro[9,10-*e*]acephenanthrylenes was known. PAP is a phenanthrene-fused acephenanthrylene (AP), which is a cyclopentannulated-PAH (CP-PAH),[23] and parent AP was known since 1985.[24] Despite various synthetic approaches for substituted AP motifs,[25−28] herein, we adopted an oxidative aromatic coupling[29] route to synthesize 1-ethoxy[9,10-*e*]PAP **8** in order to use it to construct diphenanthro-benzo[*f*]azulene **9** with [30]π-electrons in the periphery, which may be viewed as a tribenzo-fused **5-NA**. The ground-state electronic properties of **9** were studied by both experimental and computational approaches.

Commercially available bromophenol **10** was first converted to **11**, which was subjected to a Pd-catalyzed Suzuki reaction with (2-formylphenyl)boronic acid to afford **12** in 85% yield (Scheme 1). Compound **12** was subsequently converted to **13** by methyltriphenylphosphonium chloride, and then **13** was treated with methanesulfonic acid to give **14**. Compound **14** could be regioselectively brominated with *N*-bromosuccini-

https://doi.org/10.1021/acs.joc.2c03103
J. Org. Chem. 2023, 88, 5473−5482

Scheme 2. Synthesis of 9

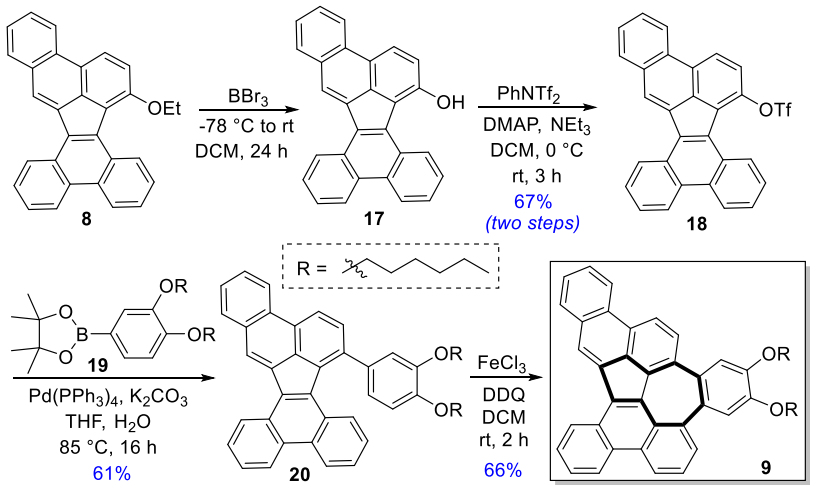

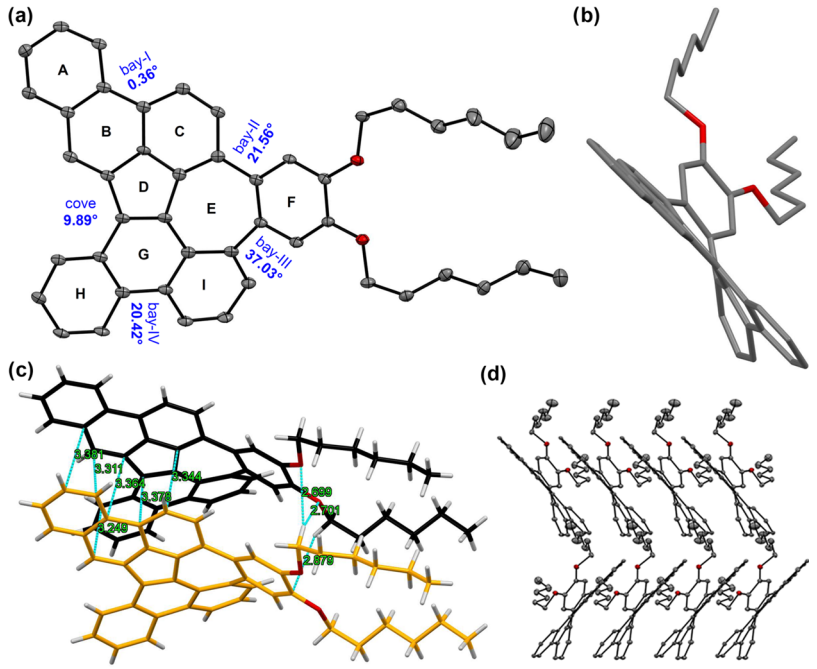

Figure 2. (a) ORTEP drawing of **9** at 30% probability of ellipsoids (hydrogens omitted). (b) Side view of **9** showing a saddle-like structure. (c) Intermolecular close C−C contacts, and hydrogen bonding distance (in Å) for **9**. (d) Herringbone packing arrangement of **9** showing columnar 1D-stacks.

mide to afford **15** in 88% yield. A Pd^0-catalyzed Suzuki reaction between **15** and 9-phenanthracenylboronic acid gave **16**, which underwent intramolecular oxidative coupling[20] in dry dichloromethane (DCM) at 0 °C with 2,3-dichloro-5,6-dicyano-1,4-benzoquinone (DDQ)[29b] and $MeSO_3H$ to form 1-ethoxy-[9,10-*e*]PAP **8**. Formation of CP-PAH **8** seems reasonable, since five-membered ring formation is thermodynamically more favorable over a six-membered ring, and the central ring of phenanthrene bearing strong olefinic C−C double bond character is also usually more reactive toward aromatic electrophilic substitutions. Furthermore, we envisaged that replacing the 1-ethoxy group of **8** with the electron-rich 3,4-dialkoxyphenyl group[30] and treating the resulting phenyl derivative under Scholl reaction[29] conditions may afford desired product **9**, as the 1-position of 2-ethoxyphenanthrene is reactive toward aromatic electrophilic substitution, which is evident from the conversion of **14** to **15** (Scheme 1).

Boron tribromide (BBr_3)-mediated dealkylation of **8** in dry DCM afforded **17**, which was converted to triflate **18** in 67% yield over two steps (Scheme 2). The Suzuki reaction between triflate **18** and pinacolboronate **19** with two hexyloxy substituents afforded **20** in 61% yield. The Scholl-type oxidative dehydrogenative aromatic coupling[20] of precursor **20** with anhydrous $FeCl_3$/DDQ[21,31] resulted in formation of desired product **9** in 66% yield with no significant byproducts, which was unambiguously confirmed by single-crystal X-ray diffraction (SCXRD) analyses. Based on the literature reports on Scholl-type oxidative aromatic coupling using DDQ,[32] the radical cation pathway could plausibly contribute to the formation of both products **8** and **9**, as proposed in the Supporting Information (Figure S30). Noticeably, when

https://doi.org/10.1021/acs.joc.2c03103
J. Org. Chem. 2023, 88, 5473−5482

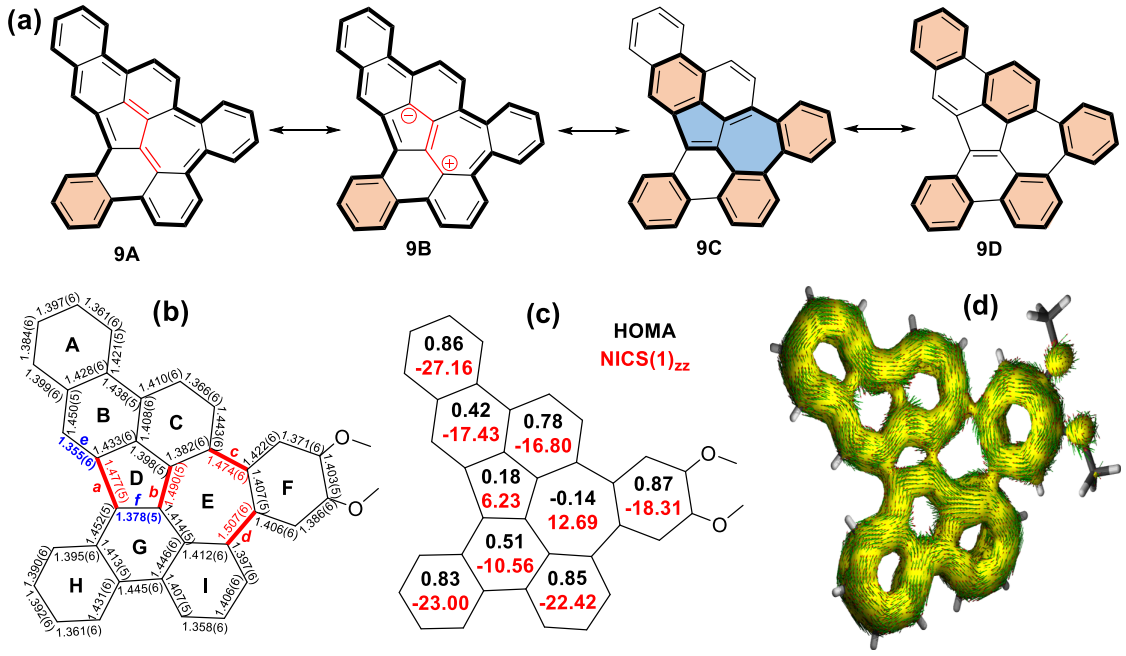

Figure 3. (a) Representative canonical forms of **9**. (b) C_{sp^2}–C_{sp^2} bond lengths (in Å) for **9** with a, b, c, d bonds suggesting weak π-bond character while e and f bonds suggested strong *trans*-diene character. (c) $NICS(1)_{zz}$ and HOMA indices of **9**. (d) ACID isosurface (0.02) of **9** showing π-contribution including the current density vectors (clock-wise currents are diatropic).

compared to Takasu's approach,[12] installation of alkoxy chains on the benzene ring was found to be quite essential to promote the Scholl cyclization-induced heptagon ring formation, which is in line with Miao's approach.[30b]

2.2. X-Ray Crystallography and Aromaticity Analyses. Single crystals of **9**, suitable for SCXRD analysis, were obtained by slow evaporation of tetrahydrofuran/toluene at ambient conditions. The benzene ring F of **9** was twisted from planarity by 21.5 and 37.0° dihedral angles at the bay-II and bay-III regions, respectively, due to steric congestions among C–E–F and I–E–F π-rings, thus resulting in a saddle-like structure (Figure 2a,b). While the dihedral angle at the bay-I (0.36°) region suggests an insignificant twist, the bay-IV region is twisted by 20.4°, as measured from the torsional angle of H–G–I rings. The cove region involving B–D–G–H rings with a dihedral angle of 9.9°, including the significant twists at the bay-II to IV regions, induced sufficient strain in the azulene unit that resulted in significant bond-length alternation (BLA), ranging from 1.378(5) to 1.507(6) Å (Figure 3b), compared to pristine azulene.[33] Furthermore, the twisted backbone forms triple helical substructures for **9** bearing *P,M,P*- and *M,P,M*-configurations in the crystal packing (Figure S21). As shown in Figure 2c, molecules of **9** were stacked cofacially within the crystal lattice with several short C–C contacts ranging from 3.249 to 3.381 Å, implying strong intermolecular π–π interactions. The C–H···π (2.879 Å) and intermolecular hydrogen bonding interactions (2.699–2.701 Å) between the alkoxy side chains and conjugated skeleton, including the strong intermolecular π–π interactions, enabled a one-dimensional columnar stack for **9** forming herringbone packing motifs (Figure 2d).

Compound **9** may be viewed in four different Kekulé forms **9A**–**9D** and regarded as a formally 30π-aromatic system **9A** with the central *trans*-diene arrangement (Figure 3a). A zwitterionic azulene in the form of **9B** with one Clar sextet[34] (shown in an orange hexagon, Figure 3a), and another neutral form **9C** with four Clar sextets and one azulene-like C_{sp^2}–C_{sp^2} alternate double/single bond arrangement for the central 5–7 π-rings (shaded in blue color) can be drawn. Additionally, the **9D** form can be drawn with five Clar sextets and a *trans*-diene arrangement at the cove region, which misses the azulene-like C_{sp^2}–C_{sp^2} bond-length arrangement in central 5–7 fused rings. Crystal structure analyses suggested that the central azulene unit did not show near equal bond-length distributions (1.378(5)–1.507(6) Å) for C_{sp^2}–C_{sp^2} bonds, like the typical parent azulene bond-length distributions (1.387–1.404 Å),[33] whereas homogeneous bond-length distributions for five outer six-membered rings A (avg. 1.398 Å), C (avg. 1.401 Å), F (avg. 1.399 Å), I (avg. 1.404 Å), and H (avg. 1.397 Å) suggested localization of benzene aromaticity (Figure 3b). The observation was further supported by the harmonic oscillator model of aromaticity (HOMA) analyses for the DFT optimized closed-shell ground-state structure of **9**,[35] implying A (0.86), C (0.78), F (0.87), I (0.85), and H (0.83) rings to be aromatic with non-significant BLA, while B and G rings are weakly aromatic (Figure 3c).[36] The small HOMA values of the D (0.18) and E (−0.14) rings suggested large BLA, indicating non-aromaticity of the azulene unit, though a negative HOMA value[37] of ring E prompted us to calculate the nucleus-independent chemical shift [$NICS(1)_{zz}$ values][38] for **9** to confirm whether heptagon E would show antiaromaticity!

$NICS(1)_{zz}$ indices for the ground state of **9** were found to be consistent with the aromatic nature of A (−27.16), C (−16.80), F (−18.31), I (−22.42), and H (−23.00) rings, showing large negative $NICS(1)_{zz}$ indices (Figure 3c). However, positive $NICS(1)_{zz}$ indices of rings D (6.23) and E (12.69) of **9** stimulated us to study the ring currents by the anisotropy of the induced current density (ACID) calculations.[39] Strong diatropic ring currents for A–B–C and H–G–I phenanthrene substructures with some localization of diatropic ring currents for A, F, I, and H benzenoid rings (Figure 3d, and see Figure S28 for a high-resolution image)

https://doi.org/10.1021/acs.joc.2c03103
J. Org. Chem. 2023, 88, 5473–5482

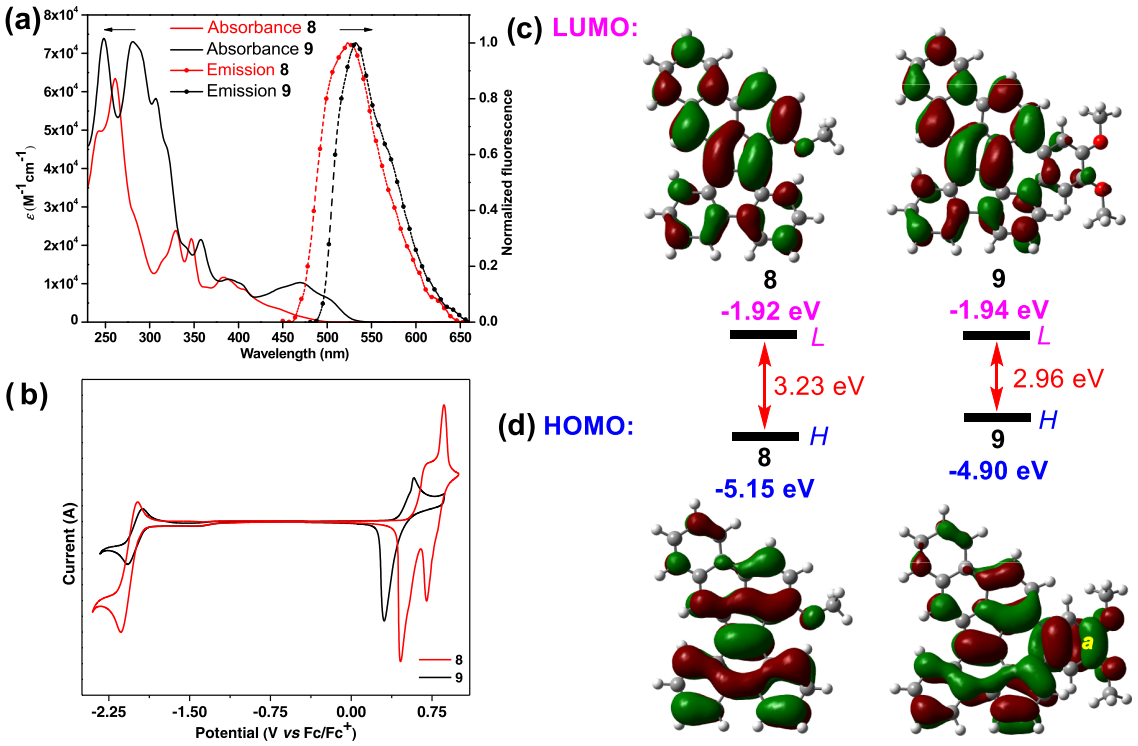

Figure 4. (a) UV−vis absorption (straight line) and emission (dash-dotted line) spectra of **8** and **9**, with inset picture under visible and 365 nm light irradiation. (b) Cyclic voltammograms for **8** and **9**. DFT optimized (c) LUMO and (d) HOMO profiles of **8** and **9**.

were observed. The large C_{sp^2}−C_{sp^2} bond lengths for a (1.477(5) Å), b (1.490(5) Å), c (1.474(6) Å), and d (1.507(6) Å) bonds of **9** suggested weak C−C π-bond character, which is in line with the absence of any ring currents above these bonds, clearly confirming D and E rings to be non-aromatic (i.e., formal azulene unit[2d,a]). The small positive $NICS(1)_{zz}$ values over the formal azulene unit could be a result of the diatropic ring currents of surrounding phenanthrene/benzene rings inducing some paratropic effect.[40,2e] Our results clearly indicated that resonance form **9D** with the five Clar sextets and a *trans*-diene (C=C bonds e: 1.355(6) Å, and f: 1.378(5) Å) arrangement in the cove region should majorly contribute to the ground state of **9** with the diminished zwitterionic contribution of the true azulene unit.

2.3. Optical and Electrochemical Properties. The UV−vis absorption spectra were measured in DCM at room temperature to study the optical properties of **8** and **9** (Figure 4a). Compound **8** displayed high energy absorption bands in the UV region[21] (absorption maxima: λ_{max} = 241 nm, ε = 49 620 M^{-1} cm^{-1}; λ_{max} = 261 nm, ε = 63 400 M^{-1} cm^{-1}; λ_{max} = 330 nm, ε = 23 980 M^{-1} cm^{-1}; λ_{max} = 346 nm ε = 21 830 M^{-1} cm^{-1}) and low energy band (λ_{max} = 382 nm, ε = 11 730 M^{-1} cm^{-1}; λ_{max} = 406 nm, ε = 8540 M^{-1} cm^{-1}) with a weak band at 446 nm due to HOMO → LUMO transition (theoretical λ_{max} = 452 nm, oscillator strength (f) = 0.0772, according to TDDFT calculations shown in Table S3), which was extended to 500 nm in the visible region. The absorption profile of compound **9** was red-shifted in comparison to **8**, with intense bands in the higher energy region (λ_{max} = 248 nm, ε = 74 100 M^{-1} cm^{-1}; λ_{max} = 280 nm, ε = 73 150 M^{-1} cm^{-1}) and low intense bands in the lower energy regions with absorption maxima λ_{max} = 358 nm (ε = 21 500 M^{-1} cm^{-1}) and 470 nm (ε = 10 300 M^{-1} cm^{-1}), accompanied with a shoulder band at λ_{max} = 500 nm (ε = 6350 M^{-1} cm^{-1}) extending till 540 nm due to extension of π-conjugation. While the lowest energy absorption of **9** at 470 nm may be attributed to the HOMO → LUMO transition, according to TDDFT calculations (theoretical λ_{max} = 489 nm, f = 0.1559, Table S4), the shoulder band red-shifted on changing solvent polarity from non-polar hexane to DCM to more polar dimethyl sulfoxide (Figure S22), suggesting that the lowest energy transition may have weak charge-transfer (CT) character.

The optical HOMO−LUMO energy gaps, measured from the absorption onsets, were found to be 2.54 and 2.33 eV for **8** and **9**, respectively (Figure 4a). Compounds **8** and **9** displayed fluorescence in DCM solution, with an emission maximum of **8** at λ_{max} = 523 nm (excited at 430 nm), and for **9**, the emission maximum was observed at λ_{max} = 532 nm (excited at 510 nm, Figure 4a). The fluorescence quantum yields (Φ) for **8** and **9** in DCM solution were 8.9 and 41.8%, respectively (with fluorescein and rhodamine 6G as standards[41] for **8** and **9**, in 1 μM ethanol, respectively). The molecular orbital profiles of **9** (Figure 4c,d) suggested that the orbital coefficients are majorly distributed over the PAP unit, suggesting the fluoroanthene[23b] subunit of **9** as the main contributor to the observed optoelectronic properties and not the azulene subunit, which is unlike other azulene-containing PAHs with greater azulene-like character[2b,5a,6,11a,12] and consistent with the SCXRD/aromaticity analyses (Figure 3b−d).

Cyclic voltammograms of **8** and **9** in DCM solution displayed reversible reduction waves with nearly identical half-wave potentials at $E^{red}_{1/2}$ = −2.05 and −2.00 V (vs Fc/Fc^+), respectively, while **8** exhibited a quasi-reversible oxidation wave at E^{ox1}_{peak} = 0.70 V (appearing at a lower oxidation potential than unsubstituted **8**),[21] and **9** appeared at a relatively lower oxidation potential E^{ox1}_{peak} = 0.58 V than **8** (Figure 4b). However, the reason for such peculiar shapes of the oxidation events is unclear, and they are similar to unsubstituted **8**.[21] The

https://doi.org/10.1021/acs.joc.2c03103
J. Org. Chem. 2023, 88, 5473−5482

electrochemical energy gaps, estimated from the first onset redox potentials, of **8** and **9** were 2.55 eV (HOMO: −5.38 eV, LUMO: −2.83 eV) and 2.34 eV (HOMO: −5.20 eV, LUMO: −2.86 eV), respectively. The nearly unaffected reversible reduction potentials for **8** and **9** could be explained by their respective frontier molecular orbital (FMO) profiles, showing that the distribution of LUMO coefficients of **9** remained almost similar to that of PAP **8** (Figure 4c). It suggested that electron density was mostly distributed over the PAP backbone of **9**, and thus, the reduction potentials of **8** and **9** were nearly identical, in line with the calculated LUMO of **9** (−1.94 eV), which is only marginally stabilized compared to that of **8** (−1.92 eV, Figure 4c). The FMO profiles of **Parent-9** (Figure S23) suggested that two *ortho*-dialkoxy substituents for **9** may destabilize the HOMO more than the two *para*-alkoxy substituents (**9-Para**, Figure S23) and thus could result in a smaller HOMO−LUMO gap for **9**. Accordingly, the theoretical HOMO of **9** increased to −4.90 eV, in comparison to **8** (−5.15 eV), and the large orbital amplitudes on ring F carbons of **9** (C═C bond with a large amplitude is labeled as *a* for **9**, Figure 4d) attached to two hexyloxy groups suggested its electron-donating ability to the PAP core of **9** with the electron-accepting[42] CP-PAH subunit with appreciable LUMO coefficients, likely explaining the CT absorption band at ∼500 nm (Figures S22 and 4a). Hence, **9** was relatively easily oxidized at a lower potential than **8**, but their reduction potentials remained identical. The theoretical HOMO−LUMO energy gap of **9** was found to be 0.27 eV smaller than that of **8**, which is similar to the decreasing trend observed for optical and electrochemical energy gaps of **8** and **9**.

3. CONCLUSIONS

In summary, a new synthetic approach for 1-substituted PAP isomer **8** and its conversion to fully conjugated PAH **9** bearing fused 5−7-membered rings was described utilizing Scholl-type oxidation, which was seldom applied to construct 7-membered ring-containing PAHs.[1,2a,c,d,43] The synthetic approach has potential to synthesize some of the hitherto unknown structural isomers of PAP, and working toward this direction is currently underway in our lab. Single-crystal analyses, HOMA, NICS, and ACID calculations suggested localization of Clar sextets in the π-backbone of **9**, which resulted in the non-aromaticity of the central azulene unit. The UV−vis absorption profile of **9** was red-shifted in comparison to **8**, suggesting an extension of π-conjugation with weak intramolecular CT character. CV analyses suggested that the smaller HOMO−LUMO energy gap of **9** than that of **8** could be due to the destabilization of the HOMO energy level, while the LUMO level remained nearly unaffected, which was supported by their identical reduction potentials, and the experimental results were in line with DFT calculations.

4. EXPERIMENTAL SECTION

4.1. General Information. Chemicals and reagents were purchased from local and international commercial suppliers (Merck, GLR innovations, BLDpharm) and used without further purification. Compound **19**, 2-(3,4-bis(hexyloxy)phenyl)-4,4,5,5-tetramethyl-1,3,2-dioxaborolane, was synthesized according to the reported procedure.[44] Thin-layer chromatography (TLC) was performed using precoated silica plates purchased from Merck (silica gel 60 PF254, 0.25 mm). Column chromatography was performed using a silica gel 100−200 mesh. NMR spectra were recorded in $CDCl_3$ (Eurisotop) at room temperature, on a JEOL JNM-ECS400 spectrometer at operating frequencies of 400 MHz (^{1}H) or 100 MHz (^{13}C), as indicated in the individual spectrum. Chemical shifts (δ) are given in ppm relative to residual solvent (chloroform δ = 7.26 for ^{1}H, and, δ = 77.16 for proton-decoupled ^{13}C NMR), and coupling constants (J) are expressed in Hz. Multiplicity is tabulated as s for singlet, d for doublet, dd for doublet of doublet, t for triplet, q for quartet, and m for multiplet. Structural assignments were made with additional information from gCOSY and gNOESY experiments. High-resolution mass spectra (HRMS) were recorded using electron spray ionization (ESI) and atmospheric pressure chemical ionization (APCI) methods on a Waters (XEVO G2-XS QTOF) mass spectrometer. UV−vis spectra were recorded in a JASCO V-770 spectrophotometer. Fluorescence spectra were recorded on a PerkinElmer LS55 fluorescence spectrophotometer. Cyclic voltammetry was performed on a CHI-1110C instrument with a glassy carbon working electrode, a Pt wire counter electrode, and a Ag wire as a pseudo-reference electrode in a DCM/Bu_4NPF_6 solvent/electrolyte couple at room temperature using a scan rate of 50 mV s^{-1}. The potential was externally calibrated against the ferrocene/ferrocenium couple (0.43 V). Melting points were determined using a BIBBY-SMP30 melting point analyzer.

4.2. Computational Methods. Density functional theory (DFT) calculations were performed using the Gaussian 09 Rev. B.01 package at the B3LYP/6-31G(d) level of theory in the gas phase. During optimization, the ethyl and hexyl chains of **8** and **9** were replaced by a methyl group. HOMA values of **9** were calculated using the Multiwfn package for the optimized singlet closed-shell ground-state structure.[45] NICS values of ground-state structure **9** were estimated at the same level of theory using the standard GIAO procedure, and the reported $NICS(1)_{zz}$ indices were averaged by the two positions (above and below the plane).[38] The ACID plot (π-only) was calculated following Herges's method.[39] Excitation energies of **8** and **9** were computed using time-dependent DFT (TDDFT) for the singlet closed-shell structures in the gas phase. Molecular orbital contributions of **8** and **9** were determined using the GaussSum 3.0 package.[46]

4.3. Syntheses. *4.3.1. 1-Bromo-4-ethoxybenzene (**11**).* To a suspension of 4-bromophenol **10** (2 g, 11.6 mmol), K_2CO_3 (2.4 g, 17.3 mmol), and KI (2.2 g, 13.3 mmol) in acetone was added bromoethane (1.4 mL, 18.5 mmol), and the mixture was heated at reflux for 12 h using an oil bath, under a nitrogen atmosphere. After being cooled to room temperature, volatile organics were removed under reduced pressure and water was added. The mixture was extracted with EtOAc (3 × 30 mL), dried over anhydrous Na_2SO_4, and filtered. The organic layer was removed under reduced pressure, and the crude product was purified by silica gel column chromatography with hexane as an eluent to obtain **11** as a colorless viscous oil (2.18 g, 94%): R_f = 0.38 (hexanes); ^{1}H NMR (400 MHz, $CDCl_3$) δ 7.38−7.34 (m, 2H), 6.79−6.74 (m, 2H), 3.99 (q, J = 7.0 Hz, 2H), 1.40 (t, J = 7.1 Hz, 3H); $^{13}C\{^1H\}$ NMR (100 MHz, $CDCl_3$) δ 158.1, 132.3, 116.3, 112.74, 63.8, 14.8; HRMS (APCI) m/z: M^+ Calcd for C_9H_9BrO 199.9837, found 199.9837.

*4.3.2. 4′-Ethoxy-[1,1′-biphenyl]-2-carbaldehyde (**12**).* An oven-dried thick-walled glass tube was charged with **11** (1 g, 4.97 mmol), 2-formylphenylboronic acid (895 mg, 5.97 mmol), K_2CO_3 (3.44 g, 24.8 mmol), 1,4-dioxane (6 mL), and water (0.6 mL) and purged with nitrogen for 30 min. The catalyst $PdCl_2$(dppf).DCM complex (82 mg, 2 mol %, DCM = dichloromethane) was added. After sealing the glass vial, the reaction mixture was warmed to 100 °C using an oil bath. After 12 h, the flask was cooled to room temperature, volatile organics were removed under reduced pressure, water was added, and the resulting mixture was extracted with EtOAc (3 × 50 mL). The organic layer was dried over Na_2SO_4, filtered, and evaporated under reduced pressure to afford a crude residue, which was purified by silica gel column chromatography (hexanes) to give compound **12** as a brown solid (960 mg, 85% yield): R_f = 0.59 (hexanes); mp 66−67 °C; ^{1}H NMR (400 MHz, $CDCl_3$) δ 10.00 (s, 1H), 8.00 (dd, J = 7.8, 1.1 Hz, 1H), 7.62 (td, J = 7.5, 1.5 Hz, 1H), 7.49−7.41 (m, 2H), 7.32−7.27 (m, 2H), 7.01−6.97 (m, 2H), 4.10 (q, J = 6.9 Hz, 3H), 1.46 (t, J = 7.0 Hz, 4H); $^{13}C\{^1H\}$ NMR (100 MHz, $CDCl_3$) δ 192.9, 159.1, 145.8,

https://doi.org/10.1021/acs.joc.2c03103
J. Org. Chem. 2023, 88, 5473−5482

133.8, 133.6, 131.4, 130.9, 129.9, 127.7, 127.4, 114.5, 63.7, 14.9; HRMS (ESI) m/z:$[M + H]^+$ Calcd for $C_{15}H_{15}O_2$ 227.1072, found 227.1063.

*4.3.3. 2-Ethoxyphenanthrene (**14**).* A solution of *t*-BuOK (1.4 g, 12.4 mmol) in dry THF (12 mL) was added dropwise to a solution of methyltriphenylphosphonium chloride (3.18 g, 9.3 mmol) in 15 mL of anhydrous THF under nitrogen at −30 °C. The mixture was stirred at −30 °C for 2 h, and then a solution of **12** in dry THF (10 mL) was added dropwise. The reaction mixture was stirred for 12 h at room temperature and then quenched with a saturated solution of NH_4Cl. The volatile organics were evaporated, and the mixture was extracted with DCM (3 × 50 mL). The organic layer was dried over anhydrous Na_2SO_4 and the solvent was subsequently removed under reduced pressure. The residue was passed through a pad of silica gel (hexanes/EtOAc, 95:5) to give a mixture of the *E*- and *Z*-isomers of **13** as a viscous yellow oil (1.42 g, 90%), and it was used directly in the next step.

To a solution of **13** (775 mg, 3.05 mmol) in dry DCM (10 mL) was added methanesulfonic acid (0.2 mL) under nitrogen at 0 °C, and the solution was stirred for 3 h at room temperature. The progress of the reaction was monitored by TLC. As the starting material was consumed, a saturated solution of $NaHCO_3$ (10 mL) was added and stirred continuously for 10 min, and the reaction mixture was extracted with DCM (3 × 30 mL). The organic layer was dried over anhydrous Na_2SO_4, filtered, and evaporated under reduced pressure. The residue was subjected to silica gel column chromatography (hexanes/EtOAc, 98:2) to give title product **14** as a white solid (560 mg, 82%): R_f = 0.48 (5% EtOAc/hexanes); mp 103−104 °C; ^{1}H NMR (400 MHz, $CDCl_3$) δ 8.59 (d, J = 8.8 Hz, 2H), 7.86 (dd, J = 8.0, 0.9 Hz, 1H), 7.72 (d, J = 8.9 Hz, 1H), 7.65 (d, J = 9.1 Hz, 1H), 7.63−7.60 (m, 1H), 7.56−7.50 (m, 1H), 7.29 (dd, J = 9.0, 2.7 Hz, 1H), 7.25 (d, 1H), 4.21 (q, J = 7.0 Hz, 2H), 1.51 (t, J = 7.0 Hz, 3H); ^{13}C{^{1}H} NMR (100 MHz, $CDCl_3$) δ 157.7, 133.5, 131.1, 130.5, 128.6, 127.5, 126.7, 126.6, 125.6, 124.6, 124.3, 122.2, 117.5, 109.4, 63.7, 15.0; HRMS (ESI) m/z: M^+ Calcd for $C_{16}H_{15}O$ 223.1123, found 223.1118.

*4.3.4. 1-Bromo-2-ethoxyphenanthrene (**15**).* To a suspension of **14** (550 mg, 2.5 mmol) in dry acetonitrile (20 mL) was added NBS (530 mg, 3 mmol) at 0 °C, and the reaction mixture was stirred for 3 h at room temperature. The progress of the reaction was monitored by TLC, and once the reactant was consumed, the reaction mixture was quenched with a saturated solution of sodium thiosulfate. The volatile organics were removed using a rotatory evaporator, and the resulting mixture was extracted with dichloromethane (3 × 30 mL), dried over sodium sulfate, and filtered. The organic layer was evaporated, and the crude residue was purified by silica gel column chromatography (hexanes) to give title product **15** as a yellow solid (660 mg, 88% yield): R_f = 0.4 (5% EtOAc/hexanes); mp 140−141 °C; ^{1}H NMR (400 MHz, $CDCl_3$) δ 8.63 (d, J = 8.9 Hz, 1H), 8.59 (d, J = 8.2 Hz, 1H), 8.24 (d, J = 9.2 Hz, 1H), 7.89 (dd, J = 7.8, 1.2 Hz, 1H), 7.82 (d, J = 9.2 Hz, 1H), 7.65 (ddd, J = 8.4, 7.1, 1.5 Hz, 1H), 7.60−7.55 (m, 1H), 7.34 (d, J = 9.1 Hz, 1H), 4.30 (q, J = 7.0 Hz, 2H), 1.56 (t, J = 7.0 Hz, 3H); ^{13}C{^{1}H} NMR (100 MHz, $CDCl_3$) δ 154.1, 132.2, 130.9, 130.2, 129.0, 128.7, 127.2, 126.4, 126.0, 125.3, 123.2, 122.4, 113.8, 111.3, 65.7, 15.1; HRMS (ESI) m/z: $[M + H]^+$ Calcd for $C_{16}H_{14}OBr$ 301.0228, found 301.0210.

*4.3.5. 2-Ethoxy-1,9′-biphenanthrene (**16**).* An oven-dried thick-walled glass tube was charged with phenanthren-9-ylboronic acid (445 mg, 2 mmol), 1-bromo-2-ethoxyphenanthrene **15** (500 mg, 1.66 mmol), K_2CO_3 (1.15 g, 8.30 mmol), toluene (8 mL), ethanol (1.5 mL), and water (1.5 mL), and the mixture was purged with nitrogen for 30 min. $Pd_2(dba)_3$ (75 mg, 5 mol %) and SPhos (136 mg, 20 mol %) were added subsequently under nitrogen, and the glass vial was sealed before being warmed to 110 °C for 12 h using an oil bath. After cooling the reaction mixture to room temperature, toluene was evaporated under reduced pressure, water was added, and the reaction mixture was extracted with DCM. The organic layer was dried over sodium sulfate and then evaporated to dryness. The crude mixture was subjected to silica gel column chromatography (hexanes/EtOAc, 95:5) to afford title product **16** as a white solid (400 mg, 60% yield): R_f = 0.33 (5% EtOAc/hexanes); mp 186-187 °C; ^{1}H NMR (400 MHz, $CDCl_3$) δ 8.85−8.80 (m, 3H), 8.71 (d, J = 8.4 Hz, 1H), 7.92 (d, J = 7.9 Hz, 1H), 7.79 (d, J = 7.8 Hz, 1H), 7.74−7.70 (m, 2H), 7.65 (dt, J = 5.8, 4.5 Hz, 3H), 7.54 (dd, J = 10.5, 5.0 Hz, 2H), 7.46 (d, J = 9.2 Hz, 1H), 7.43−7.35 (m, 2H), 7.24 (d, 1H), 4.18−4.04 (m, 2H), 1.07 (t, J = 7.1 Hz, 3H); ^{13}C{^{1}H} NMR (100 MHz, $CDCl_3$) δ 155.3, 133.7, 133.0, 132.3, 132.0, 130.9, 130.5, 130.4, 129.2, 128.8, 128.6, 127.5, 127.0, 126.8, 126.7, 126.6, 126.4, 125.9, 125.5, 125.0, 124.8, 124.0, 122.8, 122.7, 122.4, 114.0, 65.0, 14.9; HRMS (APCI) m/z: M^+ Calcd for $C_{30}H_{23}O$ 399.1749, found 399.1735.

*4.3.6. 1-Ethoxyphenanthro[9,10-e]acephenanthrylene (**8**).* To a solution of **16** (200 mg, 0.5 mmol) in dry DCM (10 mL) was added methanesulfonic acid (1 mL) at 0 °C and then added 2,3-dichloro-5,6-dicyanobenzoquinone (DDQ, 340 mg, 1.5 mmol). The reaction mixture was left to stir for 30 min at 0 °C, quenched with a saturated aq. $NaHCO_3$ solution, and then extracted with dichloromethane (3 × 20 mL). The combined organic phase was dried over anhydrous sodium sulfate, and then the solvent was removed under reduced pressure. The residue was purified by silica gel column chromatography (hexanes/EtOAc, 98:2) to afford title product **8** as a yellow solid (120 mg, 60% yield): R_f = 0.33 (5% EtOAc/hexanes); mp 235−236 °C; ^{1}H NMR (400 MHz, $CDCl_3$) δ 10.01−9.91 (m, 1H), 9.04 (d, J = 8.1 Hz, 1H), 8.92 (s, 1H), 8.79 (t, J = 8.2 Hz, 2H), 8.61 (d, J = 8.1 Hz, 1H), 8.50 (d, J = 8.8 Hz, 1H), 8.13 (d, J = 7.8 Hz, 1H), 7.80−7.74 (m, 1H), 7.73−7.60 (m, 5H), 7.44 (d, J = 8.8 Hz, 1H), 4.43 (q, J = 7.0 Hz, 2H), 1.70 (t, J = 6.9 Hz, 3H); ^{13}C{^{1}H} NMR (100 MHz, $CDCl_3$) δ 153.8, 138.1, 135.5, 133.6, 132.8, 131.3, 131.2, 131.0, 130.5, 130.3, 130.0, 129.8, 129.3, 127.5, 127.2, 127.2, 126.5, 126.0, 125.9, 125.9, 125.1, 125.0, 123.0, 122.4, 121.8, 116.5, 65.9, 15.1; HRMS (APCI) m/z: M^+ Calcd for $C_{30}H_{21}O$ 397.1592, found 397.1585.

*4.3.7. Phenanthro[9,10-e]acephenanthrylen-1-yl trifluoromethanesulfonate (**18**).* To a solution of **8** (93 mg, 0.23 mmol) in anhydrous DCM (6 mL) was added BBr_3 (1.0 M in DCM, 0.93 mL, 0.93 mmol) at −78 °C, and the reaction mixture was stirred at room temperature for 12 h. After cooling the reaction mixture to 0 °C, water was added, and then it was extracted with dichloromethane (3 × 30 mL). The combined organic layer was dried over anhydrous sodium sulfate and concentrated to afford a residue containing intermediate **17** (295 mg, yellow solid), which was used for the next step without purification.

To a solution of crude **17** in anhydrous DCM (10 mL) was added 4-dimethylaminopyridine (8.8 mg, 10 mol %) and triethyl amine (0.2 mL, 1.44 mmol), and the reaction mixture was stirred for 30 min at 0 °C, followed by addition of *N*-phenyl-bis-(trifluoromethanesulfonimide) (283 mg, 0.8 mmol). Then, the reaction mixture was stirred for 3 h at room temperature, before adding water and following extraction with DCM (3 × 20 mL). The combined organic phase was dried over anhydrous sodium sulfate and the solvent was removed under reduced pressure. The residue was purified by column chromatography on silica gel (hexanes/DCM, 99:1) to afford **18** as a yellow solid (79 mg, 67% yield over two steps): R_f = 0.22 (5% EtOAc/hexanes); mp 208-209 °C; ^{1}H NMR (400 MHz, $CDCl_3$) δ 8.93 (ddd, J = 6.1, 4.2, 2.7 Hz, 2H), 8.85 (s, 1H), 8.77 (dd, J = 11.9, 4.7 Hz, 2H), 8.61 (d, J = 8.1 Hz, 1H), 8.53 (d, J = 8.9 Hz, 1H), 8.14−8.08 (m, 1H), 7.79−7.66 (m, 7H); ^{13}C{^{1}H} NMR (100 MHz, $CDCl_3$) δ 141.9, 135.4, 134.9, 134.0, 134.0, 133.9, 131.8, 131.2, 130.8, 129.9, 129.0, 128.7, 128.6, 128.4, 127.8, 127.7, 127.5, 127.5, 127.1, 127.1, 127.0, 126.2, 125.0, 124.5, 123.7, 123.5, 123.1, 122.6; HRMS (ESI) m/z: M^+ Calcd for $C_{29}H_{15}F_3O_3S$ 500.0694, found 500.0691.

*4.3.8. 1-(3,4-Bis(hexyloxy)phenyl)phenanthro[9,10-e]-acephenanthrylene (**20**).* An oven-dried glass tube was charged with **18** (80 mg, 0.16 mmol), 2-(3,4-bis(hexyloxy)phenyl)-4,4,5,5-tetramethyl-1,3,2-dioxaborolane **19** (72 mg, 0.18 mmol), K_2CO_3 (111 mg, 0.8 mmol), THF (3 mL), and water (0.6 mL), and the mixture was purged with nitrogen for 30 min. The catalyst $Pd(PPh_3)_4$ (18 mg, 10 mol %) was subsequently added under nitrogen, and the glass tube was sealed before being warmed to 85 °C using an oil bath. After 16 h, the reaction mixture was cooled to room temperature, and THF was evaporated under reduced pressure. Water was added to the reaction

https://doi.org/10.1021/acs.joc.2c03103
J. Org. Chem. 2023, 88, 5473−5482

mixture, and then it was extracted with dichloromethane (3 × 30 mL). The organic layer was dried over anhydrous sodium sulfate, filtered, and evaporated under reduced pressure to afford a solid residue, which was subjected to silica gel column chromatography (hexanes/DCM, 95:5) to give **20** as a yellow solid. (62 mg, 61% yield): R_f = 0.37 (5% EtOAc/hexanes); mp 161-162 °C; ^{1}H NMR (400 MHz, $CDCl_3$) δ 9.03 (d, J = 8.1 Hz, 1H), 8.88 (s, 1H), 8.76 (d, J = 8.2 Hz, 1H), 8.70 (d, J = 7.8 Hz, 1H), 8.62 (d, J = 8.5 Hz, 1H), 8.53 (d, J = 8.5 Hz, 1H), 8.16 (d, J = 7.5 Hz, 1H), 7.86 (d, J = 8.3 Hz, 1H), 7.80 (t, J = 7.5 Hz, 1H), 7.74 (t, J = 6.9 Hz, 1H), 7.68 (q, J = 7.2 Hz, 2H), 7.57 (d, J = 8.1 Hz, 1H), 7.43 (t, J = 7.6 Hz, 1H), 7.18 (dd, J = 8.2, 1.9 Hz, 1H), 7.07−6.91 (m, 3H), 4.13−4.00 (m, 2H), 3.70 (s, 1H), 3.49 (s, 1H), 1.86 (dd, J = 13.8, 7.1 Hz, 2H), 1.52 (s, 2H), 1.37 (dt, J = 13.7, 5.0 Hz, 4H), 1.32−1.09 (m, 8H), 0.94 (t, J = 7.0 Hz, 3H), 0.83 (t, J = 7.1 Hz, 3H); ^{13}C{^{1}H} NMR (100 MHz, $CDCl_3$) δ 149.4, 148.9, 138.4, 137.9, 135.9, 135.7, 134.6, 133.9, 133.4, 132.8, 132.0, 131.5, 131.2, 130.6, 129.9, 128.6, 127.8, 127.7, 127.4, 126.8, 126.7, 126.2, 126.1, 125.5, 125.2, 125.1, 123.7, 123.0, 122.8, 122.2, 122.1, 116.6, 114.6, 69.6, 69.1, 31.8, 31.5, 29.3, 28.9, 25.8, 25.6, 22.8, 22.7, 14.2, 14.1; HRMS (APCI) m/z: M^+ Calcd for $C_{46}H_{45}O_2$ 629.3420, found 629.3423.

4.3.9. 2,3-Bis(hexyloxy)benzo[g]diphenanthro[9,10,1-cde:2′,1′,10′-ija]azulene (9). To a solution of **20** (55 mg, 0.09 mmol) in dry DCM (10 mL) was added DDQ (80 mg, 0.35 mmol), resulting in a color change from yellow to dark green, and then anhydrous $FeCl_3$ (142 mg, 0.9 mmol) was added to the reaction mixture. The color of the solution turned dark brown as the reaction progressed and the reaction mixture was stirred for 2 h. The progress of the reaction was monitored by TLC. Thereafter, the reaction mixture was quenched with a saturated aq. $NaHCO_3$ solution and then extracted with dichloromethane (3 × 30 mL). The organic layer was dried over anhydrous sodium sulfate, filtered, and removed under reduced pressure to afford crude residue **9**, which was further subjected to silica gel column chromatography (hexanes/DCM, 90:10) to afford pure title product **9** as an orange solid (37 mg, 66% yield) [R_f = 0.31 (5% EtOAc/hexanes)]. Recrystallization of **9** from a tetrahydrofuran/toluene (1:1) mixture at ambient temperature afforded single crystals suitable for X-ray crystallographic analysis: mp 178−179 °C; ^{1}H NMR (400 MHz, $CDCl_3$) δ 8.91 (d, J = 8.0 Hz, 1H), 8.86 (s, 1H), 8.72 (d, J = 8.2 Hz, 2H), 8.63 (d, J = 8.0 Hz, 1H), 8.56 (d, J = 8.7 Hz, 1H), 8.23 (d, J = 8.7 Hz, 1H), 8.19 (d, J = 7.5 Hz, 1H), 7.95 (d, J = 7.5 Hz, 1H), 7.82−7.73 (m, 2H), 7.68 (dd, J = 15.9, 8.0 Hz, 3H), 7.61 (s, 1H), 7.25 (s, 1H), 4.21 (t, J = 6.6 Hz, 2H), 4.15 (t, J = 6.6 Hz, 2H), 1.61−1.54 (m, 3H), 1.44−1.36 (m, 8H), 0.94 (q, J = 7.1 Hz, 6H); The ^{13}C NMR spectrum with a good signal-to-noise ratio could not be obtained for spectroscopic analysis due to insufficient solubility; HRMS (ESI) m/z: M^+ Calcd for $C_{46}H_{42}O_2$ 626.3185, found 626.3185.

■ ASSOCIATED CONTENT

Data Availability Statement

The data underlying this study are available in the published article and its online Supporting Information.

Supporting Information

The Supporting Information is available free of charge at https://pubs.acs.org/doi/10.1021/acs.joc.2c03103.

NMR spectra; X-ray crystallographic data; DFT calculations; plausible structures of seven PAP isomers; and plausible mechanisms (PDF)

Accession Codes

CCDC 2220621 contains the supplementary crystallographic data for this paper. These data can be obtained free of charge via www.ccdc.cam.ac.uk/data_request/cif, or by emailing data_request@ccdc.cam.ac.uk, or by contacting The Cambridge Crystallographic Data Centre, 12 Union Road, Cambridge CB2 1EZ, UK; fax: +44 1223 336033.

■ AUTHOR INFORMATION

Corresponding Author

Soumyajit Das − *Department of Chemistry, Indian Institute of Technology Ropar, Rupnagar 140001 Punjab, India;* orcid.org/0000-0003-0964-1958; Phone: +91)1881-232067; Email: chmsdas@iitrpr.ac.in

Authors

Priyank Kumar Sharma − *Department of Chemistry, Indian Institute of Technology Ropar, Rupnagar 140001 Punjab, India;* orcid.org/0000-0003-4360-2696

Akanksha Babbar − *Department of Chemistry, Indian Institute of Technology Ropar, Rupnagar 140001 Punjab, India;* orcid.org/0009-0006-3807-2212

Dibyendu Mallick − *Department of Chemistry, Presidency University, Kolkata 700073, India;* orcid.org/0000-0002-0650-1872

Complete contact information is available at: https://pubs.acs.org/10.1021/acs.joc.2c03103

Notes

The authors declare no competing financial interest.

■ ACKNOWLEDGMENTS

S.D. gratefully acknowledges the financial support from SERB, India (SRG/2019/000401). The central research facilities and departmental LCMS facility (supported by DST-FIST grant: SR/FST/CS-I/2018/55) at IIT Ropar are gratefully acknowledged. D.M. thanks National Supercomputing Mission (DST/NSM/R&D_HPC_Applications/2021/08) for computing resources of "PARAM Shakti" at IIT Kharagpur and "PARAM Brahma" at IISER Pune, implemented by C-DAC and supported by the Ministry of Electronics and Information Technology (MeitY) and DST, India. D.M. also thanks SERB (SRG/2019/001461) for the funding. The authors thank Devendra Mayurdhwaj Sanke (IISER Kolkata, Prof. Sanjio S. Zade group) for the single-crystal analysis. P.K.S. thanks CSIR for the senior research fellowship.

■ REFERENCES

(1) (a) Konishi, A.; Yasuda, M. Breathing New Life into Nonalternant Hydrocarbon Chemistry: Syntheses and Properties of Polycyclic Hydrocarbons Containing Azulene, Pentalene, and Heptalene Frameworks. *Chem. Lett.* **2021**, *50*, 195−212. (b) Chaolumen; Stepek, I. A.; Yamada, K. E.; Ito, H.; Itami, K. Construction of Heptagon-Containing Molecular Nanocarbons. *Angew. Chem., Int. Ed.* **2021**, *60*, 23508−23532.

(2) (a) Yang, X.; Rominger, F.; Mastalerz, M. Contorted Polycyclic Aromatic Hydrocarbons with Two Embedded Azulene Units. *Angew. Chem., Int. Ed.* **2019**, *58*, 17577−17582. (b) Zhang, X. S.; Huang, Y. Y.; Zhang, J.; Meng, W.; Peng, Q.; Kong, R.; Xiao, Z.; Liu, J.; Huang, M.; Yi, Y.; Chen, L.; Fan, Q.; Lin, G.; Liu, Z.; Zhang, G.; Jiang, L.; Zhang, D. Dicyclohepta[*ijkl,uvwx*]rubicene with Two Pentagons and Two Heptagons as a Stable and Planar Non-benzenoid Nanographene. *Angew. Chem., Int. Ed.* **2020**, *59*, 3529−3533. (c) Ma, J.; Fu, Y.; Dmitrieva, E.; Liu, F.; Komber, H.; Hennersdorf, F.; Popov, A. A.; Weigand, J. J.; Liu, J.; Feng, X. Helical Nanographenes Containing an Azulene Unit: Synthesis, Crystal Structures, and Properties. *Angew. Chem., Int. Ed.* **2020**, *59*, 5637−5642. (d) Han, Y.; Xue, Z.; Li, G.; Gu, Y.; Ni, Y.; Dong, S.; Chi, C. Formation of Azulene-Embedded Nanographene: Naphthalene to Azulene Rearrangement During the Scholl Reaction. *Angew. Chem., Int. Ed.* **2020**, *59*, 9026−9031. (e) Uehara, K.; Mei, P.; Murayama, T.; Tani, F.; Hayashi, H.; Suzuki, M.; Aratani, N.; Yamada, H. An Anomalous Antiaromaticity That Arises from the Cycloheptatrienyl Anion Equivalent. *Eur. J. Org.*

Chem. **2018**, *2018*, 4508−4511. (f) Liu, J.; Mishra, S.; Pignedoli, C. A.; Passerone, D.; Urgel, J. I.; Fabrizio, A.; Lohr, T. G.; Ma, J.; Komber, H.; Baumgarten, M.; Corminboeuf, C.; Berger, R.; Ruffieux, P.; Müllen, K.; Fasel, R.; Feng, X. Open-Shell Nonbenzenoid Nanographenes Containing Two Pairs of Pentagonal and Heptagonal Rings. *J. Am. Chem. Soc.* **2019**, *141*, 12011−12020. (g) Pigulski, B.; Shoyama, K.; Würthner, F. NIR-Absorbing π-Extended Azulene: Non-Alternant Isomer of Terrylene Bisimide. *Angew. Chem., Int. Ed.* **2020**, *59*, 15908−15912. (h) Mathey, P.; Lirette, F.; Fernández, I.; Renn, L.; Thomas, R. W.; Morin, J.-F. Annulated Azuleno[2,1,8-*ija*]azulenes: Synthesis and Properties. *Angew. Chem., Int. Ed.* **2023**, *62*, No. e202216281. (i) Wang, J.; Gámez, F. G.; Marín-Beloqui, J.; Diaz-Andres, A.; Miao, X.; Casanova, D.; Casado, J.; Liu, J. Synthesis of a Dicycloheptа[*a*,g]heptalene-Containing Polycyclic Conjugated Hydrocarbon and the Impact of Non-Alternant Topologies. *Angew. Chem., Int. Ed.* **2023**, *62*, No. e202217124.

(3) (a) Fei, Y.; Liu, J. Synthesis of Defective Nanographenes Containing Joined Pentagons and Heptagons. *Adv. Sci.* **2022**, *9*, No. 2201000. (b) Ahmed, J.; Mandal, S. K. Phenalenyl Radical: Smallest Polycyclic Odd Alternant Hydrocarbon Present in the Graphene Sheet. *Chem. Rev.* **2022**, *122*, 11369−11431. (c) Fei, Y.; Fu, Y.; Bai, X.; Du, L.; Li, Z.; Komber, H.; Low, K.-H.; Zhou, S.; Phillips, D. L.; Feng, X.; Liu, J. Defective Nanographenes Containing Seven-Five-Seven (7−5−7)-Membered Rings. *J. Am. Chem. Soc.* **2021**, *143*, 2353−2360.

(4) (a) Yazyev, O. V.; Louie, S. G. Topological defects in graphene: Dislocations and grain boundaries. *Phys. Rev. B* **2010**, *81*, No. 195420. (b) Vicarelli, L.; Heerema, S. J.; Dekker, C.; Zandbergen, H. W. Controlling Defects in Graphene for Optimizing the Electrical Properties of Graphene Nanodevices. *ACS Nano* **2015**, *9*, 3428−3435. (c) Banhart, F.; Kotakoski, J.; Krasheninnikov, A. V. Structural Defects in Graphene. *ACS Nano* **2011**, *5*, 26−41. (d) Lu, J.; Bao, Y.; Su, C. L.; Loh, K. P. Properties of Strained Structures and Topological Defects in Graphene. *ACS Nano* **2013**, *7*, 8350−8357. (e) Costa, A.; López-Castillo, A. Prediction of azulene-based nanographene-like materials. *Diamond Relat. Mater.* **2021**, *112*, No. 108235. (f) Huang, P. Y.; Ruiz-Vargas, C. S.; van der Zande, A. M.; Whitney, W. S.; Levendorf, M. P.; Kevek, J. W.; Garg, S.; Alden, J. S.; Hustedt, C. J.; Zhu, Y.; Park, J.; McEuen, P. L.; Muller, D. A. Grains and grain boundaries in single-layer graphene atomic patchwork quilts. *Nature* **2011**, *469*, 389−392.

(5) (a) Konishi, A.; Morinaga, A.; Yasuda, M. Construction of Polycyclic π-Conjugated Systems Incorporating an Azulene Unit Following the Oxidation of 1,8-Diphenyl-9,10-bis(phenylethynyl)-phenanthrene. *Chem. − Eur. J.* **2018**, *24*, 8548−8552. (b) Wang, S.; Tang, M.; Wu, L.; Bian, L.; Jiang, L.; Liu, J.; Tang, Z.-B.; Liang, Y.; Liu, Z. Linear Nonalternant Isomers of Acenes Fusing Multiple Azulene Units. *Angew. Chem., Int. Ed.* **2022**, *61*, No. e202205658. (c) Ong, A.; Tao, T.; Jiang, Q.; Han, Y.; Ou, Y.; Huang, K.-W.; Chi, C. Azulene-Fused Acenes. *Angew. Chem., Int. Ed.* **2022**, *61*, No. e202209286.

(6) Wu, F.; Ma, J.; Lombardi, F.; Fu, Y.; Liu, F.; Huang, Z.; Liu, R.; Komber, H.; Alexandropoulos, D. I.; Dmitrieva, E.; Lohr, T. G.; Israel, N.; Popov, A. A.; Liu, J.; Bogani, L.; Feng, X. Benzo-Extended Cyclohepta[*def*]fluorene Derivatives with Very Low-Lying Triplet States. *Angew. Chem., Int. Ed.* **2022**, *61*, No. e202202170.

(7) (a) Das, S.; Wu, J. Toward Singlet−Triplet Bistable Non-alternant Kekulé Hydrocarbons: Azulene-to-Naphthalene Rearrangement. *Org. Lett.* **2015**, *17*, 5854−5857. (b) Ponugoti, N.; Parthasarathy, V. Rearrangements in Scholl Reaction. *Chem. − Eur. J.* **2022**, *28*, No. e202103530.

(8) Jutz, C.; Schweiger, E. Darstellung von Benzazulenen aus Azulenderivaten. *Chem. Ber.* **1974**, *107*, 2383−2396.

(9) Munday, R.; Sutherland, I. O. Synthesis of compounds related to cyclohepta[*def*]fluorene. *J. Chem. Soc. C* **1969**, 1427.

(10) (a) Baumgartner, P.; Weltin, E.; Wagnière, G.; Heilbronner, E. Ist die Molekel ein Biradikal? *Helv. Chim. Acta* **1965**, *48*, 751−764. (b) Nendel, M.; Goldfuss, B.; Houk, K. N.; Grieser, U.; Hafner, K. Bis-periazulene: a simple Kekulé biradical with a triplet ground state. *Theor. Chem. Acc.* **1999**, *102*, 397−400.

(11) (a) Horii, K.; Kishi, R.; Nakano, M.; Shiomi, D.; Sato, K.; Takui, T.; Konishi, A.; Yasuda. Bis-periazulene (Cyclohepta[*def*]-fluorene) as a Nonalternant Isomer of Pyrene: Synthesis and Characterization of Its Triaryl Derivatives. *J. Am. Chem. Soc.* **2022**, *144*, 3370−3375. (b) Konishi, A.; Horii, K.; Yasuda, M. The road to bis-periazulene (cyclohepta[*def*]fluorene): Realizing one of the long-standing dreams in nonalternant hydrocarbons. *J. Phys. Org. Chem.* **2023**, *36*, No. e4495.

(12) Ogawa, N.; Yamaoka, Y.; Takikawa, H.; Yamada, K.; Takasu, K. Helical Nanographenes Embedded with Contiguous Azulene Units. *J. Am. Chem. Soc.* **2020**, *142*, 13322−13327.

(13) (a) Zhang, L.; Walker, B.; Liu, F.; Colella, N. S.; Mannsfeld, S. C.; Watkins, J. J.; Nguyen, T.-Q.; Briseno, A. L. Triisopropylsilylethynyl-functionalized dibenzo[*def*,*mno*]chrysene: a solution-processed small molecule for bulk heterojunction solar cells. *J. Mater. Chem.* **2012**, *22*, 4266−4268. (b) Desroches, M.; Morin, J.-F. Wurster-Type Nanographenes as Stable Diradical Dications. *Chem. − Eur. J.* **2018**, *24*, 2858−2862.

(14) Gu, Y.; Wu, X.; Gopalakrishna, T. Y.; Phan, H.; Wu, J. Graphene-like Molecules with Four Zigzag Edge. *Angew. Chem., Int. Ed.* **2018**, *57*, 6541−6545.

(15) Omist, A.; Ricci, G.; Derradji, A.; Pérez-Jiménez, A. J.; San-Fabián, E.; Olivier, Y.; Sancho-García, J. C. *peri*-Acenoacene molecules: tuning of the singlet and triplet excitation energies by modifying their radical character. *Phys. Chem. Chem. Phys.* **2021**, *23*, 24016−24028.

(16) Gu, Y.; Tullimilli, Y. G.; Feng, J.; Phan, H.; Zeng, W.; Wu, J. Wu, *peri*-Acenoacenes. *Chem. Commun.* **2019**, *55*, 5567−5570.

(17) Gu, Y.; Muñoz-Mármol, R.; Fan, W.; Han, Y.; Wu, S.; Li, Z.; Bonal, V.; Villalvilla, J. M.; Quintana, J. A.; Boj, P. G.; Díaz-García, M. A.; Wu, J. Peri-Acenoacene for Solution Processed Distributed Feedback Laser: The Effect of 1,2-Oxaborine Doping. *Adv. Opt. Mater.* **2022**, *10*, No. 2102782.

(18) Jousselin-Oba, T.; Mamada, M.; Wright, K.; Marrot, J.; Adachi, C.; Yassar, A.; Frigoli, M. Synthesis, Aromaticity, and Application of *peri*-Pentacenopentacene: Localized Representation of Benzenoid Aromatic Compounds. *Angew. Chem., Int. Ed.* **2021**, *61*, No. e202112794.

(19) Liu, T.; Qi, C.; Zhou, Q.; Dai, W.; Lan, Y.; Xu, L.; Ren, J.; Pan, Y.; Yang, L.; Ge, Y.; Qu, Y.-K.; Li, W.; Li, H.; Xiao, S. Divergent Synthesis of Contorted Polycyclic Aromatics Containing Pentagons, Heptagon, and/or Azulene. *Org. Lett.* **2022**, *24*, 472−477.

(20) Grzybowski, M.; Skonieczny, K.; Butenschön, H.; Gryko, D. T. Comparison of Oxidative Aromatic Coupling and the Scholl Reaction. *Angew. Chem., Int. Ed.* **2013**, *52*, 9900−9930.

(21) Liu, E.-C.; Chen, M.-K.; Li, J.-Y.; Wu, Y.-T. Palladium-Catalyzed Annulation of 9-Halophenanthrenes with Alkynes: Synthesis, Structural Analysis, and Properties of Acephenanthrylene-Based Derivatives. *Chem. − Eur. J.* **2015**, *21*, 4755−4761.

(22) Ogawa, N.; Yamaoka, Y.; Yamada, K.; Takasu, K. Synthesis of π-Extended Fluoranthenes via a KHMDS-Promoted Anionic-Radical Reaction Cascade. *Org. Lett.* **2017**, *19*, 3327−3330.

(23) (a) Liu, Y.-H.; Perepichka, D. F. Acenaphthylene as a building block for π-electron functional materials. *J. Mater. Chem. C* **2021**, *9*, 12448−12461. (b) Wegner, H. A.; Scott, L. T.; Meijere, A. A New Suzuki−Heck-Type Coupling Cascade: Indeno[1,2,3]-Annelation of Polycyclic Aromatic Hydrocarbons. *J. Org. Chem.* **2003**, *68*, 883−887.

(24) (a) Scott, L. T.; Reinhardt, G.; Roelofs, N. H. Acephenanthrylene. *J. Org. Chem.* **1985**, *50*, 5886−5887. (b) Amin, S.; Balanikas, G.; Huie, K.; Hussain, N.; Geddie, J. E.; Hecht, S. S. Synthesis and Fluorescence Spectra of Structural Analogs of Potential Benzo[*b*]-fluoranthene-DNA Adducts. *J. Org. Chem.* **1985**, *50*, 4642−4646.

(25) Scott, J. L.; Parkin, S. R.; Anthony, J. E. Radical-Induced Cycloaromatization: Routes to Fluoranthenes and Acephenanthrylenes. *Synlett.* **2004**, 161−164.

(26) (a) Ma, J.; Fu, Y.; Liu, J.; Feng, X. One-pot synthesis of dicyclopenta-fused peropyrene via a fourfold alkyne annulation.

https://doi.org/10.1021/acs.joc.2c03103
J. Org. Chem. 2023, 88, 5473−5482

Beilstein J. Org. Chem. **2020**, *16*, 791−797. (b) Dang, H.; Garcia-Garibay, M. A. Palladium-Catalyzed Formation of Aceanthrylenes: A Simple Method for Peri-Cyclopentenelation of Aromatic Compounds. *J. Am. Chem. Soc.* **2001**, *123*, 355−356.
(27) Ackermann, M.; Freudenberg, J.; Jänsch, D.; Rominger, F.; Bunz, U. H. F.; Müllen, K. Palladium-Catalyzed Dimerization of Bis(2-biphenylyl)acetylene toward Sterically Hindered Acephenanthrylene. *Org. Lett.* **2018**, *20*, 3758−3761.
(28) Chen, P.-T.; Yu, C.-L.; Shen, M.-H.; Cheng, M.-J.; Wu, Y.-T.; Hsu, H.-F. Highly Substituted Acephenanthrylenes and Their π-Extended Derivatives: Syntheses, Structural Analyses, and Properties. *Org. Lett.* **2022**, *24*, 4778−4782.
(29) (a) Zhai, L.; Shukla, R.; Wadumethrige, S. H.; Rathore, R. Probing the Arenium-Ion (Proton Transfer) versus the Cation-Radical (Electron Transfer) Mechanism of Scholl Reaction Using DDQ as Oxidant. *J. Org. Chem.* **2010**, *75*, 4748−4760. (b) Zhai, L.; Shukla, R.; Rathore, R. Oxidative C−C Bond Formation (Scholl Reaction) with DDQ as an Efficient and Easily Recyclable Oxidant. *Org. Lett.* **2009**, *11*, 3474−3477. (c) Wadumethrige, S. H.; Rathore, R. A Facile Synthesis of Elusive Alkoxy-Substituted Hexa-*peri*-hexabenzocoronene. *Org. Lett.* **2008**, *10*, 5139−5142.
(30) (a) Zhang, Y.; Pun, S. H.; Miao, Q. The Scholl Reaction as a Powerful Tool for Synthesis of Curved Polycyclic Aromatics. *Chem. Rev.* **2022**, *122*, 14554−14593. (b) Pun, S. H.; Cheung, K. M.; Yang, D.; Chen, H.; Wang, Y.; Kershaw, S. V.; Miao, Q. A Near-Infrared Absorbing and Emissive Quadruple Helicene Enabled by the Scholl Reaction of Perylene. *Angew. Chem., Int. Ed.* **2022**, *61*, No. e202113203. (c) Yang, Y.; Yuan, L.; Shan, B.; Liu, Z.; Miao, Q. Twisted polycyclic arenes from tetranaphthyldiphenylbenzenes by controlling the Scholl reaction with substituents. *Chem. − Eur. J.* **2016**, *22*, 18620−18627.
(31) (a) Ma, Y.; Zhang, D.; Yan, Z.; Wang, M.; Bian, C.; Gao, X.; Bunel, E. E.; Lei, A. Iron-Catalyzed Oxidative C−H/C−H Cross-Coupling between Electron-Rich Arenes and Alkenes. *Org. Lett.* **2015**, *17*, 2174−2177. (b) Jang, S. S.; Youn, S. W. The cooperative $FeCl_3$/DDQ system for the regioselective synthesis of 3-arylindoles from β-monosubstituted 2-alkenylanilines. *Org. Biomol. Chem.* **2016**, *14*, 2200−2204.
(32) (a) Jassas, R. S.; Mughal, E. U.; Sadiq, A.; Alsantali, R. I.; Al-Rooqi, M. M.; Naeem, N.; Moussa, Z.; Ahmed, S. A. Scholl reaction as a powerful tool for the synthesis of nanographenes: a systematic review. *RSC Adv.* **2021**, *11*, 32158−32202. (b) Alsharif, M. A.; Raja, Q. A.; Majeed, N. A.; Jassas, R. S.; Alsimaree, A. A.; Sadiq, A.; Naeem, N.; Mughal, E. U.; Alsantali, R. I.; Moussa, Z.; Ahmed, S. A. DDQ as a versatile and easily recyclable oxidant: a systematic review. *RSC Adv.* **2021**, *11*, 29826−29858.
(33) Hanson, A. W. The crystal structure of the azulene, s-trinitrobenzene complex. *Acta Crystallogr.* **1965**, *19*, 19−26.
(34) Solà, M. Forty years of Clar's aromatic π-sextet rule. *Front. Chem.* **2013**, *1*, 22.
(35) DFT optimization at B3LYP/6-31G(d) showed ground state of **9** to be singlet closed-shell with a large singlet-triplet energy gap (37.8 kcal mol^{-1}, Table S2). See Supporting Information for further details.
(36) (a) Kruszewski, J.; Krygowski, T. M. Definition of aromaticity basing on the harmonic oscillator model. *Tetrahedron Lett.* **1972**, *13*, 3839−3842. (b) Krygowski, T. M.; Bankiewicz, B.; Czarnocki, Z.; Palusiak, M. Aromaticity: what does it mean? *ChemTexts* **2015**, *1*, 12. (c) Sharma, P. K.; Das, S. Unveiling a Quinoidal 2,3:10,11-Dibenzoheptazethrene. *J. Org. Chem.* **2022**, *87*, 5430−5436.
(37) (a) Dominikowska, J.; Palusiak, M. EL: the new aromaticity measure based on one-electron density function. *Struct. Chem.* **2012**, *23*, 1173−1183. (b) Sharma, H.; Bhardwaj, N.; Das, S. Revisiting indeno[1,2-*b*]fluorene by steric promoted synthesis while isolating the second stable 4nπ indeno[2,1-*a*]fluorene. *Org. Biomol. Chem.* **2022**, *20*, 8071−8077.
(38) (a) Fallah-Bagher-Shaidaei, H.; Wannere, C. S.; Corminboeuf, C.; Puchta, R.; von Schleyer, P. Which NICS Aromaticity Index for Planar π Rings Is Best? *Org. Lett.* **2006**, *8*, 863−866. (b) Dobrowolski, J. C.; Lipiński, P. F. On splitting of the NICS(1) magnetic aromaticity index. *RSC Adv.* **2016**, *6*, 23900−23904. (c) Antić, M.; Furtula, B.; Radenković, S. Aromaticity of Nonplanar Fully Benzenoid Hydrocarbons. *J. Phys. Chem. A* **2017**, *121*, 3616−3626.
(39) Geuenich, D.; Hess, K.; Köhler, F.; Herges, R. Anisotropy of the Induced Current Density (ACID), a General Method To Quantify and Visualize Electronic Delocalization. *Chem. Rev.* **2005**, *105*, 3758−3772.
(40) (a) Stanger, A. The Seven-Membered Ring in Bis-Azuleno-Naphthalene is Non-Aromatic. *Eur. J. Org. Chem.* **2019**, *2019*, 857−859. (b) Stanger, A. NICS − Past and Present. *Eur. J. Org. Chem.* **2020**, *2020*, 3120−3127. (c) Uehara, K.; Mei, P.; Murayama, T.; Tani, F.; Hayashi, H.; Suzuki, M.; Aratani, N.; Yamada, H. Response to "The Seven-Membered Ring in Bis-Azuleno-Naphthalene is Non-Aromatic". *Eur. J. Org. Chem.* **2019**, *2019*, 860−861.
(41) (a) Taniguchi, M.; Lindsey, J. S. Database of Absorption and Fluorescence Spectra of >300 Common Compounds for use in PhotochemCAD. *Photochem. Photobiol.* **2018**, *94*, 290−327. (b) Kubin, R. F.; Fletcher, A. N. Fluorescence quantum yields of some rhodamine dyes. *J. Lumin.* **1982**, *27*, 455−462. (c) Kellogg, R. E.; Bennett, R. G. Radiationless Intermolecular Energy Transfer. III. Determination of Phosphorescence Efficiencies. *J. Chem. Phys.* **1964**, *41*, 3042−3045.
(42) Wood, J. D.; Jellison, J. L.; Finke, A. D.; Wang, L.; Plunkett, K. N. Electron Acceptors Based on Functionalizable Cyclopenta[*hi*]-Aceanthrylenes and Dicyclopenta[*de,mn*]Tetracenes. *J. Am. Chem. Soc.* **2012**, *134*, 15783−15789.
(43) (a) Kawasumi, K.; Zhang, Q.; Segawa, Y.; Scott, L. T.; Itami, K. A grossly warped nanographene and the consequences of multiple odd-membered-ring defects. *Nat. Chem.* **2013**, *5*, 739−744. (b) Fernández-García, J. M.; Evans, P. J.; Medina Rivero, S.; Fernández, I.; García-Fresnadillo, D.; Perles, J.; Casado, J.; Martín, N. π-Extended Corannulene-Based Nanographenes: Selective Formation of Negative Curvature. *J. Am. Chem. Soc.* **2018**, *140*, 17188−17196. (c) Nobusue, S.; Fujita, K.; Tobe, Y. Skeletal Rearrangement of Twisted Polycyclic Aromatic Hydrocarbons under Scholl Reaction Conditions. *Org. Lett.* **2017**, *19*, 3227−3230.
(44) Zhao, B.; Liu, B.; Png, R. Q.; Zhang, K.; Lim, K. A.; Luo, J.; Shao, J.; Ho, P. K. H.; Chi, C.; Wu, J. New Discotic Mesogens Based on Triphenylene-Fused Triazatruxenes: Synthesis, Physical Properties, and Self-Assembly. *Chem. Mater.* **2010**, *22*, 435−449.
(45) Lu, T.; Chen, F. Multiwfn: A multifunctional wavefunction analyser. *J. Comput. Chem.* **2011**, *33*, 580−592.
(46) O'boyle, N. M.; Tenderholt, A. L.; Langner, K. M. cclib: A library for package independent computational chemistry algorithms. *J. Comput. Chem.* **2008**, *29*, 839−845.

https://doi.org/10.1021/acs.joc.2c03103
J. Org. Chem. 2023, 88, 5473−5482

OL Organic Letters

pubs.acs.org/OrgLett

Letter

A Thiophenoradialene-Embedded Polycyclic Heteroterphenoquinone Exhibiting Dominant Antiaromatic Traits

Priyank Kumar Sharma, Dibyendu Mallick, and Soumyajit Das*

Cite This: *Org. Lett.* 2023, 25, 5089−5093

Read Online

ACCESS | Metrics & More | Article Recommendations | Supporting Information

ABSTRACT: A thiophenoradialene-embedded polycyclic heteroterphenoquinone (PHTPQ) derivative of diindeno[1,2-*b*:2′,1′-*d*]thiophene-2,8-dione, with antiaromatic characteristics, was synthesized by dehydrogenating its fluorescent dihydro PHTPQ precursor. The antiaromatic character was evidenced by the visible absorption band with a weakly intense tail extending to 800 nm in the near-infrared region (forbidden HOMO → LUMO transition) and non-emissive and amphoteric redox properties. Single-crystal and (anti)aromaticity analyses found a non-aromatic thiophene core while suggesting antiaromaticity/paratropicity of the pentafulvene subunits dominating the overall ground state properties.

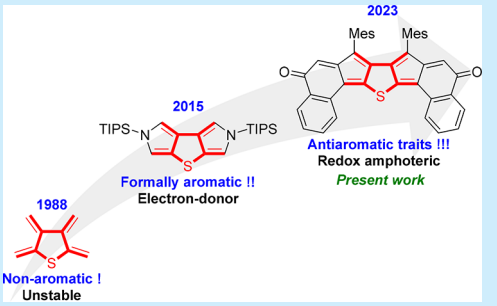

Cross-conjugation was usually regarded as being less effective in promoting electron delocalization.[1] Improved conductance properties[2] and high-performance battery[3] applications of cross-conjugated molecules made them stimulating synthetic targets. Conventional [5]radialene[4] is a cross-conjugated π-system with five exocyclic C(sp²)=C(sp²) bonds (Figure 1a) and belongs to the well-known [*n*]radialene family.[5] Studies on the hybrid [*n*]radialenes[6] with different heteroatoms (such as O, P, S, As, and Si) introduced into the radialene backbone (Figure 1a) were relatively less explored.[7] Among them, the oxa-hybrid [5]radialene and thia-hybrid [5]radialene systems were first generated as cross-conjugated reactive furanoradialene **1a**[7a,b] and thiophenoradialene **1b**[7c] by flash vacuum pyrolysis. Sulfur-centered dithienothiophene **2**[7j] or bispyrrolothiophene **3**[7h] bearing a thia-hybrid [5]radialene (or thiophenoradialene) unit was generated by attaching two aromatic heterocycles to the opposite sides of the central thiophene ring with the outer heteroatoms (S or N) facing the opposite direction. Such a ring-fusion arrangement for tricyclic **2** or **3** should better represent them as hybrid [5]radialene-like[8] molecules, considering the aromatic 14π-electron perimeter.

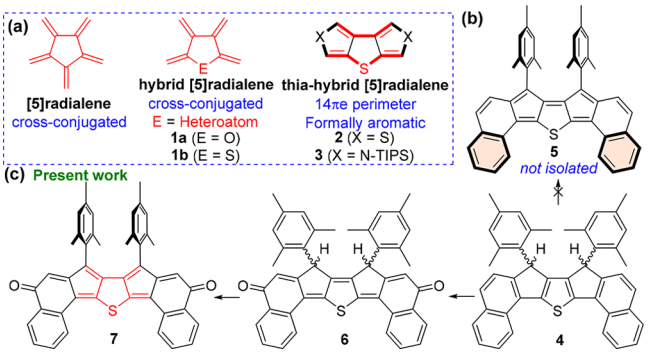

Figure 1. (a) Structures of [5]radialene, furanoradialene **1a**, and thiophenoradialene **1b**. Formally aromatic thiophenoradialenes **2** and **3** with $(4n + 2)\pi$-electrons in the outer conjugation circuit. (b) Structure of **5**, which could not be isolated from **4**. (c) Instead, **6** was isolated and dehydrogenated to afford target **7**.

An earlier attempt to isolate dicyclopenta[*b*,*d*]thiophene through linear dibenzo extension failed[9] due to the large singlet diradical character caused by the recovery of three local aromatic rings,[10] but no decomposition product was reported. We envisaged that dinaphtho fusion could be a viable approach for isolating dinaphtho-dicyclopenta[*b*,*d*]thiophene **5**, as two Clar sextets (orange hexagons in Figure 1b) would be retained for **5** while only one weakly aromatic thiophene would be dearomatized; a successful approach was adopted by the groups of both Haley and Chi to synthesize the elusive antiaromatic heterocyclic indenofluorenes.[11] We adopted the oxidative dehydrogenation approach of dihydro precursor **4** to construct **5** (Figure 1b)[12] but failed to synthesize it; instead, we isolated a fully fused polycyclic heteroterphenoquinone (PHTPQ) **6**.

Our observation was quite similar to literature reports in which π-extension of potential diradicaloid polycyclic hydrocarbons caused degradation and resulted in isolation of dione

Received: June 3, 2023
Published: June 29, 2023

as decomposition products, but their properties remained unexciting.[13] Nevertheless, to the best of our knowledge, **6** is the only example of a fully fused PHTPQ congener of π-conjugated HTPQ in which the central benzo unit was replaced by a heterocycle (thiophene for **6**).[14] Notably, a *p*-terphenoquinone (*p*TPQ) analogue with a central dihydrothiophenediylidene unit could uniquely display intense absorption in the visible region (λ_{max} = 558 nm, and log ε = 4.90)[14a] and three-stage[14a,b] or four-stage[15] amphoteric single-electron redox events, but no fluorescence for such quinones has been documented thus far. Herein, quinone **6** was characterized to explore its ground state electronic properties, including the elusive fluorescence property.

Oxidative dehydrogenation of the through-conjugated[3] (or linearly conjugated) dihydro PHTPQ **6** was envisioned to afford a dibenzo-extended diindeno[1,2-*b*:2′,1′-*d*]thiophene-2,8-dione derivative **7**, bearing a thiophenoradialene unit (Figure 1c, red). Notably, the carbonyl groups of both **6** and **7** are cross-conjugatively connected to sulfur,[16] but the carbonyl groups are through-conjugated with each other, with **7** containing one fewer π-electron pair than **6** in the conjugation path. Unlike the reported formally aromatic thia-hybrid [5]radialene with an obvious negative nucleus-independent chemical shift (NICS) for the central thiophene unit of **3** of −5.16 ppm,[7h] the thiophene unit of **7** was expected to be dearomatized, making **7** a rare example of cross-conjugated thia-hybrid [5]radialene-embedded PHTPQ that may act as electron-accepting scaffold, unlike **2** and **3**, which are electron donors. We studied the properties of **7** by single-crystal X-ray diffractometry (SCXRD), ultraviolet−visible (UV−vis) absorption, cyclic voltammetry, and density functional theory (DFT) approaches, while NICS(1)$_{zz}$,[17] HOMA (harmonic oscillator model of aromaticity),[18] and ACID (anisotropy of the induced current density)[19] calculations were performed to assess the ground state (anti)aromaticity.

Stille reaction between presynthesized 2,5-bis(trimethylstannyl)thiophene[20] **8** and commercially available **9** in toluene afforded **10** in 83% yield (Scheme 1). Nucleophilic addition of

Scheme 1. Syntheses of 6 and 7 (Mes = mesityl)

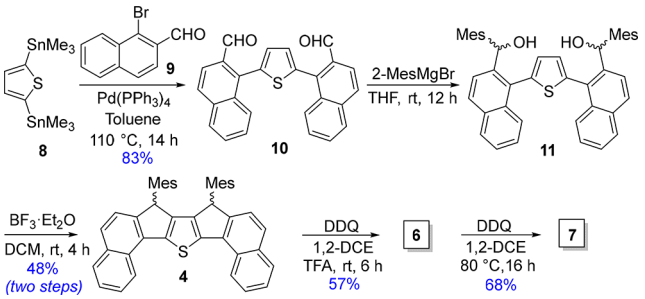

2-mesitylmagnesium bromide to **10** gave diol **11**, which was subsequently treated with $BF_3{\cdot}Et_2O$ to afford **4** in 48% yield over two steps. The oxidative dehydrogenation of **4** with only 2,3-dichloro-5,6-dicyano-1,4-benzoquinone (DDQ) did not work, but DDQ with trifluoroacetic acid (TFA) in 1,2-dichloroethane at room temperature afforded a pink solution and led to the disappearance of starting material **4**. Purification of the resulting reaction mixture through silica gel column chromatography afforded a purple-black powder in 57% yield. Unfortunately, after many attempts, we failed to grow a single crystal of the obtained purple-black solid. The high-resolution mass spectrometry (HRMS) and NMR analyses suggested the formation of PHTPQ **6**, instead of **5** (Figure 1b), as it showed intense UV−vis absorption and fluorescence in the visible region (*vide infra*).[14a] It was a quite unprecedented observation because quinones are mostly non-emissive,[21] especially HTPQ or *p*TPQ analogues.[14,15] Thus, to unambiguously confirm the structure of **6**, we aimed to oxidatively dehydrogenate **6** in the presence of DDQ to construct the first thiophenoradialene-embedded PHTPQ **7** in 68% yield. The structure of **7** was established by HRMS and one- and two-dimensional NMR analyses (see the Supporting Information), while SCXRD analysis provided further unambiguous confirmation of its formation.

Single crystals of **7** (Figure 2a) for SCXRD analysis were grown by diffusing methanol into the chloroform solution at

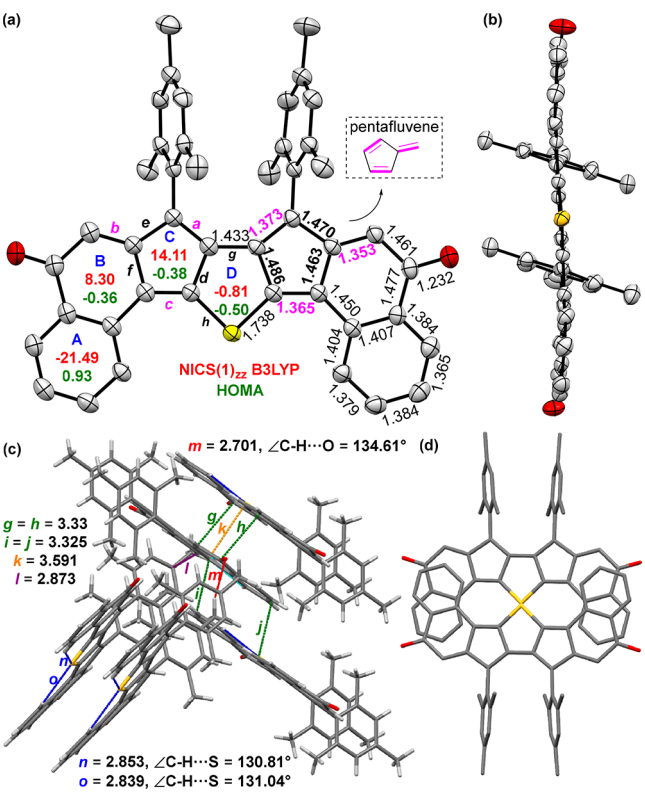

Figure 2. (a) ORTEP drawing for the top view of **7** with ellipsoids at the 30% probability level (hydrogens omitted), including mean bond lengths (angstroms), calculated NICS(1)$_{zz}$ (red) indices at the B3LYP/6-31G(d,p) level, and HOMA (green) values. (b) Side view of **7**. (c) Noncovalent interactions (Å) are labeled for **7**. (d) Pair of molecules of **7**, cofacially π-stacked about a point of inversion due to S···S interaction, forming a figure-eight-like dimeric motif.

ambient temperature. Compound **7** had a rigid and almost planar core structure (Figure 2b) with the terminal benzene rings (A) slightly deviated by ∼6.9° (average) in the covelike region, as measured from the mean plane between central ring D and terminal rings A (rings labeled in Figure 2a). However, DFT optimization revealed a planar backbone for **7** (Figure S14). The mesityl groups are nearly orthogonal to the heptacyclic π-backbone, with an average torsional angle of 69.7°. The pentafulvene subunit of **7** exhibited significant C−C bond length alternation (BLA), as shown in Figure 2a (the full bond length analysis, along with esd values, is displayed in Figure S10a) with C=C bonds *a*−*c* (see the labeling in Figure

https://doi.org/10.1021/acs.orglett.3c01815
Org. Lett. 2023, 25, 5089−5093

2a) showing a greater double bond character compared to that of the other C(sp^2)−C(sp^2) (*d*–*f*) bonds, thereby indicating an alternate double- and single-bond arrangement similar to that of unsubstituted pentafulvene.[22] The mean bond lengths for *g* (C−C) and *h* (S−C) of **7** are 1.433 and 1.738 Å, respectively, which apparently had significant single-bond character. Such bond length arrangements clearly indicated a non-aromatic thiophenoradialene motif for **7** with four exocyclic double bonds.[7g,h] On the contrary, BLA in the terminal six-membered rings (A) is less pronounced (average of 1.387 Å), suggesting benzene-like aromaticity.

In the crystal lattice, **7** (Figure 2c,d and Figure S10b) packed in a three-dimensional arrangement owing to the short S···S interaction (*k* = 3.591 Å) and intermolecular $\pi-\pi$ interaction measuring 3.33 Å (*g* = *h*) between a pair of **7** cofacially stacked about a point of inversion, with another molecule parallel-displaced at 3.325 Å (*i* = *j*), in addition to a intermolecular C−H···π (*l* = 2.873 Å) and a C−H···O hydrogen bonding (HB) (*m* = 2.701 Å, 134.6°) interactions between two neighboring molecules. Compound **7** also displayed two intramolecular C−H···S (*n* = 2.853 Å, 130.8°; *o* = 2.839 Å, 131.0°) HB interactions.[23,24]

DFT optimization of **7** at the B3LYP/6-31G(d,p) level of theory suggested a singlet closed-shell ground state with a large singlet−triplet energy gap (18.8 kcal/mol). The HOMA[18] analyses of the optimized closed-shell structure of **7** provided further support for the substantial BLA for rings C (−0.38) and B (−0.36), while insignificant BLA for terminal A rings (0.93) suggested its aromaticity. On the basis of the NICS(1)$_{zz}$[17] values of **7**, calculated using the same level of theory, ring A (−21.49) was found to be strongly aromatic while non-aromaticity for ring D (−0.81) and moderate to strong antiaromaticity for rings B (8.30) and C (14.11) were suggested. The ACID[19] plot of **7** corroborates the NICS(1)$_{zz}$ values, showing a counterclockwise ring current over ring C, indicating the significant paratropic nature of the pentafulvene subunit, while rings B and D were essentially atropic (Figure 3). A strong clockwise (diatropic) ring current observed over ring A was consistent with its large negative NICS(1)$_{zz}$ value. The strong antiaromaticity of the pentafulvene subunits could be attributed to the electron-withdrawing oxygen of carbonyl groups imposing positive charges on the attached carbons

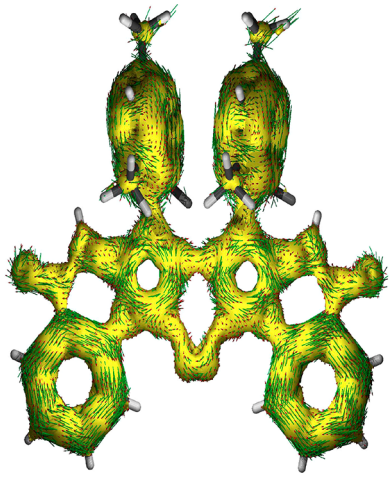

Figure 3. Current−density vectors of **7** plotted onto the ACID isosurface of 0.02 at the B3LYP/6-31G(d,p) level of theory.

(Figure S15), as analyzed by natural population analyses [NPA charges (Figure S16)] in the ground state, which may delocalize to the pentafulvene subunit, forming the antiaromatic cyclopentadienyl cation with a significant paratropic ring current.

Compounds **6** and **7** were moderately soluble in common organic solvents, with **6** exhibiting a pink color and **7** appearing to be dark yellow in dichloromethane (DCM) (Figure 4a,b). The UV−vis absorption and fluorescence spectra of **6** in DCM are depicted in Figure 4a. Compound **6** exhibited intense absorption in the visible region at λ_{max} = 557 nm (ε = 41 730 M^{-1} cm^{-1}), which looks similar to HTPQ or *p*TPQ absorption bands,[14a] resulting from the allowed HOMO → LUMO transition [theoretical λ_{max} = 513 nm; oscillator strength (*f*) = 1.29, as shown in Table S5 on the basis of time-dependent DFT (TDDFT) calculations]. Compound **7** showed an intense absorption in the visible region at λ_{max} = 504 nm [ε = 50 150 M^{-1} cm^{-1} (Figure 4b)], which is accompanied by a low-energy shoulder at ∼635 nm, despite the shortening of the linear π-conjugation path in comparison to that of **6**. Such a weakly intense shoulder band with its absorption tail extending to 800 nm (Figure 4b, inset) is reminiscent of strong ground state antiaromatic character,[23] which may be attributed to the dominant antiaromaticity of the pentafulvene subunit for **7**, as supported by NICS/ACID calculations. According to TDDFT, the absorption at 504 nm of **7** was an admixture of HOMO → LUMO+1, HOMO−1 → LUMO, and HOMO−5 → LUMO (501 nm; *f* = 0.47) transitions, while the weakly intense absorption tail in the range of 535−800 nm resulted due to the combinations of several weak and apparently forbidden transitions [*f* < 0.021 (Table S6)], including the forbidden HOMO → LUMO transition (TDDFT; 685 nm; *f* = 0.006), implying ground state antiaromatic character. The optical HOMO−LUMO energy gaps for **6** and **7**, roughly estimated from the absorption onsets, were found to be 2.12 and 1.64 eV, respectively.

Usually, chalcogen-based HTPQ derivatives are non-emissive,[14] but PHTPQ **6** exhibited fluorescence with a quantum yield (Φ) of 25% (with rhodamine B as a reference standard).[25] The emission maximum of **6** at 576 nm in DCM showed a small Stokes shift of 19 nm due to a planar and rigid backbone. Interestingly, the fluorescence disappeared upon oxidative dehydrogenation of **6** to **7**, which could likely be attributed to the dominant antiaromaticity of **7** opening the radiationless relaxation pathway due to conical intersection between the excited state and ground state potential energy surfaces.[26] Notably, formally aromatic thia-hybrid [5]-radialenes[7h] are fluorescent.

The cyclic voltammogram of **6** in DCM (Figure 4c) exhibited a two-electron reduction wave with a half-wave potential of −1.07 V ($E^{red}_{1/2}$) and two irreversible oxidations at 0.83 V (E^{ox1}_{peak}) and 1.02 V (E^{ox2}_{peak}). Compound **7** displayed redox amphotericity with two reversible reductions at half-wave potentials of −1.02 V ($E^{red1}_{1/2}$) and −1.40 V ($E^{red2}_{1/2}$) and a quasi-reversible oxidation at 1.05 V (E^{ox}_{peak}). The reversible reduction events signify the strong antiaromaticity of the pentafulvene subunit of **7**, which resulted in facile electron injections to form the 4*n* + 2 cyclopentadienyl anion.[23,27] Notably, thia-hybrid [5]radialene **3** was reported to be an electron donor[7h] and could not be reduced, while thia-hybrid [5]radialene-embedded **7** could act as an electron acceptor and donor. The electrochemical HOMO and LUMO energy levels of **6** were −5.52 and −3.82 eV, respectively, as estimated from

https://doi.org/10.1021/acs.orglett.3c01815
Org. Lett. 2023, 25, 5089−5093

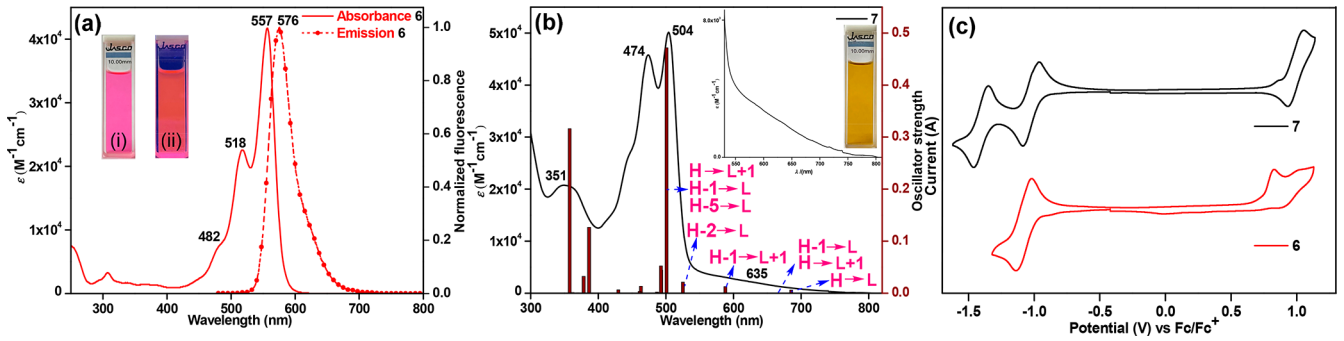

Figure 4. (a) UV−vis absorption (solid line) and emission (dashed−dotted line) spectra of **6** with the inset image under (i) visible (pink color as the DCM solution) and (ii) 365 nm light irradiation; (b) UV−vis−near-infrared absorption of **7** (inset, 535−800 nm expansion and dark yellow color of **7** as the DCM solution) with TDDFT oscillator strengths as a bar diagram. (c) Cyclic voltammograms of **6** and **7**.

the onset potentials, affording an energy gap of 1.72 eV. The electrochemical HOMO and LUMO energy levels of **7** were −5.68 and −3.86 eV, respectively, giving an energy gap of 1.82 eV. The theoretical HOMO−LUMO energy gaps were found to be 2.20 and 2.30 eV for **6** and **7**, respectively (Figure S17).

In conclusion, a fluorescent PHTPQ **6** was synthesized and oxidized to thiophenoradialene containing PHTPQ **7**, which may be regarded as an underexplored thiaradialene[28]-based π-system. SCXRD and (anti)aromaticity analyses [NICS(1)$_{zz}$ and ACID] suggested the large BLA and dominant antiaromatic character of the embedded pentafulvene subunits for **7**, as a result of the electron-withdrawing π-extended carbonyl substituents *exo* to the five-membered ring.[29] The antiaromaticity was demonstrated experimentally by the weakly intense absorption band in the range of 535−800 nm owing to a forbidden HOMO → LUMO transition, facile two-stage electron reductions with good reversibility, and non-emissive properties.[23,26,27] Our current synthetic approach has the potential to construct other heteroatom (i.e., selenium)[30] counterparts of **7** (and **6**) with tunable solid state ordering and HOMO−LUMO energy gaps for potential application as ambipolar organic semiconductors,[31] which is underway.

■ ASSOCIATED CONTENT

Data Availability Statement

The data underlying this study are available in the published article and its Supporting Information.

Supporting Information

The Supporting Information is available free of charge at https://pubs.acs.org/doi/10.1021/acs.orglett.3c01815.

General information, synthesis, and characterization of compounds and DFT calculations (PDF)

Accession Codes

CCDC 2264335 contains the supplementary crystallographic data for this paper. These data can be obtained free of charge via www.ccdc.cam.ac.uk/data_request/cif, or by emailing data_request@ccdc.cam.ac.uk, or by contacting The Cambridge Crystallographic Data Centre, 12 Union Road, Cambridge CB2 1EZ, UK; fax: +44 1223 336033.

■ AUTHOR INFORMATION

Corresponding Author

Soumyajit Das − *Department of Chemistry, Indian Institute of Technology Ropar, Rupnagar 140001 Punjab, India;* orcid.org/0000-0003-0964-1958; Email: chmsdas@iitrpr.ac.in

Authors

Priyank Kumar Sharma − *Department of Chemistry, Indian Institute of Technology Ropar, Rupnagar 140001 Punjab, India;* orcid.org/0000-0003-4360-2696

Dibyendu Mallick − *Department of Chemistry, Presidency University, Kolkata 700073 West Bengal, India;* orcid.org/0000-0002-0650-1872

Complete contact information is available at: https://pubs.acs.org/10.1021/acs.orglett.3c01815

Notes

The authors declare no competing financial interest.

■ ACKNOWLEDGMENTS

S.D. gratefully acknowledges SERB (CRG/2022/003012), India, for funding. D.M. thanks SERB (SRG/2019/001461) for funding and the National Supercomputing Mission (DST/NSM/R&D_HPC_Applications/2021/08) for computing resources of "PARAM Shakti" at IIT Kharagpur and "PARAM Brahma" at IISER Pune, implemented by C-DAC and supported by the Ministry of Electronics and Information Technology (MeitY) and DST, India. The authors thank Kamlesh Satpute (IIT Ropar) for single-crystal data. P.K.S. thanks CSIR for a senior research fellowship.

■ REFERENCES

(1) Limacher, P. A.; Lüthi, H. P. Cross-conjugation. *Wiley Interdiscip. Rev. Comput. Mol. Sci.* **2011**, *1*, 477−486.

(2) Andrews, D. Q.; Solomon, G. C.; Van Duyne, R. P.; Ratner, M. A. Single Molecule Electronics: Increasing Dynamic Range and Switching Speed Using Cross-Conjugated Species. *J. Am. Chem. Soc.* **2008**, *130*, 17309−17319.

(3) Jing, Y.; Liang, Y.; Gheytani, S.; Yao, Y. Cross-Conjugated Oligomeric Quinones for High Performance Organic Batteries. *Nano Energy* **2017**, *37*, 46−52.

(4) (a) Matsuo, T.; Fure, H.; Sekiguchi, A. Isolation and characterization of the tetralithium salt of [5]radialene tetraanion stabilized by silyl groups. *Chem. Commun.* **1999**, 1981−1982. (b) Mackay, E. G.; Newton, C. G.; Toombs-Ruane, H.; Lindeboom, E. J.; Fallon, T.; Willis, A. C.; Paddon-Row, M. N.; Sherburn, M. S. [5]Radialene. *J. Am. Chem. Soc.* **2015**, *137*, 14653−14659.

(5) Maas, G. In *Cross conjugation: Modern Dendralene, Radialene and Fulvene Chemistry*; Hopf, H., Sherburn, M. S., Eds.; Wiley-VCH: Weinheim, Germany, 2016; pp 79−116.

(6) Gholami, M.; Tykwinski, R. R. Oligomeric and Polymeric Systems with a Cross-conjugeated π-Framework. *Chem. Rev.* **2006**, *106*, 4997−5027.
(7) (a) Jullien, J.; Pechine, J. M.; Perez, F.; Piade, J. J. Preparation and characterization of "furanoradialene" (tetramethylene-tetrahydrofuran). *Tetrahedron Lett.* **1980**, *21*, 611−612. (b) Trahanovsky, W. S.; Cassady, T. J. Preparation of furanoradialene by the flash vacuum pyrolysis of diesters of 3,4-bis(hydroxymethyl)-2,5-dimethylfuran. *J. Am. Chem. Soc.* **1984**, *106*, 8197−8201. (c) Münzel, N.; Kesper, K.; Schweig, A.; Specht, H. Detection of 2,5-dimethylene-2,5-dihydrothiophene and thiophenoradialene. *Tetrahedron Lett.* **1988**, *29*, 6239−6242. (d) Miyahara, I.; Hayashi, A.; Hirotsu, K.; Yoshifuji, M.; Yoshimura, H.; Toyota, K. The first x-ray analysis of a phospha[3]-radialene. *Polyhedron* **1992**, *11*, 385−387. (e) Mahieu, A.; Miquel, Y.; Igau, A.; Donnadieu, B.; Majoral, J.-P. Versatile Behavior of a New Class of Bicyclic Compounds: Zirconacyclopentadiene Phosphiranes. *Organometallics* **1997**, *16*, 3086−3088. (f) Komen, C. M.; Horan, C. J.; Krill, S.; Gray, G. M.; Lutz, M.; Spek, A. L.; Ehlers, A. W.; Lammertsma, K. Phospha[3]radialenes. Syntheses, Structures, Strain Energies, and Reactions. *J. Am. Chem. Soc.* **2000**, *122*, 12507−12516. (g) Urushizaki, A.; Yumura, T.; Kitagawa, Y.; Hasegawa, Y.; Imoto, H.; Naka, K. Dithieno[3,4-*b*:3′,4′-*d*]arsole: A Novel Class of Hetero[5]radialenes. *Eur. J. Org. Chem.* **2020**, *2020*, 3965−3970. (h) Higashino, T.; Imahori, H. Hybrid [5]Radialenes with Bispyrroloheteroles: New Electron-Donating Units. *Chem. - Eur. J.* **2015**, *21*, 13375−13381. (i) Janssen, M. J.; De Jong, F. Synthesis, Oxidation, and Electronic Spectra of Four Dithienothiophenes. *J. Org. Chem.* **1971**, *36*, 1645−1648. (j) Iyoda, M.; Miura, M. I.; Sasaki, S.; Kabir, S. M. H.; Kuwatani, Y.; Yoshida, M. Synthesis of dithienothiophenes, cyclopentadithiophene and silacyclopentadithiophenes using palladium-catalyzed cyclization. *Tetrahedron Lett.* **1997**, *38*, 4581−4582. (k) Brieden, W.; Kellersohn, T. Synthesis and Crystal Structure of the First "1,2-Diphospha[4]radialene. *Chem. Ber.* **1993**, *126*, 845−847.
(8) Berionni, G.; Wu, J. I. C.; Schleyer, P. v. R. Aromaticity Evaluations of Planar [6]Radialenes. *Org. Lett.* **2014**, *16*, 6116−6119.
(9) Shi, X.; Chi, C. Heterocyclic Quinodimethanes. *Top. Curr. Chem.* **2017**, *375*, 68.
(10) Zeng, Z.; Shi, X.; Chi, C.; Lopez Navarrete, J. T.; Casado, J.; Wu, J. Pro-aromatic and anti-aromatic π-conjugated molecules: an irresistible wish to be diradicals. *Chem. Soc. Rev.* **2015**, *44*, 6578−6596.
(11) (a) Rudebusch, G. E.; Fix, A. G.; Henthorn, H. A.; Vonnegut, C. L.; Zakharov, L. N.; Haley, M. M. Quinoidal diindenothienoacenes: synthesis and properties of new functional organic materials. *Chem. Sci.* **2014**, *5*, 3627−3633. (b) Shi, X.; Burrezo, P. M.; Lee, S.; Zhang, W.; Zheng, B.; Dai, G.; Chang, J.; López Navarrete, J. T.; Huang, K.-W.; Kim, D.; Casado, J.; Chi, C. Antiaromatic bisindeno-[*n*]thienoacenes with small singlet biradical characters: syntheses, structures and chain length dependent physical properties. *Chem. Sci.* **2014**, *5*, 4490−4503.
(12) Marshall, J. L.; Lehnherr, D.; Lindner, B. D.; Tykwinski, R. R. Reductive Aromatization/Dearomatization and Elimination Reactions to Access Conjugated Polycyclic Hydrocarbons, Heteroacenes, and Cumulenes. *ChemPlusChem.* **2017**, *82*, 967−1001.
(13) (a) Hu, P.; Lee, S.; Park, K. H.; Das, S.; Herng, T. S.; Gonçalves, T. P.; Huang, K.-W.; Ding, J.; Kim, D.; Wu, J. Octazethrene and Its Isomer with Different Diradical Characters and Chemical Reactivity: The Role of the Bridge Structure. *J. Org. Chem.* **2016**, *81*, 2911−2919. (b) Hayashi, H.; Barker, J. E.; Cárdenas Valdivia, A.; Kishi, R.; MacMillan, S. N.; Gómez-García, C. J.; Miyauchi, H.; Nakamura, Y.; Nakano, M.; Kato, S.; Haley, M. M.; Casado, J. Monoradicals and Diradicals of Dibenzofluoreno[3,2-*b*]Fluorene Isomers: Mechanisms of Electronic Delocalization. *J. Am. Chem. Soc.* **2020**, *142*, 20444−20455.
(14) (a) Takahashi, K.; Suzuki, T.; Akiyama, K.; Ikegami, Y.; Fukazawa, Y. Synthesis and characterization of novel *p*-terphenoquinone analogs involving a central dihydrothiophenediylidene structure. *J. Am. Chem. Soc.* **1991**, *113*, 4576−4583. (b) Takahashi, K.; Suzuki, T. *p*-Diphenoquinone analogs extended by dihydrothiophenediylidene insertion. A novel amphoteric multistage redox system. *J. Am. Chem. Soc.* **1989**, *111*, 5483−5485. (c) Takahashi, K.; Gunji, A.; Akiyama, K. Novel Amphoteric 2,5-Furoquinonoid-Containing *p*-Terphenoquinone Analogues Giving Both a Stable Radical Anion and a Stable Radical Cation. *Chem. Lett.* **1994**, *23*, 863−866.
(15) Takahashi, K.; Sakai, T. Substituent Effects on Redox Potentials of Novel Amphoteric Terphenoquinone Analogues. Unsymmetrically Substituted 2,5-Bis(4-oxo-2,5-cyclohexadien-1-ylidene)-2,5-dihydrothiophenes. *Chem. Lett.* **1993**, *22*, 157−160.
(16) Phelan, N. F.; Orchin, M. Cross conjugation. *J. Chem. Educ.* **1968**, *45*, 633−637.
(17) Fallah-Bagher-Shaidaei, H.; Wannere, C. S.; Corminboeuf, C.; Puchta, R.; Schleyer, P. v. R. Which NICS aromaticity index for planar π rings is best? *Org. Lett.* **2006**, *8*, 863−866.
(18) Lu, T.; Chen, F. Multiwfn: A multifunctional wavefunction analyzer. *J. Comput. Chem.* **2012**, *33*, 580−592.
(19) Geuenich, D.; Hess, K.; Köhler, F.; Herges, R. Anisotropy of the Induced Current Density (ACID), a General Method To Quantify and Visualize Electronic Delocalization. *Chem. Rev.* **2005**, *105*, 3758−3772.
(20) Van, P. C.; Macomber, R. S.; Mark, H. B., Jr.; Zimmer, H. Lithiation reaction of 2, 5-dibromothiophene. C^{13} NMR spectra of 3-substituted derivatives. *J. Org. Chem.* **1984**, *49*, 5250−5253.
(21) Casado, J.; Ponce Ortiz, R. P.; Lopez Navarrete, J. T. Quinoidal oligothiophenes: new properties behind an unconventional electronic structure. *Chem. Soc. Rev.* **2012**, *41*, 5672−5686.
(22) Baron, P. A.; Brown, R. D.; Burden, F. R.; Domaille, P. J.; Kent, J. E. The microwave spectrum and structure of fulvene. *J. Mol. Spectrosc.* **1972**, *43*, 401−410.
(23) Sharma, P. K.; Mallick, D.; Sharma, H.; Das, S. Dominating Antiaromatic Character of *as*-Indacene Decides Overall Properties of a Formally Aromatic Dicyclopenta[*c*]fluorenothiophene. *Org. Lett.* **2023**, *25*, 2201−2206.
(24) Fargher, H. A.; Sherbow, T. J.; Haley, M. M.; Johnson, D. W.; Pluth, M. D. C−H···S hydrogen bonding interactions. *Chem. Soc. Rev.* **2022**, *51*, 1454−1469.
(25) Taniguchi, M.; Lindsey, J. S. Database of Absorption and Fluorescence Spectra of > 300 Common Compounds for use in PhotochemCAD. *Photochem. Photobiol.* **2018**, *94*, 290−327.
(26) (a) Rosenberg, M.; Dahlstrand, C.; Kilså, K.; Ottosson, H. Excited State Aromaticity and Antiaromaticity: Opportunities for Photophysical and Photochemical Rationalizations. *Chem. Rev.* **2014**, *114*, 5379−5425. (b) Grzybowski, M.; Morawski, O.; Nowak, K.; Garbacz, P. Fluorene analogues of xanthenes−low molecular weight near-infrared dyes. *Chem. Commun.* **2022**, *58*, 5455−5458.
(27) Chase, D. T.; Fix, A. G.; Rose, B. D.; Weber, C. D.; Nobusue, S.; Stockwell, C. E.; Zakharov, L. N.; Lonergan, M. C.; Haley, M. M. Electron-Accepting 6,12-Diethynylindeno[1,2-*b*]fluorenes: Synthesis, Crystal Structures, and Photophysical Properties. *Angew. Chem., Int. Ed.* **2011**, *50*, 11103−11106.
(28) Gleiter, R.; Röckel, H.; Irngartinger, H.; Oeser, T. Efficient Synthesis of Heteroradialenes by SN′ Reaction. *Angew. Chem., Int. Ed. Engl.* **1994**, *33*, 1270−1272.
(29) (a) Krygowski, T. M.; Oziminski, W. P.; Palusiak, M.; Fowler, P. W.; McKenzie, A. D. Aromaticity of substituted fulvene derivatives: substituent-dependent ring currents. *Phys. Chem. Chem. Phys.* **2010**, *12*, 10740−10745. (b) Preethalayam, P.; Krishnan, K. S.; Thulasi, S.; Chand, S. S.; Joseph, J.; Nair, V.; Jaroschik, F.; Radhakrishnan, K. V. Recent advances in the chemistry of pentafulvenes. *Chem. Rev.* **2017**, *117*, 3930−3989.
(30) Patra, A.; Bendikov, M. Polyselenophenes. *J. Mater. Chem.* **2010**, *20*, 422−433.
(31) (a) Higashino, T.; Mori, T. Small-molecule ambipolar transistors. *Phys. Chem. Chem. Phys.* **2022**, *24*, 9770−9806. (b) Sharma, H.; Ankita, A.; Bhardwaj, P.; Pandey, U. K.; Das, S. Exploring Indeno[2,1-*c*]fluorene Antiaromatics with Unsymmetrical Disubstitution and Balanced Ambipolar Charge-Transport Properties. *Organic Materials* **2023**, *5*, 72−83.

https://doi.org/10.1021/acs.orglett.3c01815
Org. Lett. 2023, 25, 5089−5093

ChemComm

COMMUNICATION

View Article Online
View Journal | View Issue

Cite this: *Chem. Commun.*, 2024, **60**, 7319

Received 9th February 2024,
Accepted 7th May 2024

DOI: 10.1039/d4cc00683f

rsc.li/chemcomm

Cyano disubstituted tetrabenzoindeno[2,1-*a*]fluorene: open-shell or closed-shell?†

Priyank Kumar Sharma,[a] Palash Jana,[b] Subhajit Bandyopadhyay[b] and Soumyajit Das *[a]

Organic diradicaloids have lately emerged as potential spintronic materials. We report the unprecedented synthesis of a near-IR absorbing indeno[2,1-*a*]fluorene derivative that displays remarkably low LUMO (−4.15 eV) and a small HOMO–LUMO gap (0.85 eV). NMR/EPR studies indicated its open-shell diradical property, which was supported by DFT calculations while suggesting a 30% diradical character and a small singlet (S)–triplet (T) gap (−2.52 kcal mol^{-1}). A large bond length alternation of the *as*-indacene core for its single-crystals indicated a quinoidal contribution with greater antiaromaticity, which is in line with the small diradical character despite showing a small S–T gap.

Exploration of polycyclic hydrocarbons (PHs) with antiaromatic and diradical properties has attracted immense interest in recent years,[1] as tuning such properties may provide paths toward new organic semiconductor materials with tunable band gaps. Formally antiaromatic indeno[1,2-*b*]fluorene[2] **1** and indeno[2,1-*a*]fluorene[3] **2** regioisomers are stable closed-shell (CS) molecules that display moderate antiaromaticity for the central *s*-indacene and *as*-indacene units,[4] respectively (Fig. 1a). Unsymmetrical disubstitution of [2,1-*a*]IF also resulted in a stable CS molecule **3**,[5] but benzo-extension of the central *as*-indacene unit of [2,1-*a*]IF afforded an open-shell (OS) molecule **benzo-2** with a large diradical character index (y_0 = 0.63), likely causing instability (half-life 77 min) and 8% synthetic yield.[6]

In continuation of efforts[7] to synthesize the elusive arene-fused dicyclopenta[*b*,*d*]thiophene (DCPT),[7a,b] a diphenanthro-DCPT (**DPDCPT**) derivative was targeted (Fig. 1b). While attempting its synthesis by a DDQ (2,3-dichloro-5,6-dicyano-1,4-benzoquinone) mediated dehydrogenation from dihydro precursor **2H-DPDCPT**, we failed to isolate it presumably due to the high reactivity (electron-rich, large y_0 = 0.51, and a small singlet–triplet energy gap (ΔE_{S-T}) = −0.64 kcal mol^{-1}; Table S2, ESI†), as analysed by density functional theory (DFT) calculation. Instead, we isolated a cyano disubstituted tetrabenzoindeno[2,1-*a*]fluorene **6** (Fig. 1b) as a degradation product, and it was confirmed by single-crystal X-ray diffraction (SCXRD) analysis (*vide infra*). Isolation of **6** was interesting since there is no straightforward synthetic approach known thus far to construct **5**, which is a constitutional isomer of known tetrabenzoindeno[1,2-*b*]fluorene **4**,[8] which displays a greater degree of antiaromaticity for the *s*-indacene unit than that of **1**. Our DFT optimization of **5** indicated its CS ground state, like **4**, and its OS singlet state was found to be isoenergetic with the CS state with a small ΔE_{S-T} = −3.46 kcal mol^{-1} (Table S2, ESI†). A lowering of the triplet state for **5**, despite showing a negligible diradical character (y_0 = 0.01), is in line with a recent report[9] by

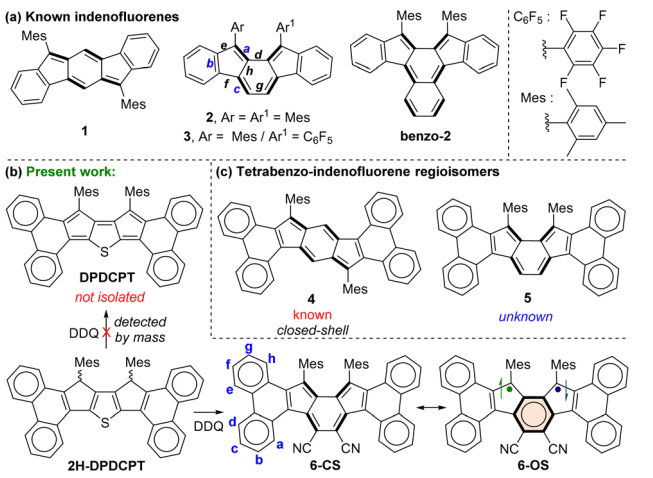

Fig. 1 (a) Indeno[1,2-*b*]fluorene **1**, indeno[2,1-*a*]fluorenes **2** & **3**, and benzo-fused [2,1-*a*]IF **benzo-2**. (b) Targeted diphenanthro-DCPT, and the synthesized tetrabenzoindeno[2,1-*a*]fluorene **6** and its resonance forms. (c) Isomeric tetrabenzoindeno[1,2-*b*]fluorene **4** and tetrabenzoindeno[2,1-*a*]fluorene **5** derivatives.

[a] *Department of Chemistry, Indian Institute of Technology Ropar, Rupnagar 140001, Punjab, India. E-mail: chmsdas@iitrpr.ac.in*
[b] *Department of Chemical Sciences, Indian Institute of Science Education and Research (IISER) Kolkata, Mohanpur 741246, West Bengal, India*

† Electronic supplementary information (ESI) available: Detailed syntheses and characterization data for **6**; X-ray crystallographic data; DFT calculations; NMR spectra; direct mass spectrum of **DPDCPT**; and plausible mechanism for formation of **6**. CCDC 2309430. For ESI and crystallographic data in CIF or other electronic format see DOI: https://doi.org/10.1039/d4cc00683f

Ottosson and Solà *et al.* explaining that diphenanthro-fused antiaromatics (pentalene, *s*-indacene) may display low-lying triplet states. Despite the lowering of the triplet excited state, **5** didn't show an OS ground state, theoretically.

We envisaged that the cyano (–CN) substituents for **6** may result in a smaller HOMO–LUMO energy spacing than that of **5**, seemingly due to the greater stabilization effect exerted by electron-withdrawing –CN groups (negative resonance effect), which are attached to *as*-indacene carbons containing large LUMO coefficients (Fig. S22, ESI†).[10] A small HOMO–LUMO energy gap is crucial to show an OS ground state, as evident from CS heptazethrene-triisopropylsilylethynyl (**HZ-TIPS**)[11] *vs.* OS heptazethrene-dicarboximide (**HZ-DI**),[12] though the number of Clar sextet recoveries remains the same for them. Therefore, in this work, compound **6** was thoroughly studied by various analytical techniques and DFT calculations to conclude its electronic ground state, while reporting its unprecedented synthesis.

Suzuki coupling between commercially available **7** and 2,5-dibromothiophene-3,4-dicarbaldehyde **8**,[13] as depicted in Scheme 1, afforded dialdehyde derivative **9**. Treatment of **9** with 2-mesitylmagnesiumbromide afforded a diol intermediate, which was subsequently treated with $BF_3{\cdot}Et_2O$ to give **2H-DPDCPT**, which is the dihydro precursor of **DPDCPT**. DDQ-mediated oxidative dehydrogenation of **2H-DPDCPT** in dichloromethane (DCM) remained partially complete, even after refluxing or increasing the reaction time, as monitored by thin layer chromatography. To ensure complete conversion, 4 equiv. DDQ was added, and the reactant was consumed within 30 minutes at room temperature (rt). The formation of the targeted **DPDCPT** could be detected from the crude reaction mixture by direct mass spectrometric (MS) analysis (Fig. S25, ESI†), but unfortunately, no desired product trace was obtained after traditional silica gel column chromatography; instead, **DPDCPT-DDQ** was isolated as a 10+2 cycloaddition adduct,[14] likely due to the reaction of **DPDCPT** and DDQ on the silica surface (Fig. S26, ESI†).

Treatment of silica gel with triethylamine, prior to loading the slurry of the crude reaction mixture containing DDQ, afforded a deep purple solid in 42% yield. However, the high-resolution mass (m/z = 739.3099) didn't match the desired mass of **DPDCPT**. It was found to be an unexpected product **6** after SCXRD analysis of the purple solid (Fig. 2), plausibly formed by

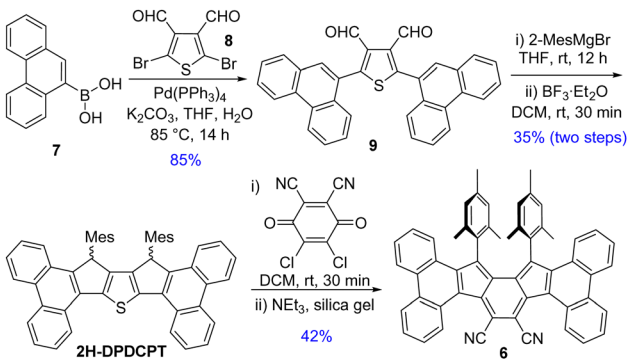

Scheme 1 Synthesis of **6**.

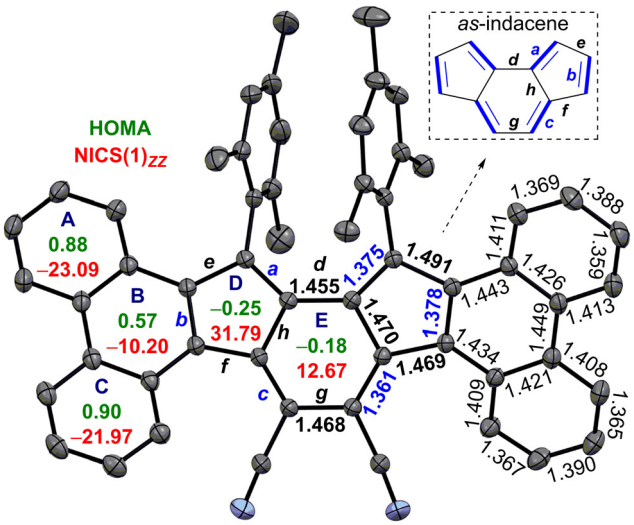

Fig. 2 ORTEP drawing of **6** with thermal ellipsoids at the 30% probability level (hydrogens and disordered solvent omitted), including the mean bond lengths (in angstroms), NICS(1)$_{zz}$ (red) and HOMA (green) indices.

the loss of a sulfur atom and ClC(═C═O)C(Cl)═C═O unit from the **DPDCPT-DDQ** adduct on neutral silica gel or an alumina column (Fig. S26, ESI†).[14b,c] Nonetheless, **6** is the first diphenanthro-*as*-indacene derivative with an *ortho*-quinoidal backbone, which is a structural isomer of **4**.

The single crystals of **6** were grown in a DCM/acetonitrile mixture (Fig. 2). SCXRD analysis of **6** revealed a contorted π-backbone (Fig. S13a, ESI†) due to the steric congestion between the –CN group and ring-C hydrogen in the cove region and repulsive interaction between the bulky mesityl groups, which are orthogonal to the IF backbone. The terminal phenanthrene units were twisted by an avg. torsional angle of 30.1°, as measured from the mean planes between central ring E and outer phenanthrene units (Fig. S13a, ESI†). The C–C double bond *b* linking *as*-indacene and the phenanthrene unit and the *exo*-methylene bond *a* for **6** are 0.032 Å and 0.016 Å, respectively, shorter than those of **2** (Fig. 2 and Table 1). The C–C single bonds *d*–*h* for **6** possess more single bond character (1.455 to 1.491 Å), with *e* and *g* bonds 0.016 and 0.037 Å longer than those of **2**. The degree of bond length alternation (BLA) in the *as*-indacene unit has significantly enhanced for **6** in comparison to **2**, suggesting a reduced extent of π-delocalization for the *as*-indacene core in **6**, indicating a greater degree of antiaromaticity for **6** than that of **2**. On the other hand, the homogeneous bond length distribution for rings A (avg. 1.394 Å) and C (avg. 1.393 Å) in **6** suggested a greater degree of benzene-like aromaticity than that of ring B (avg. 1.425 Å).

The harmonic oscillator model of aromaticity (HOMA)[15] analyses of the optimized structure **6** (at BHandHLYP/6-31G*)

Table 1 Mean C_{sp^2}–C_{sp^2} crystal bond lengths (*a*–*h*, in Å) of **6** *vs.* **2**, for *as*-indacene

	a	*b*	*c*	*d*	*e*	*f*	*g*	*h*
6	1.375	1.378	1.361	1.455	1.491	1.469	1.468	1.470
2	1.391	1.410	1.359	1.454	1.475	1.463	1.431	1.480

supported the large BLA for rings D (−0.25) and E (−0.18), whereas small (A = 0.88, C = 0.90) to moderate (B = 0.57) BLA for phenanthrene indicated its aromaticity (Fig. 2). Nuclear independent chemical shift (NICS)[16] calculation showed larger positive NICS(1)$_{zz}$ values for rings D (31.79) and E (12.67) for **6** than those of **2**, suggesting enhanced antiaromaticity of the *as*-indacene unit for **6**. The negative NICS values of rings A (−23.09), B (−10.20), and C (−21.97) for **6** are in line with the HOMA values, supporting phenanthrene ring aromaticity.

The observation of proton NMR (nuclear magnetic resonance) line broadening for **6** at rt (Fig. S5, ESI†) prompted us to study its variable temperature (VT) NMR behaviour. In $CDCl_3$, **6** exhibited broad NMR signals for some of the aromatic protons (d, c, b protons in Fig. 3a, see Fig. 1b for proton labels) at rt, while other ring protons were also broadened upon heating (Fig. S9, ESI†). These broad NMR signals became sharper upon gradual cooling and became reasonably sharper at −60 °C (213 K). This is a typical observation for OS diradicaloid PHs with small ΔE_{S-T},[11,17] due to which the excited triplet state can be thermally populated at rt or by slight heating. The observation was also supported by VT-EPR (electron paramagnetic resonance), exhibiting a featureless broad signal (g_e = 2.0041) at rt, while the signal intensity decreased as the temperature was lowered from 260 K to 150 K (Fig. 3b), which is a consequence of reduced population of magnetically active triplet species at lower temperatures.[18] A careful fitting of the VT-EPR data using the Bleaney–Bowers equation[19] gave a ΔE_{S-T} = −0.97 kcal mol^{-1} for **6** (Fig. S11a, ESI†), suggesting singlet OS ground state, which is in line with VT-EPR in solution (ΔE_{S-T} = −1.73 kcal mol^{-1}, Fig. S11b and c, ESI†).

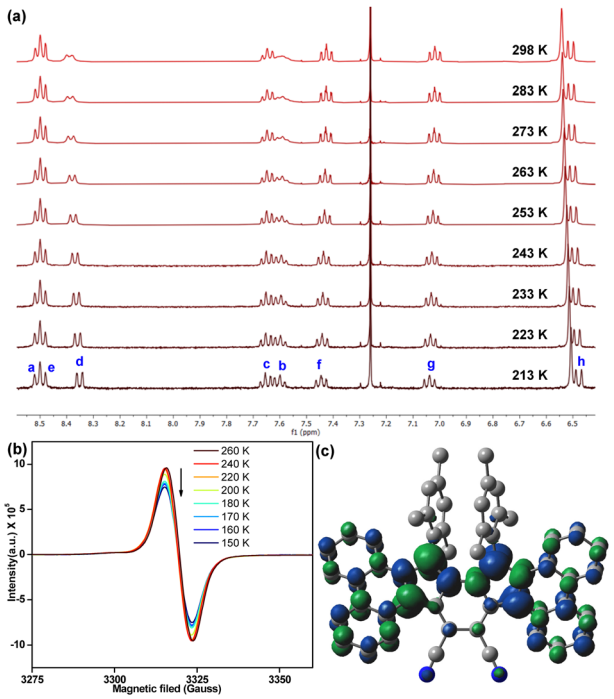

Fig. 3 (a) Partial VT-NMR of **6** in $CDCl_3$ showing aromatic protons (see Fig. 1b for proton labels); (b) VT-EPR spectra of solid sample **6**; (c) spin density distribution of singlet OS **6**.

DFT calculation of **6** at the BHandHLYP/6-31G* level of theory[20] confirmed that the energy of an OS singlet state was 1.96 kcal mol^{-1} and 2.52 kcal mol^{-1} lower than the energy of the CS singlet (quinoidal) and triplet (biradical) states, respectively (Table S2, ESI†). The y_0 for **6** was estimated to be 0.30, based on the natural orbital occupation numbers using the broken symmetry formalism. The frontier molecular orbital profiles for α- and β-spins (Fig. S21, ESI†) displayed the characteristic disjointed nature in the ground state singlet diradical form. The spin densities were observed to be uniformly dispersed across the entire π-conjugated framework (Fig. 3c), giving thermodynamic stability.

The UV-vis-NIR (UV-visible-near infrared) spectrum (Fig. 4a) of **6** exhibited intense absorption peaks at λ_{max} = 312 nm (ε = 30 000 M^{-1} cm^{-1}) and λ_{max} = 365 nm (ε = 19 000 M^{-1} cm^{-1}) in the UV region and a moderate absorption in the visible region λ_{max} = 554 nm (ε = 11 000 M^{-1} cm^{-1}), which is associated with a weak absorption band in the lowest energy region stretching from 750 to 1500 nm in the NIR region with the absorption maximum at λ_{max} = 1000 nm (ε = 650 M^{-1} cm^{-1}). Time dependent-DFT (TD-DFT) calculations of **6** in toluene (Fig. S19, ESI†) suggested that the absorption in the visible region is dominated by the HOMO−1 → LUMO transition (λ_{max} = 476 nm, oscillator strength (f) = 0.55, Table S3, ESI†), while the weaker lowest energy absorption tail has originated from a forbidden HOMO → LUMO transition (λ_{max} = 877 nm, f = 0.028). Such a long wavelength absorption tail could originate due to the admixing of the doubly excited electronic configuration (H,H → L,L) for **6** owing to its OS ground state, as observed for Kubo's diphenaleno-DCPT.[14a] Compound **6** displayed a very small optical HOMO–LUMO energy gap of 0.85 eV, as roughly estimated from the lowest energy absorption onset (1240/λ_{onset}); yet, a good photostability under ambient conditions with a half-life of 9 days was observed for **6** (Fig. S10, ESI†).

Cyclic voltammetry (CV) and differential pulse voltammetry (DPV) analyses (Fig. 4b) suggested that **6** could be easily reversibly reduced at $E_{1/2}^{red1}$ = −0.73 V and at $E_{1/2}^{red2}$ = −1.16 V (*vs.* ferrocene/ferrocenium (Fc/Fc$^+$) couple). It can also be oxidized to its radical cation and dication species at E_{peak}^{ox1} = 0.68 V and E_{peak}^{ox2} = 0.93 V, respectively. The HOMO and LUMO energy levels were −5.40 eV and −4.15 eV, as estimated from the onset potentials of the oxidation and reduction waves, respectively, giving a small electrochemical energy gap of 1.25 eV. The LUMO energy level of **6** is remarkably stabilized (low-lying) due to the electron-withdrawing cyano substituents, as hypothesized.

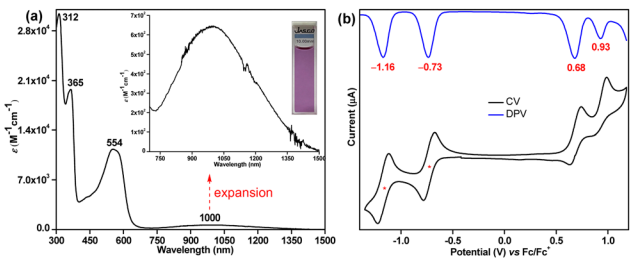

Fig. 4 (a) UV-vis-NIR absorption spectrum of **6** in toluene (715–1500 nm expansion shown in inset); (b) CV and DPV of **6**.

The greater stabilization of the LUMO basically reduced the HOMO–LUMO energy gap, and the observation is comparable to **HZ-TIPS** *vs.* **HZ-DI**, where **HZ-DI** with a small HOMO–LUMO gap displayed an OS diradicaloid ground state despite one Clar sextet being recovered for both molecules in their OS forms.[11,12] The smaller ΔE_{S-T} for **6** than that of **5** could be caused by the narrower HOMO–LUMO gap of **6** pushing its triplet excited state to locate closer to the singlet ground state.[21] As a result, the excited triplet state could be easily thermally populated at rt or by slight heating, despite showing a small y_0. Usually, the greater the y_0, the smaller the ΔE_{S-T};[22] with a few noteworthy exceptions[23] (including **benzo-2**)[6] showing a larger ΔE_{S-T} although exhibiting a larger y_0. To the best of our knowledge, compound **6** is a unique example that exhibits a small y_0 despite showing a small ΔE_{S-T}.

Typically, an OS PH with large y_0 displays a large energy difference between its CS singlet and OS singlet states, and a small energy difference between its OS singlet state and first excited triplet state.[24] Our experimental and theoretical studies confirmed that **6** exists as an OS diradicaloid in the singlet ground state with its CS quinoidal state lying in between the OS ground state and triplet excited state, which is unlike the known diradicaloid PHs[17,24] with large y_0 displaying CS quinoidal states lying vertically at a much higher energy level above the triplet state. A significant BLA for the central *as*-indacene unit of **6** in its crystalline form indicates a dominant quinoidal structure presumably due to the rt accessible low-lying CS state, which is in line with the small y_0. This observation suggested that both CS and OS resonance forms for **6** may contribute to the singlet ground state.

In summary, a formally antiaromatic diphenanthro-*as*-indacene derivative **6** was synthesized, that exhibits diradical-like and antiaromatic properties in its OS singlet ground state as a result of a low-lying CS state. Though the formation of **6** was unexpected, its detailed characterization gave newer insights in diradical chemistry as our study suggested that substitution driven HOMO–LUMO energy gap modulation can affect the ground state properties for antiaromatic PHs. The small y_0 (30%) for **6** could likely be attributed to the dominant *as*-indacene antiaromaticity owing to the low-lying quinoidal CS form, as supported by SCXRD analysis and NICS(1)$_{zz}$ calculation. The VT-NMR and VT-EPR experiments indicated its singlet diradicaloid ground state, which is the consequence of a small HOMO–LUMO energy gap. Qualitative correlations between the structural features and the properties of different diradicaloid systems usually indicate an increased y_0 as the energy separation between the singlet and triplet states decreased. However, compound **6** is an example of a rare diradicaloid exhibiting a small y_0 despite showing a small ΔE_{S-T}, implying potential for applications in organic spintronics and photonics (non-linear optics and singlet-fission) studies.[25]

S. D. thanks SERB, India (CRG/2022/003012) for funding. P. K. S. and P. J. thank CSIR for the senior research fellowship. S. B. thanks SERB for a research grant (CRG/2022/006776). The authors thank Kamlesh Satpute (IIT Ropar) for SCXRD data of **6**.

Conflicts of interest

There are no conflicts to declare.

Notes and references

1 (*a*) A. Konishi, Y. Okada, M. Nakano, K. Sugisaki, K. Sato, T. Takui and M. Yasuda, *J. Am. Chem. Soc.*, 2017, **139**, 15284; (*b*) T. Xu, X. Hou, Y. Han, H. Wei, Z. Li and C. Chi, *Angew. Chem., Int. Ed.*, 2023, **62**, e202304937.
2 D. T. Chase, A. G. Fix, S. J. Kang, B. D. Rose, C. D. Weber, Y. Zhong, L. N. Zakharov, M. C. Lonergan, C. Nuckolls and M. M. Haley, *J. Am. Chem. Soc.*, 2012, **134**, 10349.
3 A. Shimizu and Y. Tobe, *Angew. Chem., Int. Ed.*, 2011, **50**, 6906.
4 Y. Tobe, *Top. Curr. Chem.*, 2018, **376**, 12.
5 H. Sharma, N. Bhardwaj and S. Das, *Org. Biomol. Chem.*, 2022, **20**, 8071.
6 H. Miyoshi, S. Nobusue, A. Shimizu, I. Hisaki, M. Miyata and Y. Tobe, *Chem. Sci.*, 2014, **5**, 163.
7 (*a*) X. Shi and C. Chi, *Top. Curr. Chem.*, 2017, **375**, 68; (*b*) P. K. Sharma, D. Mallick and S. Das, *Org. Lett.*, 2023, **25**, 5089; (*c*) X. Shi, P. Mayorga Burrezo, S. Lee, W. Zhang, B. Zheng, G. Dai, J. Chang, J. T. López Navarrete, K.-W. Huang, D. Kim, J. Casado and C. Chi, *Chem. Sci.*, 2014, **5**, 4490; (*d*) G. E. Rudebusch, A. G. Fix, H. A. Henthorn, C. L. Vonnegut, L. N. Zakharov and M. M. Haley, *Chem. Sci.*, 2014, **5**, 3627.
8 C. K. Frederickson, L. N. Zakharov and M. M. Haley, *J. Am. Chem. Soc.*, 2016, **138**, 16827.
9 R. Ayub, O. El Bakouri, K. Jorner, M. Solà and H. Ottosson, *J. Org. Chem.*, 2017, **82**, 6327.
10 A. Casey, S. D. Dimitrov, P. Shakya-Tuladhar, Z. Fei, M. Nguyen, Y. Han, T. D. Anthopoulos, J. R. Durrant and M. Heeney, *Chem. Mater.*, 2016, **28**, 5110.
11 Y. Li, W.-K. Heng, B. S. Lee, N. Aratani, J. L. Zafra, N. Bao, R. Lee, Y. M. Sung, Z. Sun, K.-W. Huang, R. D. Webster, J. T. López Navarrete, D. Kim, A. Osuka, J. Casado, J. Ding and J. Wu, *J. Am. Chem. Soc.*, 2012, **134**, 14913.
12 Z. Sun, K.-W. Huang and J. Wu, *J. Am. Chem. Soc.*, 2011, **133**, 11896.
13 P. K. Sharma, D. Mallick, H. Sharma and S. Das, *Org. Lett.*, 2023, **25**, 2201.
14 (*a*) T. Kubo, M. Sakamoto, M. Akabane, Y. Fujiwara, K. Yamamoto, M. Akita, K. Inoue, T. Takui and K. Nakasuji, *Angew. Chem., Int. Ed.*, 2004, **43**, 6474; (*b*) Z.-L. Wang, H.-L. Li, L.-S. Ge, X.-L. An, Z.-G. Zhang, X. Luo, J. S. Fossey and W.-P. Deng, *J. Org. Chem.*, 2014, **79**, 1156; (*c*) J. S. Li, Y. Xue, Z. W. Li, W. D. Liu, C. H. Lu and P. X. Zhao, *Synlett*, 2013, **24**, 2003.
15 T. Lu and F. Chen, *J. Comput. Chem.*, 2012, **33**, 580.
16 H. Fallah-Bagher-Shaidaei, C. S. Wannere, C. Corminboeuf, R. Puchta and P. V. R. Schleyer, *Org. Lett.*, 2006, **8**, 863.
17 (*a*) S. Das, S. Lee, M. Son, X. Zhu, W. Zhang, B. Zheng, P. Hu, Z. Zeng, Z. Sun, W. Zeng, R.-W. Li, K.-W. Huang, J. Ding, D. Kim and J. Wu, *Chem. – Eur. J.*, 2014, **20**, 11410; (*b*) P. Yadav, S. Das, H. Phan, T. S. Herng, J. Ding and J. Wu, *Org. Lett.*, 2016, **18**, 2886.
18 P. Jana, S. Koppayithodi, S. Mahato, S. Molla and S. Bandyopadhyay, *J. Phys. Chem. Lett.*, 2023, **14**, 7433.
19 B. Bleaney and K. D. Bowers, *Proc. R. Soc. London, Ser. A*, 1952, **214**, 451.
20 S. Lehtola, M. Dimitrova, H. Fliegl and D. Sundholm, *J. Chem. Theory Comput.*, 2021, **17**, 1457.
21 W. Zeng, Q. Qi and J. Wu, *Eur. J. Org. Chem.*, 2018, **2018**, 7.
22 J. J. Dressler and M. M. Haley, *J. Phys. Org. Chem.*, 2020, **33**, e4114.
23 (*a*) J. J. Dressler, M. Teraoka, G. L. Espejo, R. Kishi, S. Takamuku, C. J. Gómez-García, L. N. Zakharov, M. Nakano, J. Casado and M. M. Haley, *Nat. Chem.*, 2018, **10**, 1134; (*b*) J. E. Barker, J. J. Dressler, A. Cárdenas Valdivia, R. Kishi, E. T. Strand, L. N. Zakharov, S. N. MacMillan, C. J. Gómez-García, M. Nakano, J. Casado and M. M. Haley, *J. Am. Chem. Soc.*, 2020, **142**, 1548.
24 S. S. K. Boominathan, K.-H. Chang, Y.-C. Liu, C.-S. Wang, C.-F. Wu, M.-H. Chiang, P.-T. Chou and Y.-T. Wu, *Chem. – Eur. J.*, 2019, **25**, 7280.
25 (*a*) S. Datta, Y. Cai, I. Yudhistira, Z. Zeng, Y.-W. Zhang, H. Zhang, S. Adam, J. Wu and K. P. Loh, *Nat. Commun.*, 2017, **8**, 677; (*b*) M. Nakano, *Chem. Rec.*, 2017, **17**, 27.

